

Technical Report Documentation Page

1. Report No. CA10-1130		2. Government Accession No.		3. Recipient's Catalog No.	
4. Title and Subtitle Assessment of Durability of FRP Materials for Use in Civil Infrastructure				5. Report Date March 2011	
				6. Performing Organization Code	
7. Author(s) Vistasp M. Karbhari, Soon Kook Hong, Vi Njuyen, Seth Farington, Quan Yang, Guijun Xian				8. Performing Organization Report No. UAH 11/1	
9. Performing Organization Name and Address University of Alabama in Huntsville Huntsville, AL 35899				10. Work Unit No. (TRAIS)	
				11. Contract or Grant No. 59A0602	
12. Sponsoring Agency Name and Address California Department of Transportation Division of Engineering Services 1801 30 th St., West Building MS-9 Sacramento, California 95816				13. Type of Report and Period Covered Final Report	
				14. Sponsoring Agency Code	
15. Supplementary Notes Prepared in cooperation with the State of California Department of Transportation.					
16. Abstract This report builds on the earlier research conducted in the area of durability, data for which was presented in SSRP-09/05 titled "Durability Data for FRP Rehabilitation Systems" and addresses three crucial aspects related to (1) effects of elevated temperature and aqueous exposure, (2) development of a MOL, and (3) development of a reliability based methodology for use of these data for prediction of long-term durability. Although aspects related to each are presented in separate section (A, B and C, respectively) to enable clarity in understanding the development and background of each, the end goal was to enable the development of a methodology for the reliable estimation of design data pertaining to FRP materials based on prediction of long-term durability. It is anticipated that the methodology presented in the report can be applied by designers both in the determination of threshold, MOL, values of composite performance and in the selection of appropriate levels of allowable material characteristics to include long-term durability considerations.					
17. Key Words Composite, Strengthening, Durability, Carbon/Epoxy, Temperature				18. Distribution Statement No restrictions	
19. Security Classification (of this report) Unclassified		20. Security Classification (of this page) Unclassified		21. No. of Pages 825	22. Price

DISCLAIMER

This document is disseminated in the interest of information exchange. The contents of this report reflect the views of the authors who are responsible for the facts and the accuracy of the data presented herein. The contents do not necessarily reflect the official views or policies of the State of California or the Federal Highway Administration. This publication does not constitute an endorsement by the Department of any product described herein.

For individuals with sensory disabilities, this document is available in Braille, large print, audiocassette, or compact disk. To obtain a copy of this document in one of these alternate formats, please contact: The Division of Research and Innovation, MS-83, California Department of Transportation, P.O. Box 942873, Sacramento, CA 94273-0001.



Report No.
UAH-11/1

**ASSESSMENT OF DURABILITY OF FRP
MATERIALS FOR USE IN CIVIL INFRASTRUCTURE**

Submitted by

VISTASP M. KARBHARI

Final Report Submitted to the California Department of
Transportation Under Contract No. 59A0602.

August 2011

University of Alabama in Huntsville
Huntsville, AL 35899

University of Alabama in Huntsville

Report No. UAH 11/1

**Assessment of Durability of FRP Materials For Use in Civil
Infrastructure**

Submitted by

Vistasp M. Karbhari

Professor

Final Report submitted to the California Department of Transportation
Under Contract No. 59A0602.

University of Alabama in Huntsville
Huntsville, AL 35899

August 2011

PART A

ASSESSMENT OF DURABILITY OF CARBON/EPOXY COMPOSITE MATERIALS AFTER EXPOSURE TO ELEVATED TEMPERATURES AND IMMERSION

TABLE OF CONTENTS

TABLE OF CONTENTS.....	i
LIST OF SYMBOLS.....	vi
LIST OF FIGURES.....	ix
LIST OF TABLES.....	xix
ABSTRACT.....	xxiii
1 Introduction.....	2
1.1 Introduction.....	2
1.2 Motivation.....	5
1.3 Research Objectives.....	5
1.4 Overview of Research.....	6
2 Literature Review.....	8
2.1 Fire Safety of FRP Composite Materials.....	8
2.2 Thermal Decomposition of FRP Composite Materials in Fire.....	9
2.2.1 Introduction.....	9
2.2.2 Description of Mechanisms of Thermal Degradation.....	9
2.2.2.1 Processes of Combustion in Composites.....	10
2.2.2.2 Epoxy Resin.....	10
2.2.2.3 Carbon Fibers.....	11
2.2.3 Review of Analytical Models for Effects of Fire.....	12
2.3 Effects of Seawater on FRP Composites.....	14
2.3.1 Seawater Properties.....	14
2.3.2 Seawater Effect on Mechanical Properties.....	16
2.3.2.1 Tension.....	16
2.3.2.2 Flexure.....	18
2.3.2.3 Other Mechanical Properties.....	19
2.4 Review of Naval/Marine Applications of FRP Composites.....	20
2.4.1 Introduction.....	20

	2.4.2	Surface ships	21
	2.4.3	Submarines.....	23
3		Materials and Test Methods	25
	3.1	Material Specification.....	25
	3.2	Environmental Conditions	26
	3.2.1	Mechanical Properties and Thermal Analyses	26
	3.2.2	Immersion Tests	27
	3.3	Test Procedures	29
	3.4	Data Statistics	30
	3.5	Test Methods.....	31
	3.5.1	Tension	31
	3.5.2	Off-Axis Shear	32
	3.5.3	Flexure	33
	3.5.4	Short Beam Shear	35
	3.5.5	Dynamic Mechanical Thermal Analysis (DMTA).....	36
	3.5.6	Differential Scanning Calorimetry (DSC)	38
	3.5.7	Thermogravimetric Analysis.....	39
	3.5.8	Moisture Uptake.....	41
4		Mechanical Characterization.....	42
	4.1	Tensile Testing	42
	4.1.1	Introduction.....	42
	4.1.2	Data Reduction.....	42
	4.1.3	Analyses and Results	44
	4.1.3.1	Time Dependence	44
	4.1.3.2	Temperature Dependence	56
	4.1.3.3	Morphological Analysis	61
	4.1.3.4	Strain Effect.....	68
	4.1.3.5	Volume Fraction Effect.....	74
	4.2	Off-Axis Shear Testing	79

4.2.1	Introduction.....	79
4.2.2	Data Reduction.....	80
4.2.3	Analyses and Results	82
4.2.3.1	Time Dependence.....	82
4.2.3.2	Temperature Dependence	94
4.2.3.3	Morphological Analysis	97
4.2.3.4	Strain Effect.....	100
4.2.3.5	Correlation to Tensile Test Results	102
4.3	Flexural Testing	107
4.3.1	Introduction.....	107
4.3.2	Data Reduction.....	107
4.3.3	Analyses and Results	109
4.3.3.1	Time Dependence.....	109
4.3.3.2	Temperature Dependence	121
4.3.3.3	Morphological Analysis	124
4.3.3.4	Strain Effect.....	125
4.4	Short Beam Shear Testing	128
4.4.1	Introduction.....	128
4.4.2	Data Reduction.....	129
4.4.3	Analyses and Results	130
4.4.3.1	Time Dependence.....	130
4.4.3.2	Temperature Dependence	137
4.4.3.3	Morphological Analysis	140
4.4.3.4	Correlation to Tensile Test Results	144
5	Thermal Analysis	147
5.1	Dynamic Mechanical Thermal Analysis.....	147
5.1.1	Introduction.....	147
5.1.2	Data Reduction.....	149
5.1.3	Analyses and Results	150
5.1.3.1	Glass transition temperature.....	150

5.1.3.2	Height of Tangent Delta	161
5.1.3.3	Activation Energy.....	171
5.1.3.4	Modulus.....	177
5.1.3.5	Mechanical Retention based on T_g	183
5.2	Differential Scanning Calorimetry	187
5.2.1	Introduction.....	187
5.2.2	Data Reduction.....	188
5.2.2.1	Glass Transition Temperature.....	188
5.2.2.2	Heat Capacity	189
5.2.3	Analyses and Results	190
5.3	Thermogravimetric Analysis	195
5.3.1	Introduction.....	195
5.3.2	Analyses and Results	197
5.3.2.1	Weight loss	197
5.3.2.2	Determination of Thermal Stability Parameters.....	202
5.3.2.3	Mechanical Retention based on Weight loss	211
6	Immersion Analysis.....	213
6.1	Introduction	213
6.1.1	Moisture Effect on Polymer Composites.....	214
6.1.2	Diffusion in Polymer Composites.....	215
6.2	Analyses and Results.....	219
6.2.1	Water Uptake.....	219
6.2.2	Morphological Analysis.....	242
6.2.3	Short Beam Shear Testing.....	246
6.2.3.1	Temperature Dependence	246
6.2.3.2	Time Dependence.....	251
7	Predictive Degradation Models.....	255
7.1	Introduction	255
7.2	Arrhenius Rate Degradation Model.....	256

7.2.1	Data Analysis Procedure	257
7.2.2	Results	265
7.2.2.1	Tensile Testing	265
7.2.2.2	Off-Axis Shear Testing	266
7.2.2.3	Flexural Testing	267
7.2.2.4	Short Beam Shear Testing	268
7.3	Time Temperature Superposition Model	269
7.3.1	Data Analysis Procedure	271
7.3.2	Results	275
7.3.2.1	Other Mechanical properties	275
7.3.2.2	Comparison with Arrhenius rate model	277
7.4	Weibull Statistical Strength Model	282
7.4.1	Introduction	282
7.4.2	Theory	283
7.4.3	Results	286
7.4.3.1	Predictive Data of Flexural Strength from Tensile Tests	286
7.4.3.2	Predictive Data of Tensile Strength from Flexural Tests	290
8	Conclusions	295
8.1.1	Summary	295
	REFERENCES	305

LIST OF SYMBOLS

A	Rate constant
A	Initial cross sectional area
$A_{c,f,m}$	Area of composite, fiber, and matrix, respectively
a_T	Shift factor
b	Width of the specimen tested
C_p	Specific heat of the composite material
D	Maximum deflection of the center of the beam
D	Fickian coefficient of diffusion
D_{corr}	Diffusion coefficient multiplied by a correction factor
E	Activation energy
E	Elastic modulus
E'	Storage Modulus
E''	Loss modulus
E_d	Decomposition activation energy
E_f	Elastic modulus of fiber
E_i	Initial modulus
E_m	Elastic modulus of matrix
E_M	Modulus of the polymer in the rubbery state
E_t	Modulus at time t
f	Frequency applied for DMTA test
$F_{c,f,m}$	Uniaxial load in composite, fiber, and matrix, respectively
F^{tu}	Ultimate tensile strength
G_{12}	Shear modulus
G_f	Nominal carbon fiber modulus (22 GPa)
G_m	Nominal epoxy modulus (1.308 GPa)
h	Enthalpy of the solid phase

h	Thickness of the specimen tested
h_g	Enthalpy of the volatile gas
k_x	Thermal conductivity of the composite material in the through-thickness direction
L	Support span
l	Length of the specimen
L_g	Extensometer gage length
M_∞	Weight gain after equilibrium
M_e	Final mass after decomposition
M_i	Initial mass
n	Order of reaction
n	Sample size
$P(S)$	Probability of survival
P_i	Load at the i^{th} instant
P^{max}	Maximum load prior to failure
Q_i	Heat of decomposition
Q_p	Heat of pyrolysis
R	Universal gas constant (8.3143J/mol ^o K)
s	Sample standard deviation
t	Quantile of the t-distribution
T_g	Glass transition temperature
T_{ref}	Reference temperature
T_s	Surrounding temperature
T_s	Surface temperature
V_f	Fiber volume fraction
W_i	Initial weight of the specimen (prior to immersion)
W_t	Weight of the specimen after time t
α	Degree of decomposition
α	Shape parameter

β	Constant heating rate
β	Scale parameter
Γ	Gamma function
δ	Phase angle
δ_i	Increase in gauge length at the i^{th} instant
$\Delta\tau_{12}$	Difference in applied shear strength between two shear strain points
ΔY_{12}	Difference of two strain points
ϵ_f	Emissivity of the surrounding
ϵ_f	strain of fiber
ϵ_i	Tensile strain at the i^{th} instant
ϵ_m	Strain of matrix
ϵ_s	Emissivity of the surface
ϵ_{xx}	Longitudinal normal strain
ϵ_{yy}	Lateral normal strain
μ	Mean value
ρ	Density of the composite material
σ	Stapan-Boltzman constant
σ_{11}, σ_{22}	Normal stresses in the lamina coordinate system
$\sigma_{c,f,m}$	Stress of composite, fiber, and matrix, respectively
σ_i	Tensile strength at the i^{th} instant
σ_i	Initial strength
σ_t	Strength at time t
σ_{xx}	Applied tensile stress
τ_{12}	Shear strength
τ_{xy}	Induced shear strength
Y_{12}	Sher strain
\dot{q}	Heat flow
\bar{X}	Sample mean

LIST OF FIGURES

Figure 2-1: Skjold class patrol boat built with FRP sandwich	22
Figure 2-2: Visby corvette having hybrid carbon- and glass fiber polymer laminate	23
Figure 2-3: M80 Stiletto built with new carbon-fiber materials.....	23
Figure 3-1: (a) Unidirectional panel and (b) 0/90° panel	26
Figure 3-2: (a) Humidity chamber for initial condition and (b) Oven for environmental conditions	27
Figure 3-3: (a) Test specimens for water uptake tests and (b) Test specimens for SBS tests immersed in seawater and DI water.	28
Figure 3-4: (a) Test specimens for tensile test and (b) Grip of the tensile test machine (Instron 8801)	32
Figure 3-5: (a) Test specimens for Off-axis shear test and (b) Off-axis test Machine (Instron 8801)	33
Figure 3-6: (a) Test specimens for flexure test and (b) Flexure test fixture and Instron 5583	35
Figure 3-7: (a) Test specimens for SBS and (b) SBS test fixture and Instron 5583.....	36
Figure 3-8: (a) Test specimens for DMTA and (b) DMTA test fixture and Rheometric Scientific dynamic mechanical thermal analyzer	38
Figure 3-9: (a) Schematic of DSC and (b) Rheometric Scientific DSC SP equipment .	39
Figure 3-10: (a) Mettler Toledo TGA/SDTA851° equipment, (b) Crucible and (c) Furnace for TGA tests	41
Figure 4-1: Tensile strengths and normalized tensile strengths of carbon/epoxy composite materials as a function of time at fixed temperatures, (a) ambient (b) 66 °C (c) 93°C (d) 121°C (e) 149°C (f) 177°C (g) 204°C (h) 232°C (i) 260°C.....	48
Figure 4-2: Tensile Modulus and normalized tensile modulus of carbon/epoxy composite materials as a function of time at fixed temperatures, (a) ambient (b) 66°C (c) 93°C (d) 121°C (e) 149°C (f) 177°C (g) 204°C (h) 232°C (i) 260°C.....	53
Figure 4-3: Tensile Strength of carbon/epoxy composite materials as a function of temperature at fixed periods of exposure, (a) 1 hr (b) 2 hrs (c) 4 hrs (d) 8 hrs (e) 16 hrs (f) 24 hrs (g) 48 hrs (h) 72 hrs	58

Figure 4-4: Tensile Modulus of carbon/epoxy composite materials as a function of temperature at fixed periods of exposure, (a) 1 hr (b) 2 hrs (c) 4 hrs (d) 8 hrs (e) 16 hrs (f) 24 hrs (g) 48 hrs (h) 72 hrs 59

Figure 4-5: Color distribution of the test specimens after exposure to elevated temperatures for up to 72 hrs..... 62

Figure 4-6: Test specimens fractured after tensile test after exposure to elevated temperatures at the ageing time of 72 hrs..... 64

Figure 4-7: Tensile testing results for the specimens exposed to (a) 232 °C at 72 hrs and (b) 260°C at 72 hrs 64

Figure 4-8: SEM image after tensile testing of as-received specimen: magnification 1000×..... 66

Figure 4-9: SEM images after tensile testing of specimens exposed to 232°C for (a) 1 hr, (b) 2 hrs, (c) 4 hrs, (d) 8 hrs, (e) 16 hrs, (f) 24 hrs, (g)48 hrs, (h) 72 hrs - left images: magnification 400×, right images : magnification 500×..... 66

Figure 4-10: (a) Tensile stress-ultimate failure strain curve exposed to various ageing temperatures at a fixed time of 72 hrs (b) Tensile stress-ultimate failure strain curve until the strain reaches until 0.3% (Note that the kink in figure 4-10 (a) is due to removal of the extensometer) 70

Figure 4-11: (a) Tensile Strength, (b) Tensile Modulus, (c) Load as a function of ultimate failure strains (%). Error bars indicate standard deviation..... 71

Figure 4-12: Volume fraction and the ultimate tensile strength as a function of temperature at fixed times of exposure (a) 1 hr, (b) 2 hrs, (c) 4 hrs, (d) 8 hrs, (e) 16 hrs, (f) 24 hrs, (g) 48 hrs, (h) 72 hrs 78

Figure 4-13: (a) Volume fraction versus tensile strength (b) Volume fraction versus tensile strength without specimens having volume fractions ranging from 0.2% to 0.3% 79

Figure 4-14: (a) Volume fraction versus the ultimate failure strain (b) Volume fraction versus the ultimate failure strain without specimens having volume fractions ranging from 0.3% to 0.4% 79

Figure 4-15: Off-axis shear strengths and normalized off-axis shear strengths of carbon/epoxy composite materials as a function of time at fixed temperatures, (a) ambient (b) 66°C (c) 93°C (d) 121°C (e) 149°C (f) 177°C (g) 204°C (h) 232°C (i) 260°C..... 86

Figure 4-16: Off-axis shear modulus and normalized off-axis shear modulus of carbon/epoxy composite materials as a function of time at fixed temperatures, (a) ambient (b) 66°C (c) 93°C (d) 121°C (e) 149°C (f) 177°C (g) 204°C (h) 232°C (i) 260°C..... 91

Figure 4-17: Off-axis shear strength of carbon/epoxy composite materials as a function of temperature at fixed periods of exposure 95

Figure 4-18: Off-axis shear modulus of carbon/epoxy composite materials as a function of temperature at fixed periods of exposure 96

Figure 4-19: Test specimens distorted by asymmetry in process of thermal expansion and contraction after exposure to 260°C for 8 hrs 99

Figure 4-20: Test specimens fractured after uniaxial tensile test of a $\pm 45^\circ$ laminate exposed to elevated temperatures at an ageing time of 72 hrs 99

Figure 4-21: Off-axis shear stress-ultimate failure strain curves from specimens exposed to various ageing temperatures at the fixed period of 72 hrs 101

Figure 4-22: (a) Off-axis shear strength and (b) Off-axis shear modulus as a function of ultimate failure strains (%). Error bars indicate standard deviation..... 101

Figure 4-23: (a) Off-axis shear strength and (b) Off-axis shear modulus as a function of ultimate failure strains (%) using a logarithmic scale 102

Figure 4-24: Data distribution of (a) tensile strength versus off-axis shear strength and (b) tensile modulus versus off-axis shear modulus 106

Figure 4-25: Data distribution of (a) tensile strength versus off-axis shear strength and (b) tensile modulus versus off-axis shear modulus using a logarithmic scale 106

Figure 4-26: Flexural strengths and normalized flexural strengths of carbon/epoxy composite materials as a function of time at fixed temperatures of exposure, (a) ambient (b) 66°C (c) 93°C (d) 121°C (e) 149°C (f) 177°C (g) 204°C (h) 232°C (i) 260°C..... 113

Figure 4-27: Flexural modulus and normalized flexural modulus of carbon/epoxy composite materials as a function of time at fixed temperatures, (a) ambient (b) 66°C (c) 93°C (d) 121°C (e) 149°C (f) 177°C (g) 204°C (h) 232°C (i) 260°C..... 118

Figure 4-28: Flexural strength of carbon/epoxy composite materials as a function of temperature at fixed periods of exposure 122

Figure 4-29: Flexural modulus of carbon/epoxy composite materials as a function of temperature at fixed periods of exposure 122

Figure 4-30: Test specimens fractured after flexural testing after exposure to elevated temperatures at an ageing time of 72 hrs (a) top view (b) side view..... 125

Figure 4-31: Flexural stress- strain curve resulting from specimens exposed to various ageing temperatures at a fixed time of 72 hrs..... 127

Figure 4-32: (a) Flexural strength as a function of ultimate failure strains and (b) correlations of log (Flexural strength) versus ultimate failure strain 127

Figure 4-33: (a) Flexural modulus as a function of ultimate failure strains and (b) correlations of log (Flexural modulus) versus ultimate failure strain 127

Figure 4-34: (a) Flexural load as a function of ultimate failure strains and (b) correlations of log (Flexural load) versus ultimate failure strain 128

Figure 4-35: Short Beam Shear Strengths and normalized Short Beam Shear strengths of carbon/epoxy composite materials as a function of time at fixed temperatures, (a) ambient (b) 66°C (c) 93°C (d) 121°C (e) 149°C (f) 177°C (g) 204°C (h) 232°C (i) 260°C..... 135

Figure 4-36: Short beam shear strength of carbon/epoxy composite materials as a function of temperature at fixed times of exposure..... 138

Figure 4-37: Short beam shear load of carbon/epoxy composite materials as a function of temperature at fixed times of exposure 138

Figure 4-38: SEM images after short beam shear testing of specimens exposed to (a) ambient, (b) 66°C, (c) 93°C, (d) 121°C, (e) 149°C, (f) 177°C, (g)204°C, (h) 232°C, (i) 260°C for 48 hrs in ageing time - left images : bottom section by tension, right images : top section by compression: Magnification 2000× 141

Figure 4-39: Boundary between interlaminar shear and flexural tension. $L/h = 6.09(\sigma^* > 12.17F^{sbs})$	146
Figure 4-40: Boundary between interlaminar shear and pure tension. $L/h = 6.09(\sigma^* > 12.17F^{sbs})$	146
Figure 5-1: Change in T_g based on peak tangent delta as a function of time at fixed temperatures, (a) ambient (b) 66°C (c) 93°C (d) 121°C (e) 149°C (f) 177°C (g) 204°C (h) 232°C (i) 260°C	155
Figure 5-2: Schematic diagram for detecting the glass transition temperature at peak tangent delta in conditions of elevated temperatures for 4 hrs	156
Figure 5-3: Height of tangent delta at different frequencies of test specimen exposed to 121°C for 4 hrs	157
Figure 5-4: Schematic diagram for detecting the glass transition temperature from storage modulus (Exposure temperature: 93°C, Ageing time: 72hr).....	158
Figure 5-5: Difference in T_g based on peak tangent delta at 1Hz and storage modulus as a function of time at fixed temperatures, (a) ambient (b) 66°C (c) 93°C (d) 121°C (e) 149°C (f) 177°C (g) 204°C (h) 232°C (i) 260°C.....	160
Figure 5-6: Effect of test frequency on storage modulus (specimen exposed to 121°C for 4 hrs).....	164
Figure 5-7: Effect of test frequency on loss modulus (specimen exposed to 121°C for 4 hrs).....	164
Figure 5-8: Difference of the peak of tangent delta at different frequencies on longitudinal test specimens as a function of time at fixed temperatures, (a) ambient (b) 66°C (c) 93°C (d) 121°C (e) 149°C (f) 177°C (g) 204°C (h) 232°C (i) 260°C...	167
Figure 5-9: Comparison of the height of tangent delta at 1Hz from longitudinal and transverse test specimens as a function of time at fixed temperatures, (a) ambient (b) 66°C (c) 93°C (d) 121°C (e) 149°C (f) 177°C (g) 204°C (h) 232°C (i) 260°C...	169
Figure 5-10: Comparison of the activation energies on longitudinal and transverse test specimens as a function of time at fixed temperatures, (a) ambient (b) 66°C (c) 93°C (d) 121°C (e) 149°C (f) 177°C (g) 204°C (h) 232°C (i) 260°C.....	175

Figure 5-11: Normalized inter-crosslink molecular weights on longitudinal test specimens as a function of time at fixed temperatures..... 182

Figure 5-12: Mechanical properties versus glass transition temperatures on longitudinal and transverse test specimens as a function of time at fixed temperatures, (a) ambient (b) 66°C (c) 93°C (d) 121°C (e) 149°C (f) 177°C (g) 204°C (h) 232°C (i) 260°C..... 184

Figure 5-13: Characterization of four mechanical properties in terms of strength retention (%) as a function of glass transition temperatures determined by the peak of $\tan \delta$ at 1Hz 186

Figure 5-14: Schematic diagram for detecting the glass transition temperature from heat flow versus temperature (Exposure temperature: 23°C Ageing time: 4 hrs) 189

Figure 5-15: Comparison among glass transition temperatures determined by peak height of $\tan \delta$ at 1Hz, storage modulus and DSC as a function of time at fixed temperatures, (a) ambient (b) 66°C (c) 93°C (d) 121°C (e) 149°C (f) 177°C (g) 204°C (h) 232°C (i) 260°C 193

Figure 5-16: Temperature-dependent effective specific heat capacity, thermal conductivity and E-modulus for composite materials[70] 196

Figure 5-17: Weight loss (%) on DMTA specimens exposed to elevated temperatures using balance 199

Figure 5-18: Weight loss (%) on specimens heated from 25°C to 750°C with the heating rate of 10°C/min in nitrogen environment (ageing time: 72 hrs)..... 201

Figure 5-19: Onset temperatures of decomposition on specimens exposed to elevated temperature as a time function 205

Figure 5-20: Endset temperatures of decomposition on specimens exposed to elevated temperature as a time function 205

Figure 5-21: Decomposition degree at single heat rate (10°C/min) on specimens exposed to elevated temperature for 72 hrs 207

Figure 5-22: Reaction rate of decomposition at single heat rate (10°C/min) on specimens exposed to elevated temperature for 72 hrs 207

Figure 5-23: Activation Energy of decomposition (E_d) on specimens exposed to elevated temperatures as a function of time	210
Figure 5-24: Characterization of four mechanical properties as a function of weigh loss (%)	212
Figure 6-1: Schematic curves representing four categories of recorded non-Fickian weight-gain sorption [82]	217
Figure 6-2: Contact angle of specimens in (a) top surface and (b) edge surface	219
Figure 6-3: Weight Gain (%) on specimens immersed in deionized water for 72 weeks after exposure to elevated temperatures, (a) ambient (b) 66°C (c) 93°C (d) 121°C (e) 149°C (f) 177°C (g) 204°C (h) 232°C (i) 260°C	223
Figure 6-4: Weight Gain (%) on specimens immersed in seawater for 72 weeks after exposure to elevated temperatures, (a) ambient (b) 66°C (c) 93°C (d) 121°C (e) 149°C (f) 177°C (g) 204°C (h) 232°C (i) 260°C	231
Figure 6-5: The maximum weight gain (%) on specimens immersed in (a) DI water and (b) seawater for 72 weeks	239
Figure 6-6: Diffusion coefficients on specimens immersed in (a) DI water and (b) seawater for 72 weeks	241
Figure 6-7: Scanning electron micrographs at 250× and 500× magnification fractured by short beam shear test on specimens immersed in seawater for 72 weeks after exposure to (a) 260°C for 8 hrs (b) 232°C for 72 hrs (c) 121°C for 8 hrs.....	243
Figure 6-8: Scanning electron micrographs at 250× and 500× magnification fractured by short beam shear test on specimens immersed in deionized water for 72 weeks after exposure to (a) 260°C for 8 hrs (b) 121°C for 8 hrs.....	245
Figure 6-9: Scanning electron micrographs of cross section between 2 layers on specimens immersed in seawater for 72 weeks after exposure to 260°C for 8 hrs	245
Figure 6-10: Comparison of Short Beam Shear Strengths on specimens immersed in DI water for 72 weeks after exposure to elevated temperatures in 8 hrs of ageing time	248

Figure 6-11: Comparison of Short Beam Shear Strengths on specimens immersed in sea- water for 72 weeks after exposure to elevated temperatures in 8 hrs of ageing time 250

Figure 6-12: Comparison of Short Beam Shear Strengths on specimens immersed in DI water for 72 weeks after exposure to 232°C in various ageing times 252

Figure 6-13: comparison of Short Beam Shear Strengths on specimens immersed in seawater for 72 weeks after exposure to 232°C in various ageing times 254

Figure 7-1: Percent tensile strength retentions (%) versus ln(time in minute) 258

Figure 7-2: Polynomial 2nd order curve-fit on percent tensile strength retentions versus natural logarithm of time in minute 259

Figure 7-3: Percent retentions of tensile strength versus inverse of temperature 261

Figure 7-4: Comparison of the experimental values and predicted values of tensile strength by Arrhenius rate model on specimens exposed to elevated temperatures 265

Figure 7-5: Predicted values of tensile modulus for specimens exposed to elevated temperatures using Arrhenius rate model 266

Figure 7-6: Predicted values of off-axis shear modulus for specimens exposed to elevated temperatures using Arrhenius rate model 267

Figure 7-7: Predicted values of off-axis shear strength for specimens exposed to elevated temperatures using Arrhenius rate model 267

Figure 7-8: Predicted values of flexural modulus for specimens exposed to elevated temperatures using Arrhenius rate model 268

Figure 7-9: Predicted values of flexural strength for specimens exposed to elevated temperatures using Arrhenius rate model 268

Figure 7-10: Predicted values of short beam shear strength for specimens exposed to elevated temperatures using Arrhenius rate model 269

Figure 7-11: Logarithmic scale of percent tensile strength retention (%) versus time (hr) 272

Figure 7-12: Shifted curves to yield master curve for Time-Temperature Superposition 273

Figure 7-13: Master curve of polynomial 3 rd order curve fit to log of tensile strength profile for Time-Temperature Superposition model	274
Figure 7-14: Comparison of predicted values and experimental values of tensile strength retention based on the Time-Temperature Superposition model	274
Figure 7-15: Predicted data of strengths based on Time-Temperature Superposition model - reference temperature (66°C).....	276
Figure 7-16: Predicted data of modulus based on Time-Temperature Superposition model - reference temperature (66°C).....	277
Figure 7-17: Comparison between prediction results of tensile retention for Time-Temperature Superposition and Arrhenius rate model.....	279
Figure 7-18: Comparison between prediction results of off-axis shear retention for Time-Temperature Superposition and Arrhenius rate model.....	280
Figure 7-19: Comparison between prediction results of flexure retention for Time-Temperature Superposition and Arrhenius rate model.....	281
Figure 7-20: Comparison between prediction results of short beam shear retention for Time-Temperature Superposition and Arrhenius rate model.....	282
Figure 7-21: Shape parameters on specimens exposed to elevated temperatures as a function of time from tensile test.....	287
Figure 7-22: Comparison of (a) predicted flexural strength from tensile test and (b) experimental flexural strength.....	290
Figure 7-23: Shape parameters on specimens exposed to elevated temperatures as a function of time from flexural test.....	292
Figure 7-24: Comparison of (a) predicted tensile strength from flexural test and (b) experimental tensile strength.....	294
Figure 8-1: The distribution of tensile strength retentions (%) on specimens exposed to elevated temperatures for up to 72 hrs	297
Figure 8-2: The distribution of tensile modulus retentions (%) on specimens exposed to elevated temperatures for up to 72 hrs	297
Figure 8-3: The distribution of off-axis shear strength retentions (%) on specimens exposed to the elevated temperatures for up to 72hrs	298

Figure 8-4: The distribution of off-axis shear modulus retentions (%) on specimens exposed to the elevated temperatures for up to 72hrs 298

Figure 8-5: The distribution of flexural strength retentions (%) on specimens exposed to the elevated temperatures for up to 72hrs..... 299

Figure 8-6: The distribution of flexural modulus retentions (%) on specimens exposed to the elevated temperatures for up to 72hrs 299

Figure 8-7: The distribution of Short Beam Shear strength retentions (%) on specimens exposed to the elevated temperatures for up to 72hrs 300

LIST OF TABLES

Table 2-1 Composition of seawater.....	14
Table 2-2 Comparison of seawater and pure water properties	15
Table 3-1 Test specimens for mechanical properties and thermal analysis	27
Table 3-2 Test specimens for immersion tests	29
Table 4-1 Data for tensile strength (MPa) of carbon/epoxy composite materials after exposure to various temperatures	45
Table 4-2 Data for tensile Modulus (GPa) of carbon/epoxy composite materials after exposure to various temperatures	51
Table 4-3 Time-dependent functions of tensile strength retention (%) obtained by polynomial curve fitting	55
Table 4-4 Time-dependent functions of tensile modulus retention (%) obtained by polynomial curve fitting	56
Table 4-5 Temperature-dependent functions of tensile strength retention (%) obtained by polynomial curve fitting	60
Table 4-6 Temperature-dependent functions of tensile modulus retention (%) obtained by polynomial curve fitting	60
Table 4-7 Ultimate failure strain (%) after tensile testing.....	72
Table 4-8 Volume fractions and normalized volume fractions determined by using Equation 4.11 (the elastic modulus of carbon fiber is assumed to be 230 GPa)	76
Table 4-9 Data for Off-axis shear strength (MPa) of carbon/epoxy composite materials after exposure to various temperatures.....	84
Table 4-10 Data for off-axis shear Modulus (GPa) of carbon/epoxy composite materials after exposure to various temperatures.....	89
Table 4-11 Time-dependent functions of off-axis shear strength retention (%) obtained by polynomial curve fitting	93
Table 4-12 Time-dependent functions of off-axis shear modulus retention (%) obtained by polynomial curve fitting	94

Table 4-13 Temperature-dependent functions of off-axis shear strength retention (%) obtained by polynomial curve fitting	97
Table 4-14 Temperature-dependent functions of off-axis shear modulus retention (%) obtained by polynomial curve fitting	97
Table 4-15 Comparison of experimental shear modulus and calculated shear modulus- G'_{12} : experimental off-axis shear modulus (G''_{12} = shear modulus for cylinder shaped composites, G'''_{12} = shear modulus for rectangular shaped composites)	104
Table 4-16 Data for flexural strength (MPa) of carbon/epoxy composite materials after exposure to various temperatures (N denotes normalized)	111
Table 4-17 Data for flexural modulus (GPa) of carbon/epoxy composite materials after exposure to various temperatures (N denotes normalized)	116
Table 4-18 Time-dependent functions of off-axis shear strength retention (%) obtained by polynomial curve fitting	120
Table 4-19 Time-dependent functions of off-axis shear modulus retention (%) obtained by polynomial curve fitting	120
Table 4-20 Temperature-dependent functions of flexural strength retention (%) obtained by polynomial curve fitting	123
Table 4-21 Temperature-dependent functions of flexural modulus retention (%) obtained by polynomial curve fitting	123
Table 4-22 Data for Short Beam Shear Strength (MPa) of carbon/epoxy composite materials after exposure to various temperatures (N denotes normalized)	133
Table 4-23 Time-dependent functions of Short Beam Shear Strength retention (%) obtained by polynomial curve fitting	136
Table 4-24 Temperature-dependent functions of Short Beam shear strength retention (%) obtained by polynomial curve fitting	139
Table 5-1 T_g based on the peak of tangent delta determined from longitudinal and transverse test specimens after exposure to elevated temperatures	153
Table 5-2 Comparison of glass transition temperatures determined by peak of tangent delta at 1Hz and storage modulus from longitudinal and transverse test specimens	159

Table 5-3: Height of tangent delta at the different frequencies on longitudinal and transverse test specimens after exposure to elevated temperatures.....	165
Table 5-4 Activation energies using DMTA on longitudinal and transverse test specimens after exposure to elevated temperatures.....	174
Table 5-5 Storage modulus at $T_g \pm 40^\circ\text{C}$ and normalized inter-crosslink molecular weight from longitudinal and transverse specimens	180
Table 5-6 Comparison among glass transition temperatures determined by $\tan \delta$, storage modulus and DSC (percent error means the difference between $\tan \delta$ and DSC)	192
Table 5-7 Data of weight loss (%) on DMTA specimens exposed to elevated temperatures using balance.....	199
Table 5-8 Weight percent (%) of specimens at initial and final point of decomposition using TGA	201
Table 5-9 Thermal stability parameters determined by TGA curves- T_m and α_m mean the maximum temperature and degree of decomposition at the maximum reaction	203
Table 6-1 Characteristics on specimens immersed in deionized water for 72 weeks after exposure to elevated temperatures.....	228
Table 6-2 Characteristics on specimens immersed in seawater for 72 weeks after exposure to elevated temperatures.....	236
Table 6-3 Data of Short Beam Shear Strengths on specimens immersed in DI water for 72 weeks after exposure to elevated temperatures in 8 hrs of ageing time	248
Table 6-4 Data of Short Beam Shear Strengths on specimens immersed in Seawater for 72 weeks after exposure to elevated temperatures in 8 hrs of ageing time	250
Table 6-5 Data of Short Beam Shear Strengths on specimens immersed in DI water for 72 weeks after exposure to 232°C in various ageing times	252
Table 6-6 Data of Short Beam Shear Strengths on specimens immersed in seawater for 72 weeks after exposure to 232°C in various ageing times	253
Table 7-1 Data for tensile strength retentions (%) on specimens exposed to elevated temperatures up to 72 hrs	258

Table 7-2 Equation of polynomial 2nd order curve-fit on percent tensile strength retentions versus natural logarithm of time in minute.....	259
Table 7-3 Relationship between percent retentions of tensile strength and the inverse of temperature	261
Table 7-4 Comparison of experimental data and theoretical data by Arrhenius rate relationship for specimens exposed to elevated temperatures in tensile strength	262
Table 7-5 Data for logarithmic scale of tensile strength retentions (%) on specimens exposed to elevated temperatures up to 72 hrs	271
Table 7-6 Horizontal shift factors from curve in exposure temperature (66°C) using the logarithmic scale on specimens exposed to elevated temperatures	273
Table 7-7 Predicted data of additional mechanical properties based on Time-Temperature Superposition model - reference temperature (66°C).....	275
Table 7-8 Values of shape parameters for the different exposure conditions and ageing time from tensile test	287
Table 7-9 Values of flexural strength predicted from tensile test on specimens exposed to elevated temperatures for 72 hrs	288
Table 7-10 Values of shape parameters for the different exposure conditions and ageing time from flexural test	291
Table 7-11 Values of tensile strength predicted from flexural test on specimens exposed to elevated temperatures for 72hrs	293

ABSTRACT

Carbon Fiber-Reinforced Polymer (CFRP) composites with epoxy matrices offer many advantages over conventional materials in terms of high strength-to-weight and high stiffness-to-weight ratios, design flexibility, corrosion resistance, and ease of application in rehabilitation in cases where long service-life is required. However, the assessment of durability due to environmental exposure including immersion and elevated temperature and related structural degradation represent a challenge to the structural assessment. The accurate assessment of the deterioration and degradation of a composite structure is vital in the planning for maintenance of structure critical components. In this research, carbon/epoxy composite materials have been thermally aged at nine (9) different temperatures for up to 72 hours of ageing time. In order to determine the residual mechanical properties of the specimens exposed to elevated temperatures, tensile, flexure, off-axis shear, and short beam shear tests were conducted in accordance with ASTM test procedures. In addition, the viscoelastic behavior and dynamic properties of these composites at varying ageing times and temperatures were found using Dynamic Mechanical Thermal Analysis (DMTA) and Differential Scanning Calorimetry (DSC). ThermoGravimetric Analysis (TGA) was performed to analyze the characteristics of thermal decomposition and Scanning Electron Microscopy (SEM) images were taken to investigate failure mechanisms such as interfacial debonding, delamination, and fiber fracture. Since these materials when used for rehabilitation can easily be exposed to moisture related to high relative humidity and immersion, degradation mechanisms related to moisture were investigated on specimens immersed in seawater and deionized water for 72 weeks after exposure to selected regimes of elevated temperature using gravimetric analysis, SEM and short beam shear test. Finally, well-established prediction models such as Arrhenius rate model, Time-Temperature Superposition model and Weibull statistical strength model were used with experimental data to estimate characteristic associated with long-term service life.

1 Introduction

1.1 Introduction

Fiber-Reinforced Polymer (FRP) composites offer inherent advantages over traditional materials with regard to high strength-to-weight and stiffness-to-weight ratios, design flexibility, corrosion resistance, low maintenance and enhanced service life. Carbon/epoxy composite materials are particularly useful because they exhibit better retention of mechanical properties than other FRP composites over extended periods of time. Due to these advantages, carbon/epoxy composites are a preferred materials choice for rehabilitation. The assessment of effects of environmental exposure, including due to aqueous exposure and elevated temperatures, and of related structural degradation and failure, presents a significant challenge to the safe design and accurate structural assessment of composite structures. An accurate assessment of deterioration of a composite structure subjected to exposure as represented in this study by exposure to elevated temperature is dependent on the accurate characterization of the time dependent residual mechanical characteristics of composite system as well as its viscoelastic properties. When composite materials are generally exposed to high temperatures (200~ 300°C), pyrolysis caused by chemical reactions with oxygen starts to occur from the surface and the resin component degrades to form gaseous products. In addition, the polymer matrix and organic fibers are thermally decomposed yielding volatile gases, solid carbonaceous char and airborne soot particles (smoke) via a series of chemical reaction mechanisms. Polymer composites lose not only molecular weight but also mechanical characteristics by thermal decomposition. Molecular weight is

reduced by mechanisms of random chain scission, chain-end scission and chain stripping within polymer structures. Therefore, when composite materials are thermally aged for periods of time, there is a need for the investigation of how much degradation and deterioration occurs after exposure as functions of time and temperature.

FRP composite materials are used in a variety of applications based on their stiffness, strength, reduced weight, and corrosion-free capabilities. Since degradation and deterioration of the mechanical properties of composite materials due to environmental exposure can seriously compromise structural integrity, and cause rapid creep, buckling, collapse or some other failure mode, the composite materials degraded and deteriorated must be evaluated in terms of the retention of mechanical properties to investigate whether the intrinsic functions of the material can be accomplished. In order to develop the experimental data for residual properties after exposure, tension, off-axis shear, flexure and short beam shear test were carried out according to ASTM test procedures.

Polymers show viscoelastic behavior in the presence of heat with the resin used in composite materials experiencing the change of a diversity of properties as a function of time and temperature. Thus, the severe drop of mechanical properties seen after exposure to elevated temperature is mainly attributed to the degradation of the resin than the fiber. For this reason, thermal analysis must be performed on polymeric composite materials. Dynamic Mechanical Thermal Analysis (DMTA), Differential Scanning Calorimetry (DSC) and Thermo-Gravimetric Analyses (TGA) were conducted on specimens exposed to elevated temperatures. DMTA measurements over a range of temperatures provide valuable insight into the structure, morphology and viscoelastic

behavior of polymer materials while DSC is mainly used to investigate the thermal transitions of the polymer. TGA is a powerful and simple tool to estimate the thermophysical and thermomechanical properties exposed to a controlled temperature.

The environmental conditions likely to be faced in such applications include water, humidity, moisture and seawater can result in the ingress of moisture into FRP composites. Exposure to moisture is known to cause plasticization, hydrolysis and further deterioration of the resin over time and hence it is necessary to study the moisture uptake and resulting kinetics. While general investigations regarding moisture uptake are focused on the specimens of FRP composites cured in ambient temperature, this study is concentrated on the immersion effects of specimens after exposure to elevated temperature. This estimation can be an important criterion to evaluate how long FRP rehabilitated structures can be allowed to operate after exposure. Degradation mechanisms related to moisture were investigated on specimens immersed in seawater and deionized water for 72 weeks using gravimetric analysis, SEM and short beam shear.

It is very important that predictive degradation models are used to evaluate functions for desired periods of time without failure and severe degradation, in specified environments. Based on the experimental data determined through mechanical tests, predictions of longer-term response can be obtained using well-established models such as the Arrhenius rate model, Time-Temperature Superposition (TTSP) model and Weibull statistical strength model.

This study contributes to the establishment of design factors and criteria to estimate and evaluate the performance of FRP composites used in rehabilitation

exposed to elevated temperatures and immersed in aqueous solutions using the experimental data obtained throughout various tests and analysis. It provides a further data base as well as means of accelerated test analysis.

1.2 Motivation

Significant research related to the assessment of FRP composite materials after exposure to elevated temperature has been conducted on materials such as prepreg based autoclave cured composites focused on aerospace applications. However, of late, there has been an increased interest in the development and application of composites for the rehabilitation of both primary and secondary structures. Therefore, mechanical and thermal analysis must be carried out on composite specimens exposed to both elevated temperatures and aqueous conditions for the safe design and accurate assessment of service-life.

1.3 Research Objectives

The main objectives and goals for this research can be summarized as follows.

- Development of a fundamental understanding of time-and temperature-dependent behavior of wet layup based carbon/epoxy composite materials exposed to elevated temperatures for certain time
- Verification of residual post-cure effects on specimens cured at ambient

temperatures and fabricated by manual wet layup process

- Morphological analysis of failure mechanism such as debonding between fibers and matrix, pull-out of fibers and delamination between layers using SEM
- Correlation between experimental data obtained through mechanical tests
- Thermal analysis to assess how much polymer-based composites are degraded or deteriorated by temperature and time
- Correlation of parameters such as glass transition temperature, decomposition temperature, loss tangent ($\tan \delta$), activation energy, etc determined from thermal analysis and mechanical property retention
- Verification of effects of immersion, failure mechanisms and mechanical properties on specimens immersed in seawater and deionized water
- Comparison of predictions obtained by use of established model and experimental data
- Categorization of property retention as a function of temperature, time, weight loss and weight gain due to immersion

1.4 Overview of Research

This research is focused on the assessment of durability of carbon/epoxy composite materials after exposure to elevated temperatures and immersion in aqueous solutions. For assessments, mechanical tests and thermal analysis were conducted on specimens exposed to various regimes of elevated temperature and exposure to aqueous

environments. In addition, immersion characteristics were investigated using gravimetric analysis, SEM and short beam shear test. Previous research and theories relevant to FRP composites are introduced in chapter 2. Material specifications, experimental conditions and test procedures are explained in chapter 3. Chapter 4 and chapter 5 deal with mechanical characterization and thermal analysis on specimens exposed to controlled conditions, respectively. The experimental results from immersion in seawater and deionized water for 72 weeks are presented in chapter 6. Predictions from 3 models are detailed in chapter 7.

2 Literature Review

2.1 Fire Safety of FRP Composite Materials

Over the past years, there has been significant development and application of composites for both primary and secondary load-bearing structures of Naval vessels and hence it is advantageous to use this data wherever possible for assessment of durability for rehabilitation since there is a large similarity in materials and processes, unlike with the aerospace industry. FRP composite materials are already being used in diverse areas such as deckhouse, mast, piping, valves, pumps and heat exchangers, ventilation ducts, etc. This interest in FRP composite materials is driven by needs to reduce maintenance, save weight, increase covertness and provide affordable alternatives to metallic components with lower life cycle costs[1]. It is emphasized that the use of the data from naval applications is to leverage the study for infrastructure rehabilitation and is not for use in naval vessels per-se.

The use of structural composites inside submarines is now covered by MIL-STD-2031 (SH), which includes fire and toxicity test methods such as flame spread index (FSI), specific optical density, heat release rate and ignitability, oxygen-temperature index, combustion gas generation, long-term outgassing, etc and qualification procedure for composite materials systems used in hull, machinery, and structural applications[2]. This military standard involves test methods and requirements for flammability characteristics. The following two guiding criteria were established for the use of composite systems aboard US Navy vessels[3].

1. "The composite system will not be the fire source, i.e. it will be sufficiently fire resistant not to support spontaneous combustion."
2. "Secondary ignition of the composite system will be delayed until the crew can respond to the primary fire source; i.e. the composite system will not result in rapid spreading of the fire"

2.2 Thermal Decomposition of FRP Composite Materials in Fire

2.2.1 Introduction

A major concern of FRP composite materials is poor performance during and after exposure to elevated temperatures. Therefore, it should be noted that thermal decomposition mechanisms under elevated temperatures must be investigated because the behavior of composite materials is dominated by the chemical process. This is of special interest when elevated temperatures are used as a means of accelerating aging as well.

2.2.2 Description of Mechanisms of Thermal Degradation

When a heat flux caused by heat is applied to FRP composite materials, the change of initial temperature is dependent on the rate of heat conduction into the materials and the boundary conditions. If the heat flux is applied, the surface of FRP composite materials first reaches high temperature. This change of temperature can be caused chemical reactions (pyrolysis) and gaseous products are formed by degradation of polymer component [4]. In addition, chemical reaction can result in distortion,

buckling or failure of FRP composite materials. In the process of decomposition on polymer matrix and fibers, volatile gases, char and smoke can be produced by chemical reaction mechanisms. The loss of molecular weight in polymers is attributed to the fracture mechanisms of polymer structures such as random chain scission, chain-end scission and chain stripping.

2.2.2.1 Processes of Combustion in Composites

Polymer composites exposed to high temperatures experience self-sustained combustion in air and oxygen [5]. Burning polymer composites have a highly complex combustion system. The combustion in polymer composite system occurs as combined events [6] such as heating of the polymer, decomposition, ignition, and combustion. As mentioned in previous chapter, the decomposition process for most polymers produces solid carbonaceous char and gaseous volatiles. The chemical composition and amount of the volatiles is dependent on the polymer matrix, oxygen content and temperature, although the majority of the gases are flammable polymers. Combustion of the volatiles occurs in the solid and intermittent zones of a turbulent flame.

2.2.2.2 Epoxy Resin

Epoxy resins are characterized by the presence of epoxide groups prior to cure, and they may also contain aliphatic, aromatic or heterocyclic structures in the backbone. Epoxy resin is superior to any other polymer resins in terms of the long service time and good physical properties compared to other thermosets. Like other thermoset resins, epoxy resins can be rendered fire-retardant either by incorporating fire-retardant

additives or by copolymerization with reactive fire retardants.

Three mechanisms for the oxidation of epoxies were suggested by many researches[7], [8]. Any of these mechanisms leads to the formation of carbonyl groups which further decompose and result in chain splitting.

The thermal stability of epoxy resins and their flammability depend on the structure of the monomer, the structure of the curing agent and the crosslink density.

2.2.2.3 Carbon Fibers

The structures and properties of carbon fibers are dependent on the raw material used and the process conditions of manufacture. When carbon fibers are exposed to directly to fire, their surface can be oxidized.

Severe oxidation causes carbon fibers to lose weight due to the evolution of CO or CO₂ gases. However, slight oxidation may cause carbon fibers to gain weight slightly due to the formation of chemical bonds to various. Compared to polymer matrix, reinforcing carbon fibers are generally more stable at elevated temperatures considered [9]. Thermal degradation was quantified by the amount of weight loss measured, while surface morphology changes by temperatures were monitored as attempt to investigate related physical and surface changes to the decreases in mechanical performance as a function of ageing.

In addition, trace impurities within carbon fiber act as a catalyst to the oxidation process, and this can cause thinning of the fiber. However, it should be noted that in most types of fiber the extent of oxidation is small because most carbon fibers within a

composite are surrounded by char.

2.2.3 Review of Analytical Models for Effects of Fire

In order to predict the thermal response of composite materials by fire, many models were suggested. However, thermal response mechanisms on composite materials are very complicated because many considerations were included in the process of reactions. In this section, mathematical models suggested by many researchers who studied on mathematical models for fire response will be introduced.

1) One-dimensional equation on composite materials

Assuming that heat conduction is applied to composite material in through-thickness direction, the one-dimensional equation including heat of pyrolysis determined from the theoretical mass loss rate can be expressed as Equation (2.1)[10].

$$\rho C_p \frac{\partial T}{\partial t} = \frac{\partial}{\partial x} \left[k_x \frac{\partial T}{\partial x} \right] + \frac{\partial m}{\partial x} Q_p \quad (2.1)$$

Where:

T = The temperature

t = time

x = the distance below the hot surface

ρ and C_p = the density and specific heat of the composite material

k_x = the thermal conductivity of the composite material in the through-thickness direction

2) Decomposition reaction model

To develop more precise model, new model were suggested after adding the diffusion of decomposition gases into Equation (2.4)[4]. The decomposition reactions are modeled using single or multiple-order kinetic rate theory as shown in Equation (2.2).

$$\rho C_p \frac{\partial T}{\partial t} = k \frac{\partial^2 T}{\partial x^2} + \frac{\partial k}{\partial x} \frac{\partial T}{\partial x} - \dot{m}_g C_{pg} - \frac{\partial \rho}{\partial t} (Q_i + h - h_g) \quad (2.2)$$

where:

Q_i = The heat of decomposition

h = Enthalpy of the solid phase

h_g = Enthalpy of the volatile gas

Equation (2.2) is including the effect of heat conduction, the internal convection of thermal energy and rate of heat generation The rate of chemical reaction may be described using an Arrhenius rate expression of the form shown in Equation (2.6) assuming no expansion of the materials[4].

$$\frac{\partial \rho}{\partial t} = -A \left[\frac{(\rho - \rho_f)}{\rho_0} \right]^n e^{(-E/RT)} \quad (2.3)$$

where:

A = The rate constant

E = Activation energy

n = Oder of the reaction

R = The gas constant

2.3 Effects of Seawater on FRP Composites

This research is focused on FRP composites operating in marine environments which exists surrounding seawater. There are so many considerations to assess the FRP composite materials used in the marine environmental conditions such as immersion, salinity, UV, corrosion, cycling (thaw-freeze), and so on. However, this research is concentrated on only a limited aspect of exposure, i.e. seawater immersion effects and those of elevated temperature.

2.3.1 Seawater Properties

The composition of seawater is very complex consisting of more than seventy trace elements and biological organisms, which have shown to cause some degradation. The main composition of seawater is summarized as shown in Table 2-1.

Table 2-1 Composition of seawater

Element	Symbol	Weight %
Chloride	Cl	55.04
Sulphate	SO ₄	7.68
Calcium	Ca	1.16
Sodium	Na	30.61
Magnesium	Mg	3.69
Potassium	K	1.10

Seawater is composed mostly of water (H₂O). In fact it is about 96.5 wt% water. The salinity of sea water (usually 3.5%) is made up by all the dissolved salts. Interestingly, their proportions are always the same, which can be understood if salinity differences are caused by either evaporating fresh water or adding fresh water from

rivers. Freezing and thawing also matter. Seawater properties are as follows:

- 1) Density: Any substance dissolved in a liquid has the effect of increasing the density of that liquid. The greater the amount of solute, the greater the effect.
- 2) Freezing point: Because the salt is spread on frozen path, the freezing point is depressed. Salts also lower the temperature at which water reaches its maximum density.
- 3) Boiling point: the salts have the effect of making the water molecules cluster and become more orders, thus harder to pull apart and evaporate. Therefore, boiling point is elevated.
- 4) Conductivity: If an electromagnetic field is applied to seawater, the ions will migrate, producing an electric current.

Table 2-2 shows comparison of seawater and pure water properties.

Table 2-2 Comparison of seawater and pure water properties

Property	Seawater (35%)	Pure water
Density (g/cm ³), 25°C	1.02412	1.0029
Specific conductivity (1/Ωcm), 25°C	0.0532	-
Viscosity (millipoise), 25°C	9.02	8.90
Freezing point (°C)	-1.91	0.00
Temperature of maximum density (°C)	-3.25	3.98
Specific heat (J/g°C), 17.5°C	3.898	4.182

2.3.2 Seawater Effect on Mechanical Properties

In this section, seawater effects on mechanical properties of FRP composite materials will be introduced from literatures which previous researchers have been studied. Many researches were focused on mechanical properties after immersing in deionized, distilled and tap water. Even though some researches on seawater immersion are available, studies in actual marine environments are lack because it is too difficult to test.

Accordingly, similarities and correlation factors between laboratory and real-site evaluation result need to be developed for real analyzing.

2.3.2.1 Tension

There are a lot of researches related to carbon- and glass-fiber composites immersed in saline conditions. In this section, the effects exposed to various environments will be introduced from summarizing of many studies toward tensile strength and modulus.

T.S Grant et al.[11] investigated the effect of immersion in seawater on transverse tensile properties of three graphite/epoxy composite materials. The transverse tensile strength was found to be reduced by 17% in one of the systems with essentially no change in the other two systems studied. The 17% decrease in transverse tensile strength was associated with degradation of the interfacial strength. Also they found that little difference was found in the behavior of composite immersed in distilled water and in seawater at ambient pressure or seawater at 20.7 MPa pressure. Leif A. Carlsson

et al.[12] accomplished tests using carbon/bismaleimide-epoxy, E-glass/epoxy, E-glass/polyphenylsulfide and carbon-epoxy for immersion more than 4000 hrs in distilled water and natural seawater at room temperature and 35°C. Transverse modulus, E_2 was not significantly changed after water absorption except for E-glass/polyphenylsulfide that lost about 60% of its dry modulus, despite of its low water absorption. The substantial reduction of E_2 was attributed to extensive fiber/matrix debonding induced by water. Also, all composites experienced large reduction in transverse tensile strength due to water absorption. The maximum reduction took place in E-glass/polyphenylsulfide with 85% decrease of its dry strength. An E-glass/carbon/epoxy interlayer hybrid composite has been aged by immersion in simulated seawater for varying lengths of time and then tested in transverse tension by C.A Wood et al.[13]. From transverse tests, they showed that tension properties were proportional to water uptake and then dropped rapidly after moisture saturation. Failure mechanism was verified using an environmental SEM. Resin-rich areas were found to be sources of failure initiation where debonding occurred. E-glass/Vinylester composites were fabricated using wet layup with the application of a vacuum throughout the cure to investigate tensile properties in various environmental conditions such as 23°C and 55% RH, synthetic sea water and real seawater by Lixin Wu et al.[14]. Exposure to all conditions resulted in a decrease in tensile strength and the absolute difference in response between the various exposures. The maximum reduction in tensile strength after 12 months of exposure was in sea water at a level of 13.5%, whereas the minimum, 8.26%, was recorded for the case of cycling in sea water. After immersion in sea water,

the surfaces of all the specimens showed discoloration with the initiation of blistering at areas where fibers were close to the surface, suggesting both effect of salts of the fiber-matrix integrity and the existence of osmotic processes.

2.3.2.2 Flexure

The flexural test measures the force required to bend a beam under three point or four point loading conditions. The data is often used to select materials for parts that will support loads without flexing. Flexural modulus is used as an indication of a material's stiffness when flexed. E.P. Gellert and D.M. Turley[15] performed flexural test using the polyester, phenolic and vinylester glass-fiber reinforced polymer materials immersed in 30°C seawater either unloaded or loaded at 20% of the maximum strain at flexural failure ($0.2\varepsilon_f$) to examine the effects of loading on flexural property. Flexural strength continued to degrade for the unloaded polyester and vinylester GPRs as water uptake continued toward saturation, where strength losses between 15% and 21% occurred. The unloaded phenolic lost 25% of initial strength at saturation. For ageing, loading affected the strength of only phenolic GRP with strength loss advancing from 25 to 36% loss from the initial strength. Wayne C. Tucker and Richard Brown[16] generated all data on the vinylester/graphite composite material immersed in natural filtered seawater in tubs in the laboratory at 1 atmosphere of pressure and in natural filtered seawater pressurized to a depth of 2000feet of seawater. The flexural strength and stiffness of the composite material were decreased by the high pressure exposure. In contrast, atmospheric seawater exposure did not produce any strength decrease. Both

the enhanced moisture uptake and the strength decrease at high pressure exposure were thought to be due to mechanical damage induced by the increased pressure. In 5% and 10% salt solution, the flexural properties (strength and modulus) of pultruded glass-fiber reinforced vinylester matrix composite coupons were measured for the 90° specimens as-received and after ageing by K.Liao et al.[17]. Ageing in water and salt solutions resulted in degraded flexural and tensile properties of pultruded E-glass fiber reinforced vinylester matrix composite. Salt concentration did not seem to affect flexural properties in a noticeable way. However, in terms of flexural strength, reductions were larger than those subjected to distilled water.

2.3.2.3 Other Mechanical Properties

Beside tensile and flexural test after exposure to seawater, a wide variety of tests with regard to seawater effects were accomplished because marine composite materials are increasingly using in diverse applications. These tests are including impact, fracture, fatigue, and compression test. The effects of seawater immersion on the impact resistance of two glass/epoxy composites were characterized using instrumented impact test data obtained from penetration tests by Larry H. Strait et al.[18]. Two composite materials experienced substantial reductions in peak load and energy absorbed at peak load as result of moisture-induced degradation of the fibers and fiber/matrix interface. The results of this study indicate that moisture-induced degradation can significantly reduce the impact resistance of glass fiber reinforced epoxy composites. In order to examine the interlaminar fracture toughness, the glass/polyester and glass/vinyl ester

composites panels were immersed in a large tank containing natural seawater with a salinity content of about 2.9% and temperature of 30°C for more than two years by A. Kootsookos and A.P Moritz[19]. This study reported that the mode I interlaminar fracture toughness of the composites was not affected significantly by seawater immersion, although the flexural stiffness and strength decreased with increasing amounts of water absorption. K.Y.Rhee et al.[20] conducted the compressive fracture tests of fully seawater-absorbed carbon/epoxy composites under normal atmospheric pressure and under three levels of hydrostatic pressure conditions using a high pressure tension-compression apparatus which can produce 700 MPa of hydrostatic pressure. Fracture characteristics of seawater of seawater-absorbed carbon/epoxy composites were significantly influenced by hydrostatic pressure. Compliance decreased but fracture load and fracture toughness increased with increasing hydrostatic pressure. McBagonluri et al.[21] accomplished tension-tension fatigue on E-glass/vinylester immersed in synthetic seawater. To simulate the environmental fatigue, a fluid cell was used for testing of specimens. It was found that immersion in seawater slightly improved the fatigue performance, in which degradation is attributed to a fiber-dominated process.

2.4 Review of Naval/Marine Applications of FRP Composites

2.4.1 Introduction

While the study of FRP materials for civil infrastructure rehabilitation after

exposure to sea water is sparse, FRP composite materials are being used in a variety of navy applications based on their stiffness, strength, reduced weight, and corrosion-free capabilities and hence it is advantageous to use that knowledge base as a basis for research. Until recently, the use of composite materials for military applications was limited to aerospace and US air force for high-performance applications. Currently, applications of composite materials in the U.S Navy are widely broaden into sonar bow domes, windows, hulls and so on. Moreover, there is a resurgence of interest for the use of composites in military applications including naval vessels, army combat vehicles, and unmanned vehicles. The all-composite naval ships are currently operating to perform multifunctional operation with the benefit for composite materials. Therefore, in following section, all-composite naval vessels will be introduced.

2.4.2 Surface ships

In early, use of composite materials was constrained to the construction of small patrol boats and landing craft in displacement due to relatively poor fabrication quality and low stiffness of the hulls. However, as fabrication technique and mechanical properties were improved, composite materials can be applied to larger patrol boat, minecountermeasure vessels, and corvettes.

Skjold (Figure 2-1) is the Royal Norwegian Navy's first fast patrol craft/littoral combat ship of the *Skjold*-class and is currently being evaluated by the US Navy. The ship is based on a catamaran hull where lift fans blow air into an air cushion between the hulls. The structure is built with FRP sandwich using uniaxial glass fiber and carbon

laminates with vinyl-ester or polyester resin. Polyvinyl chloride (PVC) core material is used in main structural elements below main deck and polymethacrylimide (PMI) core material is used elsewhere and for the complete superstructure. The total length of *Skjold* is approximately 157 feet at a displacement of 260 tons[22].



Figure 2-1: Skjold class patrol boat built with FRP sandwich

The Swedish Navy is operating the Visby-class corvette (Figure 2-2) from 2000. Visby class is designed to be a multi-purpose vessel with capabilities for surveillance, combat, mine laying, and anti-submarine warfare operations[23]. The visby corvette is built from sandwich composite panels having face skins of hybrid carbon- and glass fiber polymer laminate covering a poly (vinyl chloride) foam core. With carbon-reinforced composite, Visby class can get the benefit of adequate electromagnetic shielding.



Figure 2-2: Visby corvette having hybrid carbon- and glass fiber polymer laminate

The M80 Stiletto (Figure 2-3) is a prototype naval ship manufactured to meet specific requirements of the Pentagon's Office of Force Transformation. M80 Stiletto represents the next generation of military vessels. It is built with new carbon-fiber materials and has a networked architecture. It is unique for its hull design, speed, ride quality, payload capability and provision for unmanned vehicle support. The M80 Stiletto is a twin-M-hull vessel. It is 88ft in length with a 40ft beam, providing a rectangular deck area. When fully loaded, the vessel's draught is 3ft. The M80 Stiletto can reach speeds of 50kt to 60kt. The vessel is built on the advanced M-hull technology. Its carbon-fiber body ensures reduced weight and increased stiffness.



Figure 2-3: M80 Stiletto built with new carbon-fiber materials

2.4.3 Submarines

Several navies have used composites with outstanding success in a diverse range of submarine structures for nearly 50 years. Various submarine structures are made of composite materials, including sails, fins, mast strouds, casings over the upper pressure hull and bow sonar domes on nuclear submarine and combatant submarines by US Navy,

Royal Navy and French Navy. In addition, periscope fairings have been built of FRP. These autoclave-cured parts are precision machined to meet the tight tolerances required of the periscope bearing system. The fairings are all glass, with a recent switch from polyester to epoxy resins.

The defense evaluation and research agency (UK) has investigated the feasibility of lining the outside wall of the steel pressure hull with a sandwich composite material[24]. Covering the steel hull with composite cladding increased the overall buckling strength, lower fatigue strains, reduce corrosion and lower the acoustic, magnetic and electric signatures.

Composites are being used increasingly in submarine masts for communications and electronic surveillance as well as in non-hull penetrating masts. Masts made of composites have a number of advantages over those made of steel, including lighter weight and no corrosion. Composites allow moulding into complex shape without the need for machining, and the incorporation of radar absorbing materials over the entire length of the mast[25].

3 Materials and Test Methods

3.1 Material Specification

The carbon/epoxy composites were comprised of Tyfo S Epoxy and Tyfo SCH-41 reinforcing fabric supplied by FYFE Co. Composite panels comprising of two layers as shown in Figure 3-1 were fabricated using a manual wet layup process with cure under ambient conditions. Tests were conducted after a minimum of 7 days cure. The fiber content was approximately 60% by weight. The fabric reinforcement consisted of a primarily unidirectional fabric of 644 g/m² areal weight.

The fibers had a nominal tensile strength, modulus and density of 3.79 GPa, 230 GPa, 1.74g/cm³, respectively. The resin system was a two-component epoxy with a viscosity of 600-700 cps at 25 °C. After curing and then after 72 hours of post cure at 60°C, the glass transition temperature, tensile strength, modulus and elongation are specified as 82 °C, 72.4 MPa, 3.18 GPa, and 5.0%, respectively.

All mechanical tests, except for the off-axis shear test, were performed using unidirectional 2 layer panels, while 0/90 panels were used for the off-axis shear test. Because composite panels were fabricated in the field, they were uniformly preconditioned at 23 °C and 30% relative humidity (RH), in a humidity chamber to set a uniform baseline.



Figure 3-1: (a) Unidirectional panel and (b) 0/90° panel

3.2 Environmental Conditions

3.2.1 Mechanical Properties and Thermal Analyses

After cutting composites panels with a tile saw, all specimens for mechanical properties and thermal analyses were stored in a humidity chamber (Figure 3-2 (a)) to ensure an initial condition for 2 weeks. Carbon/epoxy composite specimens were exposed thermally to ambient, 66, 93, 121, 149, 177, 204, 232, and 260 °C under ageing times of 1, 2, 4, 8, 16, 24, 48, and 72 hrs. Test specimens were kept in an oven (Figure 3-2 (b)) until they reached a set time and temperature, and then they were removed to ambient conditions for testing.



Figure 3-2: (a) Humidity chamber for initial condition and (b) Oven for environmental conditions

The number of test specimens and sizes are listed in Table 3-1.

Table 3-1 Test specimens for mechanical properties and thermal analysis

Test	Specimens No	Size (mm)
Tension	temp case(9)×time case(8)×no. of test(5)+0 hour(5)=365	254×12.7×3
Off-axis shear	temp case(9)×time case(8)×no. of test(3)+0 hour(3)=219	228×12.7×3
Flexure	temp case(9)×time case(8)×no. of test(5)+0 hour(5)=365	70×12.7×3
SBS	temp case(9)×time case(8)×no. of test(5)+0 hour(5)=365	18×6×3
DMTA	temp case(9)×time case(8)×no. of test(2)+0 hour(2)=146	8.8×34×3
DSC	temp case(9)×time case(8)×no. of test(1)+0 hour(1)=146	10 ~ 15mg
TGA	temp case(9)×time case(8)×no. of test(2)+0 hour(2)=146	10 ~ 20mg
Weight Loss	temp case(9)×time case(8)×no. of test(3)+0 hour(3)=219	8.8×34×3
SEM	temp case(1)×time case(8)×no. of test[4]=32	
Total	2,003	

3.2.2 Immersion Tests

After the simulation of exposure to high temperatures such as those caused by fire in naval vessels, the characterization of mechanical properties and thermal analyses were accomplished at the various conditions to investigate how much degradation occurred in thermally aged specimens. Accurate evaluations are necessary to assess whether composite materials degraded by fire can operate at the required level of

functionality in seawater. Therefore, the specimens aged thermally at each temperatures were immersed in seawater under ambient temperature for up to 72 weeks. Simultaneously, test specimens were immersed in deionized (DI) water in the same conditions to provide a base-line comparison. Seawater from La Jolla shores was used and was periodically changed in the water bath. Figure 3-3 shows the specimens for water uptake tests and SBS tests

Moisture uptake tests were performed using gravimetric analysis. Test specimens were taken out from water bath to weigh the mass, periodically. In the case of short beam shear tests, tests were conducted after immersion in seawater and DI water under specified conditions (exposure to Ambient, 66, 93, 121, 149, 177, 204, 260 °C for 8 hr and exposure to 232 °C for 1, 2, 4, 8, 16, 24, 48 and 72hr). In addition, SEM images were taken to investigate internal fracture mechanisms caused by the exposure. The number of test specimens regarding water uptake, SBS test and SEM are summarized in Table 3-2.



Figure 3-3: (a) Test specimens for water uptake tests and (b) Test specimens for SBS tests immersed in seawater and DI water.

Table 3-2 Test specimens for immersion tests

Test	Specimens No	Size (mm)
Water Uptake	Seawater (73) + DI water (73) = 143	25.4×25.4×3
SBS	16(temp)×8(ageing)×2(case)×5(Set) = 1,280	18×12.7×3
SEM	Some of SBS specimens	
Total	1,423	

3.3 Test Procedures

The main key to obtain more accurate data depends on how erroneous factors can be eliminated. Another key is to reduce outliers from the tests set. Therefore, experiments were carried out in following sequence.

- 1) Test specimens were cut with a tile saw into ASTM recommend dimensions from carbon/epoxy composite panels. Water was used as a liquid coolant to prevent material damage caused by the build-up of heat while test specimens were cut.
- 2) Test specimens were sanded to make edges of specimens smooth after cutting. Sanding can reduce the error factors caused by cutting.
- 3) Test specimens were carefully marked using a labeling metallic pen to prevent marking from disappearing during heat and chemical reactions from exposure.
- 4) To set initial baseline conditions, test specimens were kept in a humidity chamber at ambient conditions of 23 °C and 30% RH for 2 weeks.

- 5) The initialized test specimens were put in the oven to pre-specified environmental conditions. When the required time at fixed temperatures was reached, test specimens were removed to ambient conditions.
- 6) After cooling of test specimens, to ambient levels, they were tested immediately.
- 7) Based on collected data, data analysis was carried out in accordance with MIL-HDBK-1F introduced in following section.

3.4 Data Statistics

It should be noted that wet layup composite materials have significant scatter because they are made manually and hence there is a need to check for outliers. An outlier is an observation that is much lower or much higher than most other observation in a data set. Often outliers are erroneous values, due to operator error, incorrect setting of environmental conditions during testing, or due to a defective test specimen[26].

The Maximum Normed Residual (MNR) method is used in this study for quantitative screening for outliers.

$$\text{MNR} = \frac{\max |x_i - \bar{x}|}{s}, \quad i=1,2,3,\dots,n \quad (3.1)$$

where \bar{x} is sample mean, and s is sample deviation.

The value of MNR is compared to the critical value for the sample size n . These critical values are calculated from Equation (3.2).

$$C = \frac{n-1}{\sqrt{n}} \sqrt{\frac{t^2}{n-2+t^2}} \quad (3.2)$$

If MNR is smaller than the critical value, then no outliers are detected in the sample. In addition, if an outlier is detected, this value is omitted from the calculations and the MNR procedure is applied again. This process is repeated until no outliers are detected.

3.5 Test Methods

Composite materials were characterized through a series of tests including tensile, off-axis shear, flexure, short beam shear, DMTA, DSC, TGA and moisture uptake.

3.5.1 Tension

Tensile tests are important because they are the main characterizing element that defines the in-plane strength and modulus of composites[27]. The purpose of a tensile test is to determine the ultimate tensile strength and tensile modulus of composite materials. Tensile data on unidirectional composites are often used as one of the key factors in materials selection and in laminated design.

The tensile tests on the carbon/epoxy composites were performed in accordance with ASTM D3039M[27]. Test specimens were cut to dimensions of 254 mm in length and 12.7 mm in width with the length being parallel to the fiber direction as shown in Figure 3-4 (a). For tensile tests, an Instron model 8801(Figure 3-4 (b)) was used. This enables tensile testing to be conducted with hydraulic grips. To prevent test specimens from slippage, sand paper at the ends of the specimens were used to provide additional frictional force. In this research, the gauge length was 155 mm, and the specimen was loaded in tension at a rate of 1.27 mm/min. An extensometer having a 25.4 mm gauge

length was used to measure strains. When a level of 0.3% strain was reached the extensometer was removed from test equipment so as to not have damage from subsequent fiber rupture and brooming. In addition, tensile chord modulus can be obtained from the slope of the stress-strain curve.

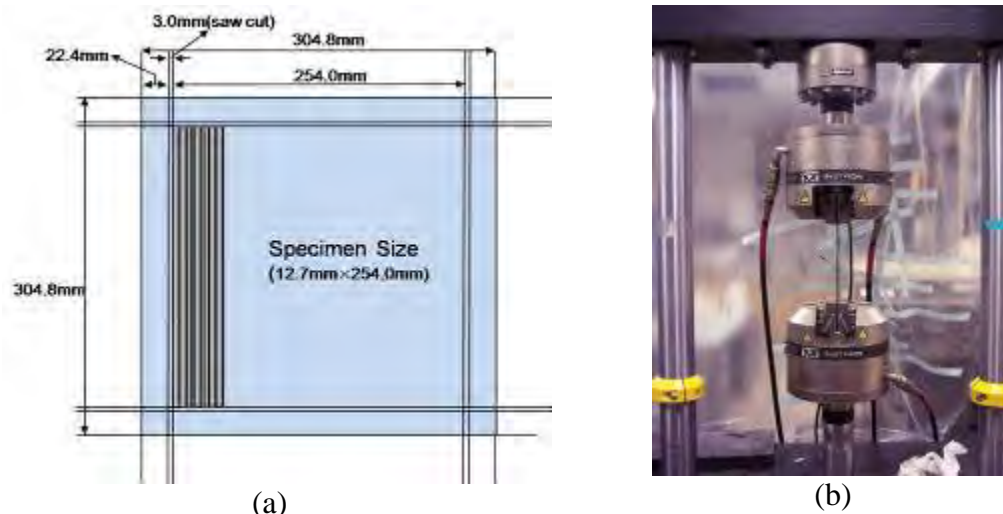


Figure 3-4: (a) Test specimens for tensile test and (b) Grip of the tensile test machine (Instron 8801)

3.5.2 Off-Axis Shear

The off-axis shear test is used to determine the in-plane shear response of polymer matrix composite materials. In these tests shear distortion occurs entirely in the plane of the composites materials. The shear strength and the shear modulus can be determined from off-axis shear test.

There are many variations of the off-axis shear test such as the uniaxial tension of a 10° off-axis laminate[28], V-notch beam shear[29], torsion tube tests[30], rail shear tests[31] and uniaxial tension of a $\pm 45^\circ$ specimen[32]. In this study, off-axis shear characteristics were determined by uniaxial tension of a $\pm 45^\circ$ coupon. Off-axis shear

test were carried out following ASTM D3518 with the same Instron 8801 as tension test.

Test specimens for off-axis shear test were cut to dimensions of 228.6 mm in length and 12.7 mm in width in the 45° direction from 0/90° carbon/epoxy panels as illustrated in Figure 3-5 (a). Sand papers at the ends of the specimens were also used to provide additional gripping force similar to that used in the tension test. The gauge length was 140 mm because the length of off-axis test specimens is smaller than that of tension test. The test procedures follow those of the unidirectional tensile test in accordance with ASTM D-3039M. When a strain level of 0.3% was attained the extensometer was removed from test equipment.

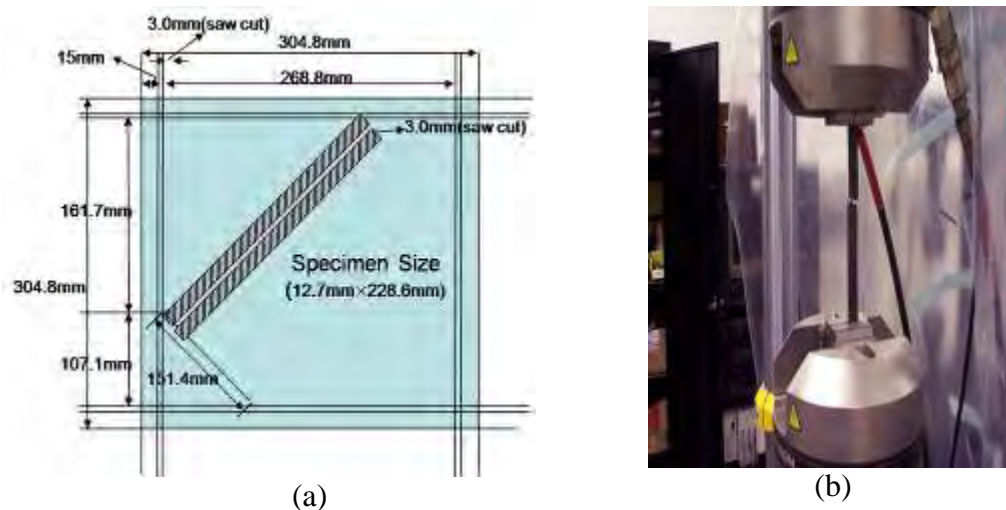


Figure 3-5: (a) Test specimens for Off-axis shear test and (b) Off-axis test Machine (Instron 8801)

3.5.3 Flexure

Flexure tests monitor the behavior of materials in simple beam loading. Specimens are supported as a simple beam, with the load applied at midpoint, and thus ultimate stress and strain can be calculated. The three point bending flexural test

measures bend or fracture strength, modulus of rupture, yield strength, modulus of elasticity in bending, flexural stress, flexural strain, and flexural stress strain materials response. Flexural strength represents the highest stress experienced within the material at its point of rupture.

Flexure tests are popular because of the simplicity of both specimen preparation and testing. Gripping of the specimen, the need for end tabs, obtaining a pure stress state and avoiding buckling are usually nonissues when conducting a flexure test[33]. In general, flexure tests are applicable to quality control and materials selection where comparative rather than absolute values are required.

The flexural tests for the carbon/epoxy composite specimens were conducted in accordance with ASTM D790[34]. For flexure test, specimens from carbon/epoxy composite panels were cut to the dimension of 12.7 mm in width and 70 mm in length as illustrated in Figure 3-6 (a). Specimens were placed on two supports and were loaded by means of a loading nose midway between the supports. The test span was 48 mm in keeping with the ASTM suggested for support span-to-depth ratio of 16:1 (the average depth of the specimens was 3 mm on 2 layers). Using Instron 5583, flexure test was carried out. As shown in Figure 3-6 (b), flexural test fixture which comprised of 2 supports and 1 load nose was used in this test. The load was applied to the specimens at a crosshead speed of 2 mm/min. The center deflection was determined throughout measurements of the vertical movement of the loading nose.

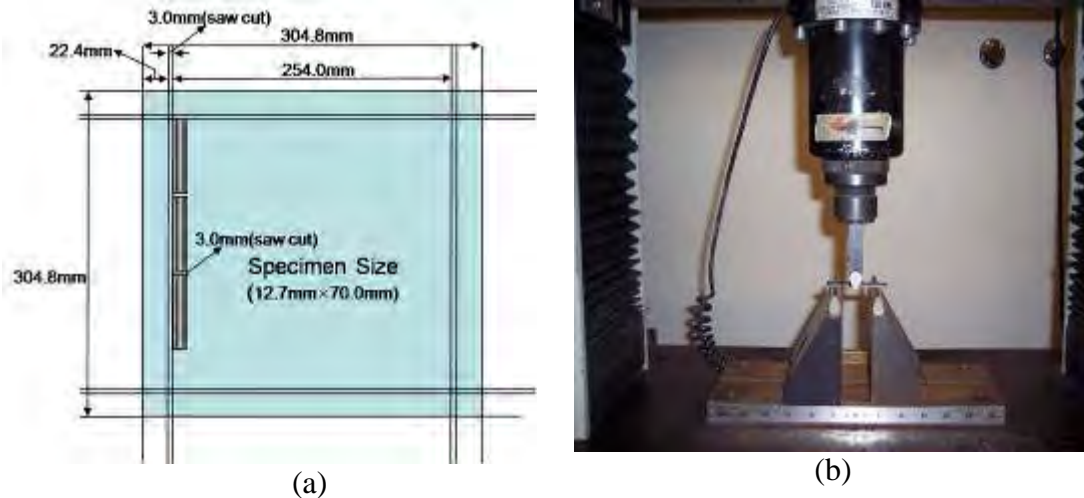


Figure 3-6: (a) Test specimens for flexure test and (b) Flexure test fixture and Instron 5583

3.5.4 Short Beam Shear

Test methods available for the determination of interlaminar shear include short beam shear, four-point shear[35], double notch shear[36] and v-notch beam shear[37]. The short beam shear test was applied to determine the interlaminar shear strength in this research.

The short beam shear tests were accomplished following ASTM D2344[38] using specimens which were cut to dimension of 6 mm in width and 18 mm in length (Figure 3-7 (a)), using test fixture, and an Instron 5583 equipment (Figure 3-7 (b)).

According to ASTM, the following geometries are recommended:

$$\text{Specimen length} = \text{thickness} \times 6$$

$$\text{Specimen width} = \text{thickness} \times 2$$

The test span in this case was 14 mm. A cross head speed of 1 mm/min was applied for all tests and the load was applied until failure of the specimens was attained.

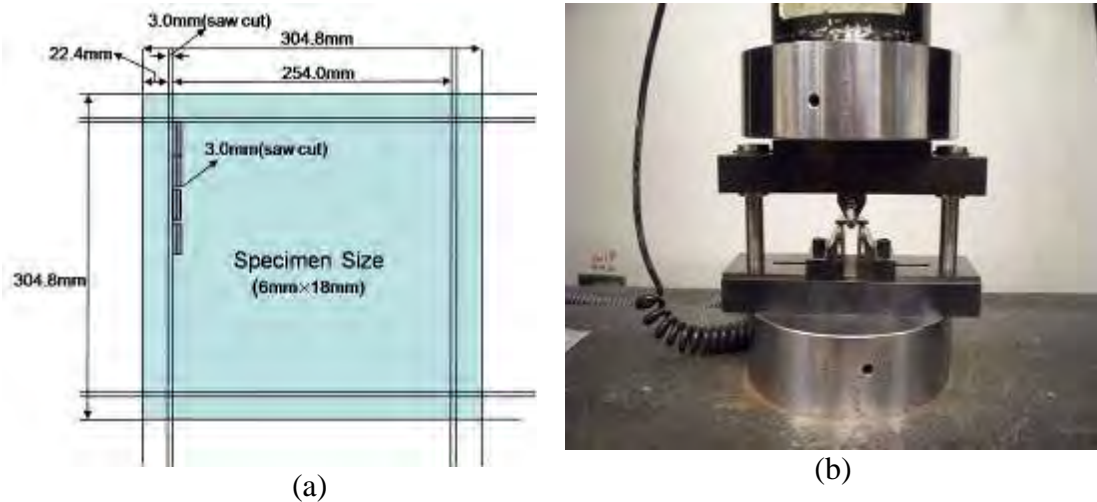


Figure 3-7: (a) Test specimens for SBS and (b) SBS test fixture and Instron 5583

3.5.5 Dynamic Mechanical Thermal Analysis (DMTA)

Dynamic Mechanical Thermal Analysis (DMTA) examines the behavior of visco-elastic materials according to temperature and frequency dependent behavior. A small strain (deformation) is imposed on the material by application of a stress. The amount of strain resulting from the applied stress enables the collection of information about the modulus of the materials, its stiffness and damping properties.

In visco-elastic behavior, an imposed stress or strain gives a response which is somewhat retarded by the viscous component of the material, its fluid-like behavior, and yet because the material has substance, solid-like behavior, there is also an elastic response. DMTA separates these two responses into separate moduli values: Elastic or Storage (denoted by E') and Loss Modulus (denoted by E''). The storage modulus, represents the elastic component of the visco-elastic behavior in-phase with the imposed deformation ($\tau = \tau_0 \cos \delta$), while the loss modulus, the viscous damping component, is

out of phase with the input signal ($\tau = \tau_0 \sin \delta$). The overall lag of the system from the input signal is a phase angle, δ . The tangent of the phase angle, $\tan \delta$, is the ratio of loss modulus to storage modulus ($\tan \delta = E''/E'$) and is a valuable indicator of the relative damping ability of the material.

Glass transition temperature, T_g , can be determined with significant levels of sensitivity through DTMA by monitoring changes in the storage modulus, E' , loss modulus, E'' , or the loss tangent, $\tan \delta$, as a function of temperature[39]. In general T_g , also changes based on the frequency used in testing and the rate of heating used. An increase in the heating rate is known to shift T_g to a higher temperatures[40] and an increase in test frequency for a constant heating rate also increases T_g [41]. Multi-frequency studies have been shown previously to be powerful tools for the determination of activation energy of glass transition and to follow crystallization and structural changes[42].

DMTA tests were performed in accordance with ASTM D5418[43] using the single cantilever frame fixture. The specimens for DMTA were cut to dimension of 8.8 mm in width and 34 mm in length as illustrated in Figure 3-8 (a). Multi-frequency DMTA tests were carried out on the specimens in longitudinal and transverse direction at 0.3, 1, 3, 10 and 30 Hz, with a heating rate of 2 °C /min and an imposed strain of 0.01%. DMTA test equipment was a Rheometric Scientific dynamic mechanical thermal analyzer as shown in Figure 3-8 (b).

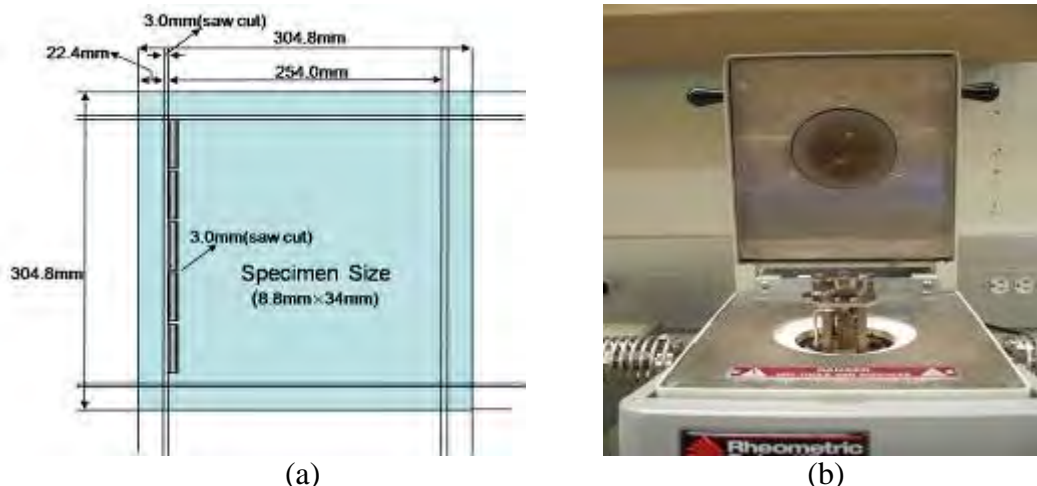


Figure 3-8: (a) Test specimens for DMTA and (b) DMTA test fixture and Rheometric Scientific dynamic mechanical thermal analyzer

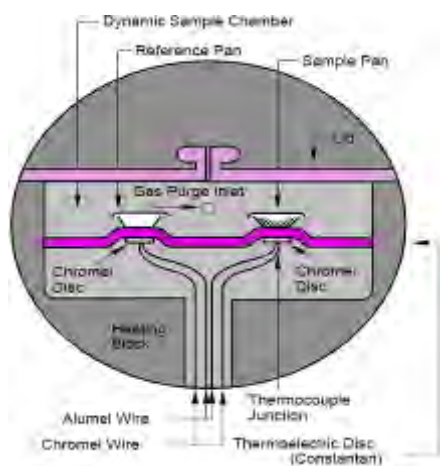
3.5.6 Differential Scanning Calorimetry (DSC)

Differential Scanning Calorimetry (DSC) measures the temperatures and heat flows related to transition in materials as a function of time and temperature in a controlled atmosphere. DSC tests provide quantitative and qualitative information about physical and chemical changes that include endothermic or exothermic process, or changes in heat capacity through the measurement of absorption or release of energy. In a DSC experiment the difference in energy input to a sample and a reference material is measured while the sample and reference are subjected to a controlled temperature program as shown in Figure 3-9 (a). DSC requires two pans equipped with thermocouples in addition to a programmable furnace, recorder, and gas controller.

In the case of polymer or polymer composite materials, glass transition temperature (T_g) is very useful aspect which can be obtained from DSC. If output DSC data shifts upward suddenly at a certain temperature, this means more heat flow is needed to balance the temperature. This shows an increase in the heat capacity of

sample. Namely, this happens because the polymer has just gone through the glass transition. Polymers have a higher heat capacity above the glass transition temperature than they do below it.

DSC tests were conducted following ASTM D 3418[44] using samples which were obtained from carbon/epoxy panels and DSC equipment by Rheometric Scientific corporation (Figure 3-9 (b)). Test samples were compressed by crimping for efficient heat transfer between the pan and the sample. Test samples of 10~15mg were heated at a ramp rate of 10 °C /min from an initial temperature of 0 °C to final temperature of 160 °C in a controlled atmosphere flowing N₂ at 10 ml/min. For cooling down until 0 °C, liquid nitrogen gas was utilized.



(a)



(b)

Figure 3-9: (a) Schematic of DSC and (b) Rheometric Scientific DSC SP equipment

3.5.7 Thermogravimetric Analysis

Thermogravimetric Analysis (TGA) is a thermal analysis technique used to measure changes in the mass of a sample as a function of temperature and/or time. TGA is commonly used to determine polymer degradation temperatures, residual solvent

levels, absorbed moisture content, and the amount of inorganic (noncombustible) filler in polymer or composite material compositions.

The volatilization of residual solvent is typically associated with the initial weight loss process in a TGA heating run. In some cases, absorbed moisture may also be liberated over this same temperature range. After the initial solvent (or moisture) weight loss process, TGA profiles typically plateau to some constant weight level until the polymer degradation temperature range is reached. Detailed and precise factors of the thermal stability based on the initial decomposition temperature (IDT), temperature of maximum rate of weight loss (T_{\max}), integral procedure decomposition temperature (IPDT), decomposition temperature range, and activation energy (E_a) of the decomposition reactions are readily determined by TGA[45].

Pyrolysis occurs through a many-stepped mechanism, where the temperature ranges for each step overlap, resulting in irregular weight-temperature curves that may be difficult to analyze. The sample weight drops slowly as pyrolysis begins, then drops precipitously over a narrow temperature range and finally turns back to a zero slope as the reactant is exhausted. The shape of the curve is determined by the kinetic parameters of the pyrolysis, such as reaction order, frequency factor, and energy of activation[46].

TGA tests were performed in accordance with ASTM E 1131[47] using samples which were cut from carbon/epoxy panels and were tested on a Mettler Toledo TGA/SDTA851^o model (Figure 3-10 (a)). Samples having 10 ~ 20 mg mass were placed into a TGA sample crucible (Figure 3-10 (b)) which was attached to a sensitive microbalance assembly. The sample holder portion of the TGA balance assembly was subsequently placed into a high temperature furnace (Figure 3-10 (c)). The balance

assembly measures the initial sample weight at room temperature and then continuously monitors changes in sample weight (losses or gains) as heat is applied to the sample. Samples were heated from 25 °C to 750 °C with the heating rate of 10 °C /min in flow of nitrogen environment (25 ml/min).

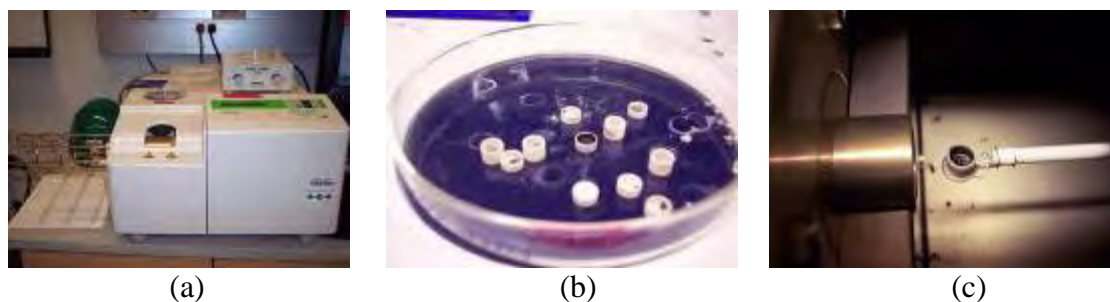


Figure 3-10: (a) Mettler Toledo TGA/SDTA851^e equipment, (b) Crucible and (c) Furnace for TGA tests

3.5.8 Moisture Uptake

For measuring the moisture uptake of the specimens immersed in sea water and de-ionized (DI) water, all samples exposed to elevated temperatures were removed from each immersion environment and kept at room temperature until measuring. All unidirectional specimens were cut to dimensions of 25.4 mm by 25.4 mm for gravimetric measurement. Wet samples from immersion environments were wiped for dryness with a paper towel prior to weighing. Weight measurements were undertaken using a Sartorius Analytical Balance with a resolution of 10^{-5} grams. Weights were recorded when the LCD display of the balance kept a stable value for 5 seconds to ensure the consistency in test method. After measurement of weight, all samples were returned to the original environment for further exposure.

4 Mechanical Characterization

Degradation and deterioration of the mechanical properties of composite materials at elevated temperature can seriously compromise structural integrity, and cause rapid creep, buckling, collapse or some other mechanisms of failure. The residual mechanical properties of thermally degraded composites following such exposure are very important factors in the design of the various applications

4.1 Tensile Testing

4.1.1 Introduction

Tensile tests in the fiber direction are important because tensile strength and modulus are the main mechanical properties that define the in-plane fiber characteristics of the composite materials. Although the tensile properties of unidirectional composites measured in the fiber direction can be considered to be fiber dominated it must be remembered that the wet layup process intrinsically results in the formation of a relatively high percentage of voids as well as significantly greater levels of variation and non-uniformity than prepreg based autoclave composites[48].

4.1.2 Data Reduction

In-plane tensile strength and modulus were determined from a standard in-plane tensile tests following ASTM D3039M. The ultimate tensile strength is determined using

$$F^{tu} = \frac{P^{\max}}{A} \quad (4.1)$$

where:

F^{tu} = Ultimate tensile strength

P^{\max} = Maximum load prior to failure

A = Initial cross sectional area

The tensile strength at each instant in time as the specimen was loaded is determined as:

$$\sigma_i = \frac{P_i}{A} \quad (4.2)$$

where:

σ_i = Tensile strength at the i^{th} instant

P_i = Load at the i^{th} instant

The tensile strain at each point of time the specimen was loaded is determined as:

$$\varepsilon_i = \frac{\delta_i}{L_g} \quad (4.3)$$

where:

ε_i = Tensile strain at the i^{th} instant

δ_i = Increase in gauge length at the i^{th} instant

L_g = Extensometer gage length

The elastic modulus can then be determined by utilizing Hook's law

$$E = \frac{\sigma_i}{\varepsilon_i} \quad (4.4)$$

The elastic modulus is calculated using data corresponding to the 0.1% to 0.3% strain range of the linear region.

4.1.3 Analyses and Results

4.1.3.1 Time Dependence

The data for tensile strength of carbon/epoxy composite materials exposed to various temperatures from ambient temperature to 260°C are shown in Table 4.1. The strength data were obtained by data reduction as described in the previous chapter. The values of normalized strength were calculated by dividing the average thickness of the specimens by 1.930 mm, the nominal thickness of 2-layers wet-layup composite panels. The values of strength retention (%) were obtained by comparing with strength on as-received specimen which is exposed to ambient temperatures without thermal ageing. At the fixed exposure temperatures, test specimens were thermally aged from 1 hr to 72 hrs in the oven to investigate time-dependent tendency. Fig 4.1 shows the tensile strength, normalized strength, and strength retention of carbon/epoxy composite materials as a function of time at fixed temperatures.

Residual Post-curing effects resulted in an increase of the tensile strength as shown in Table 4-1 and Figure 4-1. At lower exposure temperatures, more time is needed for attainment of full cure, while fully curing was attained within rapid time at higher exposure temperatures. Moreover, in the ranges of lower ageing temperatures (i.e.

66, 93, 121, 149 and 177 °C), the values of tensile strengths initially increased and then leveled off or slightly decreased after reaching the maximum strength. At the ambient temperature, the maximum strength caused by post-curing effect did not occur. In the case of specimens exposed to 204 and 232 °C, the time to reach the maximum strength was very short and the values of the maximum strength were lower compared to lower exposure temperatures. However, the values of tensile strength did not dramatically drop. On the other hand, thermal oxidation of specimens, thermal decomposition of the epoxy resin and debonding between carbon fiber and epoxy resin occurred on specimens exposed to 260 °C for more than 16 hrs and resulted in the rapid drop of tensile strengths. In particular, thermal oxidation resulting in surface deterioration causing additional decrease of the tensile strength in the case of the specimens exposed to 260 °C for more than 16 hrs.

Over the set of tensile tests, the maximum tensile strength was 775.59 MPa (154.42% in tensile strength retention) and occurred in environmental condition of 1 hr at 149 °C, while the minimum tensile strength was 188 MPa (37.55% in tensile strength retention) and as expected, under conditions of 72 hrs at 260 °C, which was the highest temperature of exposure.

In addition, standard deviations of the tensile strengths after exposure to higher temperatures were greater than those at lower exposure temperatures due to variation caused by thermal oxidation.

Table 4-1 Data for tensile strength (MPa) of carbon/epoxy composite materials after exposure to various temperatures

Exposure Temperature	Time (hr)	Thickness (mm)	Strength (MPa)	S.D (MPa)	Normalized Strength (MPa)	Strength Retention (%)
Ambient	0	3.51	502.26	15.94	913.26	100

(23 °C)	1	3.31	501.34	16.66	859.81	99.81
	2	3.21	512.68	29.32	852.70	102.07
	4	3.48	505.18	23.45	910.89	100.58
	8	3.02	507.06	19.79	793.43	100.95
	16	3.33	522.71	27.66	901.88	104.07
	24	3.05	514.71	14.11	813.40	102.47
	48	3.11	523.45	22.61	843.49	104.21
	72	3.24	519.48	16.66	872.08	103.42
66 °C	1	2.67	706.34	121.36	978.63	140.63
	2	2.43	751.05	35.12	944.65	149.53
	4	2.67	759.38	51.76	1050.53	151.19
	8	2.62	754.03	55.81	1022.62	150.13
	16	2.80	749.95	61.39	1087.03	149.31
	24	3.09	604.06	86.50	967.74	120.27
	48	2.65	584.97	43.80	804.41	116.47
	72	2.85	578.72	34.65	854.59	115.22
93 °C	1	3.22	632.60	36.84	1055.43	125.95
	2	3.02	646.52	45.32	1011.65	128.72
	4	3.20	675.49	108.19	1120.69	134.49
	8	3.12	679.70	98.29	1100.20	135.33
	16	2.97	691.43	79.60	1065.45	137.66
	24	3.26	611.17	84.19	1032.98	121.68
	48	3.14	610.71	75.52	993.59	121.59
	72	3.26	602.29	28.56	1018.59	119.92
121 °C	1	3.07	584.64	27.59	929.37	116.40
	2	3.16	583.46	77.91	954.09	116.17
	4	3.01	628.76	58.75	981.91	125.19
	8	2.73	662.12	77.57	935.20	131.83
	16	3.32	564.93	41.97	970.33	112.48
	24	3.19	524.36	48.69	866.14	104.40
	48	3.42	522.15	38.31	925.27	103.96
	72	3.21	526.22	35.73	875.90	104.77
149 °C	1	2.62	775.59	43.74	1053.20	154.42
	2	2.71	768.83	92.07	1080.87	153.07
	4	2.73	757.77	42.45	1072.19	150.87
	8	2.73	752.08	68.54	1062.78	149.74
	16	2.79	720.81	93.11	1043.49	143.51
	24	2.84	691.34	90.38	1017.79	137.65
	48	2.91	638.38	63.88	961.97	127.10
	72	2.56	684.88	43.20	909.15	136.36

Table 4-1 Continued

Exposure Temperature	Time (hr)	Thickness (mm)	Strength (MPa)	S.D (MPa)	Normalized Strength (MPa)	Strength Retention (%)
177 °C	1	2.94	612.64	80.61	932.60	121.98
	2	3.21	623.52	61.66	1037.05	124.14

	4	2.77	684.95	56.01	982.35	136.37
	8	2.77	679.07	75.74	973.21	135.20
	16	2.53	671.43	53.52	879.47	133.68
	24	3.00	624.42	125.15	969.30	124.32
	48	3.00	570.72	92.71	886.53	113.63
	72	3.12	563.94	43.88	910.49	112.28
204°C	1	3.09	577.67	57.80	923.67	115.01
	2	2.89	652.35	70.31	977.51	129.88
	4	2.70	710.17	100.84	992.03	141.39
	8	3.02	673.62	59.69	1054.06	134.12
	16	2.98	669.59	72.74	1033.18	133.32
	24	2.94	625.50	103.24	952.83	124.54
	48	3.01	595.91	31.10	929.98	118.65
	72	3.07	582.49	68.98	925.95	115.97
232°C	1	3.11	559.53	113.78	901.04	111.40
	2	3.07	594.13	72.52	945.06	118.29
	4	2.71	635.30	109.41	890.73	126.49
	8	2.79	636.98	117.50	919.49	126.82
	16	2.66	623.21	66.32	860.22	124.08
	24	2.61	611.42	48.53	826.84	121.73
	48	2.71	603.00	52.38	847.95	120.06
	72	2.59	565.29	25.92	759.19	112.55
260°C	1	3.03	627.34	118.33	984.89	124.90
	2	3.10	638.44	77.55	1024.37	127.11
	4	3.08	667.76	124.99	1066.80	132.95
	8	2.99	537.66	145.04	833.33	107.05
	16	2.89	349.88	120.66	524.40	69.66
	24	3.31	303.20	61.99	520.52	60.37
	48	2.91	248.40	107.04	375.05	49.46
	72	3.02	188.60	79.34	295.44	37.55

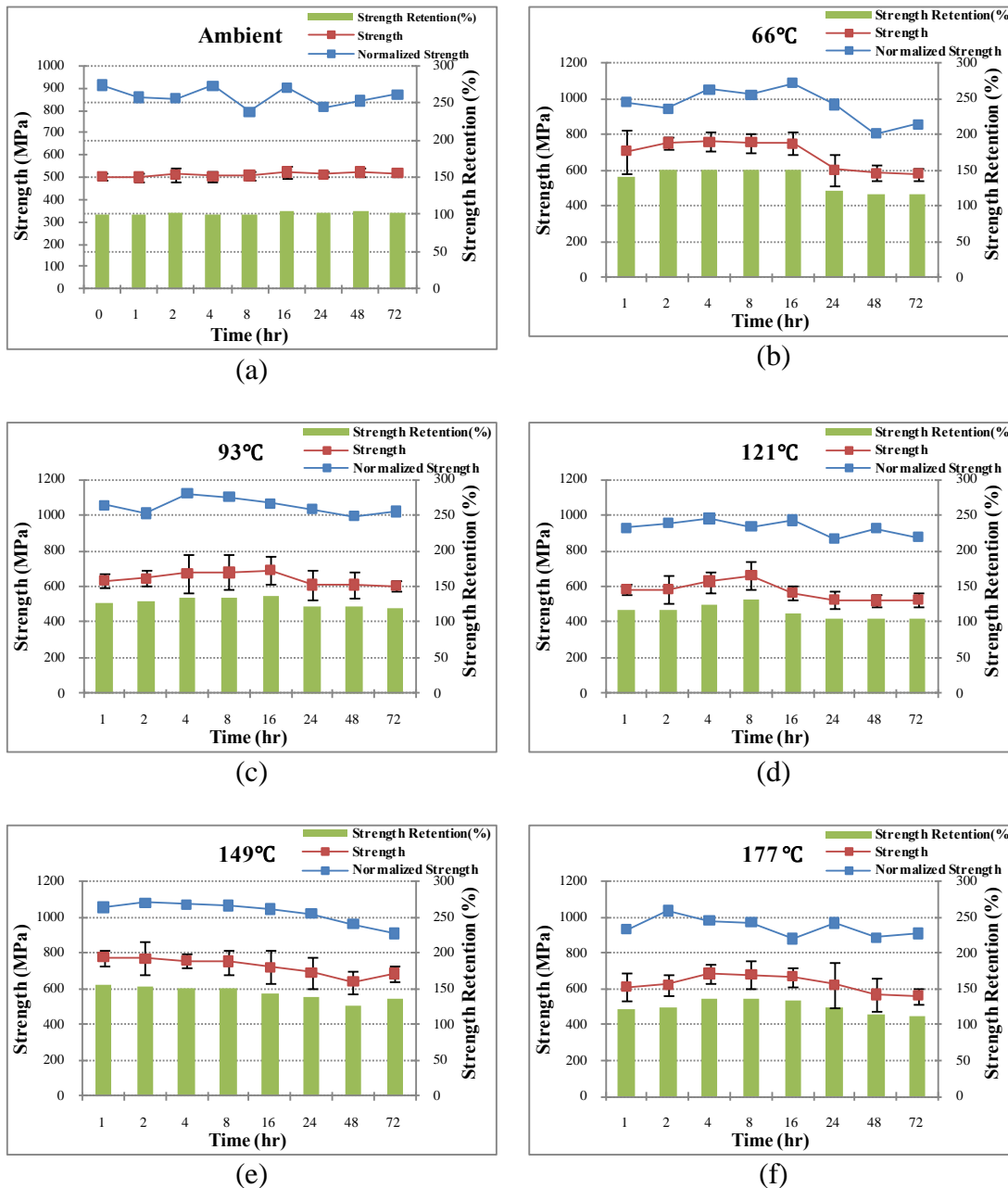
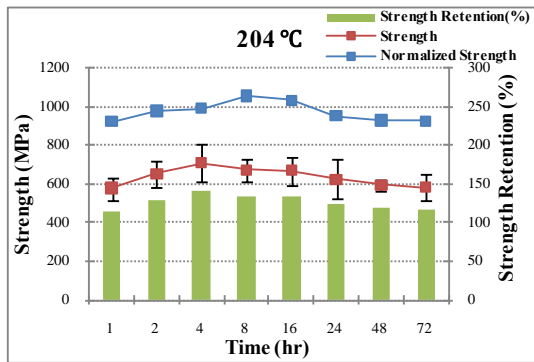
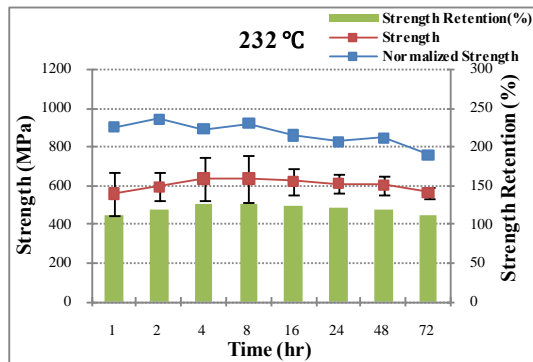


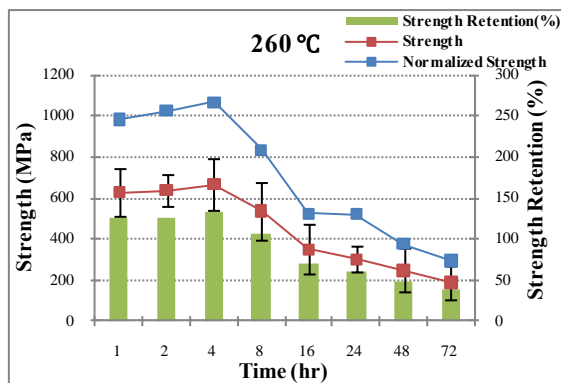
Figure 4-1: Tensile strengths and normalized tensile strengths of carbon/epoxy composite materials as a function of time at fixed temperatures, (a) ambient (b) 66 °C (c) 93°C (d) 121°C (e) 149°C (f) 177°C (g) 204°C (h) 232°C (i) 260°C



(g)



(h)



(i)

Figure 4-1: Continued

The data for tensile modulus of carbon/epoxy composite materials exposed to various temperatures from ambient temperature to 260 °C are shown in Table 4-2. The elastic modulus was calculated using data corresponding to 0.1% to 0.3% strain range within the linear region of test data.

Normalized strengths and modulus retentions (%) were obtained by same method mentioned for tensile strength. Figure 4-2 represents tensile modulus, normalized modulus, and modulus retention of the carbon/epoxy composite materials as a function of time at fixed temperatures. As shown in Figure 4-2, the data of tensile modulus show very similar tendency compared to the results of tensile strength. Initially, tensile modulus was enhanced due to post-curing effect. In all exposure temperatures, the maximum modulus values were initially attained and then showed consistency (ambient temperature) or slightly decrease (66, 93, 121, 149, 177, 204, 232 °C) or a rapid drop (260 °C). The distribution of the data within initial ageing time in terms of tensile modulus retention was mainly between 100 and 140%, while the distribution on tensile strength retention was mostly represented between 100% and 160%. This means the enhancement of the mechanical properties that would initially take place in tensile modulus was greater than that in tensile strength.

The maximum tensile modulus was 73.68 GPa (158.59% in tensile modulus retention) and occurred due to exposure of 16 hr at 66 °C, while the minimum tensile modulus was 34.08 GPa (34.08% in tensile Modulus retention) at a condition of 72 hrs at 260 °C. Tensile modulus retention of specimens exposed to 260 °C showed rapid loss in their mechanical properties compared to tensile strength retention.

Table 4-2 Data for tensile Modulus (GPa) of carbon/epoxy composite materials after exposure to various temperatures

Exposure Temperature	Time (hr)	Thickness (mm)	Modulus (GPa)	S.D (GPa)	Normalized Modulus	Modulus Retention (%)
Ambient (23°C)	0	3.51	46.46	3.60	84.48	100.00
	1	3.31	48.03	4.52	82.36	103.37
	2	3.21	50.26	3.69	83.59	108.18
	4	3.48	49.61	2.14	89.45	106.78
	8	3.02	48.24	3.56	75.48	103.83
	16	3.33	49.36	3.01	85.17	106.24
	24	3.05	53.21	4.28	84.09	114.53
	48	3.11	50.21	3.64	80.91	108.07
	72	3.24	49.52	5.22	83.13	106.59
66°C	1	2.67	56.88	4.62	78.81	122.43
	2	2.43	63.40	10.13	79.74	136.46
	4	2.67	66.18	4.48	91.55	142.43
	8	2.62	71.28	10.33	96.66	153.41
	16	2.80	73.68	9.15	106.80	158.59
	24	3.09	57.04	4.60	91.38	122.77
	48	2.65	57.08	10.82	78.49	122.86
	72	2.85	56.00	8.73	82.69	120.53
93°C	1	3.22	52.42	4.61	87.46	112.83
	2	3.02	57.86	3.39	90.54	124.54
	4	3.20	58.24	5.23	96.62	125.36
	8	3.12	60.21	8.63	97.45	129.59
	16	2.97	66.30	19.36	102.16	142.70
	24	3.26	61.20	4.09	103.44	131.73
	48	3.14	59.26	9.51	96.41	127.55
	72	3.26	51.00	8.22	86.25	109.77
121°C	1	3.07	52.54	8.67	83.52	113.09
	2	3.16	54.76	6.27	89.55	117.86
	4	3.01	56.00	2.36	87.45	120.53
	8	2.73	52.76	1.05	74.52	113.56
	16	3.32	51.49	4.37	88.44	110.82
	24	3.19	50.10	5.15	82.76	107.84
	48	3.42	45.86	7.17	81.27	98.72
	72	3.21	43.94	7.92	73.14	94.57
149°C	1	2.62	61.95	5.00	84.12	133.34
	2	2.71	60.11	5.25	84.51	129.38
	4	2.73	60.55	6.31	85.67	130.33
	8	2.73	60.58	6.63	85.61	130.40
	16	2.79	56.28	12.60	81.47	121.14
	24	2.84	56.65	5.06	83.40	121.93
	48	2.91	54.15	5.39	81.59	116.54
	72	2.56	52.78	5.40	70.06	113.59

Table 4-2 Continued

Exposure Temperature	Time (hr)	Thickness (mm)	Modulus (GPa)	S.D (GPa)	Normalized Modulus	Modulus Retention (%)
177°C	1	2.94	58.31	1.86	88.77	125.51
	2	3.21	59.44	4.67	98.86	127.94
	4	2.77	59.37	2.64	85.15	127.80
	8	2.77	56.06	4.38	80.34	120.66
	16	2.53	56.63	4.31	74.17	121.89
	24	3.00	51.76	13.28	80.35	111.41
	48	3.00	50.32	5.09	78.17	108.31
	72	3.12	49.18	5.76	79.40	105.86
204°C	1	3.09	53.46	3.57	85.48	115.07
	2	2.89	54.66	9.33	81.91	117.65
	4	2.70	60.34	2.16	84.29	129.88
	8	3.02	57.23	4.75	89.56	123.19
	16	2.98	55.18	6.39	85.14	118.77
	24	2.94	54.58	9.36	83.14	117.48
	48	3.01	53.83	5.47	84.00	115.86
	72	3.07	53.89	5.84	85.66	115.99
232°C	1	3.11	57.50	4.47	92.60	123.76
	2	3.07	59.88	3.34	95.24	128.88
	4	2.71	60.12	6.34	84.29	129.40
	8	2.79	60.82	6.11	87.80	130.91
	16	2.66	57.52	7.21	79.39	123.80
	24	2.61	55.15	3.04	74.57	118.69
	48	2.71	54.27	3.31	76.32	116.81
	72	2.59	48.15	3.68	64.66	103.63
260°C	1	3.03	49.14	6.78	77.15	105.77
	2	3.10	52.28	6.41	83.88	112.53
	4	3.08	52.61	6.37	84.05	113.24
	8	2.99	47.50	5.67	73.63	102.25
	16	2.89	35.41	4.44	53.07	76.21
	24	3.31	31.28	1.90	53.70	67.33
	48	2.91	19.68	3.86	29.71	42.35
	72	3.02	15.83	4.88	24.80	34.08

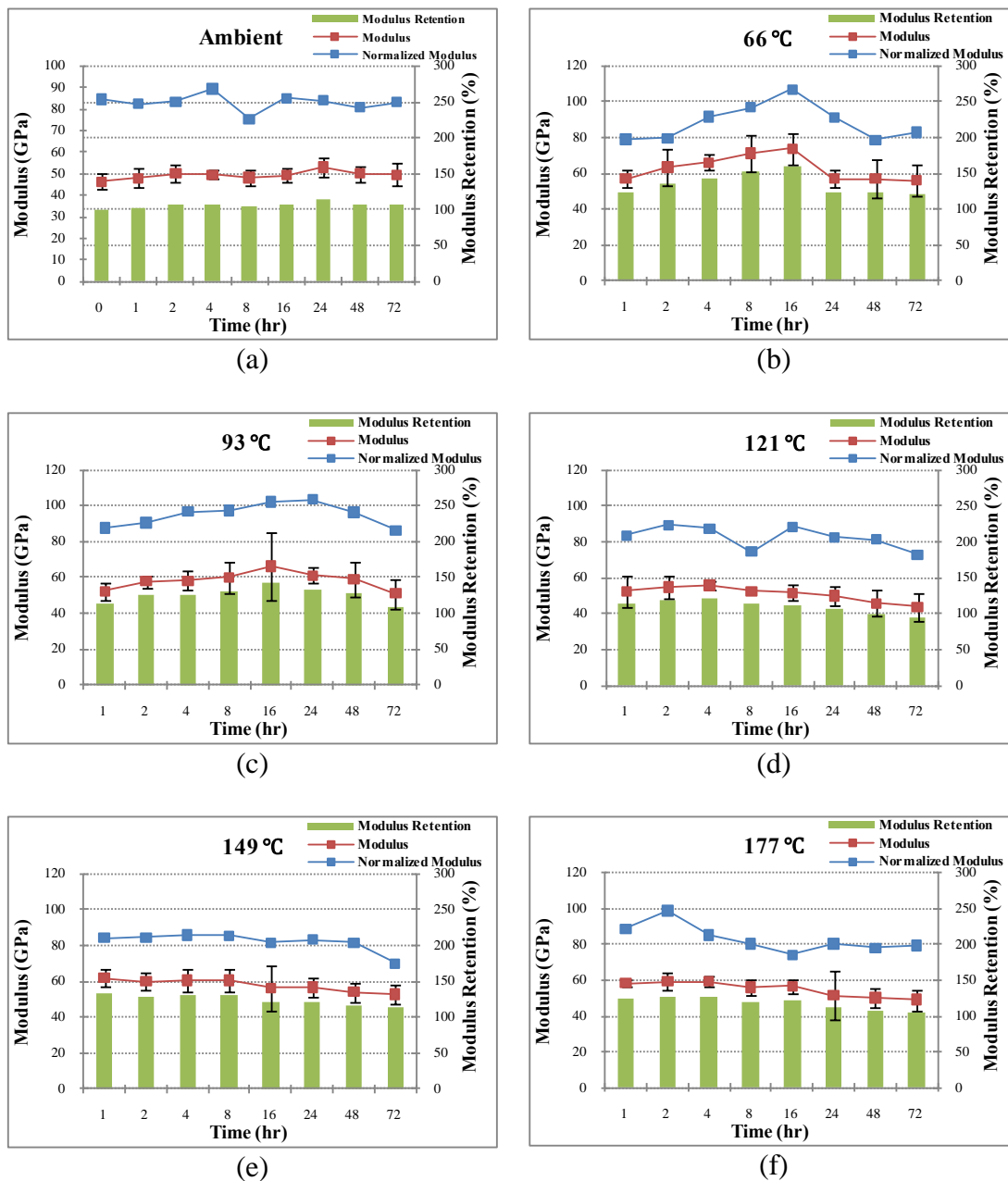


Figure 4-2: Tensile Modulus and normalized tensile modulus of carbon/epoxy composite materials as a function of time at fixed temperatures, (a) ambient (b) 66°C (c) 93°C (d) 121°C (e) 149°C (f) 177°C (g) 204°C (h) 232°C (i) 260°C

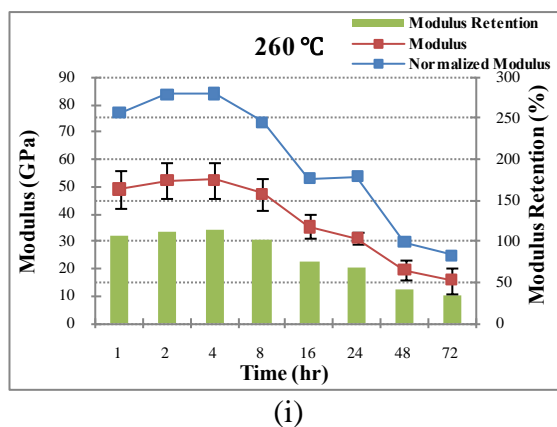
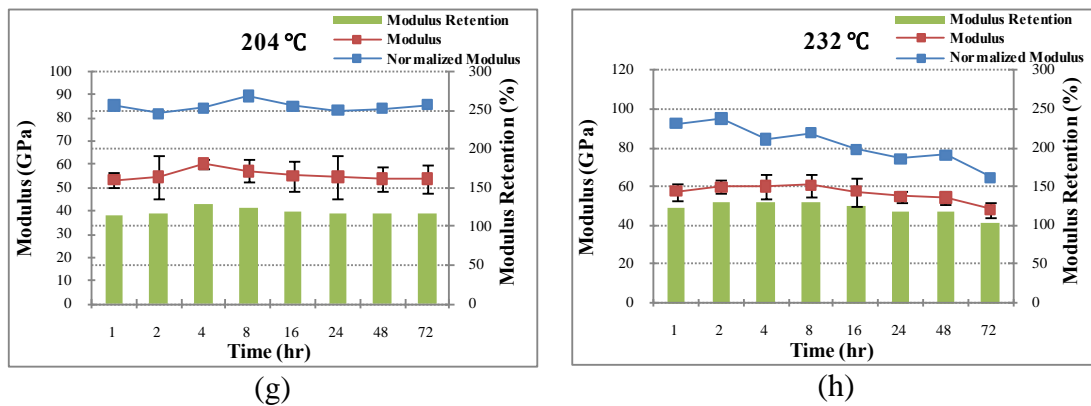


Figure 4-2: Continued

It is common engineering practice to "fit a line" to a set of data in order to determine some useful parameter in a mathematical model or perhaps to generate a calibration curve. A straight line is a simple polynomial and the goal of the fit is to determine the coefficients (the slope and intercept) of the polynomial that lead to the "best fit" of a line to the data. The fitting process can be generalized to determine the coefficients of the N^{th} -order polynomial that best fits $N+1$ (or more, usually) data points. The determination of the coefficients is usually termed "polynomial regression"

Table 4-3 and Table 4-4 show the time-dependent functions of tensile strength and modulus retention obtained by polynomial curve fittings. In looking at the data set of tensile strength and modulus retentions, it should be pointed out that time-dependent functions did not show linear tendency due to initial enhancement of the mechanical properties caused by post-curing effects. Therefore, the coefficients of regression (R^2) were relatively low compared to data sets without the initial increase and time-dependent functions were generally of the 2nd order.

Table 4-3 Time-dependent functions of tensile strength retention (%) obtained by polynomial curve fitting

Temperature(°C)	a	b	c	d	R^2
Ambient (23)		-0.0017	0.1647	100.35	0.7359
66		0.0073	-1.0516	151.96	0.7732
93	3.E-04	-0.0316	0.6298	129.13	0.5794
121		0.0062	-0.7134	123.45	0.5709
149		0.0109	-1.071	156.08	0.9743
177	5.E-04	-0.0555	1.2256	125.25	0.7931
204	4.E-04	-0.0462	1.06	126.12	0.4772
232	2.E-04	-0.0286	0.9187	117	0.5115
260		0.0317	-3.5419	132.76	0.9362

$$\text{Time-dependent function : } Y(t) = \frac{\sigma_t}{\sigma_i} \times 100 = at^3 + bt^2 + ct + d$$

Table 4-4 Time-dependent functions of tensile modulus retention (%) obtained by polynomial curve fitting

Temperature(°C)	a	b	c	d	R ²
Ambient (23)		-0.005	0.3913	103.45	0.4527
66	8.E-04	-0.0923	2.2132	131.43	0.4938
93		-0.0172	1.0672	120.23	0.7162
121		0.0022	0.4867	117.99	0.9264
149		0.0042	-0.5545	132.32	0.9344
177		0.0054	-0.6963	128.22	0.9295
204	1.E-04	-0.0136	0.2273	120.08	0.2377
232		-0.002	-0.1895	128.23	0.8882
260		0.0181	-2.4333	115.95	0.977

$$\text{Time-dependent function : } Y(t) = \frac{E_t}{E_i} \times 100 = at^3 + bt^2 + ct + d$$

4.1.3.2 Temperature Dependence

The effect of elevated temperature on the mechanical properties of composites will be discussed in this section. Changes in temperature-dependent properties can be reversibly considered up to the point where decomposition of one of the phases, usually the polymer matrix, begins. Ideally, for a particular composite system, each modulus or strength value would be measured and expressed as a function of temperature. However, there are few composite systems where all the required data are available in this form. The accurate analysis regarding relations among mechanical properties, decomposition temperature, and glass transition temperature will be discussed in the thermal analysis chapter. In this section, temperature-dependent functions for longitudinal tensile strength and modulus at fixed time periods of exposure will be demonstrated by polynomial curve fittings.

Figure 4-3 shows tensile strength of carbon/epoxy composite materials as a

function of temperature at fixed times of exposure. As shown in Figure 4-3, in cases where tensile test specimens were exposed to short time such as 1, 2, 4 and 8 hrs, the values of the tensile strength properties had fluctuation which means post-curing effect act differently on aged specimens. As ageing times were prolonged to 16, 24, 48 and 72 hrs, the data of the tensile strength strongly depended on elevated temperatures. In particular, abrupt drop of the tensile strength occurred between 232 °C and 260 °C. The amounts of tensile strength dropped by thermal decomposition at the each ageing times (16, 24, 48, 72 hrs) between 232 °C and 260 °C were 43.9, 50.4, 58.8 and 66.6% respectively. In the overall tests, when test specimens were exposed to 149 °C, tensile strengths were superior to the values on any other conditions.

Figure 4-4 represents tensile modulus of carbon/epoxy composite materials as a function of temperature at fixed periods of time. The data of the tensile modulus retention also had a similar tendency compared to those of the tensile strength retention but data fluctuation in short exposure times was not as high indicating that the values of the tensile modulus are more consistent. Similar to tensile strength retention, abrupt drop of the tensile modulus also took place between 232 °C and 260 °C. The amounts of tensile modulus decreased by thermal decomposition at the each ageing times (16, 24, 48, 72 hrs) between 232 °C and 260 °C were 38.4, 43.2, 63.7 and 67.1%, respectively.

From the data of the tensile strength and modulus retention, it can be seen that the rate of drop of the mechanical properties was higher in tensile modulus retention than in tensile strength retention in the case of high exposure temperature conditions where thermal decomposition can be expected to occur.

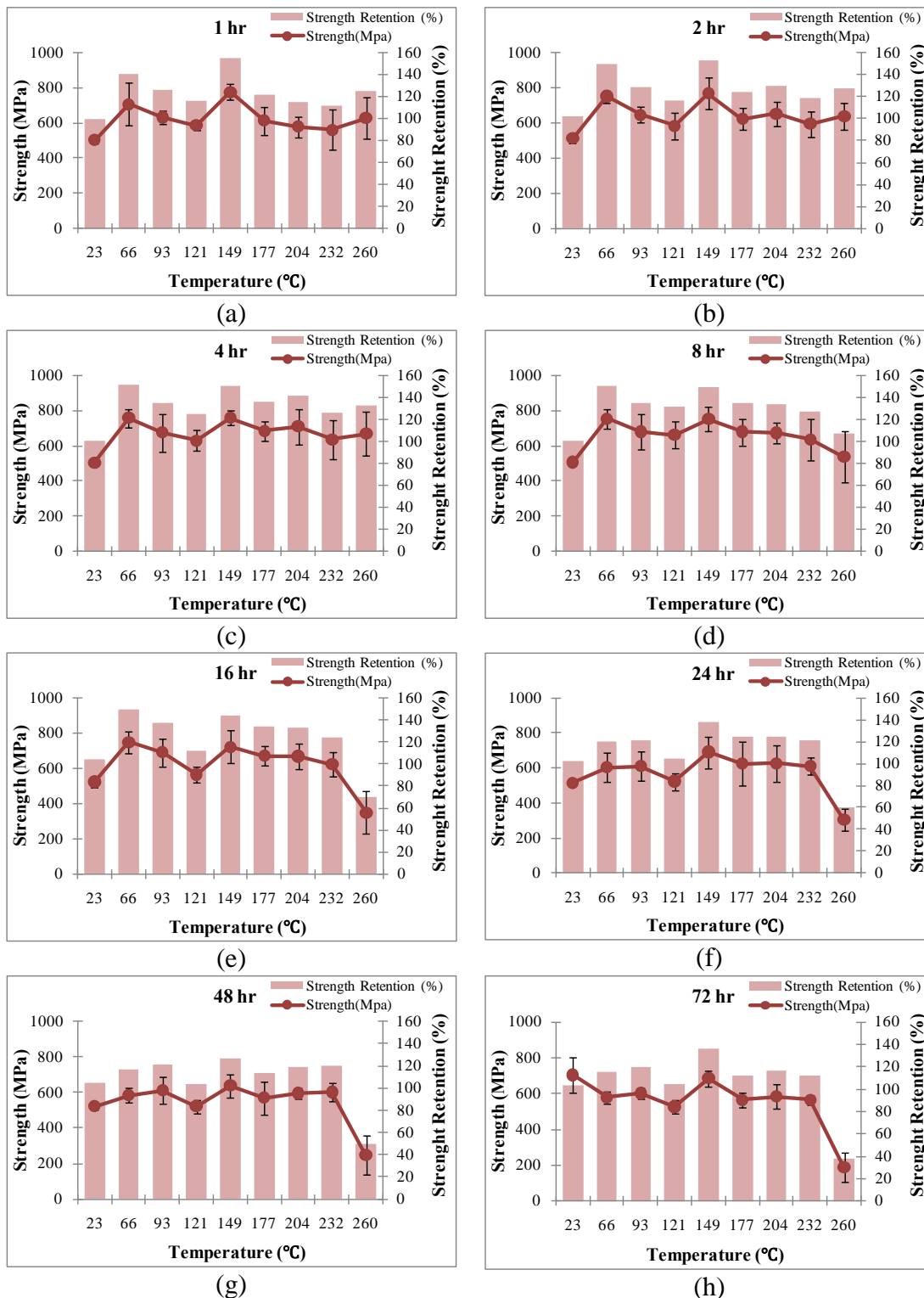


Figure 4-3: Tensile Strength of carbon/epoxy composite materials as a function of temperature at fixed periods of exposure, (a) 1 hr (b) 2 hrs (c) 4 hrs (d) 8 hrs (e) 16 hrs (f) 24 hrs (g) 48 hrs (h) 72 hrs

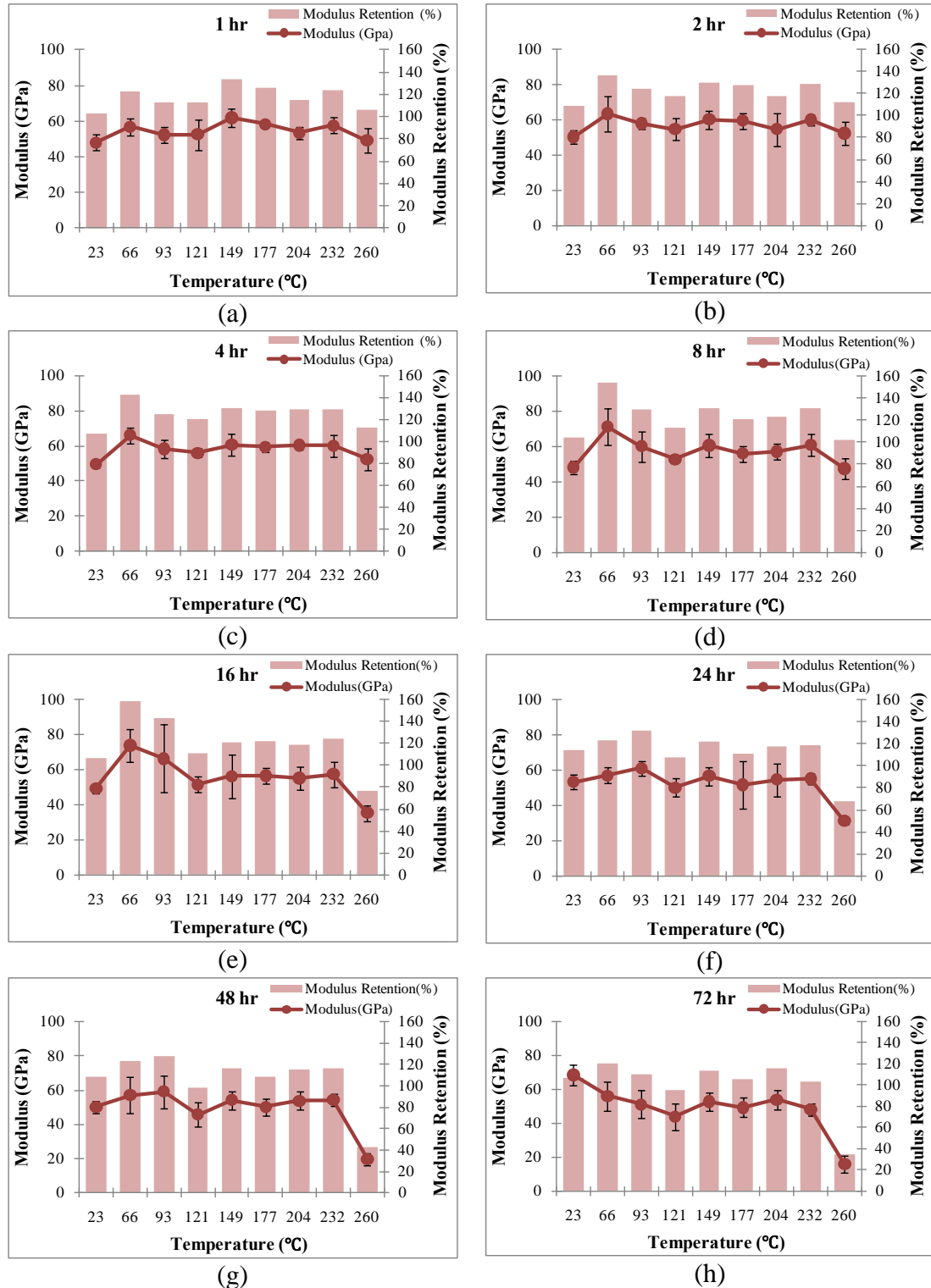


Figure 4-4: Tensile Modulus of carbon/epoxy composite materials as a function of temperature at fixed periods of exposure, (a) 1 hr (b) 2 hrs (c) 4 hrs (d) 8 hrs (e) 16 hrs (f) 24 hrs (g) 48 hrs (h) 72 hrs

Table 4-5 and Table 4-6 show the temperature-dependent functions of tensile strength and modulus retention obtained by polynomial curve fitting. Even though R-squared values are similar to the values of the time-dependent functions, temperature-dependent function had high order for good R-squared values.

Table 4-5 Temperature-dependent functions of tensile strength retention (%) obtained by polynomial curve fitting

Time (hr)	a	b	c	d	R ²
1			0.018	99.305	0.6899
2	9.E-06	-0.0044	0.5991	111.83	0.3216
4		-0.0007	0.1823	127.53	0.4414
8		-0.0016	0.3714	121.19	0.6859
16	-2.E-05	0.0073	-0.628	146.46	0.6967
24	-4.E-05	0.0141	-1.4661	159.13	0.7927
48	4.E-05	0.0151	-1.6784	168.37	0.7917
72	-5.E-05	0.0176	-1.9555	178.64	0.8552

$$\text{Temperature-dependent function : } Y(T) = \frac{\sigma_t}{\sigma_i} \times 100 = aT^3 + bT^2 + cT + d$$

Table 4-6 Temperature-dependent functions of tensile modulus retention (%) obtained by polynomial curve fitting

Time (hr)	a	b	c	d	R ²
1		-0.0003	0.1046	97.959	0.4957
2	3.E-06	-0.0019	0.3418	109.86	0.2771
4		-0.0007	0.1633	120.23	0.2374
8		-0.0004	0.0309	133.06	0.3202
16		-0.0012	0.1604	132.38	0.5564
24	-2.E-05	0.0093	-1.1203	161.39	0.7578
48	-4.E-05	0.015	-1.8075	180.99	0.7736
72	-5.E-05	0.02	-2.4561	198.97	0.8913

$$\text{Temperature-dependent function : } Y(T) = \frac{E_t}{E_i} \times 100 = aT^3 + bT^2 + cT + d$$

4.1.3.3 Morphological Analysis

First of all, if looking at the color of the test specimens exposed to elevated temperatures, the color of the specimens can be divided into five categories as represented in Figure 4-5.

Firstly, the surfaces of test specimens exposed to both ambient temperature and lower temperatures up to 121 °C kept the original morphology without the change of the color. In other words, the surfaces in ranges of these temperatures had the shining and black color. Secondly, as the aging time and exposed temperature were increased, the specimens showed a brown color and maintained a shiny surface between 149 °C and 177 °C in exposure temperature. Thirdly, in ranges of between 204 and 232 °C, the specimens had red color and shiny surface. The color change is indicative of chemical changes occurring in the epoxy due to thermal oxidation. In addition, the color change is most likely due to an optical effect from the presence of carbon fibers in the composites. Fourthly, in specimens exposed to 232 °C for more than 8 hrs of ageing time and in 260 °C for less than 8 hrs in ageing time, the test specimens had darker color than black and more shining color due to resin melting caused by severe thermal oxidation. Finally, test specimens changed to char at 260 °C for more than 16 hrs of ageing time.

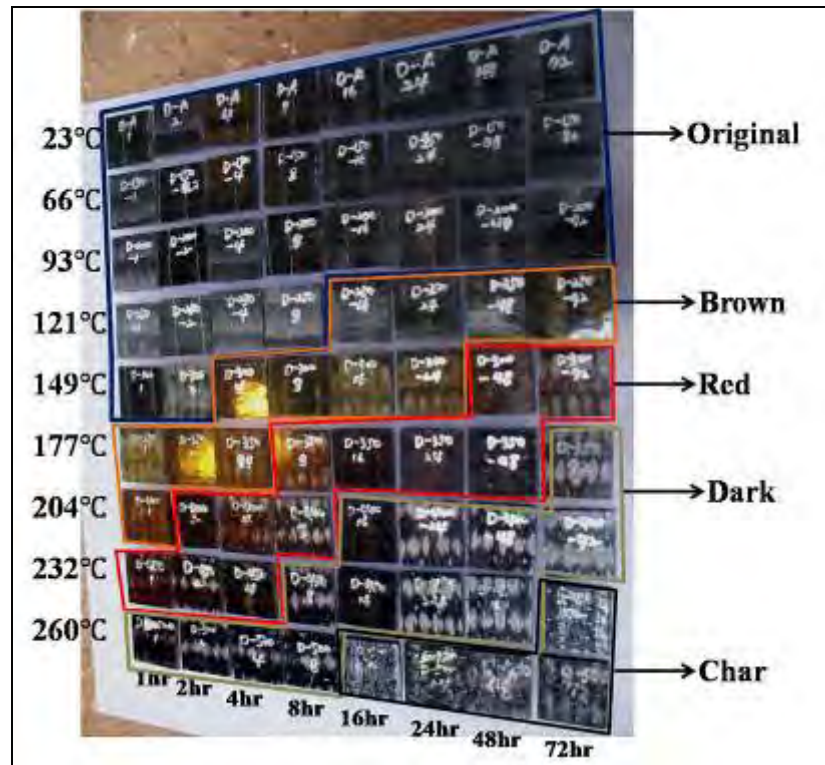


Figure 4-5: Color distribution of the test specimens after exposure to elevated temperatures for up to 72 hrs

Figure 4-6 shows test specimens fractured after tensile test after exposure to elevated temperatures at the ageing time of 72 hrs. Test coupons on unaged and lower temperature exposures revealed visible protruding carbon fibers in the cross section fractured in brittle failure. In addition, test specimens were not fractured perpendicular to the fiber directions and the cross section fractured was not clean because fracture mechanisms were affected by cracks, voids, and poor interfaces between fiber and matrix or between layers of fabric in process of manufacturing the carbon/epoxy composite materials with the manual wet layup process. It should be noted that the fibers used in composite materials do not have perfect alignment along the longitudinal direction due to the use of manual wet layup process. On the other hand, the cross sections of the test specimen fractured under high temperature exposure conditions were approximately perpendicular to the length of the tensile bar due to bonding failure between the fiber and matrix and softening of the epoxy resin. The reason why the cross section is perpendicular and clean is that poor interface between fiber and matrix by thermal oxidation resulted in fiber pulling-out. Also, damage extended along the length of test specimen and damage area was not confined to the cross section.

Figure 4-7 shows the tensile testing results for the specimens exposed to 232°C at 72 hrs and 260°C at 72 hrs. Both tensile specimens demonstrated a brooming mode of failure due to thermal degradation of the matrix. The difference of the both pictures is whether carbon fibers are thermally degraded or not. At 232°C, carbon fibers of test specimens kept the stiffness up to certain points whereas even carbon fibers were perfectly degraded by thermal oxidation after exposure to 260°C at 72 hrs.

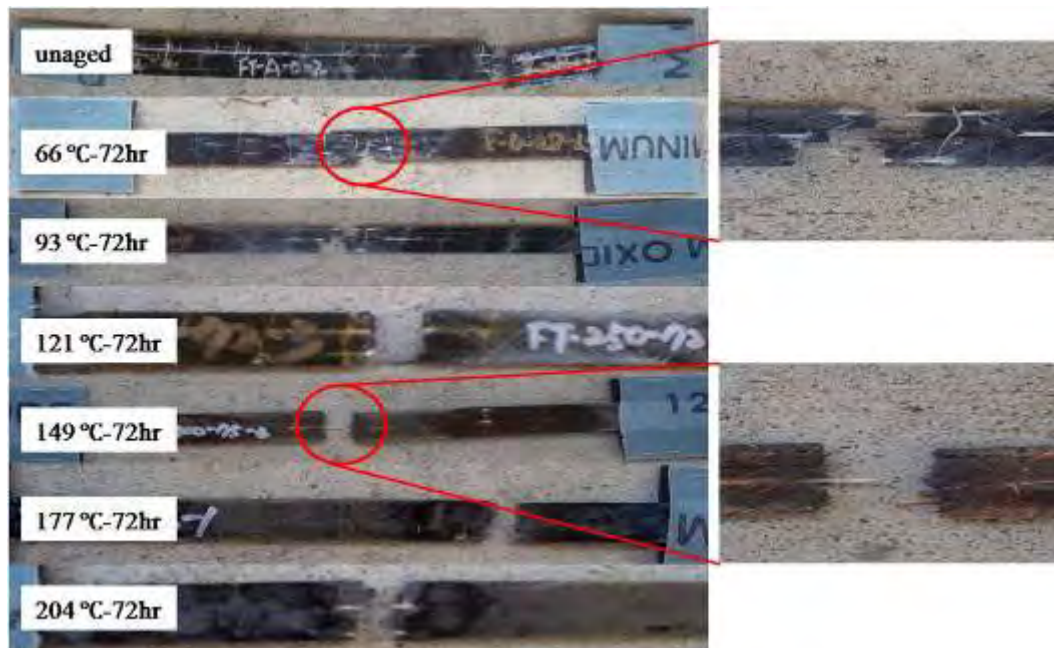


Figure 4-6: Test specimens fractured after tensile test after exposure to elevated temperatures at the ageing time of 72 hrs



(a)



(b)

Figure 4-7: Tensile testing results for the specimens exposed to (a) 232 ° C at 72 hrs and (b) 260 ° C at 72 hrs

Figure 4-8 and Figure 4-9 exhibit the SEM images for comparison of as-received specimen and specimens exposed to 232 °C at the various ageing times. On fracture surfaces of as-received specimen fibers were well covered with the matrix representing a good adhesion and fractured surface included the evidence of fracture with a significant degree of ductility. The ultimate failure strain is generally greater in unaged specimen than in aged specimen. The strain effect will be explained in following chapter. On the other hand, in the cases of the specimens exposed to 232 °C for 1, 2, 4 hr, there were a little of resin debris and the interface between fiber and resin showed the good adhesion due to the additional post curing. As the ageing times were prolonged, the entire cross section of the aged specimens exhibits micro cracking, holes which fibers were pulled out, and some of the cracks have developed into delaminations. Especially, the severe delamination occurred in the specimen exposed to 232 °C at 72 hrs due to thermal decomposition of the epoxy resin and fibers were separated from the epoxy resin, indicating a low adhesion.

If seeing the surfaces of the fibers, the cross surfaces of the specimens unaged and aged within the short exposure time were not damaged and showed the good roughness. Contrary to the above cases, the roughness of the fiber surfaces was increased and the surface was damaged by thermal degradation in the higher exposure temperatures. As circled in Figure 4-9 (e), (f), (g) and (h), there were the pits on the fractured fibers because the fibers were also damaged by thermo-oxidation.



Figure 4-8: SEM image after tensile testing of as-received specimen: magnification 1000 \times

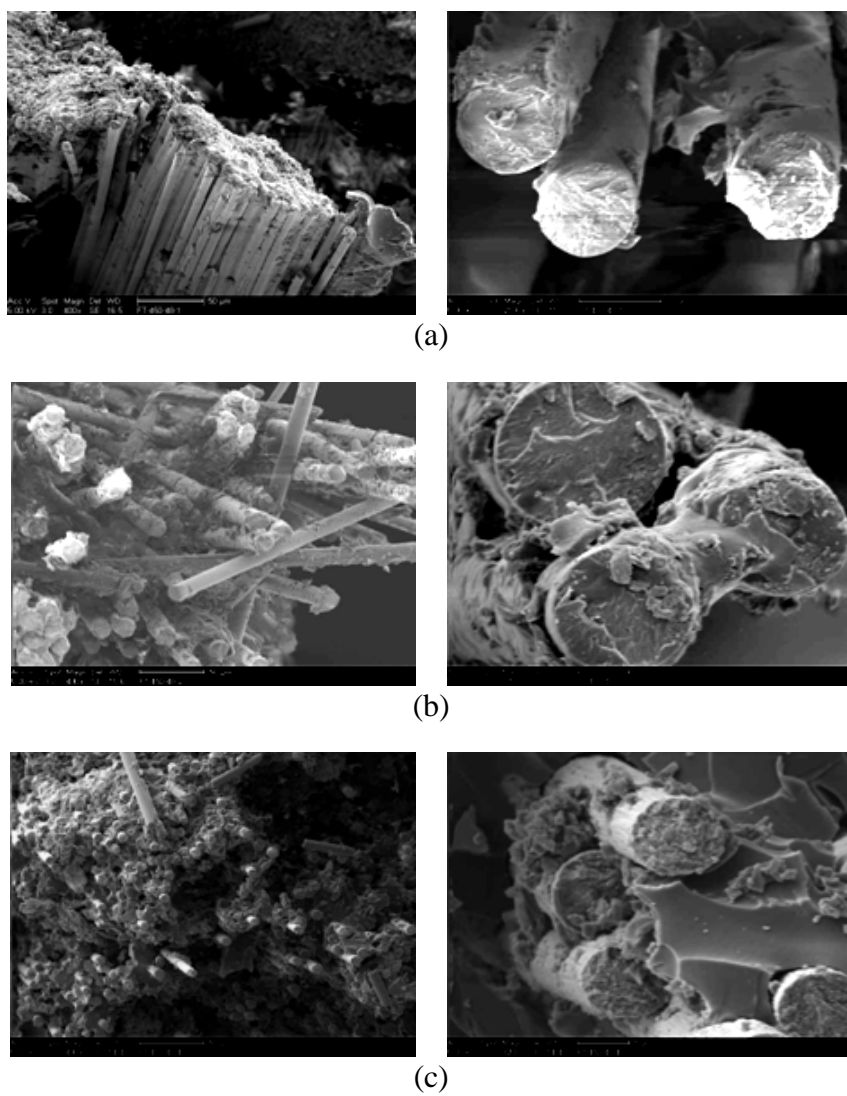
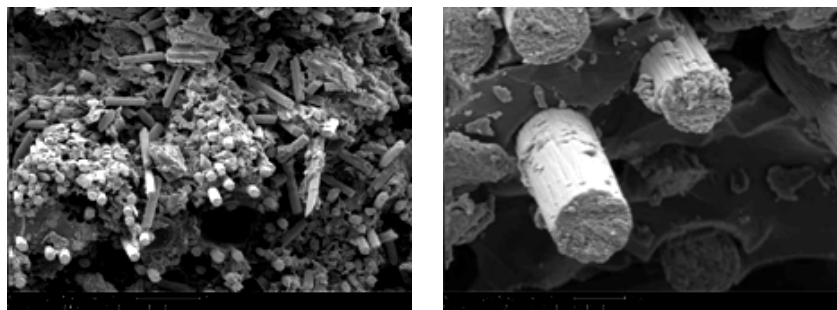
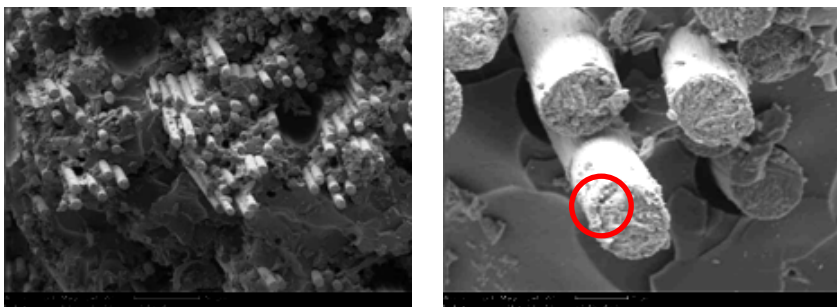


Figure 4-9: SEM images after tensile testing of specimens exposed to 232 $^{\circ}$ C for (a) 1 hr, (b) 2 hrs, (c) 4 hrs, (d) 8 hrs, (e) 16 hrs, (f) 24 hrs, (g) 48 hrs, (h) 72 hrs - left images:

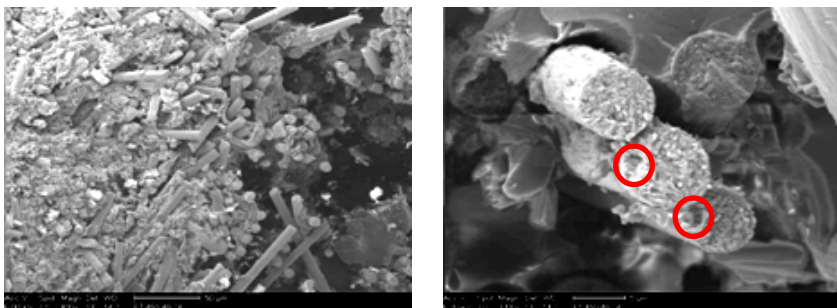
magnification 400×, right images : magnification 500×



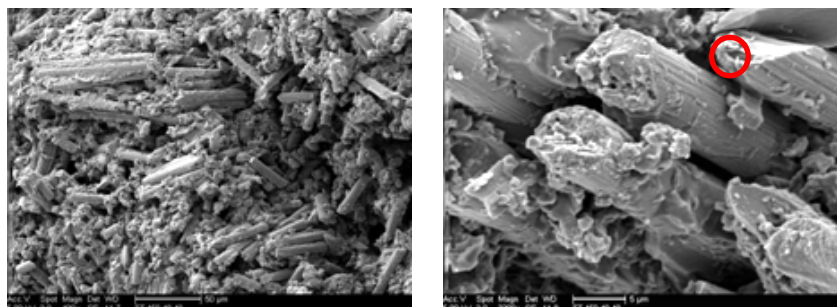
(d)



(e)



(f)



(g)

Figure 4-9: Continued

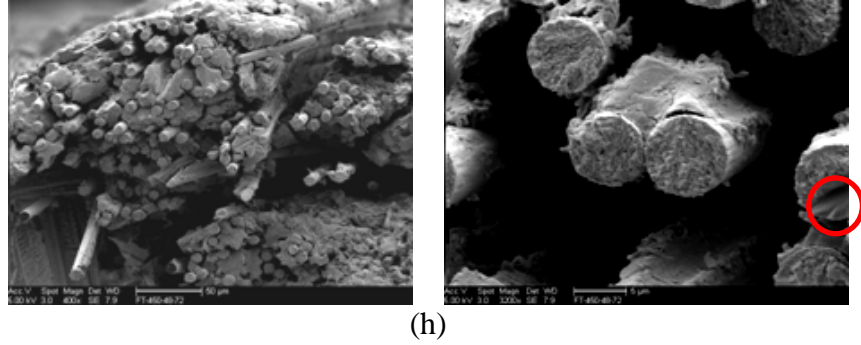


Figure 4-9: Continued

4.1.3.4 Strain Effect

Failure initiates when the fibers are elongated to their fracture strain in a unidirectional composite subjected to a longitudinal load. It is assumed that the failure strain of the fiber is less than that of the matrix and all the fibers fail at the same strain. Therefore, the ultimate longitudinal tensile strength of the composite can be assumed equal to the composite stress at the fiber fracture strain.

The ultimate failure strain of the fiber is

$$(\varepsilon_f)_{ult} = \frac{(\sigma_f)_{ult}}{E_f} \quad (4.3)$$

and the ultimate failure strain of the matrix is

$$(\varepsilon_m)_{ult} = \frac{(\sigma_m)_{ult}}{E_m} \quad (4.4)$$

Thus, the composite tensile strength is given by

$$(\sigma_1^T)_{ult} = (\sigma_f)_{ult} V_f + (\varepsilon_f)_{ult} E_m (1 - V_f) \quad (4.5)$$

Figure 4-10 shows tensile stress-ultimate failure strain curve on specimens exposed to various exposure temperatures at the fixed time, 72 hrs and tensile stress-

ultimate failure strain curve until the strain reaches until 0.3%. Ultimate tensile strains were distributed between 2.8% and 3.2% except the result of the test specimens exposed to 260 °C. The values of the ultimate failure strain were greater at the lower temperature than that at the higher temperatures. In the case of ageing time (72 hrs), perfect bonding between fibers and matrices due to fully cure occurred the strain elongation at the lower temperatures while thermal decompositions caused the ultimate failure strains to lower at the higher temperatures. The elastic modulus of the tensile test was calculated from slope between tensile stress and strain ranging from 0.1 to 0.3% before extensometer is taken off. Therefore, the slopes were changed from 0.3% strain as depicted in Figure 4-10 (a). As the slope is getting greater, test specimens are stiffer. As can be seen in Figure 4-10 (b), the slopes were increased from ambient temperature to 177°C in exposure temperature, whereas the slopes were decreased after reaching the maximum slope between 177°C and 232°C due to thermal oxidation of the resin. In the case of 260°C, thermal decomposition of the resin as well as the carbon fibers caused the elasticity to lose before reaching the ultimate failure strain of 0.3%. As depicted in Figure 4-7, the epoxy resin was perfectly decomposed and carbon fibers had a brooming mode of failure.

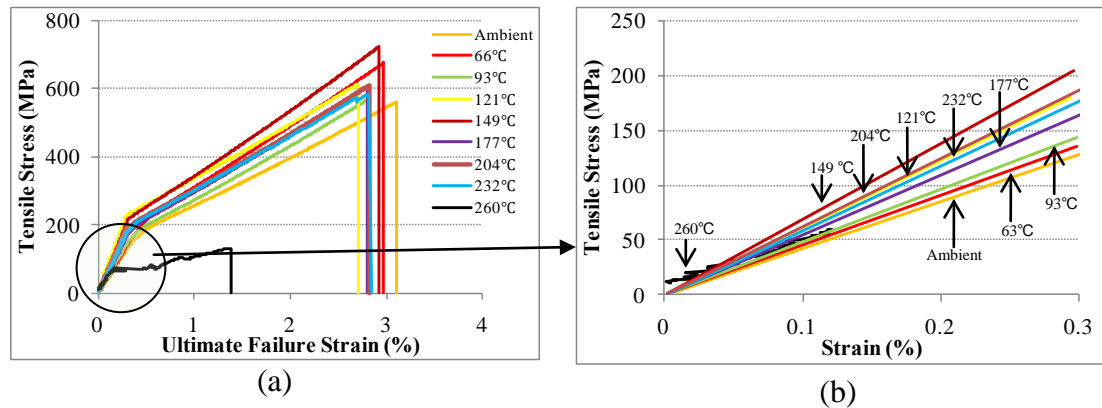


Figure 4-10: (a) Tensile stress-ultimate failure strain curve exposed to various ageing temperatures at a fixed time of 72 hrs (b) Tensile stress-ultimate failure strain curve until the strain reaches until 0.3% (Note that the kink in figure 4-10 (a) is due to removal of the extensometer)

Figure 4-11 and Table 4-7 show the relations of the ultimate tensile strength, the tensile modulus and the longitudinal load as a function of the ultimate failure strain. Except the environmental conditions exposed to 260°C for 16, 24, 48, and 72 hrs, the values of the tensile strength, the tensile modulus and load were distributed between 500 MPa and 750 MPa, 45 GPa and 73 GPa, 22 KN and 28 KN, respectively. The main range of the ultimate failure strain was between 2.4% and 3.4%. This range had the significant variation of the data because these specimens had the void due to hand wet layup process. As can be seen from R-squared values, the ultimate tensile strain showed the most linear relation with the longitudinal load. However, the linear relations between the ultimate tensile strain and the tensile modulus were poor than any other relations.

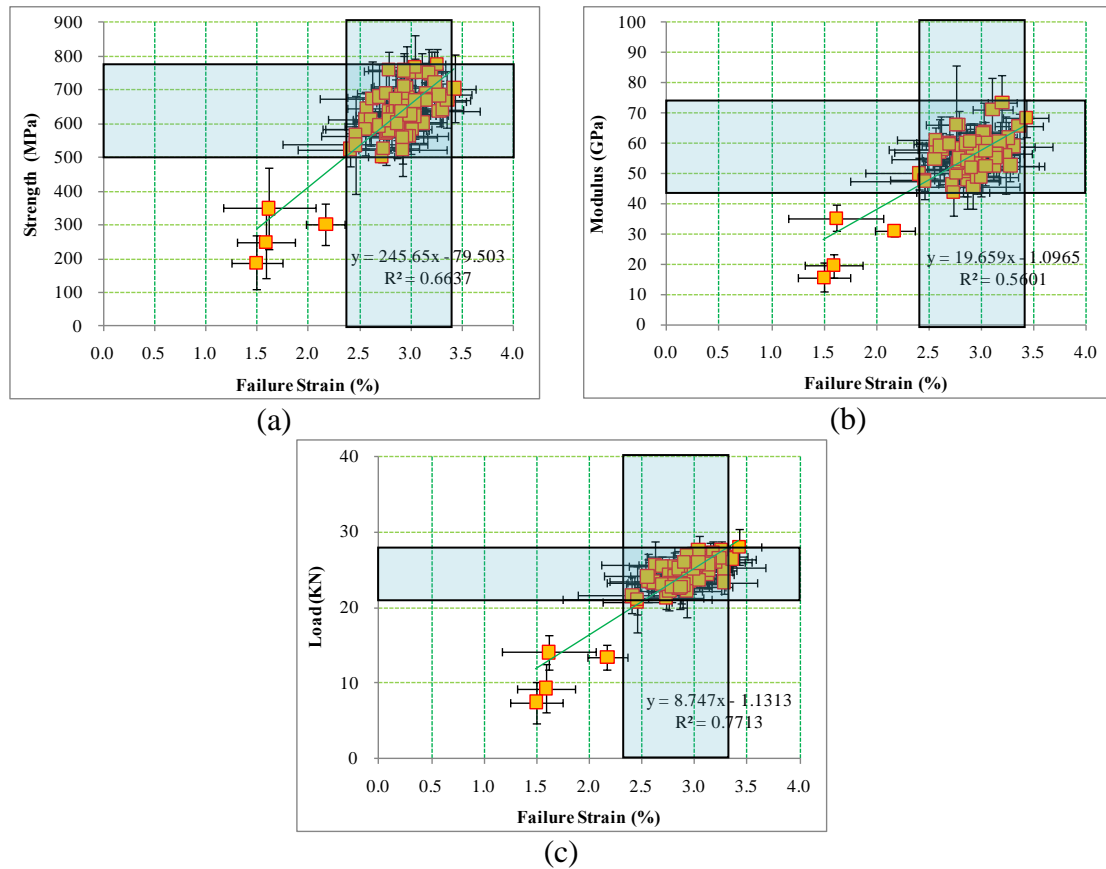


Figure 4-11: (a) Tensile Strength, (b) Tensile Modulus, (c) Load as a function of ultimate failure strains (%). Error bars indicate standard deviation

Table 4-7 Ultimate failure strain (%) after tensile testing

Exposure condition	Time (hr)	Load (KN)	S.D (KN)	Strength (MPa)	S.D (MPa)	Modulus (GPa)	S.D (GPa)	Failure strain (%)	S.D (%)
Ambient (23 °C)	0	22.88	0.98	502.26	15.94	46.46	3.60	2.713	0.13
	1	23.68	1.89	501.34	16.66	48.03	4.52	2.862	0.31
	2	24.56	2.01	512.68	29.32	50.26	3.69	3.115	0.19
	4	22.74	0.98	505.18	23.45	49.61	2.14	2.784	0.26
	8	25.04	1.33	507.06	19.79	48.24	3.56	3.275	0.40
	16	23.05	0.89	522.71	27.66	49.36	3.01	3.306	0.20
	24	24.12	0.51	514.71	14.11	53.21	4.28	3.033	0.24
	48	23.91	1.22	523.45	22.61	50.21	3.64	3.353	0.23
72	23.94	2.19	519.48	16.66	49.52	5.22	3.421	0.21	
66 °C	1	24.31	2.19	706.34	121.36	56.88	4.62	2.960	0.35
	2	24.86	1.15	751.05	35.12	63.40	10.13	3.012	0.24
	4	25.49	0.79	759.38	51.76	66.18	4.48	2.782	0.20
	8	25.54	1.24	754.03	55.81	71.28	10.33	3.102	0.19
	16	25.98	0.73	749.95	61.39	73.68	9.15	3.194	0.14
	24	24.20	1.92	604.06	86.50	57.04	4.60	2.866	0.31
	48	23.26	1.29	584.97	43.80	57.08	10.82	2.592	0.42
	72	23.61	1.25	578.72	34.65	56.00	8.73	2.933	0.22
93 °C	1	23.97	1.34	632.60	36.84	52.42	4.61	2.830	0.18
	2	24.24	0.75	646.52	45.32	57.86	3.39	2.564	0.18
	4	25.71	3.13	675.49	108.19	58.24	5.23	2.620	0.51
	8	25.44	1.36	679.70	98.29	60.21	8.63	2.685	0.31
	16	24.45	1.67	691.43	79.60	66.30	19.36	2.754	0.28
	24	23.56	2.79	611.17	84.19	61.20	4.09	2.560	0.37
	48	23.40	1.97	610.71	75.52	59.26	9.51	2.605	0.18
	72	23.30	1.02	602.29	28.56	51.00	8.22	2.827	0.46
121 °C	1	23.92	0.21	584.64	27.59	52.54	8.67	3.007	0.20
	2	24.13	2.92	583.46	77.91	54.76	6.27	2.552	0.41
	4	24.69	1.18	628.76	58.75	56.00	2.36	2.913	0.21
	8	24.01	1.55	662.12	77.57	52.76	1.05	2.916	0.25
	16	24.38	2.53	564.93	41.97	51.49	4.37	2.981	0.38
	24	21.59	2.38	524.36	48.69	50.10	5.15	2.405	0.52
	48	22.73	1.50	522.15	38.31	45.86	7.17	2.918	0.43
	72	21.31	1.51	526.22	35.73	43.94	7.92	2.726	0.35
149 °C	1	27.66	1.02	775.59	43.74	61.95	5.00	3.251	0.08
	2	27.59	1.98	768.83	92.07	60.11	5.25	3.037	0.23
	4	26.86	0.52	757.77	42.45	60.55	6.31	2.928	0.38
	8	27.33	1.51	752.08	68.54	60.58	6.63	3.170	0.06
	16	26.64	1.11	720.81	93.11	56.28	12.60	3.232	0.12
	24	26.07	2.50	691.34	90.38	56.65	5.06	3.146	0.33
	48	24.71	3.42	638.38	63.88	54.15	5.39	2.968	0.39
	72	23.39	1.47	684.88	43.20	52.78	5.40	3.274	0.32

Table 4-7 Continued

Exposure condition	Time (hr)	Load (KN)	S.D (KN)	Strength (MPa)	S.D (MPa)	Modulus (GPa)	S.D (GPa)	Failure strain (%)	S.D (%)
177 °C	1	24.21	3.13	612.64	80.61	58.31	1.86	2.809	0.13
	2	25.75	2.14	623.52	61.66	59.44	4.67	2.911	0.45
	4	25.91	0.48	684.95	56.01	59.37	2.64	2.910	0.18
	8	24.88	1.59	679.07	75.74	56.06	4.38	2.973	0.20
	16	25.03	0.93	671.43	53.52	56.63	4.31	3.138	0.26
	24	24.67	2.34	624.42	125.15	51.76	13.28	2.863	0.38
	48	22.21	2.47	570.72	92.71	50.32	5.09	2.759	0.30
	72	23.54	0.99	563.94	43.88	49.18	5.76	2.953	0.21
204 °C	1	23.19	1.85	577.67	57.80	53.46	3.57	2.766	0.28
	2	24.38	1.30	652.35	70.31	54.66	9.33	2.948	0.11
	4	24.92	2.38	710.17	100.84	60.34	2.16	2.931	0.29
	8	25.20	0.80	673.62	59.69	57.23	4.75	2.849	0.19
	16	25.80	1.27	669.59	72.74	55.18	6.39	3.137	0.22
	24	23.81	2.38	625.50	103.24	54.58	9.36	2.935	0.30
	48	23.19	1.69	595.91	31.10	53.83	5.47	2.871	0.25
	72	23.09	1.97	582.49	68.98	53.89	5.84	2.784	0.33
232 °C	1	22.16	3.42	559.53	113.78	57.50	4.47	2.921	0.33
	2	23.11	1.65	594.13	72.52	59.88	3.34	2.692	0.35
	4	22.59	2.73	635.30	109.41	60.12	6.34	2.853	0.31
	8	23.06	3.00	636.98	117.50	60.82	6.11	2.890	0.35
	16	23.71	1.44	623.21	66.32	57.52	7.21	3.039	0.15
	24	22.73	1.94	611.42	48.53	55.15	3.04	2.781	0.35
	48	22.73	2.24	603.00	52.38	54.27	3.31	2.867	0.42
	72	20.70	1.65	565.29	25.92	48.15	3.68	2.456	0.33
260 °C	1	25.16	2.87	627.34	118.33	49.14	6.78	2.993	0.35
	2	26.06	1.65	638.44	77.55	52.28	6.41	2.902	0.15
	4	25.97	2.01	667.76	124.99	52.61	6.37	3.036	0.50
	8	21.06	4.35	537.66	145.04	47.50	5.67	2.455	0.71
	16	14.11	2.36	349.88	120.66	35.41	4.44	1.613	0.45
	24	13.43	1.62	303.20	61.99	31.28	1.90	2.170	0.19
	48	9.34	3.26	248.40	107.04	19.68	3.86	1.587	0.28
	72	7.51	2.74	188.60	79.34	15.83	4.88	1.495	0.25

4.1.3.5 Volume Fraction Effect

The mechanisms applying for composite materials during loading, and the progression of damage and fracture modes, are influenced by the properties, microgeometry and the interaction amongst the composite components since composite materials are composed of the various components such as fiber, matrix, void, and interfaces[49]. The strength and the stiffness properties of the composite materials are extremely dependent on the fiber volume fraction, and this parameter thus is an important quality measure of such materials. Especially, fiber volume fraction is more important factor since the fiber is the main load-bearing component in unidirectional composite materials. The fiber volume fraction of a composite may be determined by chemical matrix digestion, the burn-off technique, or by photomicrographic techniques. In this study, the volume fractions were determined by photomicrograph in some cases.

In addition, all volume fractions can be obtained by micromechanical analysis of composites as follows,

$$F_c = F_f + F_m \quad (4.6)$$

$$F_c = \sigma_c A_c, \quad (4.7a)$$

$$F_f = \sigma_f A_f, \quad (4.7b)$$

$$F_m = \sigma_m A_m, \quad (4.7c)$$

Where:

$F_{c,f,m}$ = The uniaxial load in composite, fiber, and matrix, respectively

$\sigma_{c,f,m}$ = stress of composite, fiber, and matrix, respectively

$A_{c,f,m}$ = area of composite, fiber, and matrix, respectively

Assuming that the fibers, matrix, and composite follow Hooke's law and that the fibers and the matrix are isotropic, the stress-strain relationship is

$$\sigma_c = E_1 \varepsilon_c \quad (4.8a)$$

$$\sigma_f = E_f \varepsilon_f \quad (4.8b)$$

$$\sigma_m = E_m \varepsilon_m \quad (4.8c)$$

Where

$\varepsilon_{c,f,m}$ = strains in composite, fiber, and matrix, respectively

$E_{1,f,m}$ = elastic modulus of composite, fiber, and matrix, respectively

Accordingly, Equation 4.6 by substituting Equation 4.7 and 4.8 can be changed as following equation.

$$E_1 \varepsilon_c A_c = E_f \varepsilon_f A_f + E_m \varepsilon_m A_m \quad (4.9)$$

In the uniaxial load, the strains in the composite, fiber and matrix are equal, then from Equation 4.9,

$$E_1 = E_f \frac{A_f}{A_c} + E_m \frac{A_m}{A_c} = E_f V_f + E_m V_m \quad (4.10)$$

In the case of carbon/epoxy composite materials, the elastic modulus (230 GPa) of the carbon fiber is much greater than the elastic modulus (3.4 GPa) of the epoxy. Therefore, following equation can be yielded.

$$E_1 \approx E_f V_f \quad (4.11)$$

Table 4-8 shows the volume fractions determined by using Equation 4.11.

Table 4-8 Volume fractions and normalized volume fractions determined by using Equation 4.11 (the elastic modulus of carbon fiber is assumed to be 230 GPa)

		Ambient (23 °C)				66 °C				93 °C			
time	Modulus (GPa)	N Modulus (GPa)	V _f	N V _f	Modulus (GPa)	N Modulus (GPa)	V _f	N V _f	Modulus (GPa)	N Modulus (GPa)	V _f	N V _f	
0	46.46	84.48	0.20	0.37									
1	48.03	81.66	0.21	0.36	56.88	78.81	0.25	0.34	52.42	87.46	0.23	0.38	
2	52.48	86.69	0.23	0.38	63.40	79.74	0.28	0.35	57.86	90.54	0.25	0.39	
4	55.48	87.81	0.24	0.38	66.18	91.55	0.29	0.40	58.24	96.62	0.25	0.42	
8	58.84	91.28	0.26	0.40	71.28	96.66	0.31	0.42	60.21	97.45	0.26	0.42	
16	59.14	101.22	0.26	0.44	73.68	106.80	0.32	0.46	66.30	102.16	0.29	0.44	
24	63.84	99.21	0.28	0.43	57.04	91.38	0.25	0.40	61.20	103.44	0.27	0.45	
48	65.85	104.80	0.29	0.46	57.08	78.49	0.25	0.34	59.26	96.41	0.26	0.42	
72	68.44	108.75	0.30	0.47	56.00	82.69	0.24	0.36	51.00	86.25	0.22	0.38	
		121 °C				149 °C				177 °C			
time	Modulus (GPa)	N Modulus (GPa)	V _f	N V _f	Modulus (GPa)	N Modulus (GPa)	V _f	N V _f	Modulus (GPa)	N Modulus (GPa)	V _f	N V _f	
1	52.54	83.52	0.23	0.36	61.95	84.12	0.27	0.37	58.31	88.77	0.25	0.39	
2	54.76	89.55	0.24	0.39	60.11	84.51	0.26	0.37	59.44	98.86	0.26	0.43	
4	56.00	87.45	0.24	0.38	60.55	85.67	0.26	0.37	59.37	85.15	0.26	0.37	
8	52.76	74.52	0.23	0.32	60.58	85.61	0.26	0.37	56.06	80.34	0.24	0.35	
16	51.49	88.44	0.22	0.38	56.28	81.47	0.24	0.35	56.63	74.17	0.25	0.32	
24	50.10	82.76	0.22	0.36	56.65	83.40	0.25	0.36	51.76	80.35	0.23	0.35	
48	45.86	81.27	0.20	0.35	54.15	81.59	0.24	0.35	50.32	78.17	0.22	0.34	
72	43.94	73.14	0.19	0.32	52.78	70.06	0.23	0.30	49.18	79.40	0.21	0.35	
		204 °C				232 °C				260 °C			
time	Modulus (GPa)	N Modulus (GPa)	V _f	N V _f	Modulus (GPa)	N Modulus (GPa)	V _f	N V _f	Modulus (GPa)	N Modulus (GPa)	V _f	N V _f	
1	53.46	85.48	0.23	0.37	57.50	92.60	0.25	0.40	49.14	77.15	0.21	0.34	
2	54.66	81.91	0.24	0.36	59.88	95.24	0.26	0.41	52.28	83.88	0.23	0.36	
4	60.34	84.29	0.26	0.37	60.12	84.29	0.26	0.37	52.61	84.05	0.23	0.37	
8	57.23	89.56	0.25	0.39	60.82	87.80	0.26	0.38	47.50	73.63	0.21	0.32	
16	55.18	85.14	0.24	0.37	57.52	79.39	0.25	0.35	35.41	53.07	0.15	0.23	
24	54.58	83.14	0.24	0.36	55.15	74.57	0.24	0.32	31.28	53.70	0.14	0.23	
48	53.83	84.00	0.23	0.37	54.27	76.32	0.24	0.33	19.68	29.71	0.09	0.13	
72	53.89	85.66	0.23	0.37	48.15	64.66	0.21	0.28	15.83	24.80	0.07	0.11	

Figure 4-12 shows volume fraction and the ultimate tensile strength as a function of temperature. The composites having higher volume fraction generally showed the good mechanical properties. It should be pointed out that the range between

0.3% and 0.4% in volume fraction did not show any correlation of the tensile strength and the volume fraction. In the case of composites cured up to certain point, voids created by hand wet layup process significantly resulted in the decrease of the ultimate tensile strength. As depicted in Figure 4-13, it can be seen that the data of the tensile strength were more scattered within range between 0.3% and 0.4% in volume fraction, whereas Figure 4-13 (b) demonstrated good correlation between the tensile strength and the volume fraction in range except 0.3% and 0.4% in volume fraction.

The relations of the volume fraction and the failure strain in composite materials are also meaningful in terms of the mechanical properties. Similar to the result of correlation of the tensile strength and the volume fraction, the higher volume fraction showed the higher failure strain as shown in Figure 4-14. The data of the ultimate failure strain were more scattered within range between 0.3% and 0.4% in volume fraction as demonstrated in the correlation of the tensile strength and the volume fraction.

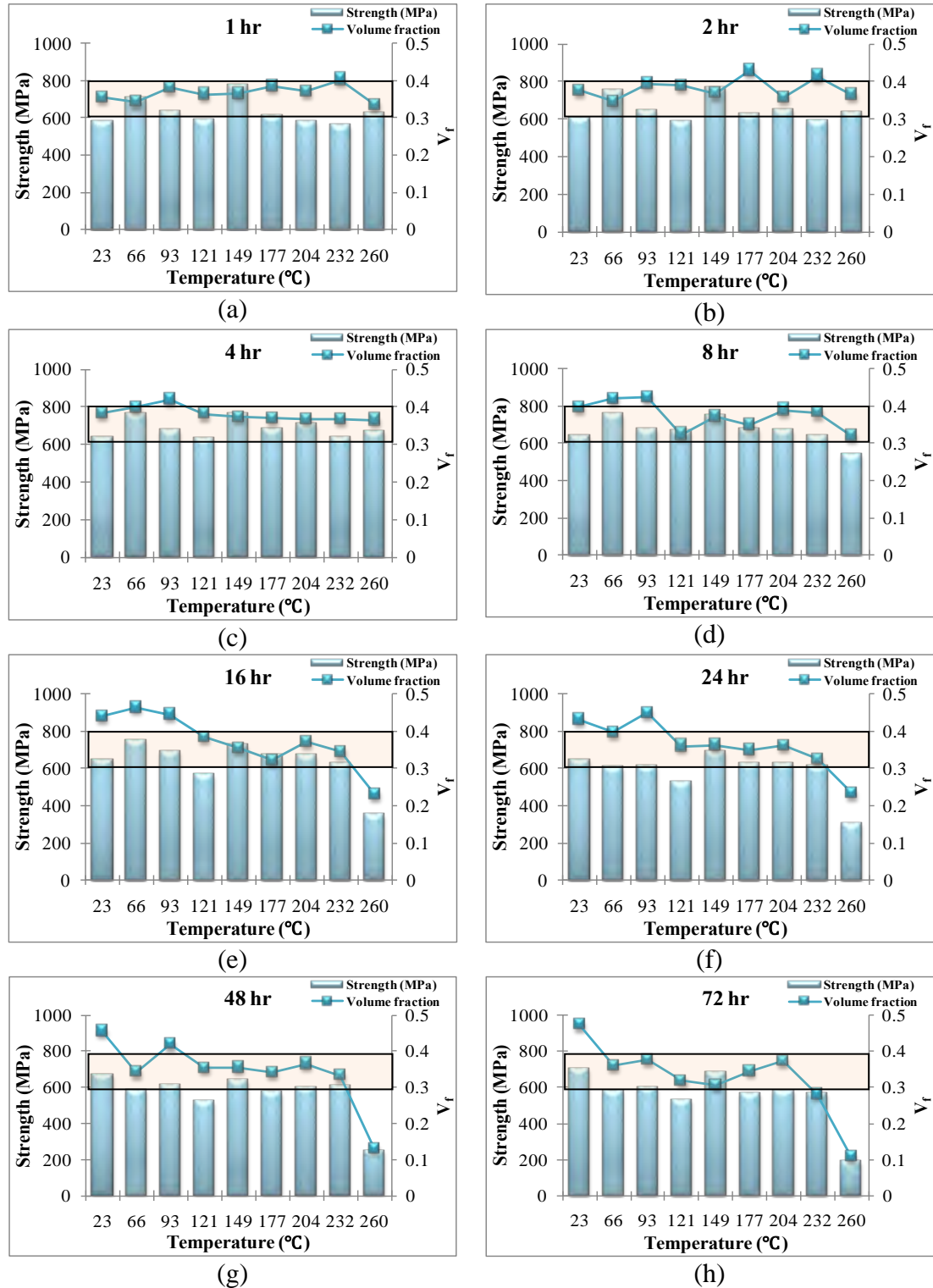


Figure 4-12: Volume fraction and the ultimate tensile strength as a function of temperature at fixed times of exposure (a) 1 hr, (b) 2 hrs, (c) 4 hrs, (d) 8 hrs, (e) 16 hrs, (f) 24 hrs, (g) 48 hrs, (h) 72 hrs

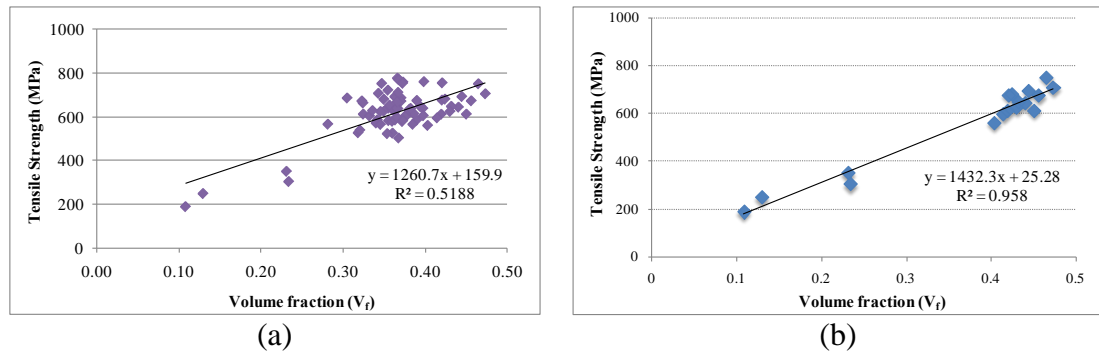


Figure 4-13: (a) Volume fraction versus tensile strength (b) Volume fraction versus tensile strength without specimens having volume fractions ranging from 0.2% to 0.3%

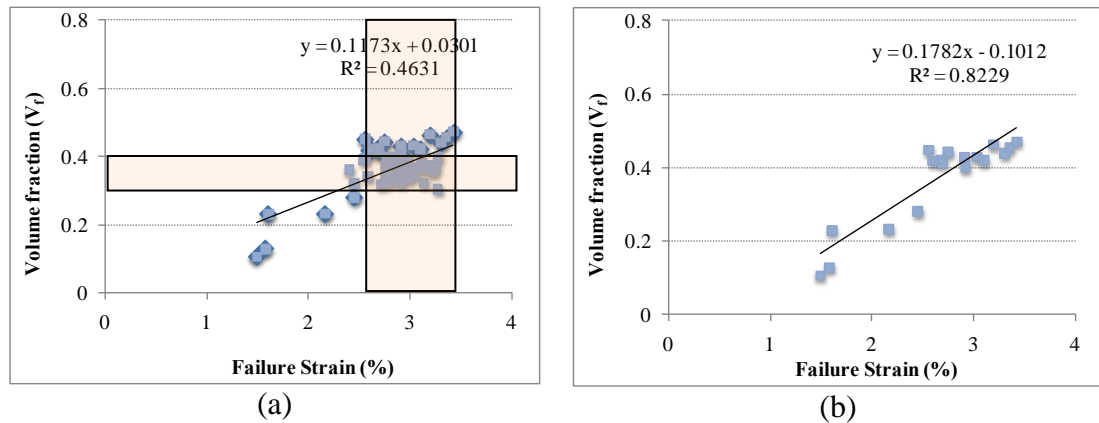


Figure 4-14: (a) Volume fraction versus the ultimate failure strain (b) Volume fraction versus the ultimate failure strain without specimens having volume fractions ranging from 0.3% to 0.4%

4.2 Off-Axis Shear Testing

4.2.1 Introduction

While the unidirectional composite is very effective in providing strength and modulus in the direction of the fibers it should be pointed out that the application of small tangential stresses may lead to matrix cracking, layer delamination and fiber-

matrix debonding, resulting in significant overall reductions in the load-bearing capacity of the composites[50]. It is obvious that off-axis shear resistance carefully assessed, especially as related to long-term response, since the efficiency of the strengthening technique can be consisted by the weakest materials characteristic. It is very important to consider the off-axis shear as a design factor. The test specimen for the off-axis shear is relatively simple to prepare and requires no special test fixture other than standard tensile grips. The test method has been standardized as ASTM D 3518.

4.2.2 Data Reduction

When a $\pm 45^\circ$ laminate is loaded in uniaxial tension, a biaxial state of stress is induced within each of the +45 and -45 lamina. In this study, off-axis shear strength and modulus were determined through a standard $\pm 45^\circ$ laminate tensile test as outlined in ASTM D 3518. The off-axis shear strength as the specimen was loaded is determined as

$$\sigma_{11} = \frac{\sigma_{xx}}{2} + \tau_{xy} \quad (4.12)$$

$$\sigma_{22} = \frac{\sigma_{xx}}{2} - \tau_{xy} \quad (4.13)$$

$$\tau_{12} = \pm \frac{\sigma_{xx}}{2} \quad (4.14)$$

Where:

σ_{11}, σ_{22} = Normal stresses in the lamina coordinate system

σ_{xx} = The applied tensile stress

τ_{xy} = Induced shear strength

τ_{12} = Shear strength

The maximum off-axis shear strength is determined as

$$\tau_{12}^{\max} = \frac{P^{\max}}{2A} \quad (4.15)$$

Where:

τ_{12}^{\max} = Maximum off-axis shear strength

P^{\max} = Maximum load

The off-axis shear strain is determined as

$$\gamma_{12} = \varepsilon_{xx} - \varepsilon_{yy} \quad (4.16)$$

Where:

γ_{12} = Shear strain

ε_{xx} = Longitudinal normal strain

ε_{yy} = Lateral normal strain

The off-axis shear modulus can be determined by using the chord shear modulus.

$$G_{12}^{chord} = \frac{\Delta\tau_{12}}{\Delta\gamma_{12}} \quad (4.17)$$

Where:

G_{12}^{chord} = Shear chord modulus

$\Delta\tau_{12}$ = Difference in applied shear strength between two shear strain points

$\Delta\gamma_{12}$ = Difference of two strain points

4.2.3 Analyses and Results

4.2.3.1 Time Dependence

The data for off-axis shear strength of carbon/epoxy composite materials exposed to various temperatures from ambient temperature to 260 °C are represented in Table 4-9. The off-axis shear strength was obtained by data reduction method. Also, the normalized off-axis shear strength and shear strength retention were calculated by same method described in tensile testing section. Figure 4-15 shows the off-axis shear strength, normalized strength, and strength retention of carbon/epoxy composite materials using uniaxial tensile test of a $\pm 45^\circ$ laminate as a function of time at fixed temperatures.

Even though uniaxial tensile test of a $\pm 45^\circ$ laminate is dominated by matrix properties, experimental results showed continuously decrease in shear strength except for test specimens exposed to ambient temperatures. Contrary to tensile testing, the effect of residual post-cure did not initially occur in off-axis shear test. As the exposure temperature was increased, the rate of decrease of the off-axis shear strength was rapidly increased. The decreases of the off-axis shear strength exposed to 66, 93, 121, 149, 177, 204, and 232 °C from 1 hr to 72 hrs in ageing time were 7.41, 17.88, 12.55, 20.36, 32.65, 34.68, and 79.30%, respectively. Especially, test specimens exposed to 232 °C abruptly underwent the decrease in off-axis shear strength. As can be seen in Table 4-9, there were no test results on test specimens exposed to 260 °C for more than 8 hrs because test specimens were already fractured when gripped for off-axis shear test.

The reason why test specimens experience continuous decrease of the off-axis shear strength is that test coupons were distorted by asymmetry when test specimens were taken out from the oven and kept in atmospheric condition before off-axis test. This phenomena means that heat transferred from the oven can be resulted in deformation of the test specimens in process of the thermal expansion and contraction. The more test specimens were exposed to high temperatures, the more distortion of the test specimens occurred.

Off-axis shear stresses applying in the plane of the laminate itself cause failure to be dominated by a single mechanism corresponding to delamination between layers and due to cracks formed across the coupon width[51].

Although the off-axis shear properties are intrinsically dependent on the resin characteristics, the increase of the shear strength which can be caused by residual post-cure effect was offset due to the distortion of the test coupons.

Table 4-9 Data for Off-axis shear strength (MPa) of carbon/epoxy composite materials after exposure to various temperatures

Exposure Temperature	Time (hr)	Thickness (mm)	Strength (MPa)	S.D (MPa)	Normalized Strength (MPa)	Strength Retention (%)
Ambient (23 °C)	0	2.98	57.51	1.81	88.80	100.00
	1	2.89	58.73	2.19	87.95	102.12
	2	3.56	58.47	2.45	107.85	101.66
	4	3.16	58.40	3.58	95.63	101.55
	8	3.00	58.14	3.99	90.27	101.08
	16	3.58	58.15	1.82	107.86	101.10
	24	3.37	59.75	3.52	104.32	103.88
	48	3.53	62.30	4.91	113.83	108.31
	72	3.02	63.38	0.80	99.29	110.20
66 °C	1	3.13	56.11	3.82	91.56	97.55
	2	3.13	55.32	5.75	90.09	96.19
	4	3.11	54.39	2.50	88.19	94.57
	8	3.27	53.79	1.47	91.61	93.52
	16	3.07	53.72	5.05	85.99	93.40
	24	3.49	52.68	6.06	95.76	91.60
	48	3.13	52.19	3.28	85.18	90.75
	72	3.25	51.95	4.61	88.03	90.33
93 °C	1	3.20	53.94	3.31	89.80	93.78
	2	3.24	51.34	1.18	86.64	89.27
	4	3.48	51.19	4.74	92.79	89.01
	8	3.27	48.16	5.31	82.10	83.73
	16	3.01	47.59	5.05	74.61	82.75
	24	3.24	44.54	1.54	75.24	77.44
	48	3.68	42.41	2.50	81.29	73.74
	72	3.26	44.29	3.57	75.13	77.01
121 °C	1	3.48	50.50	2.41	91.45	87.81
	2	3.26	50.38	3.00	85.63	87.60
	4	3.09	49.10	4.42	79.03	85.38
	8	3.29	45.19	4.57	77.44	78.57
	16	3.17	45.98	5.90	75.91	79.94
	24	3.27	44.56	4.03	75.96	77.47
	48	3.70	44.14	5.83	85.14	76.75
	72	3.32	44.16	4.78	76.37	76.79
149 °C	1	3.40	49.18	5.39	87.09	85.51
	2	3.31	48.06	3.16	82.94	83.56
	4	3.09	47.95	1.16	77.17	83.37
	8	3.25	43.23	3.37	73.25	75.16
	16	3.42	42.06	2.57	74.99	73.13
	24	3.36	39.40	6.90	69.01	68.50
	48	3.20	39.69	4.38	66.15	69.01
	72	3.31	39.17	6.48	67.45	68.10

Table 4-9 Continued

Exposure Temperature	Time (hr)	Thickness (mm)	Strength (MPa)	S.D (MPa)	Normalized Strength (MPa)	Strength Retention (%)
177 °C	1	3.20	47.90	4.91	79.75	83.28
	2	3.23	45.19	3.05	76.02	78.57
	4	3.11	41.85	5.62	67.71	72.76
	8	3.30	39.10	1.15	67.26	67.98
	16	3.32	37.82	4.06	65.33	65.75
	24	3.27	35.75	4.57	60.88	62.15
	48	3.53	33.28	8.07	61.14	57.87
	72	3.25	32.26	4.31	54.66	56.09
204 °C	1	3.35	43.90	2.06	76.52	76.33
	2	3.31	41.72	0.69	71.99	72.54
	4	3.26	38.91	0.37	65.99	67.65
	8	3.31	36.34	4.21	62.64	63.18
	16	3.42	37.57	2.13	66.92	65.32
	24	3.23	31.38	2.75	52.84	54.55
	48	3.26	30.59	2.49	51.94	53.19
	72	3.48	28.67	1.82	51.92	49.85
232 °C	1	3.28	37.22	4.30	63.52	64.71
	2	3.42	34.18	3.34	60.83	59.43
	4	3.19	33.20	3.25	55.10	57.72
	8	3.12	33.02	3.27	53.66	57.41
	16	3.40	29.09	2.11	51.56	50.57
	24	3.22	25.82	0.87	43.31	44.90
	48	3.22	16.92	5.74	28.34	29.41
	72	3.27	7.71	0.92	13.11	13.40
260 °C	1	3.24	39.58	1.56	66.73	68.82
	2	3.25	35.36	3.43	59.91	61.48
	4	3.20	33.41	2.74	55.68	58.08

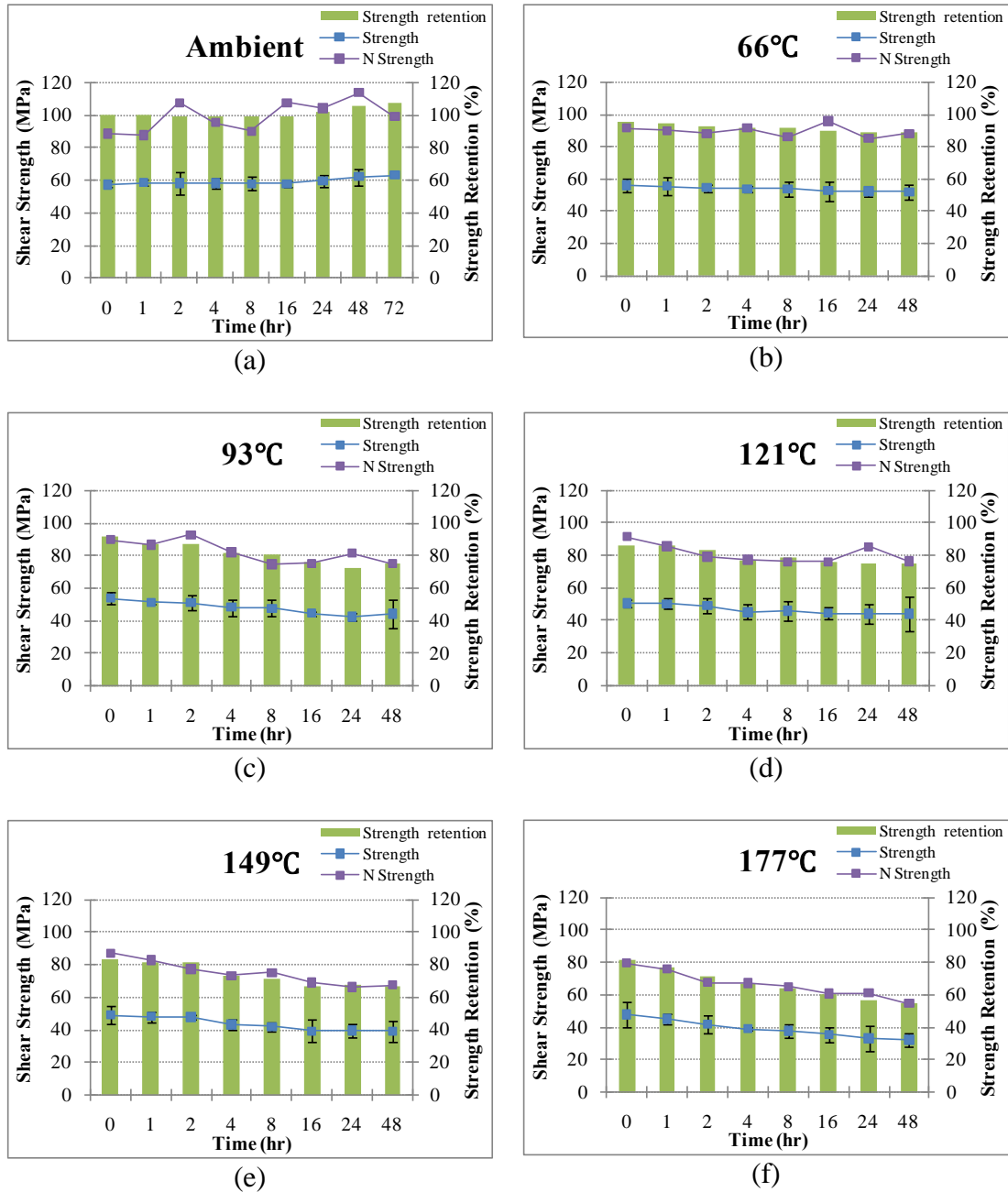


Figure 4-15: Off-axis shear strengths and normalized off-axis shear strengths of carbon/epoxy composite materials as a function of time at fixed temperatures, (a) ambient (b) 66°C (c) 93°C (d) 121°C (e) 149°C (f) 177°C (g) 204°C (h) 232°C (i) 260°C

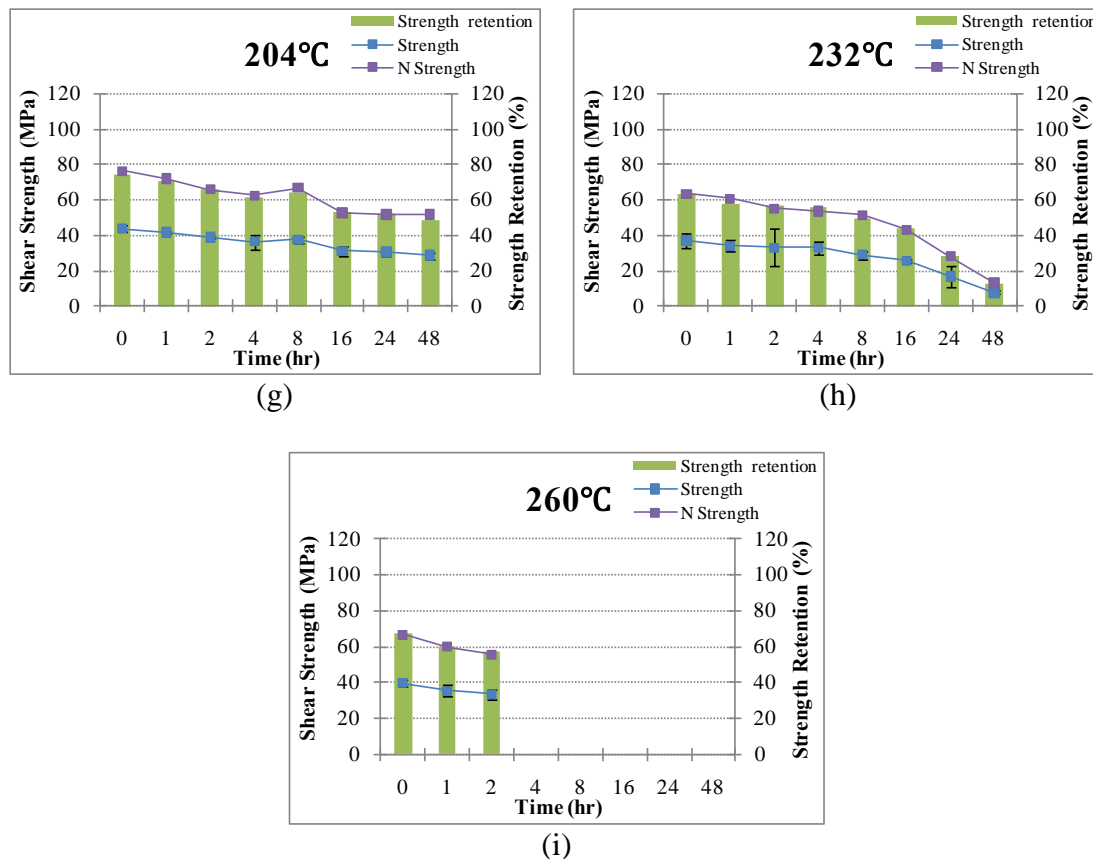


Figure 4-15: Continued

Table 4-10 lists the data for off-axis shear modulus of carbon/epoxy composite materials exposed to various temperatures from ambient temperature to 260°C. Unlike the values of the off-axis shear strength, the data of the modulus retention were relatively higher in all ageing conditions. The levels of the decreases of the off-axis shear modulus exposed to 66, 93, 121, 149, 177, 204, and 232°C from 1 hr to 72 hrs in ageing time were 5.63, 12.7, 9.14, 6.77, 5.04, 18.62, and 45.96%, respectively. These values are very low compared to the decrease of the off-axis shear strengths. This means that distortion caused by heat expansion and contraction of the test specimens did largely not affect the decrease of the shear modulus within ranges for measuring shear

chord modulus. Figure 4-16 shows off-axis shear modulus of carbon/epoxy composite materials as a function of time at fixed temperatures.

Table 4-10 Data for off-axis shear Modulus (GPa) of carbon/epoxy composite materials after exposure to various temperatures

Exposure Temperature	Time (hr)	Thickness (mm)	Modulus (GPa)	S.D (GPa)	Normalized Modulus (GPa)	Modulus Retention (%)
Ambient (23 °C)	0	2.98	6.78	0.10	10.47	100.00
	1	2.89	6.76	0.14	10.13	99.71
	2	3.56	6.88	0.38	12.70	101.47
	4	3.16	6.81	0.32	11.16	100.44
	8	3.00	6.80	0.27	10.56	100.25
	16	3.58	6.59	0.46	12.22	97.10
	24	3.37	6.71	0.18	11.72	98.92
	48	3.53	6.92	0.16	12.64	101.97
	72	3.02	7.25	0.47	11.35	106.83
66 °C	1	3.13	6.45	0.20	10.48	95.14
	2	3.13	6.29	0.27	10.18	92.68
	4	3.11	6.25	0.44	10.09	92.19
	8	3.27	6.14	0.29	10.41	90.57
	16	3.07	6.14	0.57	9.77	90.47
	24	3.49	6.15	0.27	11.13	90.71
	48	3.13	6.11	0.23	9.92	90.07
	72	3.25	6.09	0.27	10.27	89.78
93 °C	1	3.20	6.33	0.76	10.48	93.27
	2	3.24	5.75	0.29	9.66	84.82
	4	3.48	5.63	0.79	10.15	82.95
	8	3.27	5.62	0.48	9.53	82.85
	16	3.01	5.46	0.38	8.51	80.44
	24	3.24	5.32	0.28	8.93	78.38
	48	3.68	5.24	0.38	10.00	77.30
	72	3.26	5.21	0.31	8.79	76.76
121 °C	1	3.48	5.54	0.58	9.99	81.72
	2	3.26	5.40	0.56	9.14	79.66
	4	3.09	5.54	0.34	8.86	81.62
	8	3.29	5.63	0.58	9.60	83.05
	16	3.17	5.64	0.41	9.27	83.19
	24	3.27	5.58	0.14	9.47	82.31
	48	3.70	5.31	0.53	10.18	78.23
	72	3.32	5.04	0.23	8.66	74.25
149 °C	1	3.40	5.41	0.96	9.54	79.80
	2	3.31	5.40	0.95	9.27	79.61
	4	3.09	5.41	0.73	8.66	79.75
	8	3.25	5.12	0.46	8.62	75.43
	16	3.42	5.09	0.72	9.03	75.04
	24	3.36	5.01	0.57	8.74	73.91
	48	3.20	5.02	0.29	8.32	74.00
	72	3.31	5.05	0.07	8.65	74.40

Table 4-10 Continued

Exposure Temperature	Time (hr)	Thickness (mm)	Modulus (GPa)	S.D (GPa)	Normalized Modulus (Gpa)	Modulus Retention (%)
177 °C	1	3.20	5.23	0.53	8.66	77.10
	2	3.23	5.19	0.25	8.68	76.46
	4	3.11	5.23	0.19	8.41	77.05
	8	3.30	5.21	0.08	8.91	76.76
	16	3.32	5.28	0.19	9.07	77.79
	24	3.27	5.19	0.62	8.80	76.56
	48	3.53	5.11	0.84	9.34	75.33
	72	3.25	4.97	0.23	8.37	73.22
204 °C	1	3.35	6.14	0.12	10.65	90.52
	2	3.31	5.88	0.31	10.09	86.63
	4	3.26	5.24	0.62	8.85	77.30
	8	3.31	5.07	0.33	8.69	74.69
	16	3.42	5.06	0.51	8.96	74.55
	24	3.23	5.02	0.18	8.40	73.96
	48	3.26	5.02	0.19	8.49	74.05
	72	3.48	5.00	0.50	9.00	73.66
232 °C	1	3.28	5.61	0.43	9.53	82.75
	2	3.42	5.43	0.26	9.62	80.10
	4	3.19	5.25	0.73	8.67	77.40
	8	3.12	5.21	0.18	8.42	76.81
	16	3.40	5.13	0.27	9.05	75.63
	24	3.22	5.12	0.49	8.55	75.53
	48	3.22	3.80	0.26	6.33	56.02
	72	3.27	3.03	0.28	5.13	44.72
260 °C	1	3.24	5.63	0.11	9.44	82.95
	2	3.25	5.56	0.33	9.38	82.01
	4	3.20	5.55	0.50	9.21	81.87

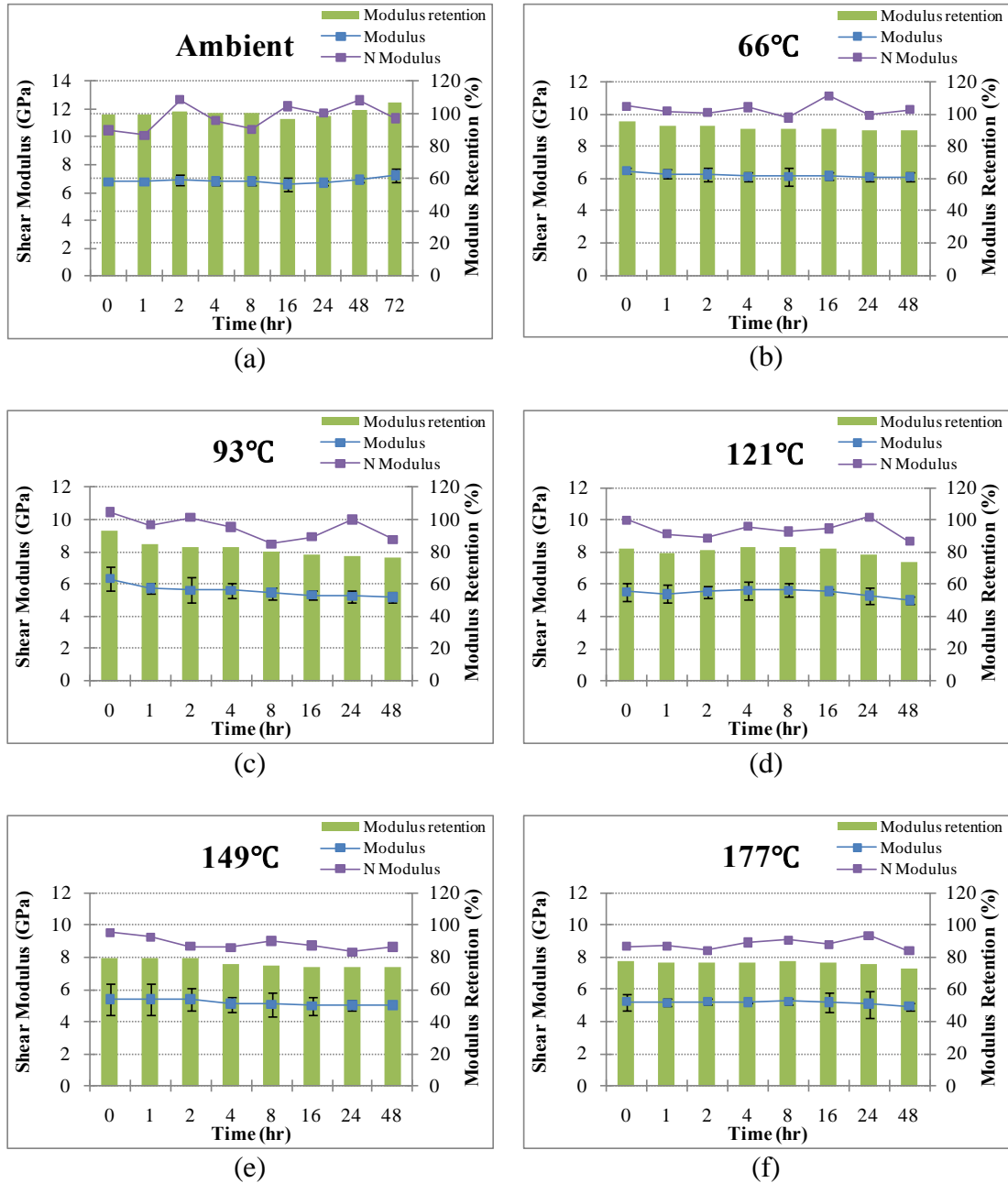
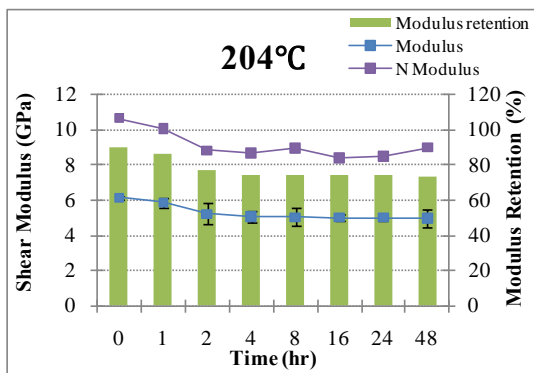
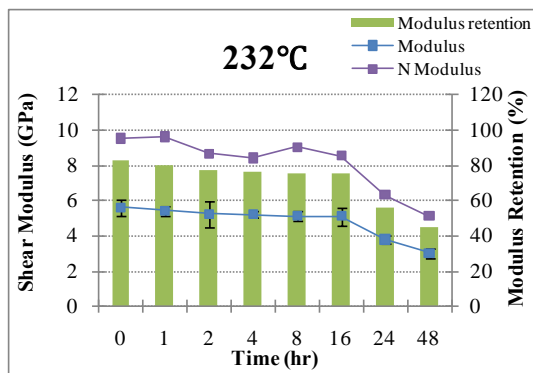


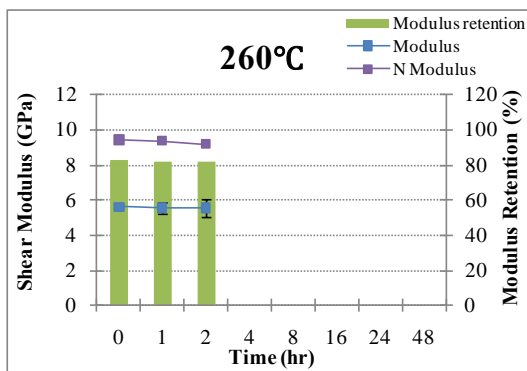
Figure 4-16: Off-axis shear modulus and normalized off-axis shear modulus of carbon/epoxy composite materials as a function of time at fixed temperatures, (a) ambient (b) 66°C (c) 93°C (d) 121°C (e) 149°C (f) 177°C (g) 204°C (h) 232°C (i) 260°C



(g)



(h)



(i)

Figure 4-16: Continued

The time-dependent functions of off-axis shear strength and modulus retention obtained by polynomial curve fittings are represented in Table 4-11 and Table 4-12. Compared to the data of the curve fitting regarding tensile strength and modulus, R-squared values were relatively higher because the residual post-cure effect did not enable the test specimens to enhance the initial shear properties. Especially, the functions showed nearly linear tendency in high temperatures such as 232 and 260 °C and R-squared values in off-axis shear strength were higher than values of modulus.

Table 4-11 Time-dependent functions of off-axis shear strength retention (%) obtained by polynomial curve fitting

Temperature(°C)	a	b	c	d	R ²
Ambient (23)			0.1257	98.966	0.9072
66	-6.E-05	0.008	-0.3787	94.915	0.9301
93		0.0078	-0.7584	90.045	0.9515
121	-2.E-04	0.0217	-0.9054	86.477	0.8911
149	-2.E-04	0.0321	-1.3697	84.936	0.9717
177	-2.E-04	0.0333	-1.5098	79.635	0.9456
204	-2.E-04	0.025	-1.2471	73.358	0.9178
232			-0.668	60.828	0.992
260			-3.2428	69.058	0.8489

$$\text{Time-dependent function : } Y(t) = \frac{\sigma_t}{\sigma_i} \times 100 = at^3 + bt^2 + ct + d$$

Table 4-12 Time-dependent functions of off-axis shear modulus retention (%) obtained by polynomial curve fitting

Temperature(°C)	a	b	c	d	R ²
Ambient (23)	-5.E-05	0.0081	-0.2603	100.82	0.8922
66	-7.E-05	0.0095	-0.3575	93.964	0.7743
93	-2.E-04	0.0216	-0.9109	89.259	0.7912
121	9.E-05	-0.0125	0.3405	80.445	0.9461
149	-9.E-05	0.0133	-0.5555	80.588	0.9234
177		-0.001	0.0226	76.882	0.9213
204	-3.E-04	0.0409	-1.4835	87.768	0.7666
232		-0.0026	-0.3337	81.123	0.9696
260			-0.3194	83.022	0.6926

$$\text{Time-dependent function : } Y(t) = \frac{\sigma_t}{\sigma_i} \times 100 = at^3 + bt^2 + ct + d$$

4.2.3.2 Temperature Dependence

Figure 4-17 represents the off-axis shear strength of the test specimens of the carbon/epoxy composite as a function of temperature at fixed time. As shown in Figure 4-17, the slopes which mean the drop of the off-axis shear strength were very steep as the ageing time is going up. The rate of decrease of the off-axis shear strength at each fixed times (1, 2, 4, 8, 16, 24, 48, 72 hrs), as the exposure time is increased, was 32.6, 39.53, 42.8, 43.2, 49.97, 56.78, 72.85 and 87.84%, respectively. It is apparent the distortion of the specimens for testing caused linear drop in off-axis shear strength and offset enhancement of the mechanical property due to residual post-cure effect. Accordingly, off-shear strength must be considered as an important design factor in many applications having high temperature variation.

Contrary to off-axis shear strength as shown in Figure 4-18 , off-axis shear modulus showed relatively a tendency to approach asymptotic levels except severe conditions (exposure temperature: more than 232 °C, ageing time: more than 48 hrs).

The level of reduction in off-axis shear modulus at fixed times (1, 2, 4, 8, 16, 24, 48, 72 hrs) from ambient temperature to 260 °C was 16.8, 19.17, 18.49, 23.38, 22.16, 23.65, 45.06, and 58.14%, respectively. Relatively, these values were very low than in the case of the off-axis shear strength.

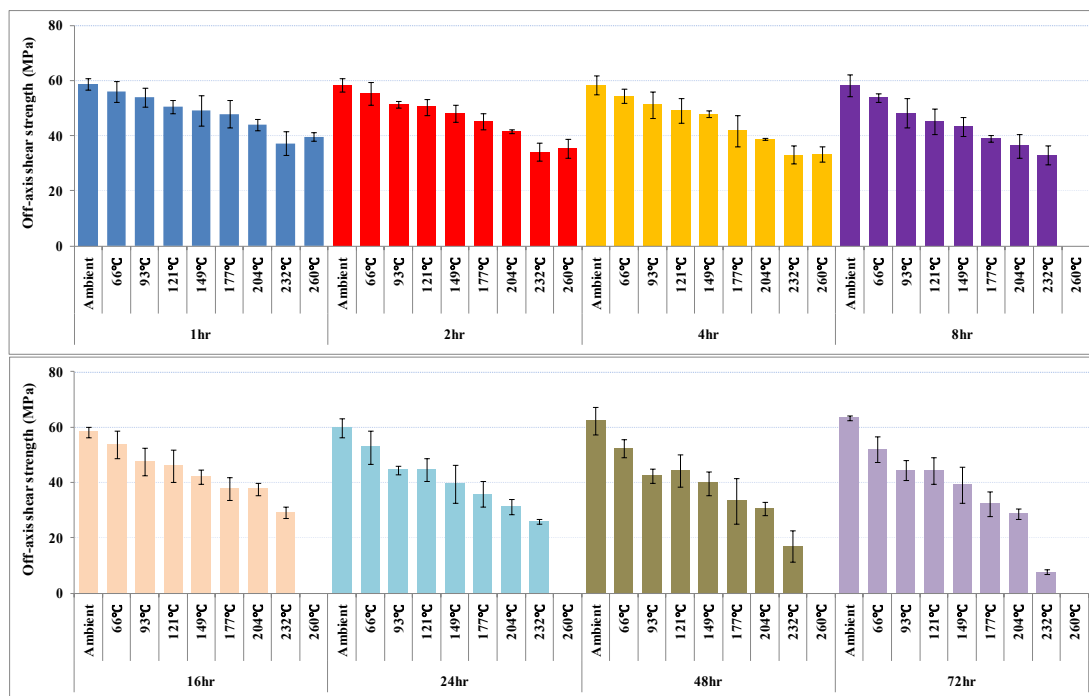


Figure 4-17: Off-axis shear strength of carbon/epoxy composite materials as a function of temperature at fixed periods of exposure

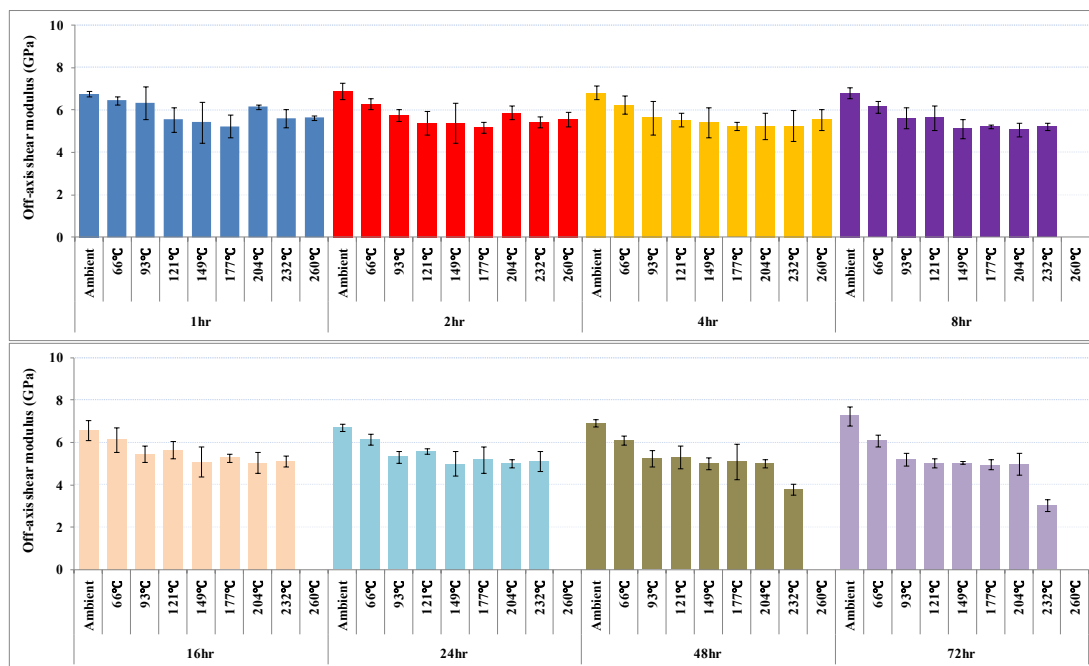


Figure 4-18: Off-axis shear modulus of carbon/epoxy composite materials as a function of temperature at fixed periods of exposure

Table 4-13 and Table 4-14 list the temperature-dependent functions of off-axis shear strength and modulus retention using polynomial curve fittings. Compared to the time-dependent functions, temperature-dependent functions showed more linear relations and R-squared values were superior to the results of the time-dependent functions. Especially, temperature-dependent functions on the off-axis strengths showed strongly linear correlation between shear strengths and exposure temperatures.

Table 4-13 Temperature-dependent functions of off-axis shear strength retention (%) obtained by polynomial curve fitting

Time (hr)	a	b	c	R ²
1	-0.0002	-0.1094	102.96	0.9539
2	-0.0002	-0.1063	101.82	0.9683
4		-0.1924	105.59	0.9742
8		-0.2047	103.21	0.9918
16		-0.222	104.46	0.974
24		-0.2634	106.13	0.9824
48		-0.3211	111.17	0.9421
72		-0.3211	117.26	0.9169

$$\text{Temperature-dependent function : } Y(T) = \frac{\sigma_t}{\sigma_i} \times 100 = aT^2 + bT + c$$

Table 4-14 Temperature-dependent functions of off-axis shear modulus retention (%) obtained by polynomial curve fitting

Time (hr)	a	b	c	R ²
1	0.0007	-0.26	107.05	0.6819
2	0.0009	-0.3192	108.13	0.8454
4	0.0008	-0.3214	107.85	0.9754
8	0.0008	-0.3212	107.44	0.9703
16	0.0006	-0.2684	103.29	0.9235
24	0.0009	-0.3294	106.29	0.9161
48	0.0003	-0.2467	104.74	0.8452
72	0.0002	-0.2656	108.03	0.7948

$$\text{Temperature-dependent function : } Y(T) = \frac{E_t}{E_i} \times 100 = aT^2 + bT + c$$

4.2.3.3 Morphological Analysis

The off-axis shear tests were accomplished in accordance with the procedure of uniaxial tensile test. Test specimens were comprised of 2 layers laminate with +45° and -45° fiber directions. Figure 4-19 shows the test coupons distorted by asymmetry in process of thermal expansion and contraction by heat transfer and dissipation when test specimens were cooled in the atmospheric temperature after taken out from the oven.

As can be seen in Figure 4-19, distortion of the test specimens by asymmetry and char formation by thermal oxidation resulted in the severe deterioration in terms of off-axial shear strength and modulus. The angles of the distortion which caused internal crack when test coupon was gripped were higher as the exposure temperatures were going up.

Figure 4-20 shows test specimens fractured after uniaxial tensile test of a $\pm 45^\circ$ laminate exposed to elevated temperatures at the ageing time, 72 hrs. All test specimens were fractured parallel to the fiber directions. In the lower exposure temperatures such as ambient temperature, 66, 93, and 121 °C, crack was found around the fractured cross section and the surface between 2 layers was well kept the shape wrapping the fibers without thermal degradation of the resin. However, the delamination between 2 layers, thermal oxidations and char formation in the internal and outer surfaces, additional cracks except the cross section were discovered in the test specimens exposed to high temperatures (204, 232, and 260 °C) as depicted in Figure 4-20.



Figure 4-19: Test specimens distorted by asymmetry in process of thermal expansion and contraction after exposure to 260°C for 8 hrs

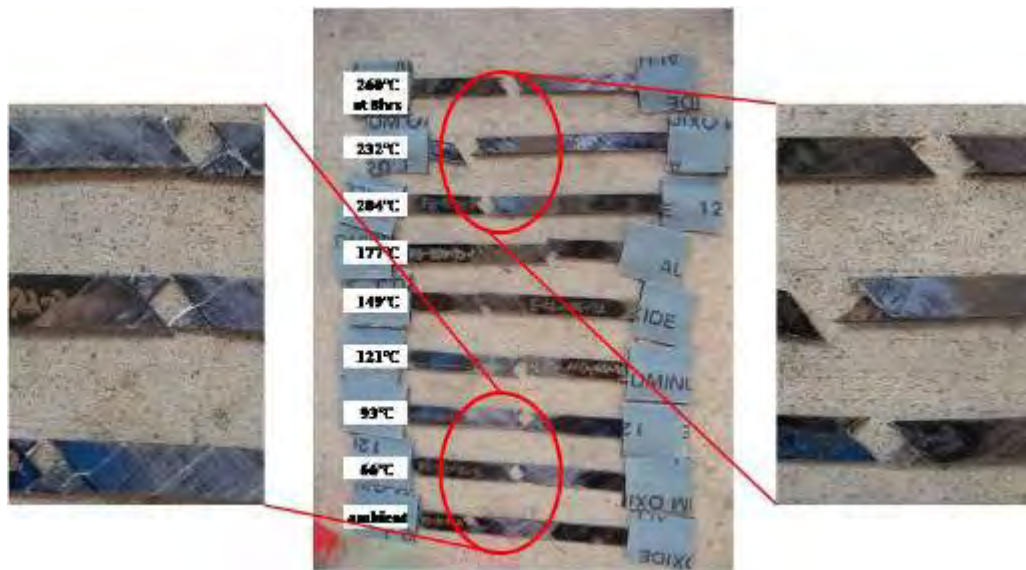


Figure 4-20: Test specimens fractured after uniaxial tensile test of a $\pm 45^\circ$ laminate exposed to elevated temperatures at an ageing time of 72 hrs

4.2.3.4 Strain Effect

Figure 4-21 shows tensile stress-ultimate failure strain curve by uniaxial tensile test of a $\pm 45^\circ$ laminate exposed to various exposure temperatures at the fixed time, 72 hrs. Like tensile test, off-axis shear modulus was calculated from slope between off-axis shear stress and strain ranging from 0.1% to 0.3% before extensometer is taken off. However, off-axis shear strain was rapidly reached to 0.3% compared to tensile strain because uniaxial tensile test of a $\pm 45^\circ$ laminate is matrix-dominant. Ultimate failure strains in off-axis shear test were lower than those of the tensile test and all test specimens were fractured before strains were reached 1.5% strain. As the exposure temperatures were going up, ultimate failure strain and off-axis shear strength were getting lower although the residual post-curing apparently happened in process of exposure to temperatures. In addition, the reason why the slopes of the off-axis shear stress versus the ultimate shear failure strains were not perfectly linear is that a $\pm 45^\circ$ laminates are ductile due to matrix-dominant characteristics. As can be seen in Figure 4-21, ductility is getting higher as the exposure temperatures are increased.

Figure 4-22 shows the off-axis shear strength and off-axis shear modulus as a function of ultimate failure strains (%). If looking at the comparison of two data related to shear strength and shear modulus, it should be pointed out that off-axis shear strengths were more strain-dependent with ultimate failure strains than in the case of off-axis shear modulus. All test coupons were fractured between 0.75% and 1.6 % in strain while off-axis shear strength and modulus were within 35 ~ 65 MPa and 5 ~ 7

GPa, respectively. Off-axis shear strengths were widely distributed compared to off-axis shear modulus as shown in Figure 4-22 (a). As shown in Figure 4-23, in the case off-axis shear strength and modulus were changed to logarithmic scale, the more linear data were obtained.

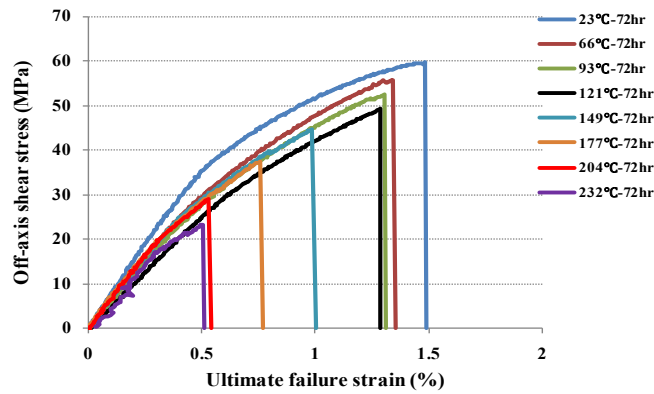


Figure 4-21: Off-axis shear stress-ultimate failure strain curves from specimens exposed to various ageing temperatures at the fixed period of 72 hrs

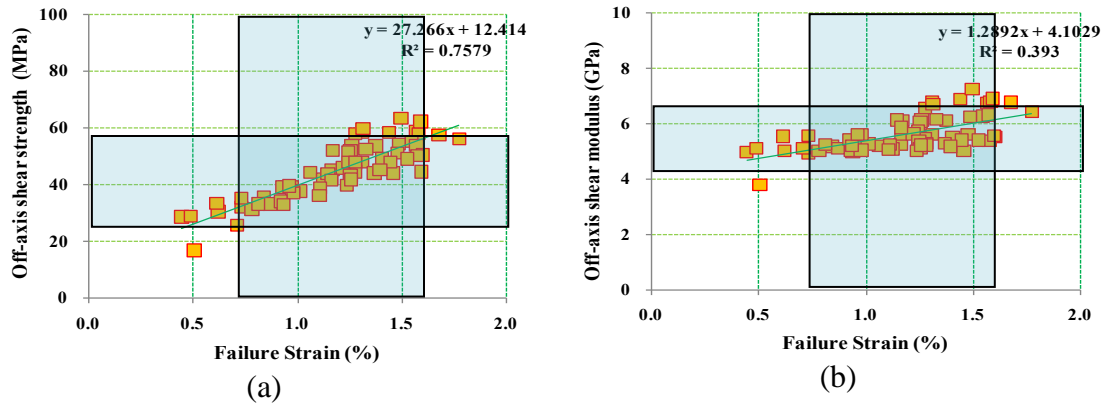


Figure 4-22: (a) Off-axis shear strength and (b) Off-axis shear modulus as a function of ultimate failure strains (%). Error bars indicate standard deviation

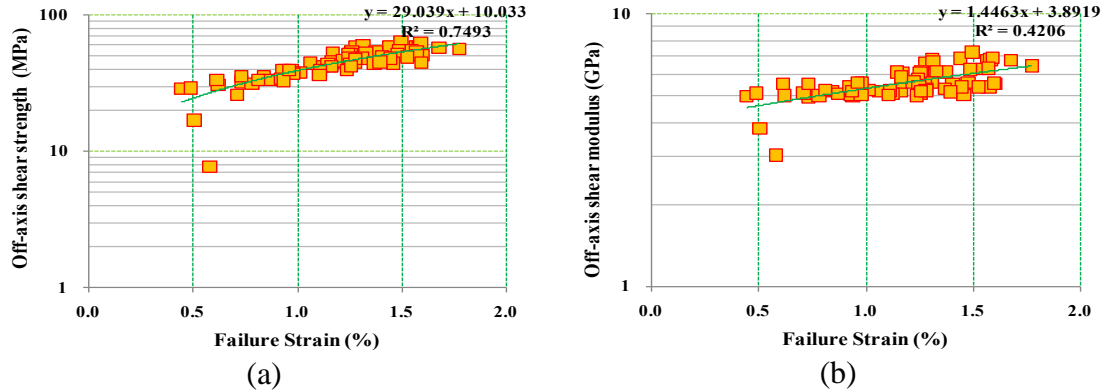


Figure 4-23: (a) Off-axis shear strength and (b) Off-axis shear modulus as a function of ultimate failure strains (%) using a logarithmic scale

4.2.3.5 Correlation to Tensile Test Results

Correlations between tensile and shear results are very important to estimate the other properties from the values obtained by useful experimental test.

First, in case an off-axis shear stress applied to a representative volume element for finding off-shear modulus of a unidirectional composite, off-shear modulus can be calculated by following equation

$$G_{12}'' = G_m \left[\frac{G_{f12}(1 + V_f) + G_m V_m}{G_{f12} V_m + G_m (1 + V_f)} \right] \quad (4.18)$$

$$G_{12}''' = \frac{G_m G_f}{G_m V_f + G_f V_m} \quad (4.19)$$

Where G_{12}'' = shear modulus for cylinder shaped composites

G_{12}''' = shear modulus for rectangular shaped composites

G_m = nominal epoxy modulus (1.308 GPa)

G_f = nominal carbon fiber modulus (22 GPa)

In addition, the data of fiber volume fraction using Equation 4.11 were used to calculate the off-axis shear modulus. As shown in Table 4-15, calculated shear modulus had good correlation in the ranges which the tensile properties were enhanced by the residual post-cure effect.

Table 4-15 Comparison of experimental shear modulus and calculated shear modulus-
 G'_{12} : experimental off-axis shear modulus (G'_{12} = shear modulus for cylinder shaped
 composites, G'''_{12} = shear modulus for rectangular shaped composites)

		Ambient (23 °C)					66 °C					
Time (hr)	V_f	G'_{12} (GPa)	G''_{12} (GPa)	error (%)	G'''_{12} (GPa)	error (%)	V_f	G'_{12} (GPa)	G''_{12} (GPa)	error (%)	G'''_{12} (GPa)	error (%)
0	0.37	6.78	5.90	13.0	4.93	27.3						
1	0.36	6.76	5.79	14.4	4.86	28.2	0.34	6.45	5.68	12.0	4.79	25.8
2	0.38	6.88	5.99	12.9	4.99	27.5	0.35	6.29	5.71	9.1	4.81	23.5
4	0.38	6.81	6.04	11.4	5.02	26.3	0.40	6.25	6.20	0.9	5.12	18.1
8	0.40	6.80	6.19	9.0	5.12	24.8	0.42	6.14	6.42	-4.6	5.27	14.2
16	0.44	6.59	6.63	-0.7	5.41	17.8	0.46	6.14	6.90	-12.5	5.60	8.8
24	0.43	6.71	6.54	2.5	5.35	20.2	0.40	6.15	6.19	-0.6	5.12	16.8
48	0.46	6.92	6.81	1.6	5.53	20.0	0.34	6.11	5.67	7.3	4.78	21.8
72	0.47	7.25	7.00	3.4	5.66	21.8	0.36	6.09	5.83	4.3	4.88	19.8
		93 °C					121 °C					
Time (hr)	V_f	G'_{12} (GPa)	G''_{12} (GPa)	error (%)	G'''_{12} (GPa)	error (%)	V_f	G'_{12} (GPa)	G''_{12} (GPa)	error (%)	G'''_{12} (GPa)	error (%)
1	0.38	6.33	6.02	4.8	5.01	20.8	0.36	5.54	5.86	-5.8	4.91	11.5
2	0.39	5.75	6.15	-7.0	5.10	11.4	0.39	5.40	6.11	-13.1	5.07	6.2
4	0.42	5.63	6.42	-14.1	5.27	6.3	0.38	5.54	6.02	-8.8	5.01	9.5
8	0.42	5.62	6.46	-14.9	5.30	5.7	0.32	5.63	5.52	2.1	4.68	16.9
16	0.44	5.46	6.68	-22.4	5.44	0.2	0.38	5.64	6.07	-7.5	5.04	10.7
24	0.45	5.32	6.74	-26.8	5.49	-3.2	0.36	5.58	5.83	-4.5	4.89	12.5
48	0.42	5.24	6.41	-22.3	5.27	-0.4	0.35	5.31	5.77	-8.8	4.85	8.6
72	0.38	5.21	5.97	-14.7	4.98	4.4	0.32	5.04	5.46	-8.5	4.65	7.7
		149 °C					177 °C					
Time (hr)	V_f	G'_{12} (GPa)	G''_{12} (GPa)	error (%)	G'''_{12} (GPa)	error (%)	V_f	G'_{12} (GPa)	G''_{12} (GPa)	error (%)	G'''_{12} (GPa)	error (%)
1	0.37	5.41	5.89	-8.8	4.92	9.1	0.39	5.23	6.08	-16.2	5.05	3.5
2	0.37	5.40	5.90	-9.3	4.93	8.7	0.43	5.19	6.52	-25.8	5.34	-3.0
4	0.37	5.41	5.95	-10.0	4.96	8.3	0.37	5.23	5.93	-13.4	4.95	5.3
8	0.37	5.12	5.95	-16.2	4.96	3.0	0.35	5.21	5.74	-10.2	4.82	7.3
16	0.35	5.09	5.78	-13.6	4.85	4.6	0.32	5.28	5.50	-4.3	4.67	11.4
24	0.36	5.01	5.86	-16.9	4.90	2.2	0.35	5.19	5.74	-10.5	4.83	7.1
48	0.35	5.02	5.79	-15.3	4.86	3.3	0.34	5.11	5.65	-10.6	4.77	6.6
72	0.30	5.05	5.35	-6.1	4.58	9.3	0.35	4.97	5.70	-14.8	4.80	3.3

Table 4-15 Continued

		204 °C					232 °C					
Time (hr)	V _f	G'12 (GPa)	G''12 (GPa)	error (%)	G'''12 (GPa)	error (%)	V _f	G'12 (GPa)	G''12 (GPa)	error (%)	G'''12 (GPa)	error (%)
1	0.37	6.14	5.94	3.2	4.96	19.3	0.40	5.61	6.24	-11.2	5.15	8.2
2	0.36	5.88	5.80	1.3	4.86	17.2	0.41	5.43	6.36	-17.0	5.23	3.7
4	0.37	5.24	5.89	-12.4	4.93	6.0	0.37	5.25	5.89	-12.3	4.93	6.2
8	0.39	5.07	6.11	-20.6	5.07	0.0	0.38	5.21	6.04	-15.9	5.02	3.6
16	0.37	5.06	5.93	-17.2	4.95	2.1	0.35	5.13	5.70	-11.1	4.80	6.4
24	0.36	5.02	5.85	-16.6	4.90	2.4	0.32	5.12	5.52	-7.7	4.68	8.6
48	0.37	5.02	5.88	-17.1	4.92	2.1	0.33	3.80	5.58	-46.9	4.73	-24.4
72	0.37	5.00	5.95	-19.1	4.96	0.7	0.28	3.03	5.16	-70.2	4.46	-47.0
		260 °C										
Time (hr)	V _f	G'12 (GPa)	G''12 (GPa)	error (%)	G'''12 (GPa)	error (%)						
1	0.34	5.63	5.61	0.2	4.75	15.7						
2	0.36	5.56	5.88	-5.7	4.92	11.6						
4	0.37	5.55	5.88	-6.0	4.92	11.4						
8	0.32		5.48		4.66							
16	0.23		4.78		4.22							
24	0.23		4.80		4.24							
48	0.13		4.11		3.82							
72	0.11		3.98		3.74							

Figure 4-24 shows the data distribution of the tensile properties and off-axis shear properties. The data of the tensile strength were distributed between 500 MPa and 790 MPa and off-axis shear strengths were widely distributed due to offset of residual post-cure effect. Meanwhile, the values of tensile and off-axis shear modulus were concentrated between 42 GPa and 75 GPa and between 5 GPa and 7 GPa, respectively. If changing the tensile properties into logarithmic scale because the values of the tensile property have more scale compared to off-axis shear property, more linear correlation can be obtained as shown in Figure 4-25.

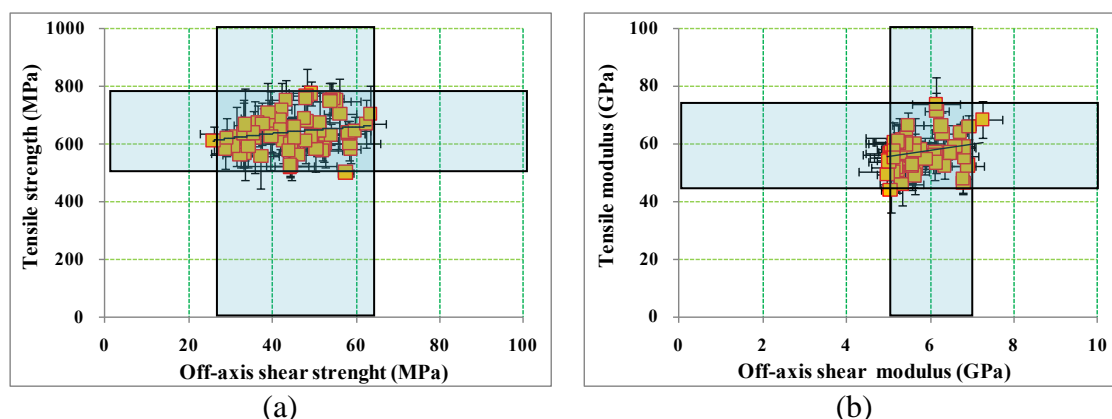


Figure 4-24: Data distribution of (a) tensile strength versus off-axis shear strength and (b) tensile modulus versus off-axis shear modulus

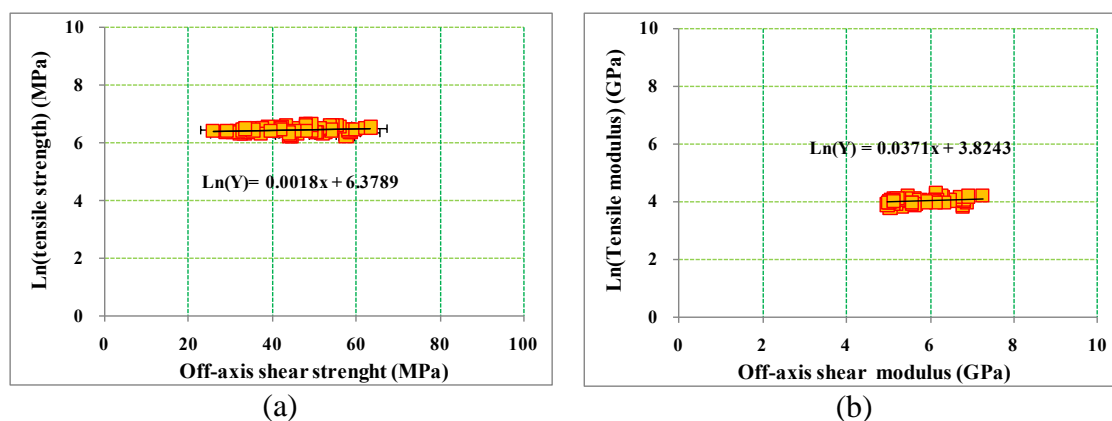


Figure 4-25: Data distribution of (a) tensile strength versus off-axis shear strength and (b) tensile modulus versus off-axis shear modulus using a logarithmic scale

4.3 Flexural Testing

4.3.1 Introduction

Flexural properties provide important characteristics of composite materials. However, it is difficult to estimate values that can be directly utilized in design because flexural testing subjects the test specimens to a mixed state of stress and a stress gradient. The flexural characteristics and their change as a function of time and temperature are important and offer the crucial data to decide the deteriorative level after exposure to high temperatures and fire.

Flexure tests are very useful for characterizing mechanical properties of layered composite materials due to simplicity of the test method for determining characteristics where relative rather than absolute data are needed. Therefore, flexural data are used to derive the other mechanical properties because of simple test method. In case composite materials are bended since flexural loading in materials imposes both tensile and compressive stresses, these tests must be considered for determining the design data. As mentioned, flexural properties are a combination of the tensile and compressive properties of the composite materials[52] .

4.3.2 Data Reduction

For test specimens in 3 point bending comprised of simple beam supported at two points and loaded at midpoint, the flexural strength and modulus are determined through a three-point flexural test following method described in ASTM D790. A support span-to-depth ratio of 16:1 was used for 2 layers laminate. The test specimens is

deflected until rupture occurs in the outer surface of the test specimen or until a maximum strain of 5.0% is reached, whichever occurs first.

The flexural strength is obtained by following equation

$$\sigma_f = \frac{3PL}{2bh^2} \quad (4.20)$$

where:

σ_f = the stress in the outer fibers at midpoint, MPa

P = the load at a given point in the load-deflection curve, N

L = the support span, mm

b = the width of the specimen tested, mm

h = the thickness of the specimen tested, mm

Flexural strain is defined as nominal fractional change in the length of an element of the outer surface of the test specimen at midspan, where the maximum stress occurs. It may be calculated for any deflection using Equation 4.21.

$$\varepsilon_f = 6Dh / L^2 \quad (4.21)$$

where:

ε_f = strain in the outer surface, mm/mm

D = maximum deflection of the center of the beam, mm

Chord modulus may be calculated from two discrete points on the load deflection curve. The chord modulus is calculated using the following equation:

$$E_f = (\sigma_{f2} - \sigma_{f1}) / (\varepsilon_{f2} - \varepsilon_{f1}) \quad (4.22)$$

where:

E_f = chord modulus, GPa

4.3.3 Analyses and Results

4.3.3.1 Time Dependence

Flexural properties with regard to strength, modulus, strain and load were determined at room temperature after the test specimens had been exposed to a controlled temperature for times up to 72 hrs. A flat rectangular specimen was simply supported close to its ends and centrally loaded in three point bending. Data were obtained by average value determined from five flexural tests. Flexural test is often utilized to characterize mechanical properties of layered laminate because they offer a simple means of determining bending response. However, Flexural tests can result in various failure modes as follows[50],

- Tensile fracture of fibers
- Tensile fracture of outer surface
- Compression fracture of outer surface
- Tensile fracture with interlaminar shear
- Compression fracture with interlaminar shear
- Interlaminar shear

Data for Flexural strength (MPa) of carbon/epoxy composite materials after exposure to various temperatures are tabulated in Table 4-16 and Flexural strengths as a

function of time at fixed temperatures are depicted in Figure 4-26. The flexural strength retentions did not largely enhanced by residual post-cure effect compared to the result of tensile test. The maximum strength retention caused by post-curing was 117.43% in condition of 177°C exposure temperature for 72hr. It should be noted that this value is much less than the maximum strength retention (154.42%) of tensile test. At lower exposure temperatures, the reason why the flexural strength data show fluctuation is that post-curing effects did not largely contribute to enhancement of the property. In other words, as mentioned previously, defects in process of hand wet layup fabrication had probably test specimens fractured in various failure modes. As ageing time was increased, the strength drops in ranges of ambient, 66, 93, 121, 149, 177, and 204 °C were only 5.23, 6.53, 3.19, 7.37, 11.54 and 13.26%, respectively. As strength enhancements were not highly affected by residual post-cure effect, strength reductions were largely not influenced by thermal degradation in low exposure temperatures. Big drop of the flexural strength took place in conditions of 232°C exposure temperature for 72 hrs and 260 °C exposure temperature for more than 8 hrs. Since thermal oxidation caused catastrophic delamination between 2 layers in high exposure temperatures, the rate of drop of the flexural strength was higher than that of the tensile strength.

Table 4-16 Data for flexural strength (MPa) of carbon/epoxy composite materials after exposure to various temperatures (N denotes normalized)

Exposure Temperature	Time (hr)	Thickness (mm)	Width (mm)	load (KN)	Strength (MPa)	S.D (MPa)	N strength (MPa)	Strength retention(%)
Ambient (23 °C)	0	2.83	12.88	0.74	513.13	36.64	753.48	100
	1	2.77	12.73	0.74	543.11	16.70	779.48	105.84
	2	2.73	12.84	0.78	565.72	15.28	799.48	110.25
	4	2.79	12.67	0.72	527.26	30.88	762.89	102.75
	8	2.84	12.73	0.75	532.05	76.51	782.91	103.69
	16	2.80	12.86	0.73	527.11	10.95	764.03	102.72
	24	2.78	12.71	0.70	515.97	75.90	742.14	100.55
	48	2.63	12.80	0.68	523.90	26.16	714.59	102.10
	72	2.88	12.49	0.73	514.70	59.23	768.72	100.31
66 °C	1	3.00	12.80	0.81	525.82	34.01	816.79	102.47
	2	3.07	12.49	0.82	520.14	9.37	826.02	101.37
	4	2.78	12.70	0.77	558.61	73.47	804.64	108.86
	8	2.84	12.85	0.78	544.49	47.94	801.21	106.11
	16	2.56	12.71	0.64	523.72	55.05	693.32	102.06
	24	2.90	12.82	0.75	543.15	81.71	815.58	105.85
	48	2.82	12.75	0.70	495.65	63.63	724.73	96.59
	72	3.03	12.64	0.80	511.71	66.01	803.36	99.72
93 °C	1	2.97	12.67	0.79	512.19	69.29	788.20	99.82
	2	2.67	12.74	0.68	540.10	24.67	747.88	105.26
	4	3.07	12.61	0.84	512.58	49.98	814.81	99.89
	8	3.08	12.73	0.79	483.48	55.38	772.19	94.22
	16	2.98	12.81	0.81	518.38	30.03	799.05	101.02
	24	3.13	12.71	0.85	495.93	109.24	804.80	96.65
	48	2.94	12.64	0.82	540.55	21.71	822.31	105.34
	72	2.91	12.84	0.84	545.66	41.23	822.03	106.34
121 °C	1	2.69	12.56	0.70	535.95	30.11	747.69	104.45
	2	2.80	12.69	0.77	554.82	36.79	805.50	108.12
	4	2.87	12.86	0.78	529.80	44.94	787.29	103.25
	8	2.91	12.55	0.78	523.24	19.17	789.61	101.97
	16	2.66	12.87	0.68	543.61	69.20	748.52	105.94
	24	2.94	12.72	0.85	555.62	26.81	846.38	108.28
	48	3.13	12.74	0.82	523.16	70.08	848.43	101.95
	72	2.67	12.57	0.70	553.06	28.91	765.11	107.78
149 °C	1	2.82	12.70	0.69	498.76	97.21	728.25	97.20
	2	2.73	12.74	0.72	574.78	46.37	814.22	112.01
	4	2.89	12.56	0.74	505.41	15.11	756.81	98.50
	8	2.78	12.73	0.81	594.22	53.17	855.16	115.80
	16	2.67	12.91	0.74	576.04	25.62	795.41	112.26
	24	2.72	12.63	0.71	553.59	48.29	779.47	107.88
	48	2.79	12.73	0.75	542.36	73.84	784.03	105.70
	72	2.99	12.78	0.73	461.98	25.12	714.51	90.03

Table 4-16 Continued

Exposure Temperature	Time (hr)	Thickness (mm)	Width (mm)	load (KN)	Strength (MPa)	S.D (MPa)	N strength (MPa)	Strength retention(%)
177 °C	1	2.87	12.77	0.79	540.21	8.04	802.62	105.28
	2	2.64	12.69	0.73	586.62	37.05	803.18	114.32
	4	3.04	12.76	0.85	529.97	85.57	834.77	103.28
	8	2.91	12.77	0.81	548.39	83.06	826.85	106.87
	16	2.80	12.99	0.75	530.45	27.08	770.25	103.37
	24	2.77	12.93	0.73	527.56	8.66	756.48	102.81
	48	2.99	12.74	0.87	549.98	42.22	852.76	107.18
	72	2.73	12.73	0.80	602.56	47.72	853.58	117.43
204 °C	1	3.08	12.72	0.89	530.27	43.87	847.33	103.34
	2	2.86	12.83	0.82	562.61	39.56	833.12	109.64
	4	3.14	12.71	0.85	492.13	48.51	800.67	95.91
	8	2.75	12.88	0.71	526.03	47.50	748.98	102.51
	16	2.80	12.62	0.76	545.35	44.81	790.47	106.28
	24	2.86	12.80	0.76	526.99	63.49	782.02	102.70
	48	3.00	12.75	0.87	548.88	68.89	853.19	106.97
	72	2.89	12.66	0.88	600.62	36.85	900.15	117.05
232 °C	1	2.95	12.75	0.85	549.63	38.76	839.54	107.11
	2	2.82	12.57	0.72	516.77	60.33	754.40	100.71
	4	3.02	12.79	0.85	528.36	61.34	826.76	102.97
	8	2.83	12.88	0.77	540.63	45.01	791.33	105.36
	16	2.98	12.65	0.79	538.35	37.20	831.94	104.92
	24	2.80	12.73	0.78	557.54	54.28	808.86	108.65
	48	2.95	12.55	0.73	534.48	73.29	816.26	104.16
	72	2.86	12.70	0.50	356.95	138.39	528.21	69.56
260 °C	1	2.99	12.95	0.80	494.27	18.27	764.46	96.32
	2	2.76	12.90	0.73	534.28	24.92	763.35	104.12
	4	2.84	12.71	0.82	575.69	12.04	847.13	112.19
	8	2.91	12.82	0.44	295.26	66.36	444.41	57.54
	16	2.68	12.78	0.15	122.17	14.30	169.33	23.81
	24	2.86	12.63	0.15	104.44	8.99	154.49	20.35
	48	3.06	12.88	0.13	76.88	13.18	122.00	14.98
	72	3.15	12.62	0.09	51.66	20.91	84.25	10.07

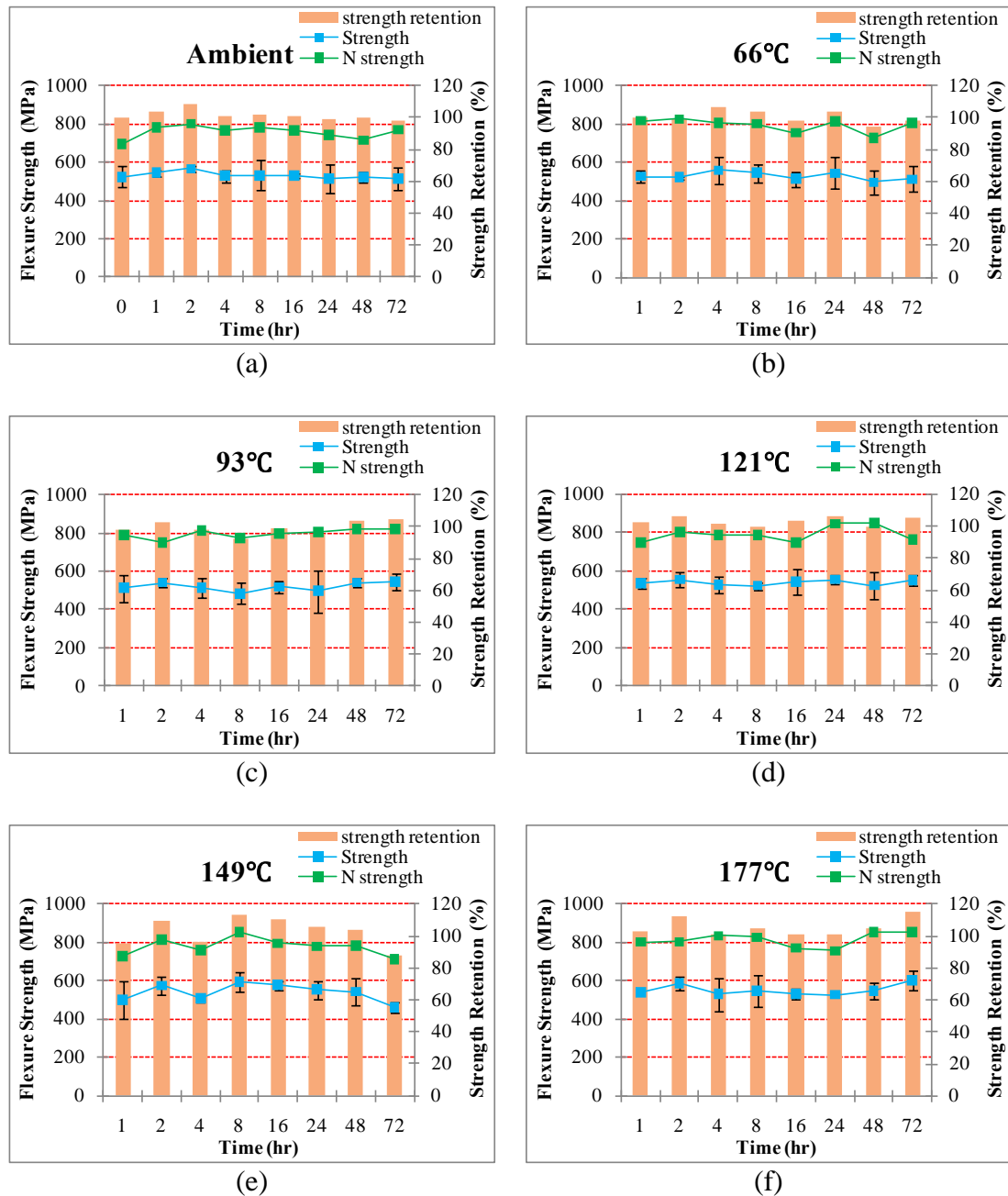


Figure 4-26: Flexural strengths and normalized flexural strengths of carbon/epoxy composite materials as a function of time at fixed temperatures of exposure, (a) ambient (b) 66°C (c) 93°C (d) 121°C (e) 149°C (f) 177°C (g) 204°C (h) 232°C (i) 260°C

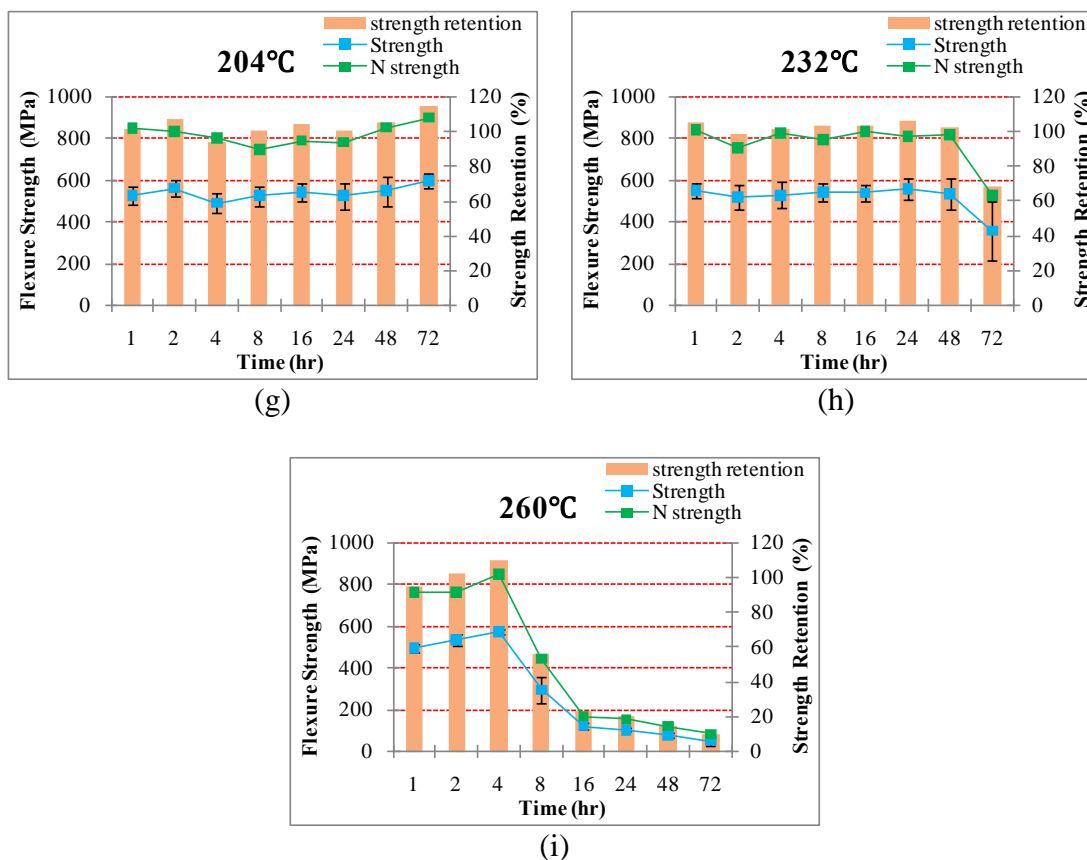


Figure 4-26: Continued

Table 4-17 shows data for flexural modulus (GPa) of carbon/epoxy composite materials after exposure to various temperatures and Figure 4-27 represents flexural modulus of carbon/epoxy composite materials as a function of time at fixed temperatures.

The chord modulus of flexural test initially showed a little increase by residual post-curing effect. The amount of increase in terms of property retention was lower than enhancement of the flexural strength. Similar to the result of flexural strength, data fluctuation existed in the low exposure temperatures and the values of the flexural modulus were rapidly reduced in high temperatures. The retention of flexural modulus

in condition of the exposure temperature (260°C) for ageing time (72 hrs) was only 6.78%. It should be noted that the thickness of test specimens affected flexural modulus. As test specimens are thinner, the flexural modulus is getting higher. Since thicker test specimen means area containing more than the maximum allowable resin content which may arise from improper curing exist, the void and defect in resin-rich area resulted in the reduction of the flexural modulus due to big deflection in centrally loading.

In case the test specimens were subjected to experimental conditions of exposure temperature (260°C) for more than 8 hrs, flexural modulus can be catastrophically reduced because test specimens supported at two points and loaded at midpoint changed to char by thermal oxidation. When nose for loading passed the section of char, rapid deflection can be measured by flexural test equipment.

Table 4-17 Data for flexural modulus (GPa) of carbon/epoxy composite materials after exposure to various temperatures (N denotes normalized)

Exposure Temperature	Time (hr)	Thickness (mm)	Width (mm)	load (KN)	Modulus (GPa)	S.D (GPa)	N Modulus (GPa)	Modulus retention(%)
Ambient (23 °C)	0	2.83	12.88	0.74	36.64	4.86	53.80	100.00
	1	2.77	12.73	0.74	41.70	1.08	59.84	113.79
	2	2.73	12.84	0.78	43.85	4.05	61.97	119.68
	4	2.79	12.67	0.72	39.52	5.26	57.18	107.85
	8	2.84	12.73	0.75	38.98	3.42	57.35	106.37
	16	2.80	12.86	0.73	40.52	3.36	58.73	110.57
	24	2.78	12.71	0.70	39.40	7.38	56.68	107.54
	48	2.63	12.80	0.68	40.78	1.62	55.62	111.28
	72	2.88	12.49	0.73	39.69	4.47	59.27	108.30
66 °C	1	3.00	12.80	0.81	36.33	9.44	56.43	99.15
	2	3.07	12.49	0.82	36.65	0.83	58.21	100.03
	4	2.78	12.70	0.77	41.11	9.37	59.22	112.20
	8	2.84	12.85	0.78	39.88	6.30	58.69	108.84
	16	2.56	12.71	0.64	39.12	4.24	51.79	106.76
	24	2.90	12.82	0.75	36.01	5.96	54.07	98.28
	48	2.82	12.75	0.70	34.55	6.38	50.52	94.30
	72	3.03	12.64	0.80	33.29	4.91	52.26	90.85
93 °C	1	2.97	12.67	0.79	35.69	7.44	54.92	97.41
	2	2.67	12.74	0.68	38.43	2.50	53.22	104.89
	4	3.07	12.61	0.84	34.13	5.58	54.26	93.16
	8	3.08	12.73	0.79	32.22	4.81	51.46	87.93
	16	2.98	12.81	0.81	31.64	4.24	48.76	86.34
	24	3.13	12.71	0.85	32.16	6.01	52.19	87.77
	48	2.94	12.64	0.82	34.50	4.54	52.49	94.16
	72	2.91	12.84	0.84	35.10	5.46	52.87	95.78
121 °C	1	2.69	12.56	0.70	38.59	1.66	53.83	105.31
	2	2.80	12.69	0.77	37.99	3.57	55.16	103.69
	4	2.87	12.86	0.78	36.21	7.52	53.81	98.82
	8	2.91	12.55	0.78	37.11	4.10	56.00	101.27
	16	2.66	12.87	0.68	38.76	8.12	53.36	105.77
	24	2.94	12.72	0.85	35.70	4.07	54.39	97.44
	48	3.13	12.74	0.82	33.72	4.00	54.68	92.01
	72	2.67	12.57	0.70	34.82	2.39	48.17	95.02
149 °C	1	2.82	12.70	0.69	34.65	10.32	50.60	94.57
	2	2.73	12.74	0.72	41.30	3.29	58.50	112.70
	4	2.89	12.56	0.74	34.99	4.78	52.39	95.48
	8	2.78	12.73	0.81	40.48	4.26	58.25	110.47
	16	2.67	12.91	0.74	36.52	3.86	50.43	99.67
	24	2.72	12.63	0.71	36.67	5.55	51.63	100.07
	48	2.79	12.73	0.75	35.46	3.93	51.25	96.76
	72	2.99	12.78	0.73	32.21	5.35	49.81	87.89

Table 4-17 Continued

Exposure Temperature	Time (hr)	Thickness (mm)	Width (mm)	load (KN)	Modulus (GPa)	S.D (GPa)	N Modulus (GPa)	Modulus retention(%)
177 °C	1	2.87	12.77	0.79	32.72	2.13	48.61	89.28
	2	2.64	12.69	0.73	40.88	3.70	55.96	111.55
	4	3.04	12.76	0.85	32.66	6.00	51.45	89.14
	8	2.91	12.77	0.81	35.52	5.96	53.56	96.95
	16	2.80	12.99	0.75	33.41	2.77	48.51	91.17
	24	2.77	12.93	0.73	34.29	4.93	49.17	93.57
	48	2.99	12.74	0.87	34.58	3.27	53.61	94.37
	72	2.73	12.73	0.80	40.87	2.98	57.90	111.55
204 °C	1	3.08	12.72	0.89	30.61	3.33	48.91	83.53
	2	2.86	12.83	0.82	36.86	4.18	54.59	100.60
	4	3.14	12.71	0.85	31.90	3.93	51.89	87.05
	8	2.75	12.88	0.71	36.98	2.35	52.66	100.93
	16	2.80	12.62	0.76	33.32	3.52	48.30	90.93
	24	2.86	12.80	0.76	33.93	6.18	50.35	92.60
	48	3.00	12.75	0.87	34.52	2.63	53.65	94.20
	72	2.89	12.66	0.88	35.56	2.50	53.29	97.04
232 °C	1	2.95	12.75	0.85	36.15	4.64	55.22	98.66
	2	2.82	12.57	0.72	34.29	2.24	50.05	93.57
	4	3.02	12.79	0.85	35.57	6.86	55.67	97.09
	8	2.83	12.88	0.77	35.54	4.42	52.01	96.98
	16	2.98	12.65	0.79	37.72	4.47	58.29	102.95
	24	2.80	12.73	0.78	37.66	4.32	54.64	102.78
	48	2.95	12.55	0.73	35.08	6.48	53.57	95.73
	72	2.86	12.70	0.50	23.45	6.88	34.70	63.99
260 °C	1	2.99	12.95	0.80	36.06	4.05	55.78	98.42
	2	2.76	12.90	0.73	35.72	2.00	51.03	97.47
	4	2.84	12.71	0.82	38.82	2.95	57.12	105.94
	8	2.91	12.82	0.44	19.24	1.80	28.96	52.51
	16	2.68	12.78	0.15	8.85	1.85	12.26	24.15
	24	2.86	12.63	0.15	8.22	1.51	12.16	22.43
	48	3.06	12.88	0.13	7.16	1.41	11.36	19.53
	72	3.15	12.62	0.09	2.48	0.86	4.05	6.78

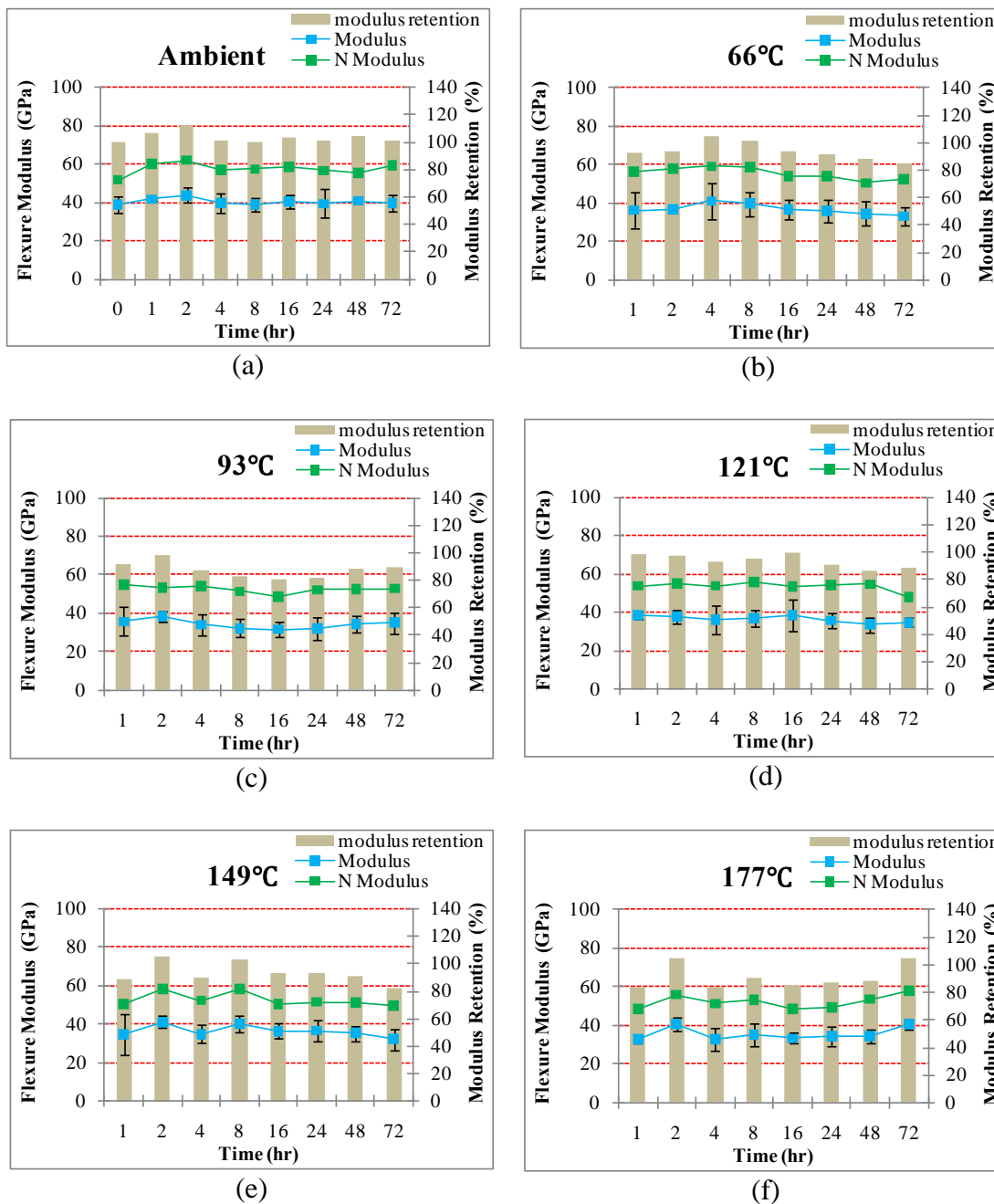


Figure 4-27: Flexural modulus and normalized flexural modulus of carbon/epoxy composite materials as a function of time at fixed temperatures, (a) ambient (b) 66°C (c) 93°C (d) 121°C (e) 149°C (f) 177°C (g) 204°C (h) 232°C (i) 260°C

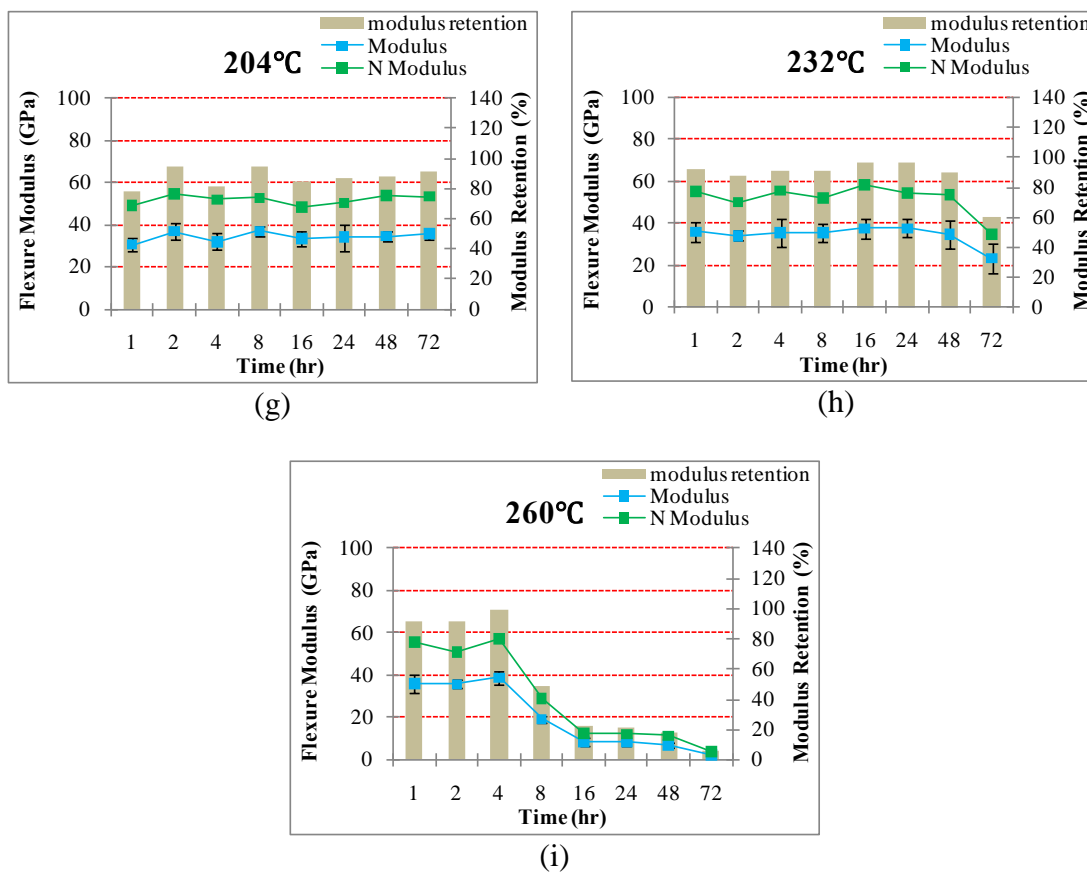


Figure 4-27: Continued

The time-dependent functions of flexural strength and modulus retention obtained by polynomial curve fittings are tabulated in Table 4-18 and Table 4-19. The coefficients of determination (R^2) of the time-dependent function in ranges of lower exposure temperatures were very low due to data fluctuation derived from thickness and defect. Especially, R-squared values in condition of ambient temperature showed the minimum values. Another reason why data variation was high than expected is that thermal oxidation did not largely affect the reduction of mechanical properties in the intermediate exposure temperatures. However, since degradations in flexural test

rapidly occurred in exposure temperature of 260 °C compared to tensile test, the coefficient of determination (R^2) showed higher values.

Table 4-18 Time-dependent functions of off-axis shear strength retention (%) obtained by polynomial curve fitting

Temperature(°C)	a	b	c	d	R^2
Ambient (23)	-7.0E-05	0.0084	-0.3353	105.73	0.4012
66	2.0E-04	-0.0189	0.3454	103.22	0.4907
93	-2.0E-04	0.0261	-0.6874	102.46	0.5865
121	1.0E-04	-0.013	0.2979	104.05	0.2465
149	1.0E-04	-0.0265	0.9694	102.19	0.5885
177	-5.0E-05	0.013	-0.5409	109.14	0.679
204	3.0E-05	0.0009	-0.039	103.49	0.6074
232	-3.0E-04	0.0156	-0.0449	103.87	0.9782
260	-1.3E-03	0.1859	-7.9962	117.97	0.932

$$\text{Time-dependent function : } Y(t) = \frac{\sigma_t}{\sigma_i} \times 100 = at^3 + bt^2 + ct + d$$

Table 4-19 Time-dependent functions of off-axis shear modulus retention (%) obtained by polynomial curve fitting

Temperature(°C)	a	b	c	d	R^2
Ambient (23)	-1.0E-04	0.0165	-0.4739	112.33	0.1408
66		0.0003	-0.2224	105.05	0.5535
93	-4.0E-04	0.0518	-1.668	101.45	0.7312
121	2.0E-04	-0.016	0.1447	102.64	0.7227
149	3.0E-05	-0.0067	0.1114	102.18	0.3991
177	-7.0E-05	0.0027	-0.3472	97.793	0.4329
204	1.0E-04	-0.0115	0.3419	91.027	0.5847
232	-1.0E-04	-0.0035	0.4771	95.199	0.9809
260	-1.5E-03	0.1968	-7.9759	114.25	0.9428

$$\text{Time-dependent function : } Y(t) = \frac{E_t}{E_i} \times 100 = at^3 + bt^2 + ct + d$$

4.3.3.2 Temperature Dependence

As shown in Figure 4-28 of flexural strength of carbon/epoxy composite materials as a function of temperature at fixed time, the majority of the flexural strengths were distributed within a range from 500 MPa to 600 MPa except the conditions of exposure temperature, 232 °C for ageing timer, 72 hrs and exposure temperature, 260 °C for ageing times of 8, 16, 24, 48 and 72 hrs. If the ageing time is less than 8 hrs, flexural strengths were not largely affected by residual post-cure and thermal degradation in exposure temperature range up to 260 °C.

Similar to the result of flexural strength, most of flexural chord modulus existed between 32 GPa and 45 GPa except the conditions mentioned in flexural strength as shown in Figure 4-29. At these conditions, data variation of the flexural modulus was much higher than in the case of flexural strength.

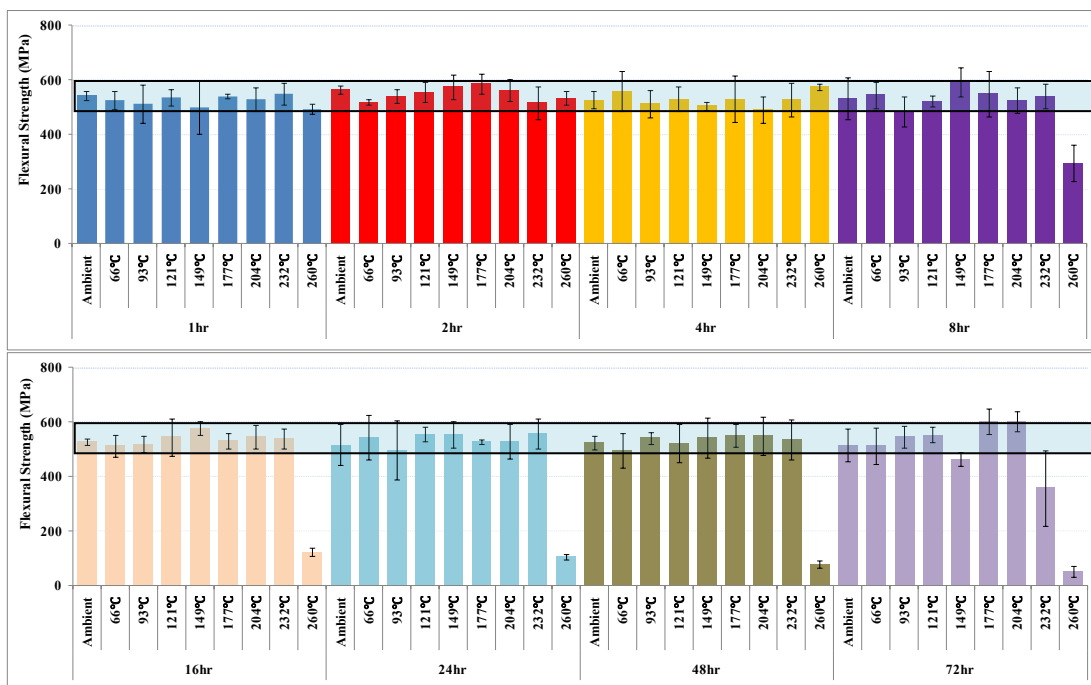


Figure 4-28: Flexural strength of carbon/epoxy composite materials as a function of temperature at fixed periods of exposure

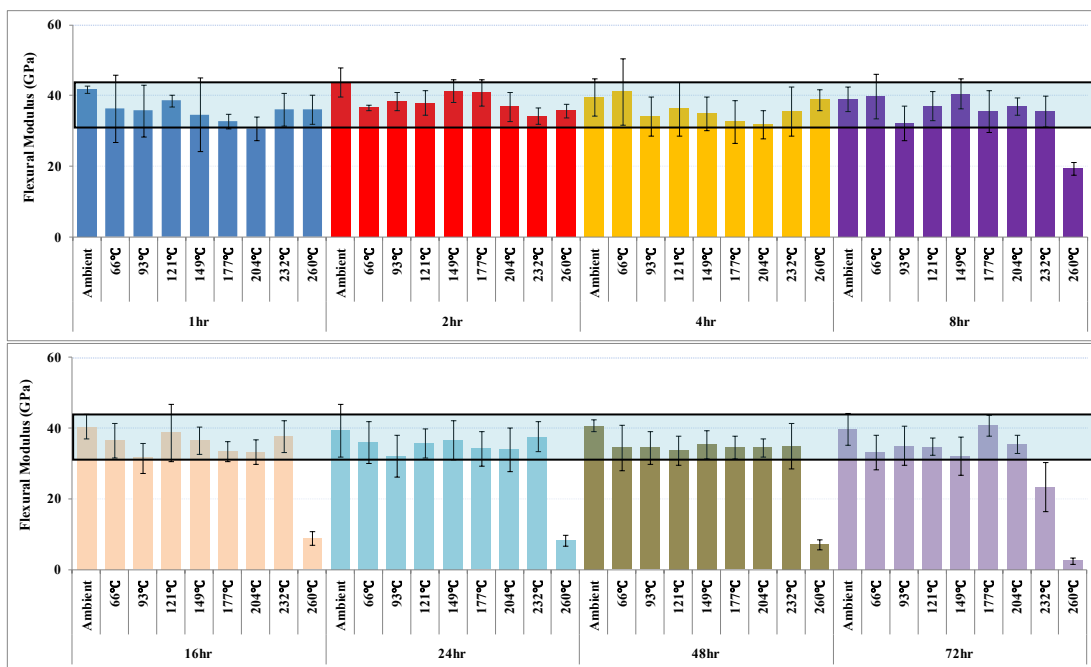


Figure 4-29: Flexural modulus of carbon/epoxy composite materials as a function of temperature at fixed periods of exposure

Based on the experimental data, temperature-dependent functions of flexural

strength and modulus retention determined by polynomial curve fitting are drawn in Table 4-20 and Table 4-21. As mentioned in time and temperature dependent analysis, since the majority of the data did not show any tendency in the ranges of lower temperatures, temperature-dependent functions had high order and the coefficient of determination (R^2) were higher compared to the values of tensile and off-shear properties.

Table 4-20 Temperature-dependent functions of flexural strength retention (%) obtained by polynomial curve fitting

Time (hr)	a	b	c	d	R^2
1	-6.E-06	0.00028	-0.3364	112.94	0.571
2	-8.E-06	0.0029	-0.2958	113.93	0.8816
4	8.E-06	-0.003	0.27	98.481	0.6546
8	-3.E-05	0.0092	-0.8728	121.99	0.8121
16	-4.E-05	0.0137	-1.2568	128.4	0.8489
24	-4.E-05	0.013	-1.1904	126.62	0.7871
48	-4.E-05	0.0155	-1.4465	131.89	0.8458
72	-4.E-05	0.0142	-1.2546	126.26	0.8901

$$\text{Temperature-dependent function : } Y(T) = \frac{\sigma_t}{\sigma_i} \times 100 = aT^3 + bT^2 + cT + d$$

Table 4-21 Temperature-dependent functions of flexural modulus retention (%) obtained by polynomial curve fitting

Time (hr)	a	b	c	d	R^2
1	4.E-06	-0.0008	-0.1093	114.44	0.7072
2	-1.E-05	0.0044	-0.5641	127.68	0.9183
4	1.E-05	-0.0033	0.1745	106.38	0.7596
8	-2.E-05	0.0091	-0.9504	127.01	0.7955
16	-4.E-05	0.0137	-1.487	141.05	0.7641
24	-4.E-05	0.048	-1.5817	140.52	0.7882
48	-4.E-05	0.0158	-1.7299	146.6	0.8586
72	-5.E-05	0.0166	-1.7061	141.49	0.9539

$$\text{Temperature-dependent function : } Y(T) = \frac{E_t}{E_i} \times 100 = aT^3 + bT^2 + cT + d$$

4.3.3.3 Morphological Analysis

Figure 4-30 represents top view and side view of the test specimens fractured after flexural test after exposure to elevated temperatures at the ageing time, 72 hrs. As exposure temperatures were going up, the color of the test specimens was also changed as described in morphological analysis of the tensile test. Except for color change, test specimens fractured by flexural test did not have characterized morphology in ranges of the lower exposure temperatures. From the side view of test specimens, there were many stains in the side section of test coupons. There were no stains in the exposure conditions of ambient and 66 °C while stains were increased as exposure temperatures were going up. The reason why there are stains in the side of the test specimens is that the polymer matrix and organic fibers decomposed thermally yield volatile gases via a series of chemical reaction mechanisms and volatile gases were emitted from side section of the test specimen.

In ranges of lower exposure temperatures (ambient, 66, 93, 121, 149 °C) for 72 hrs of ageing time, test specimens fractured by flexural test did not show the delamination between 2 layers whereas severe delamination caused by thermal oxidation occurred in ranges of the higher exposure temperatures (177, 204, 232, 260 °C) for 72 hrs. As the exposure temperatures were going up, the delaminations between 2 layers were more severe. The reason why flexural properties were rapidly reduced in range of the exposure temperature of 260 °C compared to tensile properties is that additional delamination between 2 layers caused severe deterioration of the test specimens.

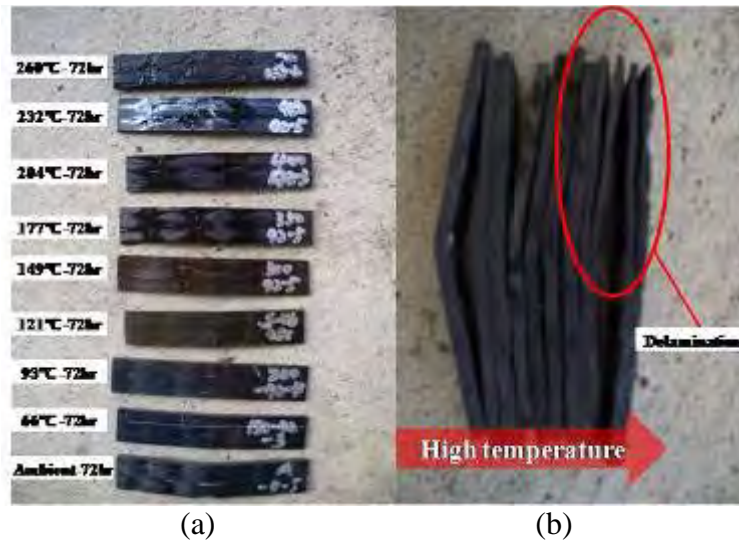


Figure 4-30: Test specimens fractured after flexural testing after exposure to elevated temperatures at an ageing time of 72 hrs (a) top view (b) side view

4.3.3.4 Strain Effect

The strains of the flexure test were calculated by using Equation 4.21. The ultimate failure strains and the maximum strains were obtained from the values which flexural stress reached the maximum and test specimens were perfectly fractured by test equipment, respectively.

Figure 4-31 shows flexural stress-ultimate failure strain curve exposed to various ageing temperatures at the fixed time, 72 hrs. The slopes of the linear range to measure the flexural chord modulus were gradually increased in exposure temperatures of from ambient to 149 °C while the values of flexural modulus were significantly reduced in ranges of high exposure temperatures more than 177 °C. The maximum stresses were increased in lower exposure temperatures and were decreased by thermal oxidation in higher exposure temperatures. Because test specimens were perfectly not cured in ambient exposure temperature, they showed the ductile property until

completely fractured after the maximum stress was reached. In case flexural modulus and strength were enhanced by residual post-cure effect, test specimen showed brittle property fractured promptly after reaching the maximum stress. In addition, the maximum strains of test specimens subjected to high temperatures of 232 and 260 °C were very high compared to any exposure temperatures. This phenomenon was attributed to softening of test specimens caused by char formation in process of thermal oxidation.

Figure 4-32 (a), Figure 4-33 (a) and Figure 4-34 (a) show flexural strength, modulus and load as a function of ultimate failure strains (%), respectively. Except for the data of the high exposure temperature (260°C), all data of the flexural strength, modulus and load were distributed between 0.014 mm/mm and 0.021 mm/mm of ultimate failure strain. If the outlier data in high exposure temperatures are extracted and the data of the flexural strength, modulus and load are changed to log scale, more linear correlations between flexural properties and ultimate strain can be obtained as represented in Figure 4-32 (b), Figure 4-33 and Figure 4-34 (b).

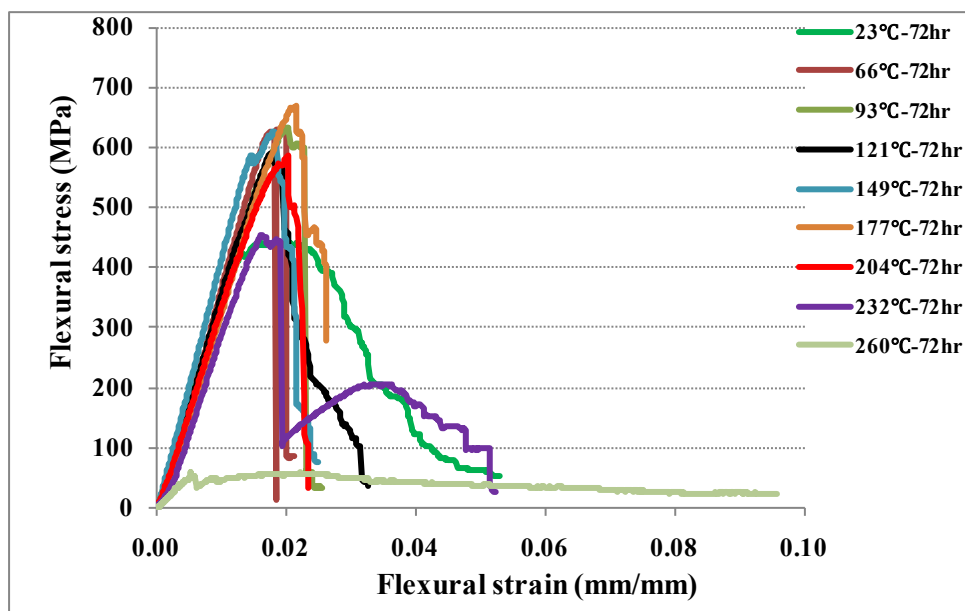


Figure 4-31: Flexural stress- strain curve resulting from specimens exposed to various ageing temperatures at a fixed time of 72 hrs

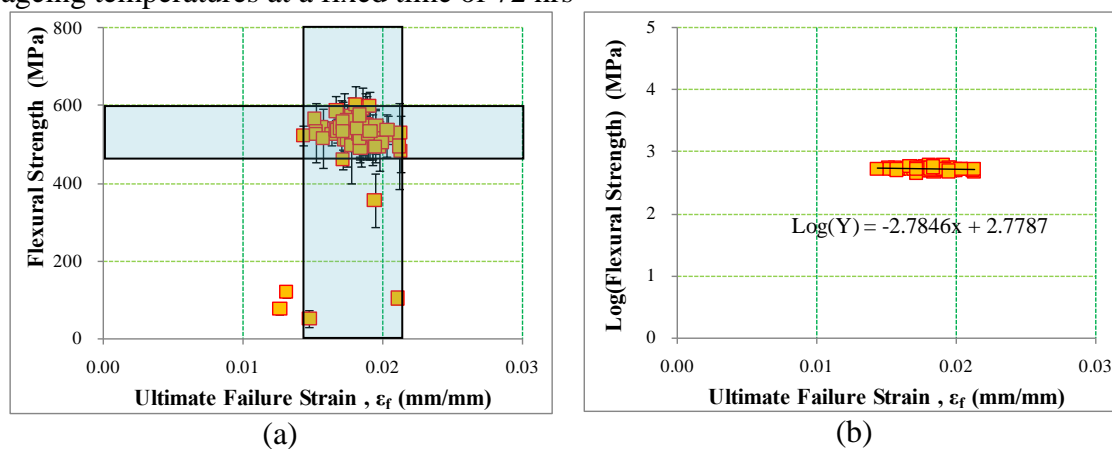


Figure 4-32: (a) Flexural strength as a function of ultimate failure strains and (b) correlations of log (Flexural strength) versus ultimate failure strain

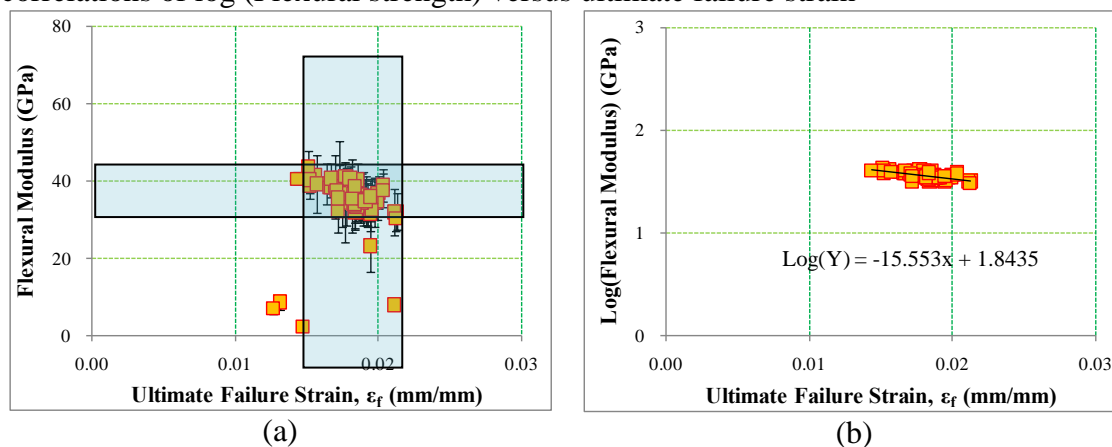


Figure 4-33: (a) Flexural modulus as a function of ultimate failure strains and (b)

correlations of log (Flexural modulus) versus ultimate failure strain

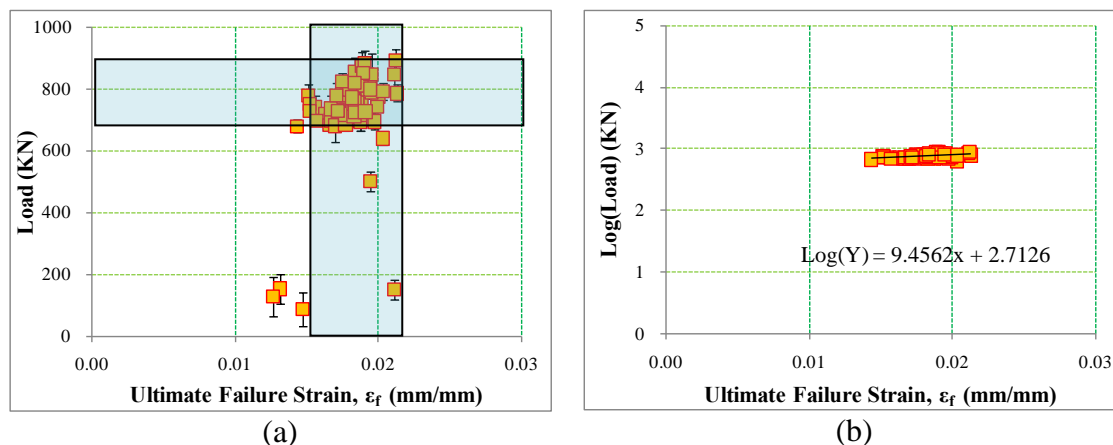


Figure 4-34: (a) Flexural load as a function of ultimate failure strains and (b) correlations of log (Flexural load) versus ultimate failure strain

4.4 Short Beam Shear Testing

4.4.1 Introduction

It is well known that the original performance of fiber reinforced polymer (FRP) composites strongly depend on the properties of the fiber reinforcement and the resin, and the interface between the two components. Layered composite materials intrinsically have a weakened zone within interlaminar regions. If the composite materials are exposed to high temperature and fire, cracks and defects within weakened zone can result in catastrophic degradations such as macrocrack formation and delamination of reinforced layers along these regions.

In case the composite materials are applied for naval applications, the majority of the fiber reinforced polymer composites are wet laid-up in ambient temperature due to huge structures. FRP composites which incompletely cured over the expected service-life can influence the properties of resin and interfaces between layers or fiber

and resin. Interlaminar shear strength (ILSS) depends primarily on the resin properties and fiber-matrix interfacial shear strengths rather than the fiber properties. Therefore, ILSS is an important characteristic to be assessed because this property can be criterion for potential failure modes. In general, ILSS refers to the shear strength parallel to the plane of lamination. In this study, short beam shear test having three-point bending fixture was executed in accordance with ASTM D2344. Because of its simplicity, the short beam shear test is widely accepted for materials screening and quality control purpose[53]. This method measures the apparent interlaminar shear strength of composite materials. Thus, short beam shear test method is not appropriate for generating design information[54].

4.4.2 Data Reduction

Short beam shear (SBS) tests were executed to obtain the interlaminar shear strength of carbon/epoxy composite materials comprised of 2 layers laminate. In the case of SBS test in three-point bending, the test specimens are center-loaded with two ends on two supports enabling lateral motion, with the force applied by a loading nose placed in midpoint of the test specimens. Detail SBS test procedure is described in Chapter 3.5.4.

SBS strength can be calculated by Equation 4.23.

$$F^{sbs} = 0.75 \times \frac{P_m}{b \times h} \quad (4.23)$$

where:

F^{sbs} = the short beam shear strength, MPa

P_m = the maximum load, N

b = the width of the specimen tested, mm

h = the thickness of the specimen tested, mm

4.4.3 Analyses and Results

4.4.3.1 Time Dependence

Although layered unidirectional composite materials offer good mechanical properties in fiber direction they have very little resistance to crack propagation and delamination under transverse and shear loading. Therefore, short beam shear test can be resulted in various failure modes as follows[55],

- Discrete shear by irregular crack and side crack
- Homogenous shear by permanent deformation and compression jamming
- Tensile fracture of outer surface
- Compression fracture of outer surface

Short beam shear test can derive complicated fractures since failure mode can be combined with other failure mode or not. Thus, it is difficult to analyze the experimental test results in short beam shear test. In particular, when used in conjunction with thin unidirectional composites, which is common with the graphite/epoxy composites, the test does not usually yield interlaminar failure[54].

Data for short beam shear strength (MPa) of carbon/epoxy composite materials

after exposure to various temperatures are tabulated in Table 4-22 and Short beam shear strength as a function of time at fixed temperatures are presented in Figure 4-35. Except for severe environments of exposure temperature ($260\text{ }^{\circ}\text{C}$) for more than 16 hrs in ageing time, all short beam shear strengths were distributed in ranging from 40 to 50 MPa. Compared to the strength retentions of tensile and flexural test, the strength retentions of short beam shear test were initially increased in the amount of more than flexural strength retention and less than tensile strength retention by residual post-curing. Therefore, the fractures of short beams shear test can be resulted in mixed failure mode. Especially, it should be pointed out that strength retention of exposure temperature ($232\text{ }^{\circ}\text{C}$) for 72 hrs in ageing time, contrary to tensile and flexural test, was not decreased by thermal degradation. Interlaminar shear stress was not contributed to fracture of the test specimens since char was only formatted in the surface of composite materials and buckling failure near the load nose in the midpoint was not occurred. However, levels of deterioration measured in the environmental condition of exposure temperature ($260\text{ }^{\circ}\text{C}$) for more than 16 hrs in ageing time were higher than strength retention in tensile and flexural test as represented in Table 4-22 and Figure 4-35.

The time-dependent functions of short beam shear retention obtained by polynomial curve fittings are tabulated in Table 4-23. Even though 3 order polynomial curve fittings were executed, the coefficient of determination (R^2) of the time-dependent function except for condition of exposure temperature ($260\text{ }^{\circ}\text{C}$) was the lowest compared to tensile and flexural strengths. As mentioned about disadvantage of short beam shear test, since short beam shear test can derive complicated fractures, particularly, in carbon/epoxy composite materials, higher variation of experimental data

resulted in lower coefficient of determination (R^2) in the ranges of intermediate exposure temperatures.

Table 4-22 Data for Short Beam Shear Strength (MPa) of carbon/epoxy composite materials after exposure to various temperatures (N denotes normalized)

Exposure temperature	Time (hr)	Thick (mm)	Width (mm)	Load (N)	Strength (MPa)	S.D (MPa)	N strength (MPa)	Strength Retention(%)
Ambient (23 °C)	0	2.26	6.54	776.69	39.45	2.01	46.15	100.00
	1	2.33	6.50	829.30	41.85	1.67	50.48	106.08
	2	2.26	6.63	843.66	42.23	1.06	49.45	107.05
	4	2.28	6.58	830.12	41.44	1.48	49.05	105.06
	8	2.34	6.50	858.81	42.43	1.41	51.35	107.55
	16	2.27	6.60	824.88	41.19	1.18	48.54	104.42
	24	2.34	6.58	857.47	41.84	2.00	50.64	106.06
	48	2.29	6.56	843.39	42.07	3.10	49.92	106.64
	72	2.26	6.54	796.31	40.28	3.17	47.21	102.11
66 °C	1	2.37	6.61	882.45	42.33	1.62	51.89	107.31
	2	2.28	6.67	930.24	45.76	3.12	54.15	115.99
	4	2.28	6.71	921.70	45.36	2.64	53.50	114.99
	8	2.34	6.46	912.26	45.45	2.25	55.02	115.22
	16	2.24	6.67	921.20	46.31	2.97	53.65	117.39
	24	2.30	6.35	909.20	46.44	3.53	55.25	117.73
	48	2.30	6.62	912.36	44.85	2.90	53.49	113.68
	72	2.30	6.56	923.86	46.02	3.23	54.75	116.66
93 °C	1	2.25	6.67	857.23	42.89	1.98	49.96	108.73
	2	2.31	6.59	902.84	44.46	3.66	53.30	112.69
	4	2.28	6.74	917.38	44.91	2.18	52.96	113.84
	8	2.23	6.68	931.75	46.94	1.12	54.24	119.00
	16	2.10	6.70	981.39	47.75	3.87	52.05	121.03
	24	2.29	6.60	892.79	44.49	3.12	52.67	112.77
	48	2.25	6.81	947.45	46.29	1.44	54.02	117.35
	72	2.32	6.70	960.55	46.37	3.07	55.70	117.55
121 °C	1	2.30	6.69	883.95	43.13	2.42	51.35	109.32
	2	2.27	6.77	926.38	45.29	2.01	53.22	114.80
	4	2.28	6.71	917.24	45.01	2.62	53.13	114.10
	8	2.29	6.65	973.76	47.93	1.50	56.87	121.51
	16	2.27	6.74	906.24	44.47	3.04	52.26	112.72
	24	2.27	6.71	914.62	44.96	1.95	52.97	113.97
	48	2.33	6.73	983.08	47.01	3.02	56.76	119.17
	72	2.29	6.40	918.65	47.01	2.86	55.83	119.16
149 °C	1	2.29	6.72	955.55	46.35	2.95	55.10	117.50
	2	2.32	6.73	959.45	46.00	1.87	55.35	116.61
	4	2.27	6.66	923.42	45.69	2.77	53.74	115.83
	8	2.28	6.69	1033.25	50.69	1.51	59.99	128.49
	16	2.26	6.61	905.01	45.46	2.40	53.23	115.23
	24	2.26	6.72	951.32	46.93	2.00	54.96	118.97
	48	2.34	6.75	973.59	46.20	2.03	56.07	117.12
	72	2.28	6.66	980.43	48.43	4.51	57.21	122.77

Table 4-22 Continued

Exposure temperature	Time (hr)	Thick (mm)	Width (mm)	Load (N)	Strengt h (MPa)	S.D (MPa)	N strength (MPa)	Strength Retention(%)
177°C	1	2.26	6.71	934.46	46.17	2.50	54.11	117.03
	2	2.28	6.69	910.04	44.63	3.10	52.82	113.14
	4	2.33	6.73	905.27	43.27	2.29	52.28	109.69
	8	2.27	6.77	941.41	46.03	1.63	54.09	116.68
	16	2.35	6.63	945.68	45.41	1.02	55.39	115.12
	24	2.34	6.62	958.83	46.39	1.07	56.29	117.60
	48	2.27	6.73	950.46	46.86	3.02	55.01	118.78
	72	2.26	6.61	940.33	47.16	4.05	55.27	119.54
204°C	1	2.23	6.72	907.45	45.54	2.26	52.57	115.45
	2	2.31	6.72	933.51	45.08	1.63	54.00	114.27
	4	2.29	6.74	894.37	43.45	1.61	51.55	110.13
	8	2.25	6.65	957.13	48.08	0.60	55.95	121.87
	16	2.27	6.47	875.64	44.73	2.22	52.60	113.37
	24	2.29	6.76	938.53	45.49	2.88	53.98	115.32
	48	2.29	6.75	921.25	44.67	4.01	52.90	113.22
	72	2.20	6.36	918.40	48.91	3.83	55.81	123.99
232°C	1	2.30	6.71	909.84	44.28	1.14	52.72	112.24
	2	2.35	6.71	958.50	45.61	3.24	55.58	115.61
	4	2.17	6.73	936.50	48.06	2.91	54.04	121.84
	8	2.30	6.67	957.24	46.71	2.66	55.76	118.41
	16	2.24	6.19	859.29	46.48	1.74	53.85	117.83
	24	2.29	6.70	955.67	46.62	4.27	55.42	118.19
	48	2.25	6.73	1003.92	49.61	3.17	57.93	125.75
	72	2.27	6.48	955.59	48.97	5.11	57.70	124.14
260°C	1	2.23	6.71	872.91	43.64	2.94	50.51	110.61
	2	2.28	6.50	950.82	48.00	1.38	56.80	121.67
	4	2.22	6.71	999.02	50.13	2.99	57.77	127.09
	8	2.22	6.56	530.95	27.34	2.46	31.45	69.31
	16	2.26	6.74	373.01	18.37	1.27	21.51	46.57
	24	2.30	6.62	191.15	9.43	1.12	11.23	23.92
	48	2.29	6.74	130.06	6.26	1.85	7.43	15.87
	72	2.33	6.43	87.46	4.42	1.47	5.32	11.20

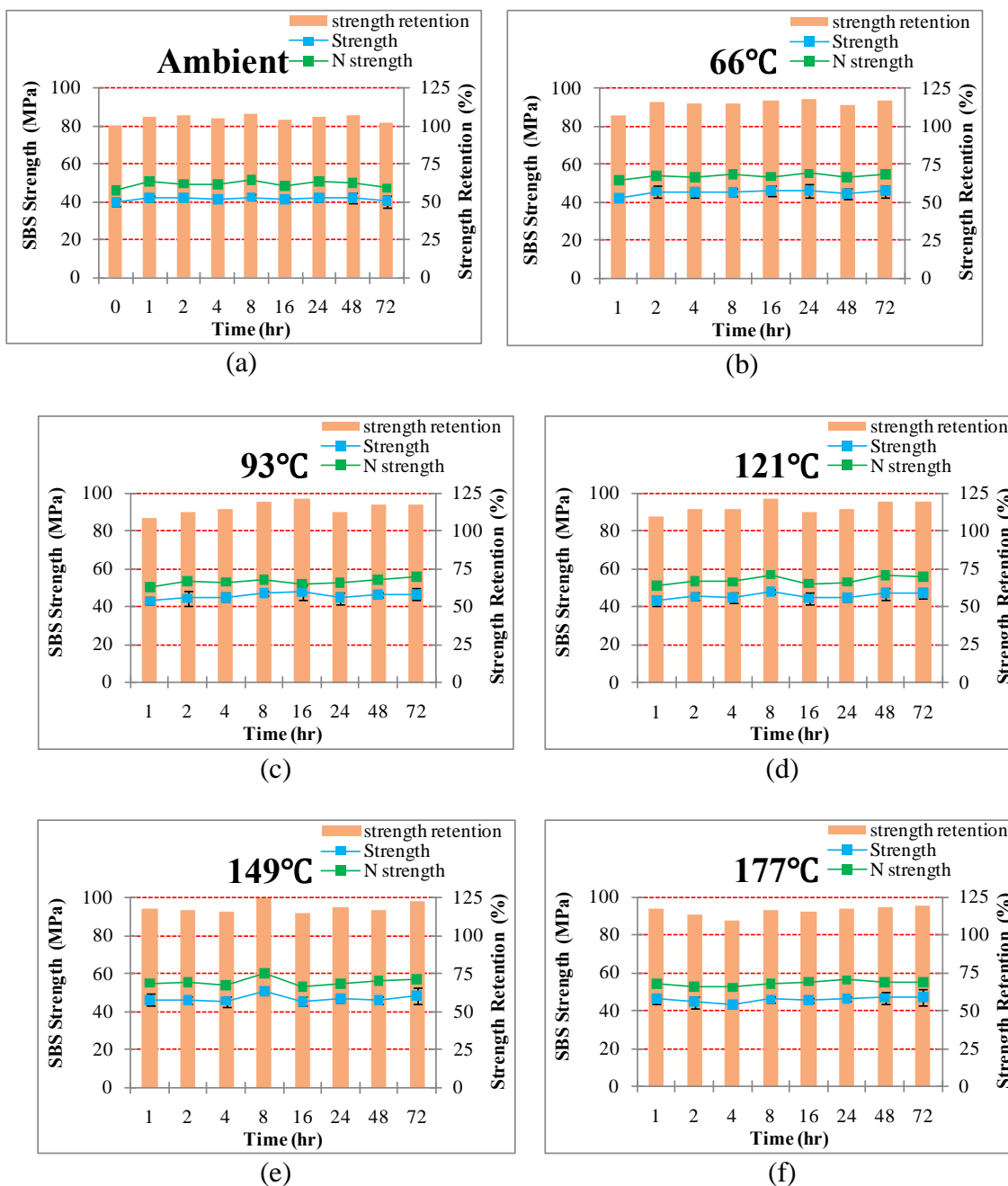


Figure 4-35: Short Beam Shear Strengths and normalized Short Beam Shear strengths of carbon/epoxy composite materials as a function of time at fixed temperatures, (a) ambient (b) 66°C (c) 93°C (d) 121°C (e) 149°C (f) 177°C (g) 204°C (h) 232°C (i) 260°C

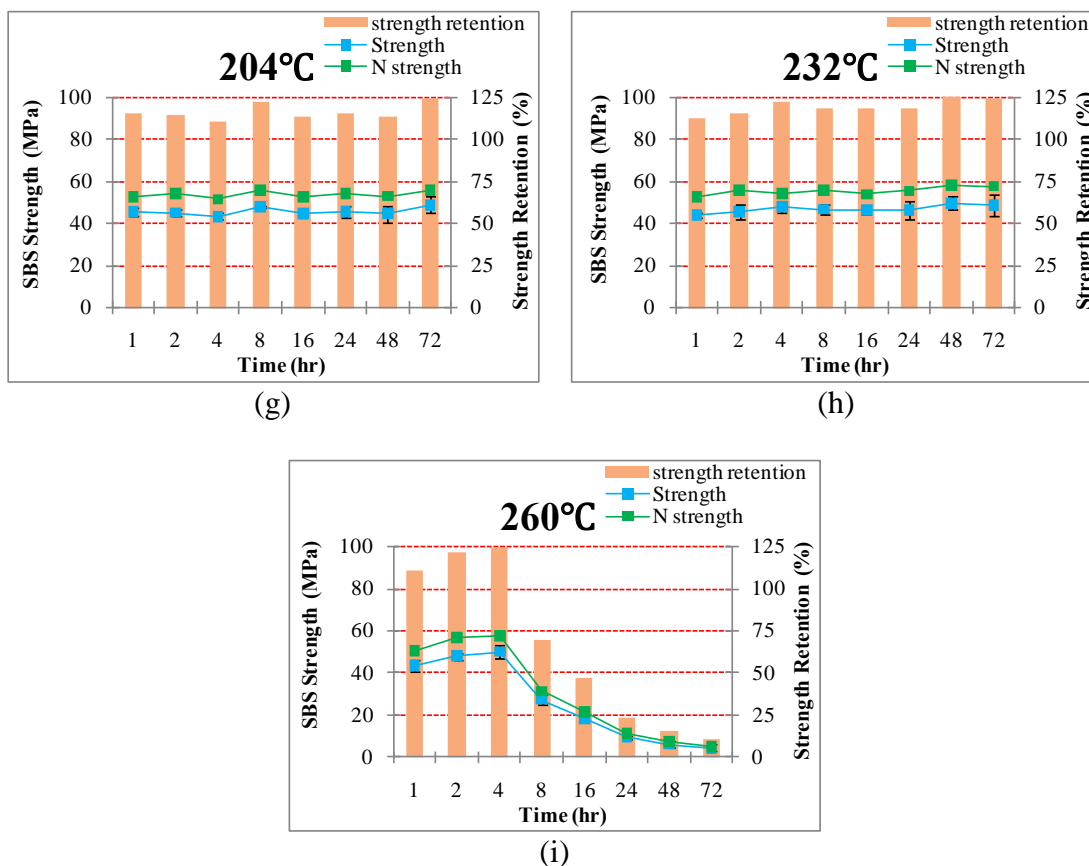


Figure 4-35: Continued

Table 4-23 Time-dependent functions of Short Beam Shear Strength retention (%) obtained by polynomial curve fitting

Temperature(°C)	a	b	c	d	R ²
Ambient(23)	-5.0E-06	-0.0021	0.1477	104.36	0.2788
66	2.0E-04	-0.027	0.8122	110.75	0.5601
93	2.0E-04	-0.024	0.7425	110.96	0.4209
121	8.0E-06	-0.0014	0.1411	113.47	0.2777
149	2.0E-04	-0.0162	0.3637	117.48	0.1819
177	-2.0E-05	0.0006	0.1239	113.66	0.5023
204	2.0E-04	-0.0176	0.3605	113.86	0.5356
232	-7.0E-05	0.0057	0.0694	116.19	0.6287
260	-1.1E-03	0.1645	-7.813	133.18	0.9469

$$\text{Time-dependent function : } Y(t) = \frac{\sigma_t}{\sigma_i} \times 100 = at^3 + bt^2 + ct + d$$

4.4.3.2 Temperature Dependence

Figure 4-36 and Figure 4-37 show the short beam shear strengths and loads of carbon/epoxy composite materials as a function of temperature at fixed time. The majority of the short beam shear strengths were distributed within ranging from 40 MPa and 50 MPa except for severe environments of exposure temperature (260°C) for more than 16 hrs in ageing time. In shorter ageing times (less than 8 hrs), short beam shear strengths were gradually increased although the exposure temperatures were going up. This phenomena means the residual post-curing effect and thermal oxidation by heat could not act on the change of short beam shear strengths. In other words, big data fluctuation appears to be stemmed from mixed failure modes of the defects and voids created in hand wet lay-up process. Data for short beam shear load were in good agreement with strength data and loads were existed between 800N and 1,000N as depicted in Figure 4-37.

Table 4-24 shows temperature-dependent functions of short beam shear strength retention (%) obtained by polynomial curve fitting. Compared to time-dependent functions, when each functions had 3 order equations, better coefficients of determination (R^2) were obtained by curve fitting.

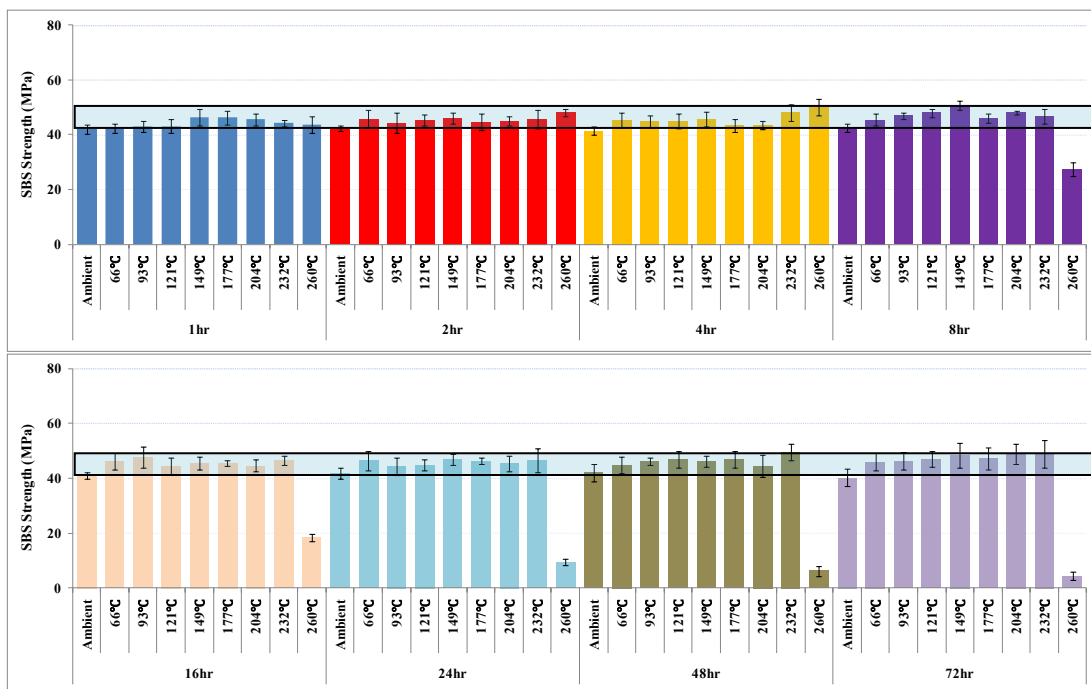


Figure 4-36: Short beam shear strength of carbon/epoxy composite materials as a function of temperature at fixed times of exposure

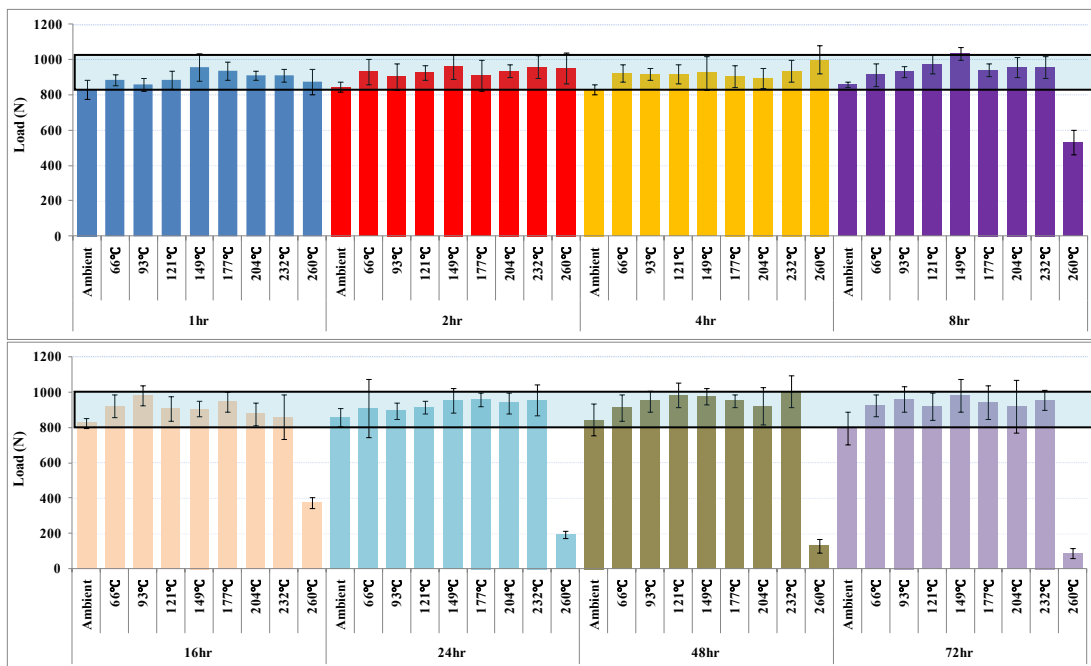


Figure 4-37: Short beam shear load of carbon/epoxy composite materials as a function of temperature at fixed times of exposure

Table 4-24 Temperature-dependent functions of Short Beam shear strength retention (%) obtained by polynomial curve fitting

Time (hr)	a	b	c	d	R ²
1	-5.E-06	0.0017	-0.0955	107.29	0.836
2	6.E-06	-0.0027	0.3598	100.4	0.8582
4	1.E-05	-0.0045	0.5412	94.954	0.8801
8	-2.E-05	0.0058	-0.3564	115.05	0.8404
16	-2.E-05	0.0073	-0.526	118.12	0.7482
24	-4.E-05	0.0131	-1.1202	131.82	0.7992
48	-4.E-05	0.0142	-1.2016	133.27	0.7595
72	-5.E-05	0.0152	-1.2157	129.9	0.7898

Temperature-dependent function : $Y(T) = \frac{\sigma_t}{\sigma_i} \times 100 = aT^3 + bT^2 + cT + d$

4.4.3.3 Morphological Analysis

Figure 4-38 shows SEM images in region between the support and the load nose at midpoint of test specimen after short beams shear testing of specimens exposed to elevated temperatures for ageing time of 48 hrs. Left images show bottom section fractured by tension and right images show top section fractured by compression. In the ranges of lower exposure temperatures, both sections showed good bonding between fibers and matrix. Since debonding between fibers and matrix and pulling-out of fibers were observed in ranges of high exposure temperatures, experimental data showed the deterioration of the interlaminar shear strengths did not occur in short beam shear testing. Pure interlaminar shear stresses were not applied for test specimens due to thin thickness. Test specimen subjected to exposure temperature (260°C) for ageing time of 48 hrs caused the catastrophic degradation due to char formation and severe debonding between fibers and matrix as shown in Figure 4-38 (i). Also, it should be noted that resin was elongated away from the original surface and moved in a fiber direction as depicted in left images of Figure 4-38 (b), (c) and (f). Such failure shapes are often defined as 'hackles', which has been corresponded to mixed-mode (combined tension and shear) interlaminar fracture[56]. Accordingly, since these fracture modes means the horizontal split is not a pure shear failure and fracture modes is very complicated, it is very difficult to obtain the accurate short beam shear strengths using the thin test specimens of carbon/epoxy composite materials.

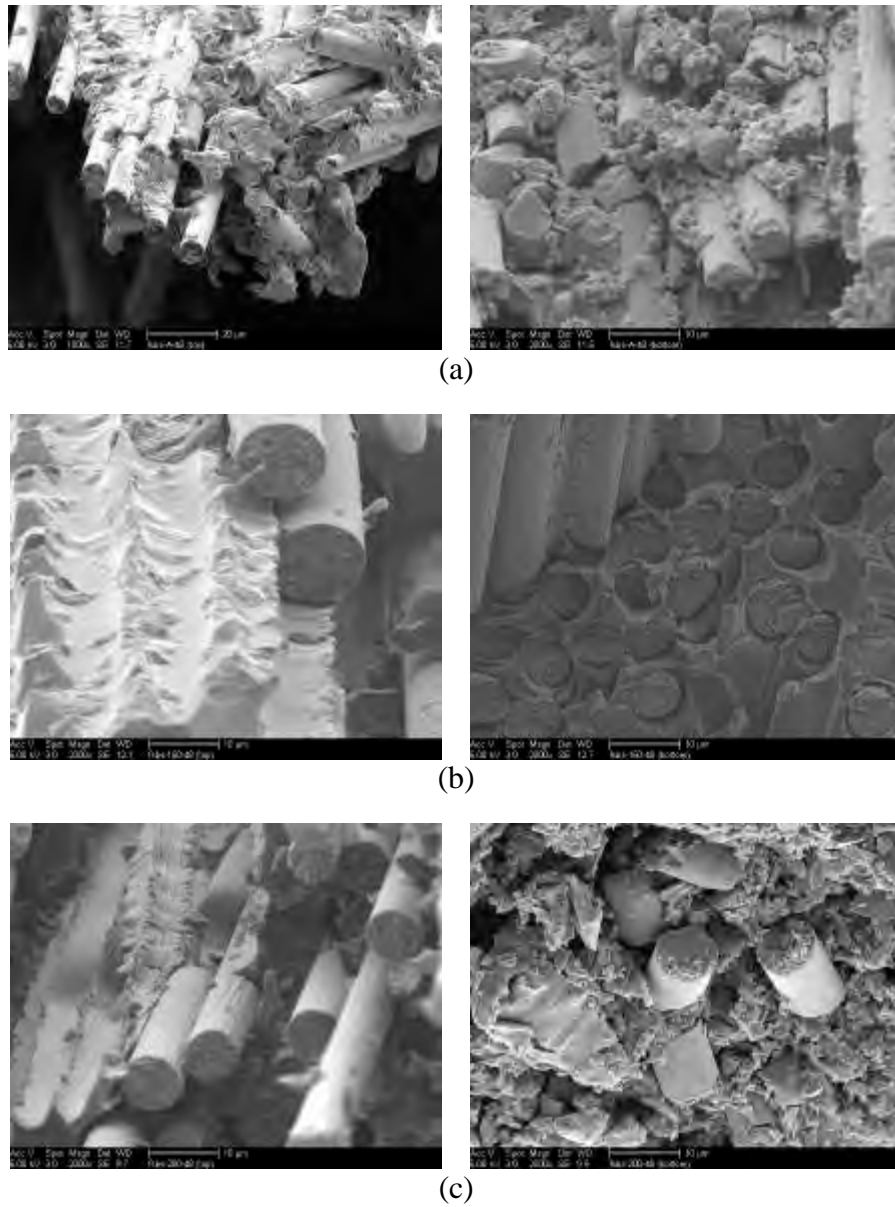
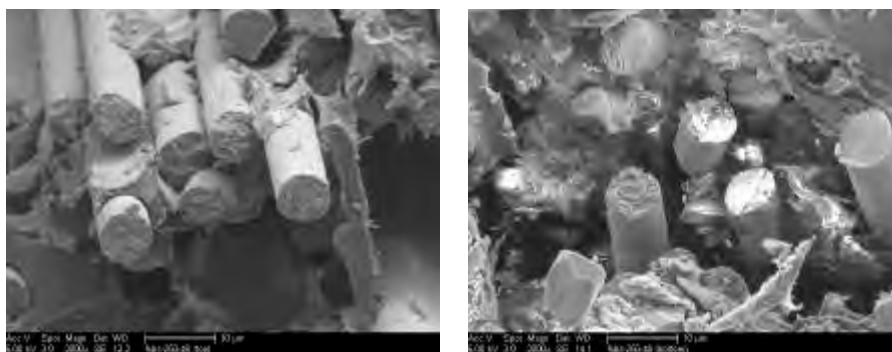
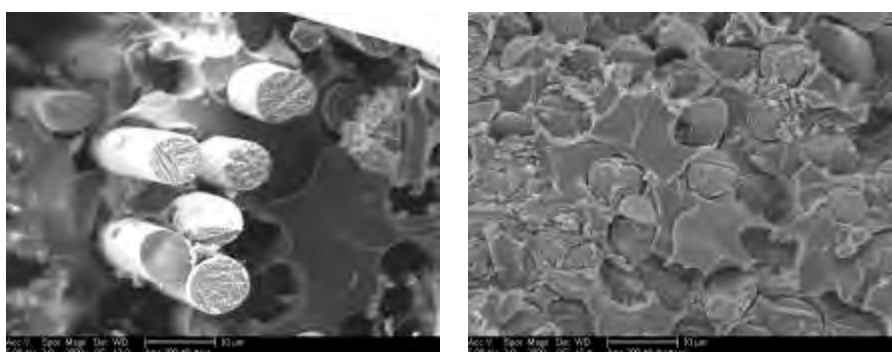


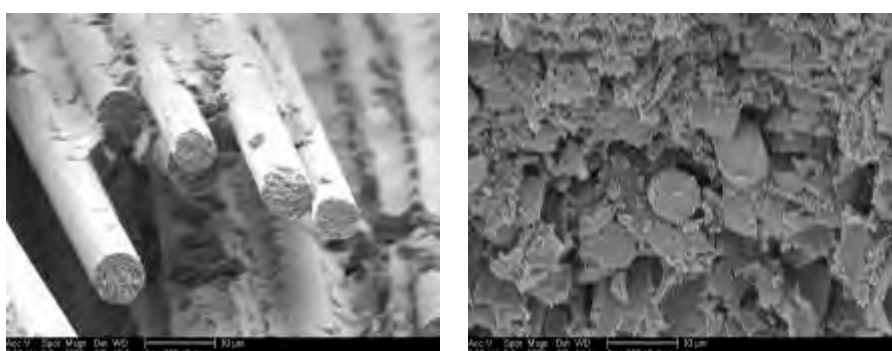
Figure 4-38: SEM images after short beam shear testing of specimens exposed to (a) ambient, (b) 66°C, (c) 93°C, (d) 121°C, (e) 149°C, (f) 177°C, (g) 204°C, (h) 232°C, (i) 260°C for 48 hrs in ageing time - left images : bottom section by tension, right images : top section by compression: Magnification 2000×



(d)

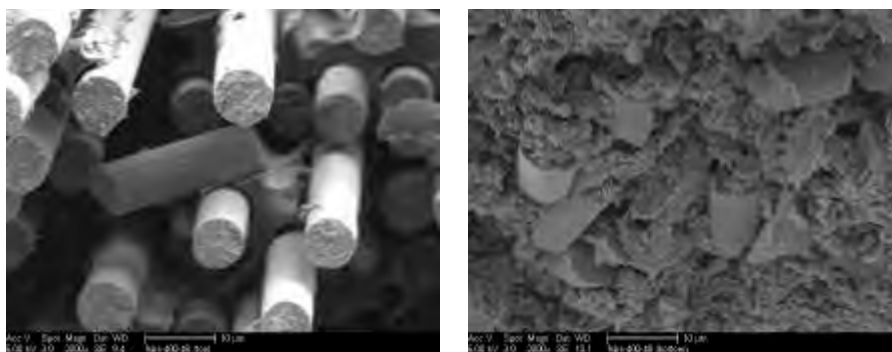


(e)



(f)

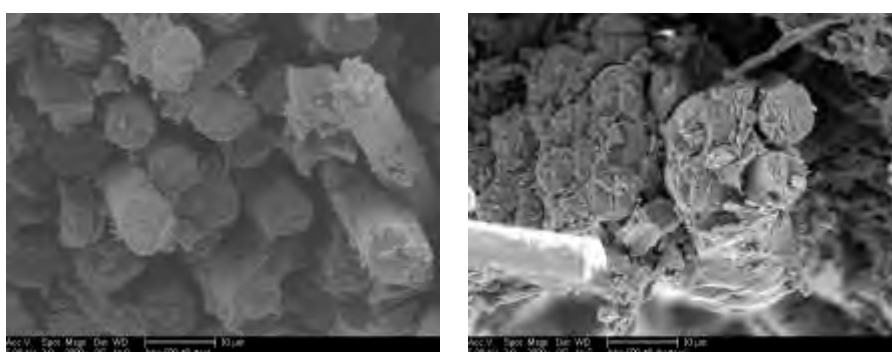
Figure 4-38: Continued



(g)



(h)



(i)

Figure 4-38: Continued

4.4.3.4 Correlation to Tensile Test Results

It is well known that the tensile properties are strongly dependent on interfacial adhesion between fibers and resin. Short beam shear testing are mainly used for the interlaminar shear strength of composite materials, though it has been recommended that short beam shear testing is proper for use as comparative measure of the fiber/matrix adhesion due to its sensitive to through thickness longitudinal shear strength. In addition, the short beam shear testing often shows a combination of failure mode such as delamination across the specimen depth, local crushing by the loading pin, bending failure, etc[57]. Therefore, through the comparison of tensile strength and short beam shear strength, it is necessary to analyze how failure mechanisms affect fracture of the test specimens in short beam shear test.

The stress applied at any point in the beam can be obtained by using strength of materials theory[58]. This theory is based on the necessary conditions for static equilibrium which pertains since the rate of deflection is small. The theory can be divided into two major components.

1. The normal stress has the maximum tensile value at midpoint between two supports. The maximum value of normal stress is

$$\sigma_x^* = \frac{3P_m L}{2bh^2} \quad (4.24)$$

2. Secondly, the longitudinal shear stress occurs at the mid-plane and is given by

$$\tau_{xy}^* \approx F^{sbs} = \frac{3P}{4bh} \quad (4.25)$$

According to Equation 4.24 and 4.25 of materials theory, test specimens of beam will be fractured by shear rather than tension or compression in outer surface at midpoint if

$$\sigma_x^* > \frac{2F^{sbs}L}{h} \quad (4.26)$$

Experimental data of tensile and flexural test are compared with materials theory as shown in Figure 4-39 and Figure 4-40. In short beam shear test, the span and average thickness of test specimens were 14 mm and 2.3 mm, respectively. Therefore, the slope of line drawn by red color in Figure 4-39 and Figure 4-40 was 12.17 according to Equation 4.26. The upper region from red line means the cases failed by short beam shear while the lower region represents the cases fractured by flexural tension at outer surface and pure tension. In particular, compared to experimental data of flexural test, the majority of failure modes of short beam shear test were occurred by not shear but flexural tension at outer surface. As a result, the reason why big variation of experimental data took place in lower exposure temperatures is that pure interlaminar shear stresses were not applied for test specimen of shear beam shear test.

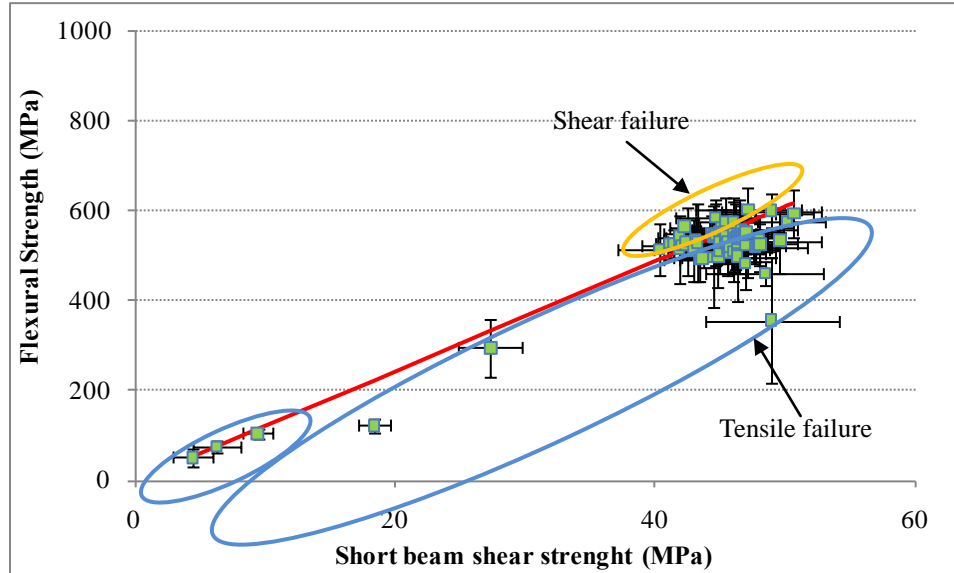


Figure 4-39: Boundary between interlaminar shear and flexural tension. $L/h = 6.09(\sigma^* > 12.17F^{sbs})$.

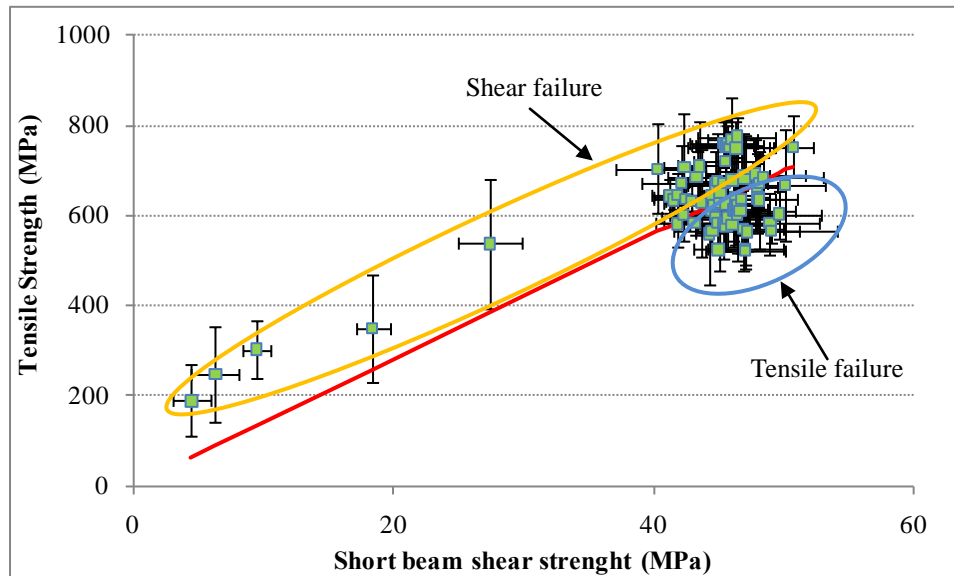


Figure 4-40: Boundary between interlaminar shear and pure tension. $L/h = 6.09(\sigma^* > 12.17F^{sbs})$.

5 Thermal Analysis

In general, thermal analysis refers to a variety of techniques in which properties of test specimens are continuously measured as the sample is programmed through a predetermined temperature profile. Therefore, thermal analysis can be used to characterize the physical and chemical properties of composite materials under conditions that simulate various environments. In particular, since polymers used in composite materials experience a diversity of properties according to temperatures, thermal analysis is necessary technique to assess the composite systems of this study focused on properties after exposure to elevated temperatures and fire.

5.1 Dynamic Mechanical Thermal Analysis

5.1.1 Introduction

Dynamic Mechanical Thermal Analysis (DMTA) is a powerful and sensitive analytical technique to determine the characteristic properties of polymer composites. DMTA measurements over a range of temperatures provide valuable insight into the structure, morphology and viscoelastic behavior of polymer materials[59]. DMTA comes from the field of rheology including the deformation and flow of materials[60]. As described in Chapter 3.5.5, an instrument is used to apply an oscillatory force on a sample in a temperature-controlled chamber. The sinusoidal stress and strain can be occurred by an oscillatory force. The instrument measures the amplitude of the peak deformation of the sine wave and the phase shift between them to determine data with

regard to modulus, viscosity, and damping. Three important parameters that can be determined from DMTA are 1) storage modulus, which is a measure of the maximum energy stored in the material during one cycle of oscillation and which gives an indication of the stiffness behavior of the sample; 2) loss modulus, which is directly proportional to the amount of energy that has been dissipated as heat by the sample; and 3) a mechanical damping term, $\tan \delta$, which is the ratio of the loss modulus to the storage modulus and is related to the degree of molecular mobility in the material[42]. Beside three important parameters, storage and loss compliance, dynamic and complex viscosity, creep compliance, and the stress-relaxation modulus can be determined by DMTA. In the case of thermoset polymers, DMTA can provide not only the glass transition temperature but also information regarding relative crosslink density and interfacial adhesion.

During measurement of the storage and loss modulus and damping property of a polymer composite over a wide range of temperatures, glass transition can be clearly detected. The glass transition is a reversible change of the polymer composite between rubbery and glassy states. The glass transition temperature can be detected as a sudden and considerable change in the elastic modulus and an attendant peak in the tangent delta curve. Since this temperature show the significant change in rigidity that polymer composites experience, glass transition temperature is a key factor in evaluating the polymer composites.

Most commonly, DMTA are accomplished in a fixed frequency in which the response of a material is studied as a function of temperature only. However, multi-frequency testing is often used for calculating activation energy, which can reveal

transitions in response and structural change in the polymer composites. By using multi-frequency test data, Time–Temperature Superposition (TTS) can be used to make long-term time-dependent predictions of some of the properties of the material. The shifting is usually done using the Arrhenius model[61] or the Williams–Landel–Ferry (WLF) model[62], depending on the reference temperature used during the master curve construction.

5.1.2 Data Reduction

DMTA test was performed in accordance with ASTM D5418[43] using the single cantilever frame fixture since the thickness of specimens was not uniform and specimen was made by wet layup process. First of all, the glass transition temperatures can be obtained by peak $\tan \delta$ or modulus data recorded from Rheometric Scientific dynamic mechanical thermal analyzer.

The storage modulus (or elastic modulus) is calculated as

$$E' = \frac{\sigma_0}{\varepsilon_0} \cos \delta \quad (5.1)$$

where:

E' = Storage Modulus

σ_0 = applied stress

ε_0 = maximum amplitude of the strain

δ = Phase angle

The loss modulus (or viscous modulus) is calculated as

$$E'' = \frac{\sigma_0}{\varepsilon_0} \sin \delta \quad (5.2)$$

where:

E'' = Loss Modulus

The tangent delta (or $\tan \delta$) is the ratio of the loss modulus to the storage modulus. The loss tangent, $\tan \delta$ is called the internal friction or damping coefficient and is the ratio of energy dissipated per cycle to the maximum potential energy stored during the cycle.

$$\tan \delta = \frac{E''}{E'} \quad (5.3)$$

5.1.3 Analyses and Results

5.1.3.1 Glass transition temperature

Identifying the glass transition and how various system modifications affect glass transition temperature is a major application for DMTA. The glass transition is easily identified from dynamic mechanical data because of the sharp decrease in storage modulus, and the corresponding loss dispersion in E'' or $\tan \delta$ that occur at glass transition temperature[63]. In general glass transition temperature, also changes based on the frequency used in testing and the rate of heating used. An increase in the heating rate is known to shift T_g to a higher temperature and an increase in test frequency for a

constant heating rate also results in the increase of T_g [41].

Glass transition temperatures based on peak $\tan \delta$ determined at different frequencies (0.3, 1, 3, 10, and 30Hz) on longitudinal and transverse test specimens after exposure to elevated temperatures are represented in Table 5-1. In addition, changes in glass transition temperature based on peak tangent delta as a function of time at fixed temperatures are shown in Figure 5-1 and Figure 5-2 shows the Schematic diagram for detecting the glass transition temperature at peak tangent delta. As shown in Table 5-1, glass transition temperatures determined from both fiber oriented test specimens showed very similar data for all environmental conditions. However, because specimens were tested in bending with single cantilever fixture in longitudinal direction, glass transition temperatures were slightly delayed compared to transverse test specimens. Thermal ageing initially caused a significant T_g increase, which is attributed to the post-cure effect on ambient cured system. As known in previous study, glass transition temperature of an epoxy resin is directly relevant to the reached crosslinkage[64]. T_g s showed no change by post-curing effect in ambient condition. In the ranges of lower exposure temperatures (66, 93 and 121°C) glass transition temperatures continuously increased as ageing time went up and the amounts of increase of the glass transition temperature by post-cure effect were 42.6, 67.2 and 69.1%, respectively. In the ranges of intermediate exposure temperatures (149, and 177°C) glass transition temperatures slightly started to decrease after reaching the maximum value. On the contrary, under 204 and 232°C condition, glass transition temperatures rapidly decrease due to serious polymer structural breakage. Under 260°C condition, glass transition temperatures dramatically decreased by thermal degradation. In the conditions of more than 24 hrs of

ageing time at 260°C, DMTA was not performed since test specimens were broken in the process of tests. The measured glass transition temperatures did not reflect the effect of the oxidation of the specimen surfaces. Therefore, specimens aged at low temperatures showed stable values in glass transition temperature after initial increase.

Glass transition is strongly influenced by the rate or frequency of mechanical energy input due to kinetic. It is well known that substantial molecular relaxation involving cooperative segmental motions of the polymer chains occurs in the region of glass transition temperature. The rate of this segmental motion depends on temperature, so that if the test frequency is increased, the relaxations corresponding to the glass transition is hard to reflect the mechanical strain input, and the polymer composites may have rigid property[63]. Therefore, glass transition temperatures increase as the rate of frequency is increased as shown in Figure 5-1. Figure 5-3 showed the height of $\tan \delta$ at different frequencies of test specimen exposed to 12°C for 4 hrs . It should be pointed out that glass transition at peak $\tan \delta$ was shifted to high temperature range and was broaden in the peak as the rate of frequencies were increased. This is related to a broadening of the relaxation spectrum in the glass transition temperature.

Table 5-1 T_g based on the peak of tangent delta determined from longitudinal and transverse test specimens after exposure to elevated temperatures

Exposure Temperature	Time	T_g (°C) Longitudinal					T_g (°C) Transverse				
		0.3Hz	1Hz	3Hz	10Hz	30Hz	0.3Hz	1Hz	3Hz	10Hz	30Hz
Ambient (23°C)	0	68.30	68.55	71.65	74.05	78.39	68.47	68.66	70.61	74.63	80.22
	1	63.89	68.75	72.68	76.64	79.33	63.79	69.53	72.38	74.89	79.30
	2	66.75	68.64	71.94	77.03	79.39	66.39	66.90	71.60	75.97	80.18
	4	64.88	69.29	73.29	74.58	77.46	63.02	67.95	73.75	73.86	81.99
	8	64.12	66.67	71.70	75.59	77.29	62.54	68.44	70.93	74.82	81.71
	16	64.29	68.95	70.25	72.63	76.50	65.46	68.95	72.54	75.44	81.55
	24	62.22	66.45	71.39	72.97	75.34	64.18	69.64	75.45	76.15	81.31
	48	64.04	67.84	70.31	73.01	75.35	71.56	71.95	73.74	78.72	84.39
72	64.15	68.82	71.81	74.88	78.58	66.17	68.08	75.25	78.52	81.83	
66°C	1	79.52	85.73	87.13	89.98	94.72	79.72	82.68	86.78	89.25	93.75
	2	84.05	84.27	87.38	91.22	95.11	80.67	82.90	88.74	93.68	97.27
	4	87.19	90.85	95.07	95.16	99.07	86.85	90.38	91.97	97.09	102.89
	8	94.86	95.94	97.10	98.79	104.09	88.15	92.02	95.56	99.33	103.00
	16	96.55	96.80	100.40	102.13	105.98	95.12	97.71	100.02	104.46	107.86
	24	98.80	100.13	100.24	102.22	106.80	93.07	96.08	98.37	101.17	103.38
	48	94.94	97.77	99.25	100.89	104.71	97.54	99.57	99.71	104.11	107.10
	72	97.44	100.12	102.62	104.43	107.45	103.80	104.01	104.15	108.76	112.96
93°C	1	89.61	93.09	98.01	101.33	104.33	92.17	93.86	97.59	102.75	105.46
	2	92.99	99.00	100.30	101.57	105.58	96.98	106.02	106.14	109.38	109.51
	4	99.55	104.49	107.31	110.25	112.62	107.20	106.59	109.97	112.78	118.42
	8	102.51	106.81	107.77	111.96	115.32	107.16	108.91	110.04	113.47	117.09
	16	102.73	107.50	112.08	114.38	115.90	108.24	111.53	113.31	117.56	121.86
	24	107.94	111.46	112.97	115.84	119.18	109.76	111.50	112.79	116.64	119.81
	48	113.53	113.89	116.05	118.52	120.90	113.51	115.19	116.75	119.26	124.64
	72	114.25	114.41	116.25	118.76	121.10	112.45	115.40	118.20	118.91	122.47
121°C	1	97.45	103.08	106.18	111.29	114.25	103.59	106.88	110.15	114.82	117.57
	2	98.50	104.05	109.96	113.99	116.00	104.12	106.81	110.87	114.29	117.62
	4	109.10	113.84	116.28	119.04	121.19	109.79	113.14	117.93	122.54	126.22
	8	111.53	117.32	117.45	122.21	124.58	111.12	115.47	119.52	122.09	124.51
	16	109.15	113.83	113.96	118.25	120.74	111.08	113.10	115.33	119.72	122.58
	24	109.23	115.30	116.63	118.71	121.82	108.18	113.97	116.22	119.32	124.64
	48	115.50	120.24	120.44	124.14	127.38	115.25	118.25	121.84	125.08	127.29
	72	114.58	120.85	119.80	124.97	127.33	115.42	119.59	119.73	123.48	128.46
149°C	1	110.43	115.56	116.52	119.06	121.24	110.71	112.40	115.70	120.94	123.95
	2	114.14	117.60	117.73	122.22	125.98	115.72	118.40	119.43	123.27	125.53
	4	113.49	117.18	117.31	121.79	124.21	114.45	119.74	118.37	124.93	127.23
	8	110.83	115.48	118.77	120.38	122.59	114.20	115.81	117.09	119.69	123.38
	16	115.91	121.17	121.27	124.39	127.53	118.98	120.80	120.93	125.23	129.92
	24	107.46	110.23	114.38	116.65	118.36	108.89	115.55	114.58	116.87	121.28
	48	108.12	113.21	113.19	118.29	119.64	112.96	115.49	116.77	120.94	125.27
	72	108.66	113.41	113.62	115.89	119.28	109.44	112.93	114.57	119.18	123.03

Table 5-1 Continued

Exposure Temperature	Time	T _g (°C)Longitudinal					T _g (°C)Transverse				
		0.3Hz	1Hz	3Hz	10Hz	30Hz	0.3Hz	1Hz	3Hz	10Hz	30Hz
177°C	1	107.52	113.47	113.69	117.42	120.53	109.92	110.14	113.70	117.81	122.10
	2	108.37	113.53	114.88	116.63	119.79	112.30	113.91	117.75	120.91	123.23
	4	109.45	113.90	114.02	118.53	121.77	109.09	112.08	114.78	118.77	121.65
	8	107.83	112.74	113.90	117.05	120.28	110.29	112.77	114.83	118.10	123.30
	16	111.00	114.60	115.97	118.88	121.93	111.23	114.02	115.42	120.08	122.32
	24	106.08	112.26	115.03	118.12	119.33	111.97	114.42	114.56	117.34	121.24
	48	111.56	112.97	114.94	117.48	119.08	103.00	109.12	114.23	116.09	121.99
	72	108.94	110.45	113.64	117.44	118.66	109.07	112.70	115.44	118.05	122.48
204°C	1	107.97	113.08	115.17	116.09	119.15	107.31	109.34	113.21	115.93	119.74
	2	112.34	112.70	114.14	117.68	120.09	110.84	112.43	111.14	115.92	119.02
	4	105.74	109.19	111.87	113.63	117.51	103.57	109.67	111.28	115.87	118.10
	8	109.98	111.92	114.79	117.22	120.16	108.62	110.36	112.00	115.32	119.69
	16	110.53	110.00	111.06	111.96	116.25	102.44	108.63	110.21	114.26	117.78
	24	106.63	107.75	111.28	113.68	116.91	101.54	106.63	109.79	112.31	115.66
	48	99.54	102.04	102.98	108.51	110.79	100.62	104.37	108.80	110.45	113.29
	72	103.39	105.64	109.07	112.37	114.56	96.54	100.69	103.71	108.13	110.29
232°C	1	107.48	112.91	112.27	115.39	119.29	109.71	111.39	114.93	119.31	122.27
	2	106.51	107.78	109.69	111.59	114.96	102.24	107.42	106.52	110.77	114.01
	4	103.45	108.56	109.61	113.90	115.39	103.96	109.88	116.00	116.12	120.57
	8	105.25	103.43	105.57	109.14	111.55	96.94	101.63	105.87	109.90	112.11
	16	91.14	98.73	101.69	103.26	106.36	90.66	96.70	99.47	103.34	105.57
	24	92.32	96.37	98.22	100.48	103.68	88.23	90.35	94.28	98.96	101.96
	48	86.24	90.57	89.94	95.44	98.63	82.43	84.74	92.89	96.05	101.74
	72	87.33	87.61	92.37	94.14	98.05	78.48	80.16	90.10	94.26	97.14
260°C	1	101.15	103.40	104.45	109.00	112.31	101.22	107.42	103.86	108.84	113.96
	2	99.00	99.30	102.77	104.57	107.68	95.12	98.70	98.83	102.58	106.29
	4	86.49	88.96	90.24	93.27	97.14	85.50	88.85	90.55	96.95	99.84
	8	68.80	71.23	81.70	81.80	86.03	75.53	80.74	85.72	89.18	93.08
	16	72.98	72.24	78.11	80.99	85.26	70.42	74.88	78.11	84.35	87.83
	24	71.71	71.53	78.06	84.28	90.29					

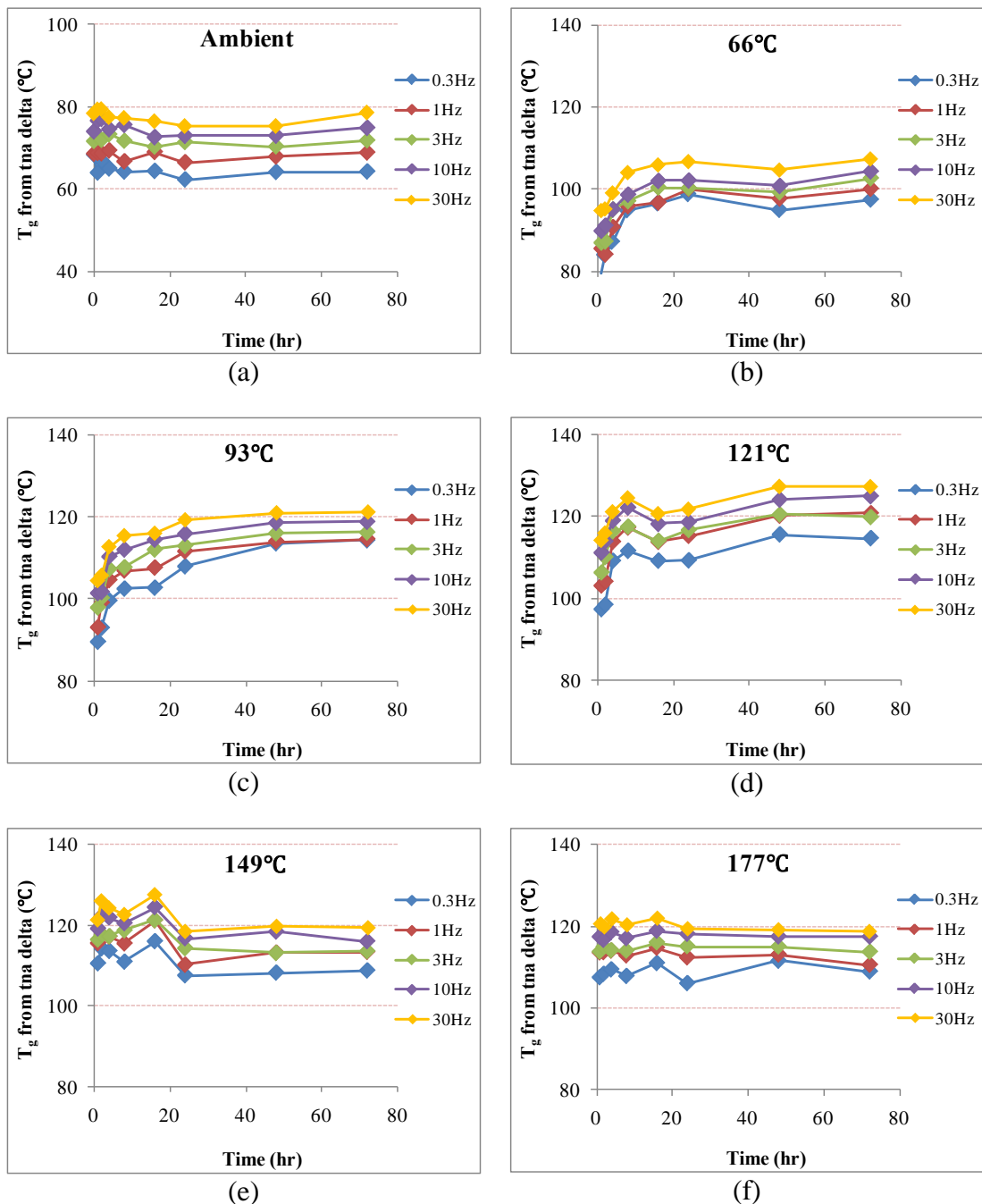


Figure 5-1: Change in T_g based on peak tangent delta as a function of time at fixed temperatures, (a) ambient (b) 66°C (c) 93°C (d) 121°C (e) 149°C (f) 177°C (g) 204°C (h) 232°C (i) 260°C

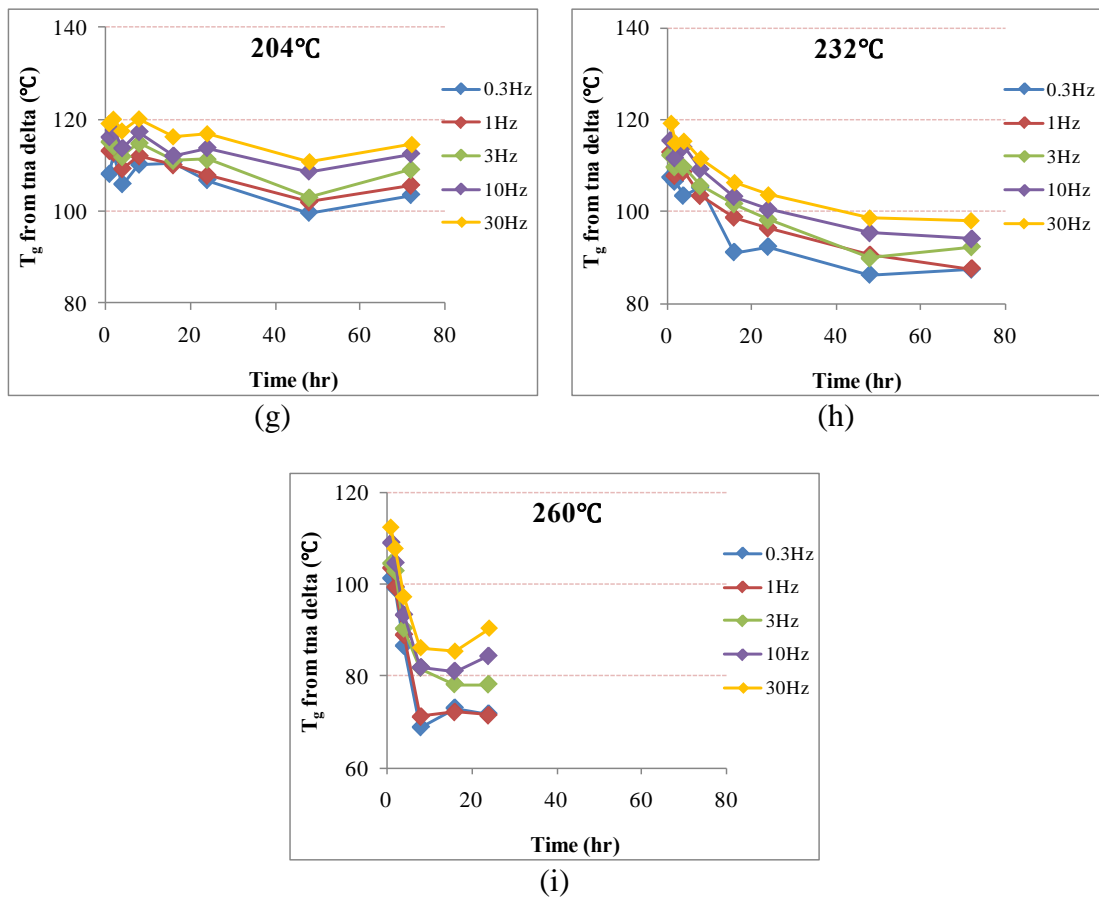


Figure 5-1: Continued

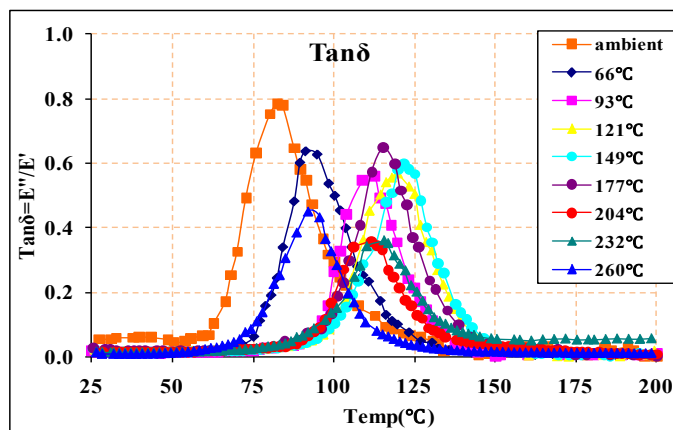


Figure 5-2: Schematic diagram for detecting the glass transition temperature at peak tangent delta in conditions of elevated temperatures for 4 hrs

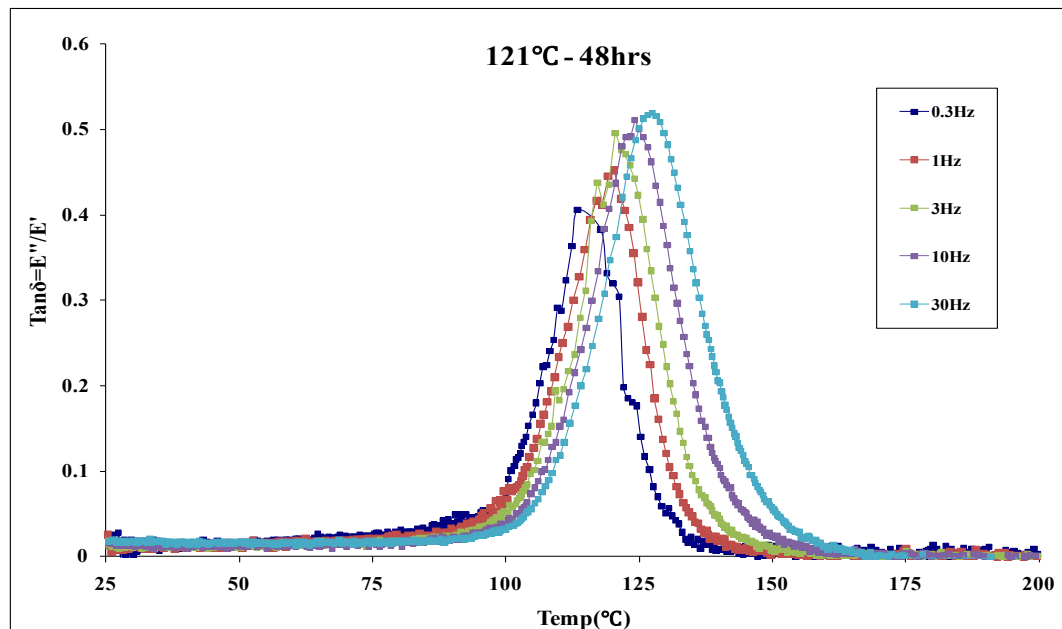


Figure 5-3: Height of tangent delta at different frequencies of test specimen exposed to 121°C for 4 hrs

Beside the method using the peak $\tan \delta$, glass transition temperature can be detected by the inflection point in the middle portion of the storage modulus profile. An analysis program of Rheometric Scientific Instruments Orchestrator can be used to detect the first derivative of the storage modulus curve, which is typically a parabolic curve. Analysis of the midpoint of the parabolic curve yields the glass transition temperature based on the storage modulus as shown in Figure 5-4. Glass transition temperatures obtained by storage modulus were lower than those of peak $\tan \delta$ in all conditions. Table 5-2 and Figure 5-5 show the comparison of glass transition temperatures determined by peak tangent delta at 1Hz and storage modulus on longitudinal and transverse test specimens. As the glass transition temperatures were increased due to post-cure effect, the differences between both values occurred. In this study, the values determined by peak $\tan \delta$ at 1Hz will be used as a representative glass

transition temperature. The reason why 1Hz values were used is that these values are close to the glass transition temperatures determined by other widely used methods such as Differential Scanning Calorimetry (DSC), dilatometry, and Thermomechanical Analysis (TMA).

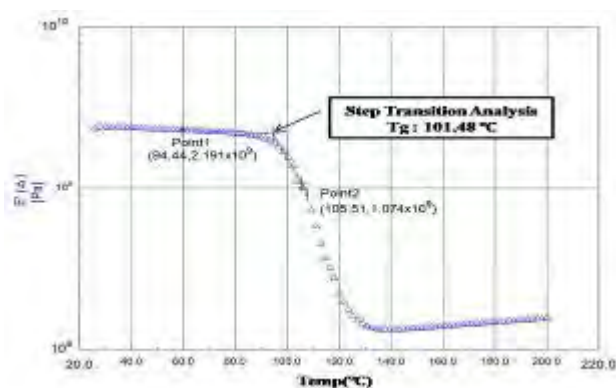


Figure 5-4: Schematic diagram for detecting the glass transition temperature from storage modulus (Exposure temperature: 93°C, Ageing time: 72hr)

Table 5-2 Comparison of glass transition temperatures determined by peak of tangent delta at 1Hz and storage modulus from longitudinal and transverse test specimens

Exposure Temperature	Time	T _g (°C)- Longitudinal		T _g (°C)- Transverse		Exposure Temperature	T _g (°C)- Longitudinal		T _g (°C)- Transverse	
		1Hz	E'	1Hz	E'		1Hz	E'	1Hz	E'
Ambient (23°C)	0	68.55	60.35	68.66	61.11	66°C				
	1	68.75	57.46	69.53	60.50		85.73	80.12	82.68	72.53
	2	68.64	68.15	66.90	58.54		84.27	80.04	82.90	77.15
	4	69.29	62.19	67.95	60.00		90.85	83.43	90.38	78.12
	8	66.67	65.64	68.44	58.07		95.94	84.95	92.02	83.84
	16	68.95	62.15	68.95	59.54		96.80	88.64	97.71	89.66
	24	66.45	61.25	69.64	60.23		100.13	90.54	96.08	88.31
	48	67.84	60.54	71.95	59.54		97.77	91.12	99.57	90.74
	72	68.82	61.16	68.08	60.12		100.12	92.34	104.01	93.06
93°C	1	93.09	91.07	93.86	87.50	121°C	103.08	97.07	106.88	100.15
	2	99.00	89.31	106.02	95.12		104.05	101.74	106.81	101.25
	4	104.49	98.87	106.59	101.46		113.84	105.12	113.14	105.34
	8	106.81	100.12	108.91	99.98		117.32	108.81	115.47	105.44
	16	107.50	103.58	111.53	102.70		113.83	105.40	113.10	104.86
	24	111.46	104.58	111.50	104.57		115.30	107.07	113.97	102.54
	48	113.89	106.31	115.19	104.64		120.24	111.84	118.25	107.62
	72	114.41	105.41	115.40	103.16		120.85	110.84	119.59	107.19
149°C	1	115.56	106.54	112.40	104.56	177°C	113.47	100.03	110.14	102.95
	2	117.60	109.64	118.40	106.30		113.53	102.45	113.91	104.43
	4	117.18	108.64	119.74	106.62		113.90	99.62	112.08	101.24
	8	115.48	103.05	115.81	106.24		112.74	103.33	112.77	101.99
	16	121.17	112.25	120.80	109.07		114.60	101.36	114.02	103.27
	24	110.23	101.58	115.55	103.20		112.26	101.41	114.42	101.19
	48	113.21	103.85	115.49	104.14		112.97	103.44	109.12	100.00
	72	113.41	103.89	112.93	102.34		110.45	98.97	112.70	99.87
204°C	1	113.08	102.22	109.34	101.21	232°C	112.91	100.00	111.39	105.90
	2	112.70	101.97	112.43	101.70		107.78	97.72	107.42	97.87
	4	109.19	100.01	109.67	102.06		108.56	97.98	109.88	98.90
	8	111.92	100.00	110.36	100.00		103.43	97.07	101.63	90.66
	16	110.00	96.36	108.63	98.52		98.73	83.24	96.70	82.95
	24	107.75	96.71	106.63	97.17		96.37	71.55	90.35	78.85
	48	102.04	86.61	104.37	95.51		90.57	68.20	84.74	80.27
	72	105.64	90.04	100.69	88.58		87.61	65.43	80.16	73.74
260°C	1	103.40	99.48	107.42	97.40					
	2	99.30	89.72	98.70	87.91					
	4	88.96	76.81	88.85	79.84					
	8	71.23	59.27	80.74	65.17					
	16	72.24	52.02	74.88	52.63					
	24	71.53	49.06							

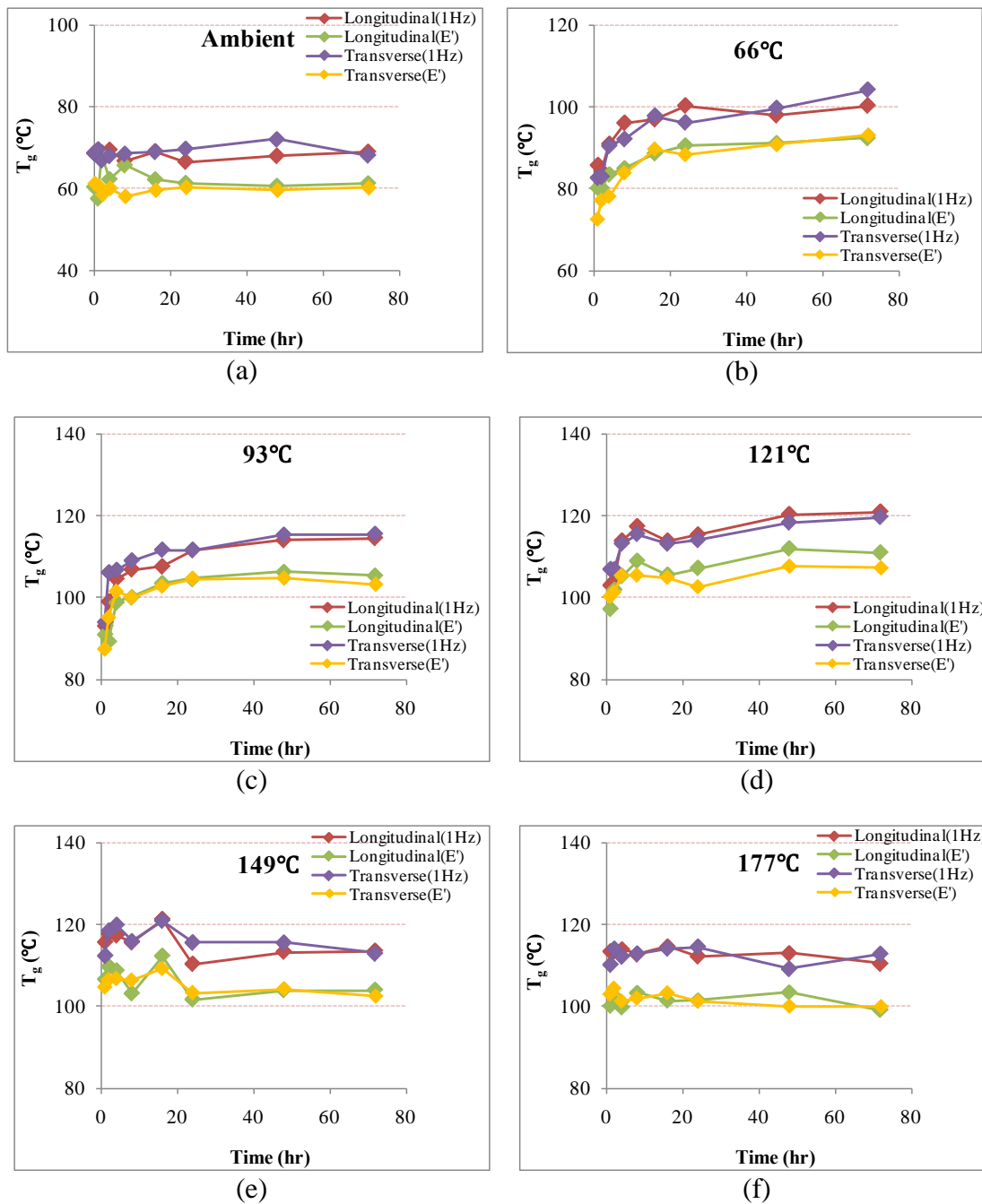


Figure 5-5: Difference in T_g based on peak tangent delta at 1Hz and storage modulus as a function of time at fixed temperatures, (a) ambient (b) 66°C (c) 93°C (d) 121°C (e) 149°C (f) 177°C (g) 204°C (h) 232°C (i) 260°C

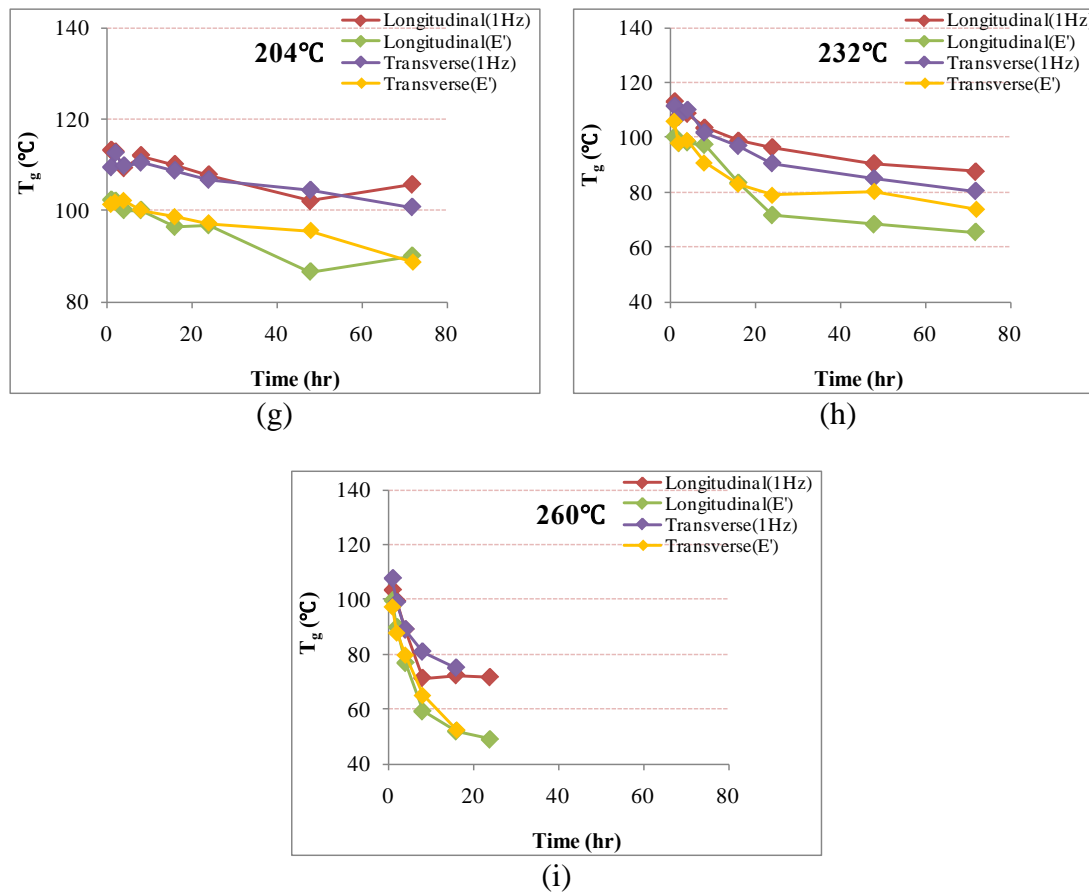


Figure 5-5: Continued

5.1.3.2 Height of Tangent Delta

The $\tan \delta$ curve provides information about the ability of a material to lose energy due to molecular rearrangements and internal friction. Moreover, this value reflects the energy dissipation ratio during dynamic strain cycles, and is relevant to the amount of epoxy chain segments undergoing the glass transition.

The storage modulus moved to higher temperature range without changing the shape or slope of change between elastic and viscoelastic region as shown in Figure 5-6.

In addition, the loss modulus shifted to higher temperatures and the level of the peak loss modulus also was increased with increase in test frequency as depicted in Figure 5-7. As described in data reduction section of chapter 5, since the $\tan \delta$ is the ratio of the loss modulus to the storage modulus, the values of $\tan \delta$ and glass transition temperatures shifted to higher levels with increase in test frequency as shown in Table 5-1.

The height of the $\tan \delta$ curve is related to interfacial adhesion performance[65]. An increase in damping loss is correlated to a loss in interfacial adhesion since perfect bonding between fibers and matrix restrict the mobility of the polymer structure, leading to a rapid response when a load is applied. Therefore, as the fiber/matrix bond performance increase, the height of peak $\tan \delta$ decreases. In other words, in case post-cure effect contributes to increase of interfacial bonding, broadened transition region and decreased $\tan \delta$ value are observed due to the stiffness or rigid of test specimen. Table 5-3 and Figure 5-8 show the variation of the height of peak $\tan \delta$ at different frequencies as a function of ageing time for both longitudinal and transverse specimens. All specimens exposed to ambient temperature showed higher height of peak $\tan \delta$ compared to other conditions. This phenomenon was attributed to increase of mobility since fully-cure was not applied for specimens. In ranges of lower exposure temperatures, the heights of peak $\tan \delta$ continued to decrease up to 72 hrs of ageing time due to residual post-cure effect. During the thermooxidative process occur, initially, the small molecules will diffuse out and evaporate into air, and the residual post-cure effect will be occurred leading to high crosslinkage. All those reactions definitely reduce epoxy segments undergoing the glass transitions, responsible for the abrupt depression

of the height of $\tan \delta$ peak.

Figure 5-9 shows comparison of the height of tangent delta at 1Hz on longitudinal and transverse test specimens as a function of time at fixed temperatures. From this figure, the heights of peak $\tan \delta$ on specimens in transverse direction were extremely higher than in longitudinal direction. The reason why the transverse specimens showed $\tan \delta$ peaks of higher value compared to the longitudinal specimens is that fibers in longitudinal specimen result in the interruption of mobility on specimens when a load is applied.

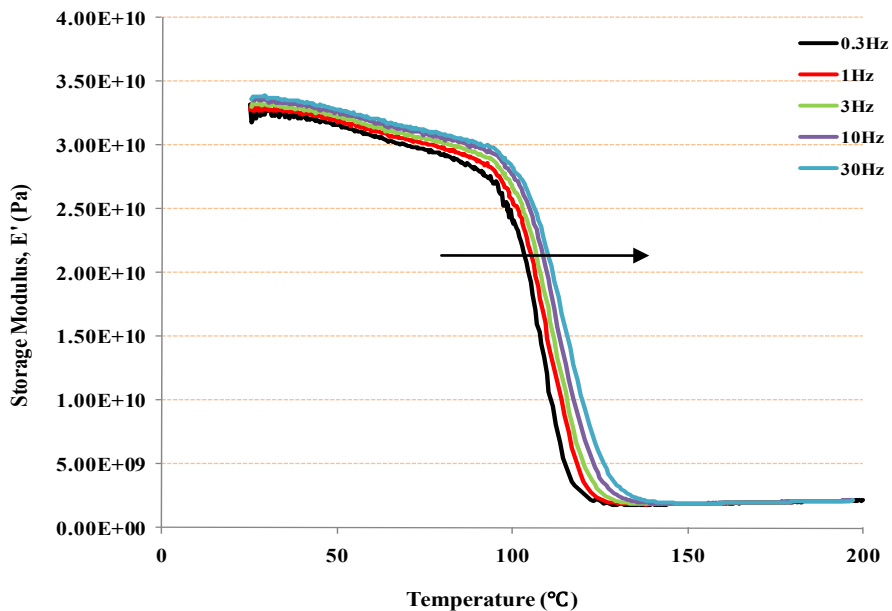


Figure 5-6: Effect of test frequency on storage modulus (specimen exposed to 121 $^{\circ}\text{C}$ for 4 hrs)

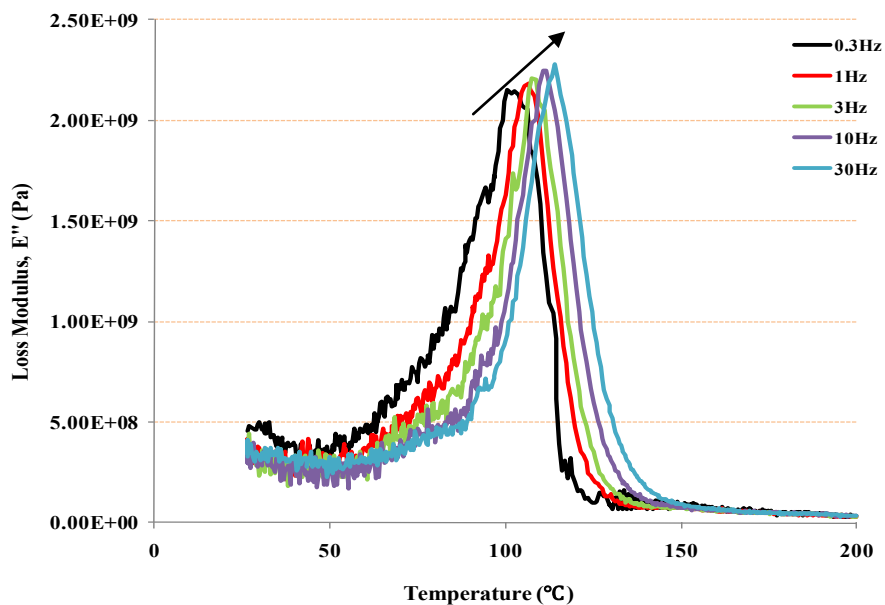


Figure 5-7: Effect of test frequency on loss modulus (specimen exposed to 121 $^{\circ}\text{C}$ for 4 hrs)

Table 5-3: Height of tangent delta at the different frequencies on longitudinal and transverse test specimens after exposure to elevated temperatures

Exposure temperature	Time	Height of tangent delta -Longitudinal					Height of tangent delta -Transverse				
		0.3Hz	1Hz	3Hz	10Hz	30Hz	0.3Hz	1Hz	3Hz	10Hz	30Hz
Ambient (23°C)	0	0.633	0.825	0.760	0.729	0.714	0.821	0.847	0.913	0.878	0.928
	1	0.598	0.645	0.601	0.578	0.588	0.945	1.060	0.945	0.986	1.004
	2	0.624	0.631	0.609	0.603	0.600	1.064	0.944	1.043	1.023	1.057
	4	0.648	0.664	0.724	0.760	0.761	0.880	0.901	0.948	0.972	0.984
	8	0.585	0.634	0.699	0.703	0.718	0.871	0.894	0.934	1.071	1.111
	16	0.615	0.649	0.683	0.685	0.698	0.887	0.900	0.925	0.965	1.025
	24	0.641	0.693	0.713	0.731	0.728	0.900	0.902	0.915	0.925	0.953
	48	0.598	0.603	0.661	0.665	0.665	0.791	0.800	0.805	0.830	0.864
72	0.625	0.645	0.687	0.704	0.699	0.785	0.792	0.817	0.858	0.909	
66°C	1	0.634	0.737	0.680	0.701	0.776	0.854	0.955	0.993	0.954	0.950
	2	0.665	0.687	0.708	0.697	0.688	0.796	0.871	0.876	0.883	0.892
	4	0.612	0.608	0.622	0.646	0.639	0.712	0.784	0.780	0.774	0.815
	8	0.568	0.581	0.592	0.596	0.682	0.832	0.865	0.850	0.861	0.866
	16	0.565	0.590	0.571	0.583	0.586	0.710	0.728	0.795	0.793	0.804
	24	0.585	0.575	0.583	0.579	0.582	0.761	0.835	0.878	0.886	0.895
	48	0.591	0.609	0.615	0.614	0.603	0.685	0.719	0.765	0.814	0.835
	72	0.595	0.570	0.619	0.634	0.632	0.583	0.657	0.672	0.684	0.757
93°C	1	0.449	0.454	0.481	0.458	0.461	0.701	0.730	0.693	0.698	0.754
	2	0.490	0.526	0.551	0.547	0.548	0.654	0.664	0.611	0.644	0.666
	4	0.436	0.448	0.457	0.459	0.477	0.624	0.647	0.633	0.658	0.686
	8	0.521	0.546	0.545	0.545	0.546	0.642	0.684	0.680	0.665	0.687
	16	0.455	0.467	0.479	0.500	0.512	0.586	0.611	0.625	0.633	0.653
	24	0.471	0.489	0.537	0.546	0.552	0.602	0.655	0.655	0.641	0.659
	48	0.487	0.443	0.466	0.489	0.494	0.596	0.616	0.623	0.633	0.660
	72	0.442	0.460	0.460	0.491	0.507	0.661	0.538	0.560	0.577	0.633
121°C	1	0.512	0.537	0.542	0.556	0.566	0.571	0.590	0.623	0.647	0.694
	2	0.501	0.549	0.523	0.514	0.520	0.602	0.638	0.691	0.688	0.708
	4	0.492	0.501	0.540	0.561	0.575	0.569	0.631	0.667	0.677	0.713
	8	0.441	0.446	0.483	0.501	0.508	0.552	0.610	0.644	0.664	0.698
	16	0.461	0.486	0.538	0.551	0.560	0.581	0.605	0.620	0.631	0.662
	24	0.469	0.504	0.513	0.553	0.568	0.508	0.551	0.587	0.595	0.660
	48	0.450	0.452	0.496	0.512	0.520	0.602	0.636	0.627	0.659	0.689
	72	0.505	0.529	0.519	0.544	0.562	0.636	0.667	0.679	0.673	0.714
149°C	1	0.475	0.496	0.530	0.557	0.570	0.631	0.654	0.646	0.652	0.691
	2	0.433	0.455	0.471	0.493	0.537	0.625	0.642	0.679	0.695	0.730
	4	0.481	0.506	0.552	0.566	0.579	0.625	0.633	0.646	0.657	0.692
	8	0.459	0.461	0.480	0.514	0.527	0.635	0.648	0.691	0.682	0.716
	16	0.501	0.518	0.518	0.562	0.570	0.591	0.617	0.630	0.656	0.709
	24	0.446	0.460	0.444	0.458	0.414	0.646	0.679	0.715	0.737	0.775
	48	0.501	0.514	0.525	0.524	0.538	0.640	0.672	0.683	0.656	0.693
	72	0.538	0.438	0.475	0.474	0.476	0.528	0.571	0.559	0.568	0.593

Table 5-3: Continued

Exposure Temperature	Time	Height of tangent delta -Longitudinal					Height of tangent delta -Transverse				
		0.3Hz	1Hz	3Hz	10Hz	30Hz	0.3Hz	1Hz	3Hz	10Hz	30Hz
177°C	1	0.495	0.514	0.526	0.531	0.544	0.621	0.638	0.618	0.640	0.665
	2	0.452	0.470	0.483	0.508	0.515	0.627	0.674	0.690	0.695	0.722
	4	0.462	0.476	0.471	0.481	0.502	0.650	0.653	0.671	0.726	0.756
	8	0.394	0.403	0.422	0.443	0.437	0.641	0.680	0.672	0.674	0.700
	16	0.390	0.416	0.421	0.425	0.434	0.433	0.453	0.465	0.453	0.473
	24	0.446	0.464	0.455	0.462	0.448	0.417	0.420	0.435	0.445	0.459
	48	0.358	0.367	0.392	0.406	0.422	0.359	0.344	0.346	0.355	0.366
	72	0.341	0.375	0.400	0.412	0.404	0.292	0.303	0.302	0.308	0.319
204°C	1	0.508	0.515	0.515	0.551	0.556	0.645	0.657	0.716	0.752	0.786
	2	0.418	0.439	0.451	0.446	0.454	0.581	0.597	0.601	0.603	0.626
	4	0.370	0.389	0.412	0.431	0.439	0.381	0.398	0.412	0.418	0.427
	8	0.345	0.354	0.376	0.380	0.387	0.327	0.359	0.353	0.352	0.365
	16	0.338	0.345	0.353	0.395	0.388	0.336	0.342	0.351	0.348	0.350
	24	0.319	0.306	0.317	0.326	0.333	0.324	0.334	0.332	0.330	0.361
	48	0.280	0.300	0.289	0.296	0.299	0.302	0.313	0.302	0.303	0.301
	72	0.294	0.314	0.326	0.340	0.341	0.301	0.312	0.300	0.301	0.300
232°C	1	0.385	0.394	0.408	0.425	0.428	0.519	0.534	0.542	0.534	0.592
	2	0.364	0.375	0.389	0.403	0.413	0.402	0.414	0.451	0.433	0.442
	4	0.345	0.358	0.362	0.377	0.386	0.332	0.363	0.367	0.372	0.378
	8	0.365	0.382	0.398	0.410	0.421	0.352	0.372	0.374	0.367	0.372
	16	0.385	0.407	0.412	0.395	0.409	0.378	0.389	0.375	0.362	0.342
	24	0.320	0.331	0.314	0.315	0.315	0.417	0.444	0.422	0.413	0.407
	48	0.305	0.323	0.332	0.325	0.329	0.313	0.334	0.332	0.329	0.329
	72	0.344	0.364	0.376	0.378	0.376	0.353	0.347	0.359	0.358	0.354
260°C	1	0.369	0.379	0.397	0.401	0.403	0.481	0.476	0.477	0.521	0.524
	2	0.475	0.477	0.520	0.517	0.518	0.470	0.474	0.470	0.463	0.466
	4	0.462	0.464	0.484	0.502	0.500	0.466	0.471	0.503	0.523	0.548
	8	0.525	0.545	0.568	0.568	0.557	0.409	0.403	0.386	0.390	0.397
	16	0.516	0.530	0.492	0.488	0.484	0.432	0.460	0.454	0.447	0.457
	24	0.534	0.536	0.503	0.488	0.483					

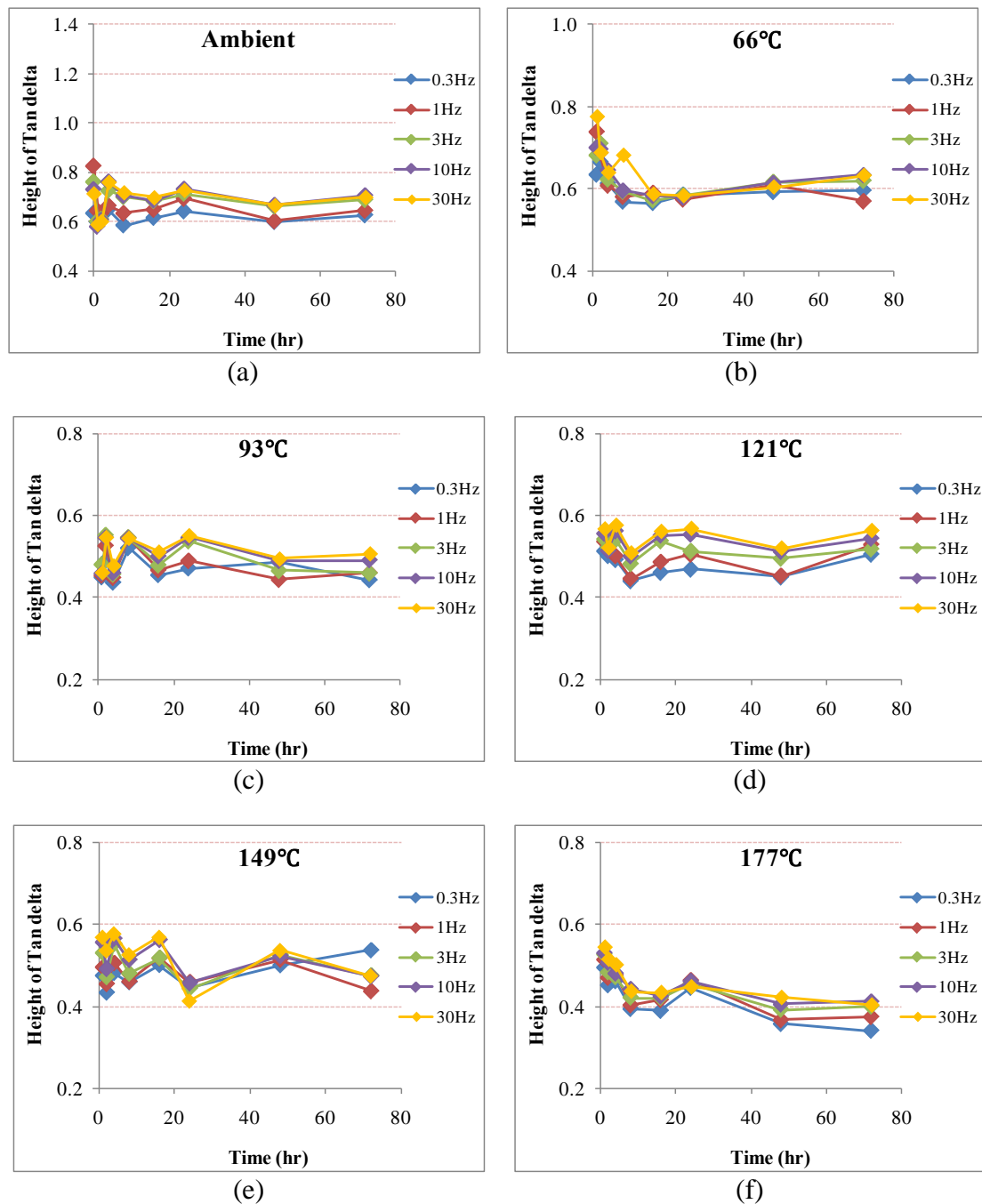


Figure 5-8: Difference of the peak of tangent delta at different frequencies on longitudinal test specimens as a function of time at fixed temperatures, (a) ambient (b) 66°C (c) 93°C (d) 121°C (e) 149°C (f) 177°C (g) 204°C (h) 232°C (i) 260°C

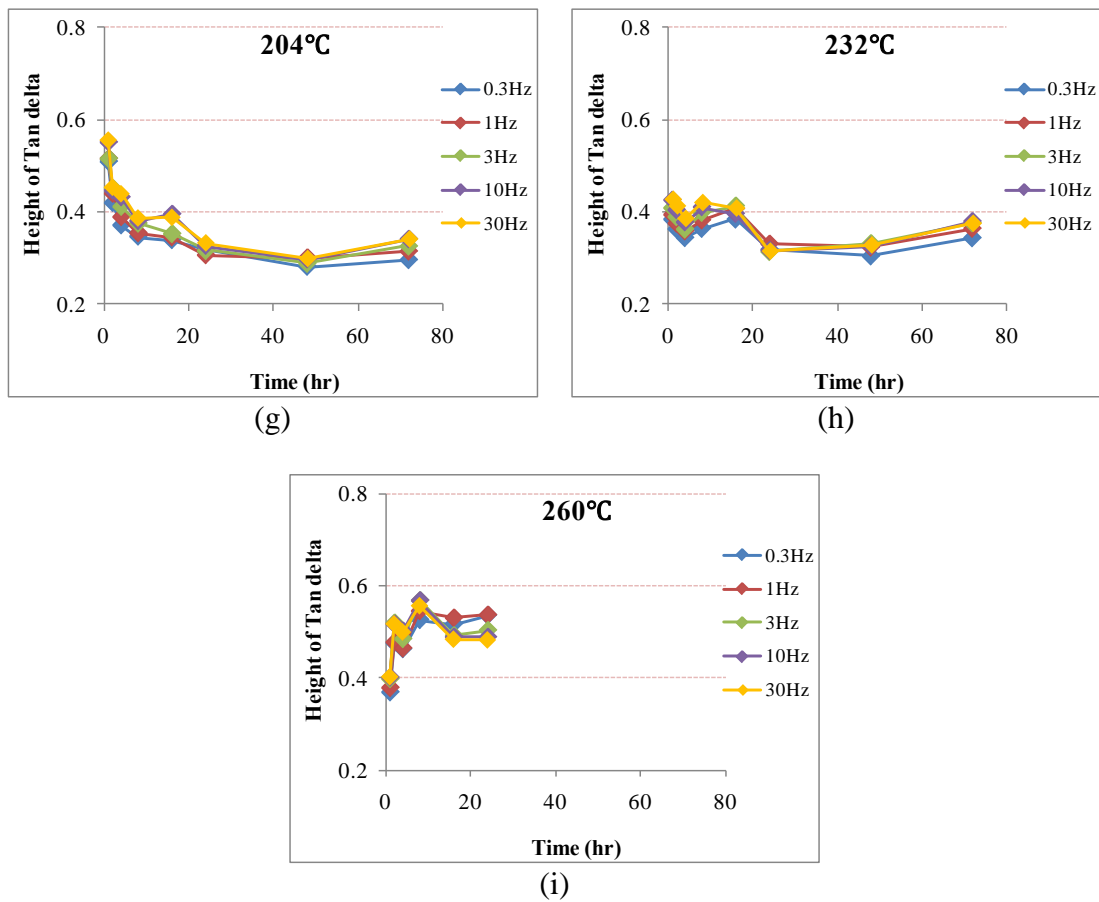


Figure 5-8: Continued

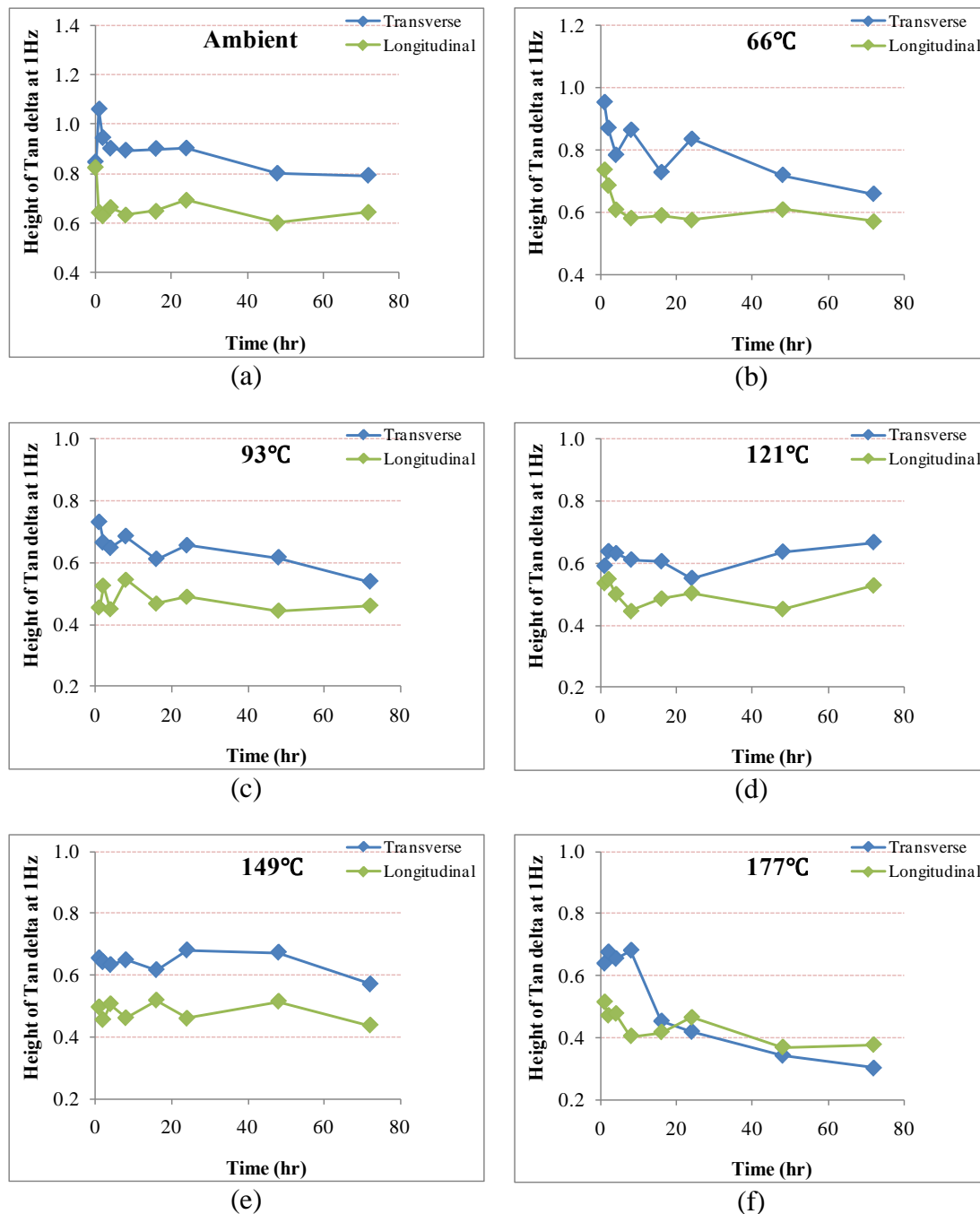


Figure 5-9: Comparison of the height of tangent delta at 1Hz from longitudinal and transverse test specimens as a function of time at fixed temperatures, (a) ambient (b) 66°C (c) 93°C (d) 121°C (e) 149°C (f) 177°C (g) 204°C (h) 232°C (i) 260°C

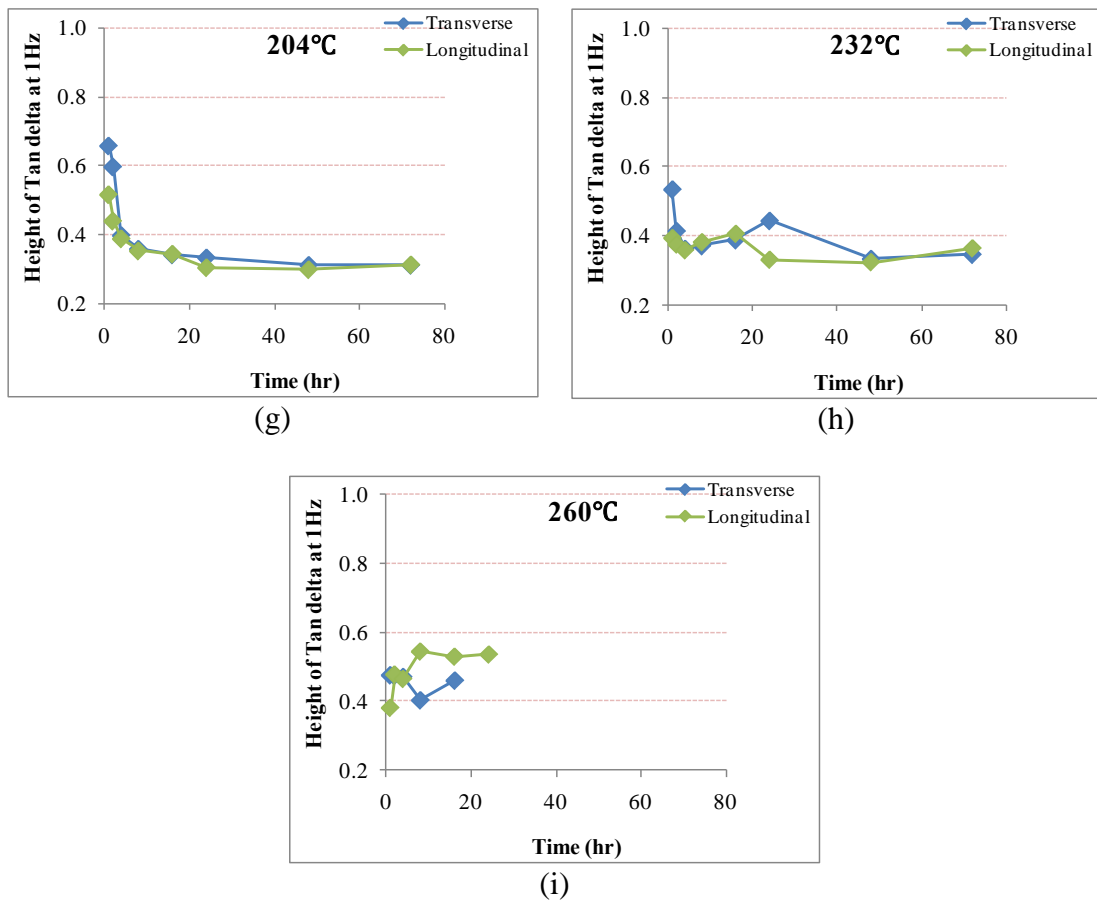


Figure 5-9: Continued

5.1.3.3 Activation Energy

The activation energy (ΔE_a) for glass transition can be obtained from the relationship between the shift of glass transition temperature and test frequency. The glass transition temperature reflects the relationship between the mobility of polymer chains and temperature while ΔE_a represents a relationship between mobility and time scale[39]. In addition, ΔE_a could be characterized as representing the energy barrier of glass transition relaxation.

Activation energy of the glass transition is calculated by Arrhenius relationship (time-temperature superposition principles) using superimposing either peak $\tan \delta$ or E'' determined over a range of frequencies.

$$f = Ae^{-(\Delta E_a/RT)} \quad (5.4)$$

where:

f = the frequency applied for DMTA test

A = a constant as the pre-exponent

R = universal gas constant

T = temperature at peak $\tan \delta$

The shift of glass transition temperatures can be related to the different frequencies from following equation.

$$\frac{f_1}{f_2} = \frac{e^{-(\Delta E_a/RT_{g1})}}{e^{-(\Delta E_a/RT_{g2})}} \quad (5.5)$$

Where:

f_1 and f_2 are corresponding values of the glass transition temperature T_{g1} and T_{g2} ,

respectively. Equation 5.5 can simply be changed as

$$\Delta E_a = -R \left[\frac{d(\ln f)}{d\left(\frac{1}{T_g}\right)} \right] \quad (5.6)$$

The value of ΔE_a can be found by plotting the natural logarithm of the frequency against the reciprocal of the glass transition temperature. Consequently, ΔE_a is yielded by multiple of the slope of curve and the universal gas constant. Activation energies are summarized on longitudinal and transverse specimens in Table 5-4 and Figure 5-10 shows comparison of the activation energy on longitudinal and transverse test specimens as a function of time at fixed temperatures.

Activation energies were continuously increased up to 72 hrs of ageing time in the ranges of lower exposure temperatures (66, 93, 121 and 149°C) Continuous increases were attributed to residual post-cure effect, which led to an intense crosslinkage and the mobility of the polymer segment was constrained significantly. In ranges of intermediate temperatures (177, 204 and 232°C), activation energies were leveled off after initially reaching to the maximum value. In light of level off, since the breakage of polymer crosslinkage was responsible for shifting easily to glass transition as the exposure temperature and ageing time were increased, activation energies were decreased. As expected, activation energies in higher exposure temperature (260°C) were catastrophically decreased in ageing time of more than 8 hrs.

Moreover, the longitudinal specimens showed higher activation energy than the transverse specimens. It should be noted that the mobility of the epoxy matrix in the unidirectional specimens is interrupted by the fibers and require more energy for the

glass transition. As the fully cure was progressed, the differences on activation energy between the longitudinal and transverse specimens were more severe compared to unaged or insufficient- cured specimens.

Table 5-4 Activation energies using DMTA on longitudinal and transverse test specimens after exposure to elevated temperatures

Exposure Temperature	Time	Activation energy (KJ/mol)		Exposure Temperature	Time	Activation energy (KJ/mol)	
		Longitudinal	Transverse			Longitudinal	Transverse
Ambient (23°C)	0	379.36	321.45	66°C			
	1	372.74	338.67		1	343.69	354.96
	2	333.36	374.25		2	335.35	325.13
	4	349.16	302.45		4	333.65	337.99
	8	383.37	347.71		8	410.29	348.47
	16	386.10	298.45		16	374.91	397.43
	24	447.51	339.54		24	448.21	394.92
	48	408.25	340.03		48	445.14	386.96
	72	368.25	291.78		72	483.75	397.38
93°C	1	381.48	364.51	121°C	1	435.58	461.90
	2	485.46	442.33		2	457.79	458.08
	4	422.35	401.29		4	479.13	543.72
	8	421.33	554.35		8	422.03	539.04
	16	384.01	425.57		16	533.90	588.25
	24	527.36	548.54		24	547.79	516.74
	48	520.79	515.99		48	520.83	541.06
	72	546.69	578.34		72	465.99	542.34
149°C	1	476.69	420.28	177°C	1	451.60	455.81
	2	518.18	437.92		2	390.80	472.61
	4	486.95	500.76		4	549.22	498.93
	8	484.50	539.56		8	477.83	386.07
	16	481.37	511.31		16	548.73	504.24
	24	493.71	516.27		24	475.25	565.73
	48	491.84	521.90		48	455.92	423.07
	72	511.35	432.74		72	488.44	446.08
204°C	1	524.85	479.24	232°C	1	508.09	487.98
	2	584.87	486.09		2	511.23	409.92
	4	499.78	435.69		4	442.32	354.50
	8	559.46	481.02		8	475.45	287.67
	16	561.32	373.18		16	488.17	275.66
	24	493.64	298.05		24	483.42	289.38
	48	421.74	313.00		48	424.63	259.42
	72	416.47	300.67		72	486.28	231.67
260°C	1	460.74	393.17				
	2	463.07	405.91				
	4	531.03	275.55				
	8	244.83	270.15				
	16	254.18	265.68				
	24	229.14					

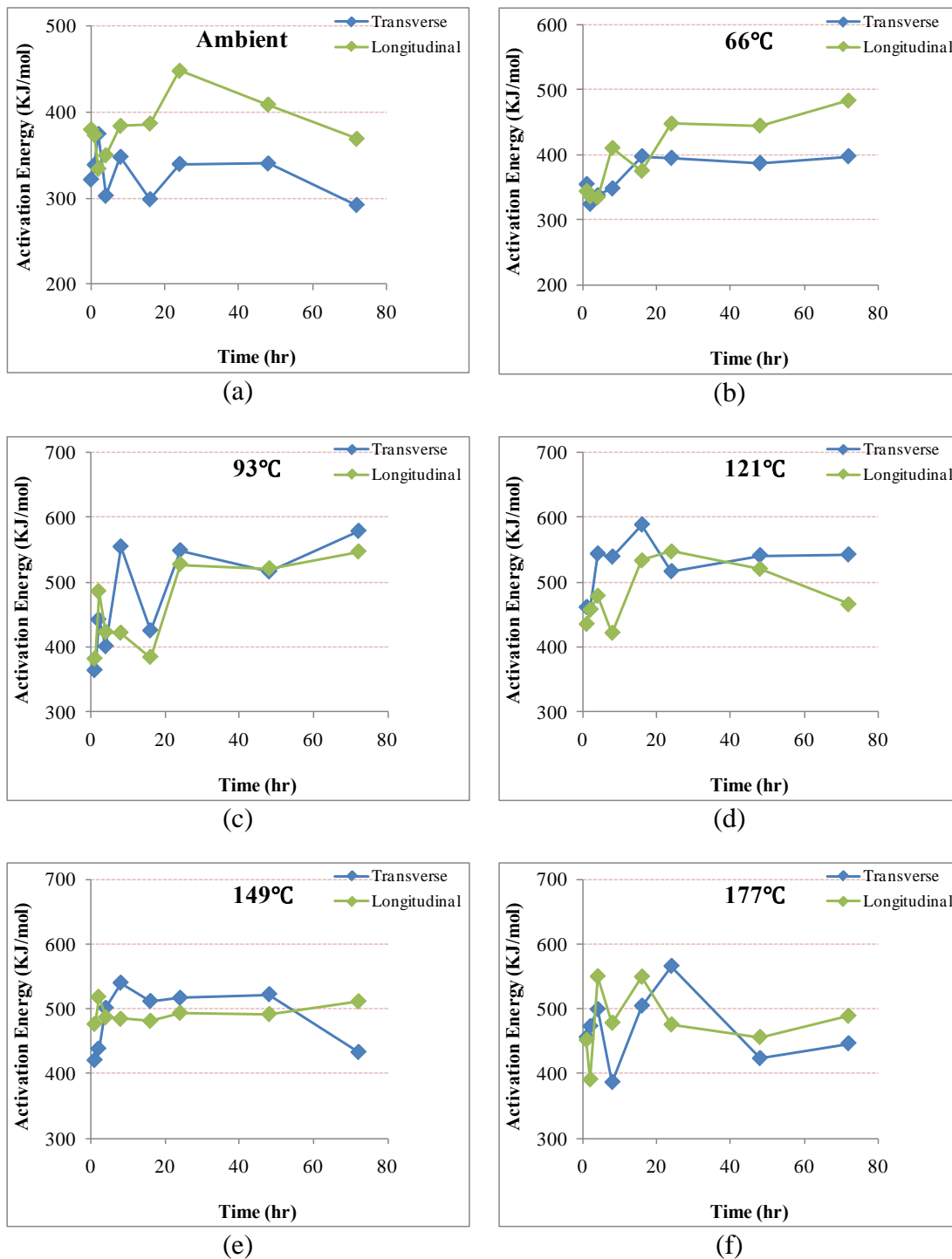
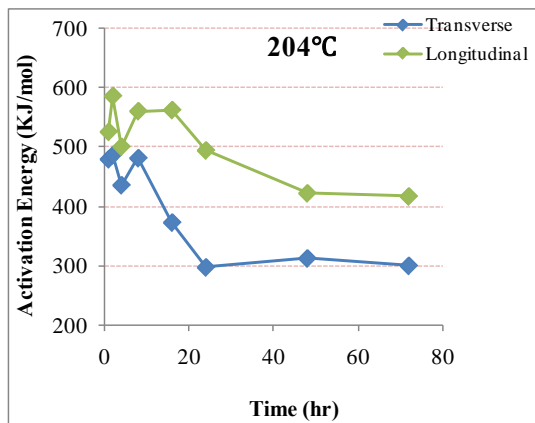
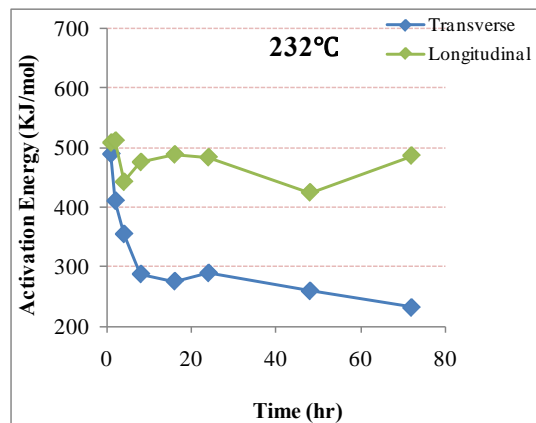


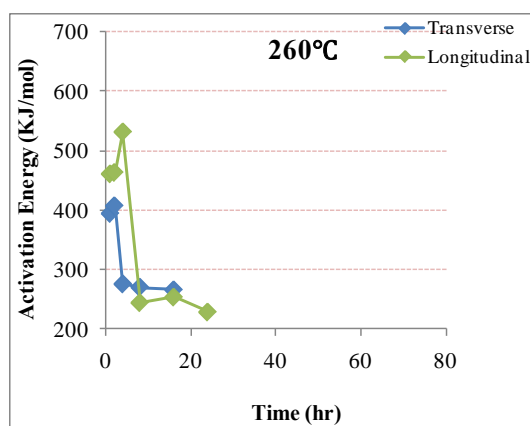
Figure 5-10: Comparison of the activation energies on longitudinal and transverse test specimens as a function of time at fixed temperatures, (a) ambient (b) 66°C (c) 93°C (d) 121°C (e) 149°C (f) 177°C (g) 204°C (h) 232°C (i) 260°C



(g)



(h)



(i)

Figure 5-10: Continued

5.1.3.4 Modulus

Storage modulus or elastic modulus (E') means, as mentioned previously, the ability of a material to store energy or the elasticity of a composite materials. It is well known that the value of the initial storage modulus is determined as $T_g-50^\circ\text{C}$ following bounds from T_g suggested by Fraga et al[66]. In this investigation, the initial storage modulus is considered as the storage modulus of $T_g-40^\circ\text{C}$ Initial storage modulus increases with degree of cross-linking and molecular weight, with post-cure not only causing a higher modulus and increased brittleness, but also stronger interfacial bonds, which result in an increase in the storage modulus as well[67]. Due to post cure effect, the values of initial storage modulus were increased in the ranges of the exposure temperature and ageing time showing higher glass transition temperatures as shown in Table 5-5. The rubber plateau region of the storage modulus is taken into account to determine the extent of chemical change occurring within the composite materials. The rubbery modulus (E'_r) was determined as values of the storage modulus at a position of $T_g+40^\circ\text{C}$ These values are taken as rubbery modulus to ensure that the asymptotic value is measured well away from the transition region. The rubbery modulus (E'_r) at a position of $T_g+40^\circ\text{C}$ are also tabulated in Table 5-5. It is known that the rubber plateau is related by the degree of crystallinity in a composite material.

A number of relationships have been developed between molecular weight and mechanical properties, as well as for unfilled polymers relating T_g to molecular weight and degree of cross-linking[68]. Therefore, it is necessary to consider changes at the level of average inter-crosslink molecular weight which is directly proportional to the ratio of materials density and cross-link density. The intercrosslink molecular weight

(M_c) can be calculated according to a method proposed by De'Neve and Shanahan[69].

The average inter-crosslink molecular weight can be expressed as:

$$M_c = \frac{3RT\rho}{E_M} \quad (5.7)$$

where:

E_M = the modulus of the polymer in the rubbery state

R = universal gas constant (8.3143J/mol^oK)

T = the temperature in the absolute scale at which the modulus was measured

ρ = the density of polymer

The rubbery modulus (E'_r) can be simplified by a rule of mixture,

$$E'_r = \frac{E_m E_f}{V_f E_m + (1 - V_f) E_f} \quad (5.8)$$

where E_f and E_m are the modulus of the fiber and matrix, respectively. If assuming that $E_f \gg E_m$, from Equation 5.7 and 5.8, a relationship between average inter-crosslink molecular weight and the rubbery modulus can be obtained by following equation,

$$M_c = \frac{3\rho RT}{(1 - V_f) E'_r} \quad (5.9)$$

In order to calculate inter-crosslink molecular weight, following values were used.

T = the temperature in Kelvin (T_g based on tan delta at 1Hz+40^oC)

V_f = volume fraction determined by tension test

E'_r = the rubber modulus corresponding to the temperature at T_g based on tan delta at 1Hz+40^oC

Table 5-5 also shows normalized inter-crosslink molecular weight obtained from

dividing inter-crosslink molecular weight on unaged specimen by cases on aged specimens as a function of temperature and time. Normalized inter-crosslink molecular weights on longitudinal test specimens as a function of time at fixed temperatures are represented in Figure 5-11. Except for the conditions of ambient temperature and high temperatures (232 and 260°C), the majority of normalized inter-crosslink molecular weights showed $M_c/(M_c)_{time} < 1$ due to residual post-cure effect. Since fully curing did not occur in ambient temperature and thermal oxidation and degradation in the ranges of severe exposure temperatures led to chain scission and breakage, normalized inter-crosslink weights showed $M_c/(M_c)_{time} > 1$.

Table 5-5 Storage modulus at $T_g \pm 40^\circ\text{C}$ and normalized inter-crosslink molecular weight from longitudinal and transverse specimens

Exposure Temperature	Time	Longitudinal (Pa)		Transverse (Pa)		Normalized inter-crosslink molecular weight	
		$T_g-40^\circ\text{C}$	$T_g+40^\circ\text{C}$	$T_g-40^\circ\text{C}$	$T_g+40^\circ\text{C}$	longitudinal	Transverse
		E'	E'	E'	E'		
Ambient (23°C)	1	4.4E+10	4.4E+09	3.96E+10	3.96E+09	1.105	0.906
	2	4.66E+10	4.66E+09	4.2E+10	4.2E+09	0.993	0.894
	4	4.14E+10	4.14E+09	3.73E+10	3.73E+09	1.032	1.020
	8	4.08E+10	4.08E+09	3.67E+10	3.67E+09	1.083	1.075
	16	4.26E+10	4.26E+09	3.84E+10	3.84E+09	1.007	1.140
	24	4.13E+10	4.13E+09	3.72E+10	3.72E+09	0.998	1.155
	48	4.29E+10	4.29E+09	3.86E+10	3.86E+09	0.984	1.185
	72	4.16E+10	4.16E+09	3.75E+10	3.75E+09	1.128	1.262
66°C	1	5.23E+10	6.02E+09	4.6E+10	5.29E+09	0.743	0.682
	2	5.28E+10	6.07E+09	4.64E+10	5.34E+09	0.741	0.683
	4	5.92E+10	6.81E+09	5.21E+10	5.99E+09	0.755	0.698
	8	5.74E+10	6.6E+09	5.05E+10	5.81E+09	0.831	0.761
	16	5.28E+10	6.07E+09	4.64E+10	5.34E+09	1.008	0.934
	24	5.19E+10	5.96E+09	4.56E+10	5.25E+09	0.881	0.807
	48	4.98E+10	5.72E+09	4.38E+10	5.04E+09	0.803	0.746
	72	4.79E+10	5.51E+09	4.22E+10	4.85E+09	0.873	0.815
93°C	1	4.28E+10	5.35E+09	3.68E+10	4.6E+09	0.927	0.879
	2	4.61E+10	5.76E+09	3.97E+10	4.96E+09	0.901	0.867
	4	4.1E+10	5.12E+09	3.52E+10	4.4E+09	0.891	1.040
	8	3.87E+10	4.83E+09	3.32E+10	4.16E+09	0.875	1.118
	16	3.8E+10	4.75E+09	3.26E+10	4.08E+09	0.865	1.203
	24	3.86E+10	4.82E+09	3.32E+10	4.15E+09	0.832	1.199
	48	4.14E+10	5.18E+09	3.56E+10	4.45E+09	0.801	1.048
	72	4.21E+10	5.26E+09	3.62E+10	4.53E+09	0.813	0.930
121°C	1	4.63E+10	6.48E+09	3.94E+10	5.51E+09	0.754	0.729
	2	4.56E+10	6.38E+09	3.88E+10	5.43E+09	0.815	0.786
	4	4.34E+10	6.08E+09	3.69E+10	5.17E+09	0.857	0.820
	8	4.45E+10	6.23E+09	3.78E+10	5.3E+09	0.742	0.708
	16	4.65E+10	6.51E+09	3.95E+10	5.53E+09	0.809	0.773
	24	4.28E+10	6E+09	3.64E+10	5.1E+09	0.833	0.795
	48	4.05E+10	5.66E+09	3.44E+10	4.81E+09	0.879	0.838
	72	4.18E+10	5.85E+09	3.55E+10	4.97E+09	0.787	0.751
149°C	1	4.16E+10	6.45E+09	3.45E+10	5.35E+09	0.786	0.765
	2	4.96E+10	7.68E+09	4.11E+10	6.38E+09	0.665	0.654
	4	4.2E+10	6.51E+09	3.48E+10	5.4E+09	0.794	0.783
	8	4.86E+10	7.53E+09	4.03E+10	6.25E+09	0.683	0.670
	16	4.38E+10	6.79E+09	3.64E+10	5.64E+09	0.736	0.721
	24	4.4E+10	6.82E+09	3.65E+10	5.66E+09	0.728	0.723
	48	4.25E+10	6.59E+09	3.53E+10	5.47E+09	0.745	0.734

	72	3.86E+10	5.99E+09	3.21E+10	4.97E+09	0.733	0.718
--	----	----------	----------	----------	----------	-------	-------

Table 5-5 Continued

Exposure Temperature	Time	Longitudinal (Pa)		Transverse (Pa)		Normalized inter-crosslink molecular weight	
		T _g -40°C	T _g +40°C	T _g -40°C	T _g +40°C	longitudinal	Transverse
		E'	E'	E'	E'		
177°C	1	3.93E+10	5.89E+09	3.34E+10	5.01E+09	0.897	0.852
	2	4.91E+10	7.36E+09	4.17E+10	6.25E+09	0.796	0.763
	4	3.92E+10	5.88E+09	3.33E+10	5E+09	0.867	0.827
	8	4.26E+10	6.39E+09	3.62E+10	5.44E+09	0.758	0.726
	16	4.01E+10	6.01E+09	3.41E+10	5.11E+09	0.762	0.729
	24	4.11E+10	6.17E+09	3.5E+10	5.25E+09	0.785	0.755
	48	4.15E+10	6.22E+09	3.53E+10	5.29E+09	0.763	0.724
	72	4.9E+10	7.36E+09	4.17E+10	6.25E+09	0.649	0.625
204°C	1	3.67E+10	4.96E+09	3.31E+10	4.46E+09	1.030	0.923
	2	4.42E+10	5.97E+09	3.98E+10	5.37E+09	0.824	0.745
	4	3.83E+10	5.17E+09	3.44E+10	4.65E+09	0.967	0.876
	8	4.44E+10	5.99E+09	3.99E+10	5.39E+09	0.885	0.798
	16	4E+10	5.4E+09	3.6E+10	4.86E+09	0.936	0.844
	24	4.07E+10	5.5E+09	3.66E+10	4.95E+09	0.896	0.808
	48	4.14E+10	5.59E+09	3.73E+10	5.03E+09	0.876	0.797
	72	4.27E+10	5.76E+09	3.84E+10	5.18E+09	0.872	0.780
232°C	1	4.34E+10	4.55E+09	3.99E+10	4.19E+09	1.203	1.061
	2	4.11E+10	4.32E+09	3.79E+10	3.97E+09	1.288	1.138
	4	4.27E+10	4.48E+09	3.93E+10	4.12E+09	1.114	0.988
	8	4.26E+10	4.48E+09	3.92E+10	4.12E+09	1.140	1.005
	16	4.53E+10	4.75E+09	4.16E+10	4.37E+09	0.977	0.860
	24	4.52E+10	4.75E+09	4.16E+10	4.37E+09	0.928	0.809
	48	4.21E+10	4.42E+09	3.87E+10	4.07E+09	0.999	0.871
	72	2.81E+10	2.95E+09	2.59E+10	2.72E+09	1.324	1.149
260°C	1	4.33E+10	3.89E+09	4.02E+10	3.62E+09	1.179	1.042
	2	4.29E+10	3.86E+09	3.99E+10	3.59E+09	1.260	1.102
	4	4.66E+10	4.19E+09	4.33E+10	3.9E+09	1.422	1.314
	8	2.31E+10	2.08E+09	2.15E+10	1.93E+09	1.971	1.767

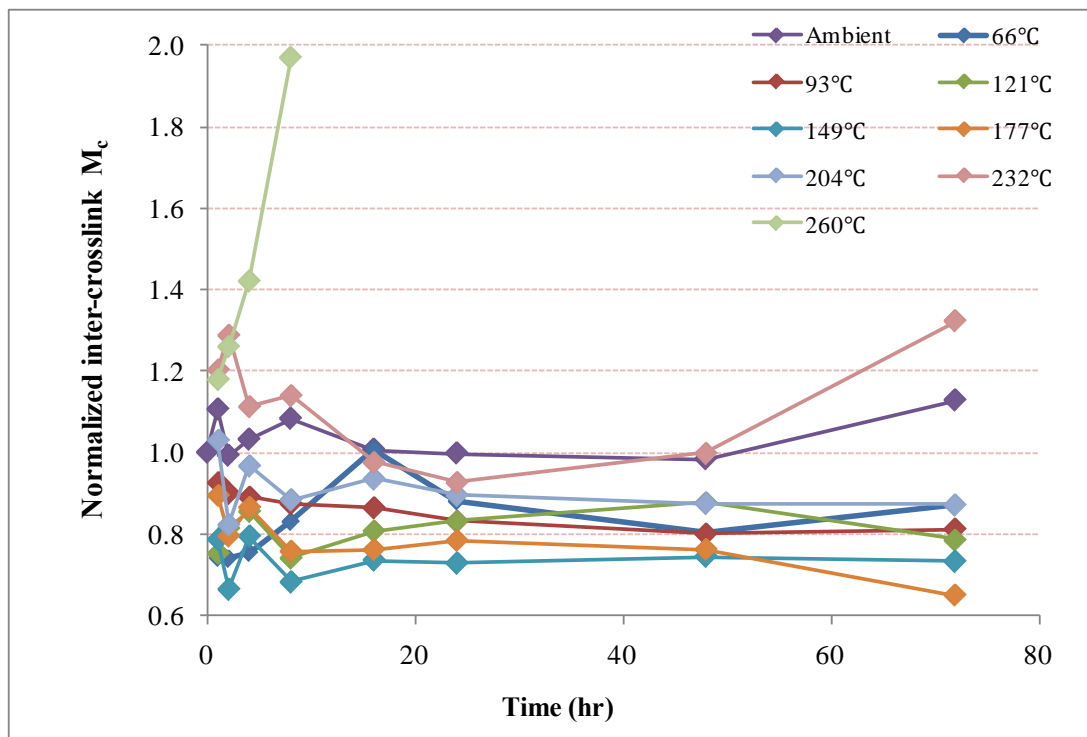


Figure 5-11: Normalized inter-crosslink molecular weights on longitudinal test specimens as a function of time at fixed temperatures

5.1.3.5 Mechanical Retention based on T_g

Mechanical properties are strongly dependent on glass transition temperature as shown in Figure 5-12. The retention of mechanical properties was enhanced with increasing glass temperatures. Tensile properties related to interfacial bond between fibers and matrix showed great enhancement due to post-cure effect compared to the properties of flexure, short beam shear and off-axis shear. As mentioned in off-axis shear test section, although glass transition temperatures increased, the distortion of test specimens caused by asymmetry led to deterioration of mechanical property. Mechanical properties on short beam shear test were slightly higher than those on flexural test in all test environments. It should be pointed out that tensile properties were rapidly and greatly increased in the ranges of lower exposure temperatures. On the other hand, if the glass transition reached the maximum due to fully curing, there was a little difference in mechanical properties such as tension, flexure and short beam shear. Therefore, glass transition temperatures can be crucial criterion to evaluate the mechanical properties on polymer-based composites.

Figure 5-13 shows the characterization of four mechanical properties in terms of strength retentions (%) as a function of glass transition temperatures determined by the peak of $\tan \delta$ at 1Hz. The majority of test data were distributed between 100°C and 120°C in glass transition temperature. Except for the exposure conditions of severe and ambient temperature and off-axis shear test, the enhancement of mechanical properties were attributed to increase of glass transition temperature. The reason why the retention of tensile properties has big variation is that tensile characteristic is greatly affected by defects created in process of hand wet layup.

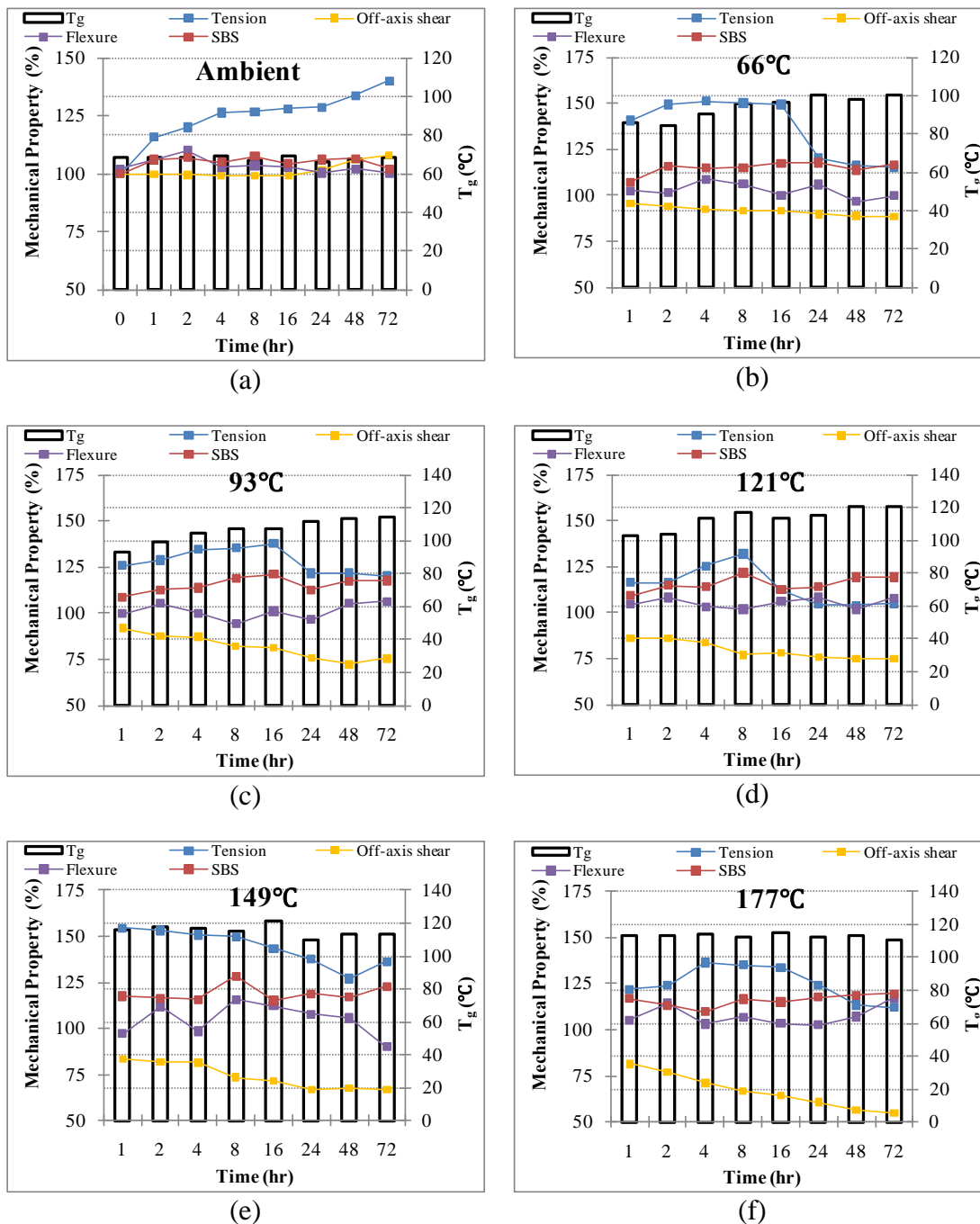


Figure 5-12: Mechanical properties versus glass transition temperatures on longitudinal and transverse test specimens as a function of time at fixed temperatures, (a) ambient (b) 66°C (c) 93°C (d) 121°C (e) 149°C (f) 177°C (g) 204°C (h) 232°C (i) 260°C

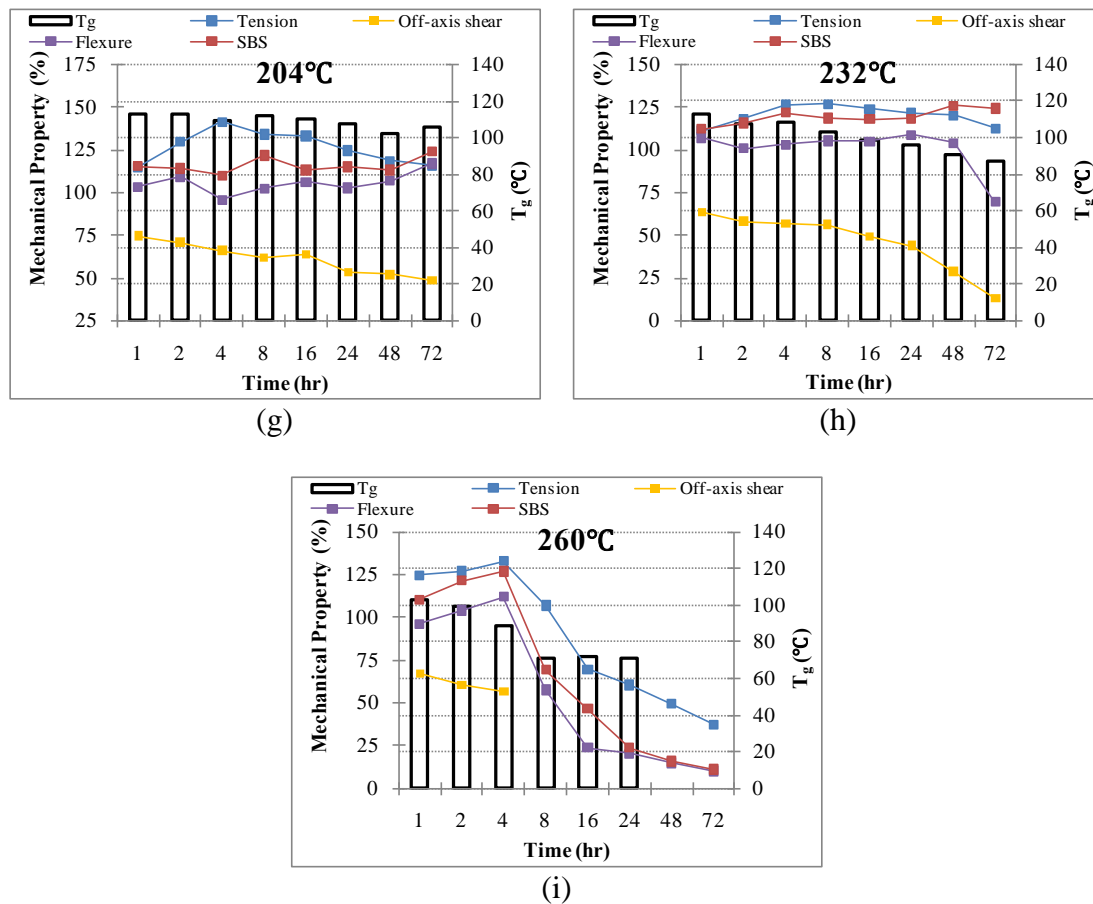


Figure 5-12: Continued

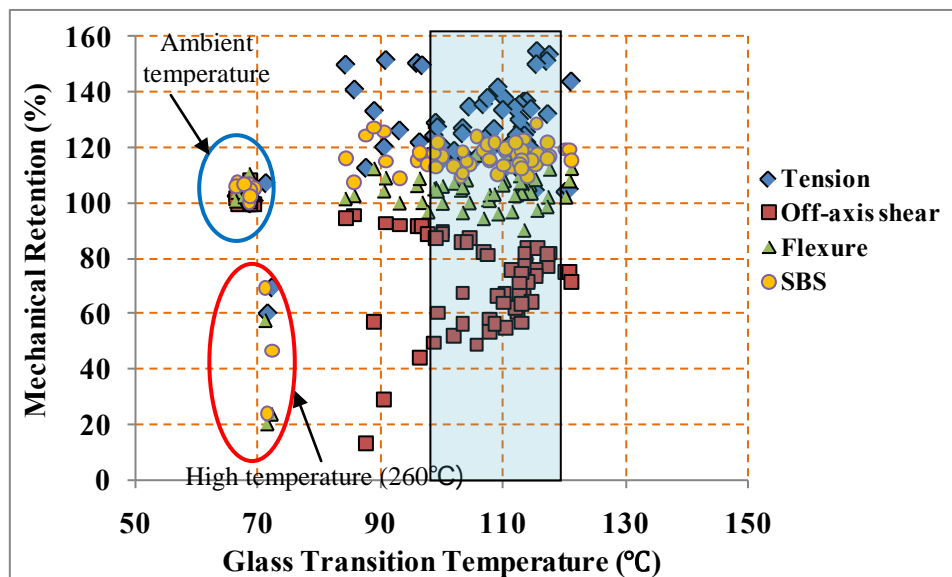


Figure 5-13: Characterization of four mechanical properties in terms of strength retention (%) as a function of glass transition temperatures determined by the peak of $\tan \delta$ at 1Hz

5.2 Differential Scanning Calorimetry

5.2.1 Introduction

As mentioned in chapter 3.5.6, Differential scanning calorimetry (DSC) is a technique to study what happens to polymers when they're heated. DSC is mainly used to investigate the thermal transitions of a polymer.

The operation of a Differential Scanning Calorimeter (DSC) is based on measurement of the thermal response of a sample pan containing polymer composites as compared with a reference pan when the two are heated uniformly at a constant rate. A flow of nitrogen gas is maintained over the samples to create a reproducible and dry atmosphere. The nitrogen atmosphere also eliminates air oxidation of the samples at high temperatures. The sample is sealed into a small aluminum pan. The reference is usually an empty pan and cover. The sample sits upon a constantan disc on a platform in the DSC cell. A thermocouple under the constantan disc measures the sample temperature. An empty reference pan sits on a symmetric platform with its own underlying wafer and thermocouple. Heat flow is measured by comparing the difference in temperature across the sample and the reference pan. The applications of DSC are as follows:

- 1) Exothermal energy of polymer cure (as in epoxy adhesives), allows determination of the degree and rate of cure.
- 2) Measurement of plastic or glassy material glass transition temperatures or softening temperatures.
- 3) Determines crystalline to amorphous transition temperatures in polymers and

plastics and the energy associated with the transition.

- 4) Determine the thermal stability of a material.
- 5) Determine the reaction kinetics of a material.

5.2.2 Data Reduction

5.2.2.1 Glass Transition Temperature

As described in dynamic mechanical thermal analysis, glass transition is a method to characterize a property of a polymeric material. The glass transition is the temperature where the polymer goes from like a hard, glass to a state of rubber. DSC defines the glass transition as a change in the heat capacity as the polymer matrix goes from the glass state to the rubber state. This is a second order endothermic transition (requires heat to go through the transition) so in the DSC the transition appears as a step transition and not a peak such as might be seen with a melting transition. In other words, polymers have a higher heat capacity above the glass transition temperature than they do below it. Because of this change in heat capacity that occurs at the glass transition, DSC is used to measure a polymer's glass transition temperature. It should be pointed out that the change doesn't occur suddenly, but takes place over a temperature range. This makes picking one discreet T_g kind of tricky. T_g is taken the middle of the incline to be the T_g as shown in Figure 5-14.

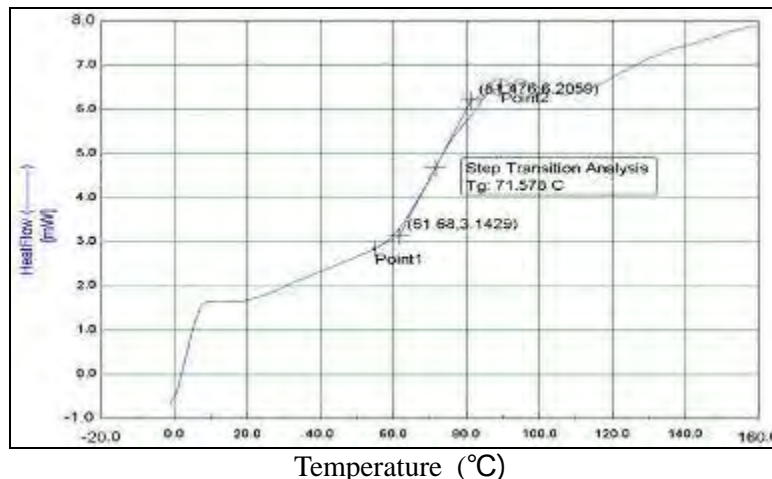


Figure 5-14: Schematic diagram for detecting the glass transition temperature from heat flow versus temperature (Exposure temperature: 23°C Ageing time: 4 hrs)

5.2.2.2 Heat Capacity

When heating reference and sample pan, the software of DSC sp equipment by Rheometric Scientific corporation will plot the difference in heat output of the two heaters against temperature. That is to say, the heat absorbed by the polymer against temperature is plotted. The heat flow is going to be shown in units of heat, q supplied per unit time, t . The heating rate is temperature increase T per unit time, t .

$$\frac{\text{Heat}}{\text{Time}} = \frac{q}{t} = \dot{q} = \text{heat flow} \quad (5.10)$$

$$\frac{\text{Temperature increase}}{\text{Time}} = \frac{\Delta T}{t} = \text{heating rate} \quad (5.11)$$

If dividing the heat flow by heating rate, heat capacity can be calculated as follow:

$$\frac{\frac{q}{t}}{\Delta T} = \frac{q}{\Delta T} = C_p = \text{heat capacity} \quad (5.12)$$

Heat capacity can be changed by variations in the material, either from its formulation or its heat history. While most investigations regarding DSC are only interested in the changes of heat capacity at the glass transition temperature to determine the glass transition temperature, information on the amount of oriented amorphous material.

5.2.3 Analyses and Results

First of all, in the analysis of differential scanning calorimetry (DSC), it should be noted that the changes affecting the mechanical properties and service life of polymer composites are often subtle and may not be seen on heating. In particular, to obtain accurate experimental results you should calibrate the DSC cell periodically. Two pans and DSC cell keep from contamination to obtain the accurate data. Since sample size is usually limited to 10-20mg and sample is extracted from big specimens, it is difficult to get consistent data. In addition, the amount of the thermal oxidation between surface and core of bulk materials can be resulted in bad data. Therefore, DSC is often used in conjunction with DMTA if reaction is endothermic or exothermic.

In this study, the analysis of DSC is only focused on detecting of the glass transition temperatures in order to compare to results determined by DMTA due to noise of DSC data.

Table 5-6 and Figure 5-15 show the comparison among glass transition temperatures determined by peak height of $\tan \delta$ at 1Hz, storage modulus and DSC on specimens exposed to elevated temperatures as a function of time. Glass transition temperatures determined by the analysis of DSC were overall higher than the results detected by the height of peak $\tan \delta$ and storage modulus using DMTA in all environmental conditions. As post-curing effect was applied to specimens, glass transition temperatures were getting higher compared to other values while glass transition temperatures show the similarity in the ranges of higher temperatures (232 and 260°C).

Table 5-6 Comparison among glass transition temperatures determined by $\tan \delta$, storage modulus and DSC (percent error means the difference between $\tan \delta$ and DSC)

Exposure Temperature	Time	T _g			Percent error(%)	Exposure Temperature	T _g			Percent error(%)
		1Hz	E'	DSC			1Hz	E'	DSC	
Ambient (23°C)	0	68.55	60.35	73.35	6.54					
	1	68.75	57.46	72.82	5.59	66°C	85.73	80.12	87.33	1.83
	2	68.64	68.15	71.79	4.39		84.27	80.04	89.45	5.79
	4	69.29	62.19	73.89	6.22		90.85	83.43	98.45	7.72
	8	66.67	65.64	72.18	7.64		95.94	84.95	102.12	6.05
	16	68.95	62.15	74.44	7.38		96.80	88.64	102.56	5.62
	24	66.45	61.25	69.45	4.33		100.13	90.54	105.37	4.97
	48	67.84	60.54	74.31	8.71		97.77	91.12	104.12	6.10
	72	68.82	61.16	69.51	1.00		100.12	92.34	103.88	3.62
93°C	1	93.09	91.07	90.57	-2.78		121°C	103.08	97.07	114.59
	2	99.00	89.31	100.58	1.57	104.05		101.74	119.78	13.13
	4	104.49	98.87	112.52	7.14	113.84		105.12	118.58	4.00
	8	106.81	100.12	115.40	7.44	117.32		108.81	115.47	-1.60
	16	107.50	103.58	117.90	8.82	113.83		105.40	118.72	4.12
	24	111.46	104.58	122.02	8.65	115.30		107.07	120.70	4.47
	48	113.89	106.31	121.81	6.50	120.24		111.84	122.92	2.18
	72	114.41	105.41	123.68	7.50	120.85		110.84	121.93	0.89
149°C	1	115.56	106.54	124.89	7.47	177°C	113.47	100.03	126.13	10.04
	2	117.60	109.64	125.34	6.18		113.53	102.45	126.69	10.39
	4	117.18	108.64	122.99	4.72		113.90	99.62	127.99	11.01
	8	115.48	103.05	125.00	7.62		112.74	103.33	126.17	10.64
	16	121.17	112.25	125.47	3.43		114.60	101.36	126.78	9.61
	24	110.23	101.58	125.28	12.01		112.26	101.41	124.61	9.91
	48	113.21	103.85	124.67	9.19		112.97	103.44	123.74	8.70
	72	113.41	103.89	124.34	8.79		110.45	98.97	121.16	8.84
204°C	1	113.08	102.22	126.58	10.67	232°C	112.91	100.00	121.63	7.17
	2	112.70	101.97	125.78	10.40		107.78	97.72	118.66	9.17
	4	109.19	100.01	125.05	12.68		108.56	97.98	121.90	10.94
	8	111.92	100.00	124.88	10.38		103.43	97.07	116.61	11.30
	16	110.00	96.36	125.47	12.33		98.73	83.24	106.27	7.10
	24	107.75	96.71	118.30	8.92		96.37	71.55	101.01	4.59
	48	102.04	86.61	112.74	9.49		90.57	68.20	91.01	0.48
	72	105.64	90.04	105.41	-0.22		87.61	65.43	86.95	-0.76
260°C	1	103.40	99.48	117.62	12.09					
	2	99.30	89.72	108.03	8.08					
	4	88.96	76.81	94.73	6.10					
	8	71.23	59.27	72.82	2.18					
	16	72.24	52.02	69.62	-3.76					
	24	71.53	49.06	70.06	-2.09					
	48			71.83						

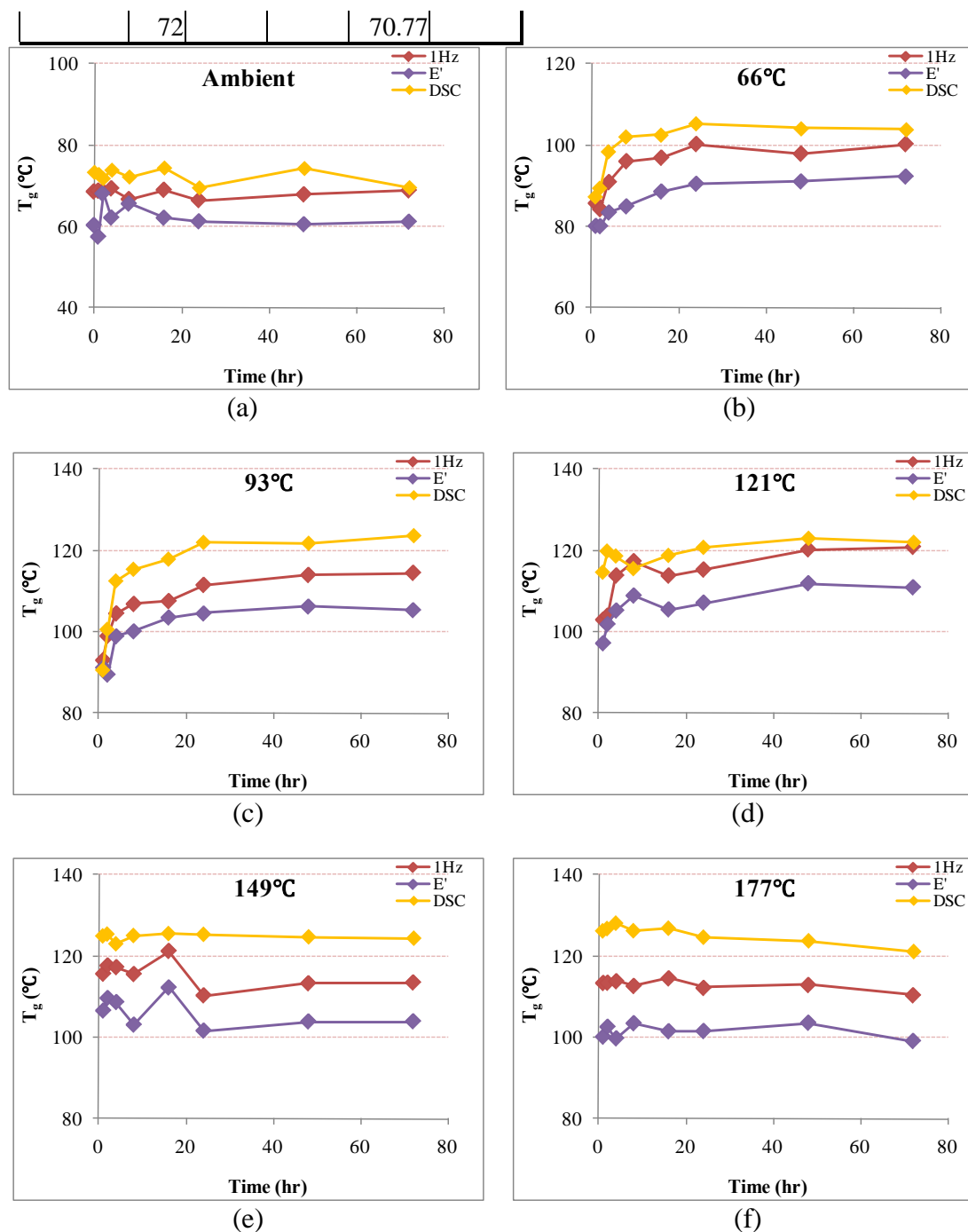


Figure 5-15: Comparison among glass transition temperatures determined by peak height of $\tan \delta$ at 1Hz, storage modulus and DSC as a function of time at fixed temperatures, (a) ambient (b) 66°C (c) 93°C (d) 121°C (e) 149°C (f) 177°C (g) 204°C (h) 232°C (i) 260°C

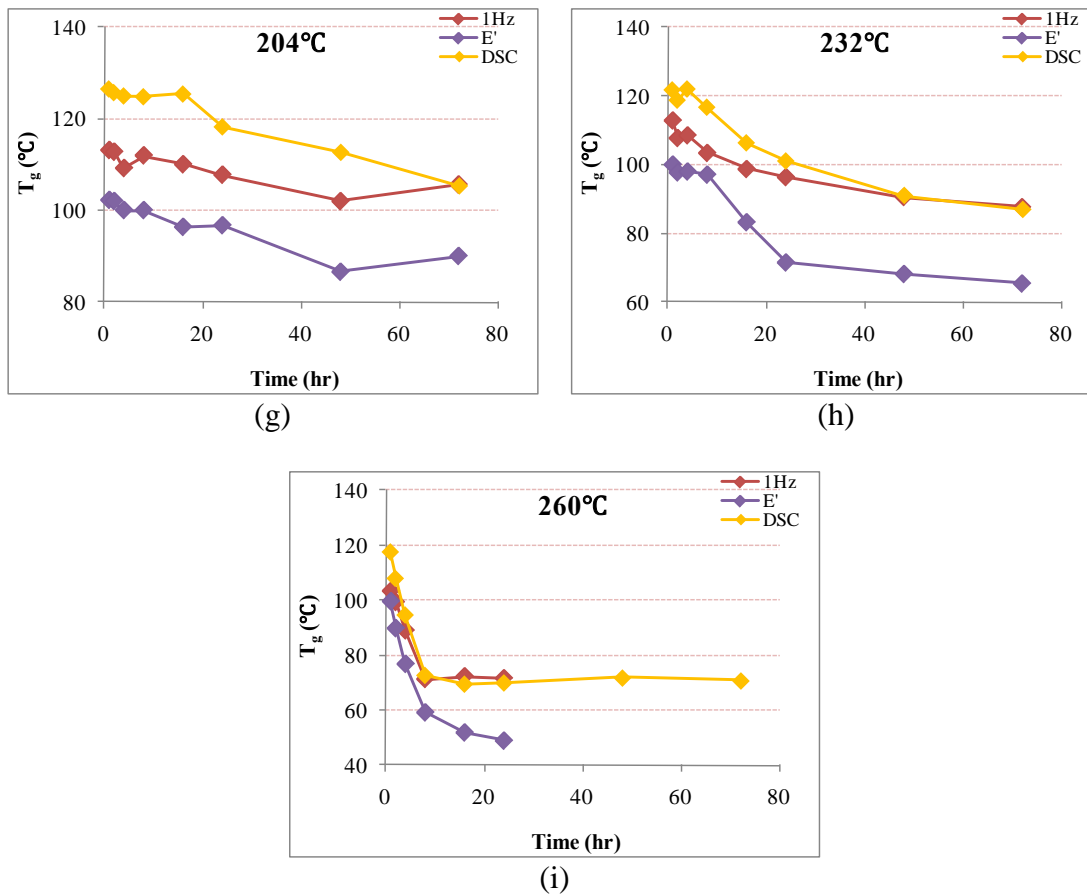


Figure 5-15: Continued

5.3 Thermogravimetric Analysis

5.3.1 Introduction

When fiber reinforced polymer composites are subjected to elevated and high temperatures, physical and chemical processes including glass transition and decomposition can greatly affect their physical and mechanical properties in various manners. To evaluate the thermal and mechanical responses of polymer composites in the ranges of the diverse exposure temperatures, thermophysical and thermomechanical properties should be considered. Thermogravimetric Analysis (TGA) is powerful and simple tool to estimate the thermophysical and thermomechanical properties exposed to a controlled temperature. In general, TGA is an analytical technique used to determine the thermal stability of composite materials and their fraction of volatile components by monitoring the mass loss that occurs when a specimen is heated. The measurement is normally performed in air or in an inert atmosphere. In this study, nitrogen gas is used to set inert condition as described in chapter 3.5.7. Mass loss can be categorized as volatile components such as absorbed moisture, residual solvents, or low-molecular-mass additive between ambient and 300°C; reaction products, such as water and amino resins, which generally form between 100°C and 250°C; and generation of volatile degradation products from polymer chain scission that generally require temperatures above 200°C but not more than 800°C [63]. All of these mass loss processes may be characterized by TGA to get information such as composition and thermal stability. In addition, kinetic information is important for estimating the times and temperatures corresponding to the processing, service lifetimes, and storage of materials. In an inert

atmosphere, the rate of many thermally activated processes can be described as a function of two variables: the temperature and the extent of conversion. The extent of conversion is conveniently determined from mass loss measurements.

The temperature-dependent effective thermophysical and thermomechanical properties of composite materials from thermal analysis using TGA combined with DMTA, DSC can be summarized in Figure 5-16. When decomposition of the composite materials due to elevated temperatures occurs, the effective specific heat capacity increases by decomposition heat emitted during endothermic process while the effective thermal conductivity definitely decreases at this region because significant thermal resistance results from the decomposed gas. As mentioned in DMTA section, the storage modulus apparently decreases in glass transition region, and drops further at decomposition.

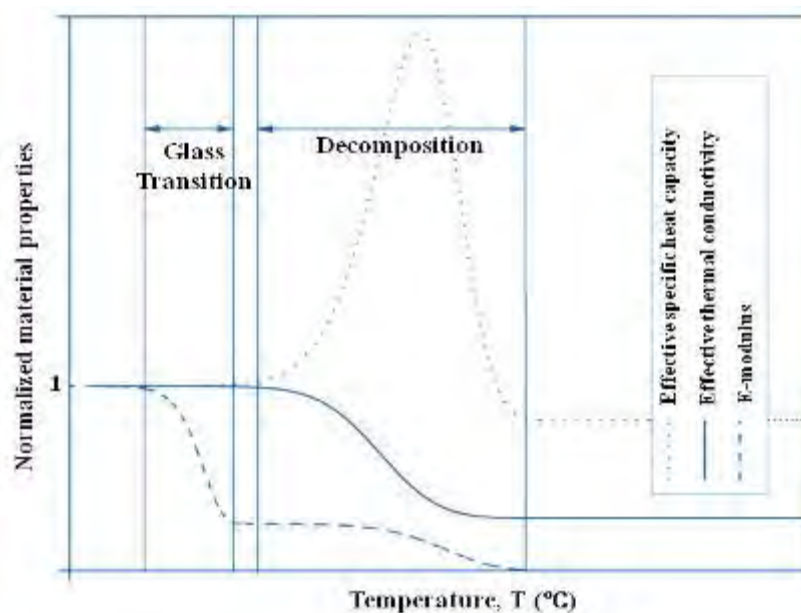


Figure 5-16: Temperature-dependent effective specific heat capacity, thermal conductivity and E-modulus for composite materials[70]

5.3.2 Analyses and Results

5.3.2.1 Weight loss

In order to compare to the results of weight loss using TGA, the characteristics of weight loss during thermooxidation process was evaluated with the weight change at various temperatures for different ageing time using DMTA specimens. When reached at required time and temperature, test specimens were removed to the atmospheric condition. After cooling in this condition, weight of DMTA specimens was recorded using analytical balance with a 10^{-5} grams resolution.

Table 5-7 and Figure 5-17 show the results of weight loss (%) on DMTA specimens exposed to elevated temperatures for up to 72 hrs using balance. In ranges of lower exposure temperatures (66, 93, 121, and 149°C), the data of weight loss only existed within 1%. As exposure temperatures were going up to 177, 204, and 232°C weight loss rapidly increased. In addition, at these temperatures, the slopes of weight loss versus time, which means the weight loss per hour, were steeper compared to lower ageing temperatures. Weight loss in 260°C was increased up to 18.2%. The slope of weight loss was 0.004, 0.005, 0.006, 0.009, 0.034, 0.039, 0.053, and 0.23 at 66, 93, 121, 149, 177, 204, 232 and 260°C respectively. In other words, characterization of weight loss can be categorized into 4 regions in this study as follows:

- 1) no-changed region: ambient temperature (~0%)
- 2) slight-changed region: 66, 93, 121, 149°C (~1.5%)
- 3) intermediate-changed region: 177, 204, 232°C (~5.6%)
- 4) catastrophic-changed region: 260°C (~18.2%)

Since the epoxy resin used in this study is cured at room temperature and is not fully cured, it is expected that the weight loss is coming from following reasons:

- 1) Evaporating of uncured small molecules
- 2) The small molecular part spilt from long polymer chain

Evaporating resulted in initial weight loss whereas separation of the small molecular part from long polymer chain due to intensive thermooxidation contributed to the abrupt weight loss. Therefore, weight loss in ranges of lower exposure temperatures was smaller than that in higher exposure temperatures since serious chain splitting was not occurred due to severe thermooxidation.

Table 5-7 Data of weight loss (%) on DMTA specimens exposed to elevated temperatures using balance

Time	Weight Loss (%)							
	66°C	93°C	121°C	149°C	177°C	204°C	232°C	260°C
1	0.1405	0.3015	0.4803	0.6380	0.8389	1.1203	1.5616	2.2166
2	0.1677	0.3431	0.5695	0.7408	0.9919	1.4126	1.9864	2.7661
4	0.2031	0.4064	0.6520	0.8425	1.1400	1.7654	2.3837	3.6499
8	0.2412	0.4801	0.7613	0.9064	1.3921	2.0724	2.8212	5.1066
16	0.2953	0.6060	0.7807	0.9668	1.8138	2.5399	3.3807	8.8491
24	0.3672	0.6474	0.8284	1.0569	2.2278	2.8100	3.9378	10.9842
48	0.4443	0.7192	0.8696	1.2555	2.9053	3.3003	4.8256	15.6297
72	0.4887	0.7334	0.8859	1.4111	3.2853	3.6310	5.6593	18.2231

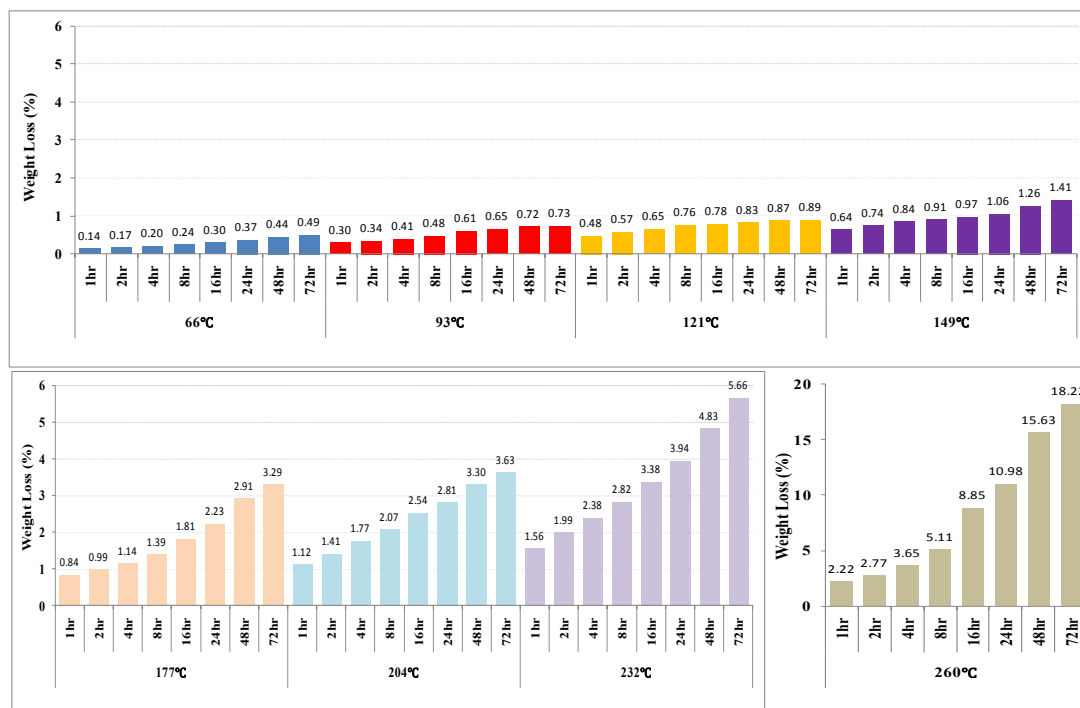


Figure 5-17: Weight loss (%) on DMTA specimens exposed to elevated temperatures using balance

Weight percent (%) of specimens at initial and final point of decomposition using TGA is presented in Table 5-8. As described in chapter 3.5.7, Samples were heated from 25°C to 750°C with the heating rate of 10°C/min in nitrogen environment (25 ml/min). m_i and m_e indicate the mass (%) that decomposition of specimens is initiated and finished and two masses can be detected using software of TGA instrument. The majority of m_i shows the value more than 99% except for some conditions (232°C more than 24 hrs of ageing time and 260°C more than 4 hrs of ageing time). This phenomenon means evaporating of uncured small molecules was only applied for weight loss before decomposition is initiated. Weakened or damaged polymer structures due to severe thermooxidation contributed to additional weight loss in higher exposure temperatures. On the contrary to the results of m_i , m_e did not show the tendency. It appears that this reason resulted from complicated mechanism of decomposition and variations having hand wet layup process.

Weight loss using TGA on specimens exposed to elevated temperatures for 72 hrs of ageing time is presented as a function of temperatures ranging from 25°C to 750°C in Figure 5-18. Based on graphs, no significant changes occurred before decomposition is initiated in all exposure temperatures except for 232°C and 260°C. However, abrupt weight loss occurred after decomposition. Finally, in ranges of 232°C and 260°C, a little of weight loss happened before decomposition while weight loss after decomposition were smaller compared to lower exposure temperatures. It should be pointed out that the un-uniformly distribution of carbon/epoxy composite materials contributed to the variation of the residual char weight.

Table 5-8 Weight percent (%) of specimens at initial and final point of decomposition using TGA

Time	Ambient (23°C)		66°C		93°C		121°C		149°C	
	m _i (%)	m _e (%)								
0	99.57	55.57								
1	99.36	43.63	99.22	48.25	99.40	52.59	99.25	52.27	99.28	52.82
2	99.34	43.70	99.37	49.27	99.18	46.25	99.64	55.97	99.52	38.14
4	99.46	52.19	99.54	49.23	99.08	39.90	99.88	45.11	99.85	45.73
8	99.32	46.43	99.36	47.29	99.39	44.58	99.81	53.34	99.76	50.01
16	99.20	49.25	99.61	56.10	99.83	55.72	99.30	57.40	99.33	52.21
24	99.43	61.09	99.21	54.11	99.76	50.27	99.08	46.63	99.57	56.15
48	99.52	59.80	99.21	42.29	99.43	55.77	99.50	46.73	99.96	45.87
72	99.27	46.30	99.59	47.17	99.27	57.93	99.51	41.52	99.90	54.38
Time	177°C		204°C		232°C		260°C			
	m _i (%)	m _e (%)								
1	99.73	51.67	99.62	43.84	99.58	53.25	99.36	46.55		
2	99.77	51.20	99.36	50.44	99.24	54.40	99.06	61.98		
4	99.50	49.30	99.15	54.28	99.41	48.04	98.24	40.97		
8	99.68	45.67	99.24	52.09	99.13	48.37	94.84	59.08		
16	99.48	44.03	99.63	59.58	99.59	58.01	93.19	64.77		
24	99.37	51.55	98.70	50.91	98.64	60.74	92.64	69.72		
48	99.21	54.71	97.02	57.03	97.00	56.39	93.47	71.21		
72	99.49	57.37	96.84	45.88	94.26	59.77	93.15	75.57		

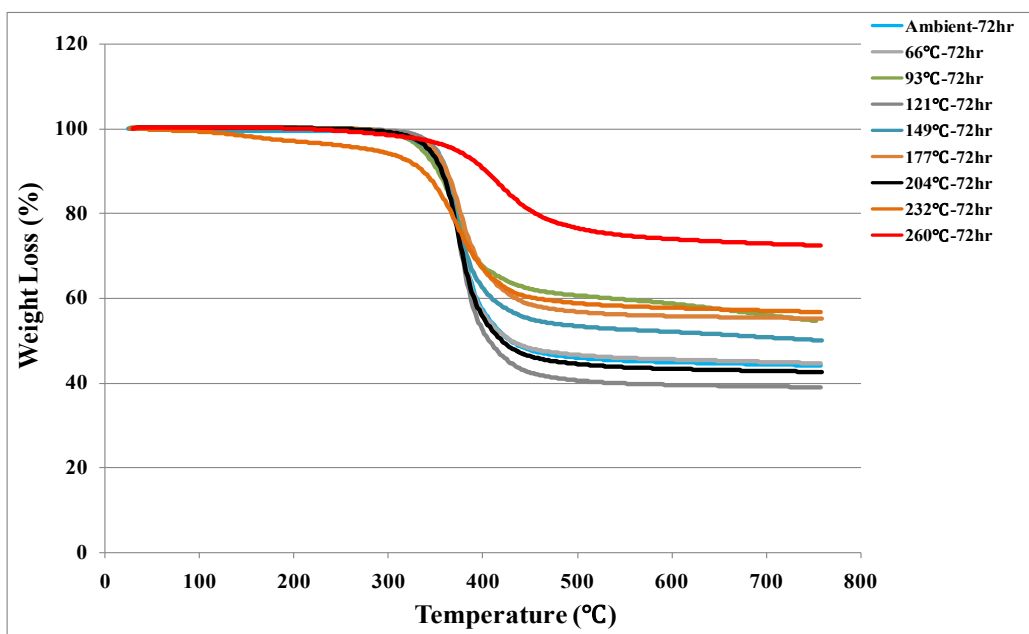


Figure 5-18: Weight loss (%) on specimens heated from 25°C to 750°C with the heating rate of 10°C/min in nitrogen environment (ageing time: 72 hrs)

5.3.2.2 Determination of Thermal Stability Parameters

Thermal stability parameters determined by the TGA curve are summarized in Table 5-9. First, the onset temperature of decomposition (T_{onset}) means what the maximum processing and manufacturing temperatures can be used without initiating decomposition. Therefore, T_{onset} is the main criteria for heat stability of polymers and polymer composites[71]. The endset temperature of decomposition (T_{endset}) indicate threshold temperature which decomposition show the asymptotic value due to char formation. T_{onset} and T_{endset} can be easily detected by software attached to TGA instrument. As shown in Figure 5-19, the values of T_{onset} initially increased due to the dominant increase of the crosslinkage with thermal treatment. For lower exposure temperatures ($\sim 149^{\circ}\text{C}$), the values of T_{onset} continuously increased even though ageing time went up. In the exposure temperatures ranging from 177 to 260 $^{\circ}\text{C}$ the values of T_{onset} continuously decreased with the extended ageing time. The higher exposure temperature led to the more serious drop in the values of T_{onset} . In the highest temperature (260 $^{\circ}\text{C}$), the absence of the initial increase of T_{onset} means the degradation of the polymer structures occurred even in a short time. After 8 hr of ageing time in 260 $^{\circ}\text{C}$ the reason why T_{onset} showed the asymptotic values is that serious thermooxidative degradation already occurred in the process of environmental conditions and this resulted in char formation. In the case of T_{endset} , the values of T_{endset} were very consistent except for exposure temperatures of more than 177 $^{\circ}\text{C}$. The values of T_{endset} were slightly increased in temperature ranging from 177 to 232 $^{\circ}\text{C}$ while these values were abruptly increased in 260 $^{\circ}\text{C}$. The increase of T_{endset} indicates decomposition occur for long time period.

Table 5-9 Thermal stability parameters determined by TGA curves- T_m and α_m mean the maximum temperature and degree of decomposition at the maximum reaction

Temperature	Time	T_{onset} (°C)	T_{endset} (°C)	T_m (°C)	α_m	E_d (KJ/mol)	n
Ambient (23°C)	0	352.25	397.56	441.00	0.881	170.10	0.89
	1	354.72	397.78	448.82	0.933	188.56	0.93
	2	353.62	399.83	444.31	0.932	185.99	0.93
	4	354.34	400.15	444.09	0.929	179.71	0.92
	8	354.85	400	444.15	0.932	179.62	0.92
	16	354.79	397.11	444.87	0.897	155.95	0.9
	24	353.25	398.67	442.67	0.921	173.83	0.91
	48	353.61	398.59	444.25	0.929	181.13	0.93
	72	355.64	400.28	445.45	0.928	176.48	0.92
66°C	1	353.81	399.49	441.20	0.923	182.52	0.93
	2	353.79	399.42	442.78	0.928	181.29	0.93
	4	354.08	399.82	439.86	0.929	196.59	0.93
	8	354.2	399.15	443.29	0.907	184.47	0.92
	16	354.13	399.53	444.50	0.928	187.47	0.93
	24	354.04	398.54	440.17	0.903	192.34	0.98
	48	354.01	399.51	443.27	0.906	235.36	0.94
	72	354.54	399.09	441.38	0.913	235.68	0.94
93°C	1	352.14	397.72	444.68	0.889	167.60	0.89
	2	351.94	397.67	441.28	0.928	190.10	0.93
	4	355.18	400.48	445.56	0.933	216.86	0.94
	8	355.35	400.71	441.76	0.931	201.87	0.93
	16	356.29	400.04	442.59	0.929	230.81	0.93
	24	356.84	398.26	444.79	0.899	183.87	0.9
	48	354.07	396.26	442.31	0.873	186.98	0.91
	72	352.74	399.06	441.43	0.914	180.71	0.92
121°C	1	348.7	396.88	440.54	0.878	144.91	0.86
	2	354.48	400.7	445.83	0.922	215.57	0.9
	4	355.9	400.66	445.62	0.937	259.41	0.95
	8	353.92	399.63	441.01	0.922	293.76	0.95
	16	354.71	400.97	445.76	0.926	200.08	0.93
	24	353.74	399.37	441.59	0.925	209.04	0.93
	48	354.17	399.92	447.59	0.939	226.32	0.94
	72	354.25	399.24	444.45	0.935	218.02	0.94
149°C	1	348.63	397.75	440.49	0.897	158.22	0.9
	2	354.75	400.24	444.53	0.930	213.24	0.94
	4	355.4	399.3	446.20	0.936	232.36	0.94
	8	353.36	399.58	441.62	0.930	204.41	0.93
	16	352.39	398.46	442.48	0.873	147.25	0.86
	24	354.07	399.39	434.34	0.887	186.80	0.9
	48	352.88	400.73	443.24	0.930	207.79	0.93
	72	347.73	400.3	446.47	0.894	154.56	0.89

Table 5-9 Continued

Temperature	Time	T _{onset} (°C)	T _{endset} (°C)	T _m (°C)	α_m	E _d (KJ/mol)	n
177°C	1	353.07	399.7	443.47	0.924	192.42	0.93
	2	353.48	399.72	440.11	0.928	205.31	0.93
	4	353.48	401.08	446.17	0.939	231.23	0.95
	8	354.48	401.01	443.04	0.929	178.93	0.93
	16	351.91	401.79	448.92	0.936	171.72	0.93
	24	350.86	400.75	442.17	0.894	145.51	0.88
	48	351.87	402.94	449.14	0.928	159.79	0.91
	72	350.63	405.18	449.03	0.925	151.22	0.91
204°C	1	354.82	400.26	447.91	0.941	236.69	0.94
	2	354.21	399.43	443.43	0.935	210.09	0.94
	4	353.08	398.52	444.20	0.882	226.16	0.94
	8	347.47	396.98	445.90	0.875	154.03	0.87
	16	347.16	397.75	448.76	0.883	175.12	0.88
	24	347.73	399.93	441.87	0.922	163.40	0.91
	48	347.02	400.47	442.47	0.894	132.06	0.89
	72	346.53	402.42	443.37	0.927	169.25	0.91
232°C	1	355.05	401.5	449.15	0.936	204.89	0.92
	2	355.26	400.61	449.32	0.936	206.11	0.92
	4	354.8	399.6	447.69	0.933	215.18	0.92
	8	348.91	402.46	447.90	0.923	167.20	0.92
	16	345.2	403.89	448.00	0.933	169.10	0.92
	24	343.28	402.56	448.93	0.876	121.83	0.84
	48	342.91	407.55	446.70	0.908	104.18	0.85
	72	335.78	409.85	441.85	0.909	66.94	0.78
260°C	1	350.96	398.86	437.40	0.929	211.91	0.94
	2	346.4	399.25	447.30	0.881	149.67	0.87
	4	346.4	404.4	446.69	0.929	148.12	0.91
	8	318.6	403.84	440.60	0.895	63.25	0.74
	16	314.23	420.3	463.72	0.848	41.64	0.75
	24	318.54	436.12	473.92	0.871	32.73	0.78
	48	323.68	456.18	498.00	0.879	29.65	0.74
	72	320.65	467.73	543.01	0.845	28.42	0.72

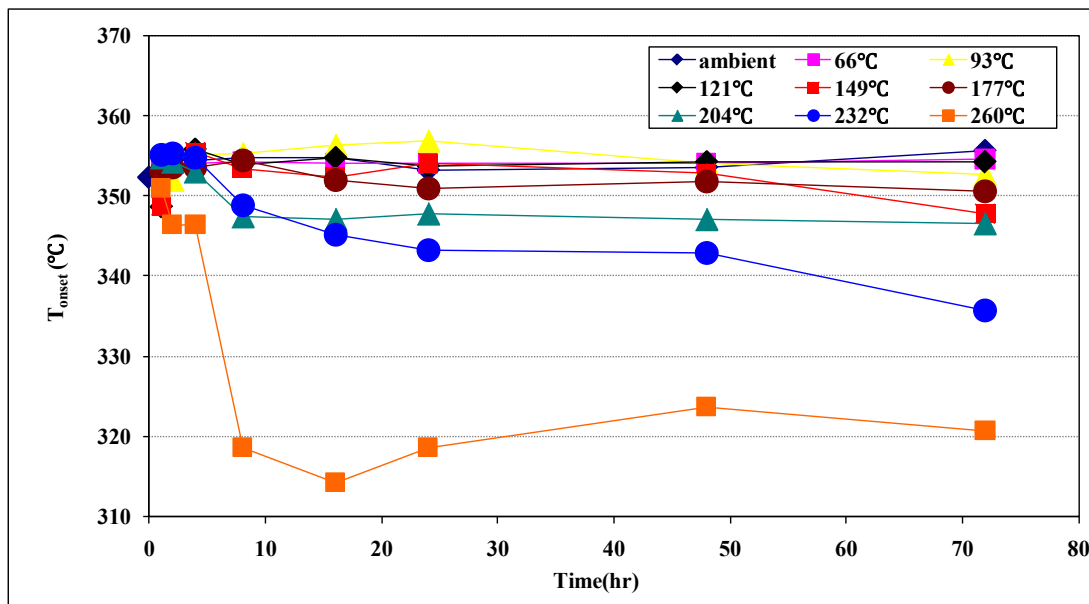


Figure 5-19: Onset temperatures of decomposition on specimens exposed to elevated temperature as a time function

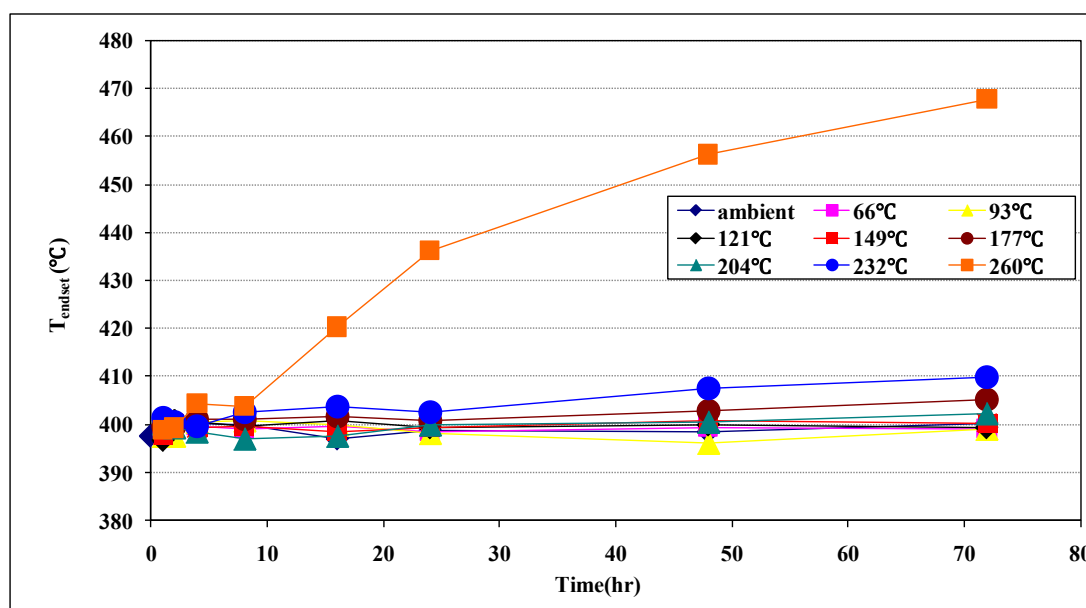


Figure 5-20: Endset temperatures of decomposition on specimens exposed to elevated temperature as a time function

In general, the mass of composite materials indicates little change until decomposition is initiated as mentioned previously. The degree of decomposition (α) can be expressed as

$$\alpha = \frac{(M_i - M)}{(M_i - M_e)} \quad (5.13)$$

where:

M = instantaneous mass

M_i = initial mass

M_e = final mass after decomposition

As can be seen in Figure 5-21, the values of decomposition degree at single heat rate ($10^\circ\text{C}/\text{min}$) on specimens exposed to elevated temperature for 72 hrs show a little change before and after decomposition in the majority of exposure temperatures. Meanwhile, from Figure 5-21 decomposition was started at lower temperatures and was finished at higher temperatures in exposure temperatures, i.e., 232 and 260°C compared to other environmental conditions. The reaction rate ($d\alpha/dT$) can be expressed by dividing the decomposition degree into temperatures and reaction rate of decomposition at single heat rate ($10^\circ\text{C}/\text{min}$) on specimens exposed to elevated temperature for 72 hrs are depicted in Figure 5-22. The maximum reaction rate occurs $d^2\alpha/dT^2 = 0$. T_m and α_m can be defined as the maximum temperature and degree of decomposition at the maximum reaction, respectively. The values of T_m and α_m are tabulated in Table 5-9. In the case of exposure temperature (260°C) for 72 hrs, T_m shows the highest value and α_m indicates the lowest value compared to other environmental conditions.

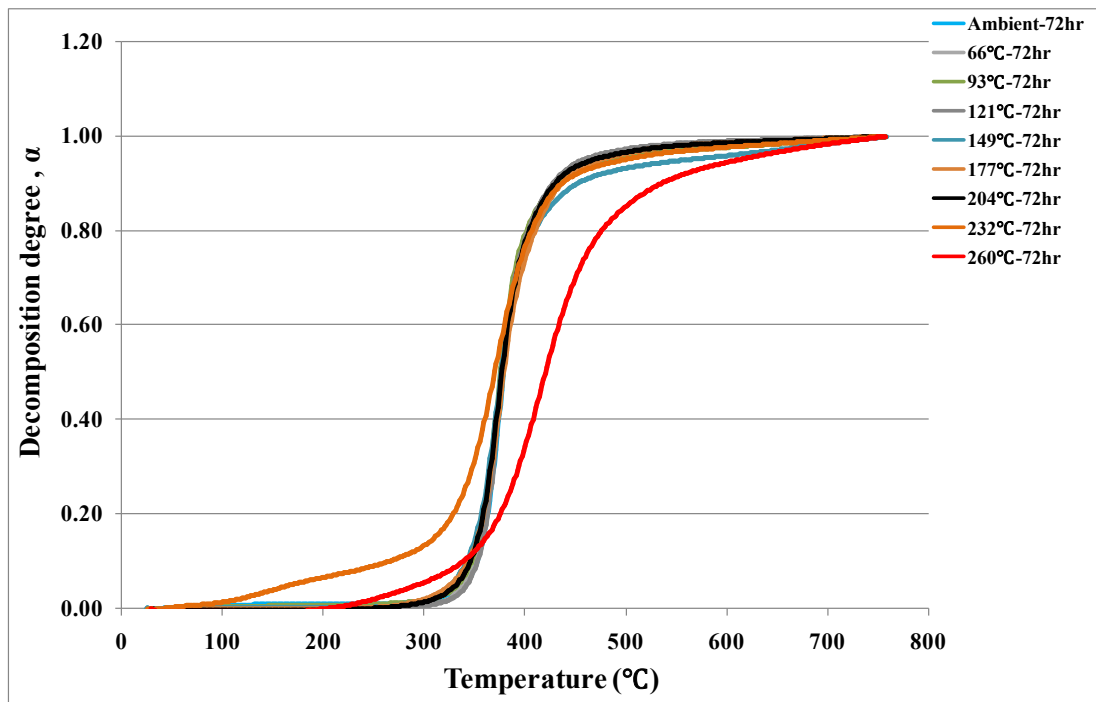


Figure 5-21: Decomposition degree at single heat rate ($10^{\circ}\text{C}/\text{min}$) on specimens exposed to elevated temperature for 72 hrs

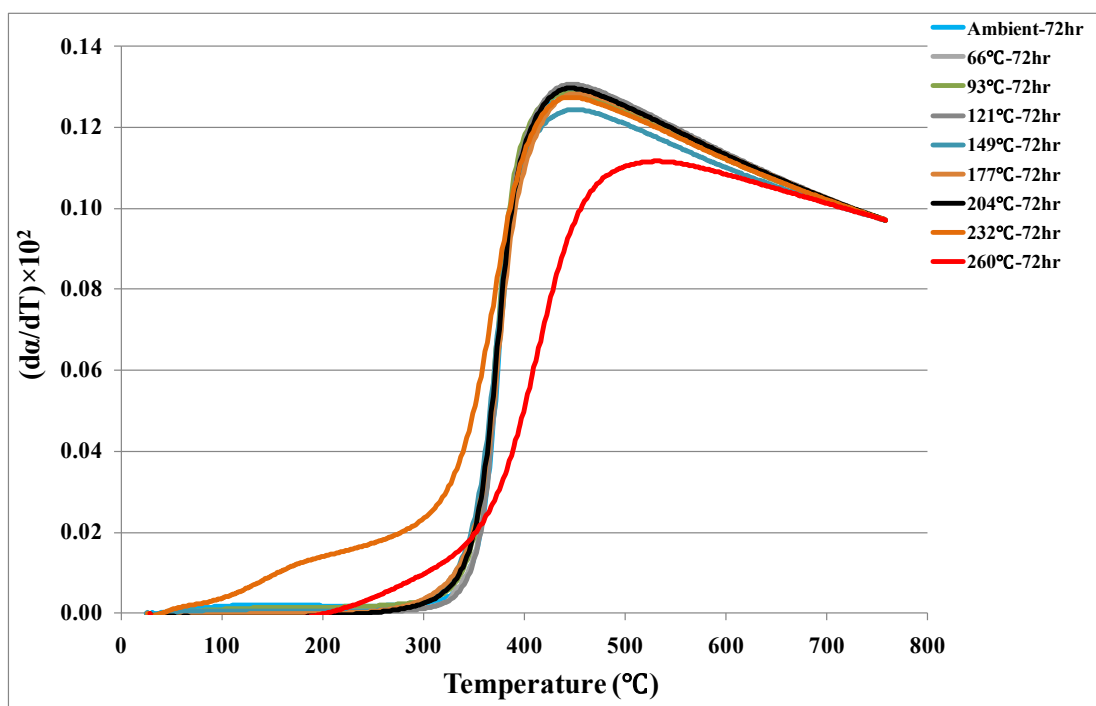


Figure 5-22: Reaction rate of decomposition at single heat rate ($10^{\circ}\text{C}/\text{min}$) on specimens exposed to elevated temperature for 72 hrs

To determine the decomposition activation energy (E_d), the modified Coats and Redfern methods[72, 73] were applied. This method is suitable for experiment with single heating rate TGA curve. The decomposition process can be expressed by the theory of chemical reaction rate and the Arrhenius law[74]. The rate of decomposition is determined by the temperature and the quantity of reactants as follows:

$$\frac{d\alpha}{dt} = k(T)f(\alpha) \quad (5.14)$$

where $k(T)$ and $f(\alpha)$ mean the effect of temperature and the effect of the reactant quantity to the reaction rate, respectively. Also, $k(T)$ and $f(\alpha)$ can be expressed as follows:

$$f(\alpha) = (1 - \alpha)^n \quad (5.15)$$

$$k(T) = A \exp\left(\frac{-E_d}{RT}\right) \quad (5.16)$$

where A is the pre-exponential factor, E_d is the activation energy, R is the universal gas constant, n is the reaction order. Moreover, a constant heating rate is expressed by

$$\frac{dT}{dt} = \beta \quad (5.17)$$

Consequently, from Equation 5.14~5.17, the rate of decomposition can be described below:

$$\frac{d\alpha}{dT} = \frac{A}{\beta} \exp\left(-\frac{E_d}{RT}\right)(1 - \alpha)^n \quad (5.18)$$

By integrating and logarithm, Equation 5.18 can be transformed as

$$\ln\left(\frac{\alpha}{T^2}\right) = \ln\left(\frac{AR}{\beta E_d}\right) \cdot \left(1 - \frac{2RT}{E_d}\right) - \frac{E_d}{RT} \quad (5.19)$$

From Equation 5.19, a slope of E_d/R can be obtained by a straight line of a plot of $\ln(\alpha/T^2)$ versus $1/T$. In this TGA, a good linearity of $\ln(\alpha/T^2)$ versus $1/T$ was found in the α range between 1% and 30%. The coefficient of determination (R^2) was more than 0.99 in linear region.

Meanwhile, Reaction order, n , of the decomposition reaction is determined according to Kissinger model[75] according to the following equations.

$$\text{For } n \neq 1, \quad n(1 - \alpha_m)^{n-1} = 1 + (n - 1) \frac{2RT_m}{E_d} \quad (5.20)$$

The values of activation energy and reaction order using Equation 5.19 and 5.20 are tabulated in Table 5-9. Figure 5-23 shows activation energy of decomposition on specimens exposed to elevated temperatures as a function of time. Activation energies for un-aged specimens were less than 190 KJ/mol. With increased exposure temperatures, the value of activation energy was increased up to 293.76 KJ/mol (exposure temperature: 121°C, ageing time: 8 hrs) due to post-cure effect. Higher activation energy is required to decompose polymer composites since the higher degree of crosslinking due to post-cure effect brings more bonds in polymer chain. As expected, activation energies catastrophically dropped less than 100 KJ/mol in severe conditions exposed to 232°C for 72 hrs and 260°C for more than 8 hrs. The breakage of polymer chains in severe conditions due to thermooxidation resulted in decrease in activation energy.

In the case of reaction order, the majority of reaction order existed between 0.85

and 0.95. The reason why reaction order showed the similar values is that the same degradation mechanisms are applied for specimens, which severe breakage of polymer chain did not occurred in the process of ageing. Similar to the results of activation energy, reaction order decreased less than 0.8 in severe conditions exposed to 232°C for 72 hrs and 260°C for more than 8 hrs. The decrease of reaction order means extreme change of degradation mechanisms. In other words, it is indicative that a serious degradation occurred in chemical structures of the molecular chains.

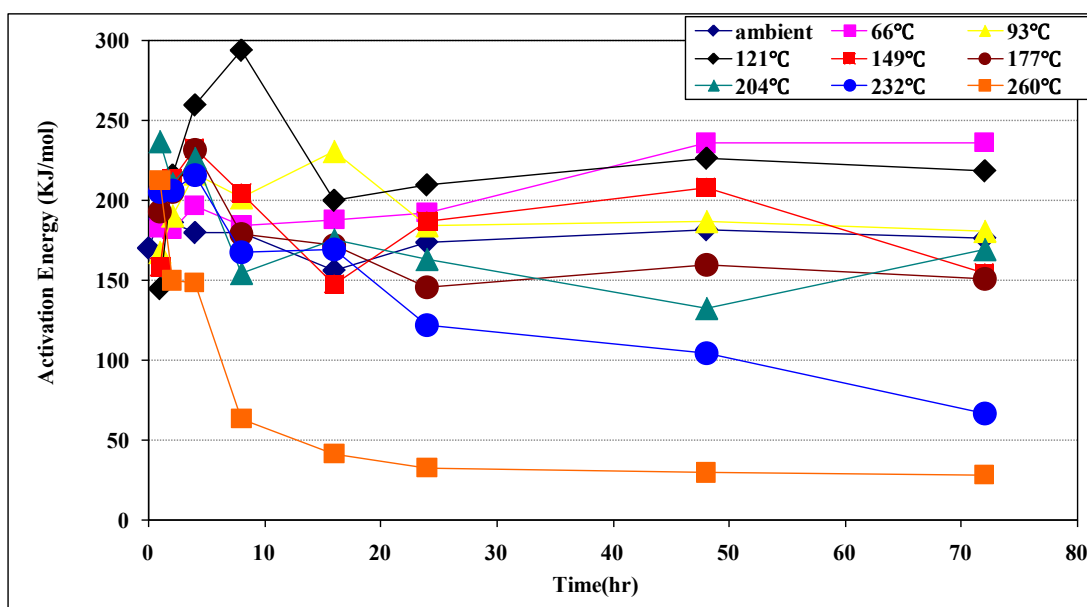
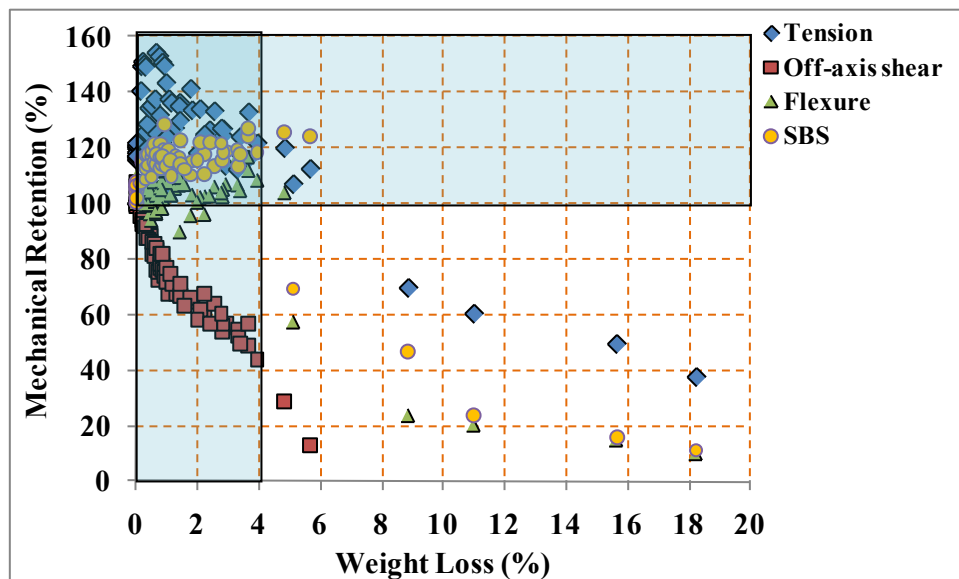


Figure 5-23: Activation Energy of decomposition (E_d) on specimens exposed to elevated temperatures as a function of time

5.3.2.3 Mechanical Retention based on Weight loss

As mechanical properties are strongly dependent on glass transition temperature, weight loss (%) of composite materials also is also associated with mechanical characterization. In Figure 5-24, mechanical retentions for four tests (Tension, off-axis shear, flexure and SBS) are represented as a function of weight loss. Most data of mechanical retention existed between 0 and 4% except for severe environmental conditions. Within 4% of weight loss, the majority of mechanical retentions showed higher values than un-aged specimens except for the properties of off-axis shear test. This phenomenon means the increase of mechanical property due to post-cure effect is more dominant than decrease of mechanical property by weight loss. The continuous decrease of off-axis shear property regardless of post-cure effect resulted from the distortion of specimens by asymmetry. In the case of tension, tensile properties showed retention more than 100% until weight loss was reached 6% and after 6%, linearly were decreased.

In the ranges within 4% of weight loss, the mechanical retentions of flexure and short beam shear test were slightly increased due to residual post-cure effect. As shown in Figure 5-24, if the weight losses of polymer composites were more than 6%, since the retentions of all mechanical properties were decreased up to 50%, polymer composites could not play a role as structures. Consequently, thermal stability parameters including weight loss and glass transition are important criteria to evaluate the performance and functionality of fiber reinforced polymer composites.



6 Immersion Analysis

6.1 Introduction

From past researches, it is known that polymer composites are very sensitive to water and moisture in any forms. Moisture in polymer composites often causes swelling and degradation. Especially, since polymer composite used in marine environments can easily be exposed to moisture regarding relative humidity and immersion, degradation mechanisms related to moisture must be investigated to evaluate the service life and long term effects. Matrix and/or interface degradation resulting from moisture absorption is a concern in most composite applications subject to normal atmospheric moisture, which can range from precipitation to mild humidity. Complete immersion in water constitutes the most severe environment, while humid air generally results in lower maximum moisture content[76]. Since this study is focused on assessment of composite materials exposed to aqueous solution, in specific – sea water, immersion analysis will be mainly performed in accordance with related theories.

While general investigations regarding moisture uptake are focused on the specimens cured in ambient temperature, this study is concentrated on the immersion effects of specimens exposed to elevated temperatures because structures of composite materials exposed to the various heat sources such as fire, ignition of flammable gases or liquids and weapon strikes must be estimated in terms of operating life. Consequently, mechanisms of complicated degradation including temperature and immersion effect can be applied to rehabilitated structures. In following section, the theories regarding moisture effects on polymer composites will be introduced.

6.1.1 Moisture Effect on Polymer Composites

The effect of moisture sorption on the degradation of polymer composite materials has been well established from a lot of investigations and studies. The degradation of polymers due to moisture can be divided into chemical and physical degradation. Chemical changes include hydrolysis of the polymer chain and interfacial bond while physical degradation means swelling, plasticization, and relaxation of the polymer[77, 78]. As swelling by moisture ingress promotes microcracking in the hydrolyzed damaged resin and interfacial debonding at the hydrolyzed interface, physio-mechanical degradation may also take place.

By moisture ingress on polymer composites, degradation mechanisms can be summarized as followings; 1) Hydrolysis: Hydrolysis is related to plasticization and this process occurs from separation of side groups from the polymer chains[17]. From the separation of polymer chains, weight loss generally occurs at the fiber-matrix interface region. This process cause permanent and irreversible degradation. 2) Plasticization: Polymer composite first experiences the plasticization due to moisture. Plasticization occurs in the matrix when bonds between ethers, secondary amines, and hydroxyl groups are broken[79]. This process involves swelling of the matrix. Unlike hydrolysis, this mechanism for degradation is reversible process on drying. 3) Microcracking: Composite materials can undergo matrix microcracking occurring when the composite reaches a stress level where the matrix begins to crack away from the fibers. Wicking created by matrix microcracking results in the ingress of large amounts of moisture into composite materials. Therefore, crack also results in high amounts of strength loss. 4) Debonding: composite materials made by hand wet layup process can have flaws in

terms of bond between the fiber and matrix. This process can be occurred by a pressure difference resulting from the moisture that is absorbed by the composite materials. This process is also irreversible degradation. 5) Delamination: Poor interface between layers can occur an acceleration of the delamination due to moisture. This is also irreversible process. Beside degradation mechanisms described above, moisture can cause fiber pitting, chain scission, leaching and microvoids in the form of reversible or irreversible degradation.

Accordingly, moisture uptake is important parameter to assess susceptibility of composite materials to deterioration and is used in the prediction of long-term durability. Under steady state conditions, moisture uptake in a composite can be expressed as a percent of the original dry mass,

$$M = \frac{(W_t - W_i)}{W_i} \times 100 \quad (6.1)$$

Where:

M = percent moisture uptake (change in weight)

W_i = initial weight of the specimen (prior to immersion)

W_t = Weight of the specimen after time t

6.1.2 Diffusion in Polymer Composites

In general definition, diffusion is the movement of molecules from a region of high concentration to a region of low concentration by means of random molecular motion. Fick's laws provide a theoretical basis for the diffusion of a fluid into a distinct

sorbing medium from a higher concentration to a lower concentration. Also, Fick's second law provides a theory for non-steady-state diffusion. Fick's law refer to that the mass of absorbed water increases linearly with the square root of time and then gradually slows until an equilibrium plateau or saturation is reached. The rate of diffusion and the attainment of an equilibrium content can be affected by materials characteristics, processing factor, environmental condition, and geometry. Since Fickian diffusion assumes no chemical reaction between the diffusion solution and composite materials, composites technically do not follow Fick's law. However, in a number of researches, the diffusion of moisture in fiber reinforced composites and crosslinking resin has been shown Fickian behavior[80, 81]. Fickian diffusion has following features.

1) Linear in the initial stage and the linear region until at least $M_t/M_m=0.6$

where:

M_t = the moisture absorbed by the composites at time t

M_m = the maximum moisture content absorbed by the composite

2) The decrease of the rate of diffusion until an equilibrium of moisture content

3) Diffusion coefficient as a function of temperature

$$D = D_0 \exp\left(\frac{-E_a}{RT}\right) \quad (6.2)$$

where:

D = diffusion coefficient

D_0 = a constant

E_a = activation energy

R = the universal gas constant

The theory of Fickian diffusion also assumes that only reversible physical reactions take place in the polymer matrix during the process of moisture sorption.

Figure 6-1 shows schematic curves representing four categories of recorded non-Fickian weight-gain sorption compared to linear Fickian diffusion. This Figure was postulated by Weitsman[82]. Curve A means pseudo-Fickian diffusion characterized by a initial uptake in the beginning stages of immersion similar to Fickian behavior. However, saturation or equilibrium is not attained in this case. In the case of curve B describing two-stage diffusion behavior, the weight of composite materials initially increases due to moisture while this process experiences a quasi-equilibrium by the competition between moisture uptake and mass loss. Curve C caused by deformations, wicking, or mechanical failure is a type of diffusion where moisture is rapidly increasing. Curve D in Figure 6-1 shows weight loss that is attributed to hydrolysis or other types of irreversible degradations. Curve LF, which has the solid line, stand for linear Fickian diffusion that follows the Fick's law.

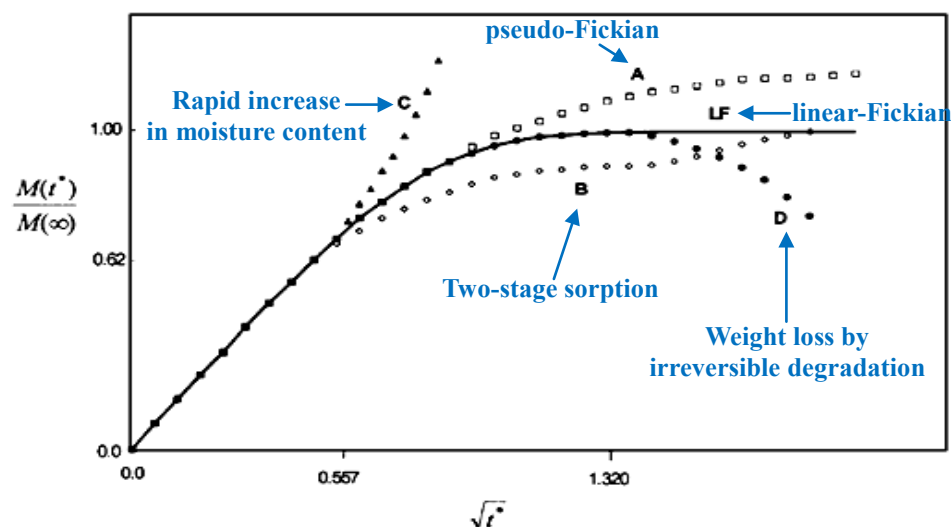


Figure 6-1: Schematic curves representing four categories of recorded non-Fickian weight-gain sorption [82]

The diffusion coefficient can be calculated either by monitoring the concentration characteristic from the volume of composite materials or via gravimetric measurements[83]. Ultimately, the diffusion coefficient can be determined according to a theoretical model used to fit experimental data trends. In case moisture uptake shows the Fickian diffusion, diffusion coefficient can be determined using the short-term approximation as expressed by Equation 6.3[84].

$$D = \frac{\pi h^2}{16M_\infty^2} \left(\frac{M_2 - M_1}{\sqrt{t_2} - \sqrt{t_1}} \right)^2 \quad (6.3)$$

where:

D = the Fickian coefficient of diffusion, mm^2/s

h = the thickness of the specimen, mm

M_∞ = the weight gain after equilibrium, g

M_1, M_2 = the percent changes in weight at time t_1 and t_2 , %

The test specimens used for moisture absorption tests are made in the form a thin plate so that the moisture enters predominantly through the surface marked by the length (l) and the width (b). However, as shown in Figure 6-2, contact angles of specimens in top and edge surface are 69° and 43° , respectively. Considering the edge effects on Equation 6.3, the diffusion coefficient multiplied by a correction factor is obtained in the form of the one-dimensional diffusion coefficient[84] as

$$D_{corr} = \frac{\pi h^2}{16M_\infty^2} \left(\frac{M_2 - M_1}{\sqrt{t_2} - \sqrt{t_1}} \right)^2 \left(l + \frac{h}{l} + \frac{h}{b} \right)^{-2} \quad (6.4)$$

where:

h = the thickness of the specimen, mm

l = the length of the specimen, mm

b = the width of the specimen, mm

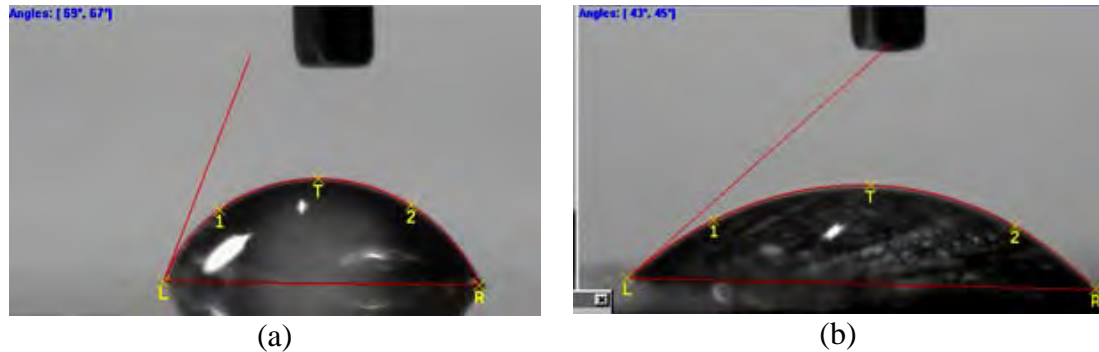


Figure 6-2: Contact angle of specimens in (a) top surface and (b) edge surface

6.2 Analyses and Results

6.2.1 Water Uptake

Glass fiber laminates have low Young's modulus, which makes it difficult to build structures with stiffness comparable to steel. Therefore, marine composite structures requiring high stiffness are often made of carbon fiber composite. However, a little of published papers are available on the effect of long-term seawater immersion on carbon fiber composite[85]. In addition, atmospheric ageing at high humidity has been reported to cause water uptake similar to that from immersion for epoxy laminates[86], while Gutierrez reported that ageing in sea air was as severe as in seawater for a range of marine composite. Especially, this study is focused on the effect of long-term seawater immersion on carbon fiber composites exposed to elevated temperatures for up to 72 hrs of ageing time using comparison with the effect of immersion in deionized water.

Before analysis of the effect of immersion on composites, the use of terms "absorption" and "adsorption" has to be clarified. Absorption is a capillary uptake by existing pores in materials and this process does not plasticize the matrix and generate little heat or swelling. Meanwhile, adsorption is the process by which a solution is formed and this process generates heat and swelling. If a polymer composite involves pores, air bubbles, or other such defects, both absorption and adsorption take place. In such a case, the term uptake is usually used[87].

The moisture uptake profiles for the carbon/epoxy composite specimens immersed in deionized water for 72 weeks are shown in Figure 6-3. Moisture uptake seems to follow two-stage diffusion response, with an initial period of linearity suggesting a diffusion-controlled process followed by a decrease in rate of moisture uptake. In other words, the results of the gravimetric measurements showed that the specimens immersed in deionized water displayed a Fickian response in all conditions. In the case of as-received specimens as shown in Figure 6-3 (a), saturation of weight gain did not occur until 1 year of immersion time and the levels of the maximum weight gain existed between 1.3% and 1.7%. These values were the lowest compared to the specimens in aged conditions. Specimens post-cured from the increase of ageing time and exposure temperature showed the rapid saturation and the higher maximum weight gain than in the case of un-cured specimens. The partially cured composite could be expected to have a greater concentration of unreacted chemical species with the epoxy resin and it appears that these were released more rapidly into water resulting in a slower net mass gain. Therefore, from experimental data, it should be pointed out that the degree of cure is proportional to the maximum mass uptake. The levels of the

maximum weight gain showed between 2.3% and 2.8% in exposure temperature, 177°C and these levels were the highest compared to any other exposure temperatures. The deterioration of composite due to thermooxidation lowered the level of the maximum weight gain from the exposure temperatures of more than 232°C. Therefore, the level of maximum weight gain can be crucial criteria to evaluate the degree of cure on specimen under-cured in ambient condition. In severe environmental conditions (ageing time: more than 16 hrs, exposure temperature: 260°C), the moisture uptake profiles did not show the Fickian behavior. The reason why Fickian behavior did not occur is that the char formed by extreme heat played a role of sponge to absorb the water and thus the amount of moisture involving in specimens was different whenever the specimens were weighed in balance.

The chemical structure and morphology of a polymer are known to influence moisture uptake. Especially, a high concentration of polar functional groups can cause increased sorption of polar penetrants. The significant concentration of hydrophilic hydroxyl groups located along the backbone exists in epoxy resin. Therefore, many investigations reported that the maximum mass gain in epoxy is higher compared to the vinyl ester, polyester and phenolic resins. In addition, it is known that glass fibers chemically react with water, usually alkali elements to leach out while carbon fibers do not absorb moisture and are resistant to any corrosive effects of water[88].

The coefficient of diffusion provides a valuable characteristic in describing the rate at which water uptake is occurring. The Fickian diffusion uses an initial linear uptake period that is characterized by saturation at the maximum moisture content. General diffusion coefficients and corrective diffusion coefficients including edge effect

on specimens immersed in deionized water for 72 weeks are obtained from experimental data and are tabulated in Table 6-1. Similar to the maximum mass uptake, diffusion coefficient was also increased with the degree of cure. The diffusion coefficients of the specimens aged in ambient condition existed between 5.5×10^{-8} mm²/s and 8.6×10^{-8} mm²/s. As the specimens reached fully cure, diffusion coefficients increased up to 29.152×10^{-8} mm²/s on specimen exposed to 121°C for 1 hr of ageing time. It is well known that although the epoxy resin exhibited the highest equilibrium uptake or solubility (i.e., the mass of sorbed penetrant per unit volume of specimen) compared to vinyl ester, polyester and phenolic resins, it has the lowest diffusion coefficients. Since diffusion coefficient is a function of permeability and solubility, this means the permeability of the epoxy is lower than that of other resins.

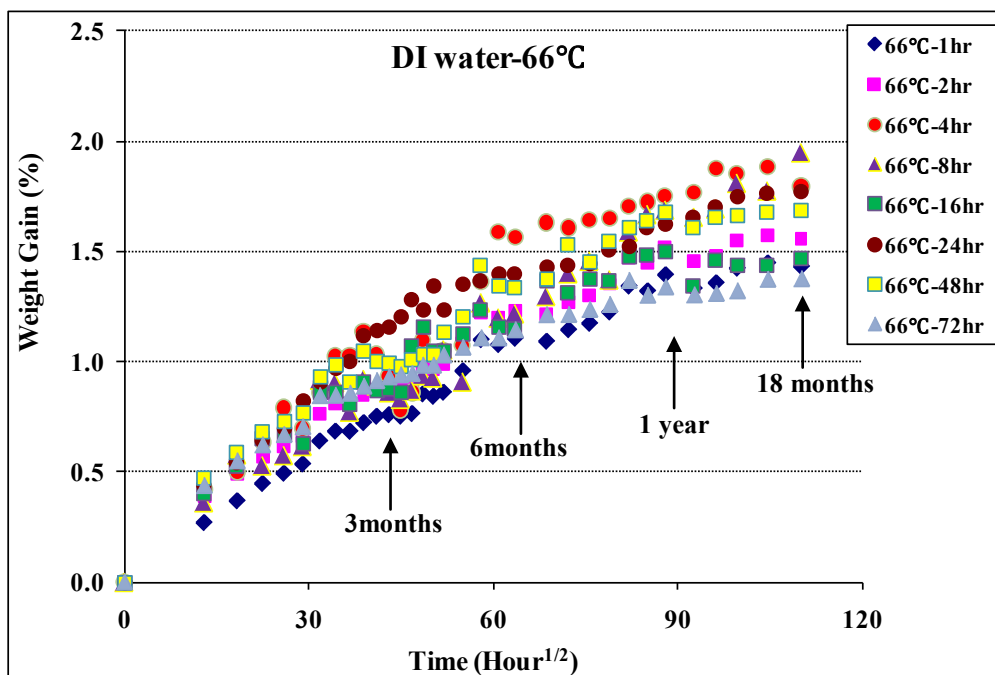
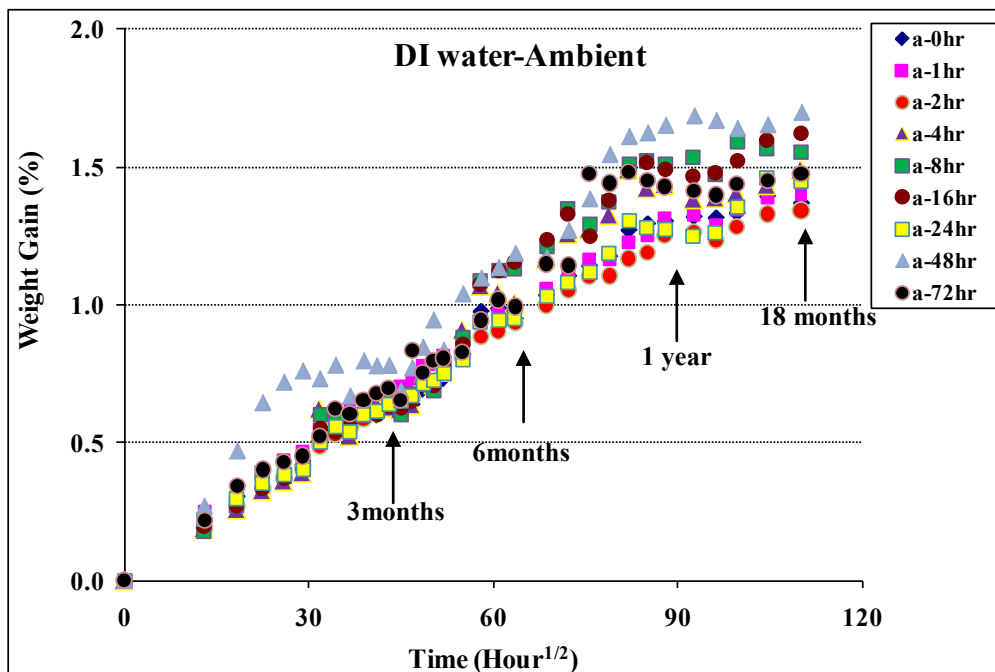
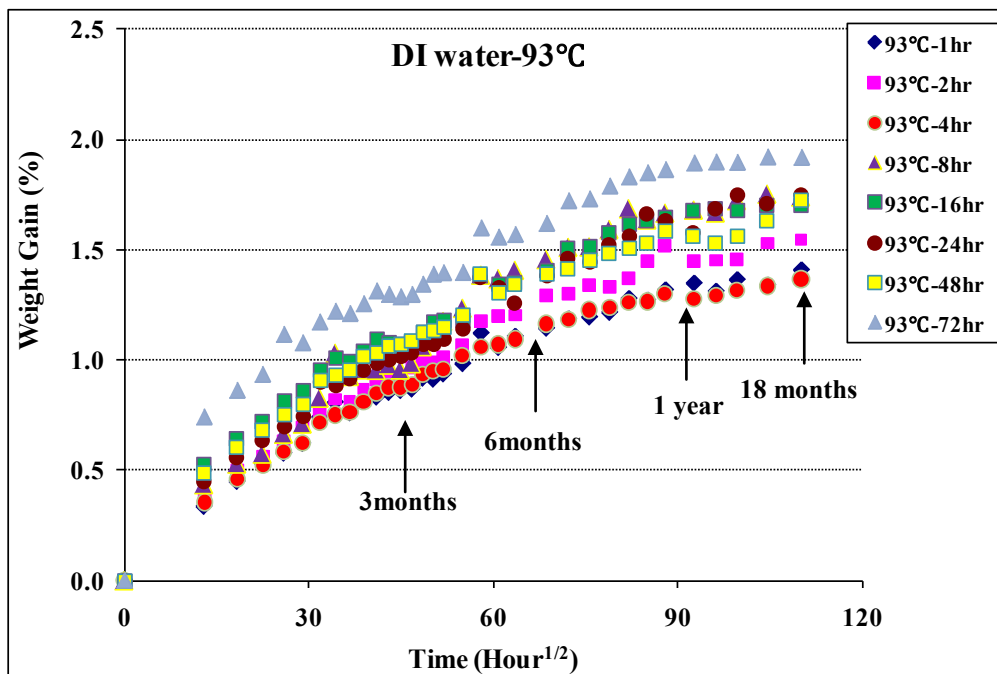
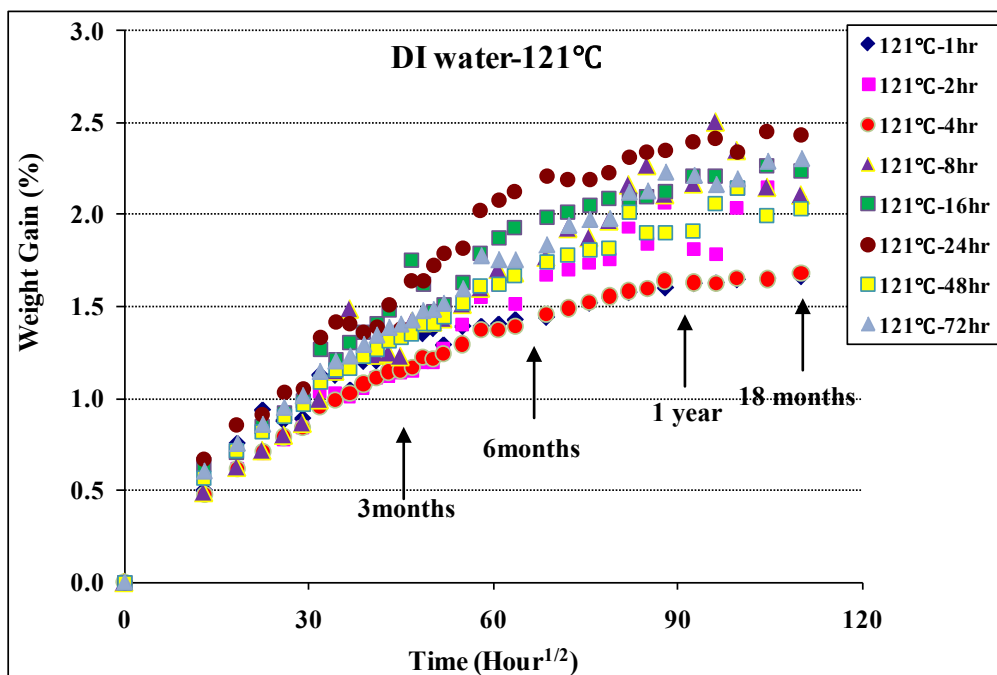


Figure 6-3: Weight Gain (%) on specimens immersed in deionized water for 72 weeks after exposure to elevated temperatures, (a) ambient (b) 66°C (c) 93°C (d) 121°C (e) 149°C (f) 177°C (g) 204°C (h) 232°C (i) 260°C



(c)



(d)

Figure 6-3: Continued

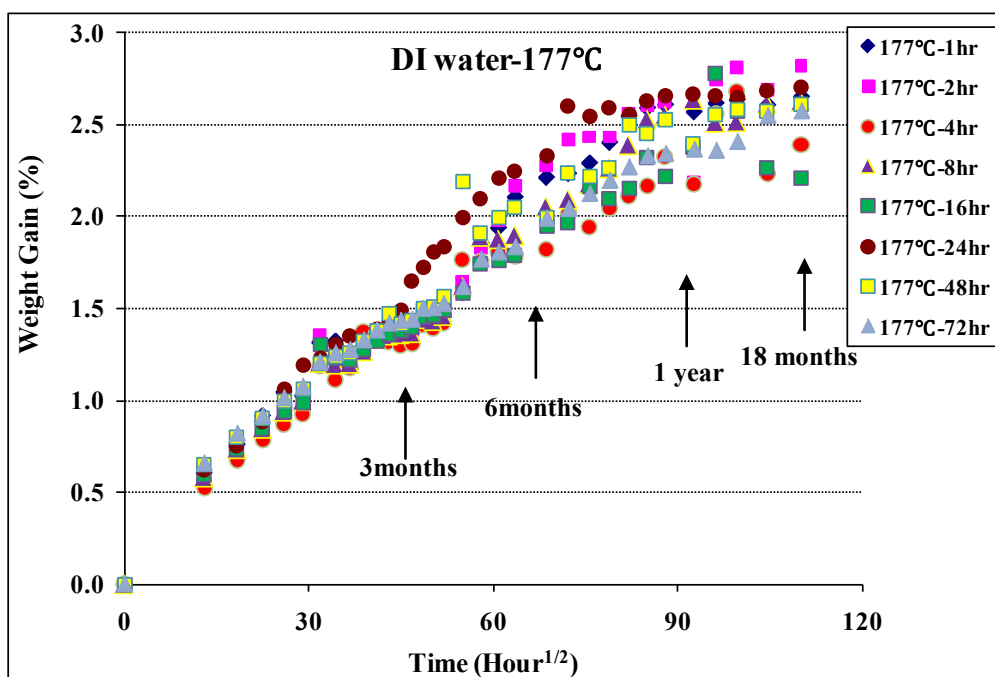
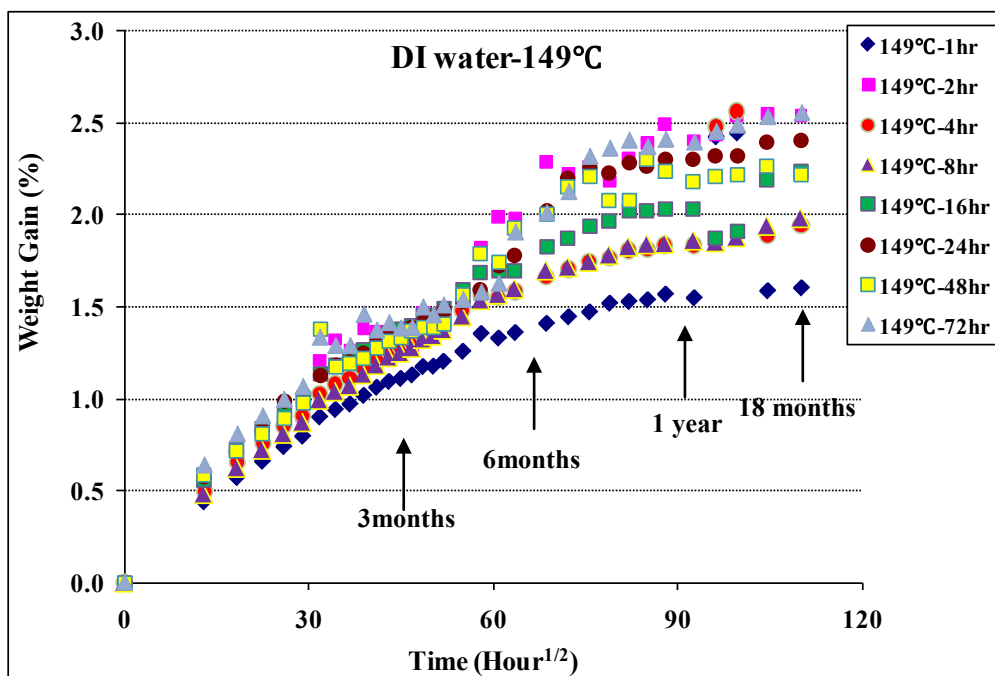


Figure 6-3: Continued

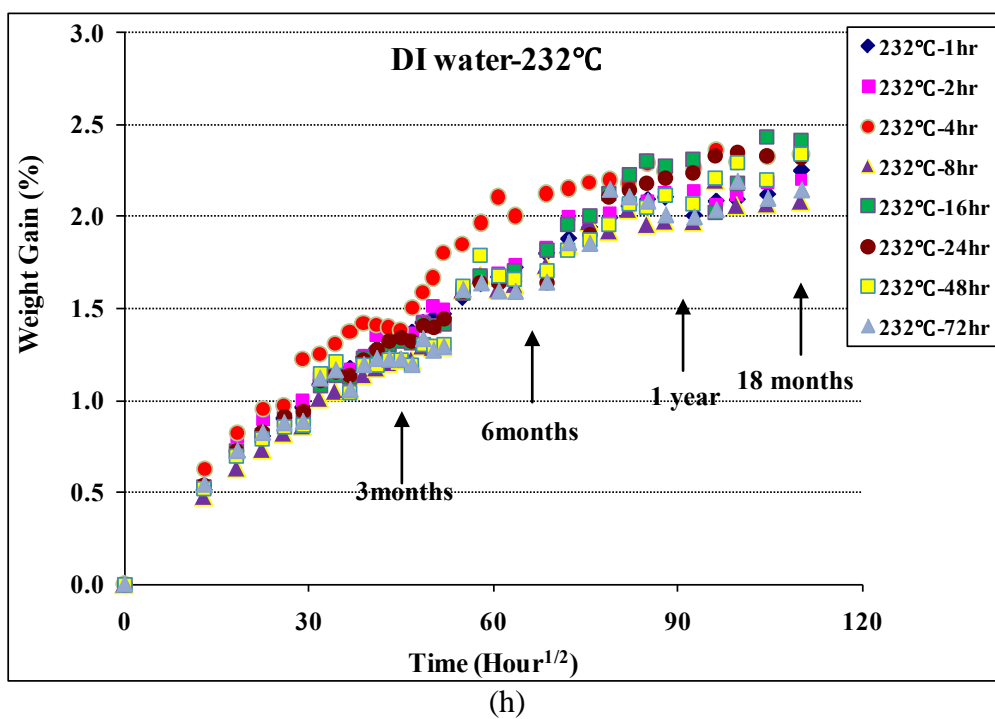
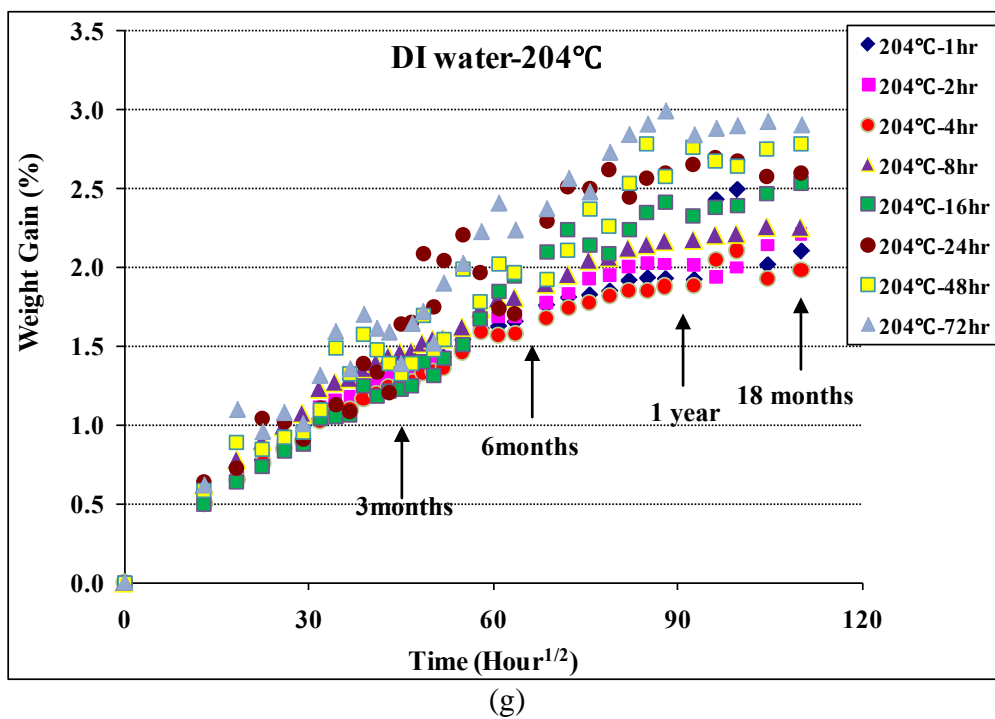


Figure 6-3: Continued

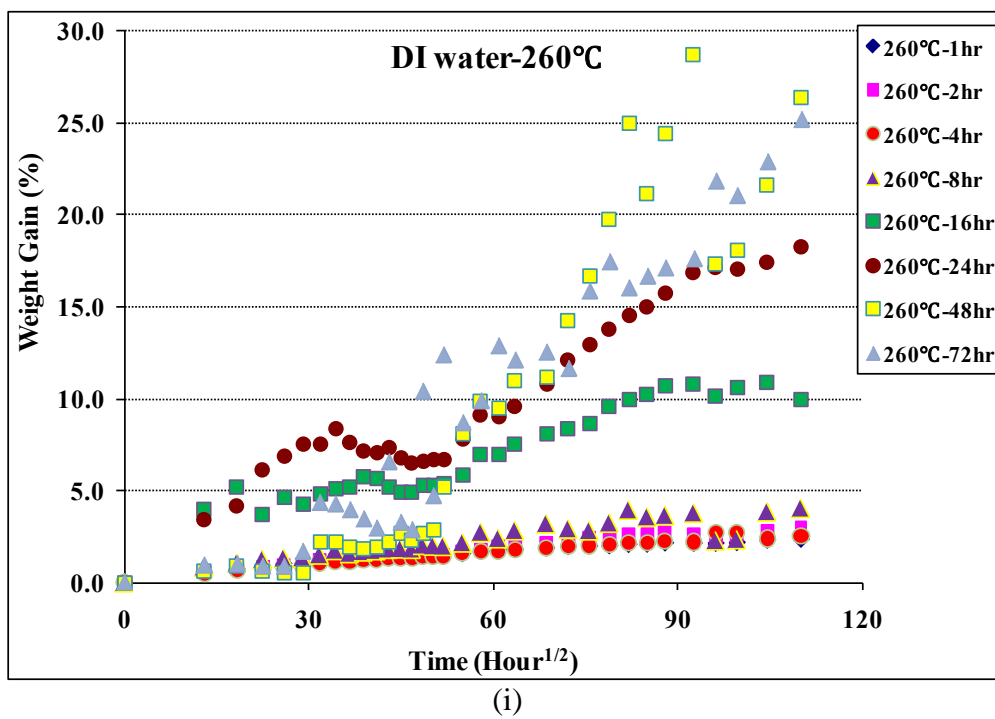


Figure 6-3: Continued

Table 6-1 Characteristics on specimens immersed in deionized water for 72 weeks after exposure to elevated temperatures

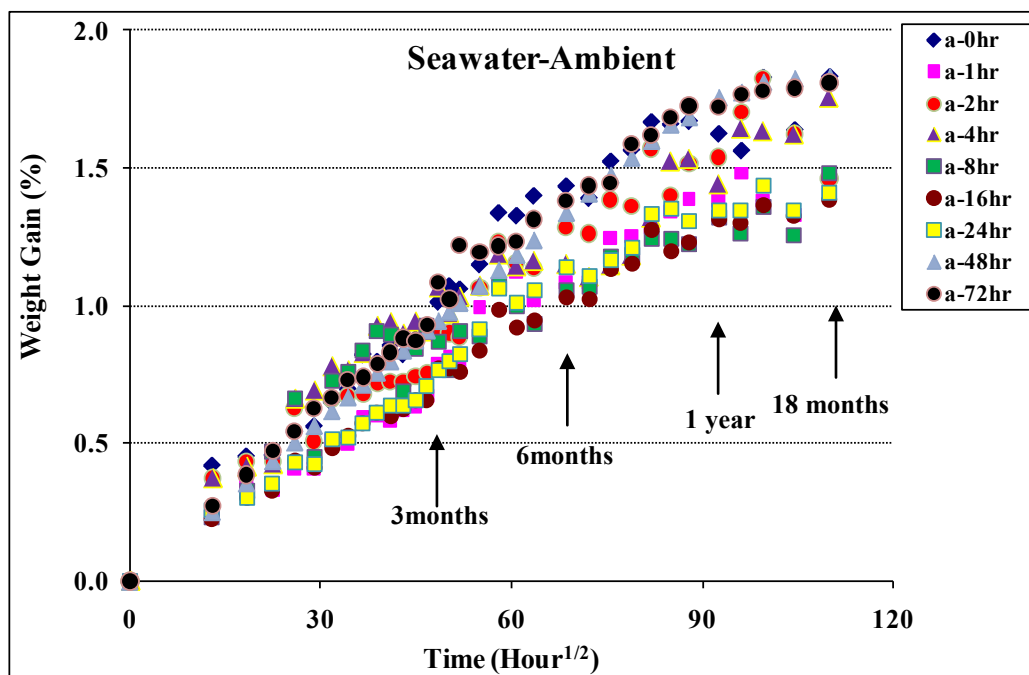
Exposure Temperature	Time	DI water							
		width (mm)	length (mm)	thickness (mm)	Mass (g)	M_{∞} (%)	$D \times 10^8$ (mm ² /s)	$D_{\text{corr}} \times 10^8$ (mm ² /s)	slope
Ambient (23°C)	0	25.9	25.74	3.01	2.235	1.392	6.762	0.0100	0.0138
	1	24.41	25.7	2.73	2.012	1.390	6.756	0.0101	0.0152
	2	25.71	25.4	3.15	2.443	1.330	8.672	0.0132	0.0146
	4	25.74	25.91	2.89	2.290	1.431	7.065	0.0103	0.0149
	8	25.63	25.88	3.01	2.325	1.566	6.363	0.0093	0.0142
	16	25.36	25.53	2.82	2.256	1.599	5.625	0.0085	0.0144
	24	25.94	25.99	3.03	2.430	1.459	6.920	0.0101	0.0142
	48	26.12	25.58	2.86	2.277	1.656	5.588	0.0084	0.0144
	72	25.83	25.72	2.9	2.427	1.450	7.599	0.0113	0.0155
66°C	1	25.86	25.74	3.15	2.423	1.448	10.050	0.0149	0.0164
	2	25.06	25.83	2.95	2.223	1.573	9.558	0.0141	0.0178
	4	25.78	24.78	3.17	2.262	1.886	10.382	0.0166	0.0189
	8	24.9	25.84	3.25	2.317	1.774	9.608	0.0141	0.0172
	16	25.87	25.61	3.15	2.390	1.439	14.300	0.0214	0.0195
	24	25.57	25.87	2.9	2.131	1.763	17.316	0.0254	0.0258
	48	25.83	26.02	3.1	2.426	1.675	11.181	0.0162	0.0189
	72	26.06	25.69	3.15	2.462	1.376	12.604	0.0187	0.0179
93°C	1	25.67	26.01	3.05	2.425	1.339	11.604	0.0168	0.0175
	2	25.94	26.02	3.17	2.530	1.530	12.799	0.0186	0.0189
	4	26	25.69	3.03	2.378	1.334	12.025	0.0179	0.0179
	8	26.04	25.68	2.87	2.307	1.752	10.673	0.0159	0.0204
	16	25.4	25.87	3	2.159	1.705	12.221	0.0179	0.0206
	24	25.96	25.83	3.08	2.365	1.709	11.992	0.0176	0.0199
	48	26.21	25.73	3.05	2.465	1.629	13.348	0.0198	0.0207
	72	25.75	25.88	3.15	2.285	1.919	14.535	0.0213	0.0227
121°C	1	25.94	25.52	2.92	2.152	1.654	29.152	0.0440	0.0322
	2	25.97	25.47	3.15	2.242	2.154	22.016	0.0333	0.0296
	4	25.94	25.2	2.95	2.184	1.648	22.905	0.0354	0.0282
	8	25.97	25.62	3.28	2.385	2.146	26.107	0.0390	0.0309
	16	25.46	26.1	2.98	2.219	2.262	23.597	0.0340	0.0332
	24	25.75	25.72	2.84	2.186	2.451	20.505	0.0305	0.0338
	48	25.47	25.81	3.12	2.512	1.991	23.516	0.0346	0.0297
	72	25.91	25.97	3.1	2.506	2.291	22.417	0.0326	0.0313
149°C	1	25.63	25.96	3.05	2.322	1.586	16.926	0.0247	0.023
	2	25.92	25.82	3.07	2.363	2.550	14.261	0.0210	0.0266
	4	25.66	25.93	3.19	2.580	1.886	25.442	0.0371	0.0294
	8	25.89	25.82	3.36	2.614	1.941	25.591	0.0376	0.0284
	16	25.94	25.61	3.17	2.550	2.193	20.730	0.0310	0.0288
	24	25.85	25.56	3.02	2.289	2.399	16.488	0.0248	0.0282
	48	25.92	25.52	3.2	2.422	2.267	19.730	0.0297	0.0283
	72	25.4	25.8	2.94	2.149	2.535	15.106	0.0223	0.0285

Table 6-1 Continued

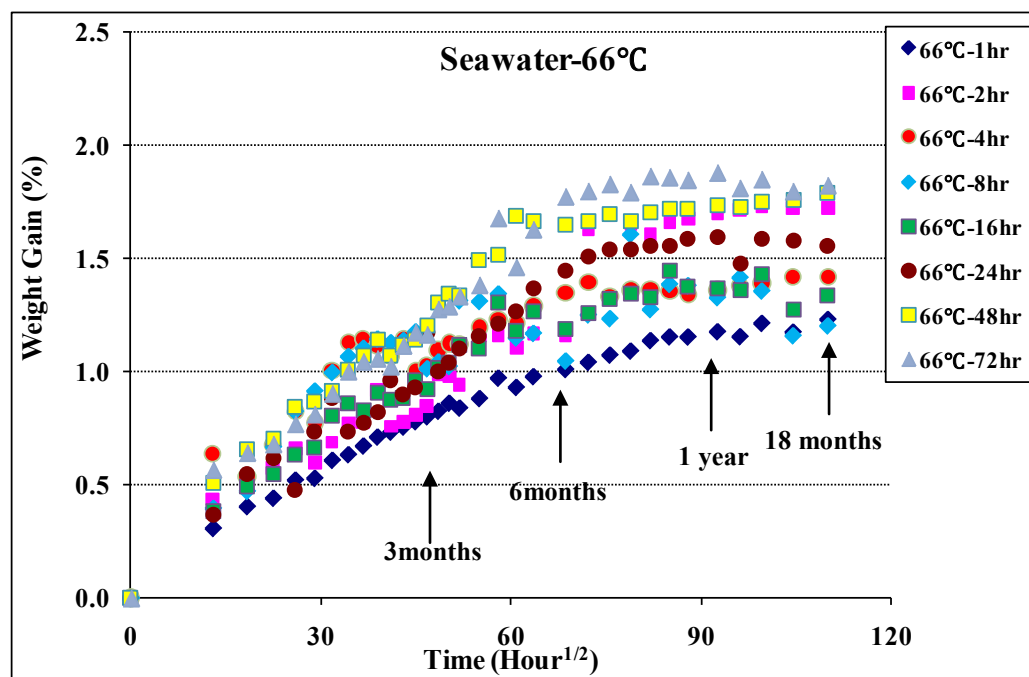
Exposure Temperature	Time	DI water							
		width (mm)	length (mm)	thickness (mm)	Mass (g)	M_{∞} (%)	$D \times 10^8$ (mm ² /s)	$D_{\text{corr}} \times 10^8$ (mm ² /s)	slope
177°C	1	25.86	25.78	2.91	2.216	2.606	11.343	0.0168	0.0253
	2	25.98	25.9	3.08	2.383	2.692	14.219	0.0208	0.272
	4	25.87	25.73	3.2	2.510	2.229	17.592	0.0261	0.0265
	8	25.68	25.89	2.99	2.312	2.615	12.797	0.0188	0.0262
	16	25.64	25.77	3.18	2.363	2.264	17.235	0.0255	0.0266
	24	24.69	25.79	3.23	2.359	2.682	22.132	0.0326	0.0323
	48	25.67	25.99	3.1	2.340	2.574	15.063	0.0219	0.0272
	72	25.4	26	3	2.306	2.553	13.810	0.0201	0.0268
204°C	1	25.94	25.74	3.16	2.570	2.015	16.620	0.0246	0.0248
	2	25.83	25.89	2.96	2.290	2.142	13.941	0.0204	0.025
	4	25.95	25.88	3.04	2.417	1.929	14.427	0.0212	0.0235
	8	25.52	25.82	3.04	2.238	2.257	14.867	0.0219	0.0258
	16	26.01	25.51	3.19	2.470	2.463	16.424	0.0248	0.027
	24	26.06	25.06	3.08	2.173	2.582	19.011	0.0297	0.0308
	48	25.86	25.97	3.25	2.553	2.747	17.638	0.0257	0.029
	72	26.08	25.9	3.3	2.538	2.930	21.946	0.0321	0.0329
232°C	1	25.8	25.82	3.14	2.529	2.118	14.872	0.0219	0.0242
	2	25.88	25.91	3	2.447	2.183	13.063	0.0191	0.0241
	4	25.07	25.81	3.08	2.358	2.326	17.938	0.0264	0.0284
	8	25.97	25.82	2.89	2.263	2.068	12.585	0.0186	0.0239
	16	24.93	25.92	2.87	2.293	2.435	10.893	0.0159	0.0243
	24	25.69	25.95	2.89	2.346	2.329	10.081	0.0147	0.0227
	48	25.48	25.89	2.98	2.212	2.203	11.936	0.0175	0.0233
	72	25.89	25.58	3.04	2.311	2.097	11.740	0.0176	0.0221
260°C	1	26.01	25.88	3.11	2.631	2.308	8.512	0.0125	0.0193
	2	25.74	25.87	3.07	2.449	2.816	13.110	0.0192	0.0268
	4	25.82	25.88	2.85	2.363	2.390	8.808	0.0129	0.0218
	8	25.77	25.98	3.06	2.274	2.846	9.512	0.0197	0.0319

Meanwhile, Figure 6-4 shows weight Gain (%) on specimens immersed in seawater for 72 weeks after exposure to elevated temperatures. Similar to the result of the immersion effect in deionized water, moisture uptake profile in seawater showed the Fickian behavior. The degree of cure is also proportional to the maximum weight gain and diffusion coefficient. If looking at Figure 6-4 (a), saturation of weight gain did not occur until 1 year of immersion time and the levels of the maximum weight gain existed between 1.3% and 1.8% similar to result of immersion in deionized water. The maximum weight gain did not largely increase until exposure temperature of 149°C. Also, in severe environmental conditions, weight gain was not accurately measured due to char created by thermooxidation and damage in the form of debonding, microcracking, and other types of morphological changes, thus allowing additional sorption to occur[89]. In this condition, although the variation of weight gain existed, continuous increase of weight gain was shown.

Table 6-2 shows diffusion coefficient and slope in linear region ($Mt/Mm < 0.6$) on specimens immersed in seawater for 72 weeks after exposure to elevated temperatures. Diffusion coefficient and corrective diffusion coefficient considering edge effect on specimens exposed to ambient temperature up to 72 hrs existed from $7.5 \times 10^{-8} \text{ mm}^2/\text{s}$ to $13.3 \times 10^{-8} \text{ mm}^2/\text{s}$ and from $0.01 \times 10^{-8} \text{ mm}^2/\text{s}$ to $0.02 \times 10^{-8} \text{ mm}^2/\text{s}$, respectively. Even though ageing time and exposure temperatures were increased, diffusion coefficient did not exceed $20 \times 10^{-8} \text{ mm}^2/\text{s}$ except for some environmental conditions.



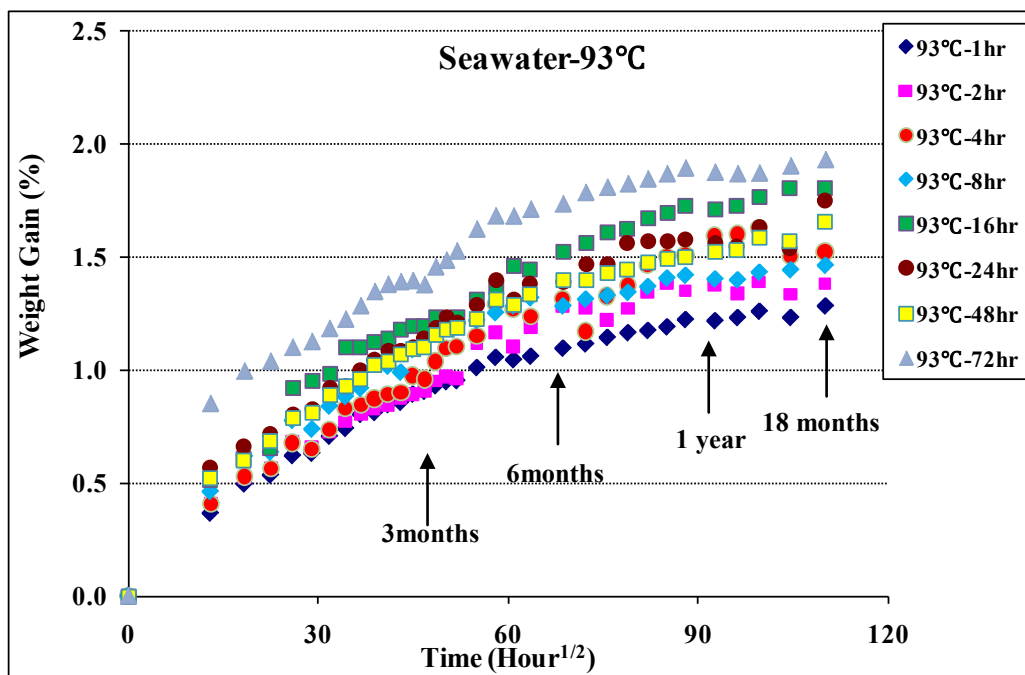
(a)



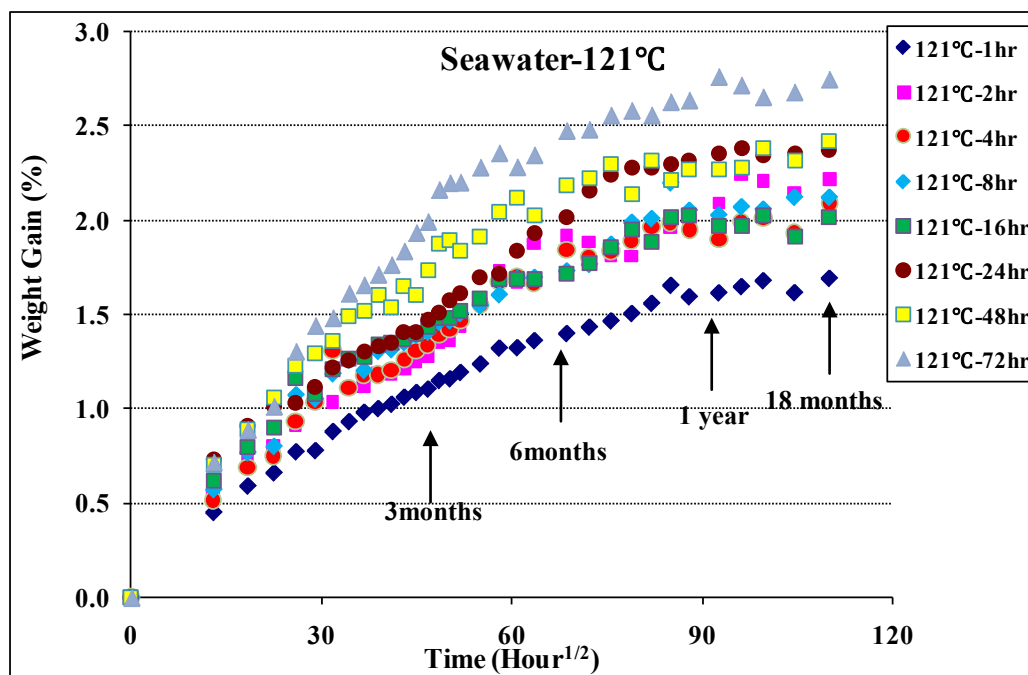
(b)

Figure 6-4: Weight Gain (%) on specimens immersed in seawater for 72 weeks after

exposure to elevated temperatures, (a) ambient (b) 66°C (c) 93°C (d) 121°C (e) 149°C (f) 177°C (g) 204°C (h) 232°C (i) 260°C

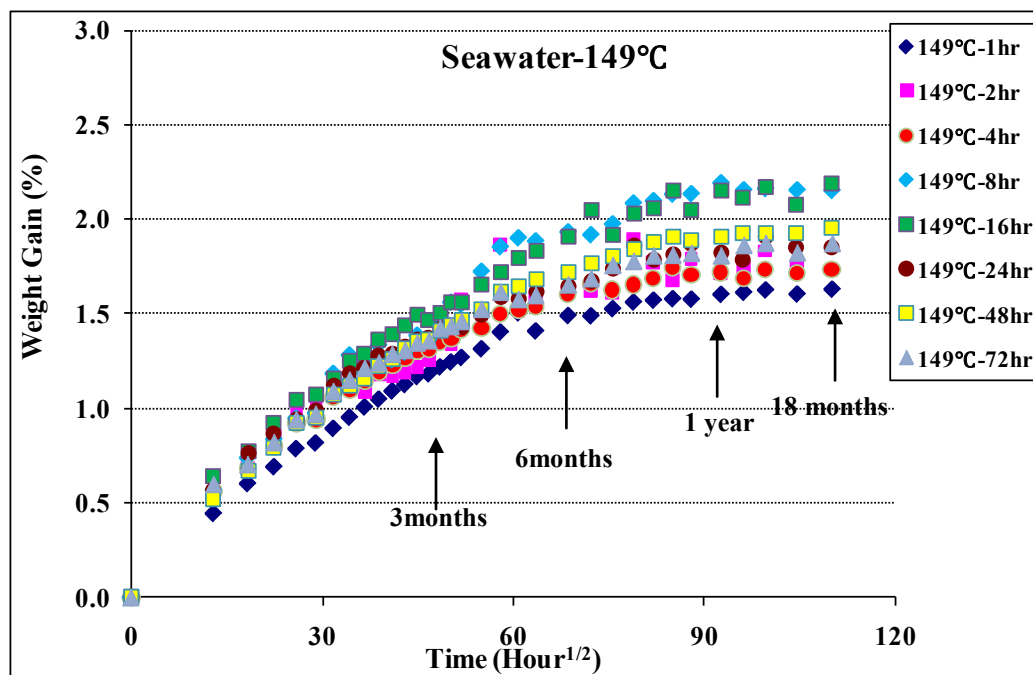


(c)

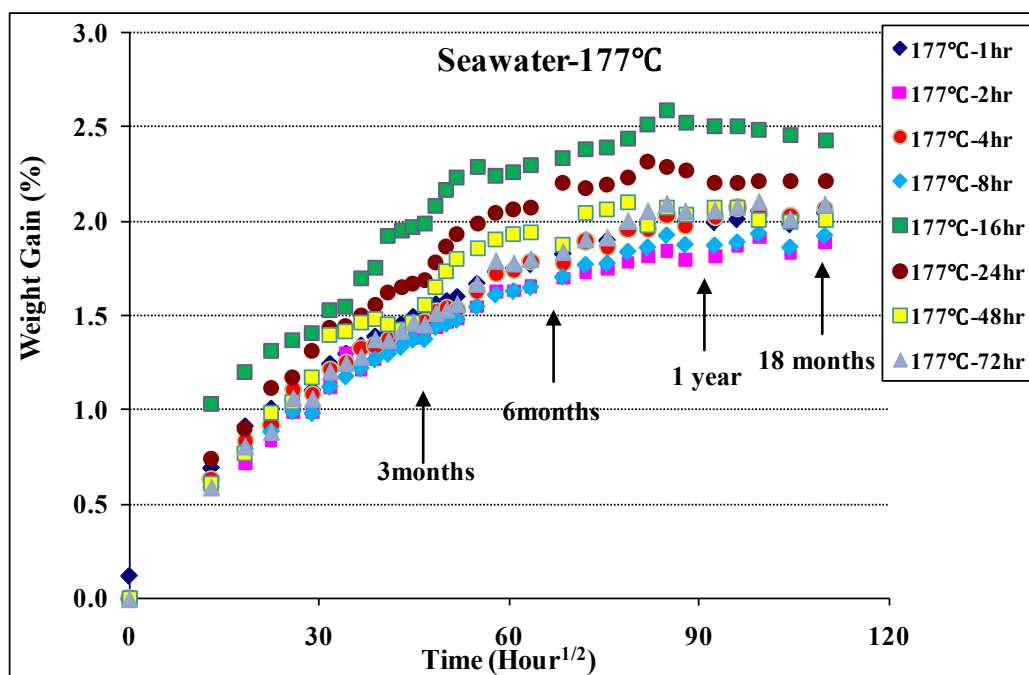


(d)

Figure 6-4: Continued



(e)



(f)

Figure 6-4: Continued

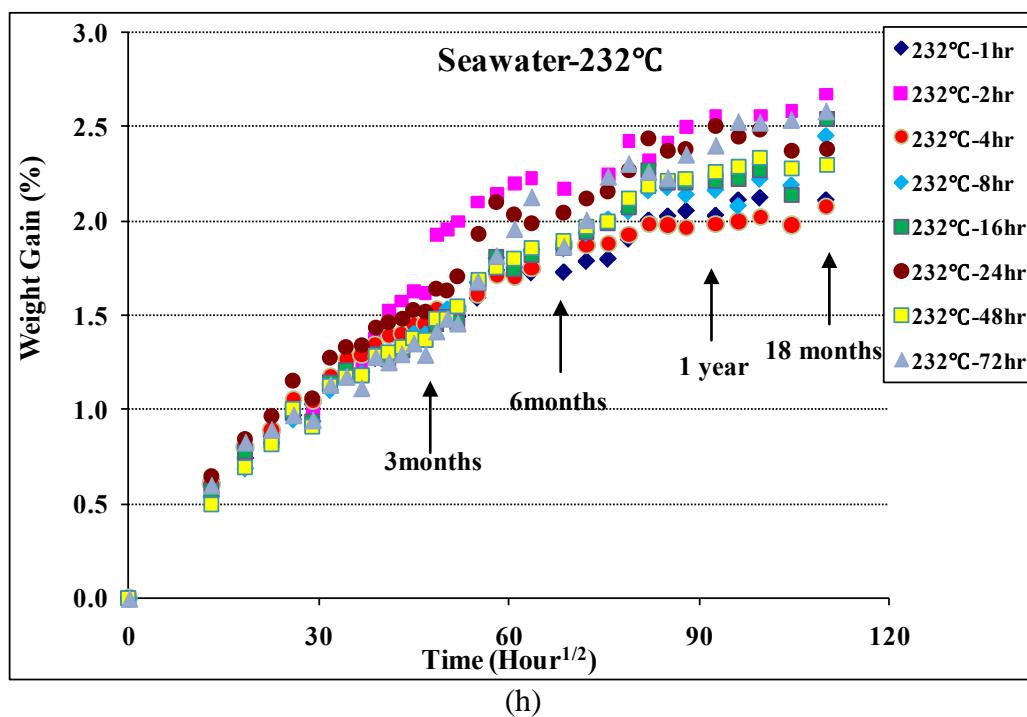
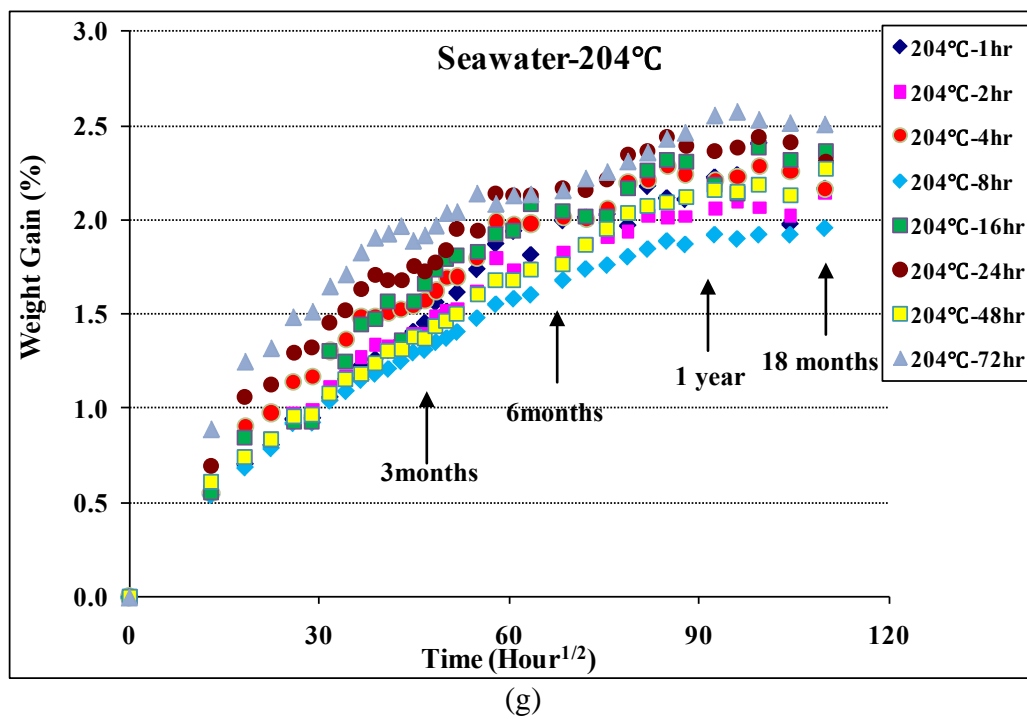


Figure 6-4: Continued

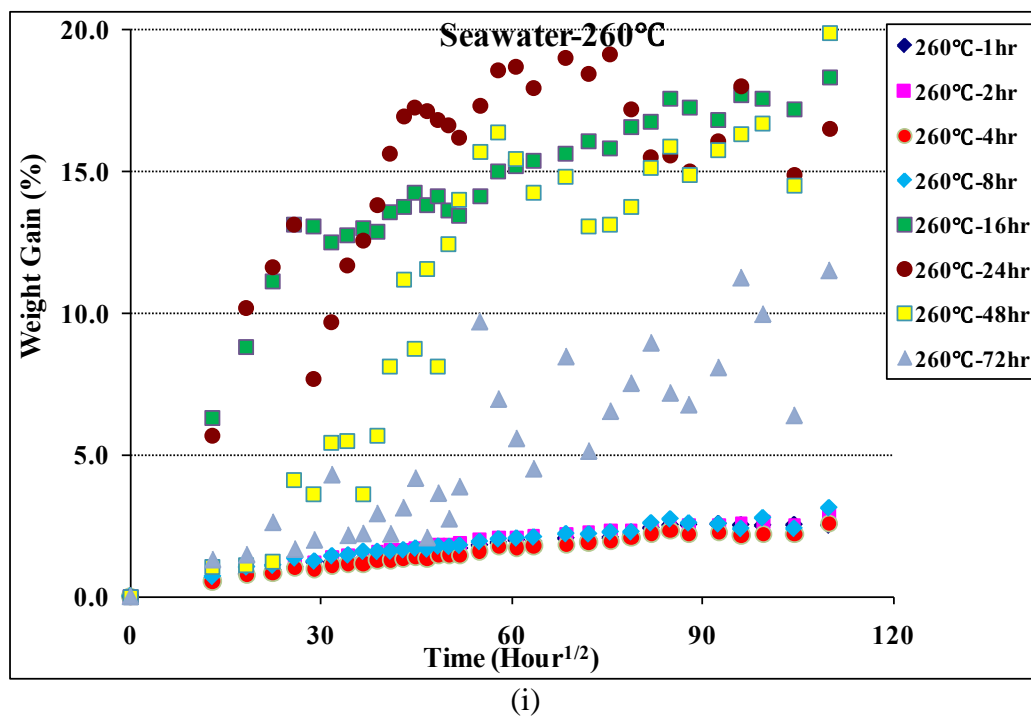


Figure 6-4: Continued

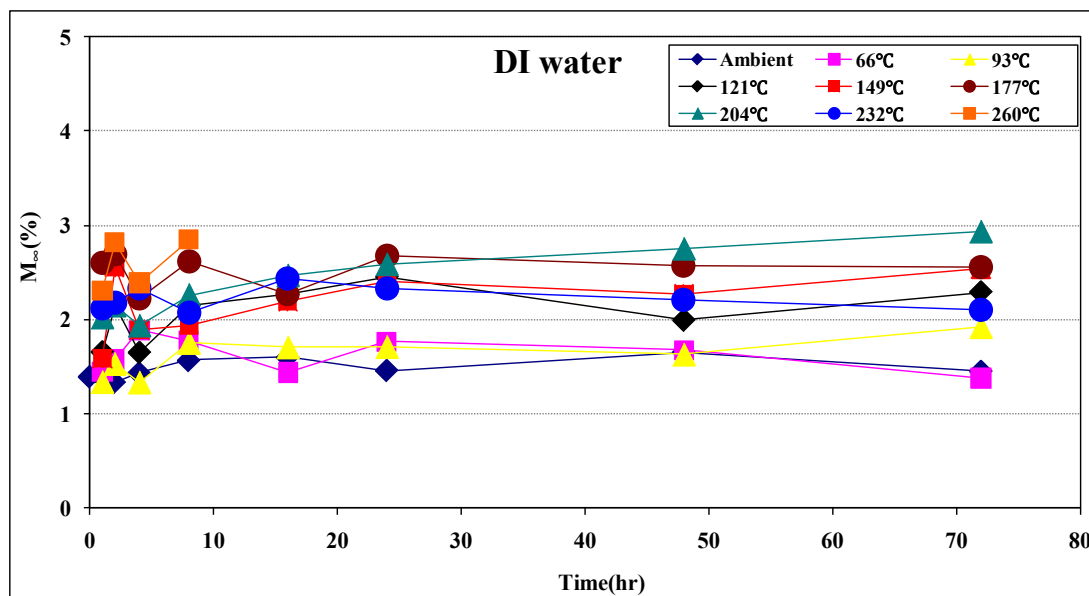
Table 6-2 Characteristics on specimens immersed in seawater for 72 weeks after exposure to elevated temperatures

Exposure Temperature	Time	seawater							
		width (mm)	length (mm)	thickness (mm)	Mass (g)	M _∞ (%)	D×10 ⁸ (mm ² /s)	D _{corr} ×10 ⁸ (mm ² /s)	slope
Ambient (23°C)	0	25.91	25.78	2.98	2.385	1.826	9.677	0.0143	0.0191
	1	25.98	24.81	3.02	2.323	1.382	7.567	0.0121	0.0145
	2	25.91	25.26	3.05	2.165	1.826	6.503	0.0100	0.0153
	4	25.97	25.95	2.99	2.320	1.633	11.354	0.0166	0.0195
	8	25.8	25.92	3.1	2.362	1.360	11.942	0.0175	0.0176
	16	25.63	25.78	3.19	2.628	1.366	8.664	0.0128	0.0146
	24	25.91	25.86	3.07	2.516	1.433	8.071	0.0119	0.0150
	48	25.48	25.92	2.82	2.161	1.811	9.105	0.0133	0.0195
	72	24.86	25.53	3.24	2.355	1.779	13.393	0.0201	0.0204
66°C	1	25.91	25.71	3	2.367	1.178	9.754	0.0145	0.0153
	2	25.99	25.95	2.98	2.253	1.723	7.935	0.0116	0.0168
	4	26.05	25	2.9	2.199	1.420	10.584	0.0166	0.0181
	8	25.92	25.97	3.3	2.589	1.160	15.912	0.0377	0.0225
	16	25.69	25.59	3.15	2.411	1.278	15.941	0.0239	0.0194
	24	25.84	24.99	3.2	2.299	1.580	13.442	0.0211	0.0195
	48	25.83	25.56	3	2.111	1.762	15.646	0.0235	0.0237
	72	25.68	25.92	3.23	2.517	1.799	16.301	0.0238	0.0227
93°C	1	25.77	25.87	3.1	2.203	1.233	12.145	0.0178	0.0169
	2	25.73	24.95	3.05	2.314	1.334	10.993	0.0173	0.0170
	4	24.84	25.74	3.15	2.196	1.503	13.276	0.0197	0.0192
	8	25.84	24.86	3.23	2.402	1.443	17.561	0.0278	0.0211
	16	25.85	25.55	3.18	2.294	1.802	14.682	0.0221	0.0219
	24	25.56	25.8	2.82	2.381	1.534	13.072	0.0193	0.0215
	48	25.83	26.15	3.2	2.430	1.571	16.436	0.0236	0.0215
	72	26.02	25.68	3.15	2.385	1.904	19.960	0.0297	0.0265
121°C	1	25.83	25.57	2.9	2.430	1.620	12.729	0.0191	0.0212
	2	26.17	25.78	3	2.320	2.149	13.376	0.0198	0.0242
	4	26.15	25.11	3.02	2.340	1.932	16.744	0.0261	0.0255
	8	25.91	25.86	3.12	2.305	2.118	16.687	0.0245	0.0258
	16	25.95	25.53	3	2.186	1.911	16.702	0.0252	0.0255
	24	26.21	25.73	3.18	2.193	2.351	15.735	0.0233	0.0259
	48	25.81	25.67	3.15	2.306	2.317	24.516	0.0365	0.0324
	72	25.84	25.8	3.14	2.234	2.676	32.632	0.0481	0.0403
149°C	1	25.81	25.78	3.2	2.471	1.605	17.462	0.0258	0.0224
	2	24.56	26.01	3.1	2.338	1.745	17.879	0.0259	0.0244
	4	25.8	25.08	2.93	2.259	1.718	14.293	0.0223	0.0229
	8	25.81	25.74	2.88	2.316	2.152	16.598	0.0246	0.0281
	16	25.77	25.93	3.04	2.411	2.081	16.884	0.0247	0.0264
	24	25.9	25.7	2.74	2.201	1.853	12.517	0.0186	0.0238
	48	25.87	25.97	3.24	2.543	1.926	19.175	0.0279	0.0254
	72	25.56	25.66	3.2	2.240	1.857	17.759	0.0265	0.0243

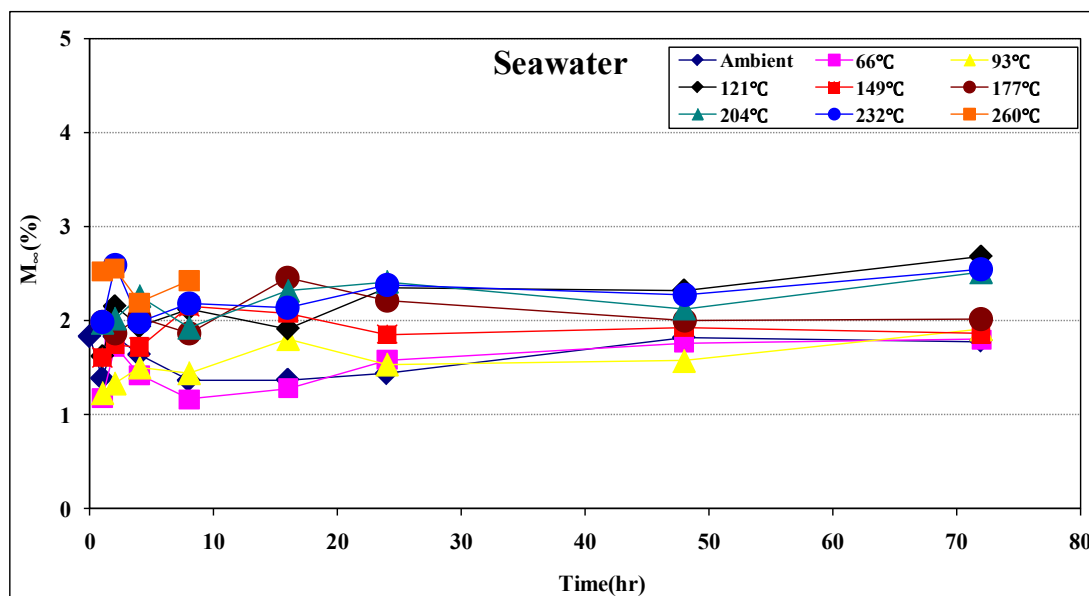
Table 6-2 Continued

Exposure Temperature	Time	seawater							
		width (mm)	length (mm)	thickness (mm)	Mass (g)	M _∞ (%)	D×10 ⁸ (mm ² /s)	D _{corr} ×10 ⁸ (mm ² /s)	slope
177°C	1	25.87	25.37	3.06	2.195	1.980	15.107	0.0230	0.0242
	2	25.93	25.87	2.9	2.330	1.866	15.115	0.0222	0.0248
	4	25.5	26.64	2.9	2.224	2.026	14.605	0.0202	0.0254
	8	26.05	24.86	2.98	2.242	1.860	15.126	0.0240	0.0241
	16	25.7	24.78	3.08	2.333	2.453	24.242	0.0387	0.0339
	24	25.79	25.84	3.04	2.358	2.213	22.032	0.0324	0.0311
	48	25.87	25.91	2.94	2.300	1.996	20.695	0.0303	0.0296
	72	25.73	25.82	3.12	2.259	2.012	18.670	0.0275	0.0266
204°C	1	25.86	25.8	3.12	2.411	1.975	23.552	0.0347	0.0296
	2	25.4	25.77	2.87	2.254	2.020	15.974	0.0236	0.0268
	4	25.33	25.73	3.07	2.297	2.258	19.815	0.0294	0.0295
	8	25.84	25.77	2.91	2.381	1.923	13.604	0.0201	0.0238
	16	25.93	25.83	2.89	2.367	2.313	19.912	0.0293	0.0318
	24	25.89	25.67	2.9	2.211	2.409	18.415	0.0275	0.0311
	48	25.89	25.82	3.2	2.540	2.127	16.809	0.0247	0.0253
	72	25.61	25.87	3.2	2.333	2.510	20.566	0.0301	0.0304
232°C	1	25.43	25.77	3.05	2.181	1.984	17.555	0.0260	0.0262
	2	25.65	25.95	3.18	2.430	2.584	22.964	0.0335	0.0328
	4	25.6	25.93	2.95	2.353	1.981	18.121	0.0265	0.0275
	8	26	25.74	3.21	2.594	2.187	20.291	0.0300	0.0281
	16	25.98	25.02	3.09	2.470	2.142	16.688	0.0261	0.0262
	24	25.66	25.82	3.13	2.383	2.370	19.616	0.0289	0.0295
	48	25.85	26.17	3	2.324	2.278	16.771	0.0241	0.0279
	72	25.89	25.76	2.96	2.532	2.542	11.751	0.0174	0.0250
260°C	1	25.86	26.02	3.13	2.327	2.519	16.397	0.0238	0.0278
	2	25.76	25.93	3.18	2.531	2.549	23.993	0.0350	0.0333
	4	25.89	25.03	2.94	2.201	2.189	15.011	0.0235	0.0264
	8	25.87	23.96	2.89	2.023	2.421	18.549	0.0317	0.0314

Figure 6-5 shows the maximum weight gain (%) on specimens immersed in deionized water and seawater at atmospheric temperature for 72 weeks. There is a little difference in the maximum weight gain. In particular, the maximum weight gain of all specimens which ageing time is less than 8 hrs in entire exposure temperatures was almost identical. All data of the maximum weight gain in these conditions existed between 1.2% and 2.8%. In both immersion conditions, the maximum weight gains were slightly increased in proportion to ageing time and exposure temperature. The difference among the maximum weight gains in lower (ambient, 66 and 93°C) and higher (121, 149, 177, 204, and 232°C) exposure temperatures existed on specimens immersed in deionized water. However, this gap was not shown on specimens immersed in seawater. This means that the unreacted chemical species in partially cured composite were released more rapidly into deionized water. In addition, it should be pointed out that the maximum weight gains in seawater were slightly lower than those in deionized water in overall environmental conditions. Apparently, the sorption of salts into the epoxy by diffusion and along fiber-matrix interface debonds and bulk material cracks by wicking can be resulted in the higher mass retention in seawater while the organic species leached from the specimens were separated from the salty residue by solvent extraction. The organic species were even found visually in seawater container. Consequently, mass loss by leaching of organic species than mass uptake by sorption of salts largely contributed to lower maximum weight gain in seawater compared to the values of deionized water.



(a)



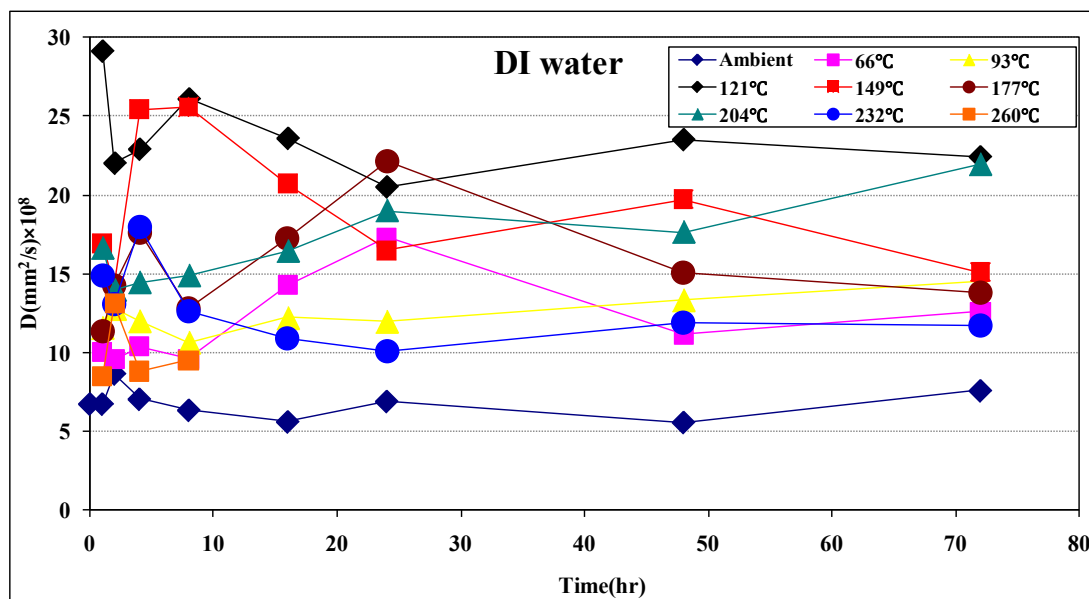
(b)

Figure 6-5: The maximum weight gain (%) on specimens immersed in (a) DI water and (b) seawater for 72 weeks

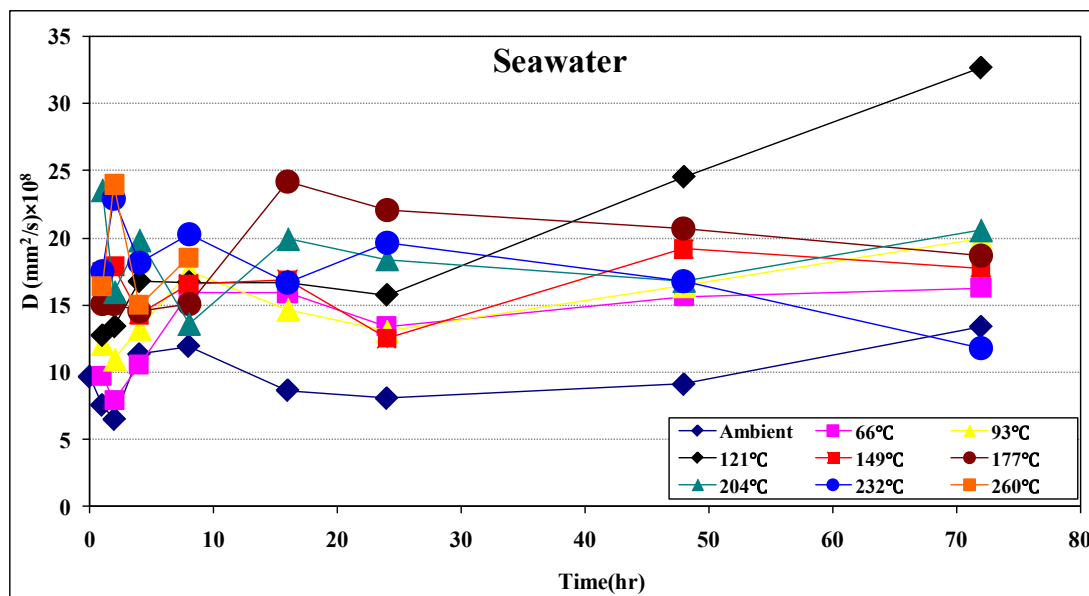
Figure 6-6 shows comparison of diffusion coefficients on specimens immersed in deionized water and seawater for 72 weeks. Overall diffusion coefficients calculated for deionized water immersion were higher than those for seawater immersion in all environmental conditions. Diffusion coefficients in deionized water were widely distributed with increase of ageing time and exposure temperatures. In other words, the degree of cure on specimens was strongly dependent on the diffusion coefficient. On the other hand, the variation of diffusion coefficients in immersion of seawater was less than that in deionized water. Lower diffusion coefficient in seawater seems to be attributed to mass loss by leaching out of organic species.

Epoxy resins have relatively high moisture absorption by the presence of hydroxyl groups in the epoxy chains attracting polar water molecules[90] whereas epoxy resins have superior chemical resistance compared to other resins. Therefore, although carbon/epoxy composites for this study showed higher maximum weight gain until saturation reach, this composite material showed the lowest diffusion coefficient compared to other composite materials.

It should be noted that both faces of the composite specimens were exposed to the deionized water and seawater. However, in actual service conditions, only one of the two flat faces of the externally bonded FRP is exposed to water. Therefore, moisture uptake and diffusion coefficient were obtained by more severe conditions.



(a)



(b)

Figure 6-6: Diffusion coefficients on specimens immersed in (a) DI water and (b) seawater for 72 weeks

6.2.2 Morphological Analysis

Swelling of the carbon/epoxy laminate composite by water uptake is the following mechanisms such as the increase of the free volume between the molecules due to water penetration into small pores, interface between carbon fiber and the epoxy resin and the delamination interface between layers. By water uptake, the epoxy is plasticized and caused cracks by creating volume expansion and increased stress. These mechanisms can result in the degradations of the epoxy and interface.

Morphological analysis regarding degradations caused by water uptake was accomplished using SEM images on specimens immersed in deionized water and seawater. Figure 6-7 shows SEM images at 250 \times and 500 \times magnification fractured by short beam shear test on specimens immersed in seawater for 72 weeks after exposure to the various conditions. As shown in Figure 6-7 (a), specimens after exposure to 260 $^{\circ}$ C for 8 hrs showed severe fracture of the epoxy, pulling-out of the carbon fibers and smooth surface of the carbon fibers without resin particles in the section fractured by tension. In particular, the epoxy surrounding carbon fibers showed more severe cracks. Hydrolysis, swelling and plasticization by water uptake resulted in destruction of the epoxy and trail of carbon fibers in the section fractured by compression. Delamination between 2 layers was found on specimens exposed to 232 $^{\circ}$ C for 72 hrs as presented in Figure 6-7 (b). Beside delamination, the evidences of degradation occurred on specimens exposed 260 $^{\circ}$ C for 8 hrs were also found by short beam shear test. Specimens exposed to 121 $^{\circ}$ C for 8 hrs showed relatively good fiber-matrix bonding and thus epoxy resin was closely adhered to carbon fibers as shown in Figure 6-7 (a).

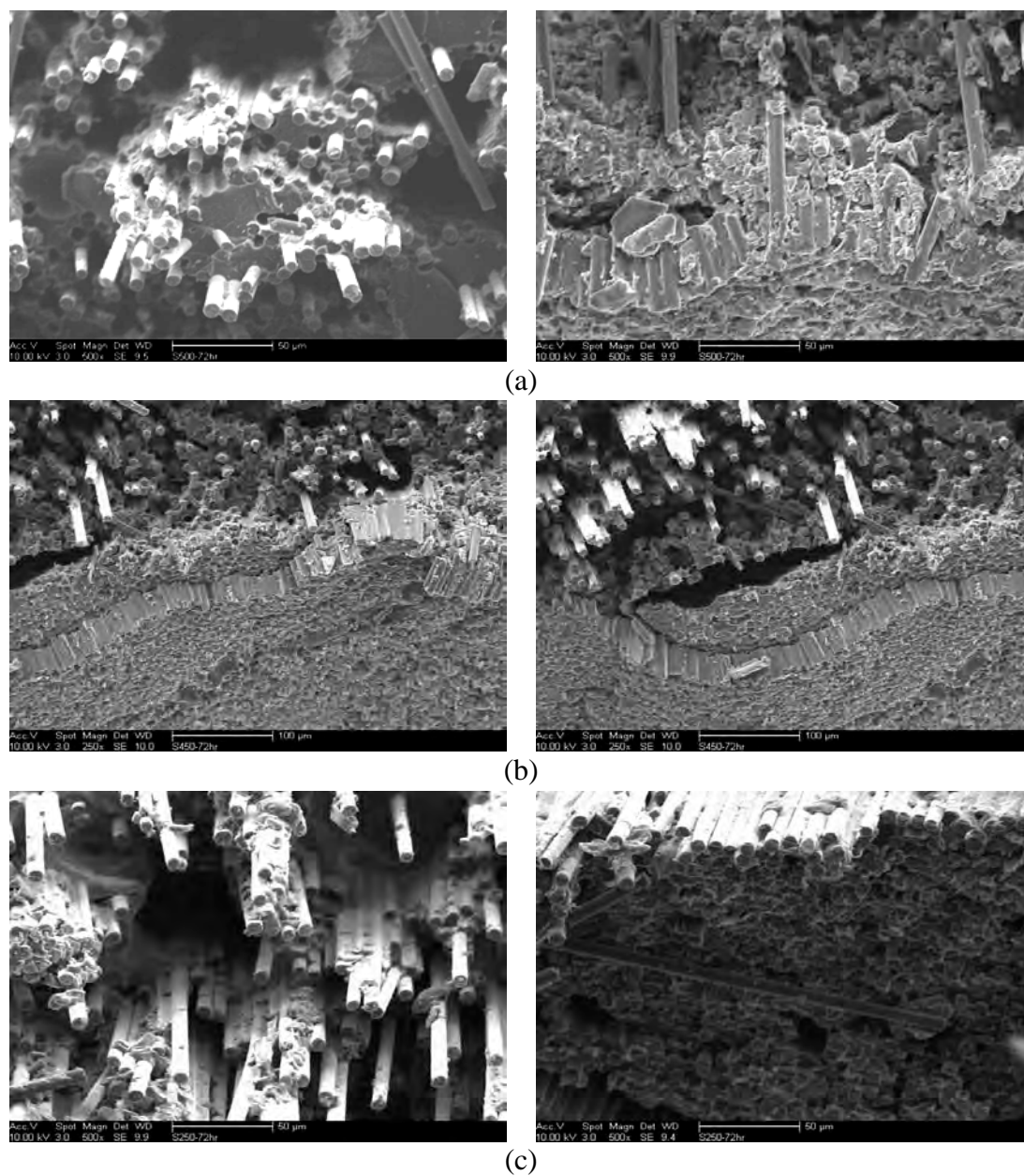


Figure 6-7: Scanning electron micrographs at 250 \times and 500 \times magnification fractured by short beam shear test on specimens immersed in seawater for 72 weeks after exposure to (a) 260 $^{\circ}$ C for 8 hrs (b) 232 $^{\circ}$ C for 72 hrs (c) 121 $^{\circ}$ C for 8 hrs

Compared to the morphological analysis on specimen immersed in seawater, the specimens fractured by short beam shear test after immersion in deionized water did not showed different degradation mechanisms. As depicted in Figure 6-8 (a), specimens immersed in deionized water for 72 weeks after exposure to 260°C for 8 hrs showed catastrophic cracks in the epoxy and interface and the delaminations between 2 layers. Cracks and cavities created by thermooxidation when the specimens were heated to high temperature accelerated the severe degradations from rapid water uptake and hydrolysis within carbon/epoxy composite materials. Since specimens exposed to 121°C for 8 hrs showed good mechanical properties by post-curing effect without degradation due to thermooxidation, bonding between the fibers and matrix was relatively superior to specimens exposed to high temperature as shown in Figure 6-8 (b) although immersion was progressed for 72 weeks.

Figure 6-9 shows SEM images of cross section delaminated between 2 layers on specimens immersed in seawater for 72 weeks after exposure to 260°C for 8 hrs . Particles, cracks and cavities of the epoxy by water uptake and hydrolysis were founded in the cross section delaminated between 2 layers. No failure shape of 'hackles' as shown in Figure 4-38 (b), (c) and (f) were occurred on specimens immersed in deionized water for 72 weeks. This phenomenon is attributed to the deterioration of interfacial bonding between the carbon fibers and the epoxy resin.

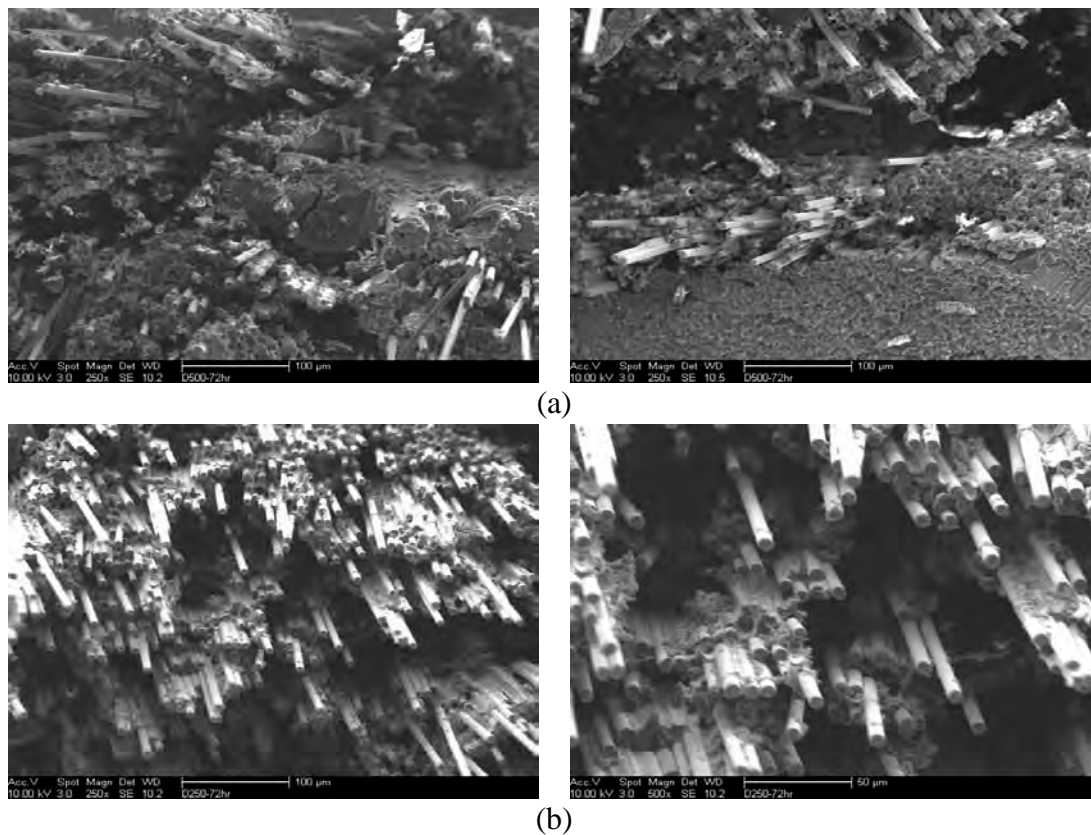


Figure 6-8: Scanning electron micrographs at 250 \times and 500 \times magnification fractured by short beam shear test on specimens immersed in deionized water for 72 weeks after exposure to (a) 260 $^{\circ}$ C for 8 hrs (b) 121 $^{\circ}$ C for 8 hrs

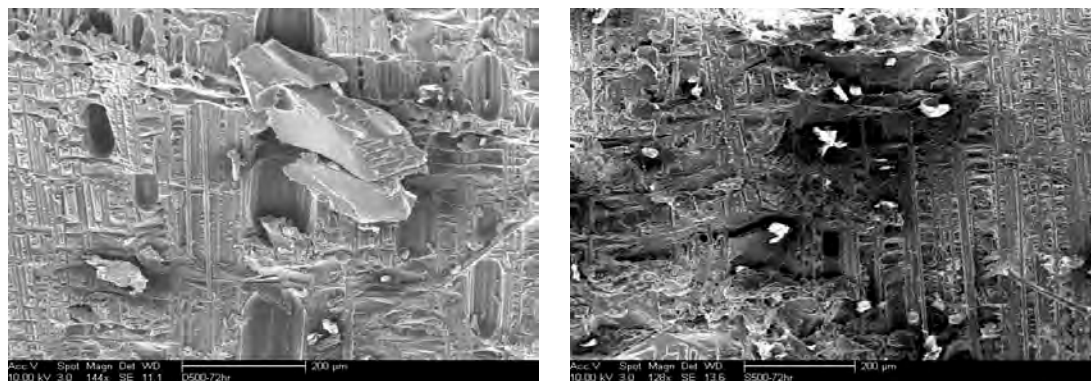


Figure 6-9: Scanning electron micrographs of cross section between 2 layers on specimens immersed in seawater for 72 weeks after exposure to 260 $^{\circ}$ C for 8 hrs

6.2.3 Short Beam Shear Testing

To investigate the mechanical property of specimens immersed in deionized water and seawater for 72 weeks after exposure to elevated temperatures for up to 72 hrs, short beam shear test was accomplished in accordance with ASTM D2344. In case the specimens of all conditions tested in chapter 4.4 are used to characterize the immersion effect, so many specimens and times are required for short beam shear test immersed in deionized water and seawater. Therefore, the specimens aged for 8 hrs at elevated temperatures were used to investigate the temperature-dependent characterization after immersion while, for time-dependent characterization, the specimens exposed to 232°C for up to 72 hrs of ageing time were utilized. Total specimens used in short beam shear test for immersion effect were 1,280 since 5 specimens were tested in each of conditions such as 4, 8, 12, 16, 24, 36, 48 and 72 weeks in immersion period.

6.2.3.1 Temperature Dependence

Data and comparison of short beam shear strength on specimens immersed in deionized water for 72 weeks after exposure to elevated temperatures in 8 hrs of ageing time are presented in Table 6-3 and Figure 6-10. Except for the specimens immersed in deionized water after exposure to 260°C for 8 hrs, all specimens showed similar characterizations which had initially decrease (~ 16 weeks), asymptotic trend or slightly increase (16 ~ 48 weeks) and rapidly decrease after 48 weeks in terms of short beam shear strengths. Initially rapid drop and asymptotic trend were corresponded to Fick's law which the mass of absorbed water increases linearly with the square root of time

and then gradually slows until equilibrium. The rate of decrease in short beam shear strengths after immersion from original state to 72 weeks in deionized water was 23.0, 28.1, 35.7, 38.7, 36.0, 33.7, 35.2, 35.9 and 30.7% on specimens exposed to ambient, 66, 93, 121, 149, 177, 204, 232 and 260°C respectively. Post-cured specimens in intermediate exposure temperatures (121, 149, 177, 204, 232°C) had higher rate of decrease in short beam shear strengths compared to other conditions since, as investigated in chapter 6.2.1, specimens post-cured from the increase of ageing time and exposure temperature showed the rapid saturation and the higher maximum weight gain compared to un-cured specimens. Contrary to specimens in other conditions, specimens exposed to 260°C for 8 hrs showed initially a little of increase in short beam shear strengths. However, after 48 weeks in immersion time, rapid decrease of short beam shear strengths occurred by delamination between 2 layers due to moisture uptake.

From many researches, it is well known that epoxy has the superior durability and the lowest diffusion coefficient compared to vinylester, polyester and phenolic resins in water environmental conditions. In addition, it is known that glass fibers chemically react with water while carbon fibers do not absorb moisture and are resistant to any corrosive effects of water. Therefore, intrinsic properties of epoxy and carbon fiber against water resulted in a slight decrease or asymptotic trend in terms of short beam shear strengths until 48 weeks in immersion period. However, it appears that catastrophic drop of short beam shear strengths after 48 weeks of immersion was derived from irreversible degradations such as hydrolysis, microcracking, microvoids and epoxy relaxation.

Table 6-3 Data of Short Beam Shear Strengths on specimens immersed in DI water for 72 weeks after exposure to elevated temperatures in 8 hrs of ageing time

Strength (MPa) - DI water									
weeks	Ambi	66°C	93°C	121°C	149°C	177°C	204°C	232°C	260°C
0	42.43	45.45	46.94	47.93	50.69	46.03	48.08	46.71	27.34
4	38.79	41.61	41.55	40.15	42.35	41.98	39.99	42.73	31.74
8	39.45	42.47	41.08	38.35	39.12	40.90	40.95	40.75	30.63
12	39.51	40.82	40.48	40.42	38.54	38.37	37.45	41.85	30.48
16	36.25	41.50	40.88	39.89	38.67	38.99	36.16	40.81	31.57
24	36.97	39.72	41.23	38.89	38.47	40.31	39.11	41.05	30.66
36	39.13	40.21	39.46	38.65	39.28	39.68	38.11	39.39	30.65
48	39.37	41.47	39.23	38.27	40.20	42.00	37.29	38.92	27.60
72	31.69	32.68	30.17	29.39	32.44	30.51	31.15	29.95	18.94

Standard deviation (MPa)									
weeks	Ambi	66°C	93°C	121°C	149°C	177°C	204°C	232°C	260°C
0	1.41	2.25	1.12	1.50	1.51	1.63	0.60	2.66	2.46
4	3.08	0.90	3.48	1.25	1.59	2.84	2.14	3.24	1.85
8	2.29	1.67	1.16	1.56	1.17	2.22	2.52	1.79	5.23
12	2.35	2.51	1.40	1.89	1.36	1.97	3.28	1.25	5.61
16	1.59	2.57	0.47	3.03	0.41	1.54	1.48	1.48	2.65
24	1.97	2.22	0.80	2.92	2.74	1.15	3.33	3.64	5.96
36	2.50	1.48	1.81	2.06	1.61	1.75	1.77	1.41	5.86
48	2.22	1.44	2.38	2.27	1.83	2.94	0.64	5.15	3.48
72	2.45	1.89	2.97	2.67	2.24	3.21	1.21	5.41	5.98

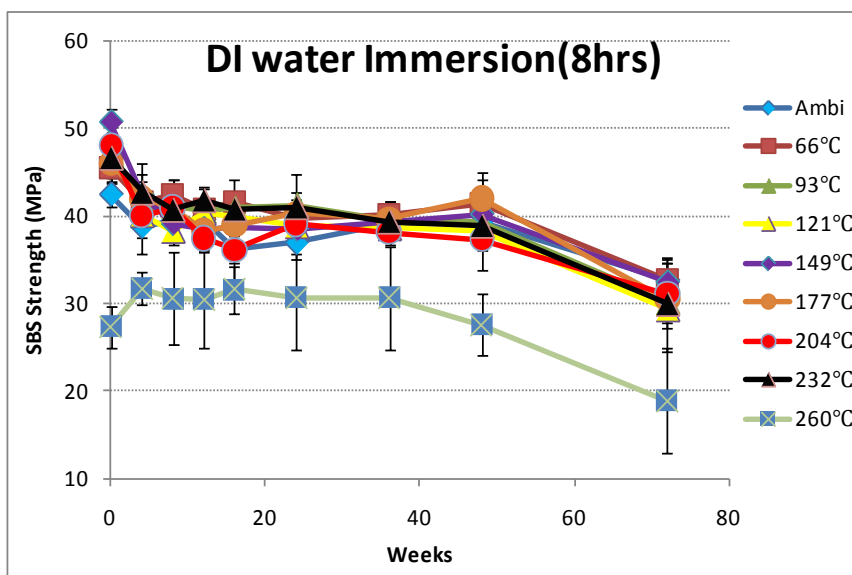


Figure 6-10: Comparison of Short Beam Shear Strengths on specimens immersed in DI water for 72 weeks after exposure to elevated temperatures in 8 hrs of ageing time

To compare of results of short beam shear test immersed in deionized water, short beam shear tests were conducted using specimens immersed in seawater under same environmental conditions. Data and comparison of short beam shear strength on specimens immersed in seawater for 72 weeks after exposure to elevated temperatures in 8 hrs of ageing time are shown in Table 6-3 and Figure 6-10. As demonstrated in chapter 6.2.1, although a little difference between specimens immersed in deionized water and seawater existed with regard to diffusion coefficient and the maximum water uptake, the results of short beam shear strengths on specimens immersed in seawater were in good agreement with the data immersed in deionized water as shown in Figure 6-10 and Figure 6-11. In addition, it seems that salt or salinity involving in seawater did not influence deterioration and degradation in short beam shear property.

The rate of decrease in short beam shear strengths after immersion from original state to 72 weeks in seawater was 22.7, 25.2, 32.8, 36.3, 40.7, 33.4, 31.0, 35.3 and 22.7% on specimens exposed to ambient, 66, 93, 121, 149, 177, 204, 232 and 260 respectively. These rates of decrease in short beam shear strengths were slightly lower than the values after immersion in deionized water. However, the difference of rate of decrease was negligible.

Table 6-4 Data of Short Beam Shear Strengths on specimens immersed in Seawater for 72 weeks after exposure to elevated temperatures in 8 hrs of ageing time

Strength (MPa) - seawater									
weeks	Ambi	66°C	93°C	121°C	149°C	177°C	204°C	232°C	260°C
0	42.43	45.45	46.94	47.93	50.69	46.03	48.08	46.71	27.34
4	39.59	41.56	39.39	40.15	39.48	40.18	36.40	41.57	32.52
8	39.18	39.22	40.99	39.22	41.56	39.71	39.49	40.58	31.10
12	39.84	41.79	40.31	38.63	40.54	39.52	40.40	41.70	32.70
16	37.24	42.31	41.12	38.95	39.43	38.62	40.10	39.06	31.06
24	41.84	41.73	40.64	41.22	38.46	39.19	42.22	38.13	32.19
36	38.18	40.37	39.96	38.86	38.36	38.64	39.27	39.50	31.85
48	40.87	43.89	39.68	38.30	38.76	39.61	42.40	37.29	30.87
72	32.79	34.01	31.54	30.55	30.07	30.65	33.17	30.22	21.12

Standard deviation (MPa)									
weeks	Ambi	66°C	93°C	121°C	149°C	177°C	204°C	232°C	260°C
0	1.41	2.25	1.12	1.50	1.51	1.63	0.60	2.66	2.46
4	1.68	3.63	3.62	1.25	3.08	2.08	3.83	2.23	0.83
8	0.79	2.08	1.29	2.79	3.31	0.76	1.91	2.11	2.41
12	2.48	1.99	1.53	2.39	2.30	1.52	1.66	1.87	6.54
16	0.51	2.92	2.39	0.70	1.06	2.94	2.73	1.78	7.96
24	9.92	0.74	0.55	3.03	3.01	2.29	1.14	5.48	5.08
36	2.04	2.18	2.87	2.04	2.85	2.47	1.90	1.52	5.90
48	2.66	0.31	1.88	0.71	1.27	2.45	4.49	2.10	6.51
72	2.81	0.67	2.01	1.45	2.07	2.87	4.97	3.04	6.64

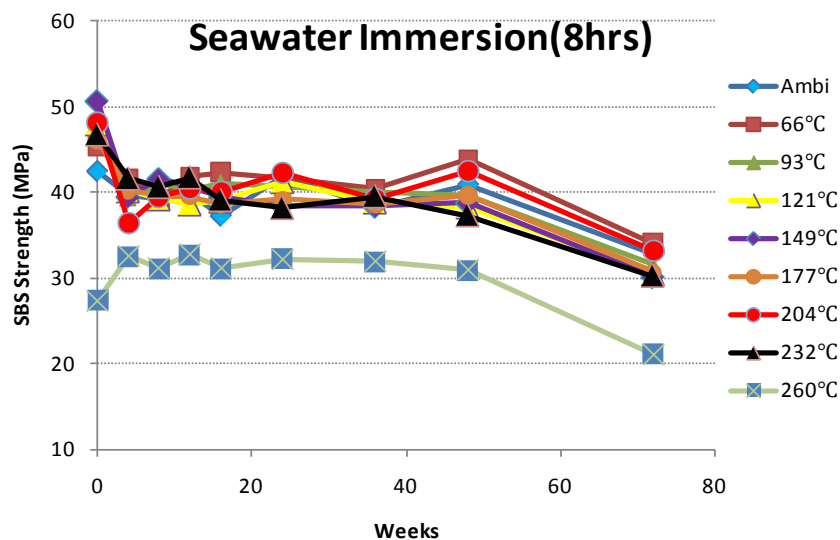


Figure 6-11: Comparison of Short Beam Shear Strengths on specimens immersed in sea- water for 72 weeks after exposure to elevated temperatures in 8 hrs of ageing time

6.2.3.2 Time Dependence

For time-dependent characterization on carbon/epoxy composite materials immersed in deionized water and seawater, specimens aged from 1 hr to 72 hrs under 232°C of exposure temperature were immersed until 72 weeks in water bath at the atmospheric temperature. Table 6-5 and Figure 6-12 show data and comparison of short beam shear strengths on specimens immersed in deionized water for 72 weeks after exposure to 232°C in various ageing times. Contrary to the results of tensile and flexural test, short beam shear strengths of specimens exposed to 232°C were continuously and slightly increased without degradation caused by thermooxidation as ageing time was extended from 1 hr to 72 hrs as demonstrated in chapter 4.4.

The specimens exposed to 232°C before immersion showed increasing short beam shear strengths with extended ageing time as shown in Table 6-5. The rate of decrease in short beam shear strengths after immersion until up to 72 weeks in deionized water was 26.1, 31.9, 35.5, 35.9, 34.5, 35.4, 37.5 and 38.7% on specimens exposed to 232°C for 1, 2, 4, 8, 16, 24, 48, and 72 hrs, respectively. Namely, the increased short beam strengths by post-cure effect resulted in more degradation by water ingress. Consequently, the rapid drop of short beam shear strengths was attributed to water ingress and hydrolysis on fully post-cured specimens. Also, immersion effects and time-dependent characterization in terms of short beam shear strengths on specimens exposed to 232°C were identical regardless of ageing times.

Table 6-5 Data of Short Beam Shear Strengths on specimens immersed in DI water for 72 weeks after exposure to 232°C in various ageing times

Strength (MPa) - DI water								
weeks	1hr	2hr	4hr	8hr	16hr	24hr	48hr	72hr
0	44.28	45.61	48.06	46.71	46.48	46.62	49.61	48.97
4	41.44	39.54	39.95	42.73	41.77	43.77	41.27	41.16
8	39.93	42.94	40.48	40.75	42.26	42.47	40.37	43.60
12	39.25	38.28	38.45	41.85	41.63	42.45	41.75	43.58
16	41.73	40.05	39.30	40.81	41.14	42.47	43.25	42.17
24	40.99	42.50	42.25	41.05	42.86	42.96	41.10	41.00
36	38.37	40.46	38.84	39.39	41.35	43.50	42.02	39.49
48	41.53	39.36	39.65	38.92	42.16	43.07	39.51	41.41
72	32.71	31.07	31.00	29.95	30.46	30.12	31.02	30.01

Standard deviation (MPa)								
weeks	1hr	2hr	4hr	8hr	16hr	24hr	48hr	72hr
0	1.14	3.24	2.91	2.66	1.74	4.27	3.17	5.11
4	1.24	1.72	2.78	3.24	2.09	0.88	4.72	4.27
8	2.46	2.02	3.75	1.79	1.28	3.35	4.39	3.97
12	2.27	3.35	5.25	1.25	0.84	2.84	1.31	1.08
16	3.34	3.14	2.48	1.48	1.52	2.02	3.38	5.42
24	4.16	1.96	5.34	3.64	2.93	2.95	5.66	5.20
36	2.55	1.98	6.62	1.41	2.29	2.59	3.57	1.45
48	1.15	0.61	2.51	5.15	3.87	1.58	2.86	4.01
72	1.87	1.21	2.48	5.41	3.41	2.41	3.04	4.57

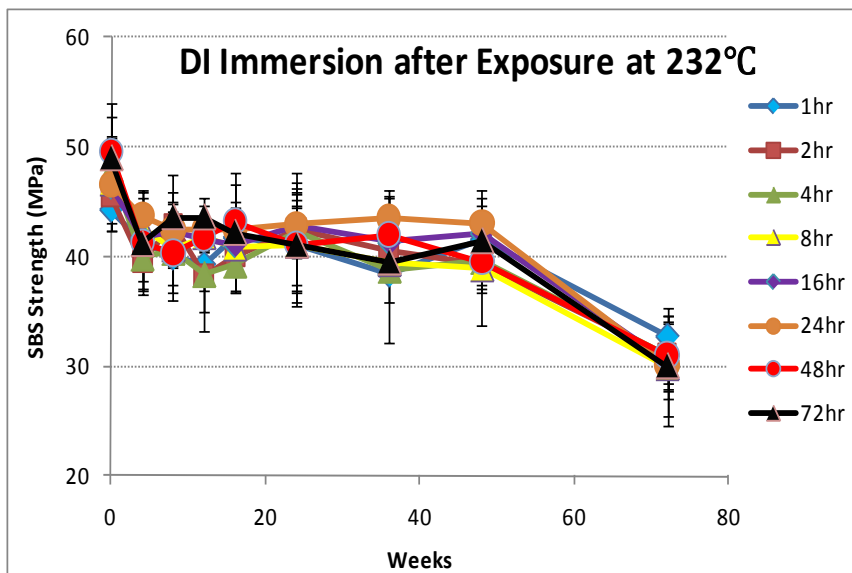


Figure 6-12: Comparison of Short Beam Shear Strengths on specimens immersed in DI water for 72 weeks after exposure to 232°C in various ageing times

As shown in Table 6-6 and Figure 6-13, compared to the results of specimens immersed in deionized water, any specific characterization was not found on specimens immersed in seawater. Similar to temperature-dependent characterization, salt or sanity involving seawater did not affect additional decrease in terms of short beam shear strengths. The rate of decrease in short beam shear strengths after immersion until up to 72 weeks in seawater was 28.0, 27.6, 32.8, 35.3, 33.3, 35.0, 39.6 and 41.5% on specimens exposed to 232°C for 1, 2, 4, 8, 16, 24, 48, and 72 hrs, respectively

Table 6-6 Data of Short Beam Shear Strengths on specimens immersed in seawater for 72 weeks after exposure to 232°C in various ageing times

Strength (MPa) - Seawater								
weeks	1hr	2hr	4hr	8hr	16hr	24hr	48hr	72hr
0	44.28	45.61	48.06	46.71	46.48	46.62	49.61	48.97
4	40.60	40.33	42.68	41.57	42.07	45.67	44.79	42.30
8	38.32	38.30	40.40	40.58	38.44	42.26	43.26	37.36
12	38.27	39.76	40.50	41.70	40.94	41.00	42.77	40.70
16	38.50	40.33	39.99	39.06	42.31	40.82	41.90	42.25
24	37.54	40.13	42.11	38.13	43.11	39.48	42.38	41.33
36	38.60	40.92	39.78	39.50	41.37	41.71	40.28	39.13
48	39.12	40.48	41.14	37.29	40.65	40.77	39.56	38.94
72	31.88	33.02	32.32	30.22	31.01	30.31	29.97	28.64
Standard deviation (MPa)								
weeks	1hr	2hr	4hr	8hr	16hr	24hr	48hr	72hr
0	1.14	3.24	2.91	2.66	1.74	4.27	3.17	5.11
4	0.60	0.71	1.35	2.23	3.01	3.53	4.05	4.35
8	1.25	1.80	2.05	2.11	2.84	3.93	2.88	1.11
12	2.48	0.57	0.76	1.87	1.69	5.63	3.11	3.62
16	3.44	3.94	3.66	1.78	2.00	2.01	4.04	3.77
24	1.70	3.10	2.67	5.48	3.00	1.00	2.09	4.15
36	2.59	2.85	0.82	1.52	1.01	2.93	2.66	2.64
48	2.85	3.68	2.36	2.10	1.74	1.17	1.22	4.41
72	3.04	3.74	2.44	3.04	1.97	1.79	1.41	4.97

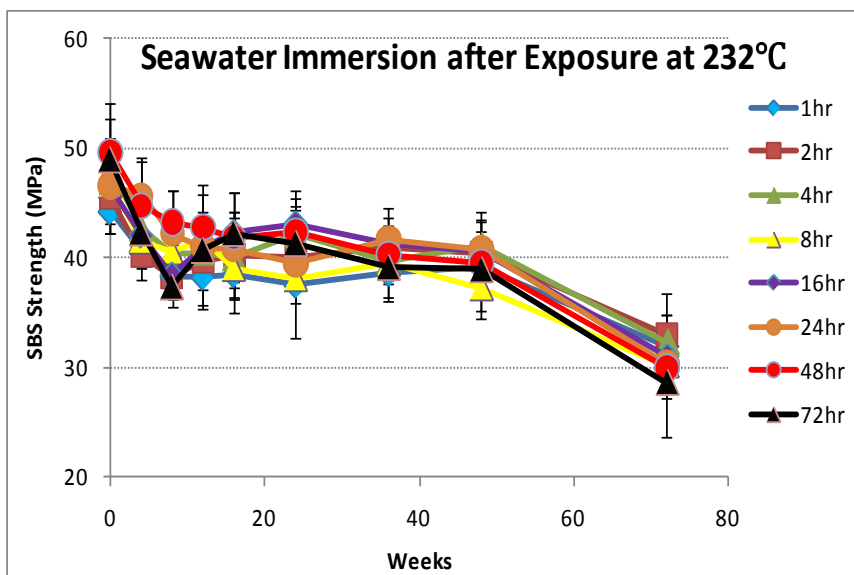


Figure 6-13: comparison of Short Beam Shear Strengths on specimens immersed in seawater for 72 weeks after exposure to 232°C in various ageing times

7 Predictive Degradation Models

7.1 Introduction

A concern caused by using FRP composites in rehabilitation applications is their high flammability and poor fire resistance. As mentioned in chapter 4, the mechanical properties of FRP composites can be severely degraded by fire and elevated temperatures. Therefore, based on the data of mechanical properties determined in chapter 4, it is very important that predictive degradation models must be performed to evaluate functions for desired periods of time without failure and severe degradation, in specified environments. For some period of exposure the strengths and the moduli may remain above their allowable limits. However, after some time, the mechanical properties may decrease that the composite materials cannot sustain the imposed loads or maintain the allowable desire. From this problem, a knowledge of long term strength retention under working conditions is required to estimate the accurate service life. Since the degradation caused by fire and elevated temperatures occurs rapidly and initial increase of mechanical properties due to post-cure effect must be considered, estimation of service life can be different with long term predictive degradation model applied for immersion which degradations continuously occurred.

Firstly, one of the earliest and most successful acceleration models, Arrhenius rate degradation model will be introduced. The Arrhenius rate model predicts how time-to-fail varies with temperature. Secondly, Time-Temperature Superposition (TTSP) will be used for analyzing of service life. This model is a well-known principle that works well for certain types of viscoelastic materials and related effects of time and

temperature, thereby allowing for an exchange between the effects of time and elevated temperature. Lastly, Weibull statistical strength model will be carried out to correlate between tension and flexure results.

7.2 Arrhenius Rate Degradation Model

The Arrhenius Rate degradation model is the most common model regarding life-stress relationships used in accelerated life estimation. The rate of a chemical reaction can be affected by several parameters, including temperature. The Arrhenius rate relationship is derived from the Arrhenius reaction rate equation suggested by Arrhenius in 1887[91]. The reaction rate can be expressed by

$$R(T) = A \exp\left(\frac{-E_a}{KT}\right) \quad (7.1)$$

where:

R = Speed of reaction

A= Non-thermal constant

E_a= activation energy (J/mol)

K = Boltzman's constant (1.38×10⁻²³J/K)

T = Temperature (Kelvin)

In Equation 7.1, activation energy means the energy which molecules in composite materials shall possess to react. Therefore, the activation energy is a criterion of the effect that temperature has on the reaction.

Assuming that life is proportional to the inverse reaction rate of the process, the

Arrhenius life-stress relationship can be expressed as

$$L(T) = C \exp\left(\frac{B}{T}\right) \quad (7.2)$$

where:

L = a quantifiable life measure or material property

C = a model parameter to be determined (C>0)

B = another model parameter

T = Temperature (Kelvin)

A linear relationship can be obtained by taking the natural logarithm of both sides of Equation 7.2 as following.

$$\ln(L(T)) = \ln(C) + \frac{B}{T} \quad (7.3)$$

B is the slope of the line and $\ln(C)$ is the intercept of the line. The variable in this equation is the inverse of the temperature. Therefore, a quantifiable life measure is commonly drawn against the inverse temperature. The constant B and C can be identified from experimental data and relationships can be estimated for other temperatures than those used to determine these relationships.

7.2.1 Data Analysis Procedure

The analysis process (i.e., tensile strength) on Arrhenius rate model will be demonstrated in this section. The goal of the Arrhenius rate model is to determine the long-term degradation of the composites. Table 7-1 shows the tensile strength retentions (%) on specimens exposed to elevated temperatures up to 72 hrs.

Table 7-1 Data for tensile strength retentions (%) on specimens exposed to elevated temperatures up to 72 hrs

Time [hr]	Time [min]	Percent Strength Retention (%)								
		Ambient (23°C)	66°C	93°C	121°C	149°C	177°C	204°C	232°C	260°C
0	0	100.0	100.0	100.0	100.0	100.0	100.0	100.0	100.0	100.0
1	60	99.8	140.6	126.0	116.4	154.4	122.0	115.0	111.4	124.9
2	120	102.1	149.5	128.7	116.2	153.1	124.1	129.9	118.3	127.1
4	240	100.6	151.2	134.5	125.2	150.9	136.4	141.4	126.5	133.0
8	480	101.0	150.1	135.3	131.8	149.7	135.2	134.1	126.8	107.0
16	960	104.1	149.3	137.7	112.5	143.5	133.7	133.3	124.1	69.7
24	1440	102.5	120.3	121.7	104.4	137.6	124.3	124.5	121.7	60.4
48	2880	104.2	116.5	121.6	104.0	127.1	113.6	118.6	120.1	49.5
72	4320	103.4	115.2	119.9	104.8	136.4	112.3	116.0	112.5	37.6

More linear line can be plotted by taking natural logarithm of time versus the percent strength retentions as shown in Figure 7-1.

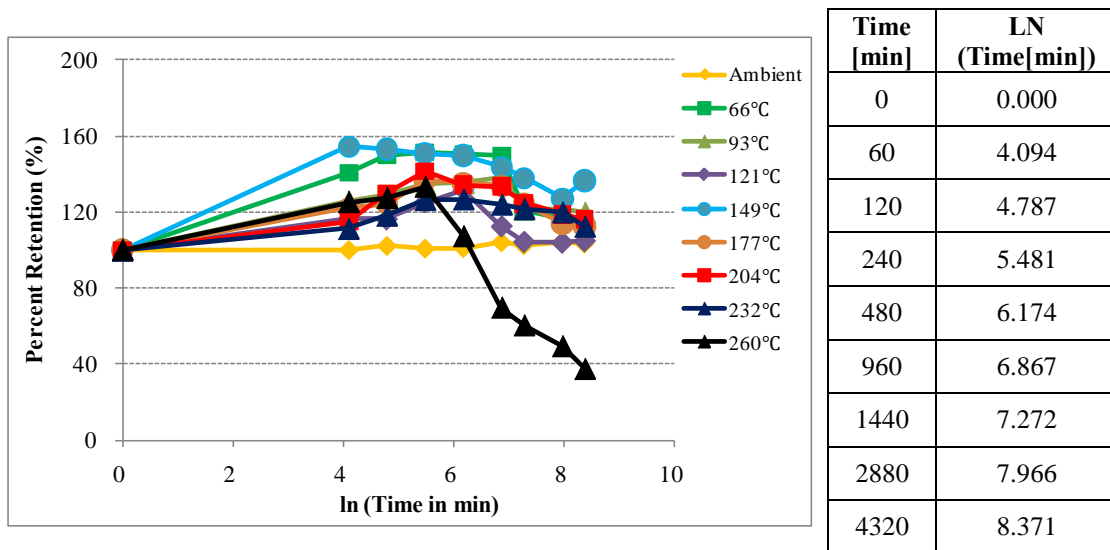


Figure 7-1: Percent tensile strength retentions (%) versus ln(time in minute)

In general, since degradation is more severe as time increase, linear line can be obtained from percent retention of property and logarithm of time. However, in this

study, perfect linear line cannot be yielded due to initial increase of strengths by residual post-cure effect. Therefore, using polynomial 2nd order curve-fit can bring higher R-squared values as demonstrated in Figure 7-2 and Table 7-2.

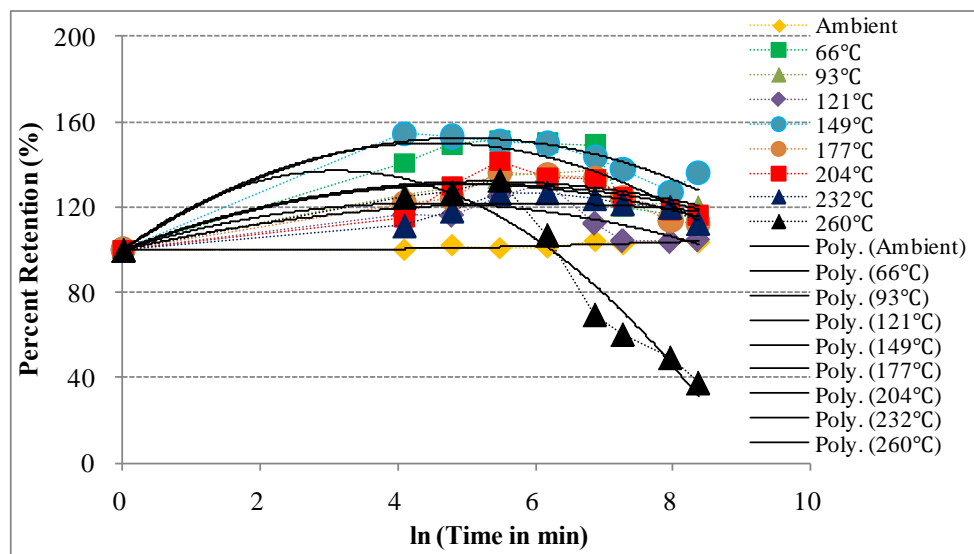


Figure 7-2: Polynomial 2nd order curve-fit on percent tensile strength retentions versus natural logarithm of time in minute

Table 7-2 Equation of polynomial 2nd order curve-fit on percent tensile strength retentions versus natural logarithm of time in minute

Exposure temperature	A	B	C	R ²
Ambient(23°C)	100	-0.239	0.0874	0.7081
66°C	100	22.206	-2.4564	0.8532
93°C	100	12.202	-1.1602	0.8420
121°C	100	10.075	-1.1651	0.6245
149°C	100	21.115	-2.1243	0.9412
177°C	100	12.547	-1.2788	0.7584
204°C	100	11.910	-1.1495	0.6876
232°C	100	7.3001	-0.6134	0.7249
260°C	100	23.811	-3.8236	0.9292

$$\sigma(t) = \frac{\sigma_i}{100} (A + B \ln(t) + C \ln(t)^2)$$

Using equations in Table 7-2 , the tensile strength of the specimens for longer time at different temperatures can be yielded to predict the response of the composite materials.

Next step to get the Arrhenius rate analysis is to establish a relationship between percent tensile strength retention and temperature. Since the function between percent tensile strength retention and temperature is different for each time step and life is proportional to the inverse reaction rate of the process, a percent retention can be plotted against the inverse of temperature as Figure 7-3. Also, linear relationship between percent retention of tensile strength and inverse of temperature can be obtained from Figure 7-3. The reason why Figure 7-3 did not show perfect linear relationship is that post-curing effect was applied for specimens. However, the relationship and tendency in Table 7-3 can be used to determine the tensile strength of composite materials at different time steps for a particular temperature. From Table 7-4, the intercept of line was decreased and the slope of line was increased with increasing time. In particular, the slope of line showed minus values until ageing time reached 8 hrs. This means degradation of tensile strength did not occur in ranges of exposure temperatures (~ 260°C) in this study. Actually, test specimens did not lose the original property (100% in terms of percent tensile strength retention) in tensile test until ageing

time reached 8 hrs in exposure temperature of 260°C

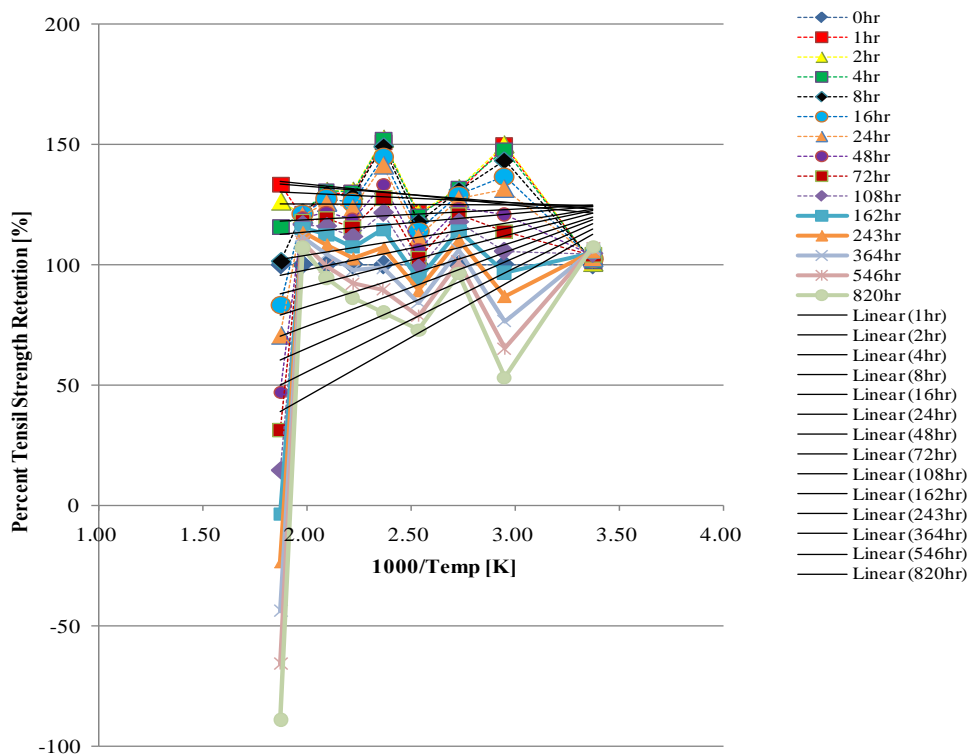


Figure 7-3: Percent retentions of tensile strength versus inverse of temperature

Table 7-3 Relationship between percent retentions of tensile strength and the inverse of temperature

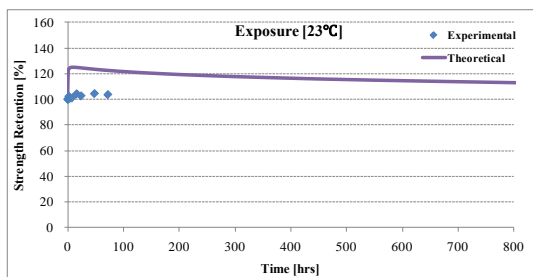
Time [hr]	A	B
1	150.69	-8.61
2	146.13	-6.77
4	137.76	-3.98
8	125.58	-0.24
16	109.60	4.46
24	98.49	7.65

1.0	115.0	132.7	111.4	133.7	124.9	134.5
2.0	129.9	131.9	118.3	132.7	127.1	133.4
4.0	141.4	129.4	126.5	129.9	133.0	130.3
8.0	134.1	125.1	126.8	125.1	107.1	125.1
16.0	133.3	118.9	124.1	118.4	69.7	118.0
24.0	124.5	114.5	121.7	113.6	60.4	112.8
48.0	118.7	105.5	120.1	103.9	49.5	102.5
72.0	116.0	99.4	112.6	97.3	37.6	95.5
108.0		92.7		90.1		87.8
162.0		85.3		82.2		79.4
243.0		77.4		73.7		70.3
364.5		68.8		64.5		60.6
546.8		59.6		54.6		50.1
820.1		49.8		44.1		39.0

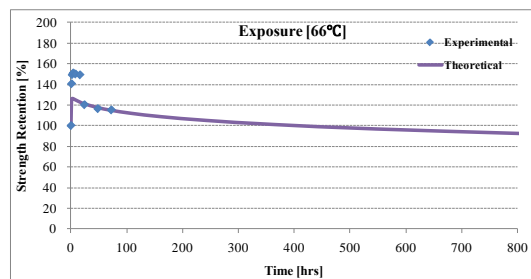
Figure 7-4 shows comparison between the experimental values and predicted values of tensile strength determined by Arrhenius rate model for specimens exposed to elevated temperatures. Except for the conditions of exposure temperatures such as ambient, 66°C, and 260°C, predicted values of tensile strength were relatively in good agreement with experimental data. In other words, good relationships between theoretical and experimental data were shown in ranges of intermediate exposure temperatures. Tensile strengths in these exposure temperatures showed decrease or level-off after initial increase due to post-cure effect. Furthermore, since the rate of degradation by Arrhenius rate model in intermediate exposure temperatures showed higher rate compared to experimental data, it is possible to apply for design factor to predict the long-term service life in terms of tensile strength of carbon/epoxy composite materials.

The analysis procedure of Arrhenius rate model can be applied to experimental data from all tensile, off-axis shear, flexural and short beam shear tests and results are presented in the following section. From analysis in chapter 7.2.2, it can also be observed that Arrhenius rate model provides rather conservative estimates for all mechanical properties such as tension, off-axis shear, flexure and short beam shear in

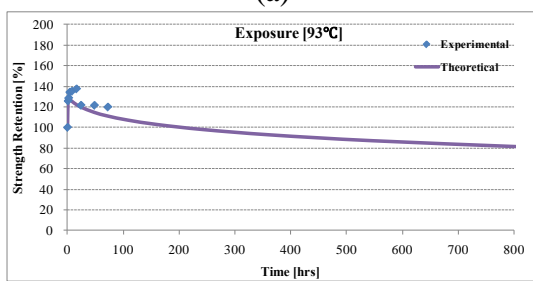
ranges of intermediate exposure temperatures.



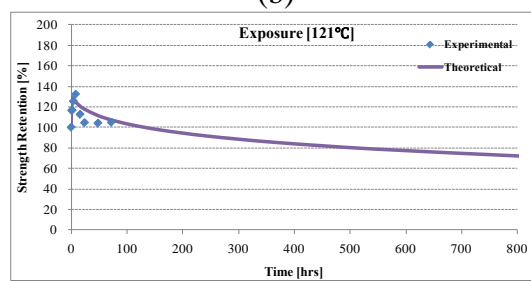
(a)



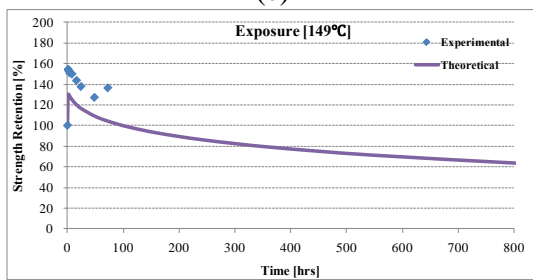
(b)



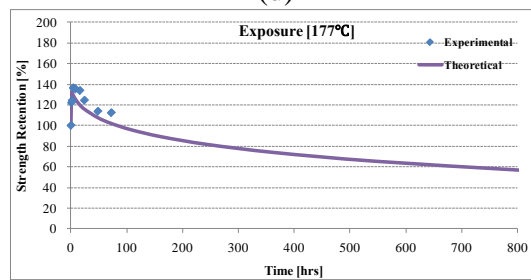
(c)



(d)



(e)



(f)

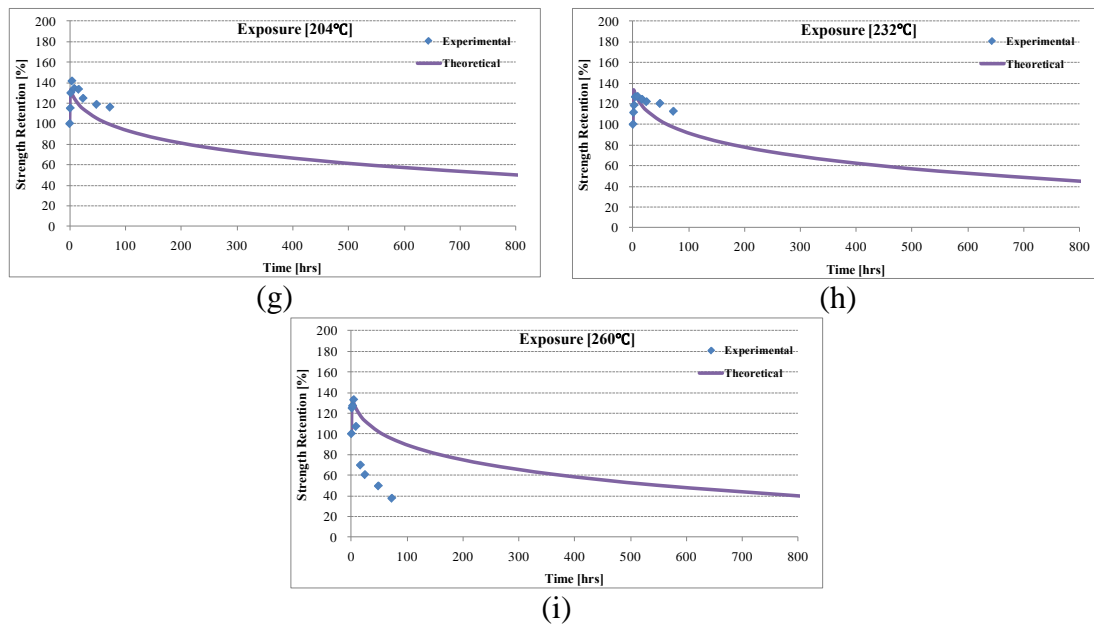


Figure 7-4: Comparison of the experimental values and predicted values of tensile strength by Arrhenius rate model on specimens exposed to elevated temperatures

7.2.2 Results

Predicted data related to strength and modulus on all mechanical tests determined by Arrhenius rate models will be presented in this section. Since predicted data are difficult to distinguish in same graph from experimental data, just predictive data will be introduced.

7.2.2.1 Tensile Testing

Tensile strengths based on Arrhenius rate model already were introduced in chapter 7.2.1. Predicted values of tensile modulus using Arrhenius rate model are presented in Figure 7-5. Similar to the results of predicted tensile strengths, until 72 hrs of ageing time which means the maximum time in this study, predicted values were corresponded well with experimental data except for the conditions of exposure

temperatures (ambient and 260°C). Experimental data started to lose original properties of tensile modulus in conditions (exposure temperature: 260°C ageing time: ~8 hrs) while predicted data showed decrease of original properties in lower environmental conditions.

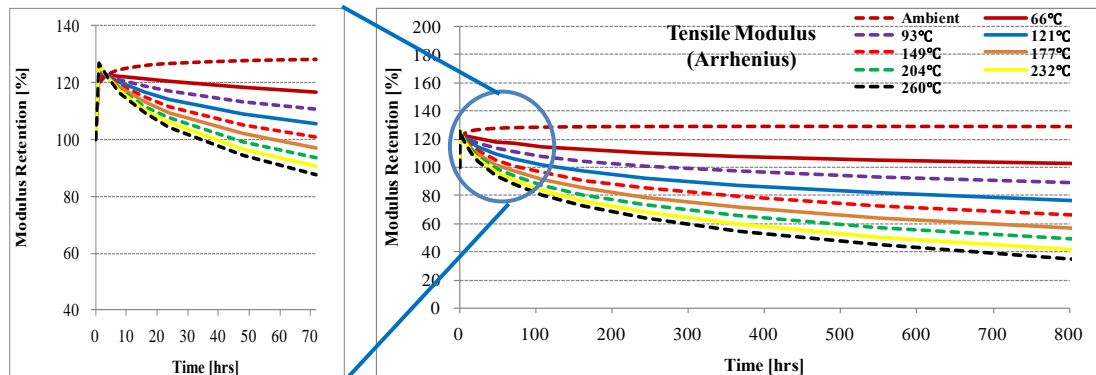


Figure 7-5: Predicted values of tensile modulus for specimens exposed to elevated temperatures using Arrhenius rate model

7.2.2.2 Off-Axis Shear Testing

Predicted values of off-axis shear modulus and strength using Arrhenius rate model are presented in Figure 7-6 and Figure 7-7. Predicted data were comparatively in good agreement with experimental data in both cases. Also, since post-cure effect was not applied to off-axis shear specimens, predicted data of off-axis shear test showed the best agreement with experimental data compared to other mechanical properties affected by post-cure effect.

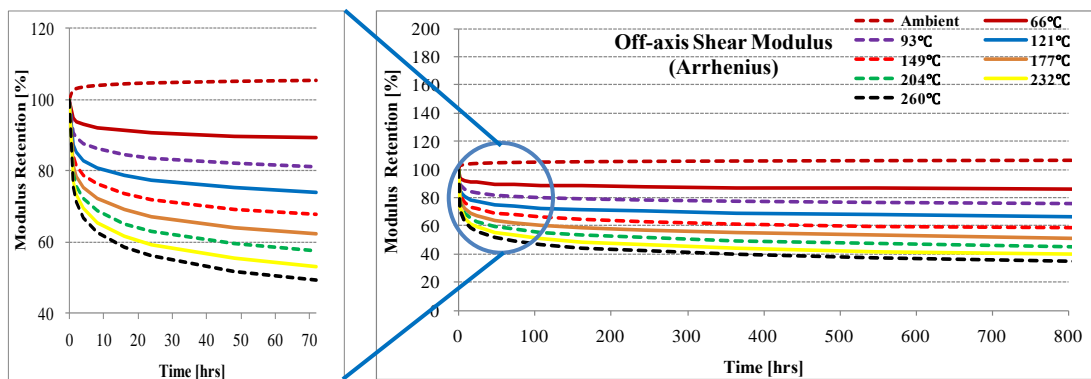


Figure 7-6: Predicted values of off-axis shear modulus for specimens exposed to elevated temperatures using Arrhenius rate model

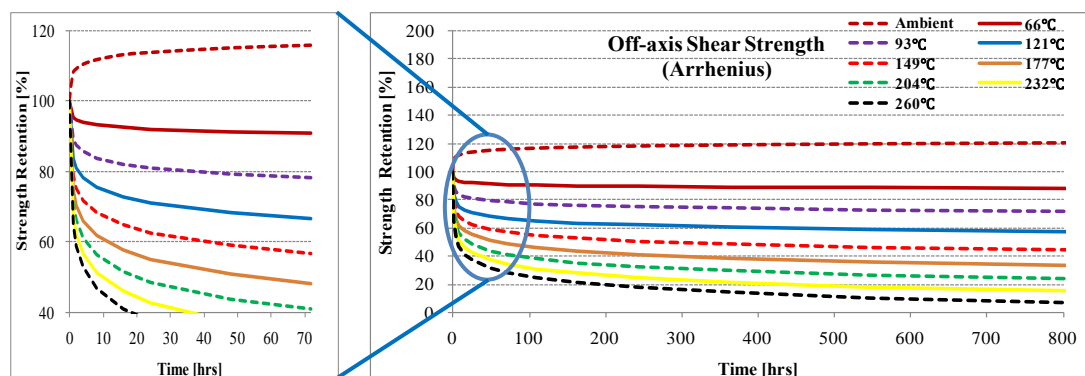


Figure 7-7: Predicted values of off-axis shear strength for specimens exposed to elevated temperatures using Arrhenius rate model

7.2.2.3 Flexural Testing

The Arrhenius predictions of flexural modulus and strength, for the specimens exposed to elevated temperatures are depicted in Figure 7-8 and Figure 7-9. Since the increase of mechanical properties by initial post-cure effect was not higher than the cases of tensile and short beam shear test, predicted data obtained by Arrhenius rate model showed rapid drop in terms of strength and modulus with extension of ageing time.

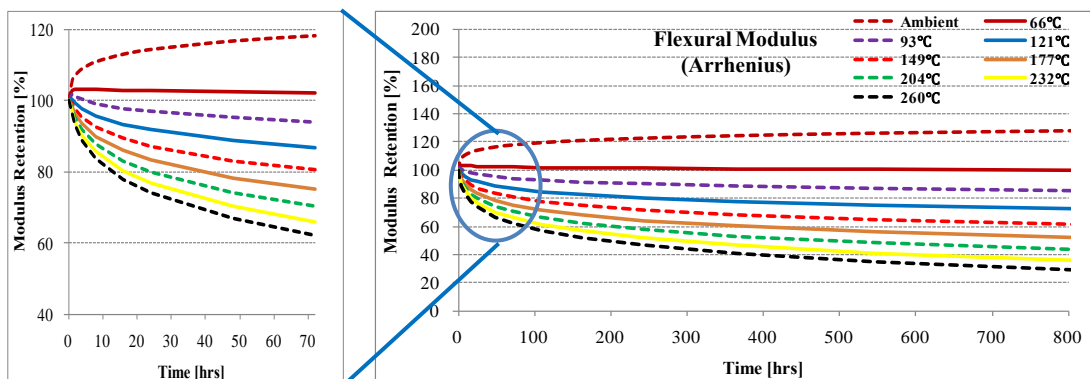


Figure 7-8: Predicted values of flexural modulus for specimens exposed to elevated temperatures using Arrhenius rate model

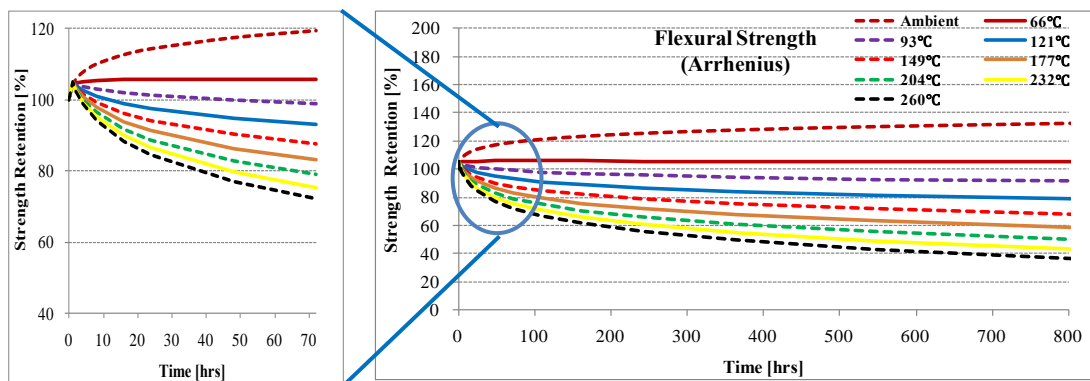


Figure 7-9: Predicted values of flexural strength for specimens exposed to elevated temperatures using Arrhenius rate model

7.2.2.4 Short Beam Shear Testing

The Arrhenius predictions of short beam shear strength, for the specimens exposed to elevated temperatures are presented in Figure 7-10. As seen from the Figure 7-10, predicted data for short beam shear strength showed the values between tensile and flexural strengths similar to experimental data.

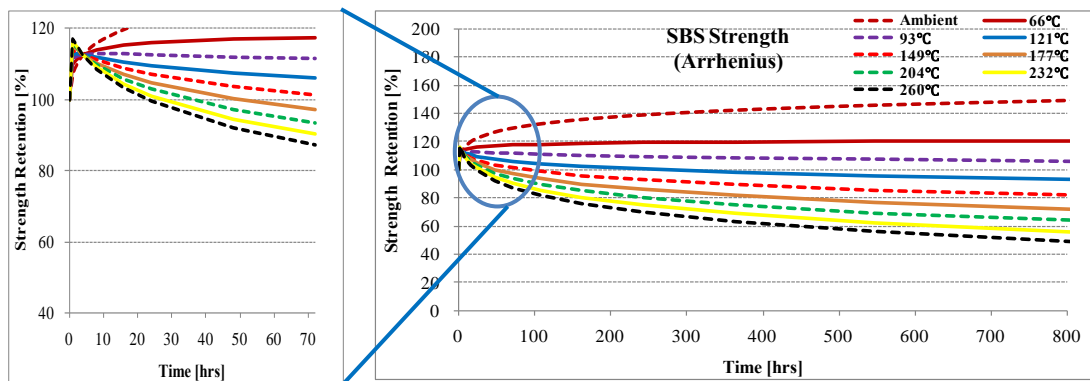


Figure 7-10: Predicted values of short beam shear strength for specimens exposed to elevated temperatures using Arrhenius rate model

7.3 Time Temperature Superposition Model

Time-Temperature Superposition (TTSP) principle comes from the concept that molecular relaxation occurs at faster rate in higher temperature and thus TTSP is a well-

known methodology that frequently used to describe the mechanical and electrical relaxation behavior of polymer composites[92]. If the failure of composite materials occurs by one mechanism, TTSP provides a powerful tool for accurate prediction[93].

TTSP is based on the assumption that the effects of changing temperature on the time-dependent characteristic of a composite material are equivalent to the shift in the actual time scale of the measurement. If time-dependent data at a chosen temperature is selected as a reference curve, the shift on the time scale is dependent on the test temperature to obtain a master curve. A master curve can be generated by shifting the short term data on a logarithmic scale to the reference temperature. Therefore, master curve is the function of time and temperature. The horizontal shift is expressed as

$$f(T_0, t) = f(T_1, t / a_T) \quad (7.4)$$

where:

f = the property in the model

T₀ = the reference temperature (Kelvin)

t = time (hours)

T = the temperature that is being shifted (Kelvin)

a_T = shift factor

Based on the Williams-Landel-Ferry (WLF)[94], shifting for master curve can be derived from two criteria which the same shift factor should be capable of use in superposition of all viscoelastic functions and the adjacent curves must match exactly over a reasonable distance. Beside the usual horizontal shift, reasonable master curve often needs vertical shift because of the inherent changes in the property of polymer composites. The vertical shift is based on the reference temperature whereas the

horizontal shift is based on the Arrhenius relationship. All of shift factors are quantitatively in good agreement with two Arrhenius' equations with different activation energies ΔE [95]:

$$\text{Log}(a_T) = -\frac{\Delta E}{2.303R} \left(\frac{1}{T} - \frac{1}{T_{ref}} \right) \quad (7.5)$$

where:

$\text{Log}(a_T)$ = the shift factor using the logarithmic scale

ΔE = the activation energy (KJ/mol)

R = the gas constant (8.3143×10^{-3} [KJ/(K.mol)])

T = the temperature that is being shifted (Kelvin)

T_{ref} = the reference temperature (Kelvin)

7.3.1 Data Analysis Procedure

The analysis process (i.e., tensile strength) on TTSP model will be demonstrated in this section. Once the experimental data is shifted as Equation 7.5, the master curve can be generated in order to provide predicted data over long time. Table 7-5 and Figure 7-11 show the logarithm scale of tensile strength retentions (%) and time on specimens exposed to elevated temperatures up to 72 hrs for TTSP model.

Table 7-5 Data for logarithmic scale of tensile strength retentions (%) on specimens exposed to elevated temperatures up to 72 hrs

Time [hr]	Log(percent short beam shear strength retention)							
	66°C	93°C	121°C	149°C	177°C	204°C	232°C	260°C
0	2.000							
1	2.148	2.100	2.066	2.189	2.086	2.061	2.047	2.097
2	2.175	2.110	2.065	2.185	2.094	2.114	2.073	2.104

4	2.180	2.129	2.098	2.179	2.135	2.150	2.102	2.124
8	2.176	2.131	2.120	2.175	2.131	2.127	2.103	2.030
16	2.174	2.139	2.051	2.157	2.126	2.125	2.094	1.843
24	2.080	2.085	2.019	2.139	2.095	2.095	2.085	1.781
48	2.066	2.085	2.017	2.104	2.055	2.074	2.079	1.694
72	2.062	2.079	2.020	2.135	2.050	2.064	2.051	1.575

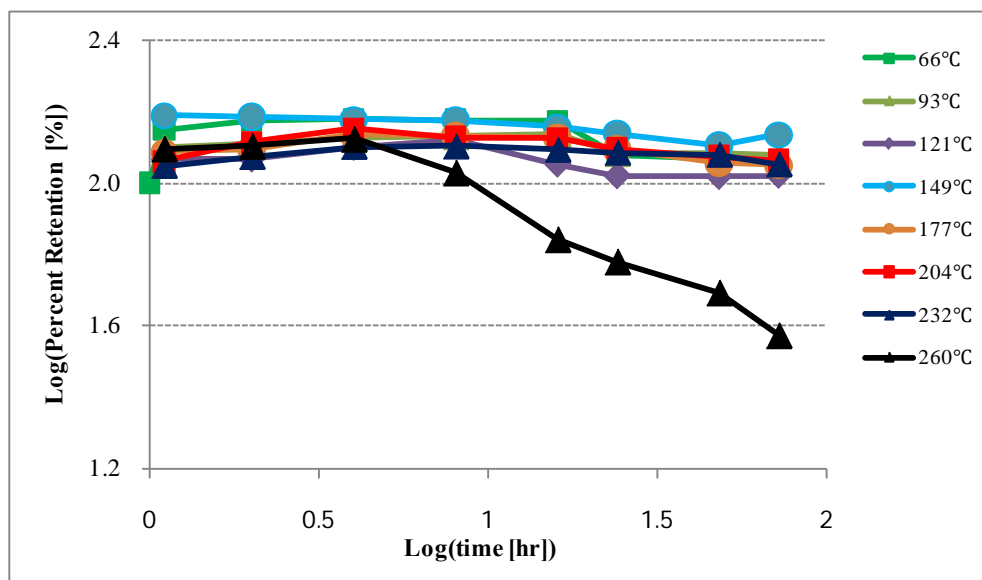


Figure 7-11: Logarithmic scale of percent tensile strength retention (%) versus time (hr)

According to Equation 7.5, the logarithmic horizontal shifts for the curves of Figure 7-11 are tabulated in Table 7-6. These shift factors were calculated by using activation energies obtained by Dynamic Mechanical Thermal Analysis. For accurate master curve, vertical shifts were slightly performed with curve of reference exposure

temperature (66°C) Shifted curves to generate master curve for Time-Temperature Superposition model are shown in Figure 7-12. Based on Figure 7-12, master curve of good relationship ($R^2 = 0.95745$) using polynomial 3rd order curve fit was generated as shown in Figure 7-13. Using master curve, long-term service life in terms of tensile strength retentions can be estimated as shown in Figure 7-14.

Table 7-6 Horizontal shift factors from curve in exposure temperature (66°C) using the logarithmic scale on specimens exposed to elevated temperatures

ΔT	~93°C	~121°C	~149°C	~177°C	~204°C	~232°C	~260°C
$\log(a_T)$	0.429	1.974	4.027	4.098	8.068	8.319	9.599

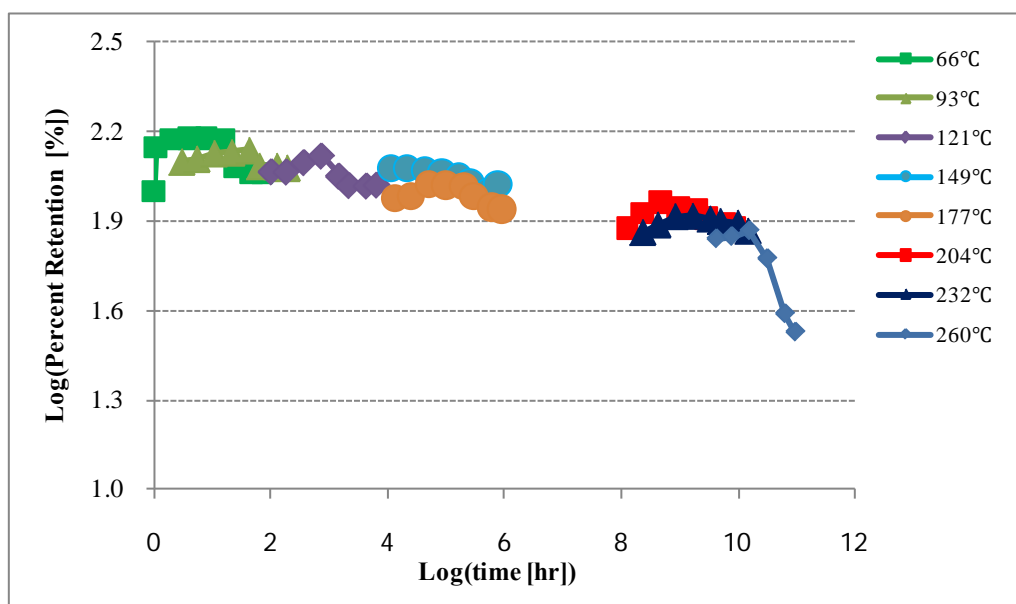


Figure 7-12: Shifted curves to yield master curve for Time-Temperature Superposition

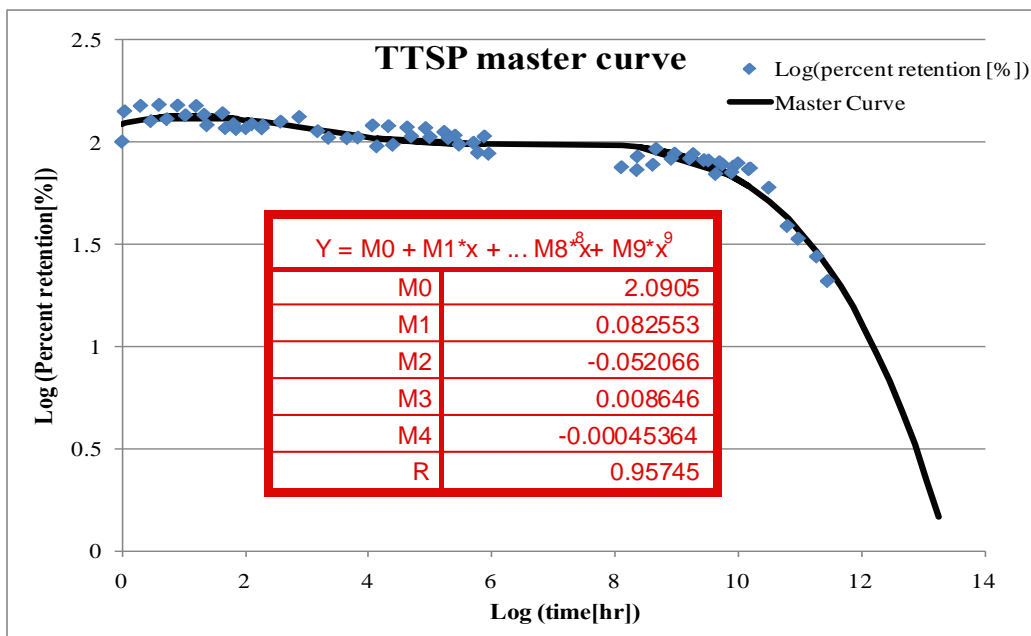


Figure 7-13: Master curve of polynomial 3rd order curve fit to log of tensile strength profile for Time-Temperature Superposition model

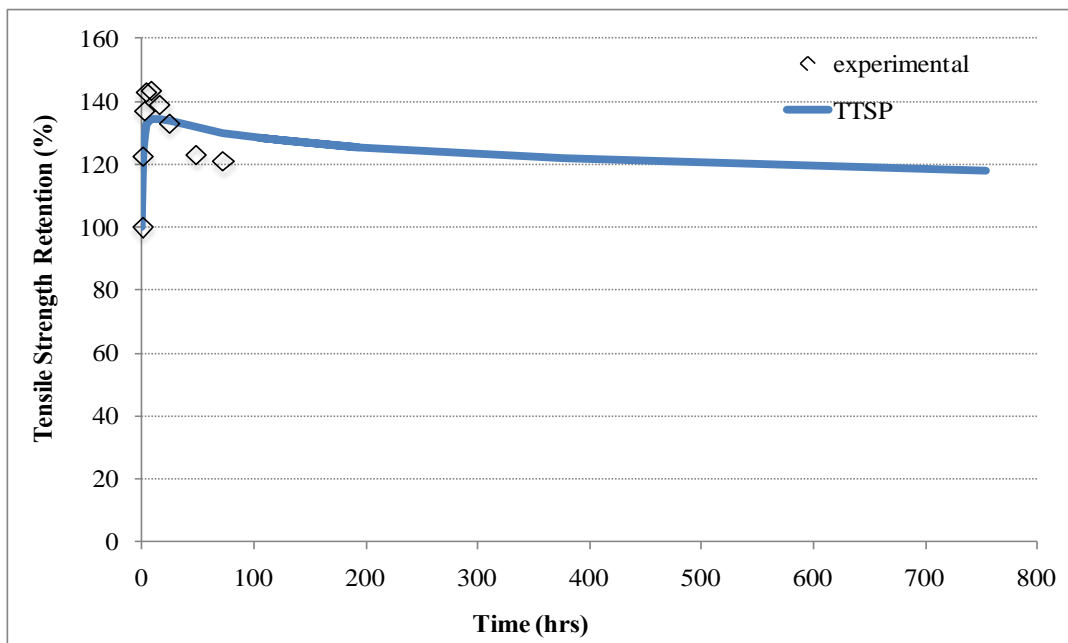


Figure 7-14: Comparison of predicted values and experimental values of tensile strength retention based on the Time-Temperature Superposition model

7.3.2 Results

Predicted data related to strength and modulus on all mechanical tests determined by Time-Temperature Superposition model will be presented in this section.

7.3.2.1 Other Mechanical properties

Results for the other mechanical properties as derived from Time-Temperature Superposition model are presented in Table 7-7, Figure 7-15 and Figure 7-16.

Table 7-7 Predicted data of additional mechanical properties based on Time-Temperature Superposition model - reference temperature (66°C)

Time (hr)	Strength Retention (%)				Modulus Retention (%)		
	Tension	Off-axis shear	Flexure	SBS	Tension	Off-axis shear	Flexure
0	100	100	100	100	100	100	100
1	124.12	82.87	87.76	92.18	112.50	83.95	87.19
2	129.08	90.22	96.68	103.83	121.62	89.42	95.20
4	132.79	95.93	104.49	114.57	129.26	93.36	101.95
8	134.48	98.62	109.47	121.92	133.70	94.87	105.93
16	134.45	98.62	111.76	125.88	135.17	94.32	107.35
24	133.76	97.58	112.00	126.76	134.83	93.22	107.17
48	131.70	94.44	110.89	126.21	132.56	90.35	105.47
72	130.08	92.02	109.53	124.89	130.43	88.25	103.84
103.7	128.43	89.58	107.97	123.21	128.13	86.19	102.08
128.9	127.38	88.05	106.92	122.03	126.62	84.90	100.93
188.6	125.45	85.28	104.91	119.72	123.79	82.60	98.78
193.4	125.32	85.09	104.78	119.56	123.60	82.45	98.63
377.1	121.75	80.11	100.93	114.96	118.22	78.35	94.62
754.3	117.99	75.07	96.82	109.91	112.45	74.26	90.43

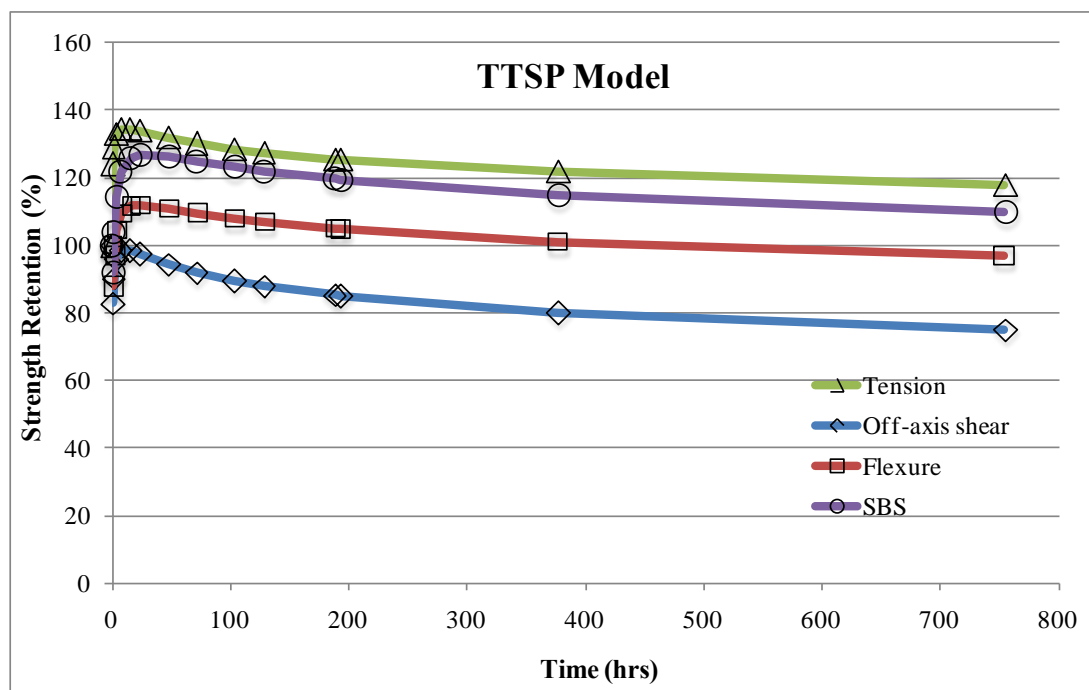


Figure 7-15: Predicted data of strengths based on Time-Temperature Superposition model - reference temperature (66°C)

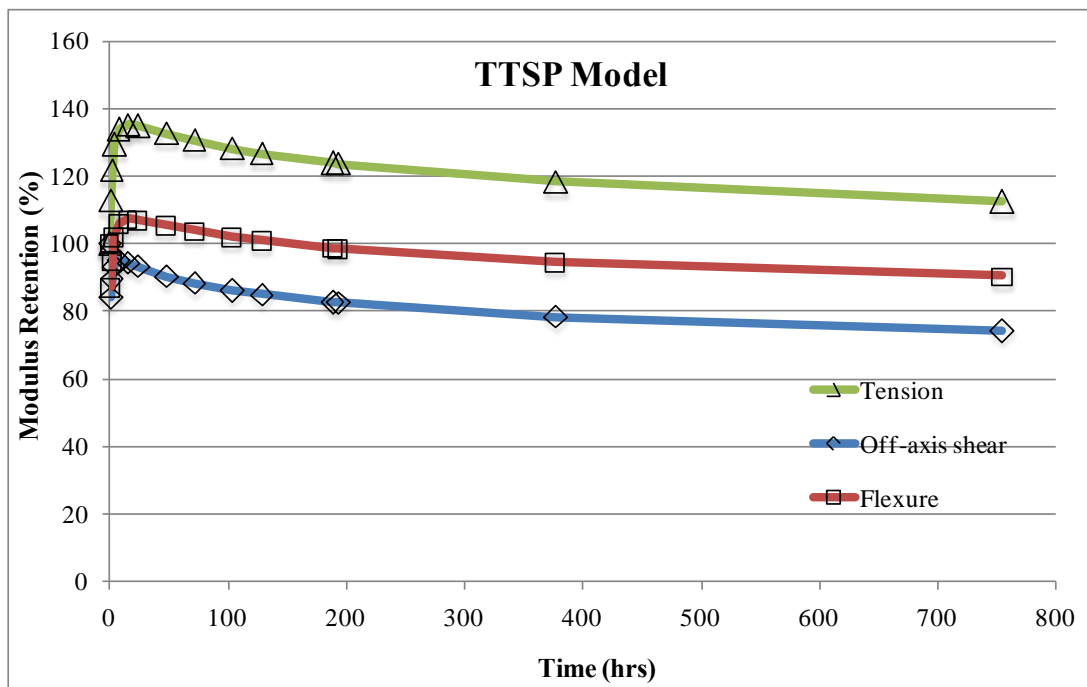


Figure 7-16: Predicted data of modulus based on Time-Temperature Superposition model - reference temperature (66°C)

7.3.2.2 Comparison with Arrhenius rate model

In this section, a direct comparison between Arrhenius rate model and Time-Temperature Superposition model will be accomplished to estimate which model is closer to experimental data. Since both models could not exactly reflect the increase of mechanical property due to residual post-cure effect, predicted data generated by two models were slightly different from experimental data. The difference between predictive model and experimental data is attributed to assumption to simply the process of analysis on predictive models. It is well known that the Arrhenius based prediction model assumes degradation processes to proceed in linear characteristic and hence can only be used in cases where self-consistent damage progression can be expected to occur. Also, in the case of TTSP model, it is assumed that the same mechanism of

degradation occurs across all temperatures. Although some difference exists, two predictive models are useful for estimating the long-term service life because predicted data showed similar trend with experimental data and more conservative estimations in the majority of exposure temperatures compared to experimental results.

Figure 7-17, Figure 7-18, Figure 7-19 and Figure 7-20 illustrate comparison among prediction results of tension, off-axis shear, flexure and short beam shear retentions for Time-Temperature Superposition and Arrhenius rate model.

If looking at the results of tension retention, the modulus and strength retentions were almost identical at same model. However, the rate of degradation obtained by Arrhenius rate model was more conservative than that of TTSP model. The experimental data of tensile test on specimens exposed to 66°C were initially or largely affected by post-cure effect and were superior to other mechanical properties. Since TTSP model was shifted from reference temperature (66°C) and initial increase was well reflected in predicted data, predicted data by TTSP model were similar with actual experimental data with minimal percent differences as shown in Figure 7-17.

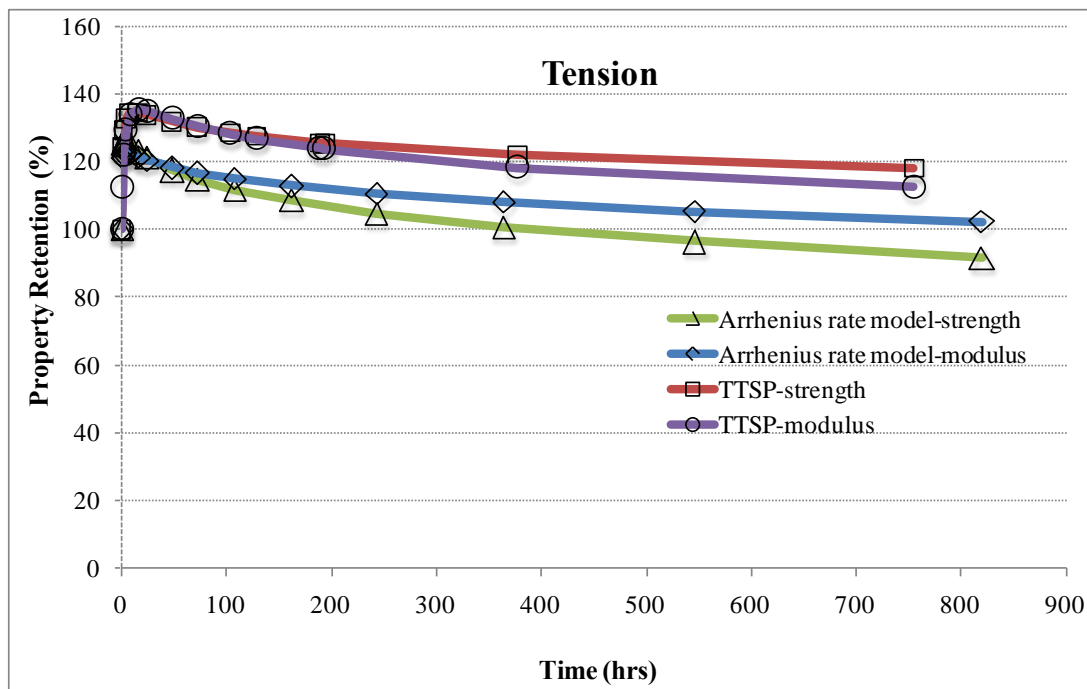


Figure 7-17: Comparison between prediction results of tensile retention for Time-Temperature Superposition and Arrhenius rate model

Since asymmetry on $\pm 45^\circ$ specimens did not result in initial increase, as depicted in Figure 7-18, predicted data by two models were in good agreement with experimental data contrary to other mechanical properties because both models do not take into account effects of post-cure. Until ageing time (72 hrs) applied for this study, Arrhenius rate model showed higher rate of degradation than TTSP model while as ageing time is longer, TTSP model was reversely more conservative compared to Arrhenius rate model.

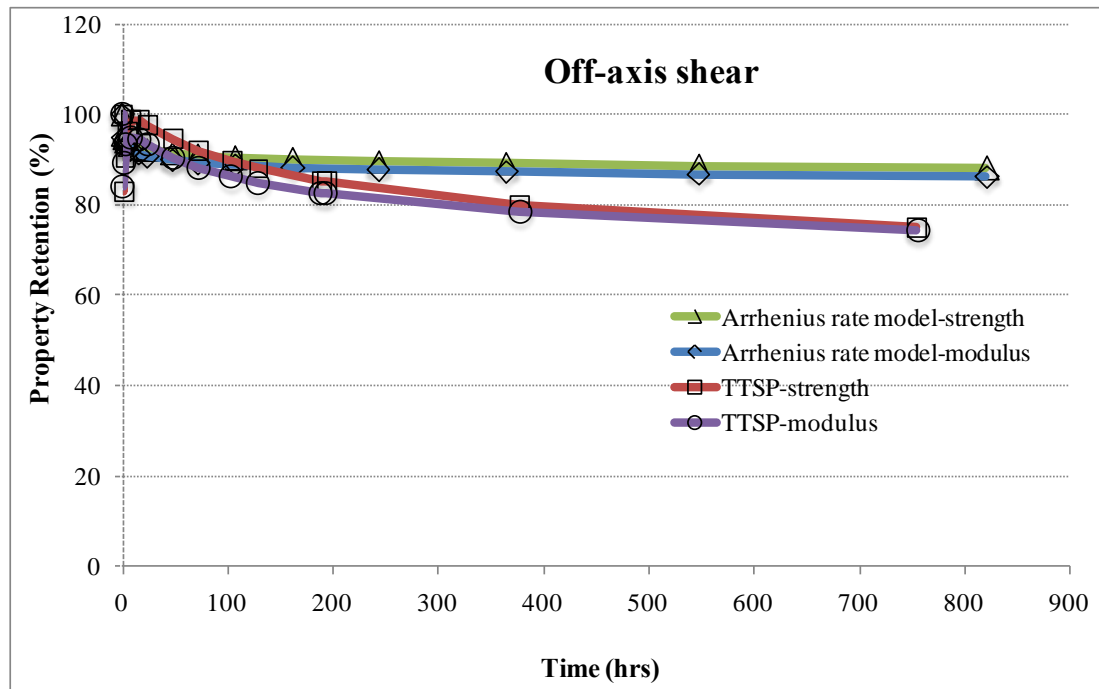


Figure 7-18: Comparison between prediction results of off-axis shear retention for Time-Temperature Superposition and Arrhenius rate model

As shown in Figure 7-19 and Figure 7-20, in the cases of flexural and short beam shear test on specimens exposed to temperature (66°C), initial increase of property retentions did not largely occur compared to the results of tension. In addition, continuous decrease like off-axis shear did not also take place. Therefore, predicted data generated by two models were almost identical regardless of extension of time. Two models can be equally applied for prediction of flexural and short beam shear retention on specimen exposed to 66°C .

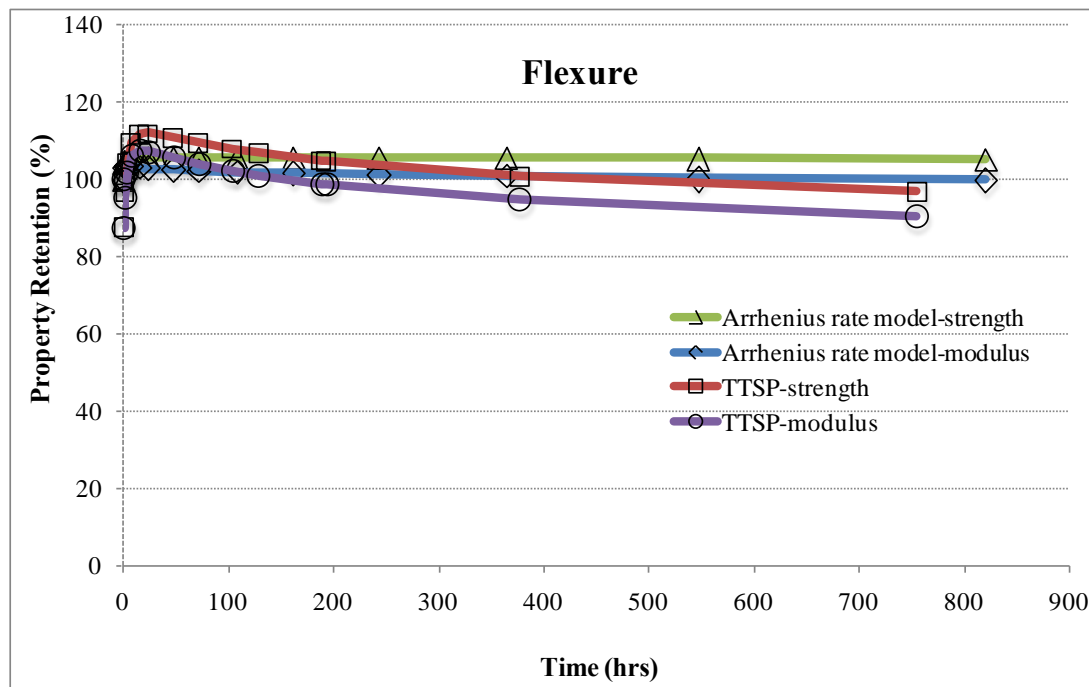


Figure 7-19: Comparison between prediction results of flexure retention for Time-Temperature Superposition and Arrhenius rate model

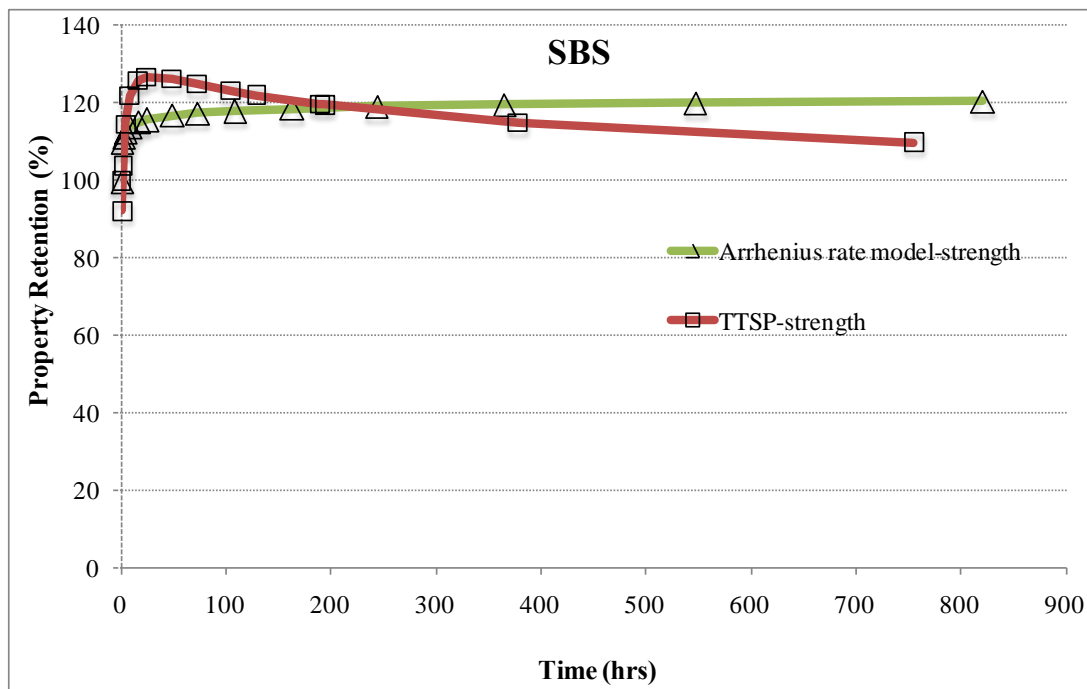


Figure 7-20: Comparison between prediction results of short beam shear retention for Time-Temperature Superposition and Arrhenius rate model

7.4 Weibull Statistical Strength Model

7.4.1 Introduction

If unidirectional composite materials are used in rehabilitation applications, bending and tension are both major forms of loading. To characterize these properties, design practice relies strongly on testing which can be both expensive and time-consuming. For this problem, many researchers have been tried to develop unique tests that can provide multiple performance attributes or develop analytical approaches that would enable use of data from a series of other test results. Therefore, the ability to predict the strength of components subject to flexural, tensile or a combination of these types of loading is important practical interest[96].

Tensile data on unidirectional composite materials are usually used as design

factor in composite materials selection and design of composite laminates. Flexural test is often accomplished in industry for material specification and quality control purpose. Even though flexural test is easier compared to tensile test, data generated from a unidirectional flexural test usually yield higher strength than data obtained from tensile test[97]. The tensile strength measured in flexural test is often 30% to 100% higher than the strength determined from unidirectional tensile test[98]. The presence of a stress gradient in the flexure-test results an increase in tensile strength compared to the tensile test under uniform stress. However, tensile strengths were higher than those measured by flexural test in this study. This phenomenon appears to be stemmed from good load-bearing of carbon fibers and superior interfacial bond between carbon fibers and epoxy resin.

In general, a statistical-strength theory based on a weibull distribution can be used to describe the difference between unidirectional-tensile data measured from a flexural test and a pure tensile specimen. In this chapter, the results of 3-point flexure test will be correlated with the data of a standard tensile coupon test for unidirectional carbon/epoxy composite materials. Also, theoretical results calculated by two parameter Weibull distribution model will be compared to the experimental data for tensile and flexural strength.

7.4.2 Theory

Ratios of flexural strengths to tensile strengths for wide varieties of brittle materials have been found to agree very well with Weibull's statistical strength theory.

Weibull theory defines the probability of survival of composite materials that a test specimen involving a distribution of flaws throughout its volume can survive the application of a stress distribution is expressed by[99],

$$P(S) = \exp \left\{ - \int_V \left[\frac{\sigma(x, y, z) - \sigma_u}{S_0} \right]^\alpha \right\} dx dy dz \quad (7.6)$$

where:

$P(S)$ = the probability of survival

α = the flaw-density exponent that determines the scatter of strength for the materials (shape parameter)-this is related to the relative variance of the distribution

S_0 = the normalizing scale parameter that locates the strength distribution

σ_u = the threshold stress below which the material will never fail (usually taken to be zero)

V = the volume of the specimen that is being stressed

For simpler form, taking σ_u as zero because tensile stress is uniform throughout the specimen, Equation 7.6 can be rewritten by,

$$P(S_t) = \exp \left[-V_t \left(\frac{\sigma_t}{S_0} \right)^\alpha \right] \quad (7.7)$$

where the subscript t denotes tension and V_t is the volume of the tensile coupon used in the tensile tests.

On the other hand, test specimen used in three-point bending flexural tests is subjected to non-uniform stress throughout the rectangular coupon. Therefore, Equation 7.8 including non-uniform factor can be made from Equation 7.6 as,

$$P(S_f) = \exp \left[-V_f \left(\frac{\sigma_f}{S_0} \right)^\alpha \left(\frac{1}{2(\alpha + 1)^2} \right) \right] \quad (7.8)$$

where the subscript f denotes flexure and V_f is the volume of the specimen used in the flexural tests. $\frac{1}{2(\alpha + 1)^2}$ means the non-uniform stress distribution.

The ratio of the median failure stress in three-point bending flexure to that in tension is obtained by setting $P(S_t)=P(S_f)$ as,

$$\frac{\sigma_f}{\sigma_t} = \left[2(\alpha + 1)^2 \frac{V_t}{V_f} \right]^{\frac{1}{\alpha}} \quad (7.9)$$

The shape parameter (α) provides indications of scatter and is related to the relative variation of the distribution[100]. The shape parameter can be correlated to the coefficient of variation (COV) as

$$COV = \left\{ \frac{\Gamma \left(1 + \frac{2}{\alpha} \right)}{\Gamma^2 \left(1 + \frac{2}{\alpha} \right)} - 1 \right\}^{0.5} \quad (7.10)$$

where Γ means the gamma function. Two approximations are often used to explain this relationship with a high degree of accuracy, as follows,

$$COV = \alpha^{-0.926} \quad (7.11)$$

$$COV = \frac{1.2}{\alpha} \quad (7.12)$$

A relationship between the mean value, μ , the shape factor, α , and the scale parameter, β , can be described as[101]

$$\mu = \beta \Gamma \left(1 + \frac{1}{\alpha} \right) \quad (7.13)$$

7.4.3 Results

According to Weibull statistical strength theory, predicted data for tensile and flexural test will be presented in this section.

7.4.3.1 Predictive Data of Flexural Strength from Tensile Tests

First of all, the Weibull shape parameter must be obtained in order to predict data of flexural strength from tensile test. Equation 7.12 and coefficient of variation (COV) are used to calculate the shape parameter in all environmental conditions. Shape parameters obtained are tabulated in Table 7-8 and Figure 7-21 depicts the shape parameters as a function of ageing time from tensile test. If looking at the shape parameters obtained from tensile test, shape parameters showed very high values in under-cure conditions (ambient and low exposure temperature for short ageing time). Namely, coefficients of variation in under-cure conditions were lowered by the lowest standard deviation although mean values were lower compared to post-cure conditions. As post-cure effects are applied for specimens, shape parameters were getting lower. Since tensile failure mode can be largely affected by defects or voids in the process of hand layup fabrication, the standard deviation was getting higher in post-cure conditions. In high exposure temperature (260°C), lower mean values contributed to lower shape parameters.

Table 7-8 Values of shape parameters for the different exposure conditions and ageing time from tensile test

Time	Shape parameters for elevated exposure temperatures from tensile tests								
	Ambient (66°C)	66°C	93°C	121°C	149°C	177°C	204°C	232°C	260°C
0	37.8								
1	14.03	6.98	20.60	25.42	21.28	9.12	11.99	5.90	6.36
2	12.17	25.66	17.12	8.99	10.02	12.13	11.13	9.83	9.88
4	35.54	17.61	7.49	12.84	21.42	14.67	8.45	6.97	6.41
8	16.88	16.21	8.30	10.24	13.17	10.76	13.54	6.51	4.45
16	20.84	14.66	10.42	16.15	9.29	15.06	11.05	11.28	3.48
24	16.77	8.38	8.71	12.92	9.18	5.99	7.27	15.12	5.87
48	19.74	16.03	9.70	16.36	11.99	7.39	12.99	13.81	2.78
72	18.42	20.04	15.31	17.67	19.02	15.42	10.13	12.15	2.85

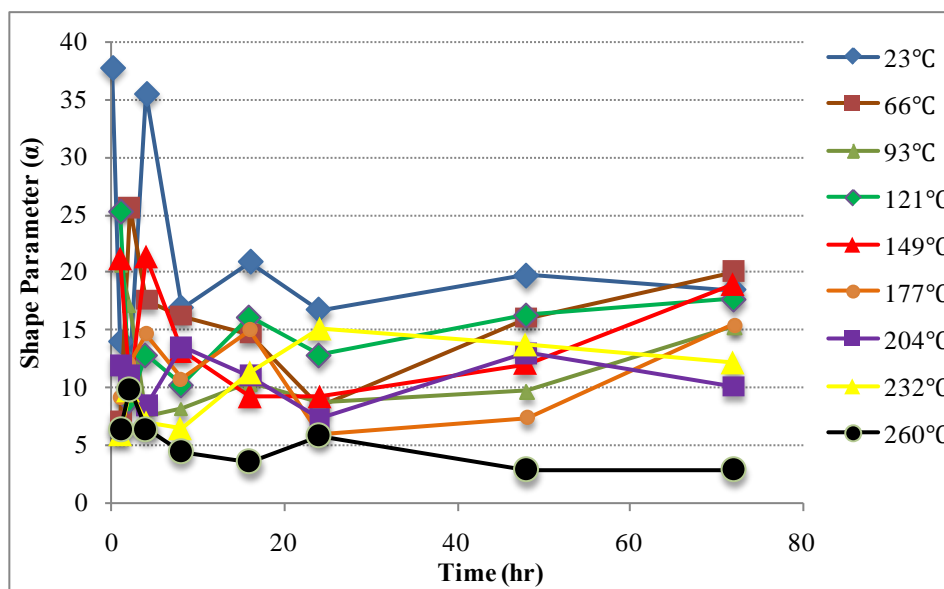


Figure 7-21: Shape parameters on specimens exposed to elevated temperatures as a function of time from tensile test

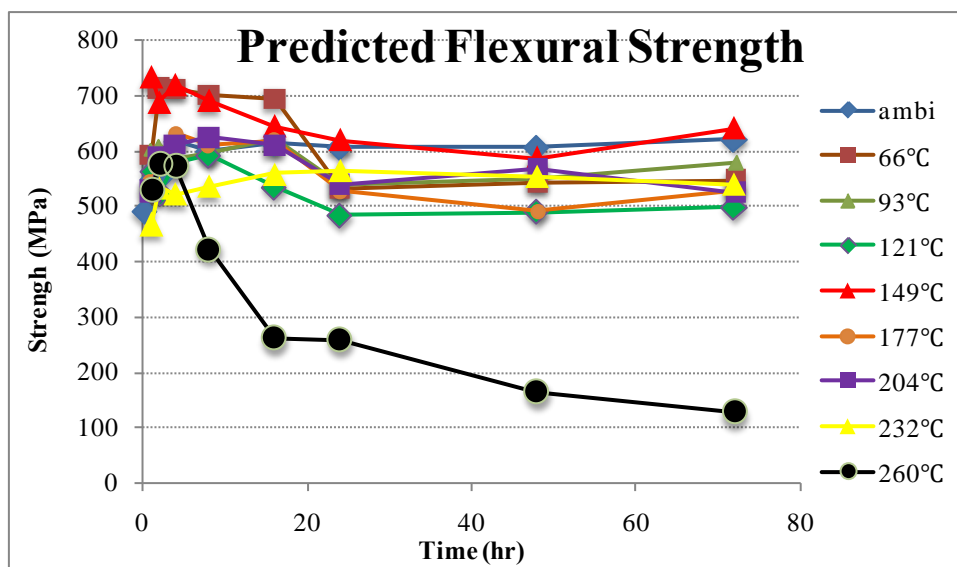
Table 7-9 and Figure 7-22 show values of flexural strength predicted from tensile test on specimens exposed to elevated temperatures for 72 hrs. It can be seen from Figure 7-22 that predictions of flexural strength are fairly close to the

experimental values of flexural strength. In addition, predictive data of flexural strength were overall shifted to high values compared to the experimental data. Especially, predictive data for flexural strength were in good agreement with experimental data in the ranges showing high values of flexural strength due to post-cure effect. Also, predictive data were widely distributed compared to experimental data.

Table 7-9 Values of flexural strength predicted from tensile test on specimens exposed to elevated temperatures for 72 hrs

Time	Predicted Flexural Strength (MPa) : non-uniform term								
	Ambient (23°C)	66°C	93°C	121°C	149°C	177°C	204°C	232°C	260°C
0	493.69								
1	549.31	592.78	601.55	563.03	734.66	545.30	526.86	466.83	529.01
2	554.62	713.58	609.91	523.38	689.35	579.80	590.69	535.00	578.06
4	617.23	711.68	586.40	578.81	718.92	632.19	612.34	521.15	571.33
8	599.12	700.71	595.68	592.76	691.82	610.90	625.55	535.63	423.05
16	614.39	693.48	620.75	534.42	644.02	619.90	609.61	560.20	261.72
24	608.51	533.13	540.67	484.10	618.01	527.04	538.95	565.87	259.40
48	608.65	544.14	549.40	490.18	585.16	491.64	567.74	554.20	165.02
72	623.60	546.08	579.09	498.79	641.40	529.55	525.32	540.13	127.90
Time	Experimental Flexural Strength (MPa)								
	Ambient (23°C)	66°C	93°C	121°C	149°C	177°C	204°C	232°C	260°C
0	547.72								
1	543.11	525.82	512.19	535.95	498.76	540.21	530.27	549.63	494.27
2	585.72	520.14	540.10	554.82	574.78	586.62	562.61	516.77	534.28
4	527.26	558.61	512.58	529.80	505.41	529.97	492.13	528.36	575.69
8	532.05	544.49	483.48	523.24	594.22	548.39	526.03	540.63	295.26
16	527.11	513.13	518.38	543.61	576.04	530.45	545.35	538.35	122.17
24	515.97	543.15	495.93	555.62	553.59	527.56	526.99	557.54	104.44
48	523.90	495.65	540.55	523.16	542.36	549.98	548.88	534.48	76.88
72	514.70	511.71	545.66	553.06	461.98	602.56	600.62	356.95	51.66

Time	Percentage error (%)								
	Ambient (23°C)	66°C	93°C	121°C	149°C	177°C	204°C	232°C	260°C
0	-10.94								
1	1.13	11.30	14.85	4.81	32.11	0.93	-0.65	-17.74	6.57
2	-5.61	27.11	11.45	-6.01	16.62	-1.18	4.75	3.41	7.57
4	14.58	21.51	12.59	8.47	29.70	16.17	19.63	-1.38	-0.76
8	11.19	22.29	18.84	11.73	14.11	10.23	15.91	-0.93	30.21
16	14.21	26.01	16.49	-1.72	10.56	14.43	10.54	3.90	53.32
24	15.21	-1.88	8.28	-14.77	10.42	-0.10	2.22	1.47	59.74
48	13.92	8.91	1.61	-6.73	7.31	-11.87	3.32	3.56	53.41
72	17.46	6.29	5.77	-10.88	27.97	-13.79	-14.34	33.92	59.61



(a)

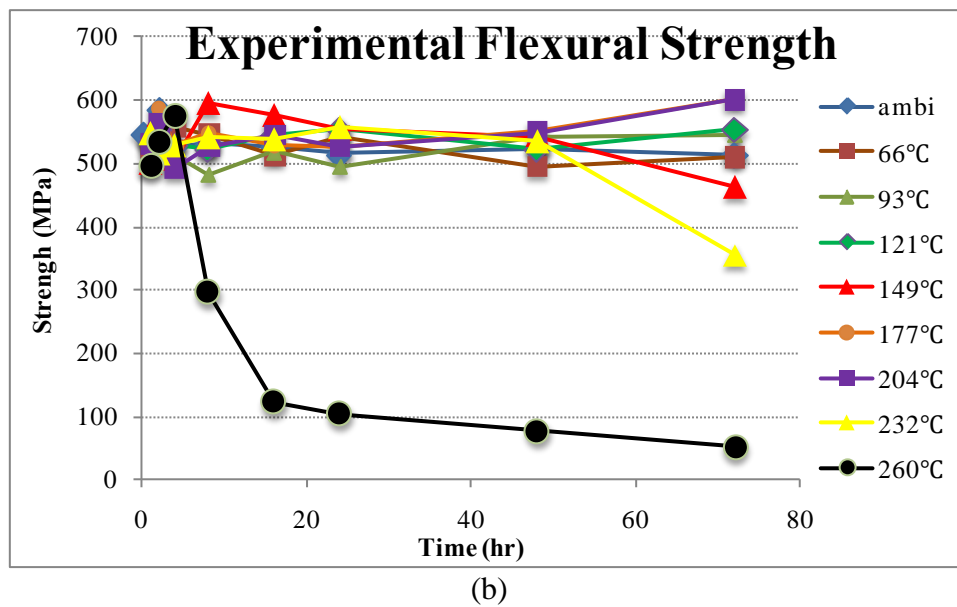


Figure 7-22: Comparison of (a) predicted flexural strength from tensile test and (b) experimental flexural strength

7.4.3.2 Predictive Data of Tensile Strength from Flexural Tests

As investigated in previous section, predicted data of flexural strength from tensile test showed good correlation with experimental data. On the contrary to this, if tensile strengths can be estimated from flexure test which has easier method compared to other mechanical tests, it can be more efficient prediction to avoid cost and time-consuming. The Weibull parameters for each of the flexural test data sets are evaluated as shown in Table 7-10 and Figure 7-23. Similar to shape parameters of tensile strength,

shape parameters from flexure test showed high values in under-cure conditions and low values in high exposure temperatures (204, 232 and 260°C). In additions, the reasons why the high variation of shape parameters show compared to tensile strengths are that flexure test intrinsically has stress gradient in bending and failure mechanisms are very complicated.

Table 7-10 Values of shape parameters for the different exposure conditions and ageing time from flexural test

Time	Shape parameters for elevated exposure temperatures from flexural tests								
	Ambient (23°C)	66°C	93°C	121°C	149°C	177°C	204°C	232°C	260°C
0	29.11								
1	39.03	18.55	8.87	21.36	6.16	20.61	14.50	17.02	32.47
2	46.00	26.64	26.27	18.10	14.88	19.00	17.07	10.28	25.73
4	20.49	9.12	12.31	14.15	40.14	7.43	12.17	10.34	27.38
8	8.34	13.63	10.48	32.75	13.41	7.92	13.29	14.41	5.34
16	37.75	15.42	20.71	9.43	26.98	23.51	14.61	17.36	10.25
24	8.16	7.98	5.45	24.87	13.76	23.09	9.96	12.32	9.94
48	24.03	9.35	29.88	8.96	8.81	15.63	9.56	8.75	7.00
72	10.43	9.30	15.88	22.96	22.07	15.15	19.56	3.10	2.96

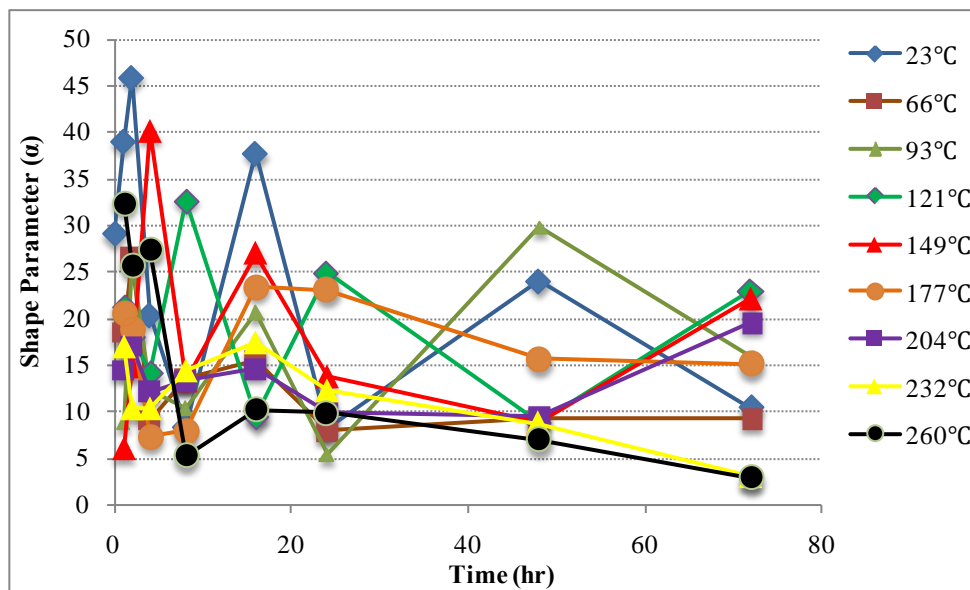
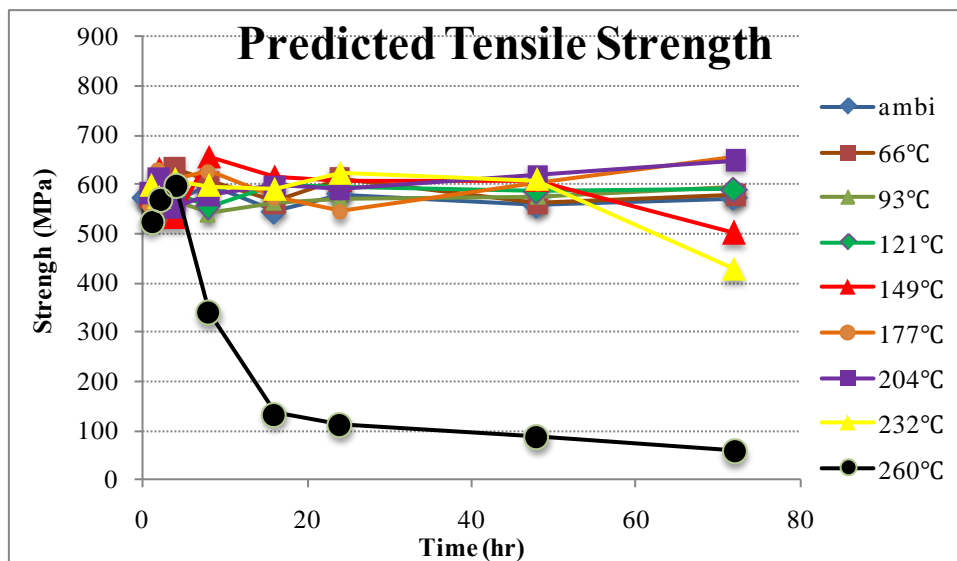


Figure 7-23: Shape parameters on specimens exposed to elevated temperatures as a function of time from flexural test

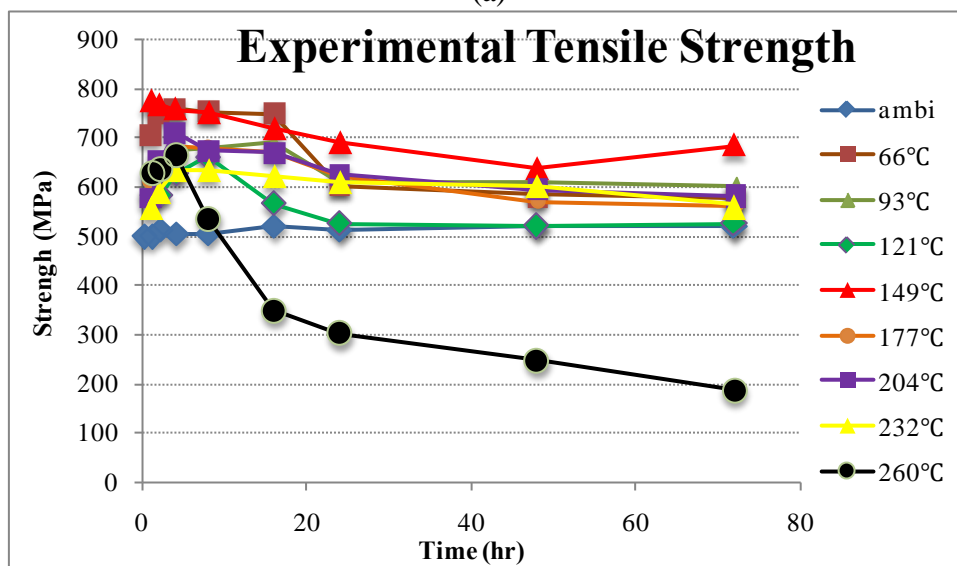
Table 7-11 and Figure 7-24 present values of tensile strength predicted from flexural test on specimens exposed to elevated temperatures for 72 hrs. As shown Figure 7-24, predicted data of tensile strength from flexural test showed a similar tendency with experimental tensile strengths. On the contrary to the predictive data of flexural strength, predictive data of tensile strength were overall shifted to lower values in intermediate exposure temperatures. In other words, the increase of strength due to post-cure effect was reduced by weibull statistical strength model. Except for severe condition (exposure temperature: 260°C), experimental data of tensile strength were scattered between 500 MPa and 800 MPa while predictive data were distributed between 500 MPa and 650 MPa.

Table 7-11 Values of tensile strength predicted from flexural test on specimens exposed to elevated temperatures for 72hrs

Time	Predicted Tension Strength (MPa)								
	Ambient (23°C)	66°C	93°C	121°C	149°C	177°C	204°C	232°C	260°C
0	575.20								
1	568.39	576.14	575.29	575.57	579.31	557.46	584.55	599.69	524.58
2	613.04	541.27	576.26	600.50	632.32	630.48	615.08	576.11	570.15
4	568.88	633.87	567.93	583.09	532.82	611.14	554.29	609.12	598.58
8	599.17	605.95	541.84	555.98	657.54	626.96	578.11	597.12	339.77
16	547.49	565.45	561.88	599.86	615.07	573.44	598.18	591.33	135.95
24	580.70	613.66	570.48	594.93	608.63	545.31	591.45	623.28	113.82
48	560.20	562.69	574.47	587.11	609.80	603.83	619.31	609.56	88.50
72	572.98	581.35	594.57	591.94	502.05	656.91	650.28	428.97	60.38
Time	Experimental Tension Strength (MPa)								
	Ambient (23°C)	66°C	93°C	121°C	149°C	177°C	204°C	232°C	260°C
0	502.26								
1	581.68	706.34	632.60	584.64	775.59	612.64	577.67	559.53	627.34
2	602.68	751.05	646.52	583.46	768.83	623.52	652.35	594.13	638.44
4	635.18	759.38	675.49	628.76	757.77	684.95	710.17	635.30	667.76
8	637.06	754.03	679.70	662.12	752.08	679.07	673.62	636.98	537.66
16	643.02	749.95	691.43	564.93	720.81	671.43	669.59	623.21	349.88
24	646.80	604.06	611.17	524.36	691.34	624.42	625.50	611.42	303.20
48	672.05	584.97	610.71	522.15	638.38	570.72	595.91	603.00	248.40
72	704.18	578.72	602.29	526.22	684.88	563.94	582.49	565.29	188.60
Time	Percentage error (%)								
	Ambient (23°C)	66°C	93°C	121°C	149°C	177°C	204°C	232°C	260°C
0	12.68								
1	-2.34	-22.60	-9.96	-1.58	-33.88	-9.90	1.18	6.70	-19.59
2	1.69	-38.76	-12.19	2.84	-21.59	1.10	-6.06	-3.13	-11.98
4	-11.65	-19.80	-18.94	-7.83	-42.22	-12.08	-28.12	-4.30	-11.56
8	-6.32	-24.44	-25.44	-19.09	-14.38	-8.31	-16.52	-6.67	-58.24
16	-17.45	-32.63	-23.06	5.82	-17.19	-17.09	-11.94	-5.39	-157.37
24	-11.38	1.56	-7.13	11.86	-13.59	-14.51	-5.76	1.90	-166.39
48	-19.97	-3.96	-6.31	11.06	-4.69	5.48	3.78	1.08	-180.67
72	-22.90	0.45	-1.30	11.10	-36.42	14.15	10.42	-31.78	-212.33



(a)



(b)

Figure 7-24: Comparison of (a) predicted tensile strength from flexural test and (b) experimental tensile strength

8 Conclusions

8.1.1 Summary

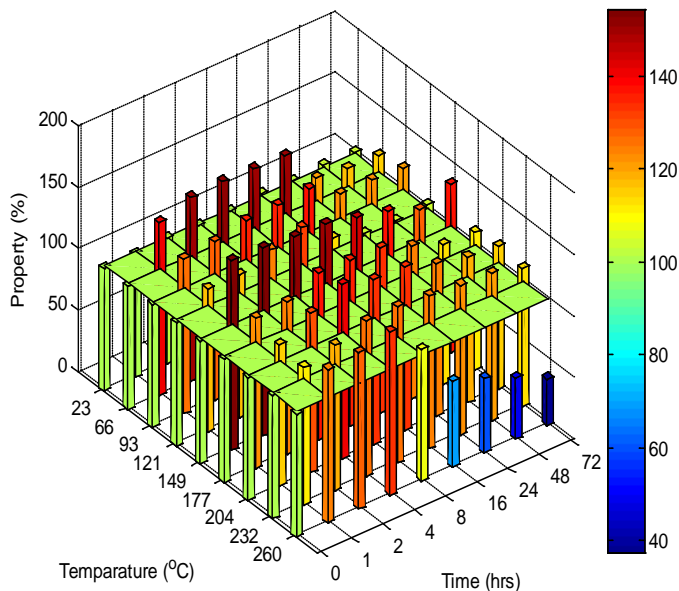
The various characterizations in conjunction with immersion effect were investigated for assessments of carbon/epoxy composite materials after exposure to elevated temperatures. This research can be summarized into mechanical characterization, thermal analysis, immersion analysis and predictive degradation model.

- Mechanical characterizations:

- (1) As shown in Figure 8-1 and Figure 8-2, all tensile property retentions (%) within test conditions were more than 100% due to residual post-cure effect except for specimens exposed to temperature of 260 °C for 16 hrs of ageing time.
- (2) The increase of tensile strength retentions by post-cure effect was superior to that of tensile modulus retention
- (3) As expected, increase of tensile property occurred with extension of ageing time in the ranges of lower exposure temperatures whereas the enhancement of tensile property initially took place in the ranges of higher exposure temperatures and then tensile properties including strength and modulus were decreased due to degradation of thermooxidation.
- (4) The color of the specimens exposed to elevated temperatures can be divided into five categories- no change, brown color with shiny surface, red color with shiny surface, dark color with shiny surface and char formation. Therefore, color of the specimen exposed to temperature can be used in estimate the degree of curing

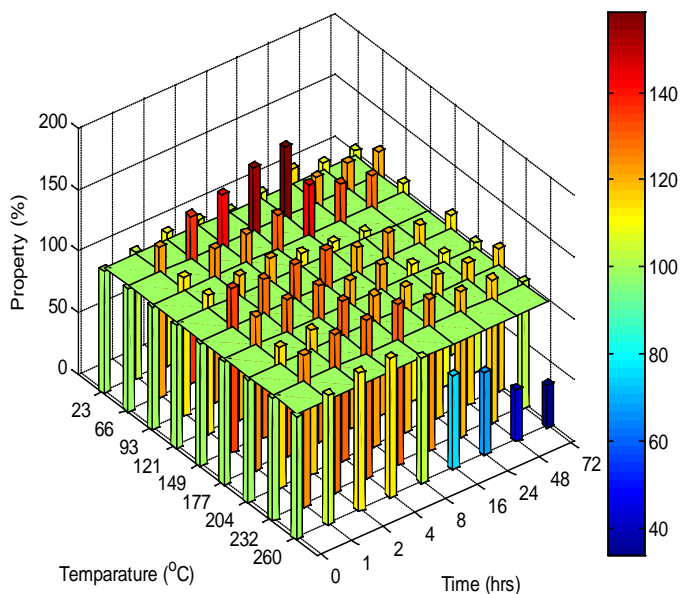
and ageing as well as degradation in FRP composite materials.

- (5) Specimens exposed to 260 °C for more than 16 hrs demonstrated a brooming mode of failure due to thermally perfect degradation of the matrix. Tensile strength and modulus were catastrophically dropped in these ranges.
- (6) As shown in Figure 8-3 and Figure 8-4, the majority of the retentions (%) of off-axis shear property were less than 100% since test coupons were distorted by asymmetry when taken out from the oven and kept in atmosphere before off-axis shear test.
- (7) Most retentions of flexural property existed between 80% and 120% as shown in Figure 8-5 and Figure 8-6. The residual post-cure effect did not largely lead to increase of flexural properties compared to tensile results. Since thermal oxidation caused catastrophic debonding between 2 layers in high exposure temperatures, the rate of drop of the flexural property was higher than that of the tensile property.
- (8) Compared to the strength retentions of tensile and flexural test, the strength retentions of short beam shear test were initially increased in the amount of more than flexural strength retention and less than tensile strength retention by residual post-curing as shown in Figure 8-7. Therefore, the fractures of short beams shear test can be resulted in mixed failure mode. In particular, compared to experimental data of flexural test, the majority of failure modes of short beam shear test were occurred by not shear but flexural tension at outer surface.



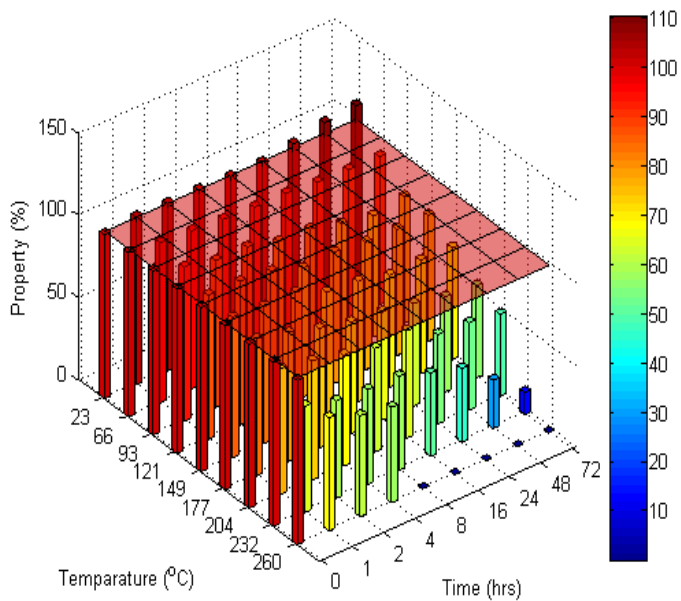
Retention (%) range	Tensile strength (count)
140~	11
120~140	31
100~120	26
80~100	1
60~80	2
~60	2
Total	73

Figure 8-1: The distribution of tensile strength retentions (%) on specimens exposed to elevated temperatures for up to 72 hrs



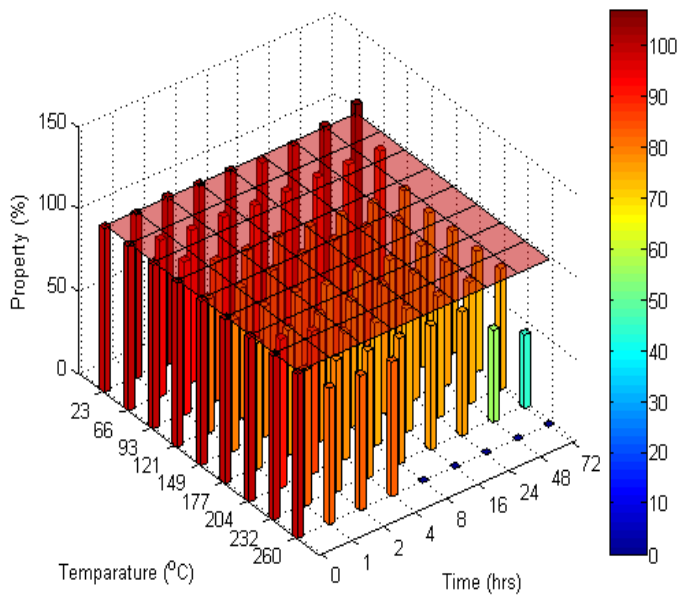
Retention (%) range	Tensile modulus (count)
140~	4
120~140	29
100~120	34
80~100	2
60~80	2
~60	2
Total	73

Figure 8-2: The distribution of tensile modulus retentions (%) on specimens exposed to elevated temperatures for up to 72 hrs



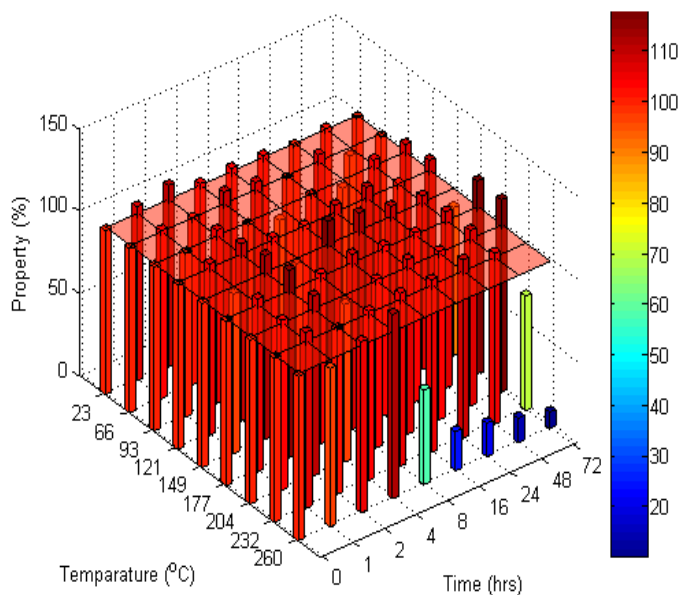
Retention (%) range	Off-axis shear strength (count)
140~	
120~140	
100~120	9
80~100	20
60~80	26
~60	18
Total	73

Figure 8-3: The distribution of off-axis shear strength retentions (%) on specimens exposed to the elevated temperatures for up to 72hrs



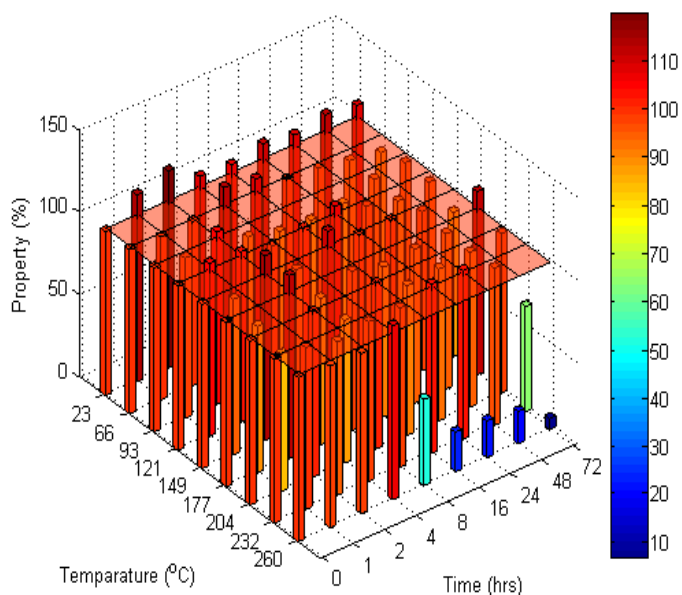
Retention (%) range	Off-axis shear modulus (count)
140~	
120~140	
100~120	6
80~100	28
60~80	32
~60	7
Total	73

Figure 8-4: The distribution of off-axis shear modulus retentions (%) on specimens exposed to the elevated temperatures for up to 72hrs



Retention (%) range	flexural strength (count)
140~	
120~140	
100~120	49
80~100	18
60~80	1
~60	5
Total	73

Figure 8-5: The distribution of flexural strength retentions (%) on specimens exposed to the elevated temperatures for up to 72hrs



Retention (%) range	flexural modulus (count)
140~	
120~140	
100~120	28
80~100	39
60~80	1
~60	5
Total	73

Figure 8-6: The distribution of flexural modulus retentions (%) on specimens exposed to the elevated temperatures for up to 72hrs

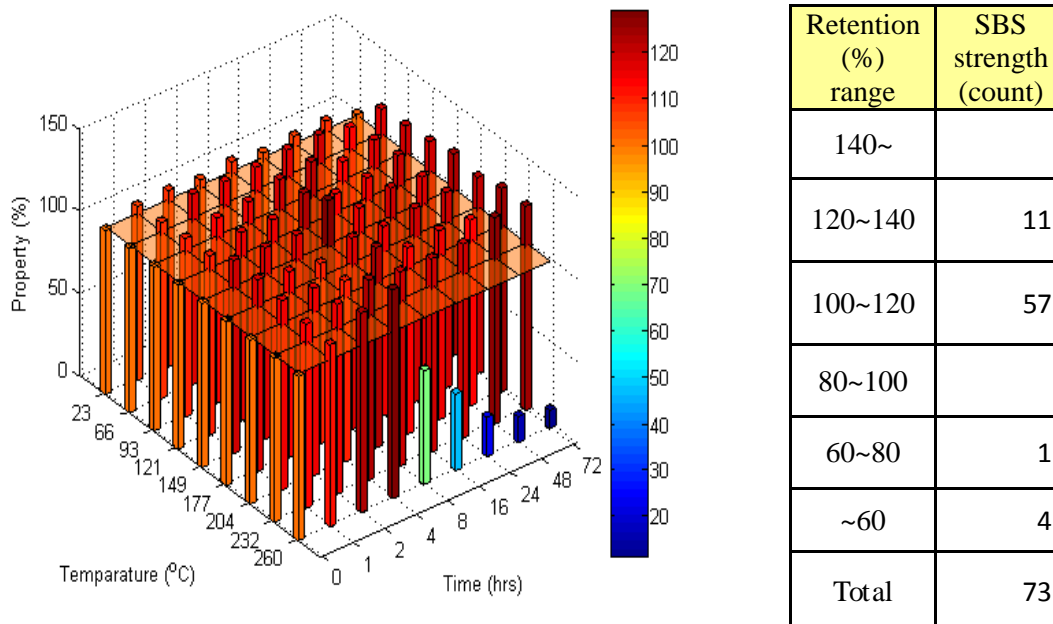


Figure 8-7: The distribution of Short Beam Shear strength retentions (%) on specimens exposed to the elevated temperatures for up to 72hrs

- *Thermal analysis:*

- (1) Thermal ageing initially caused a significant increase of the glass transition temperature, which is attributed to the post-cure effect on ambient cured system.
- (2) Glass transition temperatures determined from both fiber oriented test specimens using DMTA showed very similar data for all environmental conditions. However, because specimens were tested in bending with single cantilever fixture in longitudinal direction, glass transition temperatures of longitudinal specimen were slightly delayed compared to transverse test specimens.
- (3) If the test frequency is increased, the relaxations corresponding to the glass transition is hard to reflect the mechanical strain input, and the polymer

composites may have rigid property. Therefore, glass transition temperatures increase as the rate of frequency is increased.

- (4) Since the $\tan \delta$ is the ratio of the loss modulus to the storage modulus, the height of $\tan \delta$ and glass transition temperatures shifted to higher levels with increase in test frequency. From increase of interfacial bonding by post-cure effect, broadened transition region and decreased $\tan \delta$ value were observed due to the stiffness or rigid of test specimen.
- (5) Activation energies were continuously increased up to 72 hrs of ageing time in the ranges of lower exposure temperatures (66, 93, 121 and 149 °C). Continuous increases were attributed to residual post-cure effect, which led to an intense crosslinkage and the mobility of the polymer segment was constrained significantly. In ranges of intermediate temperatures (177, 204 and 232 °C), activation energies were leveled off after initially reaching to the maximum value.
- (6) Except for the conditions of the severe exposure temperature (260 °C), ambient temperature and off-axis shear test, the enhancement of mechanical properties were associated with increase of glass transition temperature.
- (7) Glass transition temperatures determined by the analysis of DSC were overall higher than the results detected by the height of peak $\tan \delta$ and storage modulus using DMTA in all environmental conditions.
- (8) Since the epoxy resin used in this study was cured at room temperature and was not fully cured, weight loss of specimens was attributed to evaporating of

uncured small molecules and spilt of the small molecular part from long polymer chain.

- (9) The values of T_{onset} initially increased due to the dominant increase of the crosslinkage with thermal treatment. For lower exposure temperatures ($\sim 149^\circ\text{C}$), the values of T_{onset} continuously increased even though ageing time go up. In the exposure temperatures ranging from 177 to 260°C , the values of T_{onset} continuously decreased with the extended ageing time. The higher exposure temperatures resulted in the more serious drop in the values of T_{onset} by thermal decomposition of specimens.

- Immersion analysis:

- (1) The results of the gravimetric measurements on specimens immersed in deionized water and seawater showed a Fickian response in all conditions.
- (2) Specimens post-cured from the increase of ageing time and exposure temperature showed the rapid saturation and the higher maximum weight gain compared to un-cured specimens.
- (3) The partially cured composite could be expected to have a greater concentration of unreacted chemical species with the epoxy resin and it appears that these species were released more rapidly into water resulting in a slower net mass gain.
- (4) Mass loss by leaching of organic species than mass uptake by sorption of salts largely contributed to lower maximum weight gain in seawater compared to the values of deionized water.

- (5) Overall diffusion coefficients calculated for deionized water immersion were higher than those for seawater immersion in all environmental conditions. Diffusion coefficients in deionized water were widely distributed with increase of ageing time and exposure temperatures.
- (6) All specimens immersed in deionized water and seawater showed similar characterizations which had initially decrease (~ 16 weeks), asymptotic trend or slightly increase (16 ~ 48 weeks) and rapidly decrease after 48 weeks in terms of short beam shear strengths.
- (7) Intrinsic properties of epoxy and carbon fiber against water resulted in a slight decrease or asymptotic trend in terms of short beam shear strengths until 48 weeks in immersion period. However, catastrophic drop of short beam shear strengths after 48 weeks of immersion was derived from irreversible degradations such as hydrolysis, microcracking, microvoids and epoxy relaxation.
- (8) Specimens immersed in deionized water and seawater for 72 weeks after exposure to 260 °C for 8 hrs showed catastrophic cracks in the epoxy and interface and the delaminations between 2 layers by the increase of the free volume and water ingress into cracks and cavities created by thermooxidation when the specimens were heated to high temperature.

- Predictive degradation models:

- (1) In tensile tests, the rate of degradation obtained by Arrhenius rate model was more conservative than that of TTSP model.

- (2) Since asymmetry on $\pm 45^\circ$ specimens did not result in initial increase, predicted data by two models (Arrhenius rate model and TTSP model) were in good agreement with experimental data contrary to other mechanical properties.
- (3) Predicted data of flexural and short beam shear test generated by two models (Arrhenius rate model and TTSP model) were almost identical regardless of extension of ageing time. Therefore, two models can be equally applied for prediction of flexural and short beam shear retention.
- (4) Predictions of flexural strength generated by Weibull statistical strength model were fairly close to the experimental values of flexural strength. In addition, predictive data of flexural strength were overall shifted to high values compared to the experimental data.
- (5) On the contrary to the predictive data of flexural strength, predictive data of tensile strength by Weibull statistical strength model were overall shifted to lower values in intermediate exposure temperatures.

Implementation: Based on this study it is recommended that a MOL be defined and used for implementation in the field. Further, results from this study should be extended to other composite systems used by Caltrans so as to provide a chart for inspectors and engineers related to safer operating time-temperature plots with residual performance characteristics. These should also be assessed for integration into design variables. An example of its implementation is shown in the next section of this report.

REFERENCES

1. Caplan I, *Marine composites-First International Workshop on Composite Materials for Offshore Operation*. University of Houston, TX, 26-28, October 1993.
2. MIL-STD-2031, *Fire and Toxicity test methods and qualification procedure for composite materials systems used in Hull, Machinery, and Structural Application inside Naval Submarines*. 1991.
3. MeMarco RA, *36th International SAMPE Symposium*. 1991. 36.
4. Henderson, J.B., J.A. Wiebelt, and M.R. Tant, *A Model for the Thermal Response of Polymer Composite Materials with Experimental Verification*. *Journal of Composite Materials*, 1985. 19(6): p. 579-595.
5. Landrock, A.H., *Handbook of Plastics Flammability and Combustion Toxicology*. Noyes Publication, 1983. Park Ridge.
6. C.F.Cullis and M.M.Hirschler, *The Combustion of Organic Polymers*. Clarendon Press, 1981. Oxford.
7. Le Huy, H.M., Bellenger, V.,Verdu, J. and M. Paris, *Thermal oxidation of anhydride cured epoxies. I--mechanistic aspects*. *Polymer Degradation and Stability*, 1992. 35(1): p. 77-86.
8. Bruce, L.B., *The thermooxidative stability of cured epoxy resins. I*. *Journal of Applied Polymer Science*, 1993. 47(10): p. 1821-1837.
9. McMahon PE, *Oxidative resistance of carbon fibers and their composites*. In: *Advanced Composite Materials-Environmental Effects*. ASTM STP 658, 1978: p. 254-266.

10. Pering, G.A., P.V. Farrell, and G.S. Springer, *Degradation of tensile and shear properties of composites exposed to fire or high-temperature*. Journal of Composite Materials, 1980. 14(JAN): p. 54-68.
11. Grant, T.S. and W.L. Bradley, *In-Situ Observations in SEM of Degradation of Graphite/Epoxy Composite Materials due to Seawater Immersion*. Journal of Composite Materials, 1995. 29(7): p. 852-867.
12. Leif A. Carlsson, F.P., *Influence of sea water on transverse tensile properties of PMC, NIST Special Publication 887*. National Institute of Standards and Technology, 1995: p. 203-221.
13. Wood, C.A. and W.L. Bradley, *Determination of the effect of seawater on the interfacial strength of an interlayer E-glass/graphite/epoxy composite by in situ observation of transverse cracking in an environmental SEM*. Composites Science and Technology, 1997. 57(8): p. 1033-1043.
14. Lixin Wu. Karen Murphy. Vistap M. Karbhari and J.S. Zhang, *Short-term effects of sea water on E-glass/vinylester composites*. Journal of Applied Polymer Science, 2001. 84: p. 2760-2767.
15. Gellert, E.P. and D.M. Turley, *Seawater immersion ageing of glass-fibre reinforced polymer laminates for marine applications*. Composites Part A: Applied Science and Manufacturing, 1999. 30(11): p. 1259-1265.
16. Tucker, W.C. and R. Brown, *Moisture Absorption of Graphite/Polymer Composites Under 2000 Feet of Seawater*. Journal of Composite Materials, 1989. 23(8): p. 787-797.

17. Liao, K., C.R. Schultheisz, and D.L. Hunston, *Effects of environmental aging on the properties of pultruded GFRP*. Composites Part B: Engineering, 1999. 30(5): p. 485-493.
18. Strait, L.H., M.L. Karasek, and M.F. Amateau, *Effects of Seawater Immersion on the Impact Resistance of Glass Fiber Reinforced Epoxy Composites*. Journal of Composite Materials, 1992. 26(14): p. 2118-2133.
19. Kootsookos, A. and A.P. Mouritz, *Seawater durability of glass- and carbon-polymer composites*. Composites Science and Technology, 2004. 64(10-11): p. 1503-1511.
20. Rhee, K.Y.H., S. R. Park, S. J. Kim, H. J. and D.H. Jung, *Fracture behavior of seawater-absorbed carbon/epoxy laminated composites in the hydrostatic pressure condition*. Materials Science and Engineering: A, 2006. 419(1-2): p. 209-213.
21. McBagonluri, F.G., K. Hayes, M. Verghese, K. N. E. and J.J. Lesko, *Characterization of fatigue and combined environment on durability performance of glass/vinyl ester composite for infrastructure applications*. International Journal of Fatigue, 2000. 22(1): p. 53-64.
22. Roger M.Crane, J.W.G., Dirk Hieder, S. Yarlagadda, S. G. Advani, *Intelligent processing and inspection of Naval composites*. AMPTIAC Quarterly, 2003. 7, number 3(navy experts explain the newest materials & structural technologies).
23. Mouritz, A.P., Gellert, E. Burchill, P. and K. Challis, *Review of advanced composite structures for naval ships and submarines*. Composite Structures, 2001. 53(1): p. 21-42.

24. Smith J., *Novel submarine hulls*. naval composite news, 1999. 3:13-4.
25. Newan MR., *Development of non hull penetrating masts and perisopes*. In: *proceedings of Warship'99*. The International Symposium on Naval structures 6, 1999. June 14-16(paper No 6).
26. *MIL-HDBK-17-1F: composite Materials Handbook*. Polymer Matrix Composites Guidelines for Characterization of Structural Materials. 1.
27. ASTM D3039M, *Standard Test Method for Tensile Properties of Polymer Matrix Composite Materials*. Amercian Society of Testing Materials, 2003. Vol.15.03.
28. C.C. Chamis and J.H. Sinclair, *Ten-Degree Off-Axis Test for Shear Properties in Fiber Composites*. Experimental Mechanics, 1977. Vol.17: p. 339-346.
29. ASTM D5379, *Standard Test Method for Shear Properties of Composite Materials by the V-notch Beam Method*. Amercian Society of Testing Materials, 100 Barr Harbo Drive, West Conshohocken, PA 19428, 1997. Vol.15.03.
30. ASTM D5488, *Standard Test Method for In-plane Shear Properties of Hoop Wound Polymer Matrix Composite Cylinders*. Amercian Society of Testing Materials, 1998. Vol.04.10.
31. ASTM D4255, *Standard Test Method for Testing In-Plane Shear Properties of Composite Laminates*. Amercian Society of Testing Materials, 1997. Vol. 15.03.
32. ASTM D3518/D3518M-94, *Standard Test Method for In-Plane Shear Response of Polymer Matrix Composite Materials by Tensile Test of a $\pm 45^\circ$ Laminate*. Amercian Society of Testing Materials, 2001. Vol. 15.03.

33. Donald F. Adams, L.A.C., R. Byron Pipes,, *Experimental characterization of advanced composite materials*. CRC Press, 2003. Third edition.
34. ASTM D790M, *Standard Test Method for Flexural Properties of Unreinforced and Reinforced Plastics and Eletrical Insulated Materials*. Amercian Society of Testing Materials, 2003. Vol.08.01.
35. C.E. Browning, F.L.A., and J.M. Whitney, *A Four-Point Shear Test for Graphite/Epoxy Composites: Quality Assurance and Processing, STP 797*. Amercian Society of Testing Materials, Philadelphia, 1983(54-74).
36. ASTM D3846, *Standard Test Method for In-Plane Shear of Reinforced Plastics*. americian Society of Testing Materials, 100 Barr Harbo Drive, West Conshohocken, PA 19428, 1998. Vol.08.02.
37. ASTM D5379, *Standar Test Method for Shear Properties of Composite Materials by the V-notch Beam Method*. Amercian Society of Testing Materials, 1997. Vol.15.03.
38. ASTM D2344/D2344M-00, *Standard Test Method for Short-Beam Strength of Polymer Matrix Composite Materials and Their Laminates*. Amercian Society of Testing Materials, 2006. Vol.15.03.
39. Karbhari, V.M. and Q. Wang, *Multi-frequency dynamic mechanical thermal analysis of moisture uptake in E-glass/vinylester composites*. *Composites Part B: Engineering*, 2004. 35(4): p. 299-304.
40. Chartoff RP, Weissman PT, and S. A., *Application of dynamic mechanical methods to Tg determination in polymers: an overview*. ASTM STP 1249, 1994: p. 88-107.

41. G. Li, P. Lee-Sullivan, and R.W. Thring, *Determination of Activation Energy for Glass Transition of an Epoxy Adhesive Using Dynamic Mechanical Analysis* Journal of Thermal Analysis and Calorimetry, 2000. Volume 60: p. 377-390.
42. Stephen, G.K. and S. Arun, *Dynamic mechanical analysis of fiber-reinforced phenolics*. Journal of Applied Polymer Science, 1999. 73(5): p. 649-658.
43. ASTM D5418-07, *Standard Test Method for Plastics: Dynamic Mechanical Properties: In Flexure*. American Society of Testing Materials, 2001. Vol.08.03.
44. ASTM D3418-03, *Standard Test Method for Transition Temperatures of Polymers By Differential Scanning Calorimetry*. American Society of Testing Materials, 2005. Vol.08.02.
45. Wu, C.S., Liu, Ying Ling, Chiu, Yie Chan and Y.S. Chiu, *Thermal stability of epoxy resins containing flame retardant components: an evaluation with thermogravimetric analysis*. Polymer Degradation and Stability, 2002. 78(1): p. 41-48.
46. H.H.Horovitz and Gershon.Metzger, *A New Analysis of Thermogravimetric Traces*. Anal. Chem, 1963. 35(10): p. 1464-1468.
47. ASTM E1131-03, *Standard Test Method for Compositional Analysis by Thermogravimetry*. American Society of Testing Materials, 2003. Vol.14.02.
48. Abanilla, M.A., Y. Li, and V.M. Karbhari, *Durability characterization of wet layup graphite/epoxy composites used in external strengthening*. Composites Part B: Engineering, 2005. 37(2-3): p. 200-212.

49. Rochardjo, H.S.B., et al., *Effects of the fiber content on the longitudinal tensile fracture behavior of uni-directional carbon/epoxy composites*. Journal of Materials Processing Technology, 1997. 67(1-3): p. 89-93.
50. J.M.Hodgkinson, *Mechanical Testing of advanced Firber Composites*. Cambrige, Eglan: CRC Press, 2000.
51. Abanilla, M.A., V.M. Karbhari, and Y. Li, *Interlaminar and intralaminar durability characterization of wet layup carbon/epoxy used in external strengthening*. Composites Part B: Engineering, 2006. 37(7-8): p. 650-661.
52. L.A. Carlsson and R.B. Pipes, *Experimental Characterization of Advanced Composite Materilas*. New Jersy:prentice-Hall, Inc., 1987.
53. W.W. Stinchcomb, E.G.H., and H.L.Price, *Use of the short-beam shear test for quality control of graphite-polyimide laminates*. Reproducibility and Accuracy of Mechanical Tests, 1977. ASTM STP, 626:96.
54. Whitney, J.M. and C.E. Browing, *On short-beam shear tests for composite materials*. Experimental Mechanics, 1985. volume 25(3): p. page 294-300.
55. Daniels, B.K., N.K. Harakas, and R.C. Jackson, *Short beam shear tests of graphite fiber composites*. Fibre Science and Technology, 1971. 3(3): p. 187-208.
56. Richards-Frandsen, R. and Y. Nærheim, *Fracture Morphology of Graphite/Epoxy Composites*. Journal of Composite Materials, 1983. 17(2): p. 105-113.
57. Drzal, L.T. and M. Madhukar, *Fiber matrix adhesion and its relationship to composite mechanical-properties*. Journal of Materials Science, 1993. 28(3): p. 569-610.

58. S.Timoshenko, *Strength of Materials, Part I*. Van Nostrand, Princeton, 3rd edition, 1955: p. 95,118.
59. Akay, M., *Aspects of dynamic mechanical analysis in polymeric composites*. Composites Science and Technology, 1993. 47(4): p. 419-423.
60. Menard, K.P., *A Practical Introduction to Dynamic Mechanical Analysis*. Boca Raton, Florida, CRC Press, 1999.
61. Ward, I.M.H., D. W., *An Introduction to the mechanical Properties of Solid Polymer*. Wiley, New York, 1993.
62. Ferry, J.D., *Viscoelastic Properties of Polymers, 3rd edition*. Wiley, New York, 1980.
63. Joseph D. Menczel and R. Bruce Prime, *Thermal Analysis of Polymers*. Wiley, A John Wiley & Sons, inc., Publication, 2008.
64. Pascault, J.P. and R.J.J. Williams, *Glass transition temperature versus conversion relationships for thermosetting polymers*. Journal of Polymer Science Part B: Polymer Physics, 1990. 28(1): p. 85-95.
65. Kennedy, J.M., et al., *Characterization of Interfacial Bond Strength by Dynamic Analysis*. Journal of Composite Materials, 1992. 26(6): p. 869-882.
66. Fraga, A.N., et al., *Relationship between Dynamic Mechanical Properties and Water Absorption of Unsaturated Polyester and Vinyl Ester Glass Fiber Composites*. Journal of Composite Materials, 2003. 37(17): p. 1553-1574.
67. Karbhari, V.M., *Dynamic Mechanical Analysis of the Effect of Water on E-glass-Vinylester Composites*. Journal of Reinforced Plastics and Composites, 2006. 25(6): p. 631-644.

68. Fox, T.G. and S. Loshaek, *Influence of molecular weight and degree of crosslinking on the specific volume and glass temperature of polymers*. Journal of Polymer Science, 1955. 15(80): p. 371-390.
69. De'Neve, B. and M.E.R. Shanahan, *Water absorption by an epoxy resin and its effect on the mechanical properties and infra-red spectra*. Polymer, 1993. 34(24): p. 5099-5105.
70. Bai, Y.U. and T. Keller, *Time Dependence of Material Properties of FRP Composites in Fire*. Journal of Composite Materials, 2009. 43(21): p. 2469-2484.
71. Remiro, P.M., et al., *The effect of crosslinking and miscibility on the thermal degradation of an uncured and an amine-cured epoxy resin blended with poly (epsilon-caprolactone)*. Polymer Degradation and Stability, 2002. 78: p. 83-93.
72. Coats, A.W. and J.P. Redfern, *Kinetic parameters from thermogravimetric data*. nature 201:68, 1964.
73. Coats, A.W. and J.P. Redfern, *Kinetic parameters from thermogravimetric data. II*. Journal of Polymer Science Part B: Polymer Letters, 1965. 3(11): p. 917-920.
74. Lee, J.Y., M.J. Shim, and S.W. Kim, *Thermal decomposition kinetics of an epoxy resin with rubber-modified curing agent*. Journal of Applied Polymer Science, 2001. 81(2): p. 479-485.
75. Kissinger, H.E., *Reaction Kinetics in Differential Thermal Analysis*. Analytical Chemistry, 1957. 29(11): p. 1702-1706.
76. Collings, T.A. and S.M. Copley, *On the accelerated ageing of CFRP*. Composites, 1983. 14(3): p. 180-188.

77. Antoon, M.K. and J.L. Koenig, *The Structure and Moisture Stability of the Matrix Phase in Glass-Reinforced Epoxy Composites*. 1980. 19(1): p. 135 - 173.
78. Mijovic J, K.F.L., *The Effect of Hygrothermal Fatigue on Physical/Mechanical Properties and Morphology of Neat Epoxy Resin and Graphite/Epoxy Composite*. Journal of Applied Polymer Science, 1985. Vol.30, No.6: p. 2527-2549.
79. Fried, N., *Degradation of Composite Materials: The Effect of Water on Glass-Reinforced Plastics*. Proceedings of the Fifth Symposium on Naval Structural Mechanics, Philadelphia, 1967: p. 813-837.
80. Tsotsis, T.K. and S.M. Lee, *Long-Term Durability of Carbon and Glass-Epoxy Composite Materials in Wet Environments*. Journal of Reinforced Plastics and Composites, 1997. 16(17): p. 1609-1621.
81. Liao, K., Schultesiz, C. R., Hunston, D. L., Brinson, L. C, *Long-Term Durability of Fiber-Reinforced Polymer-Matrix Composite Materials for Infrastructure Applications: A Review*. Journal of Advanced materials, 1998. 30, No.4: p. 3-40.
82. Weitsman, Y.J., K. Anthony, and Z. Carl, *Effects of Fluids on Polymeric Composites--A Review*, in *Comprehensive Composite Materials*. 2000, Pergamon: Oxford. p. 369-401.
83. Marshall, J.M., G.P. Marshall, and R.F. Pinzelli, *The diffusion of liquids into resins and composites*. Polymer Composites, 1982. 3(3): p. 131-137.
84. Shen, C.-H. and G.S. Springer, *Moisture Absorption and Desorption of Composite Materials*. Journal of Composite Materials, 1976. 10(1): p. 2-20.

85. Mouritz, A.P., A. Kootsookos, and G. Mathys, *Stability of polyester- and vinyl ester-based composites in seawater*. Journal of Materials Science, 2004. 39(19): p. 6073-6077.
86. Bonniau, P. and A.R. Bunsell, *A Comparative Study of Water Absorption Theories Applied to Glass Epoxy Composites*. Journal of Composite Materials, 1981. 15(3): p. 272-293.
87. Joannie, W.C., N. Tinh, and A. Khaled, *Sorption and diffusion of water, salt water, and concrete pore solution in composite matrices*. Journal of Applied Polymer Science, 1999. 71(3): p. 483-492.
88. Prian, L. and A. Barkatt, *Degradation mechanism of fiber-reinforced plastics and its implications to prediction of long-term behavior*. Journal of Materials Science, 1999. 34(16): p. 3977-3989.
89. Apicella, A. and L. Nicolais, *Environmental aging of epoxy resins: synergistic effect of sorbed moisture, temperature, and applied stress*. Industrial & Engineering Chemistry Product Research and Development, 1981. 20(1): p. 138-144.
90. Tejraj, M.A., *Liquid diffusion into epoxy resin composites*. Journal of Applied Polymer Science, 1988. 35(5): p. 1251-1256.
91. Reliasoft(2000), *Reliasoft's Life Data Analysis Reference*. Reliasoft Publishing, Tucson, Arizona.
92. Ding, H.Z. and Z. Wang, *Time-temperature superposition method for predicting the permanence of paper by extrapolating accelerated ageing data to ambient conditions*. Cellulose, 2007. 14(3): p. 171-181.

93. A. Kuraishi, *Durability Analysis of Composite Structure Using the Accelerated Testing Methodology*. Ph.D dissertation, Stanford University, 2001.
94. Wang, J.Z.P., H. Chang, T. Iyengar, N. Dillard, D. A. and K.L. Reifsnider, *Physical aging behavior of high-performance composites*. Composites Science and Technology, 1995. 54(4): p. 405-415.
95. Nakada, M.M., Yasushi Kinoshita, Masaya Koga, Ryuju Okuya, Tsuguyuki and R. Muki, *Time-Temperature Dependence of Tensile Strength of Unidirectional CFRP*. Journal of Composite Materials, 2002. 36(22): p. 2567-2581.
96. Wisnom, M.R., *The Relationship between Tensile and Flexural Strength of Unidirectional Composites*. Journal of Composite Materials, 1992. 26(8): p. 1173-1180.
97. Whitney, J. and M. Knight, *The relationship between tensile strength and flexure strength in fiber-reinforced composites*. Experimental Mechanics, 1980. 20(6): p. 211-216.
98. Holmberg, J.A., *On Flexural and Tensile Strength for Composites Manufactured by RTM*. Journal of Reinforced Plastics and Composites, 1992. 11(11): p. 1302-1320.
99. Bullock, R.E., *Strength Ratios of Composite Materials in Flexure and in Tension*. Journal of Composite Materials, 1974. 8(2): p. 200-206.
100. Karbhari, V.M. and M.A. Abanilla, *Design factors, reliability, and durability prediction of wet layup carbon/epoxy used in external strengthening*. Composites Part B: Engineering, 2007. 38(1): p. 10-23.

101. He, X. and S.O. Oyadiji, *Application of coefficient of variation in reliability-based mechanical design and manufacture*. Journal of Materials Processing Technology, 2001. 119(1-3): p. 374-378.
102. J. Wu and D.D.L. Chung, *Increasing the electromagnetic interference shielding effectiveness of carbon fiber polymer–matrix composite by using activated carbon fibers*. Carbon, 2002. 40: p. 445-467.

PART B

DEVELOPMENT OF MOL LIMITS FOR FRP COMPOSITES

TABLE OF CONTENTS

Table of Contents.....	i
List of Symbols.....	vi
List of Figures.....	viii
List of Tables.....	xv
1. PROBLEM DEFINITION.....	1
1.1. Introduction.....	1
1.2. Synopsis of Research.....	2
2. LITERATURE REVIEW.....	4
2.1. INTRODUCTION.....	4
2.1.1. Marine Composites.....	5
2.1.2. Seawater Degradation.....	7
2.2. MOISTURE UPTAKE.....	8
2.2.1. Degradative Mechanisms.....	9
2.2.2. Diffusion.....	15
2.2.3. Coefficient of Diffusion.....	16
2.3. TENSION.....	19
2.3.1. Salt Water Immersion.....	20
2.3.2. Seawater Immersion.....	21
2.3.3. Seawater Cycling.....	22
2.3.4. Immersion in Seawater Under Pressure.....	23
2.4. SHORT BEAM SHEAR.....	24
2.4.1. Salt Water Immersion.....	25
2.4.2. Seawater Immersion.....	26
2.4.3. Immersion in Seawater and Salt Water Under Pressure.....	27
2.4.4. Long-term Studies in Seawater Aging Environments.....	28
2.5. SEAWATER EFFECT ON OTHER MECHANICAL PROPERTIES.....	28
2.5.1. Flexure.....	28
2.5.2. Fracture Toughness.....	29
2.5.3. Dynamic Mechanical Thermal Analysis.....	29
2.5.4. Fatigue.....	30
2.5.5. Fiber Pull-Out.....	30
2.6. CORRELATION BETWEEN DEGRADATION FROM ACTUAL MARINE ENVIRONMENTS AND LABORATORY TESTING.....	30
2.7. SUMMARY.....	32

3.	MATERIALS AND TEST METHODS.....	33
3.1.	INTRODUCTION.....	33
3.2.	MATERIAL SYSTEM DETAILS.....	33
3.3.	DETERMINATION OF FIBER LOADING.....	34
3.4.	ENVIRONMENTAL CONDITIONS.....	35
3.5.	TESTING PERIODS.....	37
3.6.	TEST METHODS.....	37
3.6.1.	Moisture Uptake.....	37
3.6.2.	Tension.....	38
3.6.3.	Flexure.....	39
3.6.4.	Short Beam Shear.....	40
3.6.5.	Dynamic Mechanical Thermal Analysis (DMTA).....	41
4.	MOISTURE.....	42
4.1.	INTRODUCTION.....	42
4.2.	RESULTS AND DISCUSSION.....	45
4.2.1.	Moisture Absorption Profiles.....	45
4.2.2.	Comparison of Continuous and Non-Continuous Uptake.....	49
4.2.3.	Coefficient of Diffusion.....	53
4.2.4.	Activation Energy.....	59
4.3.	SUMMARY.....	60
5.	TENSION.....	61
5.1.	INTRODUCTION.....	61
5.2.	RESULTS AND DISCUSSION.....	62
5.2.1.	Tensile Strength.....	62
5.2.2.	Tensile Modulus.....	76
5.2.3.	Failure Modes.....	88
5.3.	SUMMARY.....	92
6.	FLEXURE.....	94
6.1.	INTRODUCTION.....	94
6.2.	RESULTS AND DISCUSSION.....	96
6.2.1.	Flexural Strength.....	96
6.2.2.	Flexural Modulus.....	112
6.2.3.	Failure Modes.....	122
6.3.	SUMMARY.....	126
7.	SHORT BEAM SHEAR.....	127
7.1.	INTRODUCTION.....	127
7.2.	RESULTS AND DISCUSSION.....	128
7.2.1.	Short Beam Shear Strength.....	128
7.3.	COMPARISON OF MECHANICAL PROPERTIES.....	148
7.4.	SUMMARY.....	156

8.	DYNAMIC MECHANICAL THERMAL ANALYSIS.....	158
8.1.	INTRODUCTION.....	158
8.2.	RESULTS AND DISCUSSION.....	159
8.2.1.	Tan Delta.....	159
8.2.1.1.	Glass Transition Temperature.....	160
8.2.1.2.	Height of Tan Delta.....	173
8.2.1.3.	Area Between Curves.....	185
8.2.1.4.	Activation Energy.....	189
8.2.2.	Storage Modulus.....	199
8.2.2.1.	Glass Transition Temperature.....	200
8.2.2.2.	Verification of Flexural Modulus.....	200
8.2.2.3.	Rubber Plateau.....	204
8.2.2.4.	Intercrosslink Molecular Weight.....	208
8.2.3.	Loss Modulus.....	211
8.2.3.1.	Glass Transition Temperature.....	212
8.2.3.2.	Activation Energy.....	212
8.3.	SUMMARY.....	213
9.	MODELING AND LIFE PREDICTION.....	216
9.1.	INTRODUCTION.....	216
9.2.	ARRHENIUS RATE RELATIONSHIP.....	216
9.2.1.	Application to Data.....	218
9.3.	TIME-TEMPERATURE SUPERPOSITION.....	225
9.3.1.	Application to Data.....	227
9.4.	COMPARISON OF PREDICTIVE MODELS.....	232
9.5.	SUMMARY.....	236
10.	SUMMARY AND APPLICATION TO DESIGN.....	237
10.1.	DEVELOPMENT OF A BASIS FOR DESIGN.....	237
10.2.	MATERIAL OPERATIONAL LIMIT.....	239
10.3.	CONFIDENCE LEVEL.....	241
	APPENDIX.....	250
	REFERENCES.....	273

LIST OF SYMBOLS

D	Coefficient of Diffusion
h	Thickness of Specimen
M_{∞}	Moisture Weight Gain at Saturation
M_1	Percentage Weight Gain at Time t_1
M_2	Percentage Weight Gain at Time t_2
M_m	Moisture Content of Specimen
D_{∞}	Coefficient of Diffusion with One-Dimensional Correction Factor
l	Height of Specimen
b	Width of Specimen
T_g	Glass Transition Temperature
SBS	Short Beam Shear
RH	Relative Humidity
V_f	Fiber Volume Fraction
w_f	Weight of Fiber
ρ_f	Density of Fiber
ρ_m	Density of Matrix
w_c	Weight of Composite in Air
W_w	Weight of Composite in Wet State
W_d	Weight of Composite at Baseline
α	Probability Per Unit Time That a Free Water Molecule Becomes Bound
β	Probability Per Unit Time That a Bound Water Molecule Becomes Free
D_c	Value of the coefficient of diffusion in $\text{mm}^2/\text{second}$
t	Length of the Immersion in Hours
E_d	Diffusion Activation Energy
R	Universal Gas Constant
T	Temperature
F^{tu}	Ultimate Tensile Strength
P^{max}	Maximum Load at Failure
A	Average Cross Sectional Area
P_{dry}	property after drying
P_{wet}	property measured as a result of testing immediately after removing the specimen from conditions of exposure
P_o	initial baseline data determined at the outset
P_t	property at time t
P_0	property at time = 0
σ	Strength
E	Modulus
σ_f	Stress in the Outer Fibers at Midpoint
P	Load at a Given Point in the Load-Deflection Curve
l	Support Span
d	Depth of the Sample Tested
E_B	Modulus of Elasticity in Bending
m	Slope of the Tangent to the Initial Straight-Line Portion of the Load-Deflection Curve
F^{sbs}	Short Beam Shear Strength
P_m	Maximum Load Observed During the Test
$\tan\delta$	Tangent Delta

E''	Loss Modulus
E'	Storage Modulus
h_α	Height of Tan Delta
ΔE_a	Apparent Activation Energy Based on T_g
σ°	Sinusoidal Stress
ε°	Sinusoidal Strain
δ	Phase Angle
E_r'	Rubber Modulus
M_c	Intercrosslink Molecular Weight
ρ	Density
$R(T)$	Speed of the Reaction
A	Unknown Non-thermal Constant
K	Boltzman's constant
L	Quantifiable Measure of Life or the Material Property
B	Model Parameters
C	Model Parameters
T_o	Reference Temperature
f	Property Being Considered in the TTSP Model
T_1	Temperature Being Shifted in the TTSP Model
a_T	Shift Factor in the TTSP Model
T_{ref}	Reference Temperature in the TTSP Model
M.O.L.	Material Operational Limit
F.S.	Safety Factor.
\hat{A}	Maximum Likelihood Estimators
m	Maximum Likelihood Estimators
\bar{Y}	Mean Value of the Y Test Data
\bar{X}	Mean Value of the X Test Data.
n	Number of Points in the Data Set,
X_i	Value of the X Test Data at i
Y_i	Value of the Y Test Data at i .
R_i	Residuals
σ_y	Standard Deviation of the Residuals
$c_{1-\alpha,\gamma}$	c-Multiplier
σ_x	Standard Deviation of the Stress Data.
X^*	Confidence Level

LIST OF FIGURES

Figure 2.1. :	Typical Vinylester.....	7
Figure 2.2. :	Non-Fickian Diffusion Patterns.....	15
Figure 2.3. :	Correlation Between Natural and Accelerated Aging Studies.....	31
Figure 3.1. :	Unidirectional and Chopped Strand Mat E-Glass Fibers.....	34
Figure 3.2. :	Wet/Dry Cycle Set-up.....	36
Figure 3.3. :	Tension Test Set-up.....	39
Figure 3.4. :	Test set-up for 3-Point Bending.....	40
Figure 3.5. :	Test set-up for Short Beam Shear.....	40
Figure 3.6. :	Test Set-up for DMTA.....	41
Figure 4.1. :	Change in Moisture Uptake As a Function of Temperature and Time of Immersion-Continuous.....	46
Figure 4.2. :	Change in Moisture Uptake As a Function of Temperature and Time of Immersion-Non-Continuous.....	46
Figure 4.3. :	Change in Moisture Uptake As a Function of Time and Type of Cyclic Exposure-Continuous.....	48
Figure 4.4. :	Change in Moisture Uptake As a Function of Time and Type of Cyclic Exposure-Non-Continuous.....	48
Figure 4.5a. :	Change in Moisture Uptake After Immersion in 23°C Seawater as a Function of Immersion Time and Procedure.....	49
Figure 4.5b. :	Change in Moisture Uptake After Immersion in 40°C Seawater as a Function of Immersion Time and Procedure.....	50
Figure 4.5c. :	Change in Moisture Uptake After Immersion in 60°C Seawater as a Function of Immersion Time and Procedure.....	50
Figure 4.6a. :	Change in Moisture Uptake After Exposure to Freeze/Thaw Cycle as a Function of Time and Procedure.....	51
Figure 4.6b. :	Change in Moisture Uptake After Exposure to Wet/Dry Cycle as a Function of Time and Procedure.....	51
Figure 4.7. :	Fit for Coefficient of Diffusion After Immersion in 23°C Seawater As a Function of Procedure a) Continuous and b) Non-Continuous.....	54
Figure 4.8. :	Fit for Coefficient of Diffusion After Immersion in 40 °C Seawater As a Function of Procedure a) Continuous and b) Non-Continuous.....	55
Figure 4.9. :	Fit for Coefficient of Diffusion After Immersion in 60 °C Seawater As a Function of Procedure a) Continuous and b) Non-Continuous.....	56
Figure 4.10. :	Fit for Coefficient of Diffusion After Wet/Dry Cyclic Exposure As a Function of Procedure a) Continuous and b) Non-Continuous.....	57
Figure 5.1. :	Change in Tensile Strength as a Function of Temperature and Time of Immersion in Seawater.....	66

Figure 5.2. :	SEM Micrograph Showing Damage at 4 weeks in 40°C Seawater.....	67
Figure 5.3. :	SEM Micrograph Showing Damage at 4 weeks in 60°C Seawater.....	68
Figure 5.4. :	Change in Tensile Strength as a Function of Time and Type of Cyclic Exposure.....	70
Figure 5.5a. :	Effect of Redrying on Tensile Strength Retention after Immersion 23°C in Seawater.....	72
Figure 5.5b. :	Effect of Redrying on Tensile Strength Retention after Immersion 40°C in Seawater.....	73
Figure 5.5c. :	Effect of Redrying on Tensile Strength Retention after Immersion 60°C in Seawater.....	73
Figure 5.5d. :	Effect of Redrying on Tensile Strength Retention after Immersion -10°C in Seawater.....	74
Figure 5.6a. :	Effect of Redrying on Tensile Strength After Exposure to Freeze/Thaw Condition.....	74
Figure 5.6b. :	Effect of Redrying on Tensile Strength After Exposure to Wet/Dry Condition.....	75
Figure 5.7. :	Relationship Between Moisture Content and Tensile Strength Retention for Specimens Immersed in 23°C, 40°C, and 60°C Seawater.....	76
Figure 5.8. :	Change in Tensile Modulus as a Function of Temperature and Time of Immersion in Seawater.....	79
Figure 5.9. :	SEM Micrograph Demonstrating Degree of Fiber/Matrix Debonding After Exposure to 60°C Seawater for 78 weeks.....	81
Figure 5.10. :	Change in Tensile Modulus as a Function of Time and Type of Cyclic Exposure.....	83
Figure 5.11a. :	Effect of Redrying on Tensile Modulus Retention after Immersion in 23°C Seawater.....	85
Figure 5.11b. :	Effect of Redrying on Tensile Modulus Retention after Immersion in 40°C Seawater.....	86
Figure 5.11c. :	Effect of Redrying on Tensile Modulus Retention after Immersion in 60°C Seawater.....	86
Figure 5.11d. :	Effect of Redrying on Tensile Modulus Retention after Immersion in -10°C Seawater.....	87
Figure 5.12a. :	Effect of Redrying on Tensile Modulus After Exposure to Freeze/Thaw Exposure.....	87
Figure 5.12b. :	Effect of Redrying on Tensile Modulus After Exposure to Wet/Dry Cycling.....	88
Figure 5.13. :	Failed Tension Specimens Immersed in 23°C, 40°C, and 60°C after 78 weeks.....	89
Figure 5.14. :	Failed Tension Specimens Immersed in 40°C Seawater for 4, 35, 52, and 78 weeks.....	90
Figure 5.15. :	Typical Failed Tension Specimens, Unexposed.....	91
Figure 5.16. :	Failed Tension Specimens Subjected to Freeze/Thaw and Wet/Dry Cycling after 72 weeks.....	92
Figure 6.1. :	Change in Flexural Strength as a Function of Temperature and Time of Immersion in Seawater.....	99

Figure 6.2. :	SEM Micrograph of E-glass/vinylester in As-Received State.....	101
Figure 6.3. :	SEM Micrograph of E-glass/vinylester After Exposure to 40°C Seawater for 4 weeks.....	101
Figure 6.4. :	SEM Micrograph of E-glass/vinylester After Exposure to 60°C Seawater for 4 weeks.....	102
Figure 6.6. :	SEM Micrograph of E-glass/vinylester After Exposure to Freeze/Thaw Cycle for 72 weeks.....	105
Figure 6.7. :	SEM Micrograph of E-glass/Vinylester After Exposure to Wet/Dry Cycle for 72 weeks.....	106
Figure 6.8a. :	Effect of Redrying on Flexural Strength Retention after Immersion at 23°C in Seawater.....	108
Figure 6.8b. :	Effect of Redrying on Flexural Strength Retention after Immersion at 40°C in Seawater.....	109
Figure 6.8c. :	Effect of Redrying on Flexural Strength Retention after Immersion at 60°C in Seawater.....	109
Figure 6.8d. :	Effect of Redrying on Flexural Strength Retention after Immersion at -10°C in Seawater.....	110
Figure 6.9a. :	Effect of Redrying on Flexural Strength After Exposure to Freeze/Thaw Condition.....	110
Figure 6.9b. :	Effect of Redrying on Flexural Strength After Exposure to Wet/Dry Condition.....	111
Figure 6.10. :	Relationship Between Moisture Content and Flexural Strength Retention for Specimens Immersed in 23°C, 40°C, and 60°C Seawater.....	112
Figure 6.11. :	Change in Flexural Modulus as a Function of Temperature and Time of Immersion in Seawater.....	115
Figure 6.12. :	Change in Flexural Modulus as a Function of Time and Type of Cyclic Exposure.....	117
Figure 6.13a. :	Effect of Redrying on Flexural Modulus Retention after Immersion in 23°C Seawater.....	119
Figure 6.13b. :	Effect of Redrying on Flexural Modulus Retention after Immersion in 40°C Seawater.....	120
Figure 6.13c. :	Effect of Redrying on Flexural Modulus Retention after Immersion in 60°C Seawater.....	120
Figure 6.13d. :	Effect of Redrying on Flexural Modulus Retention after Immersion in -10°C Seawater.....	120
Figure 6.14a. :	Effect of Redrying on Flexural Modulus After Exposure to Freeze/Thaw Cycling.....	121
Figure 6.14b. :	Effect of Redrying on Flexural Modulus After Exposure to Wet/Dry Cycling.....	121
Figure 6.15. :	Bottom Surfaces of Failed 3-Point Bending Specimens For Different Conditions.....	123
Figure 6.16. :	Bottom Surfaces of Failed Three-Point Bending Specimens Immersed in 60°C Seawater.....	125
Figure 7.1. :	Change in SBS Strength as a Function of Temperature and Time of Immersion in Seawater.....	132
Figure 7.2. :	Optical Micrograph Showing Coalescence of Debonds Present at Chopped Strand Mat Layers (100X Magnification) After Immersion in Seawater at 23°C For 78 Weeks.....	133

Figure 7.3. :	Optical Micrograph Showing Cracks Resulting from Immersion in 23°C Seawater after 4 weeks (100X Magnification).....	134
Figure 7.4. :	Optical Micrograph Revealing Coalescence of Debonds After Exposure to 40°C Seawater For 4 Weeks (100X Magnification).....	135
Figure 7.5. :	Optical Micrograph Showing Development of Cracks at 78 weeks in 40°C Seawater (100X Magnification).....	136
Figure 7.6. :	Optical Micrograph Showing Substantial Losses in ILSS Validated by Presence of Large Width Cracks after 60°C Seawater Immersion for 52 Weeks (100X Magnification).....	137
Figure 7.7. :	Optical Micrograph Showing Large Amounts of Cracking and Debonding for E-glass/Vinylester After Immersion in 60°C Seawater Immersion for 52 Weeks (100X Magnification).....	138
Figure 7.8. :	Change in SBS Strength as a Function of Time and Type of Cyclic Exposure.....	140
Figure 7.9. :	Optical Micrograph Showing Sites for Wicking After Exposure to Wet/Dry Cycles At 72 Weeks (100X Magnification).....	141
Figure 7.10. :	Optical Micrograph Showing Microcracking Characterized by Connection of Crescent Shaped Debonds at 72 Weeks in the Wet/Dry Cycle (500X Magnification).....	142
Figure 7.11a. :	Effect of Redrying on SBS Strength Retention after Immersion at 23°C in Seawater.....	144
Figure 7.11b. :	Effect of Redrying on SBS Strength Retention after Immersion at 40°C in Seawater.....	144
Figure 7.11c. :	Effect of Redrying on SBS Strength Retention after Immersion at 60°C in Seawater.....	145
Figure 7.11d. :	Effect of Redrying on SBS Strength Retention after Immersion at -10°C in Seawater.....	145
Figure 7.12a. :	Effect of Redrying on SBS Strength After Exposure to Freeze/Thaw Condition.....	146
Figure 7.12b. :	Effect of Redrying on SBS Strength After Exposure to Wet/Dry Condition.....	146
Figure 7.13. :	Relationship Between Moisture Content and SBS Strength Retention for Specimens Immersed in 23°C, 40°C, and 60°C Seawater.....	147
Figure 7.14. :	Relationship Between Moisture Content and Interlaminar Shear Strength Retention for Specimens Exposed to Cycling Conditions.....	148
Figure 7.15. :	Comparison of Strength Retention Properties in 23°C Seawater.....	149
Figure 7.16. :	Comparison of Strength Retention Properties in 40°C Seawater.....	149
Figure 7.17. :	Comparison of Strength Retention Properties in 60°C Seawater.....	150
Figure 7.18. :	Comparison of Strength Retention Properties in -10°C Seawater.....	151
Figure 7.19. :	Comparison of Strength Retention Properties in Freeze/Thaw Cycle Exposure.....	151
Figure 7.20. :	Comparison of Strength Retention Properties in Wet/Dry Cycle Exposure.....	152
Figure 7.21. :	Comparison of Modulus Retention Properties in 23°C Seawater.....	153

Figure 7.22. :	Comparison of Modulus Retention Properties in 40 °C Seawater.....	154
Figure 7.23. :	Comparison of Modulus Retention Properties in 60 °C Seawater.....	154
Figure 7.24. :	Comparison of Modulus Retention Properties in -10°C Seawater.....	155
Figure 7.25. :	Comparison of Modulus Retention Properties in Freeze/Thaw Cycle Exposure.....	155
Figure 7.26. :	Comparison of Modulus Retention Properties in Wet/Dry Cycle Exposure.....	156
Figure 8.1. :	Change in T_g at 1 Hz Based on Tan Delta as a Function of Temperature and Time of Immersion in Seawater.....	166
Figure 8.2a. :	Effect of Redrying on T_g at 1 Hz Based on Tan Delta After Immersion in 23°Seawater.....	166
Figure 8.2b. :	Effect of Redrying on T_g at 1 Hz Based on Tan Delta After Immersion in 40°Seawater.....	167
Figure 8.2c. :	Effect of Redrying on T_g at 1 Hz Based on Tan Delta After Immersion in 60°Seawater.....	167
Figure 8.2d. :	Effect of Redrying on T_g at 1 Hz Based on Tan Delta After Immersion in -10°Seawater.....	168
Figure 8.3. :	Change in T_g at 1 Hz Based on Tan Delta As a Function of Time and Type of Cyclic Exposure.....	172
Figure 8.4a. :	Effect of Redrying on T_g at 1 Hz Based on Tan Delta as a Function of Freeze/Thaw Exposure.....	172
Figure 8.4b. :	Effect of Redrying on T_g at 1 Hz Based on Tan Delta as a Function of Wet/Dry Exposure.....	173
Figure 8.5. :	Change in Height of Tan Delta at 1 Hz as a Function of Temperature and Time of Immersion in Seawater.....	179
Figure 8.7a. :	Effect of Redrying on Height of Tan Delta after Immersion in 23°C Seawater.....	179
Figure 8.7b. :	Effect of Redrying on Height of Tan Delta after Immersion in 40°C Seawater.....	180
Figure 8.7c. :	Effect of Redrying on Height of Tan Delta after Immersion in 60°C Seawater.....	180
Figure 8.7d. :	Effect of Redrying on Height of Tan Delta after Immersion in -10°C Seawater.....	181
Figure 8.8.	Change in Height of Tan Delta at 1 Hz As a Function of Time and Type of Cyclic Exposure.....	184
Figure 8.9a. :	Effect of Redrying on Height of Tan Delta as a Function of Freeze/Thaw Exposure.....	184
Figure 8.9b. :	Effect of Redrying on Height of Tan Delta as a Function of Wet/Dry Exposure.....	185
Figure 8.10a. :	Change in Area Between Tan Delta Curves at 1 Hz as a Function of Temperature of Immersion in Seawater and Period of Exposure.....	186
Figure 8.10b. :	Change in Area Between Tan Delta Curves at 1 Hz as a Function of Cyclic Exposure and Period of Exposure.....	189
Figure 8.11. :	Change in Activation Energy Based on Tan Delta as a Function of Temperature and Time of Immersion in Seawater.....	193

Figure 8.12a. :	Effect of Redrying on Activation Energy Based on Tan Delta After Immersion in 23°C Seawater.....	194
Figure 8.12b. :	Effect of Redrying on Activation Energy Based on Tan Delta After Immersion in 40°C Seawater.....	194
Figure 8.12c. :	Effect of Redrying on Activation Energy Based on Tan Delta After Immersion in 60°C Seawater.....	195
Figure 8.12d. :	Effect of Redrying on Activation Energy Based on Tan Delta After Immersion in -10°C Seawater.....	195
Figure 8.13. :	Change in Activation Energy Based on Tan Delta As a Function of Time and Type of Cyclic Exposure.....	198
Figure 8.14a. :	Effect of Redrying on Activation Energy Based on Tan Delta as a Function of Freeze/Thaw Exposure.....	198
Figure 8.14b. :	Effect of Redrying on Activation Energy Based on Tan Delta as a Function of Wet/Dry Exposure.....	199
Figure 8.15. :	Comparison Between Calculated Flexural Modulus Based on DMTA Parameters and Experimental Data For Immersion in 23°C Seawater.....	202
Figure 8.16. :	Comparison Between Calculated Flexural Modulus Based on DMTA Parameters and Experimental Data For Immersion in 40°C Seawater.....	203
Figure 8.17. :	Comparison Between Calculated Flexural Modulus Based on DMTA Parameters and Experimental Data For Immersion in 60°C Seawater.....	203
Figure 8.18. :	Change in Rubbery Modulus as a Function of Temperature and Time of Immersion in Seawater.....	206
Figure 8.19. :	Change in Rubbery Modulus as a Function of Time and Type of Cyclic Exposure.....	207
Figure 8.20. :	Change in Intercrosslink Molecular Weight As a Function of Temperature and Time of Immersion in Seawater.....	209
Figure 8.21. :	Change in Intercrosslink Molecular Weight As a Function of Time and Type of Cyclic Exposure.....	211
Figure 9.1. :	Tensile Strength Retention vs. Time.....	219
Figure 9.2. :	Tensile Strength Retention vs. ln (Time in Days).....	220
Figure 9.3. :	Tensile Strength Retention vs. Inverse Temperature.....	221
Figure 9.4. :	Determination of Correction Factor for Arrhenius Rate Relationship.....	223
Figure 9.5. :	Comparison of Predicted and Experimental Values of Tensile Strength Retention Based on Arrhenius Rate Relationship.....	224
Figure 9.6. :	Predicted Strength Values Using Arrhenius Rate Relationship.....	225
Figure 9.7. :	Predicted Modulus Values Using Arrhenius Rate Relationship.....	225
Figure 9.8. :	Plot of Log Strength versus Log Time.....	228
Figure 9.9. :	Shifted Curves to Generate Master Curve for Time-Temperature Superposition.....	228
Figure 9.10. :	Master Curve for Time-Temperature Superposition.....	229

Figure 9.11. :	Power Curve Fit to Log of Strength Profile for Time-Temperature Superposition.....	229
Figure 9.12. :	Comparison of Predicted and Experimental Values of Tensile Strength Retention Based on the Time-Temperature Superposition.....	230
Figure 9.13. :	Strength Prediction Values Based on Time-Temperature Superposition...	231
Figure 9.14. :	Modulus Prediction Values Based on Time-Temperature Superposition...	232
Figure 9.15. :	Comparison Between Prediction Results of Tensile Strength Retention for Time-Temperature Superposition and Arrhenius Rate Relationship....	233
Figure 9.16. :	Comparison Between Prediction Results of Flexural Strength Retention for Time-Temperature Superposition and Arrhenius Rate Relationship....	234
Figure 9.17. :	Comparison Between Prediction Results of SBS strength Retention for Time-Temperature Superposition and Arrhenius Rate Relationship.....	234
Figure 9.18. :	Comparison Between Prediction Results of Tensile Modulus Retention for Time-Temperature Superposition and Arrhenius Rate Relationship....	235
Figure 9.19. :	Comparison Between Prediction Results of Flexural Modulus Retention for Time-Temperature Superposition and Arrhenius Rate Relationship....	236
Figure 10.1. :	Log-Linear Fit of Strength-Life Data.....	242
Figure 10.2. :	Distribution of Residuals.....	244
Figure 10.3. :	Inverse Normal Distribution of the Data.....	244

LIST OF TABLES

Table 2.1. :	Types of Glass Fibers.....	6
Table 2.2. :	Composition of Seawater.....	8
Table 2.3. :	Moisture Studies in Salt Water and Seawater.....	13
Table 2.4. :	Table of Coefficient of Diffusion in Various Marine Environments.....	18
Table 3.1. :	Typical Properties of Vinyl ester Resin.....	34
Table 4.1. :	Maximum Weight Gain Determined For Continuous and Non-Continuous Monitoring.....	52
Table 4.2a. :	Coefficient of Diffusion Based on Fickian and Langmuir Diffusion Models Determined By Continuous Monitoring Procedure.....	58
Table 4.2b. :	Coefficient of Diffusion Based on Fickian and Langmuir Diffusion Models Determined By Non-Continuous Monitoring Procedure.....	58
Table 5.1a. :	Tensile Strength Determined At Ambient Conditions of 23°C and 30%RH.....	63
Table 5.1b. :	Tensile Strength Determined After Immersion in 23°C Seawater (“Wet” Testing) and as a Result of Subsequent Drying (“Dry Testing”).....	64
Table 5.1c. :	Tensile Strength Determined After Immersion in 40°C Seawater (“Wet” Testing) and as a Result of Subsequent Drying (“Dry Testing”).....	64
Table 5.1d. :	Tensile Strength Determined After Immersion in 60°C Seawater (“Wet” Testing) and as a Result of Subsequent Drying (“Dry Testing”).....	65
Table 5.1e. :	Tensile Strength Determined After Immersion in -10°C Seawater (“Wet” Testing) and as a Result of Subsequent Drying (“Dry Testing”).....	65
Table 5.2a. :	Tensile Strength Determined After Exposure to Freeze/Thaw Cyclic Exposure (“Wet” Testing) and as a Result of Subsequent Drying (“Dry Testing”).....	69
Table 5.2b. :	Tensile Strength Determined After Exposure to Wet/Dry Cyclic Exposure (“Wet” Testing) and as a Result of Subsequent Drying (“Dry Testing”).....	69
Table 5.3a. :	Effect of Redrying for Tensile Strength After Immersion In Seawater.....	71
Table 5.3b. :	Effect of Redrying for Tensile Strength After Exposure to Freezing Conditions.....	71
Table 5.3c. :	Effect of Redrying for Tensile Strength After Exposure to Cyclic Conditions.....	72
Table 5.4a. :	Tensile Modulus Determined At Ambient Conditions of 23°C and 30%RH.....	77
Table 5.4b. :	Tensile Modulus Determined After Immersion in 23°C Seawater (“Wet” Testing) and as a Result of Subsequent Drying (“Dry Testing”).....	77
Table 5.4c. :	Tensile Modulus Determined After Immersion in 40°C Seawater (“Wet” Testing) and as a Result of Subsequent Drying (“Dry Testing”).....	78
Table 5.4d. :	Tensile Modulus Determined After Immersion in 60°C Seawater (“Wet” Testing) and as a Result of Subsequent Drying (“Dry Testing”).....	78

Table 5.4e. :	Tensile Modulus Determined After Immersion in -10°C Seawater (“Wet” Testing) and as a Result of Subsequent Drying (“Dry Testing”)...	79
Table 5.5a. :	Tensile Modulus Determined After Exposure to Freeze/Thaw Cycle (“Wet” Testing) and as a Result of Subsequent Drying (“Dry Testing”)...	82
Table 5.5b. :	Tensile Modulus Determined After Exposure to Wet/Dry Cycle (“Wet” Testing) and as a Result of Subsequent Drying (“Dry Testing”).....	82
Table 5.6a. :	Effect of Redrying for Tensile Modulus After Immersion In Seawater....	84
Table 5.6b. :	Effect of Redrying for Tensile Modulus After Exposure to Freezing Conditions.....	84
Table 5.6c. :	Effect of Redrying for Tensile Modulus After Exposure to Cycling Conditions.....	85
Table 6.1a. :	Flexural Strength Determined At Ambient Conditions of 23°C and 30%RH.....	97
Table 6.1b. :	Flexural Strength Determined After Immersion in 23°C Seawater (“Wet” Testing) and as a Result of Subsequent Drying (“Dry Testing”).....	97
Table 6.1c. :	Flexural Strength Determined After Immersion in 40°C Seawater (“Wet” Testing) and as a Result of Subsequent Drying (“Dry Testing”).....	98
Table 6.1d. :	Flexural Strength Determined After Immersion in 60°C Seawater (“Wet” Testing) and as a Result of Subsequent Drying (“Dry Testing”).....	98
Table 6.1e. :	Flexural Strength Determined After Immersion in -10°C Seawater (“Wet” Testing) and as a Result of Subsequent Drying (“Dry Testing”)...	99
Table 6.2a. :	Flexural Strength Determined After Exposure to Freeze/Thaw Cycling (“Wet” Testing) and as a Result of Subsequent Drying (“Dry Testing”)...	103
Table 6.2b. :	Flexural Strength Determined After Exposure to Wet/Dry Cycling (“Wet” Testing) and as a Result of Subsequent Drying (“Dry Testing”)...	104
Table 6.3a. :	Effect of Redrying for Flexural Strength After Immersion In Seawater...	107
Table 6.3b. :	Effect of Redrying for Flexural Strength After Exposure to Freezing Conditions.....	107
Table 6.3c. :	Effect of Redrying for Flexural Strength After Exposure to Cyclic Conditions.....	108
Table 6.4a. :	Flexural Modulus Determined At Ambient Conditions of 23°C and 30%RH.....	112
Table 6.4b. :	Flexural Modulus Determined After Immersion in 23°C Seawater (“Wet” Testing) and as a Result of Subsequent Drying (“Dry Testing”)...	113
Table 6.4c. :	Flexural Modulus Determined After Immersion in 40°C Seawater (“Wet” Testing) and as a Result of Subsequent Drying (“Dry Testing”)...	113
Table 6.4d. :	Flexural Modulus Determined After Immersion in 60°C Seawater (“Wet” Testing) and as a Result of Subsequent Drying (“Dry Testing”)...	114
Table 6.4e. :	Flexural Modulus Determined After Immersion in -10°C Seawater (“Wet” Testing) and as a Result of Subsequent Drying (“Dry Testing”)...	114
Table 6.5a. :	Flexural Modulus Determined After Exposure to Freeze/Thaw Cycle (“Wet” Testing) and as a Result of Subsequent Drying (“Dry Testing”)...	116
Table 6.5b. :	Flexural Modulus Determined After Exposure to Wet/Dry Cycle (“Wet” Testing) and as a Result of Subsequent Drying (“Dry Testing”).....	116
Table 6.6a. :	Effect of Redrying for Flexural Modulus After Immersion In Seawater...	117

Table 6.6b. :	Effect of Redrying for Flexural Modulus After Exposure to Freezing Conditions.....	118
Table 6.6c. :	Effect of Redrying for Flexural Modulus After Exposure to Cycling Conditions.....	118
Table 7.1a. :	SBS Strength Determined At Ambient Conditions of 23°C and 30%RH..	129
Table 7.1b. :	SBS Strength Determined After Immersion in 23°C Seawater (“Wet” Testing) and as a Result of Subsequent Drying (“Dry Testing”).....	130
Table 7.1c. :	SBS Strength Determined After Immersion in 40°C Seawater (“Wet” Testing) and as a Result of Subsequent Drying (“Dry Testing”).....	130
Table 7.1d. :	SBS Strength Determined After Immersion in 60°C Seawater (“Wet” Testing) and as a Result of Subsequent Drying (“Dry Testing”).....	131
Table 7.1e. :	SBS Strength Determined After Immersion in -10°C Seawater (“Wet” Testing) and as a Result of Subsequent Drying (“Dry Testing”).....	131
Table 7.2a. :	SBS Strength Determined After Exposure to Freeze/Thaw Cycling (“Wet” Testing) and as a Result of Subsequent Drying (“Dry Testing”)...	139
Table 7.2b. :	SBS Strength Determined After Exposure to Wet/Dry Cycling (“Wet” Testing) and as a Result of Subsequent Drying (“Dry Testing”).....	139
Table 7.3a:	Effect of Redrying for SBS Strength After Immersion In Seawater.....	142
Table 7.3b. :	Effect of Redrying for SBS Strength After Exposure to Freezing Conditions.....	143
Table 7.3c. :	Effect of Redrying for SBS Strength After Exposure to Cyclic Conditions.....	143
Table 8.1a. :	T _g Based on Tan Delta for Ambient Condition at 23°C and 30% RH.....	161
Table 8.1b. :	T _g Based on Tan Delta Determined After Immersion in 23°C Seawater (“Wet Testing”) and as a Result of Subsequent Redrying (“Dry Testing”)	162
Table 8.1c. :	T _g Based on Tan Delta Determined After Immersion in 40°C Seawater (“Wet Testing”) and as a Result of Subsequent Redrying (“Dry Testing”)	163
Table 8.1d. :	T _g Based on Tan Delta Determined After Immersion in 60°C Seawater (“Wet Testing”) and as a Result of Subsequent Redrying (“Dry Testing”)	164
Table 8.1e. :	T _g Based on Tan Delta Determined After Immersion in -10°C Seawater (“Wet Testing”) and as a Result of Subsequent Redrying (“Dry Testing”)	165
Table 8.2a. :	T _g Based on Tan Delta Determined as a Function of Time During Freeze/Thaw Exposure.....	170
Table 8.2b. :	T _g Based on Tan Delta Determined as a Function of Time During Wet/Dry Exposure.....	171
Table 8.3a. :	Height of Tan Delta for Ambient Condition at 23°C and 30%RH - Values are Unitless.....	174
Table 8.3b. :	Height of Tan Delta Determined After Immersion in 23°C Seawater (“Wet Testing”) and as a Result of Subsequent Redrying (“Dry Testing”) – Values are Unitless.....	175
Table 8.3c. :	Height of Tan Delta Determined After Immersion in 40°C Seawater (“Wet Testing”) and as a Result of Subsequent Redrying (“Dry Testing”) – Values are Unitless.....	176
Table 8.3d. :	Height of Tan Delta Determined After Immersion in 60°C Seawater (“Wet Testing”) and as a Result of Subsequent Redrying (“Dry Testing”) – Values are Unitless.....	177

Table 8.3e. :	Height of Tan Delta Determined After Immersion in -10°C Seawater (“Wet Testing”) and as a Result of Subsequent Redrying (“Dry Testing”) – Values are Unitless.....	178
Table 8.4a. :	Height of Tan Delta Determined as a Function of Time and Freeze/Thaw Exposure – Values are Unitless.....	182
Table 8.4b. :	Height of Tan Delta Determined as a Function of Time and Wet/Dry Exposure – Values are Unitless.....	183
Table 8.5a. :	Area Between Tan Delta Curves at 1 Hz (Exposed Sample Compared to As-Received Sample) Determined as a Function of Temperature of Immersion in Seawater and Period of Exposure.....	186
Table 8.5b. :	Area Between Tan Delta Curves at 1 Hz (Exposed Sample Compared to As-Received Sample) Determined as a Function of Type of Cyclic Exposure and Period of Exposure.....	188
Table 8.6a. :	Activation Energy Based on Tan Delta Determined After Exposure to Ambient Conditions at 23°C and 30% RH.....	191
Table 8.6b. :	Activation Energy Based on Tan Delta Determined After Immersion in 23°C Seawater (“Wet Testing”) and as a Result of Subsequent Redrying (“Dry Testing”).....	191
Table 8.6c. :	Activation Energy Based on Tan Delta Determined After Immersion in 40°C Seawater (“Wet Testing”) and as a Result of Subsequent Redrying (“Dry Testing”).....	192
Table 8.16d. :	Activation Energy Based on Tan Delta Determined After Immersion in 60°C Seawater (“Wet Testing”) and as a Result of Subsequent Redrying (“Dry Testing”).....	192
Table 8.16e. :	Activation Energy Based on Tan Delta Determined After Immersion in -10°C Seawater (“Wet Testing”) and as a Result of Subsequent Redrying (“Dry Testing”).....	193
Table 8.17a. :	Activation Energy Based on Tan Delta Determined as a Function of Freeze/Thaw Exposure.....	197
Table 8.17b. :	Activation Energy Based on Tan Delta Determined as a Function of Wet/Dry Exposure.....	197
Table 8.18. :	Comparison of Flexural Modulus Calculated From DMTA and Experimental Data.....	201
Table 8.19. :	Percent Difference Between Flexural Modulus Calculated From DMTA and Experimental Data.....	202
Table 8.20a. :	Rubbery Modulus at $T_g + 50^\circ\text{C}$ At Ambient Conditions, 23°C and 30%RH.....	204
Table 8.20b. :	Rubbery Modulus at $T_g + 50^\circ\text{C}$ After Immersion in Seawater.....	205
Table 8.20c. :	Rubbery Modulus at $T_g + 50^\circ\text{C}$ After Exposure to -10°C Seawater.....	205
Table 8.21. :	Rubbery Modulus at $T_g + 50^\circ\text{C}$ Determined as a Function of Type and Period of Cyclic Exposure.....	207
Table 8.22. :	Intercrosslink Molecular Weight Determined After Immersion in Seawater as a Function of Temperature.....	209
Table 8.21. :	Intercrosslink Molecular Weight Determined as a Function of Time and Type of Cyclic Exposure.....	210
Table 9.1. :	Tensile Strength Retention as a Function of Time (in months).....	218

Table 9.2. :	Linear Relationships Between Tensile Strength and Time.....	220
Table 9.3. :	Least Square Fit Between Strength and Inverse Temperature.....	221
Table 9.4. :	Predicted Values of Strength Retention Based on Arrhenius Rate Relationship.....	222
Table 9.5. :	Values of Predicted Strength Retention Based on Modified Arrhenius Rate Relationship[%].....	223
Table 9.6. :	Retention [%] Values For Mechanical Properties Based on Modified Arrhenius Rate Relationship.....	224
Table 9.7. :	Tensile Strength Values As a Result of Immersion in Seawater.....	227
Table 9.8. :	Comparison of Predicted Values from Time-Temperature Superposition and Experimentally Obtained Values.....	230
Table 9.9. :	Additional Mechanical Property Predictions Based on Time-Temperature Superposition.....	231
Table 10.1. :	Characteristics that Reached M.O.L.....	240
Table 10.2. :	M.O.L. Based on Predictive Models, Differing Values Based on TTSP are in Brackets.....	241
Table 10.3. :	Maximum Likelihood Estimators and Standard Deviation of the Residuals.....	245
Table 10.4. :	One-Sided Tolerance Limit.....	246
Table 10.5. :	Confidence Level Multipliers.....	246
Table 10.6. :	Confidence Levels Based on Predicted Service Life Using Time-Temperature Superposition After Exposure to 23°C Seawater For 20 Years.....	247
Table 10.7. :	Confidence Levels Based on Predicted Service Life Using Time-Temperature Superposition After Exposure to 23°C Seawater For 20 Years.....	247
Table A.4.1. :	Average Weight Gain for 23°C Immersion.....	250
Table A.4.2. :	Average Weight Gain for 40°C Immersion.....	251
Table A.4.3. :	Average Weight Gain for 60°C Immersion.....	252
Table A.4.4. :	Average Weight Gain for Freeze/Thaw Cycling.....	253
Table A.4.5. :	Average Weight Gain for Wet/Dry Cycling.....	254
Table A.8.1a. :	T _g Based on Storage Modulus for Ambient Condition at 23°C and 30%RH.....	255
Table A.8.1b.:	T _g Based on Storage Modulus Determined After Immersion in 23°C Seawater (“Wet Testing”) and as a Result of Subsequent Redrying (“Dry Testing”).....	256

Table A.8.1c. :	T _g Based on Storage Modulus Determined After Immersion in 40°C Seawater (“Wet Testing”) and as a Result of Subsequent Redrying (“Dry Testing”).....	257
Table A.8.1d.:	T _g Based on Storage Modulus Determined After Immersion in 60°C Seawater (“Wet Testing”) and as a Result of Subsequent Redrying (“Dry Testing”).....	258
Table A.8.1e. :	T _g Based on Storage Modulus Determined After Immersion in -10°C Seawater (“Wet Testing”) and as a Result of Subsequent Redrying (“Dry Testing”).....	259
Table A.8.2a. :	T _g Based on Storage Modulus Determined as a Function of Cyclic Exposure.....	260
Table A.8.2b.:	T _g Based on Storage Modulus Determined as a Function of Wet/Dry Exposure.....	261
Table A.8.3a. :	T _g Based on Loss Modulus for Ambient Condition at 23°C and 30% RH..	262
Table A.8.3b.:	T _g Based on Loss Modulus Determined After Immersion in 23°C Seawater (“Wet Testing”) and as a Result of Subsequent Redrying (“Dry Testing”).....	263
Table A.8.3c. :	T _g Based on Loss Modulus Determined After Immersion in 40°C Seawater (“Wet Testing”) and as a Result of Subsequent Redrying (“Dry Testing”).....	264
Table A.8.3d.:	T _g Based on Loss Modulus Determined After Immersion in 60°C Seawater (“Wet Testing”) and as a Result of Subsequent Redrying (“Dry Testing”).....	265
Table A.8.3e. :	T _g Based on Loss Modulus Determined After Immersion in -10°C Seawater (“Wet Testing”) and as a Result of Subsequent Redrying (“Dry Testing”).....	266
Table A.8.4a. :	T _g Based on Loss Modulus Determined as a Function of Cyclic Exposure.....	267
Table A.8.4b.:	T _g Based on Loss Modulus Determined as a Function of Cyclic Exposure.....	268
Table A.8.5a. :	Activation Energy Based on Loss Modulus for Seawater Immersion.....	269
Table A.8.5b.:	Activation Energy Based on Loss Modulus for Seawater Immersion.....	269
Table A.8.5c. :	Activation Energy Based on Loss Modulus for Seawater Immersion.....	270
Table A.8.5d.:	Activation Energy Based on Loss Modulus for Seawater Immersion.....	270
Table A.8.5e. :	Activation Energy Based on Loss Modulus for Seawater Immersion.....	271
Table A.8.6a. :	Activation Energy Based on Loss Modulus After Exposure to Freeze/Thaw Cycling.....	271
Table A.8.6b.:	Activation Energy Modulus After Exposure to Wet/Dry Cycling Based on Loss.....	272

CHAPTER 1 – PROBLEM DEFINITION

1.1. INTRODUCTION

Commercial interest in the use of E-glass reinforced polymer composites is increasing in both civil and offshore applications due to the inherent performance attributes, damping qualities, tailorability, and light-weight of components fabricated of this class of materials as compared to metallic components used conventionally. In addition to weight savings, ease of handlability and significantly reduced thermal conductivity make them increasingly attractive for offshore platforms and associated structural elements. Despite anecdotal evidence of the durability of these materials in a marine environment [1,2,3] especially with the appropriate use of gel-coats [4], there is still a critical lack of validated durability data resulting in the application of conservative design safety factors [4-7].

Vinylester resins, produced from various epoxides and ethylenically unsaturated carboxylic acids are increasingly preferred to unsaturated polyesters because of their higher resistance to solvents and chemicals, as well as their intrinsic higher toughness. However, there is still insufficient data of their durability, especially over the long-term [8-10]. It should be noted that in general, these systems are comprised of low molecular weight polyhydroxyether chains with reactive groups at the chain ends, and which undergo cross-linking by free radical polymerization using organic peroxides and hydroperoxides as initiators. In addition, styrene is used as a diluent in the monomeric form, resulting in cure proceeding as a combination of individual polymerizations of styrene (homopolymerization), the vinylester monomer, and combined interactions between the two resulting in the formation of microgels in the bulk resin, which can result in quenching of the reaction prior to the full polymerization. Further, cure kinetics of thermosets are known to be dependent on local viscosity which again can cause reaction quenching due to the premature vitrification. This complicates characterization and modeling of

the degradation process, especially when the resin or its composites are immersed in aqueous solutions since the incomplete polymerization can not only induce lower heat stability, lower resistance to hydrolysis and a greater degree of susceptibility of swelling in the solvents [11], but can also result in earlier hydrolysis of the ester groups causing formation of carboxyl groups which autocatalyze leading to further decomposition [12]. In addition, aqueous immersion also results in development of a water/moisture induced residual cure [13,16].

Although there is some evidence that immersion in salt water results in lower equilibrium mass uptake than that in distilled water [15,16], other data suggest that an increase in salinity can result in increased loss in composite properties [17,18]. A recent study by Chin et al. [19] on unreinforced resin samples, however, showed that solubility, equilibrium mass uptake, and values of diffusion coefficients, all measured at 22°C for a Dow Derakane 411-350 PA were slightly higher for samples immersed in salt solution than for these immersed in distilled water. Given the lack of data, especially over the long-term that could be used for purposes of design of civil infrastructure components there is a critical need for the development of both validated data sets and for predictions of long-term durability, especially in cases without gel coats since it is unlikely, at present, that substantial routine maintenance would be done at this level on civil structures.

1.2. SYNOPSIS OF RESEARCH

Detailed and controlled characterization of an E-glass/vinylester system under simulated marine conditions was conducted using both immersion and cyclic exposure in order to obtain a more accurate representation of the material's failure due to the exposure. Past studies often provided overly conservative results where composites are fully immersed in severe conditions. Realistically, several components in structures are more likely to be partially saturated in a marine environment, thus degradation could be less severe.

In order to provide full characterization of varying environmental conditions, a complete set of mechanical and dynamic tests are performed in conjunction with one another. Moisture uptake is monitored as a means of obtaining a history of uptake and weight changes in the composite over specific periods of time. Changes in mechanical characteristics such as tensile strength and modulus, flexural strength and modulus, and SBS strength are monitored. Dynamic mechanical thermal analysis is conducted to provide insight into the viscoelastic response of the composite due to the exposure. The combination of these analyses provides a clearly defined material response.

The research includes a literature survey focused on the durability of carbon and glass fiber composites subjected to a variety of marine environments including natural seawater, synthetic seawater, and NaCl solution. Following this, individual chapters provide data from mechanical tests and analysis of the results. Dynamic mechanical thermal analysis (DMTA) results are reported and used to provide further correlation of effects. In each chapter, damage characterization is emphasized through micrographs showing typical degradation at critical time periods with pictorial evidence of fiber/matrix debonding and coalescence of debonds. Finally, life prediction methodologies are employed to extrapolate long-term data from the current short-term investigation.

While the focus of the research is on development of a process for determination of the MOL, the research is based on exposure to aqueous environments, and especially sea water as a specific example. It is emphasized that the procedure developed and shown by example in the last chapter of this section of the report can be applied to other exposure conditions, and combinations thereof, as well.

CHAPTER 2 – LITERATURE REVIEW

2.1. INTRODUCTION

From the early the 1940's onwards there has been interest in construction of piers, decks, wharves, and boats for the marine industry using fiber reinforced polymer (FRP) composites. While a majority of the research focused on aerospace applications, there was a high level of interest in the use of FRP materials in the marine industry, and its use has increased over the years, despite lack of data at the same level as in the aerospace field. Designers considered composites very attractive as a new material because of its potential to resist corrosion, resulting in less maintenance costs over long periods of time. Issues regarding long-term durability were assuaged through the incorporation of large safety factors, which ensured a high level of conservatism. Many projects using composites in the marine industry have been successfully completed and their inspection after longer periods of service has demonstrated good survivability [3,20-24].

Anchorage, Inc., a company that pioneered the use of resin glass construction built three 40-foot patrol boats for the Coast Guard in the early 1950's [23]. These patrol boats, constructed of glass fiber and polyester resin, were subjected to harsh marine environments for a period of ten years. After considerable use in fresh and salt water environments, it was noted that their hulls had not corroded, deformed, or cracked. In fact, use of these boats were eventually diverted to the Houston Ship Canal where the waters were highly corrosive due to effluents from oil and gas refineries, which had turned the water into a degradative environment with high concentrations of sulphuric acid. Evaluation after service had shown that the strength of the laminates still met the vessel's design requirements. Final analysis also showed that maintenance costs were 80% less than boats constructed of steel or aluminum.

One of the early interesting investigations was in 1953 when the USS Halfbeak, a submarine, was reinforced with glass fiber composites [24]. This was one of the largest structural applications with glass-fiber reinforced polymers (GRP) composites at the time. The structure was designed with a safety factor of 4.0 because of the lack of knowledge surrounding the area of durability. After eleven years of service, the structure was evaluated by the Naval Applied Science Laboratory. Specimens were cut from the structure and tested in flexure and hardness. Although the specimens had been covered in marine growth, it did not seem to affect the strength of the composite. Mechanical test results showed that the properties did not substantially deviate from the original properties and still met design requirements. However, the high-quality laminate and safety factor used incurred a cost of two times that of the previous aluminum model.

In 1967, the U.S. Navy did a survey of composite boats in service from 1947 to ascertain their structural integrity [3]. The survey included 74 boats belonging to 21 different classes. The boats ranged from 12-foot Wherry's to 52-foot LCSR's (Landing Craft Swimmer Recovery). Older boats were constructed of mat-cloth fabric and the newer boats were constructed of woven roving. Initial visual inspection showed some cracking and crazing on the surface from impact damage, but otherwise they were overall in excellent condition. Characterization included core bond, flexure, and tensile tests. There was no evidence of degradation as a function of age, even for the 16-year-old boats. Repairs were less frequent and inexpensive.

2.1.1. Marine Composites

The variety of reinforcing fibers is wide in variety, however carbon, aramid, and glass are most commonly used in the marine industry. Carbon fibers are especially advantageous because they exhibit high properties in tension, stiffness, and flexure [25]. In fact, carbon exhibits the highest specific stiffness of any fiber commercially available. However, their low impact strength, low thermal and electrical resistance, and high cost often deter their use in the marine

industry. Aramid, more commonly known as Kevlar, also exhibits fairly high strength, good impact resistance, and resistance to thermal degradation [25]. However, its high cost, low compressive and flexural strength, and susceptibility to moisture and UV based degradation contribute to its modest use in the industry.

Glass is commonly used in the marine industry because of its high strength, low weight, corrosion resistance, and its dielectric and non-magnetic properties [25]. Its low cost and ease of processing using wet-layup techniques also contribute to its popular use in the marine construction field. Several types of glass fibers are available including E-glass “electrical”, C-glass “corrosion resistant”, S-glass “silica”, R-glass “high strength”, and T-glass “high modulus”. Table 2.1 summarizes their uses and differences [26].

Table 2.1. Types of Glass Fibers [26]

Type of Fiber	Characteristics
E-glass	Low alkali content, high tensile and compressive strength, low cost, low impact resistance, most commonly used in marine industry
C-glass	Most resistant to chemical attack
R, S, and T-glass	Higher tensile strength and modulus than E-glass, high SBS strength, good wet strength retention, mainly used for aerospace industry, high cost

Most resins used for marine composites are vinylesters, epoxies, and polyesters. Polyesters are common in the marine industry, specifically for use in yachts. They are often referred to as unsaturated polyesters. The most common types used are orthophthalic polyester and isophthalic polyester. The latter is used when water resistance is desired. Epoxies are known for their high performance and resistance to environmental degradation. They are most commonly used in the aerospace field but are increasingly being used in marine applications as well. Epoxies are tough and resilient through absorption of chemical and thermal stresses, which is attributed to the two ring groups at the center of its molecular chain.

Vinylester resins were developed to incorporate the properties of epoxies with additional advanced corrosion resistance [25]. As shown in Figure 2.1, vinylesters have backbones similar to epoxies, except all the reactive sites (unsaturated vinyl groups) are at the end of the molecular chain. There are a reduced number of ester groups, which results in improved chemical resistance. Ester groups are more susceptible to hydrolysis, which can lead to degradation. The reduced amount of ester groups indicates this resin is a good candidate in applications where moisture is a factor. Longer backbones and cross-linked network chains contributes to its higher extensibility, resilience, and fracture toughness.

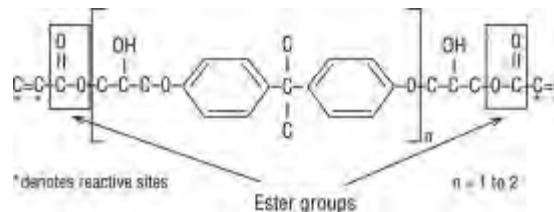


Figure 2.1. Typical Vinylester [25]

2.1.2. Seawater Degradation

Past research has used simulated seawater or NaCl solutions for assessment of durability. The composition of seawater is very complex consisting of more than seventy trace elements and biological organisms, which have shown to cause some degradation [27]. Seawater is 96.5% pure water in addition to 3.5% salts [28]. Table 2.2 summarizes the six main elements that make up the bulk of seawater.

Table 2.2. Composition of Seawater [28]

Element	Symbol	Weight %
Chloride	Cl	55.04
Sulphate	SO ₄	7.68
Calcium	Ca	1.16
Sodium	Na	30.61
Magnesium	Mg	3.69
Potassium	K	1.10

Looking at the complex nature of seawater, its effect on the mechanical properties of a composite can be greatly affected. Once a composite has been exposed to moisture, this ingress can often cause a number of different types of damage including a softening of the matrix that ultimately affects matrix dominated mechanical properties, such as transverse tensile strength [29]. Interestingly, the pH of seawater can have an affect on the diffusion process in which the presence of OH⁻ ions hydrolyze ester linkages present in vinylesters [30]. In contrast to degrading the composite, the opposite can also occur in which high temperatures can cause a post-cure in the composite and thus increase its properties. Post-cure affects the cross-linking density, in which a high density allows for better interfacial bonding between the fibers and the matrix. Marine composites are normally cured at ambient conditions; therefore a slow progressive post-cure can be a likely scenario.

2.2. MOISTURE UPTAKE

Through extensive past research, it is known that composites are sensitive to water. Although very similar in appearance, the type of water used as a medium can vary the diffusion process and ultimately the amount of moisture absorbed. Specifically, deionized water is one of the harshest solutions used in aging experiments because ions with negative charges are filtered out of the water resulting in a greater diffusion rates. Distilled water is another type of solution that is less harsh and is formulated from tap water purified through use of high temperatures,

which rid the water of hard chemicals and bacteria. It is fairly neutral in terms of pH. Seawater typically contains large Na particles, which can obstruct diffusion, resulting in a smaller amount of absorption. However, some experiments have shown that Na crystals can form within the composite due to their wicking in solution form along fiber-matrix debonds and macrocracks. The salinity in seawater lowers the vapor pressure of water, contributing to the retardation of moisture ingress. Typical values of pH for seawater are around 8, which makes seawater more alkaline than neutral. If a multi-layer composite is immersed in the above solutions, deionized water will most likely degrade it the fastest because it will be able to reach the composite's vulnerable site at midplane the earliest.

2.2.1. Degradative Mechanisms

An overview of degradative mechanisms is summarized below. Moisture ingress can cause a number of different types of damage including:

- Plasticization and Swelling
- Hydrolysis
- Blistering
- Matrix Cracking
- Leaching
- Fiber/Matrix Debonding
- Delamination

When moisture first encounters a composite, it can cause a phenomenon known as plasticization. Plasticization occurs in the matrix when bonds between ethers, secondary amines, and hydroxyl groups are broken [31-33]. Physical effects include swelling of the matrix, which introduces additional hygrothermal stresses in addition to the existing residual stresses

[32,34,35,36,37]. Immersion in salt water and seawater have shown a loss in glass transition temperature (T_g) [32,34,35], a reduction in Young's modulus [32,34], and a shift of maximum loss tangent to lower temperatures [38]. Also possible is an increase in transverse strength [39]. Although these are significant, they are often reversible upon drying [35,36,37].

Hydrolysis is often associated with plasticization. This process occurs when there is a separation of side groups from the existing polymer chain [35,36]. Hydrolysis is often accelerated from plasticization at the surface of the composite [32]. Because portions of the polymer chain are being separated, weight loss usually occurs around the fiber matrix interface region [32,36,40]. Unlike plasticization, the separation of side groups is a permanent degradation process and is not reversible upon drying [35,36,37].

Blistering occurs due to an osmotic process. Blistering was observed and evaluated by Tucker [30,41] when a composite was galvanically coupled to an active metal in seawater. Water diffuses into the matrix of the composite and forms new molecules, which create a pressure difference within the solution surrounding it [42]. Once the pressure inside the composite exceeds the surrounding pressure, a blister forms and deforms the adjacent matrix. Blistering has been noted to commonly occur in boats and yachts fabricated with fiber reinforced polymers, but have generally been found to not affect the strength or integrity of the material in the short-term and has shown to only be a cosmetic defect [2]. However, lack of maintenance can lead to severe degradation as these areas allow faster moisture uptake and serve as initiators for delamination and cracking.

A composite can also experience matrix microcracking. Microcracking occurs when the composite reaches a stress level where the matrix begins to crack away from the fibers. This process can allow the composite to continuously uptake large amounts of moisture through the cracks, eventually resulting in high amounts of strength loss (wicking). This point in stress is the commencement of breakdown. It is a well known fact that glass fiber composites are susceptible

to moisture degradation [44]. Durability research in salt water by Liao, Kajorncheappunngam, and Graner have resulted in identification of microcracking [3,36,45], while others have experienced microcracking as a result of environmental cycling in salt water or seawater [18,49,46,47]. Microcracking can also result from immersion in elevated temperatures in which permanent loss of material can occur [48,49].

Leaching is a process by which soluble oxides such as K_2O and Na_2O are lost from the composite and result in mass loss [35]. This is an irreversible process [37] that can increase the brittleness of the molecular network [18] and promote pitting of glass fibers, which is an indication of moisture-induced corrosion [50]. Research by Chin et al. [19] and Wu et al. [18] under salt water and seawater have both shown leaching. It is important to note that accelerated aging can increase the probability of leaching [48].

Fiber/matrix debonding occurs when there is insufficient bond between the fiber and resin. This can result because of poor construction (i.e. incomplete wet-out or resin rich regions in manufacture), a pressure difference resulting from the moisture that is sorbed by the composite, or environmental freeze/thaw cycling [46]. When this occurs, large reductions in tensile strength can be experienced [35,45,51,52,53]. This is an irreversible process [36] and is also associated with immersion in elevated temperatures [48].

Delamination can occur in a multi-layer composite when the bond at the interface between layers is poor. This is an irreversible process [36] and can cause disastrous effects to the properties of a composite. Liao et al [36] and Castaing et al. [54] experienced delamination in the durability of composites in salt water, which resulted in loss of properties. Delamination is also common in applications of composites to boats and yachts. In a study by Graner, some minor skin delaminations were seen after considerable periods of service [32].

Table 2.3 summarizes conditions from a collection of durability studies, in which moisture absorption is monitored, involving glass and carbon fiber composites under salt water, seawater, or synthetic seawater environments.

Table 2.3. Moisture Studies in Salt Water and Seawater

Author	Fiber	Resin	Testing Temperature	Environment	Testing Duration
Wu, Karbhari, Zhang [18]	E-glass	Vinylester	23°C	Synthetic Seawater, Natural Seawater	12 months
Tucker [30,41,64]	Graphite	Polymer	23°C	Seawater	7 months
Grant, Bradley [32,62,63]	Graphite	Epoxy	23°C	Simulated Seawater	3 months
Subramaniam, Blum, Dharani [33]	Glass/Carbon Hybrid		23°C, 50°C	Salt Water	400 days
Pomies [35]	Carbon, E-glass	Epoxy, Polyphenylsulfide	23°C, 35°C	35% Salinity Seawater	5000 hours
Liao, Schultheisz, Hunston [36]	E-glass	Vinylester	23°C	5% NaCl, 10% NaCl	6570 hours
Davies, Pomies, Carlsson [37]	E-glass	Epoxy	20°C	Seawater	8 months
Soulier, Berruet, Chateauminois, Chabert, Gauthier [38]	Glass, Carbon	Epoxy	23°C	35%, 70%, 150%, 350% Seawater	
Letton, Bradley [39]	Graphite	Epoxy	23°C	Salt Water	2000 hours
Bradley, Chiou, Grant [44]	Carbon, Glass	Epoxy, Vinylester	23°C	Seawater	90 days
Karbhari, Rivera, Zhang [46,47]	E-glass, Carbon	Vinylester	-10°C, Freeze/Thaw	5% NaCl	2400 hours
Hodgkiss, Cowling, Mulheron [48]	Glass	Epoxy, Polyester	23°C	Seawater	18 months
Loos, Springer, Sanders, Tung [49]	E-glass	Polyester	23°C, 50°C	Saturated NaCl Solution	200 days
Pomies, Carlsson, Gillespie [51,53]	Carbon, E-glass	Epoxy, Polyphenylsulfide	23°C, 35°C	Seawater	5000 hours

Table 2.3. (Continued) Moisture Studies in Salt Water and Seawater

Sonawala, Spontak [52]	Glass	Isophthalic Polyester, Vinylester	25°C	5% NaCl	270 days
Zhang, Karbhari, Ye, Mai [55]	E-glass	Vinylester	23°C	2.5% NaCl	17 months
Strait, Karasek, Amateau [56]	E-glass	Epoxy	60°C	Synthetic Seawater	3 months
Davies, Mazeas, Casari [57]	Glass	Orthophthalic Polyester, Isophthalic Polyester, Vinylester, Epoxy	20°C, 50°C	Seawater	18 months
Liao, Atkorn, Milkovich, Gomez, Schultheisz, Brinson, Fildes, Brailsford [58]	E-glass	Vinylester, Isophthalic Polyester	Freeze/Thaw	2% NaCl, 0.05g NaCl and (NH ₄) ₂ SO ₄	900 hours
Springer, Sanders, Tung [59]	E-glass	Vinylester, Polyester	23°C, 93°C	Saturated Salt Solution	200 days
Davies, Pomies, Carlsson [60]	Glass	Polypropylene	23°C	Seawater	5 months
Pollard, Baggott, Wostenhom, Yates [61]	E-glass	Isophthalic Polyester	23°C, 40°C, 60°C, 80°C	Seawater	900 days
Kosuri, Weitsman [65]	Graphite	Epoxy	23°C	Seawater	10,000 hours
Loos, Springer [66]	Graphite	Epoxy	300-322K	Saturated Salt Water	200 days
Macander, Silvergleit [67]	Graphite	Epoxy	23°C	Synthetic Seawater	26 weeks
Adams, Singh [68]	Carbon, Glass	Epoxy, Polyester	10°C, 20°C	Seawater	625 days
Kootsookos, Mouritz, St. John [69]	Glass, Carbon	Polyester, Vinylester	30°C	2.9% Salinity	10 months
Rege, Lakkad [70]	Carbon, Glass	Epoxy	100°F, 140°F, 175°F	0.5128 M Salt Water	120 hours
Steckel, Hawkins, Bauer [71]	E-glass, Carbon	Epoxy, Vinylester, Polyester	23°C	Salt Water	471 days
Wood, Bradley [72]	E-glass/Carbon Hybrid	Epoxy	23°C	Synthetic Seawater	5 months

2.2.2. Diffusion

Diffusion is a process by which matter is transported from one part of the system to another by random molecular motion [35]. Most researchers studying moisture absorption state that the diffusion they are observing is Fickian. This diffusion type is characterized by initial linear weight gain and saturation thereafter. Composites are not a homogeneous material and technically do not fall under the category of Fick's laws. However, since fibers sorb negligible amounts of water, most researchers use these laws under specific simplifying assumptions. Non-fickian diffusion is often characterized by mass loss or fluctuations in weight gain.

When monitoring weight gain in a composite, it is often convention to plot mean weight gain (%) versus square root time. Figure 2.2 is adapted from a review by Weitsman that summarizes the main patterns of diffusion [73].

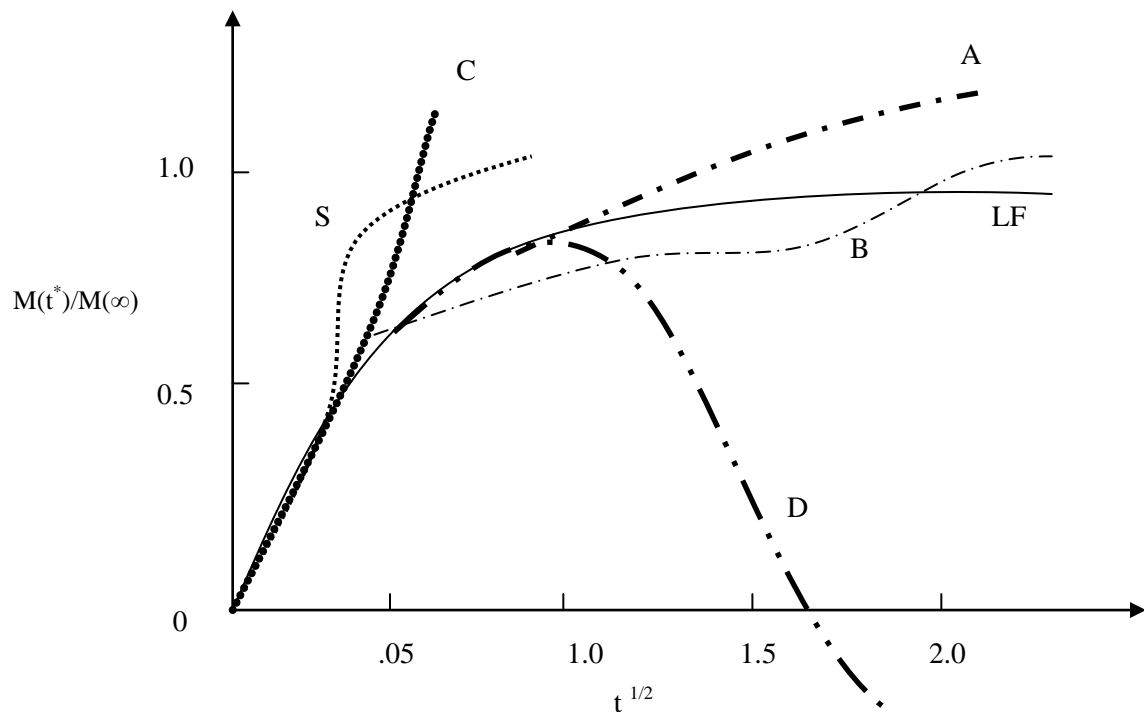


Figure 2.2. Non-Fickian Diffusion Patterns [73]

According to Weitsman, there are six main diffusion patterns that are often observed in moisture uptake studies. Depending on the degradation, they can either be reversible or irreversible. Following is a summary of these patterns [73].

- LF: The solid line stands for linear Fickian diffusion. Following Fick's Laws, diffusion is linear in the initial uptake region and constant thereafter.
- A: Curve A is designated as Pseudo-Fickian diffusion. This type of diffusion is characterized by a initial uptake in the beginning stages of immersion similar to Fickian diffusion, however saturation is never achieved.
- B: Curve B describes a Two-Stage Diffusion Behavior. The composite initially takes up weight due to moisture. Simultaneously, some mass loss is occurring. A competition between moisture uptake and mass loss occurs, until finally the moisture overtakes the concurrent mass loss and reaches an asymptote.
- C: Curve C is a type of diffusion where moisture is rapidly increasing. This can be caused by deformations, wicking, or mechanical failure.
- D: Curve D is a severe type of diffusion where at a point through immersion, sudden mass loss occurs due to hydrolysis or other types of irreversible degradation.
- S: Curve S describes a moving diffusion front.

2.2.3. Coefficient of Diffusion

The coefficient of diffusion is a numerical value that is convenient in representing the rate at which moisture is diffusing into the composite. These values can be extremely helpful when designing with a specific composite. For example, since most degradation usually occurs in the initial period of exposure for E-glass/vinylester composites, it would be beneficial to determine the rate at which moisture can cause damage in the composite.

Most studies use a short-term approximation of the Fickian coefficient of diffusion, which is determined by equation 2-1 [25].

$$D = \frac{\pi h^2}{16M_\infty^2} * \left(\frac{M_2 - M_1}{\sqrt{t_2} - \sqrt{t_1}} \right)^2 \quad (2-1)$$

where:

D is the Fickian coefficient of diffusion,

h is the thickness of the specimen,

M_∞ is the weight gain at saturation, and

M_1 and M_2 are percentage weight gains at times t_1 and t_2 such that t_1 and t_2 are in the initial linear portion of the curve.

The moisture content, M_m , is found by equation 2-2.

$$M_m = \frac{(\text{weight of specimen} - \text{weight of control})}{\text{weight of control}} * 100 \quad (2-2)$$

To obtain the one-dimensional coefficient D_∞ , a correction factor suggested by Shen and Springer is used as shown in equation 3 [25].

$$D_\infty = D \left[1 + \left(\frac{h}{b} \right) + \left(\frac{h}{l} \right) \right]^{-2} \quad (2-3)$$

where:

h is the thickness,

l is the height of the specimen, and

b is the width of the specimen

Table 2.4 provides a list of Fickian coefficients of diffusion from various researchers who have conducted studies immersing carbon and glass fiber composites in salt water, seawater, or synthetic seawater.

Table 2.4. Table of Coefficient of Diffusion in Various Marine Environments

Authors	Year	Fiber	Matrix	Process	Salt Environment	Coefficient of Diffusion [mm ² /sec]
Wu, Murphy, Karbhari & Zhang [18]	2002	E-glass	Vinylester	Wet layup	23°C Synthetic Seawater	0.429 x 10 ⁻⁶
					23°C Natural Seawater	0.498 x 10 ⁻⁶
Tucker [30]	1987	Graphite	Vinylester	Pre-preg	23°C Seawater	0.399 x 10 ⁻⁶
			Epoxy			0.413x10 ⁻⁶
Tucker & Brown [41]	1989	Graphite	Vinylester	Wet layup	21°C Seawater at 2000 fsw	0.599 x 10 ⁻⁶
					21°C Seawater at 1 atm	0.399 x 10 ⁻⁶
Zhang, Rivera & Karbhari [47]	2000	Carbon	Vinylester	Wet layup	Freeze/Thaw in 5% NaCl	0.55 x 10 ⁻⁶
Loos, Springer, Sanders & Tung [49]	1980	E-glass (SMC-25)	Polyester	Wet layup	23°C Saturated NaCl	8.3 x 10 ⁻⁵
		E-glass (SMC-65)			50°C Saturated NaCl	33 x 10 ⁻⁵
					23°C Saturated NaCl	0.8 x 10 ⁻⁵
		E-glass (SMC-30)			50°C Saturated NaCl	2.5 x 10 ⁻⁵
					23°C Saturated NaCl	21 x 10 ⁻⁵
		50°C Saturated NaCl			30 x 10 ⁻⁵	
Pomies, Carlsson & Gillespie [53]	2000	Glass	Polyphenylene Sulfide	Wet layup	35°C Seawater	0.217 x 10 ⁻⁶
Zhang, Karbhari, Ye & Mai [55]	2000	Glass Woven Roving	Vinylester	Wet layup	2.5% NaCl Room Temperature	0.52 x 10 ⁻⁶
		Glass Roving + CSM				0.78 x 10 ⁻⁶

Table 2.4. (Continued) Table of Coefficient of Diffusion in Various Marine Environments

Springer, Sanders & Tung [59]	1980	E-glass	Polyester	Wet layup	23°C Saturated Salt Water	10.0×10^{-5}
					93°C Saturated Salt Water	5.0×10^{-5}
		Vinylester			23°C Saturated Salt Water	5.0×10^{-5}
					93°C Saturated Salt Water	30.0×10^{-5}
Davies, Pomies & Carlsson [60]	1996	Glass	Polypropylene	Wet layup	23°C Seawater	0.833×10^{-6}
Pollard, Baggott, Wostenholm & Yates [61]	1989	E-glass	Isophthalic Polyester	Wet layup	Seawater 2°C, atm pressure	0.139×10^{-6}
					Seawater 80°C, atm pressure	0.690×10^{-6}
					Seawater 60°C, atm pressure	1.085×10^{-6}
					Seawater 40°C, atm pressure	0.273×10^{-6}
Loos & Springer [66]	1979	Graphite (Fiberite)	Epoxy	Pre-preg	Saturated Salt Water Room Temperature	0.113×10^{-7}
		Graphite (Hercules)				0.229×10^{-7}
		Graphite (Narmco)				0.172×10^{-7}
Adams & Singh [68]	1995	Woven Carbon	Epoxy	Wet layup	10°C Natural Seawater	0.04×10^{-6}
					20°C Natural Seawater	0.25×10^{-6}

2.3. TENSION

There are a number of investigations involving durability of carbon and glass fiber composites subjected to various environmental conditions in saline conditions. Comparing immersion in salt water and natural seawater, reductions in properties for tensile strength seem to be more affected by salt-water solutions. It seems that seawater contains less aggressive components and diffuse less moisture into the composite. Various environmental conditions

studied include salt-water immersion, seawater immersion, cycling conditions, and pressure induced environments. The following sections summarize the effects of these environmental conditions towards tensile strength and modulus.

2.3.1. Salt Water Immersion

Common durability investigations involve immersion in salt-water solutions for short periods of time. A report by Faza et al. described the response of glass/polyester and glass/vinylester composites immersed in 4% salt solution at temperatures ranging from 74°F to 200°F [74]. This study used a testing structure in which tension tests were performed while immersed in solutions. They reported losses in longitudinal tensile strengths ranging from 10% to 20%. The tensile modulus showed negligible reductions. Kajorncheappunngam et al. immersed E-glass/epoxy composites in salt solution for 5 months [45]. Observation showed an initial increase in ultimate tensile strength which was attributed to post cure and then a decrease in strength thereafter. Similar to Faza et al. [74], little effect was seen in tensile modulus. For a period of 7 months, Springer et al. immersed E-glass/vinylester and E-glass polyester composites in a saturated salt solution at 23°C and 93°C [59]. Similar trends in tensile strength and modulus were found. Sonawala et al. looked at glass/polyester and glass/vinylester composites in 5% NaCl solutions for a period of 9 months [52]. A slightly larger reduction in ultimate tensile strength was recorded at 31%.

Investigations involving durability of E-glass/vinylester composites in salt-water solutions for long periods of immersion have shown a general reduction of properties on the order of 20% to 30%. An experiment by Liao et al. immersed E-glass/vinylester composites in room temperature salt solutions of concentrations of 5% and 10% for a period of 2 years [36]. Liao reported failure modes of matrix cracking, delamination and weight loss resulting from hydrolysis. Changes in longitudinal tensile strength and modulus were reported to be 29% and

23%, respectively [36]. Likewise, an investigation by Zhang et al. immersed E-glass/vinylester composites in 2.5% NaCl solution for a period of 1.5 years [55]. Analogous results were found with changes in longitudinal tensile strength and modulus of 25% and 15%, respectively.

Common characteristics among the studies cited above are the initial drops in tensile strength within the first three months. Also, all of these investigations noted small changes in modulus, which may be beneficial in design, since calculations are stiffness driven. For long-term immersion, a leveling off of properties was seen after an initial reduction [36,55]. This change has been reported as an irreversible process in which only partial regain in properties was seen after redrying [55].

2.3.2. Seawater Immersion

Some laboratory experiments attempt to mirror conditions related to real-site evaluations by introducing composites to actual seawater or synthetic seawater prepared according to ASTM standards (if seawater is not readily available due to location).

The statements following are an account of durability research in seawater for short periods of time. Grant and Bradley did research on graphite and glass composites exposed to simulated seawater for a period of 3 months [32]. Transverse tension tests were performed because of the sensitivity of fiber/matrix interfacial strength towards moisture, and changes in matrix strength were also analyzed. Reductions after 21 days were small for most tests and reductions were on the order of 20%. However, after a 90-day immersion, the graphite/vinylester samples lost 56-68% strength. These reductions were attributed to plasticization and swelling. Pomies and Carlsson considered carbon/epoxy and E-glass/epoxy composites subjected to seawater at 23°C and 35°C [35,51,53]. Transverse tension tests were also performed. Reductions in transverse tensile strength were seen as large as 70% in the E-glass/epoxy samples. Grami et al. exposed glass/polyurethane composites for 3 months in simulated seawater at 25°C and 100°C [75]. At

25°C, loss in longitudinal tensile strength was at most 14%. However at 100°C, samples lost 51% strength, indicating degradation mechanisms attributed to accelerated aging. Losses were attributed to interfacial degradation. As can be seen from the data above, degradation in the transverse direction, where the matrix is most sensitive to moisture, are large compared to losses in the fiber direction.

Some assessments have subjected composites immersed in seawater to longer periods of immersion of around 1 year. Al-Bastaki and Al-Madani found that glass/polyester samples fabricated to simulate sporting equipment (immersed in natural seawater) had increased in modulus and reduced in tensile strength by very small amounts [76]. The increase in modulus was attributed to the woven glass on the outside layers being pulled in tension during mechanical testing. Typical brittle failures were seen after tensile testing, with fiber pull-out being the dominant failure mechanism. An E-glass/graphite/epoxy hybrid composite was studied by Wood and Bradley, who immersed their samples in synthetic seawater [72]. Transverse tension tests showed that tension properties increased with moisture content and then dropped after saturation. Failure was verified in an environmental SEM; resin-rich areas were found to be sources of failure initiation where debonding occurred. An interesting long-term exposure to seawater examination was a study by Davies et al. in which glass fibers with a variety of resins including polyester, vinylester, and epoxy, were evaluated [57]. Tension tests were performed with fibers oriented along the 45° direction in order to determine shear modulus, a property not commonly assessed for. Results showed that the shear modulus of the glass/polyester decreased significantly while the reductions in values for the glass/epoxy and vinylester were less severe.

2.3.3. Seawater Cycling

Use of composites in marine structures can imply use in areas where a tidal splash zone is applicable; or in cold environments where seasonal changes can melt and freeze the upper layers of

water. Often, laboratory experiments simulate these cycles in a controlled environment. Interest in the effect of tensile properties subjected to cycling in seawater has sparked research resulting in the following investigations.

Analyses by Wu et al. [18], Karbhari et al. [46], and Zhang et al. [47] have shown concurring results when studying E-glass/vinylester composites exposed to cycling. Wu et al. exposed samples to a wet/dry cycle in seawater and found an 8% drop in tensile strength [18]. The small loss in properties can be validated through the minimum amount of moisture that was sorbed. Also notable was the high amount of variability that was seen amongst specimens tested. Hypothesis of these effects was attributed to microcracking in samples from wet/dry cycling. Karbhari et al. exposed samples to a freeze/thaw cycle in 5% NaCl solution, where similar results were found [46]. Failure was attributed to fiber matrix debonding and matrix microcracking. These samples also experienced wicking, which caused the maximum degradation. Zhang et al. exposed samples to a freeze/thaw cycle in salt solution and concurrently found small reductions in tensile strength and modulus [47].

In a study by Steckel et al., glass/polymer composites were subjected to freeze/thaw cycling [71]. As opposed to the researchers cited above, no reductions in tensile strength were experienced. Moisture profiles showed the cycling retarded moisture intake and as a result, did not cause any degradation. A report by Hulatt and Thorne studying carbon and glass composites subjected to wet/dry cycling of a road salt solution showed that there were no adverse affects on the longitudinal modulus or ultimate tensile strength; in fact, a slight increase was noted for the modulus [19].

2.3.4. Immersion in Seawater Under Pressure

Composites have been aimed for use in some applications where pressure may be a factor. For instance, since oil deposits of increasing importance, the future may call for drilling at greater

depths. Use of composites in this field will reduce weight as compared to the weight of steel that is currently used. Hence, researchers have induced samples to varying pressures in seawater environments.

Bradley and coworkers performed extensive research on various composites subjected to seawater and pressurized environments [39,44,62,63]. Bradley et al. summarizes the effect of pressure in two statements: “1) it can reduce the free volume in the resin reducing the locations where molecules can accumulate and 2) it can increase the driving force for moisture absorption” [44]. In papers by Grant and Bradley [62,63], various graphite fibers placed in epoxy and fluorine were immersed in synthetic seawater at a pressure of 20.7 MPa in order to simulate ocean depths of 1900 meters (6000 feet). Transverse tension tests show reductions from 4% to 17%. Compared to control samples immersed in seawater at atmospheric pressure, it was concluded that pressure and salt did not affect the rate of degradation.

2.4. SHORT BEAM SHEAR

Another mechanical testing procedure valuable in analyzing the durability of a composite is the short beam shear test, which determines the short beam shear (SBS) strength. This data can describe the degree of strength between layers, an indicator of the relative degradation of the composite at the interfacial bond level [77]. This mechanical test, although not as common as the tension test, is investigated by some researchers and will be described in four sections: salt water immersion, seawater immersion, immersion in seawater and salt water under pressure, and long-term studies in natural aging environments.

2.4.1. Salt Water Immersion

Several investigators have studied the effects of short beam shear as a result of immersion in salt water. It is known that salt can degrade the fiber/matrix interface, which is crucial to the SBS strength.

Rege and Lakkad reported on CFRP and GFRP composites immersed in 0.5128 M salt solution and distilled water for a period of 120 hours in order to reach saturation [70]. A varying number of temperatures were used: 100°F, 140°F, and 175°F. Results showed that the carbon fiber composites saw the most damage when testing in SBS mode. A 58.5% decrease at 175°F was experienced. Also interesting to note was that immersion in salt water resulted in a higher amount of moisture weight gain than in distilled water, which contradicts previous surveys [41,64,68]. Another interesting observation was that more moisture was sorbed in the composite than in the neat resin samples. According to theory, glass and carbon fibers in a composite absorb negligible amounts of moisture and hence absorption in a neat resin sample and a composite sample should not differ by large amounts, after accounting for fiber volume fraction. Ultimately, Rege and Lakkad found that SBS strength was more affected by the salt water than distilled water.

Steckel et al. studied E-glass and carbon fiber reinforced with epoxy, vinylester and polyester [71]. They immersed the samples in salt water at room temperature for 417 days. Similar to Rege and Lakkad [70], the carbon fiber composites experienced a greater amount of degradation on the order of 20% reduction as compared the glass fiber composites. A comparable study by Gellert and Turley with similar composites and immersion time showed 12-21% drop in SBS strength [78].

Springer, Sanders, and Tung considered E-glass/vinylester and E-glass/polyester composites in saturated salt water for a period of 6 months at 23°C and 93°C [59]. After investigating the

environmental effects on SBS strength, it was found that at 23°C, the strength did not change, while at 93°C, a more pronounced effect was seen. This difference was attributed to accelerated aging effects.

Chin, Hughes, and Signor researched glass/vinylester and glass/polyester composites immersed in salt water for 427 days at 23°C, 40°C, 60°C, and 80°C [40]. The most degradation in SBS strength occurred in the polyester samples, while the vinylester samples experienced a 20% reduction, analogous to the study by Steckel et al. [71] and Gellert et al. [78]. Degradation was attributed to hydrolysis and disruption at the fiber matrix interface.

Similar among the papers cited above are that SBS strength in salt water is one of the most degradative effects, as compared to other mechanical tests. Reductions on the order of 20% to 60% were shown, depending on immersion temperature.

2.4.2. Seawater Immersion

The following reports are accounts of researchers studying the SBS strength of glass and carbon fiber composites in synthetic and natural seawater.

An investigation by Wu et al. immersed E-glass/vinylester composites in synthetic seawater and natural seawater at room temperature for 12 months [18]. Decreases in SBS strength were very close for the synthetic and natural seawater, with reductions of 15.6% and 15.4%, respectively. Because the architectures of the samples were not unidirectional, the values of SBS strength cannot be taken as absolutes. Similar to the study by Wu et al. [18], several graphite/epoxy samples were immersed in synthetic seawater at room temperature for 12 months by Macander and Silvergleit [67]. A 20% reduction in SBS strength was seen. The rate of degradation was greatest in the initial portion of the immersion period. Notable was the similar trends in degradation for tests in short beam shear, compression, and flexural tests, indicating a correlation between all three.

Davies, Pomies, and Carlsson looked at E-glass/epoxy composites immersed in natural seawater for 8 months [37]. Different from those cited above, Davies et al. used a four-point shear test and found failure modes of compressive buckling and yielding. However, only a 2% drop in SBS strength was found when exposed to seawater at room temperature.

2.4.3. Immersion in Seawater and Salt Water Under Pressure

Some researchers have exposed samples to saline environments under varying pressures and have actually found that this environment can cause increases in SBS strength. Although in most papers a clear explanation is not stated, it may be that since the vapor pressure of the water is reduced by the salinity, moisture is unable to reach the mid-plane to degrade the composite.

Tucker found that graphite/epoxy exposed to natural seawater at a pressure of 666 psi for 6 months increased the SBS strength by 10% [30]. No evidence of degradation was found when examining the samples. However, an explanation of the increase was mentioned implying that some of the samples failed in flexure and not in shear. Grant had similar findings when they exposed graphite/epoxy and graphite/vinylester samples to synthetic seawater at pressures of 3000 psi [32]. A comparable increase of 11.1% was also found.

Some studies exposed carbon and glass fibers to seawater and pressure induced environments. Nakanishi and Shindo exposed samples varying salinities of NaCl solution (0-23%) and 78.5 MPa at room temperature for 12 months [17]. They found that SBS strength increased with salt content and that the presence of salt showed no signs of accelerating deterioration. In general, they observed that glass was more affected than carbon from this environment. Dukes and Griffiths reported on the superiority of carbon when doing a study comparing carbon and glass [79]. They subjected pressure to samples at 7 MN/m² for 12.5 months. In terms of SBS strength, retention of properties varied from 90%-120%.

2.4.4. Long-term Studies in Seawater Aging Environments

J. Gutierrez, F. Le Lay, and P. Hoarau were one of the first to evaluate the environmental durability of composites in seawater [80]. In 1968, the Direction des Constructions Navales (DCN) chose 50 composites varying from carbon and glass fibers to epoxy, vinylester, and polyester resins. The composites were exposed to sea air for periods of 9,13,17, and 21 years and were then tested for short beam shear. They stated that aging in sea air was as severe as in seawater. Since real time tests were performed, an accelerated aging study was done in parallel. Main findings included that the fibers reinforced with pre-impregnated epoxy samples performed in shear better than other specimens, but were sensitive to aging. They explained this was because of the complete polymerization of the resin, leading to the creation of a number of hydrophilic groups, which favor hydrolytic degradation of the material. Fibers reinforced with epoxy post-cured at 80°C and vinylester at 120°C improved SBS strength properties for accelerated aging tests, but had little effect on natural aging tests. They concluded that post-cured samples were not justified for natural aging tests.

2.5. SEAWATER EFFECT ON OTHER MECHANICAL PROPERTIES

Other tests have often been utilized to determine the properties of composites. These can include a wide variety of measurements including: flexural strength, fracture toughness, glass transition temperature, fatigue, and ultimate bond strength. Each of these will be described briefly in the following sections.

2.5.1. Flexure

Standards, such as ASTM D790 and ASTM D6272, are commonly used to test for flexure in three-point or four-point bending configurations. This test measures the bending strength and

bending modulus (stiffness). When composites are subjected to seawater, it has been found that the flexural modulus does not seem to be affected. However, in terms of flexural strength, reductions are larger than those subjected to distilled water [36].

2.5.2. Fracture Toughness

Fracture toughness tests determine the resistance of a material to fracture. A typical form of this test uses an end notch flexure fracture specimen. The crack growth in the specimen is then measured to determine properties in mode I (tensile mode), mode II (sliding mode), and mode III (tearing mode). Davies et al. assessed the mode II fracture toughness of glass/polypropylene composites exposed to seawater. It was determined that values of the strain energy release rate reduced with exposure to seawater. In addition, crack growth was found to be less affected by the immersion [60].

2.5.3. Dynamic Mechanical Thermal Analysis

Dynamic mechanical thermal analysis (DMTA) can be performed in order to obtain a material's viscoelastic response and glass transition temperature (T_g). In this technique, specimens are dynamically excited by a sinusoidal force and are exposed to conditions of increasing temperature. The natural frequencies of the specimens are used to derive stiffness properties of the material [81]. For composites, the T_g corresponds to the temperature at which it was cured. Wu et al. found that, when exposed to seawater, the T_g remains unchanged until 6 months. The T_g decreased as much as 14% after 1.5 years. It was explained that leaching could cause this, in which the brittleness of the network is increased [18].

2.5.4. Fatigue

This test determines the behavior of a material under cyclic/periodic loading. Environmental fatigue can also be introduced where moisture and temperature become a factor [82]. McBagonluri et al. investigated tension-tension fatigue in E-glass/vinylester exposed to synthetic seawater [83]. Specimens were tested in a fluid cell to introduce environmental fatigue. It was found that exposure to seawater slightly improved the fatigue performance, in which degradation is attributed to a fiber-dominated process.

2.5.5. Fiber Pull-Out

The fiber pull-out test is used to measure ultimate bond strength. In this test, a force is applied to a single fiber, causing it to debond from the rest of the composite. A testing mechanism records the debond force and this is used to determine the ultimate bond strength. In a study by Meyer et al., carbon fiber composites were exposed to varying temperatures and salt water [84]. It was found that salt-water saturation reduces the bond strength as a function of time and temperature.

2.6. CORRELATION BETWEEN DEGRADATION FROM ACTUAL MARINE ENVIRONMENTS AND LABORATORY TESTING

A large portion of the data presented in the above sections reviews mechanical testing characterization based on laboratory data. Gutierrez et al. presented results that show symmetry exists between natural aging and accelerated aging studies [80]. A study was conducted in parallel with glass fiber composites reinforced with various resins subjected to ambient cure conditions and post-cured conditions. Natural aging tests took place over a period of thirty years with an accelerated aging test in parallel that subjected the composites to artificial seawater at room temperature and 70°C [81]. Results on a semi-log graph are shown in Figure 2.3.

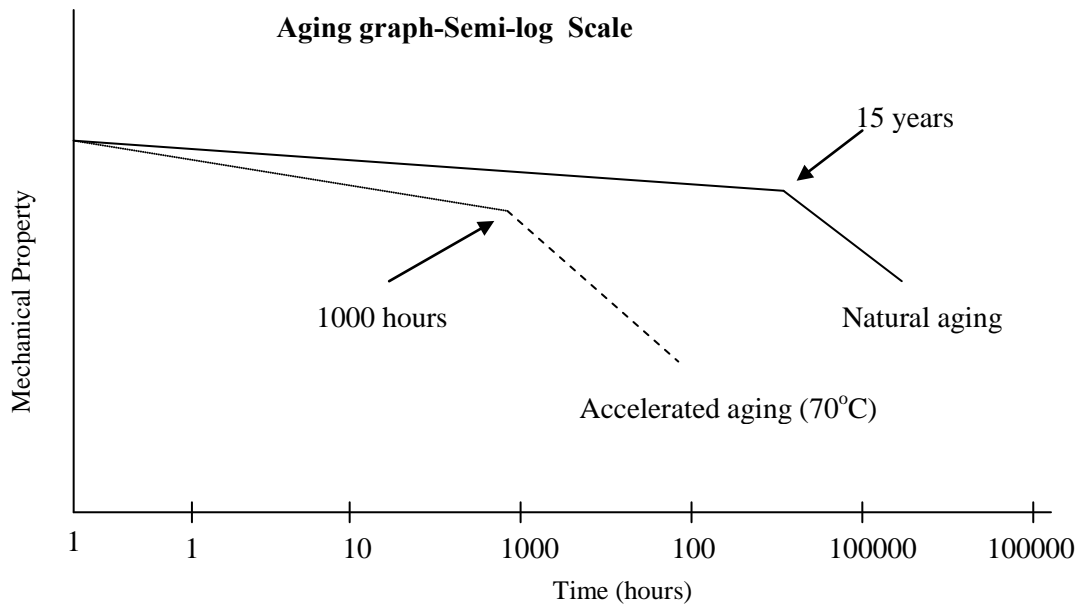


Figure 2.3. Correlation Between Natural and Accelerated Aging Studies [68]

A limited number of studies that provide aging in actual marine environments have been published. Comparisons show that similarities exist between laboratory and real-site evaluation results. Katawaki and Sasaki immersed carbon fiber composites in the splash zone of Suruga Bay in Japan for 1.5 years and tested for tensile characterization [85]. Changes in tensile strength and modulus were on the order of 12% and 1.3%, respectively. Researchers have simulated the effect of the tidal splash zone by creating a wet/dry cycle in the laboratory, as Wu et al. presented [18]. Results showed strength was affected by 9% and modulus was little affected.

Takayanagi and Kemmochi studied glass/polyester composites on a floating structure in Tokyo Bay for 2 years [86]. Testing showed increases in tensile strength by 13%, while changes in tensile modulus were minimal [86]. The increases were attributed to radiation that resulted in post-cure of the specimens. Hulatt, Hollaway, and Thorne studied the effect of UV and found very similar results as compared to Takayanagi and Kemmochi [19]. Changes in tensile strength increased by 15%, while changes in tensile modulus were insignificant [19].

Fried and Graner reported on results of a glass boat hull in service for 11 years [24]. Flexural tests were performed that resulted in 11% changes in flexural strength and 5% changes in flexural modulus. Gellert and Turley [78], Liao, Schultheisz, and Hunston [36], Nakanishi and Shindo [17], and Macander and Silvergeit [67] all reported changes on the same order when submerging composites in room temperature saline environments. No adverse effects in flexural properties were found by Mazor and Broutman [87], and Tucker and Brown [41]. It should be noted that flexural characterization is a combination of fiber and resin dominated properties that can result in insignificant changes if fibers, such as carbon, are evaluated at high fiber volume fractions

2.7. SUMMARY

After surveying numerous papers, it is apparent that studies in deionized, distilled and tap water are more common than those in salt water or seawater. It is important to note that seawater can be less harmful, and in some cases more harmful than exposure to water. These factors may be important in design. Although a wide variety of parameters are available for testing the properties of a composite, the ones most commonly examined are moisture absorption, tension, and short beam shear. Although some studies are available [85], lacking in the available literature are composite exposures to actual marine environments. Most researchers confine their samples to a controlled environment and comparisons show that significant correlation exists.

CHAPTER 3 – MATERIALS AND TEST METHODS

3.1. INTRODUCTION

The development of rational design guidelines is predicated on the availability of a validated and comprehensive set of data which can be used to describe characteristics of a materials system in terms of mode of loading and effects of exposure type and time. This requires that the data be collected in a well-defined and documented fashion following established protocols. This is especially true when minor changes in test conditions or procedures could result in errors which can confound materials level changes, or when the process used to fabricate the material has itself a variability that needs to be considered. The latter aspect is critical when using newer processes such as resin infusion, which while extremely attractive for fabrication of large, complex and highly integrated systems [88], also do not as yet have a processing science base. Further, the changes in properties over time, as a result of slow progression of cure, also need to be considered in non-autoclave processes and processes conducted in ambient temperature conditions since these can often cause difficulties in interrogating materials deterioration due to environmental exposure.

3.2. MATERIALS SYSTEM DETAILS

Specimens were fabricated in panel form in sizes of 1000 mm by 1000 mm using the resin infusion process under ambient conditions. The reinforcement consisted of 2 layers of unidirectional e-glass fabric with a stitched backing of chopped strand mat. The layers were symmetrical about the midplane with the chopped strand mat towards the center (Figure 3.1). Typical properties of the vinyl ester are given in Table 3.1. Cure was conducted under vacuum pressure at 23°C and 56% relative humidity (RH). It should be noted that the use of an ambient temperature cure results in incomplete polymerization which leads to lowered resistance to

hydrolysis, enhanced susceptibility to early moisture induced degradation, and swelling due to solvent uptake [89].

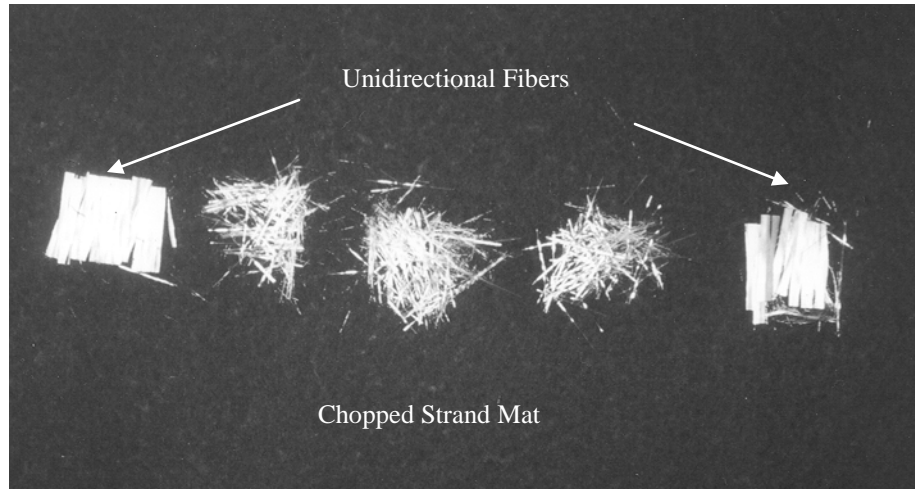


Figure 3.1. Unidirectional and Chopped Strand Mat E-Glass Fibers

Table 3.1. Typical Properties of Vinyl ester Resin [88]

Property	Value	Units
Tensile Strength	90	MPa
Tensile Modulus	4	GPa
Specific Weight	1.07	
Coefficient of Linear Expansion	80	mm/m/°C

3.3. DETERMINATION OF FIBER LOADING

Fiber volume fraction was determined using the matrix burn-off method. Four 25.4 mm by 25.4 mm specimens were placed in an oven at 600°C for six hours until only the fibers remained. Using equation 3-1, the fiber volume fraction was obtained to be on average 46.5%.

$$V_f = \frac{\frac{w_f}{\rho_f}}{\frac{w_f}{\rho_f} + \frac{w_c - w_f}{\rho_m}} \quad (3-1)$$

where:

V_f is the fiber volume fraction

w_f is the weight of the fiber in grams

ρ_f is the density of the fiber in g/cm^3 (taken to be 2.54 g/cc herein)

ρ_m is the density of the matrix in g/cm^3 (taken to be 1.03 g/cc herein)

w_c is the weight of the composite in air in grams

3.4. ENVIRONMENTAL CONDITIONS

The selection of exposure conditions was based on typical service conditions that marine industry construction would normally encounter. To obtain baseline data, specimens were first placed in an environmental conditioning chamber at 23°C and 30% RH for thirty days, after which they were exposed to one of the 7 listed conditions.

1. Immersion in 23°C seawater
2. Immersion in 40°C seawater
3. Immersion in 60°C seawater
4. Immersion in seawater at -10°C after saturation was attained under ambient (23°C) conditions (8 months room temperature immersion)
5. Freeze/Thaw Cycling alternating between -10°C and 20°C every hour
6. Wet/Dry Cycling in seawater over intervals of 12 hours each
7. Ambient at 23°C and 30% RH

Conditions 2 and 3 were used to obtain data under accelerated aging conditions and to provide service life predictions. Condition 4 was chosen to simulate marine structures in cold regions. Initial saturation was performed in order to simulate changing seasons (i.e. summer to winter). Condition 5 simulates freeze/thaw exposure. Condition 6 simulates the effect of the tidal splash zone for a structure such as a pier. Condition 7 is employed to determine a general characterization of the response when specimens are unexposed and to serve as a base-line for comparison. Results can be grouped into two categories: Conditions 1-4 are labeled “Immersion” and Conditions 5-6 are labeled “Cycling.”

Samples were placed in rectangular plastic containers in which holes were drilled in order for the seawater to permeate the samples. For immersion conditions, large temperature controlled baths were filled with purified seawater lined with plastic sheeting (to prevent rusting of the container). The plastic containers were then submerged into the solution at the appropriate temperature with thermocouples to provide verification of conditions. The freeze/thaw specimens were placed in a large plastic container inside a freeze/thaw chamber that was programmed to change between -10°C and 20°C . In order to simulate the tidal splash zone, 2 rectangular acrylic containers were connected with a pump. Samples were placed in a container and water was drained and filled at 12 hour intervals. Figure 3.2 shows the set-up used for the wet/dry exposure.

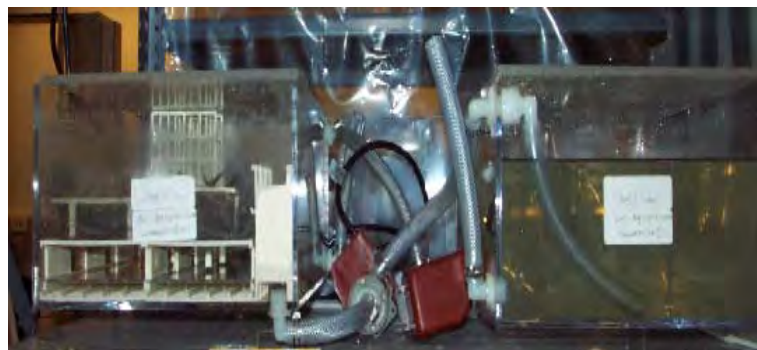


Figure 3.2. Wet/Dry Cycle Set-up

Seawater was collected from La Jolla Shores Beach in La Jolla, California and purified in the laboratory using HgCl_2 . The seawater had a pH of 8.58 and a salinity of 3.46%.

3.5. TESTING PERIODS

Since it is known that glass fiber reinforced polymer composites often undergo the highest amount of degradation during the initial phase of environmental exposure, specimens were tested more frequently during the first 16 weeks and less frequently over the subsequent time period. Specimens were exposed to the conditions listed in Section 3.4 for a total of 72 weeks. The frequency of testing was determined to be: 0, 4, 8, 12, 16, 24, 32, 52, and 72 weeks. During these testing periods, two sets of specimens for each test were removed from their exposures. One set of specimens was tested immediately and will be referred to as “wet” properties. The second set of specimens was re-dried in a conditioning chamber in order to examine regain in properties. These specimens were conditioned at 23°C and 30% RH for thirty days. These results will be referred to as “dry” properties.

3.6. TEST METHODS

A total of five replicates were used for each condition to obtain a statistically significant set of properties for the E-glass/vinyl ester system tested. Moisture uptake was measured to assess whether there was a direct relationship between mechanical properties and moisture uptake.

3.6.1. Moisture Uptake

Moisture uptake measurements were taken in an attempt to assess the relationship between uptake and degradation that occurs in a composite when exposed. In correlation with other mechanical tests, the change in specimen weight observed during that time period could be an indication of the damage mechanism that is occurring. The type of diffusion that is occurring can

also provide a large indication of different types of damage. The diffusion coefficient is an indicator of the rate of diffusion, or how fast moisture transport occurs through the material.

The frequency of measurement was higher during the initial stages of exposure for moisture uptake measurements, and less frequent during later periods. The frequency was determined as: 0, 1, 4, 8, 24, 96 (4 days), 168 (1 week), 336 (2 weeks), 672 (1 month), 1344 (2 months), 2016 (3 months), 2688 (4 months), 4032 (6 months), 5376 (8 months), 8640 (12 months), and 12960 (18 months) hours.

Sets of specimens were cut to a size of 25.4 mm x 25.4 mm and the edges were left unsealed for each condition listed in Section 3.4. Test methods follow the procedure described in ASTM D5229 [90]. Ten specimens were monitored for weight change using gravimetric means using an analytic Sartorius balance having an accuracy of 60.0000 g. These specimens were then placed back in their conditions thereafter. In addition to the continuously monitored moisture specimens, four additional specimens were measured at each of the time intervals mentioned in the preceding paragraph and were not placed back in their conditions. This was done in an attempt to differentiate between the two methods and to assess the effects, if any, of periodic atmospheric exposure. Specimens which were weighed and placed back into their exposure conditions will be referred to as “Continuous,” while the specimens that were not placed back in their conditions will be referred to as “Non-continuous.”

The diffusion coefficient (D), weight gain (M_m) and activation energy are calculated from the collected for each condition and are described in more detail in Chapter 4.

3.6.2. Tension

Following ASTM D3039, specimens were cut to dimensions of 254 mm length and 25.4 mm in width, with the length being parallel to the fiber direction [91]. An Instron model 5583 was used to carry out mechanical tests. Use of a plumber’s sand paper (230 grit) was used to

provide additional gripping force at the ends of the specimen to avoid slippage. A gauge length of 177.8 mm was used and the specimen was pulled in tension at a rate of 1.27 mm/min. Data was sampled at 2 points per second. An extensometer with a 25.4 mm gage length was used to measure strains. A 40% drop in load characterized specimen failure. Results pertaining to ultimate tensile strength and modulus are described in Chapter 5. Test setup using an Instron 5583 is shown in Figure 3.3.



Figure 3.3. Tension Test Set-up

3.6.3. Flexure

A total of five specimens were tested from each testing period for flexure. Specimens were cut to 33 mm in length and 12.7 mm in width following ASTM D790 [92]. Specimens were cut with the direction of the fiber being parallel to the length. Specimens were placed on support span of 25 mm and loaded at a rate of 0.76 mm/min at the midpoint until failure. Data was sampled at 5 points per second. Failure was noted when maximum strain in the outer surface of the specimen reached 0.05 mm/mm. Results pertaining to flexural strength and modulus are shown in Chapter 6. The test set-up using an Instron 5053 is shown in Figure 3.4.



Figure 3.4. Test set-up for 3-Point Bending

3.6.4. Short Beam Shear

A total of five specimens were tested for SBS. Specimens were cut to 12.7 mm in length and 3.8 mm in width according to ASTM D 2344 [93]. Specimens were cut with the fibers being parallel to the length. Specimens were placed on a support span of 8 mm and loaded at a rate of 1.00 mm/min at the midpoint until failure. Data was sampled at 5 points per second. Failure was characterized by a drop in load of 30%. Results of SBS strength are discussed in Chapter 7. A typical test set-up using an Instron 5053 is shown in Figure 3.5.



Figure 3.5. Test set-up for Short Beam Shear

3.6.5. Dynamic Mechanical Thermal Analysis (DMTA)

Specimens were cut to dimensions of 46 mm in length and 9 mm in width according to ASTM E1640 [94]. Specimens were cut with the fiber being parallel to the length. Tests were performed in order to obtain the material's viscoelastic response and glass transition temperature (T_g). Specimens were tested in a Rheometric Scientific DMTA V at a temperature range between 25°C and 200°C. A medium three-point-bending frame was used for testing, under multifrequency mode, i.e. 1, 5, 10, and 30 Hz at a rate of 3°C/min. The multifrequency mode was used to obtain activation energies for the glass transition temperature. These energies are an indication of the mobility of the polymer chain, which can assist in determining the crosslinking density. Results are described in Chapter 8. A typical test set-up is shown in Figure 3.6.



Figure 3.6. Test Set-up for DMTA

CHAPTER 4 – MOISTURE

4.1. INTRODUCTION

It is known that moisture can cause short-term and long-term effects including plasticization and hydrolysis in composites. Knowing when these phenomena occur can help relate the changes in mechanical properties with environmental effects.

It is important to differentiate between the terms absorption and adsorption. While often used interchangeably in the literature, they describe two dramatically different aspects. As described by Chin et al., absorption occurs through capillary uptake in voids or microcracks [19]. On the contrary, adsorption involves uptake through heat and swelling. Since confusion among the terms is common, a more appropriate term to use is moisture uptake, which describes a combination of both trends [19].

Weight change is monitored by the amount of moisture that is being sorbed. Equation 4-1 determines the percentage weight change at a specific time [90].

$$M_m = \frac{(W_w - W_d)}{W_d} * 100 \quad (4-1)$$

where:

W_w is the weight of the specimen in the wet state at time t in grams and

W_d is the weight of the composite at the dry state (i.e. at the base-line condition) at time zero in grams.

Moisture uptake can follow a variety of patterns depending on the diffusion mechanism. Diffusion is based on the idea that there is a net transfer of molecules from an area of higher concentration to one of lower concentration. Fickian diffusion is described as a steady linear initial uptake followed by a sharp change in slope after which a steady saturation phase occurs. Rate of diffusion is dependent upon temperature as described by Fick in 1885 [95]. In the present

study, it is observed that moisture absorption is initially Fickian for specimens immersed in seawater. However, there is a net decrease after a period of time. Periods of mass loss are not included in the calculation in order to determine the rate before degradation occurs. It is important to note that moisture is continually being sorbed. A decrease in weight gain means the amount of moisture being sorbed is dominated by the loss of material. This type of response has also been noted by other researchers such as Liao et al. [58], Gellert and Turley [78], and Mouritz et al. [96]. Since the initial part of the profile exhibits Fickian diffusion, it is worthwhile analyzing the coefficients of diffusion for comparison with other published studies. It is determined using the short-term approximation as described by equation 5-2 [25].

$$D = \frac{\pi h^2}{16M_\infty^2} * \left(\frac{M_2 - M_1}{\sqrt{t_2} - \sqrt{t_1}} \right)^2 \quad (4-2)$$

where:

D is the Fickian coefficient of diffusion in mm²/second,

h is the thickness of the specimen in mm,

M_∞ is the weight gain after saturation at the specified immersion temperature in grams,

and

M₁ and M₂ are the percentage changes in weight at time t₁ and t₂ (in seconds) such that both times are within the initial linear regime for moisture uptake.

To obtain the one-dimensional coefficient D_∞, a correction factor by Shen and Springer is used [97].

$$D_{\infty} = D \left[1 + \left(\frac{h}{b} \right) + \left(\frac{h}{l} \right) \right]^{-2} \quad (4-3)$$

where:

D_{∞} is the corrected coefficient of diffusion in $\text{mm}^2/\text{second}$,

h is the thickness in mm, and

l and b are the height and width in mm, respectively.

It is known that anomalous behavior is also possible as described by Carter and Kibler [98]. A Langmuir type model based on the assumptions that bulk absorption in the resin occurs and that the effects of surfaces can be neglected is used. This model can provide a view incorporating both mobile and bound phases. Molecules of the mobile phase diffuse with an independent diffusion rate and concentration. Once they are sorbed, they become bound with a certain probability. Diffusion of Langmuir type is generally characterized by an initial linear uptake followed by a less severe change in slope before reaching saturation. The Langmuir coefficient of diffusion is based on a first term approximation and is determined by equation 4-4 [98]. Similar to the Fickian coefficient of diffusion, periods of mass loss are not included in the calculation in order to determine the rate before degradation occurs.

$$M = M_{\infty} \left[1 - \frac{\alpha}{\alpha + \beta} \exp(-\beta t) - \frac{\beta}{\alpha + \beta} \exp(-\alpha t) - \frac{8}{\pi^2} \exp\left(\frac{-D_c t}{b^2} \pi^2\right) \right] \quad (4-4)$$

where:

M_{∞} is the moisture at saturation in grams,

b is the specimen width in mm,

α is the probability per unit time that a free water molecule becomes bound,

β is the probability per unit time that a bound water molecule becomes free,

D_c is the value of the coefficient of diffusion in $\text{mm}^2/\text{second}$, and

t is the length of the immersion in hours (until the point of mass loss, if this occurs).

An indication of the energy barrier that has to be overcome for diffusion of moisture to take place is the activation energy determined by the Arrhenius relationship [89] in equation 4-5.

$$D = D_o \exp\left(\frac{-E_d}{RT}\right) \quad (4-5)$$

where:

D is the diffusion coefficient in mm²/second,

D_o is a constant coefficient,

E_d is the activation energy in J/mol,

R is the universal gas constant (R=8.3143 J/mol^oK), and

T is the temperature in degrees Kelvin.

The activation energy is usually found by plotting ln (D) vs. 1/T, taking the slope of that curve, and multiplying by R [89].

4.2. RESULTS AND DISCUSSION

4.2.1. Moisture Absorption Profiles

Moisture uptake profiles are shown for “Immersed” exposures for both “Continuous” and “Non-continuous” measurements in Figures 4.1 and 4.2. Moisture uptake was not monitored for specimens frozen at -10°C because of difficulties in obtaining accurate data, without causing temperature variations.

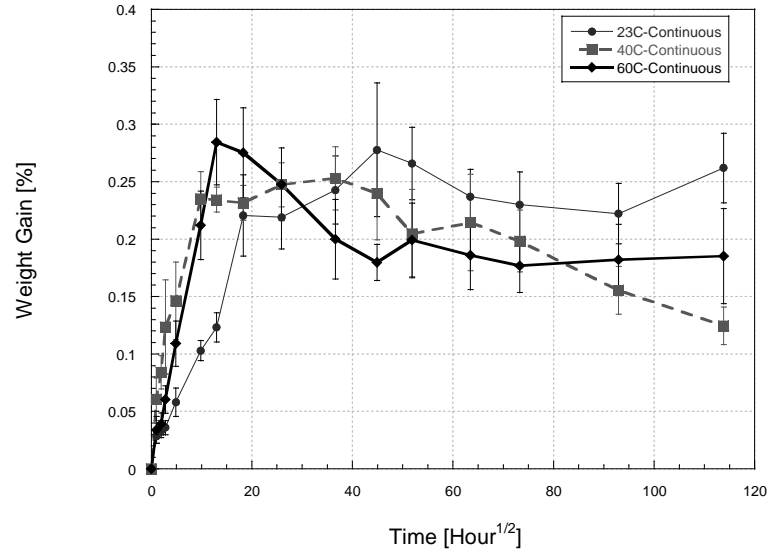


Figure 4.1. Change in Moisture Uptake As a Function of Temperature and Time of Immersion-Continuous

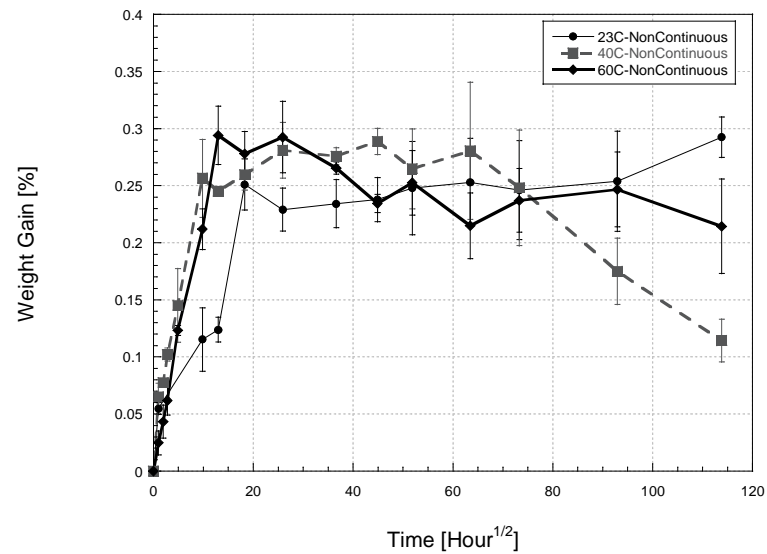


Figure 4.2. Change in Moisture Uptake As a Function of Temperature and Time of Immersion-Non-Continuous

When examining the moisture profiles for the immersed specimens, of immediate attention is the diffusion rate of the samples exposed to 40°C and 60°C seawater. Considering that the initial region of the curves for these samples overlap within bounds of standard deviation, the diffusion rate for these two exposures can be considered essentially the same. Other researchers

that have composites immersed in seawater have found maximum weight gain to be larger than that found in the current study, on the order of 1%-2% [46,56,72,99], while some have found comparable weight gain comparable at about 0.3% [18,58,69]. Others such as Davies, Pomies, and Carlsson [60], Loos and Springer [66], and Rege and Lakkad [70], who have conducted accelerated aging tests in seawater have observed a rate of diffusion dependence on temperature. The similar rates of diffusion indicate a similarity in degradation mechanisms insofar as moisture uptake is concerned. Plasticization can be noted as occurring in the specimens immersed in seawater at 40°C that causes swelling and residual stresses. The residual stresses create a pressure difference that creates an environment for rapid diffusion to occur. Plasticization is a reversible process, but once these residual stresses reach a certain point, it can cause permanent damage to the matrix resulting in debonding from fibers and even leaching of material. As seen from the profiles, at the end of the overall investigation, the specimens immersed in seawater at 40°C have the lowest weight gain out all immersion exposures. For samples immersed in 60°C seawater, a fluctuation in weight gain is seen.

The general decrease in weight under elevation temperatures of immersion after initial saturation is an indication of physical damage or chemical degradation [58]. This damage can be in the form of matrix cracking or fiber/matrix debonding [32,48,53]. It has been found that at 23°C severe degradation is rare [69] and this is consistent with the current findings. The general decrease in weight in the specimens immersed in seawater at 60°C is attributed to the leaching of low molecular weight species, which is commonly seen in high temperature immersion in seawater [69]. Generally, hydrolysis initiates the permanent mass loss in the form of styrene and glycols [69].

Figure 4.3 and 4.4 describe the moisture uptake characteristics of E-glass/vinylester composites after exposure to cyclic conditions.

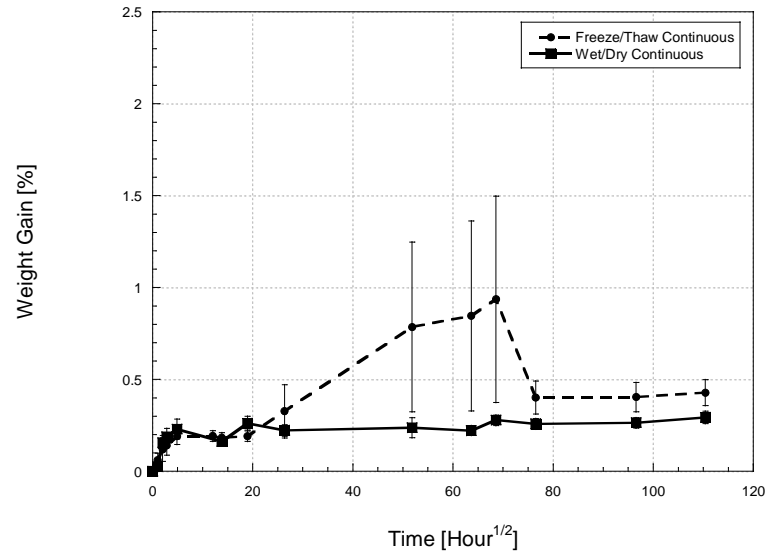


Figure 4.3. Change in Moisture Uptake As a Function of Time and Type of Cyclic Exposure-Continuous

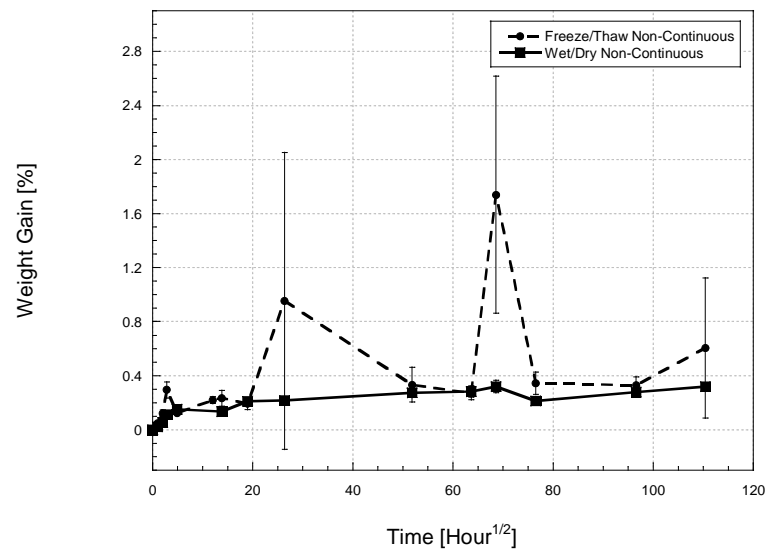


Figure 4.4. Change in Moisture Uptake As a Function of Time and Type of Cyclic Exposure-Non-Continuous

For samples cycled under freeze/thaw or wet/dry exposures, large standard deviations between samples are experienced. The composite swells when immersed and shrinks when dried, creating microcracks that can vary from specimen to specimen. Large standard deviations resulting from microcracking have also been observed by Wu et al. [18], Liao et al. [58], and

Hulatt et al. [100]. As can be seen from the figures, the freeze/thaw cycle is a less severe environment than the wet/dry cycle because samples are continually immersed and do not experience the sudden change in moisture content and the consequent swelling and shrinkage. As seen in the moisture uptake profiles, freeze/thaw samples show a higher overall moisture content than the wet/dry specimens because they are continually immersed. The possibility of wicking can introduce higher moisture contents in the cycled specimens as compared to the continuously immersed specimens.

4.2.2. Comparison of Continuous and Non-Continuous Uptake

A comparison of Continuous and Non-Continuous measurements is useful in order to assess if an extraneous effect in the procedure (removing and replacing the specimens into their environments) has any effect on moisture uptake. Figure 4.5 shows moisture uptake profiles that were monitored according to the 2 different procedures outlined in Chapter 3 (Continuous and Non-Continuous).

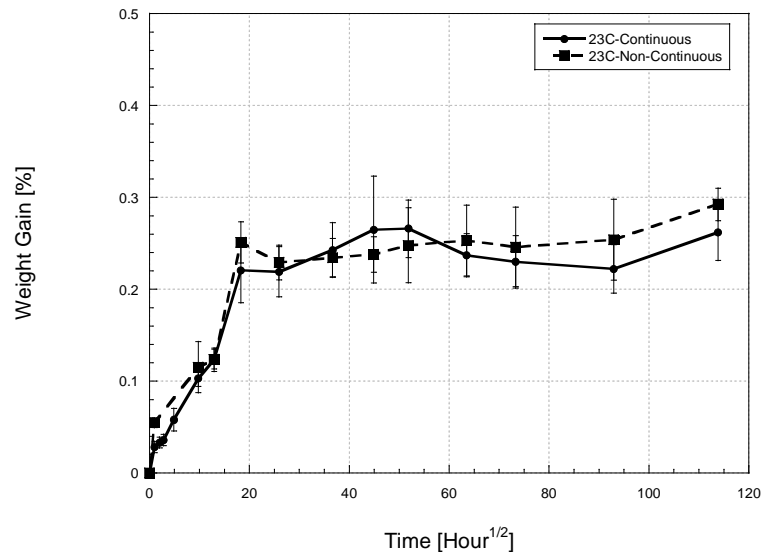


Figure 4.5a. Change in Moisture Uptake After Immersion in 23°C Seawater as a Function of Immersion Time and Procedure

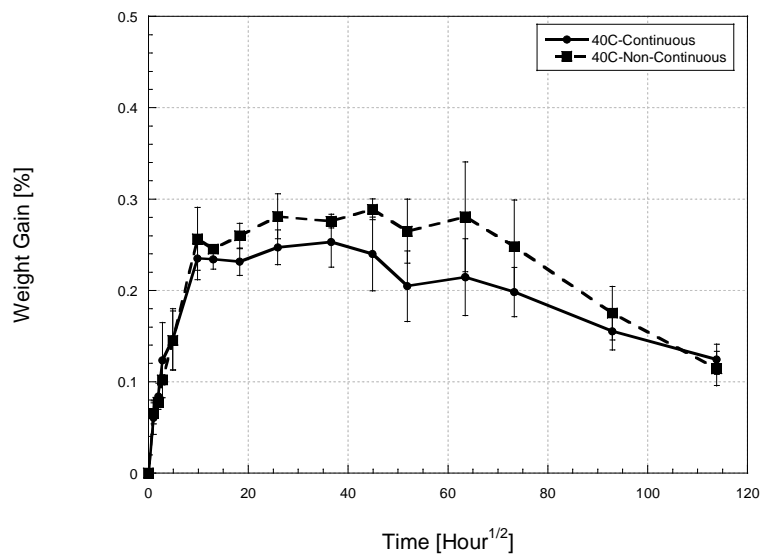


Figure 4.5b. Change in Moisture Uptake After Immersion in 40°C Seawater as a Function of Immersion Time and Procedure

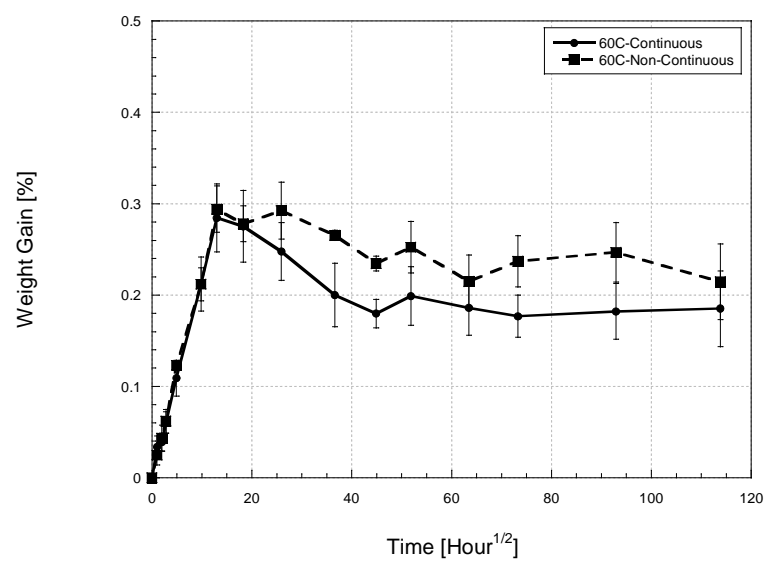


Figure 4.5c. Change in Moisture Uptake After Immersion in 60°C Seawater as a Function of Immersion Time and Procedure

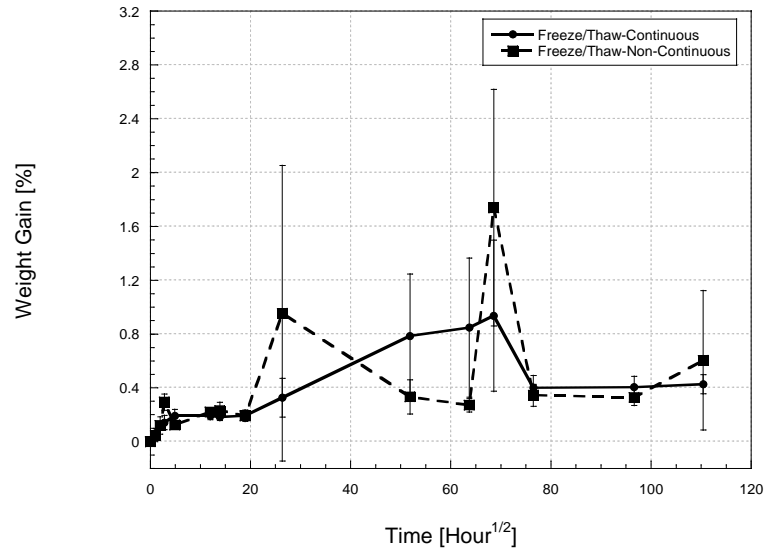


Figure 4.6a. Change in Moisture Uptake After Exposure to Freeze/Thaw Cycle as a Function of Time and Procedure

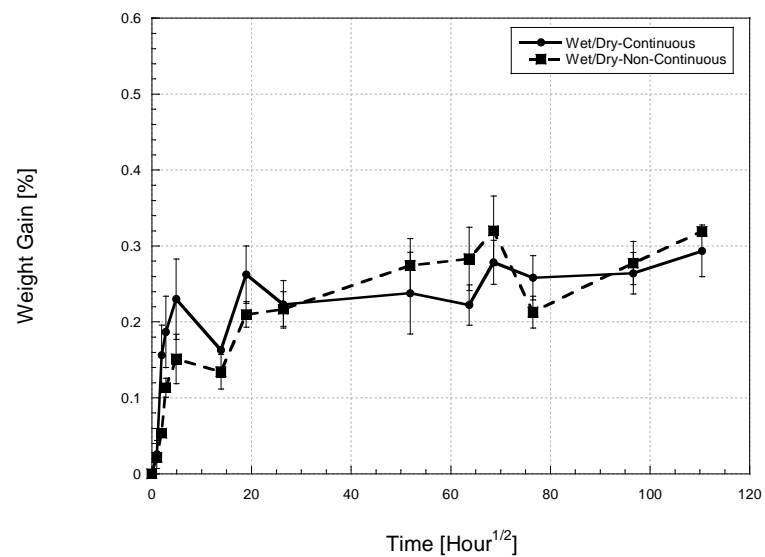


Figure 4.6b. Change in Moisture Uptake After Exposure to Wet/Dry Cycle as a Function of Time and Procedure

Observation of superimposed moisture profiles for Continuous and Non-Continuous monitoring of immersed samples show that similar trends are seen under both conditions. Examination shows that the Non-Continuous specimens yield a slightly higher moisture content. This higher moisture content is attributed to the cycle that is introduced when Continuous

specimens are taken out of their environment, dried, and then replaced in their environment. As described in the previous section, cycling can cause microcracking and material losses.

Table 4.1 is provided to show the maximum weight gain encountered for both types of monitoring.

Table 4.1. Maximum Weight Gain Determined For Continuous and Non-Continuous Monitoring

Condition	Continuous		Non-continuous	
	Maximum Moisture Content (%)	Time for Maximum Moisture Content (hours)	Maximum Moisture Content (%)	Time for Maximum Moisture Content (hours)
23°C	0.266	2688	0.293	12960
40°C	0.268	1344	0.289	2016
60°C	0.285	168	0.294	168
Freeze/Thaw	0.937	4704	1.734	4704
Wet/Dry	0.279	4704	0.320	4704

It can be seen that in most cases, weight gains of the same magnitude are attained. However, specimens exposed to the freeze/thaw exposure for Non-continuous monitored specimens reached 1.734% as compared to 0.937% for Continuous monitoring. This 180% increase is considerable, but has to be assessed in terms of the larger scatter bounds. In general, most specimens reached the maximum moisture content over the same period of time. However some Non-Continuous specimens took longer to reach the maximum moisture content. For specimens immersed in 23°C seawater, the maximum moisture content at Continuous and Non-continuous monitoring was reached at 4 and 18 months, respectively. Seemingly, these time periods are of substantial difference. Looking closer at the data, at 4 months for the Continuously monitored specimens, the standard deviation is somewhat high. If one were to exclude that data point, then the next highest moisture content would coincide at 18 months. Similar observations of large standard deviations need to be taken into account in the time to reach maximum moisture

content for the 40°C immersed and cycled specimens. At 60°C, the specimens take the same time to reach maximum moisture content and follow the same trends.

4.2.3. Coefficient of Diffusion

The coefficient of diffusion provides a valuable characteristic in describing the rate at which uptake is occurring. The short-term Fickian approximation utilizes an initial linear uptake period that is characterized by saturation at the maximum moisture content. The Langmuir model takes into account moisture profiles before any mass loss occurs and reaches a plateau at the maximum moisture content before mass loss. Figures 4.7-4.10 show both fits applied to the Continuous and Non-continuous data. The corresponding coefficients of diffusion are listed in Table 4.2. The R^2 value describes the fit of the data to the model; a value close to 1 shows a good fit. It should be noted that in cases where attainment of a peak in weight gain is followed by overall mass loss, the peak is assumed to be the end point and hence the predicted diffusion response considers asymptotic behavior thereafter.

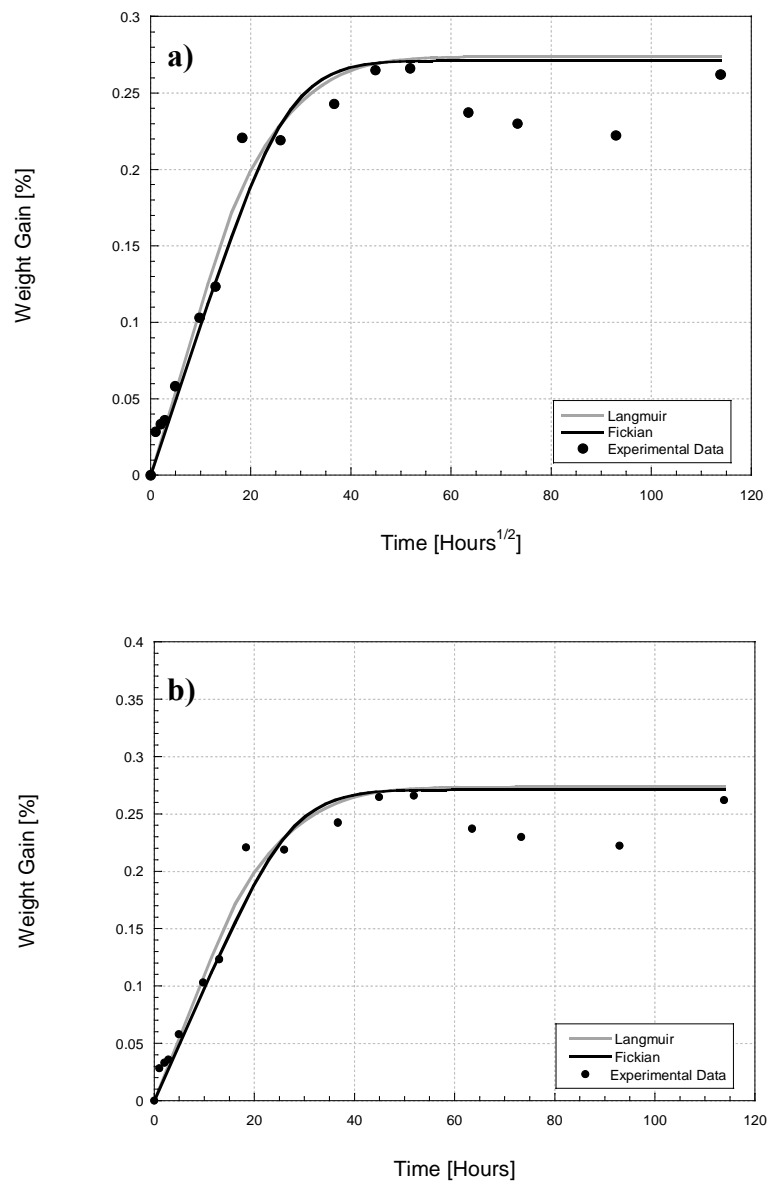


Figure 4.7. Fit for Coefficient of Diffusion After Immersion in 23°C Seawater As a Function of Procedure a) Continuous and b) Non-Continuous

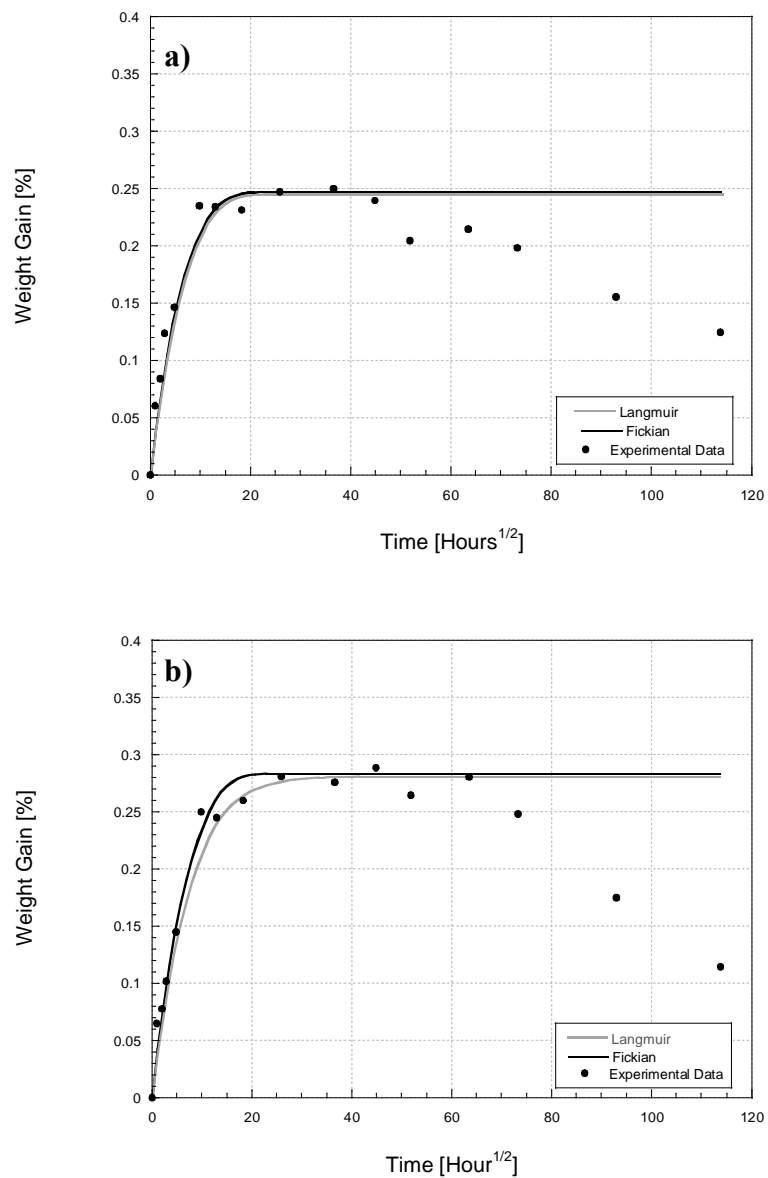


Figure 4.8. Fit for Coefficient of Diffusion After Immersion in 40°C Seawater As a Function of Procedure a) Continuous and b) Non-Continuous

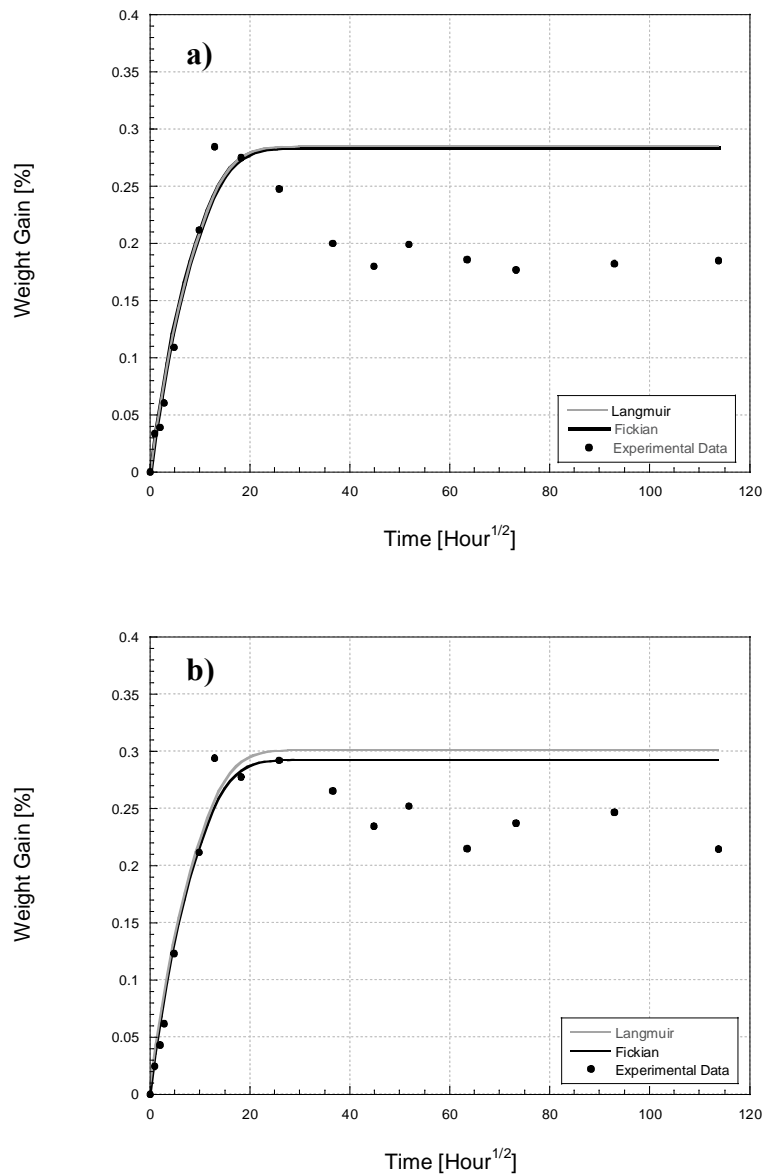


Figure 4.9. Fit for Coefficient of Diffusion After Immersion in 60°C Seawater As a Function of Procedure a) Continuous and b) Non-Continuous

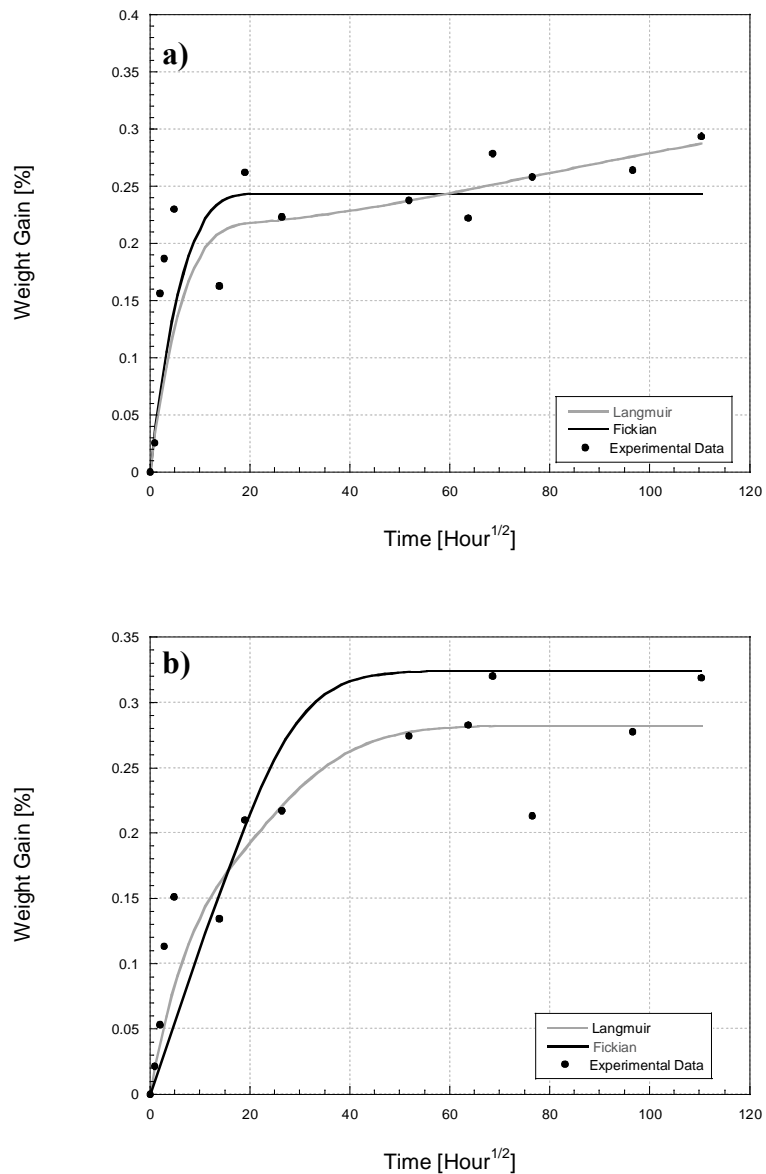


Figure 4.10. Fit for Coefficient of Diffusion After Wet/Dry Cyclic Exposure As a Function of Procedure a) Continuous and b) Non-Continuous

Table 4.2a. Coefficient of Diffusion Based on Fickian and Langmuir Diffusion Models Determined By Continuous Monitoring Procedure

Condition	Continuous				
	Fickian [mm ² /s]	Langmuir [mm ² /s]	R ²	α	β
23°C	1.63 x 10 ⁻⁶	7.36 x 10 ⁻⁵	0.98	2.4 x 10 ⁻³	2.18 x 10 ⁻³
40°C	4.35 x 10 ⁻⁶	8.63 x 10 ⁻⁵	0.95	1.13 x 10 ⁻⁴	3 x 10 ⁻⁴
60°C	5.16 x 10 ⁻⁶	7.93 x 10 ⁻⁵	1.00	3.36 x 10 ⁻²	5.83 x 10 ⁻³
Wet/Dry	5.10 x 10 ⁻⁷	8.05 x 10 ⁻⁵	0.9	4.5 x 10 ⁻⁵	8.3 x 10 ⁻⁵

Table 4.2b. Coefficient of Diffusion Based on Fickian and Langmuir Diffusion Models Determined By Non-Continuous Monitoring Procedure

Condition	Non-Continuous				
	Fickian [mm ² /s]	Langmuir [mm ² /s]	R ²	α	β
23°C	1.35 x 10 ⁻⁶	7.81 x 10 ⁻⁵	0.95	2.6 x 10 ⁻⁵	7.2 x 10 ⁻⁵
40°C	5.57 x 10 ⁻⁶	1.44 x 10 ⁻⁴	0.97	2.72 x 10 ⁻⁴	2.21 x 10 ⁻⁴
60°C	4.73 x 10 ⁻⁶	1.54 x 10 ⁻⁴	1.00	2.1 x 10 ⁻²	3.54 x 10 ⁻³
Wet/Dry	2.29 x 10 ⁻⁷	7.84 x 10 ⁻⁵	0.93	1.55 x 10 ⁻³	1.32 x 10 ⁻³

The values for coefficients of diffusion are listed in Table 4.2. It can be seen that the Fickian coefficients of diffusion reiterate the fact that the initial rates of diffusion are very similar for specimens immersed in 40°C and 60°C seawater. The coefficient of diffusion for the 23°C seawater immersion specimens is considerably smaller; consistent with Fick's law that shows rate dependence on temperature [95]. Comparing the Continuous and Non-Continuous coefficient of diffusion, the values show very slight differences. Considering the large fluctuations in mass gain for the cycled specimens, the coefficients are difficult to fit to a Fickian model, therefore, the corresponding coefficients for Continuous and Non-continuous immersion vary slightly. Pomies, Carlsson, and Gillespie [53] found similar Fickian coefficients of diffusion at 23°C seawater immersion. Similarly, Pollard, Baggott, Wostenholm, and Yates [61] found similar Fickian coefficients of diffusion at 60°C seawater immersion.

Determining a Langmuir fit shows the diffusion for 40°C and 60°C seawater immersion are very similar. The 23°C seawater immersion specimens show a slight decrease in rate. Also noticeable is the change in magnitude from Langmuir to Fickian, the Langmuir coefficients show a higher value. For most conditions, the value of R^2 is close to 1, describing a good fit. Cycling does not fit the Langmuir model as well and reflects an R^2 -value less than 1 ($R^2=0.918$).

4.2.4. Activation Energy

Using the coefficients of diffusion calculated in Section 4.2.3, the activation energy can be calculated. Low activation energies indicate a weak diffusion barrier and can relate to a high moisture uptake. Conversely, high activation energies indicate a strong barrier, therefore less moisture sorption can be expected to occur [89]. The activation energies determined from the Fickian coefficients of diffusion are 44.7 kJ/mol and 47.6 kJ/mol for Continuous and Non-continuous monitoring, respectively.

The energy barrier that has to be overcome in order for diffusion of moisture to take place is determined from an Arrhenius type relationship [89]. Comparing the values from both Continuous and Non-continuous monitoring, there is a 6% difference between the two. Standard deviations overlap, indicating that rates diffusion are essentially the same.

Values of activation energy fitted to the Fickian coefficient of diffusion values were similar to those found by previous researchers. Phani and Bose found the activation energy of glass fiber composites immersed in water to be slightly higher than the current investigation at 51.76 kJ/mol [101]. Bonniau and Bunsell [102] studied water diffusion in glass-epoxy composites for diamine-cured resin and found the activation energy to be 47.28 kJ/mol. Similar values were also reported by Edwards and Sridharan who immersed polyester laminates in water and found the activation energy to be 45 kJ/mol [103]. However, Karbhari found the activation of unidirection e-

glass/vinyl ester in deionized water to be much lower at 9.8 kJ/mol [89] due to an incomplete cure.

4.3. SUMMARY

Analyzing the moisture uptake in composites has revealed evidence of degradation at specific time periods. These can be summarized as follows:

- The small amount of moisture sorbed in the present experiment is important to note.
- Similar rates of moisture uptake in 40°C and 60°C specimens are significant and show similar effects of plasticization.
- Specimens subjected to Non-Continuous and Continuous monitoring generally take the same period of time to reach the maximum moisture content.
- The statistical variation associated with cycling is evident in the moisture profiles.
- Activation energies determined using the Fickian coefficients of diffusion are similar to those reported by previous researchers who subjected composites to elevated temperature regimes.

CHAPTER 5 – TENSION

5.1. INTRODUCTION

The strength of a unidirectional composite can degrade as a result of seawater immersion for a number of reasons including deterioration of the resin, or the fiber/matrix interphase bond. In addition, moisture uptake can enhance effects of the process induced residual stresses. Residual stresses arise from the differing thermal coefficients of expansion present in the fiber and the resin. Once the composite is left to cure, additional stresses can form in the composite. The interaction of moisture with the residual stresses introduces swelling and differential stresses that can deteriorate the bond of a fiber and matrix. These effects in total can thus alter the properties of the composite over time.

The use of tensile properties (strength, elastic modulus, and failure strain) in design is reliant on the values obtained from experimental testing. Design parameters are often based on “wet” properties (tested immediately after removal from environments to take account of the lower bound). These properties are obviously conservative. It has been shown that partial regain of properties is possible through redrying. In the case of the tidal splash zone on a pier, for example, constant submergence at the water line is not a realistic condition, since the area could be subject to changes in water level due to tides. As a result, it is of importance to examine both the wet and redried strengths and characterize the reversible and irreversible effects of exposure.

Following ASTM D3039, the calculation of ultimate strength is based on the maximum load carried before failure [91] and is found by equation 5-1.

$$F^u = \frac{P^{\max}}{A} \quad (5-1)$$

where:

F^u is the ultimate tensile strength in MPa,

P^{\max} is the maximum load at failure in N, and

A is the average cross sectional area in mm^2 taken prior to testing.

The coupons behave in linear elastic fashion until failure and hence Hooke's Law can be directly used for determination of modulus. The strains are measured using an extensometer and for purposes of calculation of modulus, strains in the initial region are considered. Since measurements are taken in both the "wet" and "dry" states, the regain of properties due to elimination of absorbed water can be determined. The regain is computed as

$$\% \text{Regain} = \frac{P_{dry} - P_{wet}}{P_o - P_{wet}} \times 100 \quad (5-2)$$

where:

P_{dry} is the property after drying in a humidity chamber at 23°C and 30% RH for 30 days (which is the time period also used for initial conditioning),

P_{wet} is the property measured as a result of testing immediately after removing the specimen from conditions of exposure, and

P_o is the initial baseline data determined at the outset.

5.2. RESULTS AND DISCUSSION

The following tables report the values of tensile strength and tensile modulus as a function of time for specimens after immersion, after cyclic exposure, and after redrying. Results for specimens exposed to baseline "ambient" conditions are also reported.

5.2.1. Tensile Strength

Changes in tensile strength as a result of immersion in seawater, and after redrying are shown in Table 5.1 and Figure 5.1, whereas the corresponding results after cyclic exposure are shown in Table 5.2 and Figure 5.4. The effects of redrying are shown in Table 5.3 and Figures 5.5 and 5.6. In the figures percentage retention is determined by equation 5-3.

$$\% \text{ Retention} = \frac{P_t}{P_o} * 100 \quad (5-3)$$

where:

P_t is the property at time t and

P_o is the property at time = 0.

Table 5.1a. Tensile Strength Determined At Ambient Conditions of 23°C and 30%RH

Time [weeks]	Ambient	
	σ [MPa]	Std. Dev. [MPa]
0	729.6	77.6
4	670.0	23.7
8	671.2	43.0
12	745.1	18.0
16	664.6	130.9
24	678.1	67.1
32	722.7	76.5
48	711.2	102.3
72	709.5	30.9

Table 5.1b. Tensile Strength Determined After Immersion in 23°C Seawater (“Wet” Testing) and as a Result of Subsequent Drying (“Dry Testing”)

Time [weeks]	23°C			
	<i>Wet Testing</i>		<i>Dry Testing</i>	
	σ [MPa]	Std. Dev. [MPa]	σ [MPa]	Std. Dev. [MPa]
0	729.6	77.6	729.6	77.6
4	646.0	62.9	647.0	30.9
8	702.9	23.4	657.4	30.8
12	682.8	113.1	630.6	74.7
16	614.9	19.8	610.6	46.6
26	619.9	63.2	658.4	51.3
35	603.4	22.4	-	-
52	592.6	43.0	555.2	30.3
78	561.4	72.8	599.8	40.4

Table 5.1c. Tensile Strength Determined After Immersion in 40°C Seawater (“Wet” Testing) and as a Result of Subsequent Drying (“Dry Testing”)

Time [weeks]	40°C			
	<i>Wet Testing</i>		<i>Dry Testing</i>	
	σ [MPa]	Std. Dev. [MPa]	σ [MPa]	Std. Dev. [MPa]
0	729.6	77.6	729.6	77.6
4	543.3	38.2	616.5	58.5
8	463.8	29.0	493.4	34.4
12	457.2	3.4	-	-
16	467.0	11.9	512.3	27.0
26	448.8	55.3	467.8	12.2
35	453.4	68.6	441.8	37.8
52	438.8	24.2	476.1	35.4
78	424.6	16.4	437.8	59.7

Table 5.1d. Tensile Strength Determined After Immersion in 60°C Seawater (“Wet” Testing) and as a Result of Subsequent Drying (“Dry Testing”)

Time [weeks]	60°C			
	<i>Wet Testing</i>		<i>Dry Testing</i>	
	σ [MPa]	Std. Dev. [MPa]	σ [MPa]	Std. Dev. [MPa]
0	729.6	77.6	729.6	77.6
4	428.9	57.4	476.4	47.9
8	393.5	36.6	446.8	26.2
12	391.1	37.3	395.7	43.5
16	393.3	41.8	-	-
26	365.9	17.2	395.3	1.3
35	374.7	12.8	397.1	40.0
52	379.9	15.6	368.2	40.8
78	375.9	23.4	376.6	5.0

Table 5.1e. Tensile Strength Determined After Immersion in -10°C Seawater (“Wet” Testing) and as a Result of Subsequent Drying (“Dry Testing”)

Time [weeks]	-10°C			
	<i>Wet Testing</i>		<i>Dry Testing</i>	
	σ [MPa]	Std. Dev. [MPa]	σ [MPa]	Std. Dev. [MPa]
0	729.6	77.6	729.6	77.6
4	655.8	55.0	705.1	80.9
8	668.7	39.3	678.1	120.1
12	638.6	58.3	721.9	45.4
16	633.1	28.6	647.2	114.7
24	667.0	38.2	688.5	77.2
35	642.9	24.8	701.5	32.1
48	609.9	102.6	646.1	32.4
72				

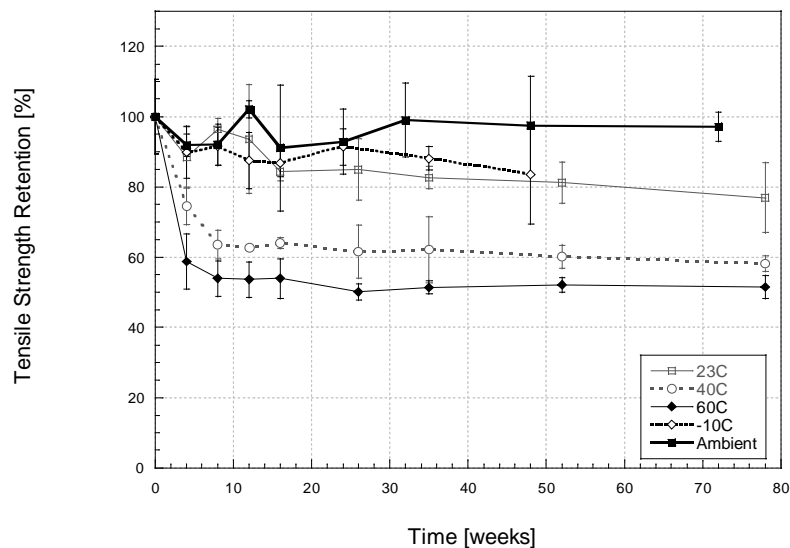


Figure 5.1. Change in Tensile Strength as a Function of Temperature and Time of Immersion in Seawater

As can be seen from Table 5.1 and Figure 5.1, tensile strength decreases both with time and temperature of immersion. In general, at all temperatures, there is an initial drop in strength followed by a slower decrease with time. Specimens immersed in seawater at 23°C seawater show a small level of residual post-cure at the 8-week level resulting in a minor increase in strength after the initially rapid increase of 11.5% in the first 4 weeks. After this point, there is a continuous decrease in strength, almost at asymptotic levels from about the 32-week time period with the loss at the end of the exposure time period of 78 weeks being about 23%. In an earlier study by Wu et al. [18] also showed similar trends, as have other researchers for glass fiber composites immersed in room temperature saline solutions [36,47,52,71,74,75,104].

In the case of specimens immersed in seawater at 40°C, the drop in strength over the initial 4-weeks was greater, at the level of about 25% with asymptotic behavior being seen after about 12-weeks of immersion. The drop in strength over the entire period was about 42%. This is, however, lower than that reported by Grami et al. [75] for glass/polyurethane specimens where drops of 51% were reported as a result of 4 weeks of immersion.

For specimens immersed in seawater at 60°C, the drop in strengths were even greater and more rapid with a 46% decrease resulting from just 8-weeks immersion. It should be noted that at these high temperatures matrix microcracking and fiber matrix debonding also take place with cracking being accelerated by plasticization [36]. The presence of debonding as early as 4 weeks is seen in Figures 5.2 and Figure 5.3.

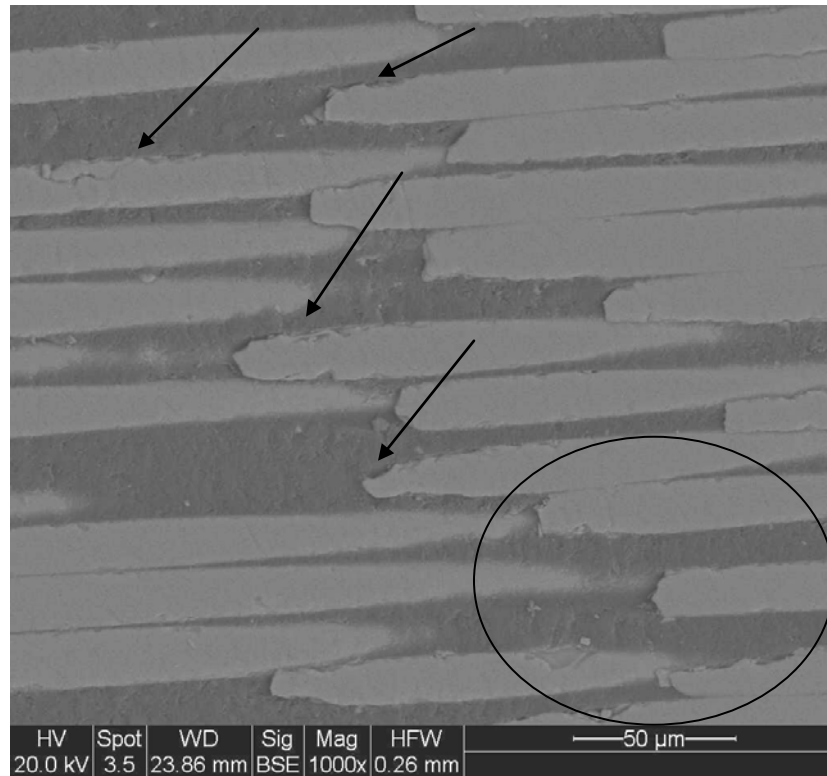


Figure 5.2. SEM Micrograph Showing Damage at 4 weeks in 40°C Seawater

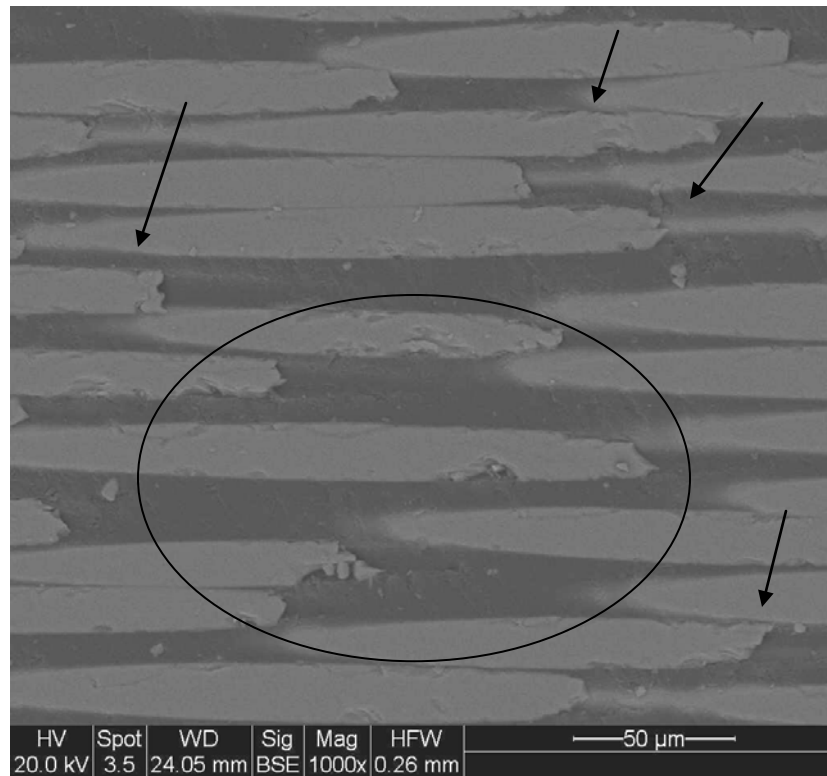


Figure 5.3. SEM Micrograph Showing Damage at 4 weeks in 60°C Seawater

Patterns of degradation as a result of immersion at elevated temperatures coincides with results reported by Matthewson [105] who suggested that for GFRP composites, nonlinear behavior is seen with an abrupt change in strength. The significant change that occurs initially results from the effect of plasticization and the results of the residual stresses that are created from the varying coefficients of expansion for the fiber and resin. Plasticization is the dominant degradation mechanism during initial immersion. Mechanisms after this period of time can occur from fiber matrix debonding, interface degradation, or fiber degradation.

Freezing conditions showed degradation similar to specimens immersed in 20°C seawater. This trend can be attributed to saturation in room temperature seawater for eight months before freezing. Others that have investigated the effects of freezing have found small changes in tensile strength [106], while some have found freezing to cause an increase in strength [46], caused by

the embrittlement of the matrix. However, it should be noted that the results of previous researchers differ because the initial saturation period was not executed.

The following section describes changes in tensile strength after exposure to cyclic conditions. Table 5.2 and Figure 5.4 show the effect of the exposure with time.

Table 5.2a. Tensile Strength Determined After Exposure to Freeze/Thaw Cyclic Exposure (“Wet” Testing) and as a Result of Subsequent Drying (“Dry Testing”)

Time [weeks]	Freeze/Thaw			
	<i>Wet Testing</i>		<i>Dry Testing</i>	
	σ [MPa]	Std. Dev. [MPa]	σ [MPa]	Std. Dev. [MPa]
0	729.6	77.6	729.6	77.6
4	635.6	89.8	570.8	62.8
8	726.3	-	730.1	59.1
12	649.1	109.0	637.4	24.0
16	652.0	62.7	661.5	50.5
24	663.6	75.7	644.0	92.6
35	644.7	26.5	710.4	28.6
54	644.0	53.1	740.5	30.6
72	630.7	37.9	617.2	27.4

Table 5.2b. Tensile Strength Determined After Exposure to Wet/Dry Cyclic Exposure (“Wet” Testing) and as a Result of Subsequent Drying (“Dry Testing”)

Time [weeks]	Wet/Dry			
	<i>Wet Testing</i>		<i>Dry Testing</i>	
	σ [MPa]	Std. Dev. [MPa]	σ [MPa]	Std. Dev. [MPa]
0	729.6	77.6	729.6	77.6
4	644.6	86.7	656.2	25.5
8	658.8	21.0	639.5	40.5
12	639.8	15.8	659.1	26.9
16	563.4	53.5	631.5	67.0
24	632.4	38.3	612.7	-
35	608.2	33.6	677.6	19.6
54	588.4	26.5	660.4	-
72	599.9	82.6	599.2	67.8

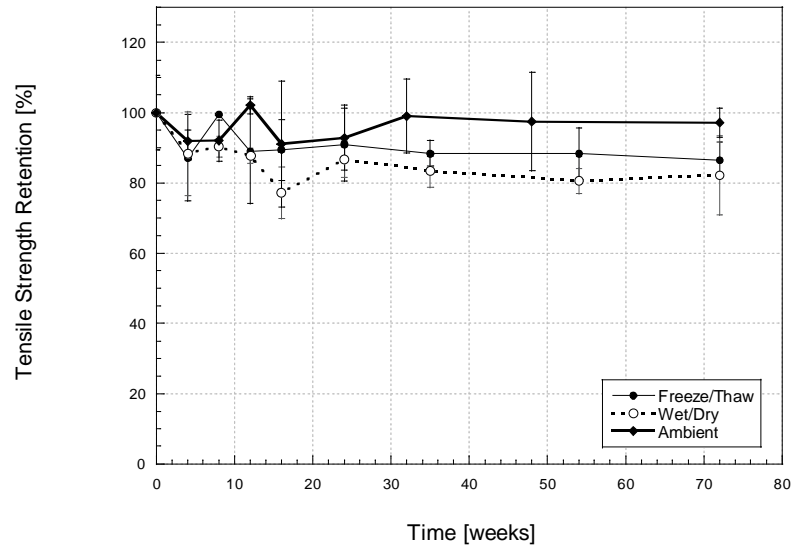


Figure 5.4. Change in Tensile Strength as a Function of Time and Type of Cyclic Exposure

Cycling in seawater proved to show subtle differences in degradation response as compared to accelerated aging. These results can be seen in Figure 5.4. When exposed to Freeze/Thaw, the tensile strength fluctuated from 0-8 weeks and then showed decreases lower than 13%. The variation in properties is attributed to the matrix microcracking and increasing brittleness that is introduced from continuous swelling and shrinking caused by the cycle [18,55]. Strength loss is caused by wicking and crystallization that consequently cause interfacial debonding [46]. From 12-72 weeks, the properties seemed to reach an asymptote, similar to what was observed for the immersed specimens. Others who have exposed glass fiber composites to freeze/thaw conditions have found changes in strength on the same order [47,46], while others have found little or no effect [71].

Exposure to the wet/dry cycling was slightly more severe than from the freeze/thaw conditions, with variation occurring from 0-8 weeks. The largest drop occurred at 16 weeks with a 23% drop in strength. An asymptotic trend was seen after 16 weeks exposure. Variation and failure is caused by mechanisms that were explained previously with freeze/thaw exposures.

Other researchers exposing glass fiber composites to wet/dry conditions in saline solutions have found both small decreases in strength [18] and increase in properties [100].

After exposure to immersion and cycling, specimens were tested after being redried in a conditioning chamber for 30 days at 23°C and 30%RH. Table 5.3 and Figures 5.5 and 5.6 demonstrate the effect of redrying.

Table 5.3a. Effect of Redrying for Tensile Strength After Immersion In Seawater

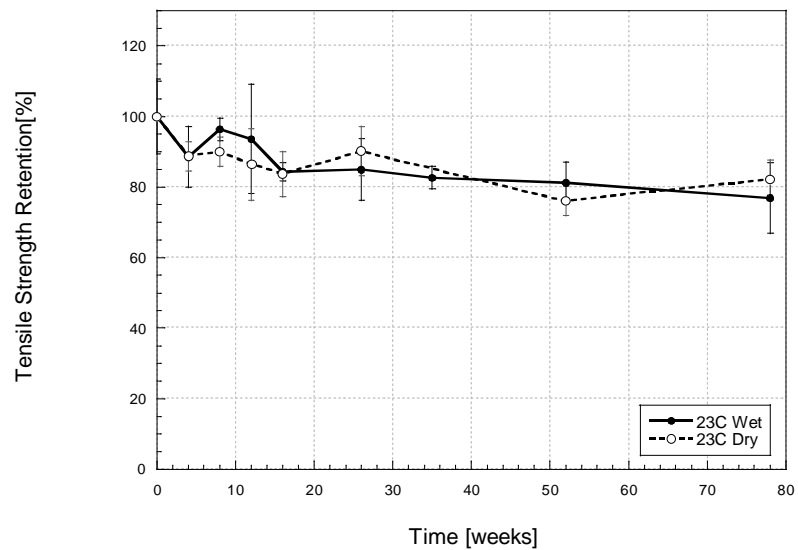
Time [weeks]	Regain [%]		
	23°C	40°C	60°C
0	100.0	100.0	100.0
4	1.2	39.3	15.8
8	-170.0	11.1	15.9
12	-111.3	-	1.4
16	-3.7	17.2	-
26	35.1	6.8	8.1
35	-	-	-
52	-27.3	12.8	-3.4
78	22.8	4.3	0.2

Table 5.3b. Effect of Redrying for Tensile Strength After Exposure to Freezing Conditions

Time [weeks]	Regain [%]
	-10°C
0	100.0
4	66.8
8	15.5
12	91.6
16	14.7
26	34.3
35	-
52	30.3
78	

Table 5.3c. Effect of Redrying for Tensile Strength After Exposure to Cyclic Conditions

Time [weeks]	Regain [%]	
	Cyclic Exposure	
	Freeze/Thaw	Wet/Dry
0	100.0	100.0
4	-68.8	13.6
8	114.4	-27.2
12	-14.6	21.5
16	12.3	41.0
26	-29.7	-20.2
35	-	-
52	112.7	50.9
78	-13.7	-0.5

**Figure 5.5a. Effect of Redrying on Tensile Strength Retention after Immersion 23°C in Seawater**

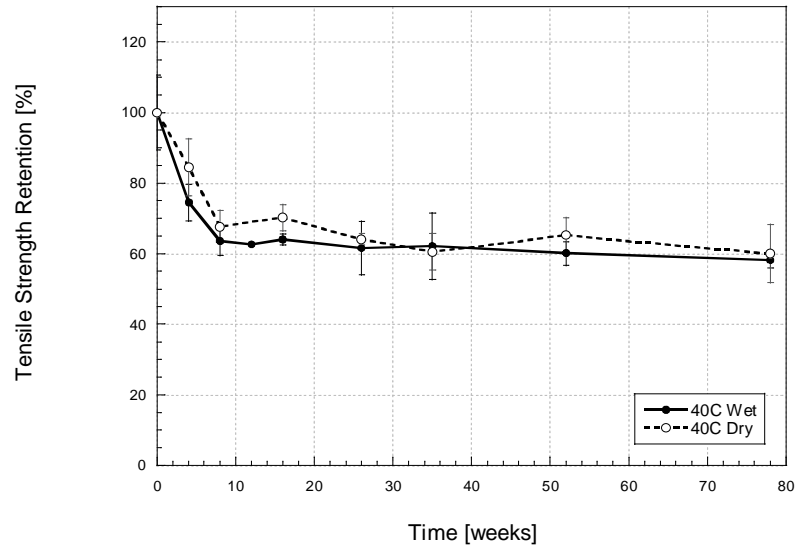


Figure 5.5b. Effect of Redrying on Tensile Strength Retention after Immersion 40°C in Seawater

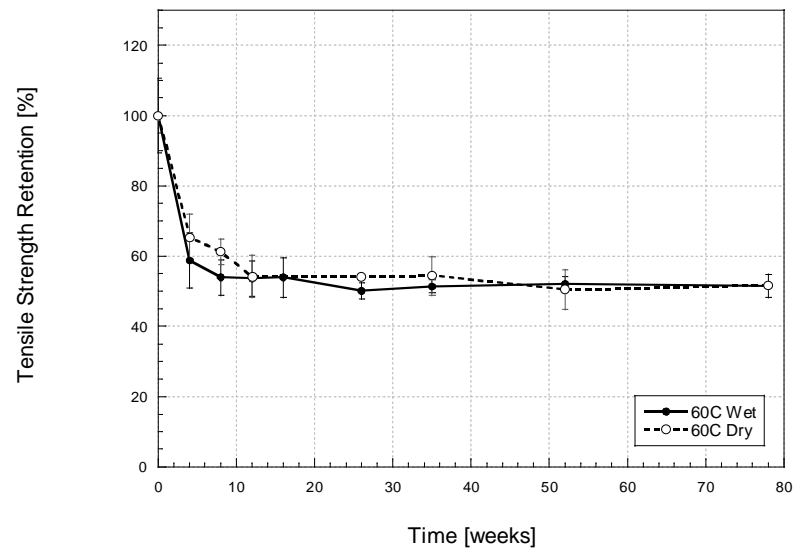


Figure 5.5c. Effect of Redrying on Tensile Strength Retention after Immersion 60°C in Seawater

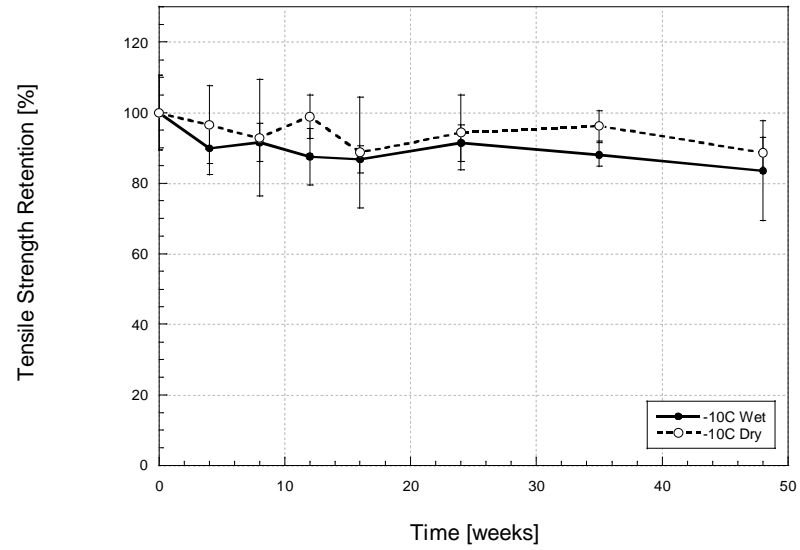


Figure 5.5d. Effect of Redrying on Tensile Strength Retention after Immersion -10°C in Seawater

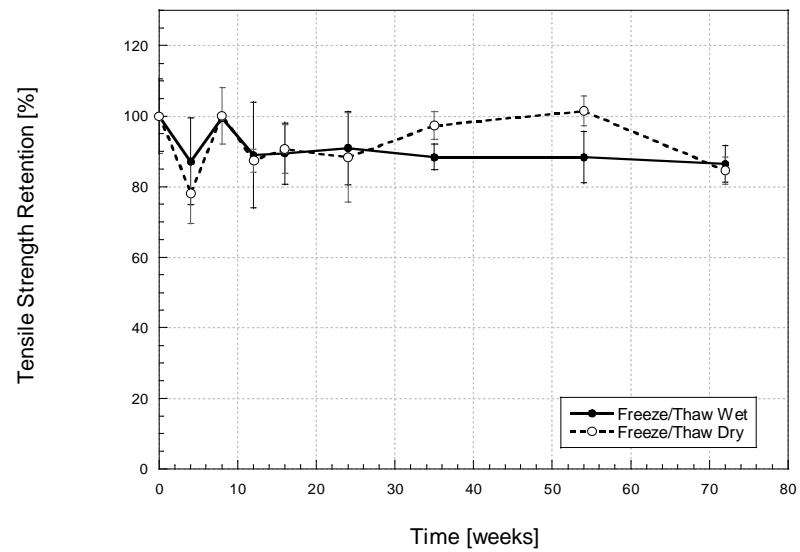


Figure 5.6a. Effect of Redrying on Tensile Strength After Exposure to Freeze/Thaw Condition

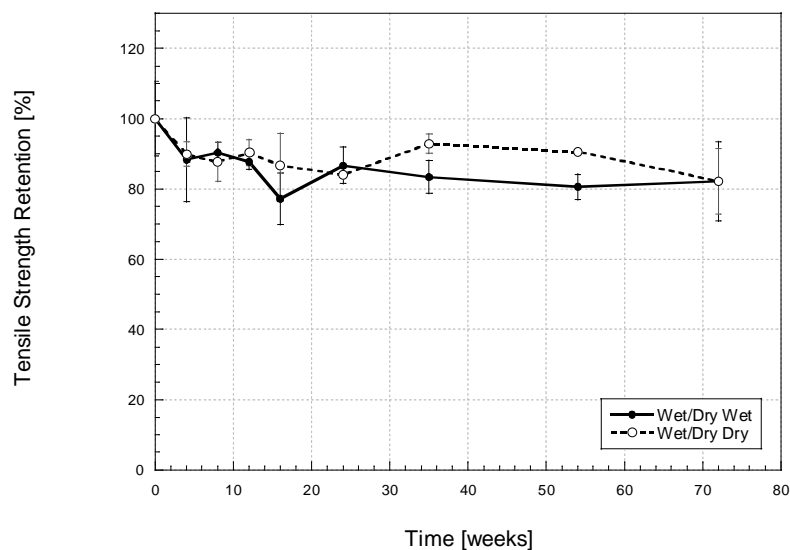


Figure 5.6b. Effect of Redrying on Tensile Strength After Exposure to Wet/Dry Condition

As seen from Figures 5.5 and 5.6 there is very little effect of redrying emphasizing that in general effects are largely irreversible. It is interesting to note that some level of regain is seen in the specimens exposed to -10°C conditions but that the results are within scatter bounds. Samples exposed to cyclic conditions appear to show effects of regain, but between the 24 and 72 week periods, suggesting that some of these could be due to reversal of swelling stresses and of crack closure, which could lead to erroneous interpretations since these are not truly reversible.

Degradation in strength due to exposure to environmental conditions can be reversible, irreversible, or a combination of both [36]. Initial degradation is usually associated with plasticization and has been found to be reversible upon drying [36]. Properties have been shown to provide partial, but not full regain [55,59]. To distinguish the effects of plasticization, a linear relationship of percent retention and weight gain, as shown in Figure 5.7 is utilized [107]. Because the slopes of the curves vary, it can be concluded that the effect of plasticization occurring in the 40°C and 60°C immersion occurs only prior to 4 weeks. Tension tests were not performed between 0 and 4 weeks, therefore it cannot be definitively concluded when plasticization occurs for these exposures.

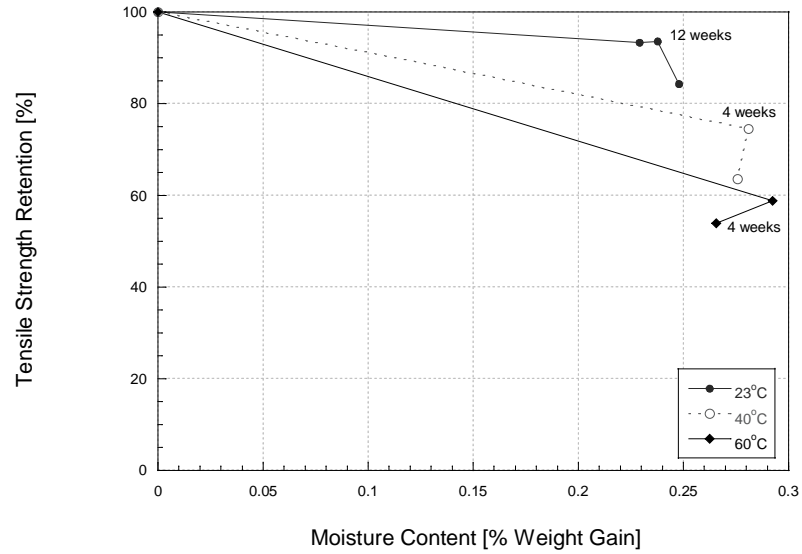


Figure 5.7. Relationship Between Moisture Content and Tensile Strength Retention for Specimens Immersed in 23°C, 40°C, and 60°C Seawater

5.2.2. Tensile Modulus

Changes in tensile modulus as a result of immersion in seawater, and after redrying are shown in Table 5.4 and Figure 5.8, whereas the corresponding results after cyclic exposure are shown in Table 5.5 and Figure 5.10. The effects of redrying are shown in Table 5.6 and Figures 5.11 and 5.12.

Table 5.4a. Tensile Modulus Determined At Ambient Conditions of 23°C and 30%RH

Time [weeks]	Ambient	
	E [GPa]	Std. Dev. [GPa]
0	37.4	1.0
4	33.9	1.5
8	35.8	0.4
12	33.8	3.5
16	37.8	-
24	30.9	3.1
32	34.6	3.2
48	31.3	2.4
72	29.7	1.4

Table 5.4b. Tensile Modulus Determined After Immersion in 23°C Seawater (“Wet” Testing) and as a Result of Subsequent Drying (“Dry Testing”)

Time [weeks]	23°C			
	<i>Wet Testing</i>		<i>Dry Testing</i>	
	E [GPa]	Std. Dev. [GPa]	E [GPa]	Std. Dev. [GPa]
0	37.4	1.0	37.4	1.0
4	33.0	2.5	34.7	0.5
8	36.4	3.7	34.8	1.8
12	36.8	2.1	33.4	4.0
16	33.3	3.3	34.2	2.1
26	34.2	0.6	32.3	0.5
35	30.2	-	-	-
52	30.0	0.3	33.6	4.9
78	30.1	-	28.0	2.4

Table 5.4c. Tensile Modulus Determined After Immersion in 40°C Seawater (“Wet” Testing) and as a Result of Subsequent Drying (“Dry Testing”)

Time [weeks]	40°C			
	<i>Wet Testing</i>		<i>Dry Testing</i>	
	E [GPa]	Std. Dev. [GPa]	E [GPa]	Std. Dev. [GPa]
0	37.4	1.0	37.4	1.0
4	35.9	4.1	37.1	1.3
8	34.4	2.7	-	-
12	34.3	1.1	-	-
16	35.2	3.6	34.8	2.6
26	29.2	4.4	32.6	2.3
35	34.2	3.5	32.9	0.5
52	30.0	5.0	29.9	4.5
78	32.3	0.4	27.5	2.2

Table 5.4d. Tensile Modulus Determined After Immersion in 60°C Seawater (“Wet” Testing) and as a Result of Subsequent Drying (“Dry Testing”)

Time [weeks]	60°C			
	<i>Wet Testing</i>		<i>Dry Testing</i>	
	E [GPa]	Std. Dev. [GPa]	E [GPa]	Std. Dev. [GPa]
0	37.4	1.0	37.4	1.0
4	39.1	1.9	33.1	1.6
8	29.2	1.4	28.8	2.0
12	29.3	3.1	27.6	3.1
16	34.2	4.1	-	-
26	32.6	4.6	33.7	6.3
35	30.9	1.6	32.3	2.7
52	30.7	6.0	31.7	2.5
78	26.1	4.7	25.7	4.1

Table 5.4e. Tensile Modulus Determined After Immersion in -10°C Seawater (“Wet” Testing) and as a Result of Subsequent Drying (“Dry Testing”)

Time [weeks]	-10°C			
	<i>Wet Testing</i>		<i>Dry Testing</i>	
	E [GPa]	Std. Dev. [GPa]	E [GPa]	Std. Dev. [GPa]
0	37.4	1.0	37.4	1.0
4	27.3	3.8	36.8	7.8
8	27.3	1.6	34.5	0.9
12	30.6	3.6	28.7	1.7
16	27.5	2.5	29.7	2.9
24	25.2	3.2	34.0	3.6
35	26.9	2.3	31.3	1.7
48	27.2	1.4	29.6	2.4
72				

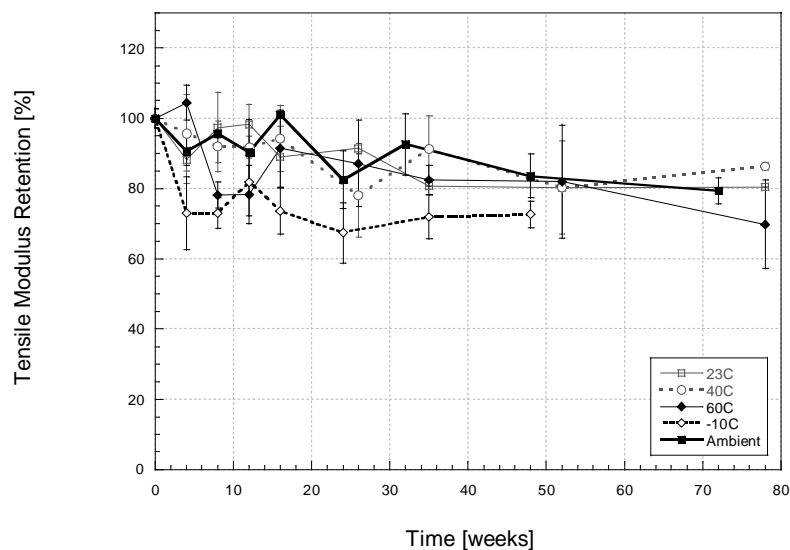


Figure 5.8. Change in Tensile Modulus as a Function of Temperature and Time of Immersion in Seawater

Tension specimens subjected to immersion temperatures of 23°C, 40°C, and 60°C seawater show minimal changes in modulus with a level of fluctuating behavior. The initial fluctuations in tensile modulus can be due to effects of residual cure. Vinyl ester based composites manufactured under ambient cure have shown to result in incomplete polymerization. Full

polymerization progresses over extended periods of time [55]. Immersion in seawater shows a maximum change of 20% at 78 weeks. Immersion at 40°C shows a maximum change of 22% at 26 weeks after which there is a minor increase, albeit still within scatter bounds. At 60°C immersion, larger scatter is noticed with changes at a maximum of 30% at 78 weeks.

In general, the increase in temperature of immersion causes an increase in degradation of the modulus [58]. As shown from the results above, degradation for this study was 20%, 22%, and 30% for 23°C, 40°C, and 60°C immersion in seawater. Accordingly, the small changes in modulus are in agreement with the results of a number of researchers who have shown that immersion in saline solution at room temperature and elevated temperatures have small effects on the tensile modulus [2,18,55,68,71,74,85]. Decreases in tensile modulus result from the diffusion of Na particles and moisture through cracks that propagate from fiber/matrix debonding [18]. Figure 5.9 shows a SEM micrograph demonstrating the amount of fiber/matrix debonding that occurs.

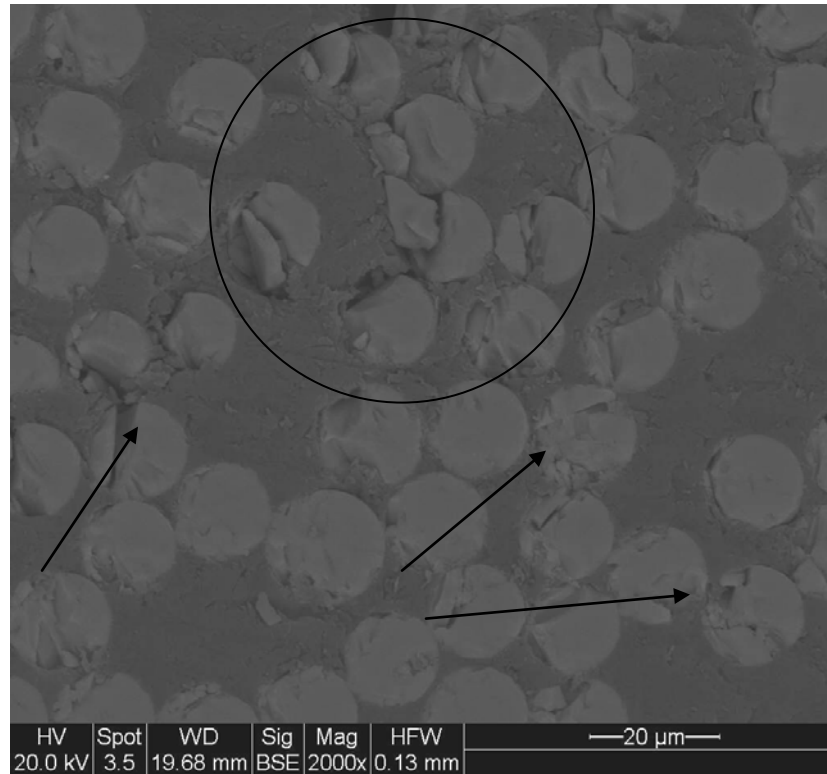


Figure 5.9. SEM Micrograph Demonstrating Degree of Fiber/Matrix Debonding After Exposure to 60°C Seawater for 78 weeks

Exposure to freezing conditions shows a more stable pattern in tensile modulus, where from 8-48 weeks a change on average of 30% is observed. While freezing has previously shown to increase stiffness [46], the initial saturation over an 8-month period governs the drop in modulus and freezing provides stability in the network.

The following section reviews the changes in tensile modulus after exposure to cyclic conditions.

Table 5.5a. Tensile Modulus Determined After Exposure to Freeze/Thaw Cycle (“Wet” Testing) and as a Result of Subsequent Drying (“Dry Testing”)

Time [weeks]	Freeze/Thaw			
	<i>Wet Testing</i>		<i>Dry Testing</i>	
	E [GPa]	Std. Dev. [GPa]	E [GPa]	Std. Dev. [GPa]
0	37.4	1.0	37.4	1.0
4	30.9	3.1	36.8	2.9
8	37.6	0.5	35.1	2.2
12	33.4	3.2	31.4	1.9
16	31.7	1.4	30.3	0.0
24	33.3	2.2	27.9	3.6
35	27.9	1.5	32.1	0.7
54	29.5	2.4	30.5	2.2
72	28.1	4.0	24.2	2.8

Table 5.5b. Tensile Modulus Determined After Exposure to Wet/Dry Cycle (“Wet” Testing) and as a Result of Subsequent Drying (“Dry Testing”)

Time [weeks]	Wet/Dry			
	<i>Wet Testing</i>		<i>Dry Testing</i>	
	E [GPa]	Std. Dev. [GPa]	E [GPa]	Std. Dev. [GPa]
0	37.4	1.0	37.4	1.0
4	30.7	0.8	34.4	4.9
8	32.2	1.5	33.3	0.7
12	31.6	0.3	30.6	1.3
16	31.4	0.7	30.7	0.1
24	34.7	0.9	29.3	1.1
35	26.7	5.4	30.4	2.5
54	26.4	5.5	33.1	3.5
72	27.3	2.6	27.5	0.6

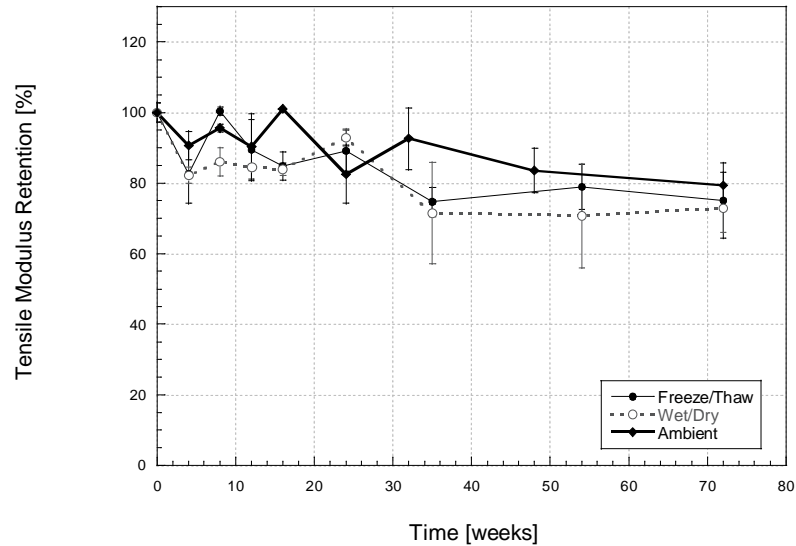


Figure 5.10. Change in Tensile Modulus as a Function of Time and Type of Cyclic Exposure

Cycling shows large standard deviations in modulus and a fluctuating behavior. Wet/Dry cycling has a more severe effect than freeze/thaw cycling. For specimens subjected to freeze/thaw cycling, maximum changes of 25% occur at 32 weeks. Specimens subjected to wet/dry cycling experience an average change of 30% at 48 weeks. Similar reductions in tensile modulus due to freeze/thaw cycling were found by Karbhari et al. [46] and Zhang et al. [47]. Previous results found from wet/dry cycling were similar in magnitude of change [18,100]. Larger reductions in tensile modulus from wet/dry cycling arise from the wicking of moisture through the increased amount of microcracks introduced from the cyclic exposure.

The following section reviews the effect of redrying for all exposures after being redried in a conditioning chamber for 30 days at 23°C and 30%RH.

Table 5.6a. Effect of Redrying for Tensile Modulus After Immersion In Seawater

Time [weeks]	Regain [%]		
	23°C	40°C	60°C
0	100.0	100.0	100.0
4	38.1	80.6	362.8
8	-172.4	-	-5.6
12	-509.3	-	-20.9
16	21.9	-20.7	-
26	-57.8	40.8	24.0
35	-	-38.8	21.3
52	48.0	-2.6	14.4
78	-28.3	-94.0	-3.6

Table 5.6b. Effect of Redrying for Tensile Modulus After Exposure to Freezing Conditions

Time [weeks]	Regain [%]
	-10°C
0	100.0
4	93.9
8	71.6
12	-27.9
16	22.2
26	72.3
35	42.3
52	23.1
78	

Table 5.6c. Effect of Redrying for Tensile Modulus After Exposure to Cycling Conditions

Time [weeks]	Regain [%]	
	Freeze/Thaw	Wet/Dry
0	100.0	100.0
4	91.1	55.2
8	1851.9	21.5
12	-50.6	-15.7
16	-24.7	-11.6
26	-132.1	-204.4
35	44.3	34.1
52	12.7	60.8
78	-41.3	2.1

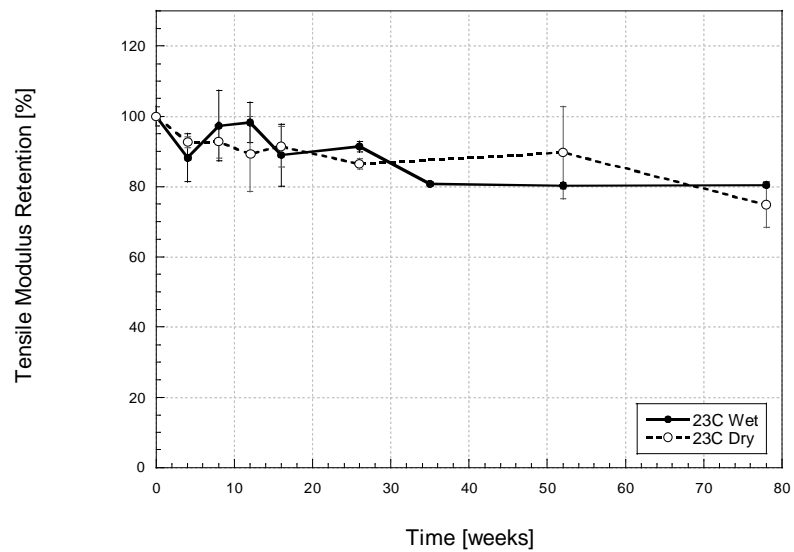


Figure 5.11a. Effect of Redrying on Tensile Modulus Retention after Immersion in 23°C Seawater

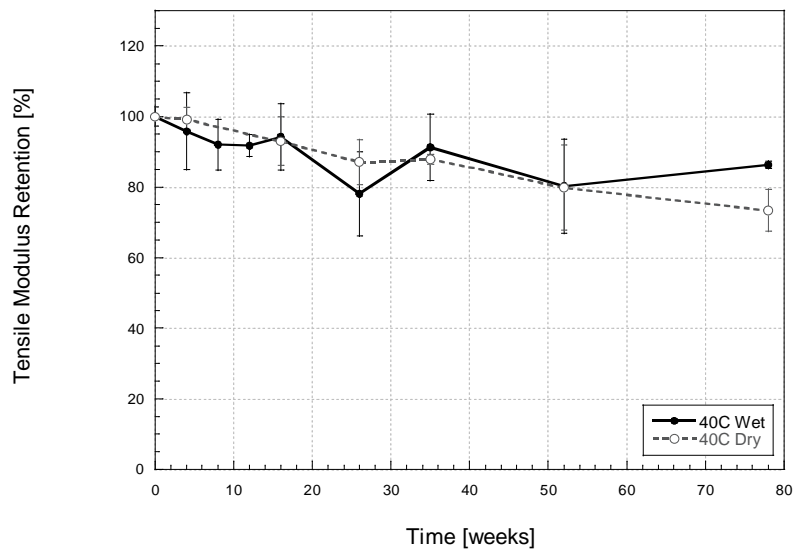


Figure 5.11b. Effect of Redrying on Tensile Modulus Retention after Immersion in 40°C Seawater

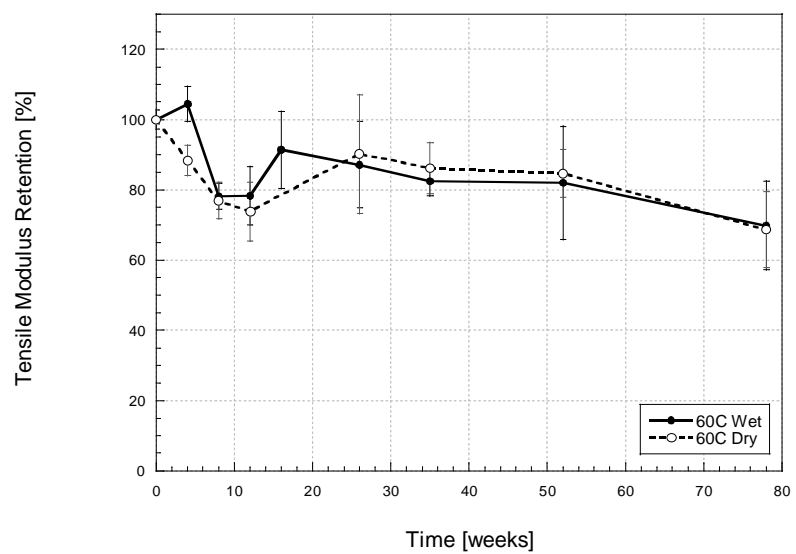


Figure 5.11c. Effect of Redrying on Tensile Modulus Retention after Immersion in 60°C Seawater

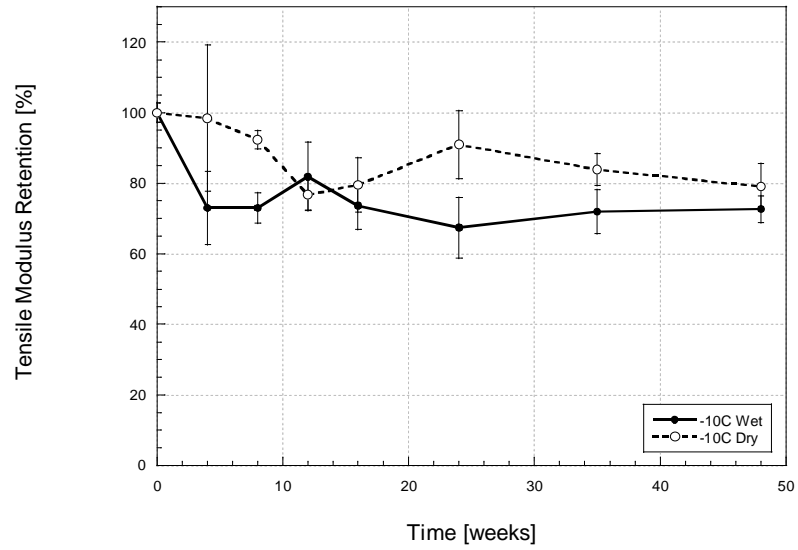


Figure 5.11d. Effect of Redrying on Tensile Modulus Retention after Immersion in -10°C Seawater

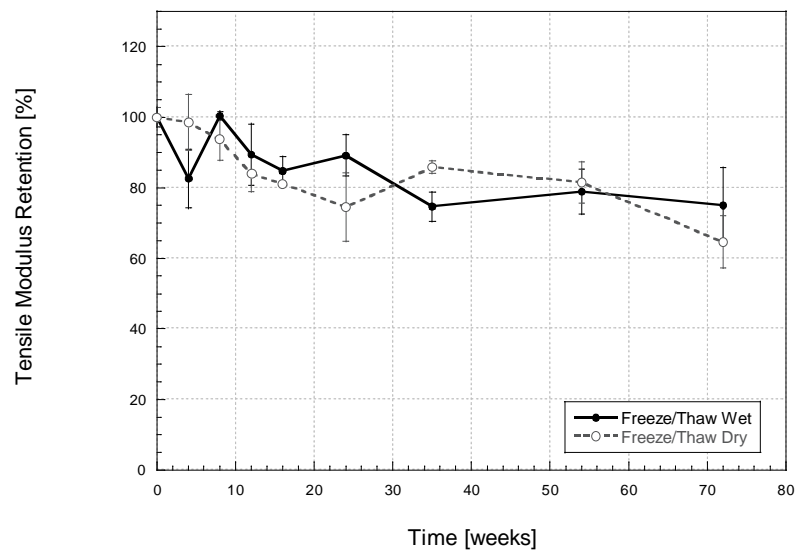


Figure 5.12a. Effect of Redrying on Tensile Modulus After Exposure to Freeze/Thaw Exposure

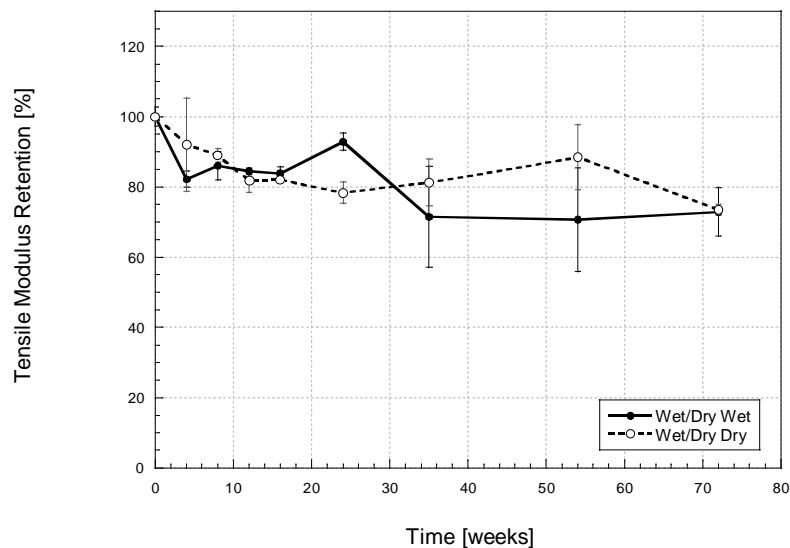


Figure 5.12b. Effect of Redrying on Tensile Modulus After Exposure to Wet/Dry Cycling

Referring to Figure 5.11 and 5.12, there seems to be little indication of regain in properties. Considering the substantial amount of scatter (such as in Figure 5.11a), the error bars are within bounds of the wet and dry properties. This is an indication that permanent degradation occurs.

5.2.3. Failure Modes

The failure mode for the immersed samples was constant throughout the experiment and was characterized by ASTM D3039 [91] as “XGM” (explosive, occurring in the gage length, middle). The failure typically occurred midspan of the specimen, however some tests yielded failures that were slightly off-centered. Failures that were not centered were attributed to the manufacturing process, which resulted in local resin-rich areas. Discoloration was observed in elevated immersion temperatures of 40 and 60°C and is illustrated in Figure 5.13. The discoloration is an indication of the Na particles present in seawater, which has shown to affect the fiber/matrix region [18]. Figure 5.13 also shows the explosive behavior that is most apparent in the specimens exposed to 23°C seawater. This behavior seemed to decrease with the elevation

in temperature of immersion. The figure shows typical failures after 78 weeks immersion in 23°C, 40°C, and 60°C seawater.

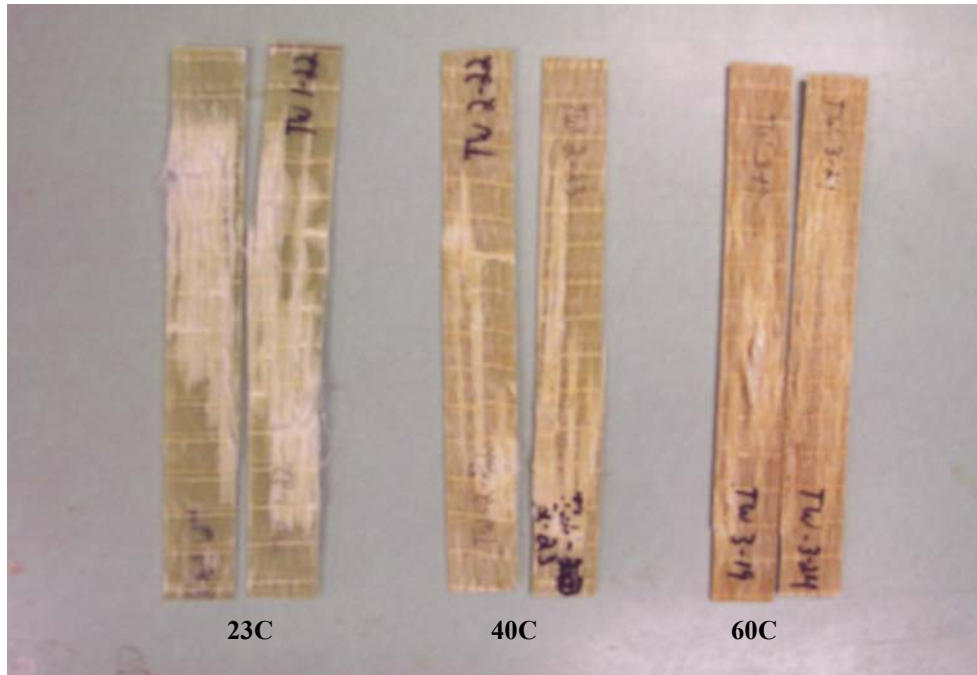


Figure 5.13. Failed Tension Specimens Immersed in 23°C, 40°C, and 60°C after 78 weeks

Explosive behavior also seemed to decrease with time for all immersion conditions. Figure 5.14 illustrates this trend for specimens immersed in 40°C seawater.

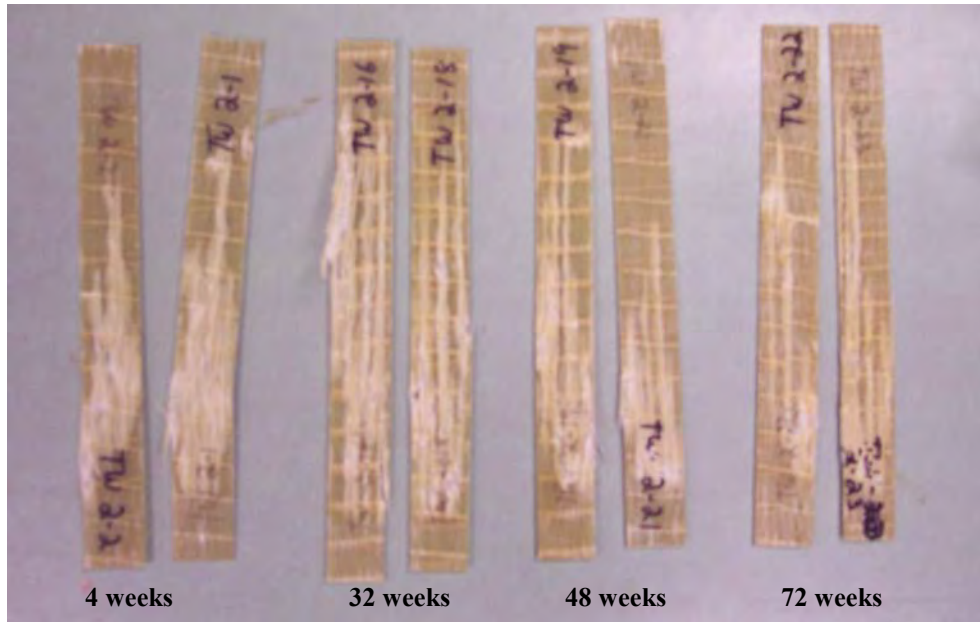


Figure 5.14. Failed Tension Specimens Immersed in 40°C Seawater for 4, 35, 52, and 78 weeks

Comparing the above failed specimens to typical control specimens stored in an environmental chamber at 23C and 30% RH, shows a considerable decrease in the amount of explosive intertow fracture behavior. Figure 5.15 shows failed tension samples that were unexposed to a seawater environment.

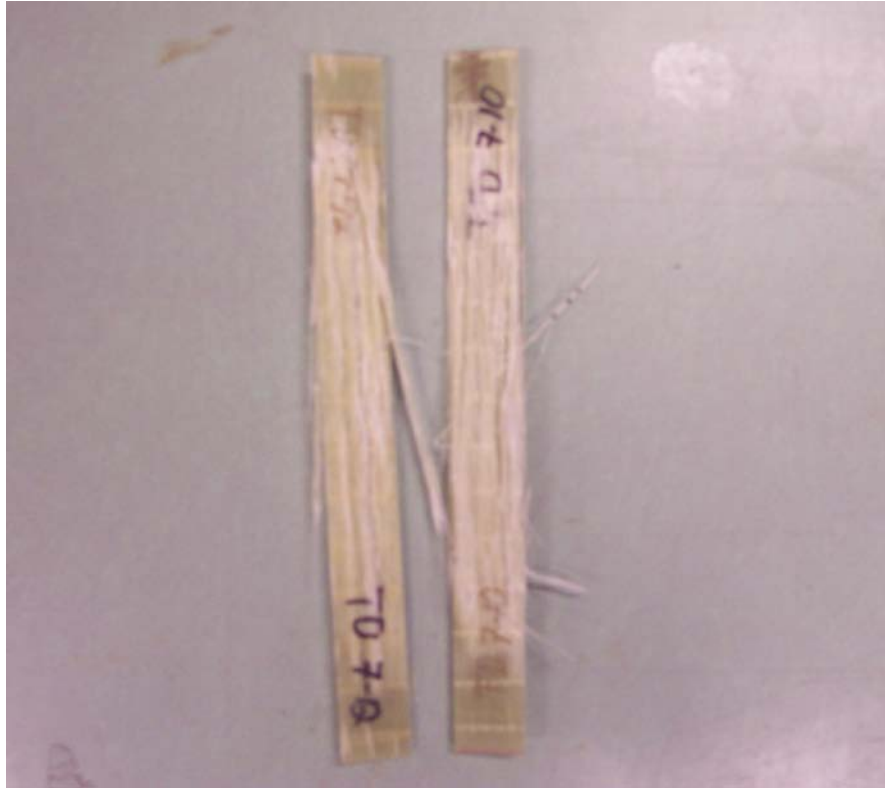


Figure 5.15. Typical Failed Tension Specimens, Unexposed

Failure modes did not change when exposed to cycling conditions. Figure 5.16 shows typical failed tension specimens after 72 weeks exposure for freeze/thaw and wet/dry conditions. Failure is similar to what is observed to unexposed specimens (shown in Figure 5.15).

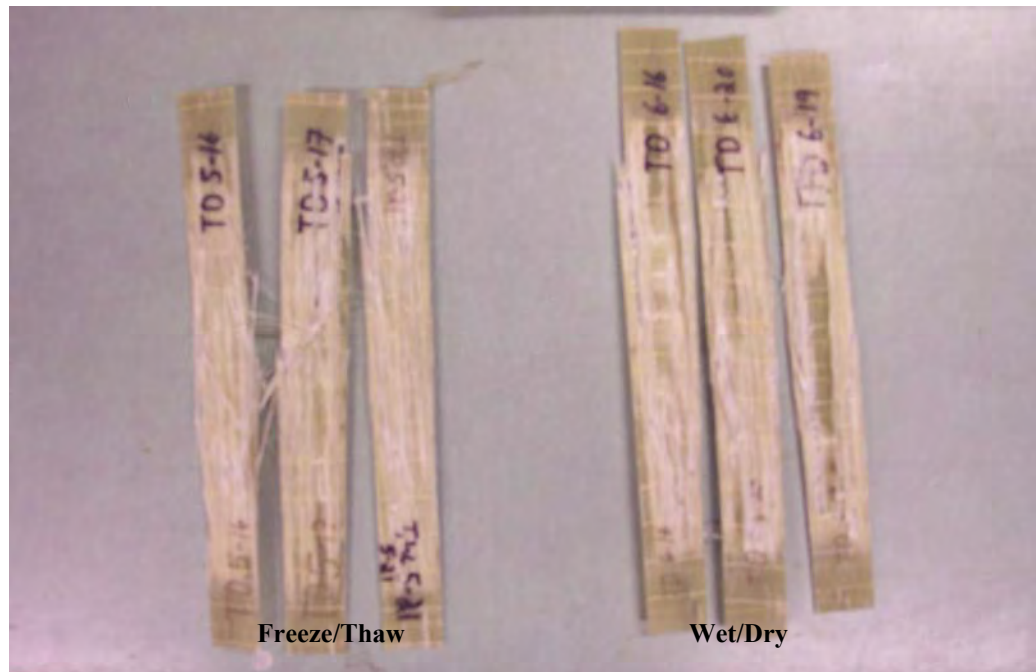


Figure 5.16. Failed Tension Specimens Subjected to Freeze/Thaw and Wet/Dry Cycling after 72 weeks

5.3. SUMMARY

The following highlights the significant findings for this section:

- Postcure is prevalent in tensile strength results for immersion in room temperature seawater
- Immersion at elevated temperatures reflect an increase in rate and level of degradation of tensile strength with temperature
- Freezing showed results similar to immersion in room temperature seawater, caused by initial saturation at room temperature seawater for 8 months
- Cycling showed significant fluctuations and larger levels of standard deviations due to matrix microcracking
- Plasticization occurs for 12 weeks at room temperature seawater; while immersion in elevated temperature shows plasticization occurred before 4 weeks, although the exact time period cannot be determined from the current data. Exposure to cycling showed

plasticization can not be the dominant mechanism because regain in properties was not achieved

- Failure modes remained constant throughout the experiment, however the amount of explosive behavior decreased with time and increase in immersion temperature
- Degradation at the fiber level does not occur in short-term immersion

CHAPTER 6 – FLEXURE

6.1. INTRODUCTION

Flexural data provide important characteristics of materials as related to structural response. However, since the flexural testing at coupon level subjects the material to a mixed state of stress and a stress gradient, it is difficult to derive values that can be directly used in design. Nonetheless, the determination of flexural characteristics and their change as a function of type and period of exposure is important and gives the engineer crucial data to understand the effects of exposure on long-term response. This is especially true in unidirectional composites wherein tensile strength is largely fiber dominated and hence may not provide a full picture of level of deterioration over the short term.

Flexural strength is defined as the strength of a material in bending, expressed as the stress on the outermost fibers of a bent test specimen, at the instance of failure. When exposed to moisture, both the resin and interface can be altered, thus changes in flexural characteristics can be expected even at time scales where no apparent changes are seen at the fiber level. As performed in the current study, tests were performed to establish the durability in flexure.

For a specimen supported in 3 point bending (simple beam supported at two points and loaded at midpoint), flexural strength is calculated as shown in equation 6-1.

$$\sigma_f = \frac{3PL}{2bd^2} \quad (6-1)$$

where:

σ_f is the stress in the outer fibers at midpoint in MPa,

P is the load at a given point in the load-deflection curve in N,

L is the support span in mm,

b is the width of the sample tested in mm, and

d is the depth of the sample tested in mm

The ultimate failure strength is found as the maximum of the calculated stresses.

The flexural modulus is determined as calculated in equation 6-2.

$$E_B = \frac{L^3 m}{4bd^3} \quad (6-2)$$

where:

E_B is the modulus of elasticity in bending in MPa,

L is the support span in mm,

b is the width of the sample tested in mm,

d is the depth of the sample tested in mm, and

m is the slope of the tangent to the initial straight-line portion of the load-deflection curve in N/mm.

Strains for the determination of the slope correspond to the predominantly linear region between stress levels of 50 and 300 MPa.

Percent regain is calculated according to equation 5-4.

6.2. RESULTS AND DISCUSSION

The following tables report the values of flexural strength and flexural modulus as a function of time for specimens after immersion, after cyclic exposure, and after redrying. Results for ambient specimens are also reported.

6.2.1. Flexural Strength

Changes in flexural strength as a result of immersion in seawater, and after redrying are shown in Table 6.1 and Figure 6.1, whereas the corresponding results after cyclic exposure are shown in Table 6.2 and Figure 6.5. The effects of redrying are shown in Figures 6.8 and 6.9. In the figures, percentage retention is determined by equation 6-3.

$$\% \text{ Retention} = \frac{P_t}{P_o} * 100 \quad (6-3)$$

where:

P_t is the property at time t and

P_o is the property in its as-received state.

Table 6.1a. Flexural Strength Determined At Ambient Conditions of 23°C and 30%RH

Time [weeks]	Ambient	
	σ [MPa]	Std. Dev. [MPa]
0	880.8	118.0
4	889.2	31.2
8	913.7	84.4
12	817.7	89.8
16	830.7	56.1
24	760.9	104.7
32	824.7	132.8
48	-	-
72	879.9	23.4

Table 6.1b. Flexural Strength Determined After Immersion in 23°C Seawater (“Wet” Testing) and as a Result of Subsequent Drying (“Dry Testing”)

Time [weeks]	23°C			
	<i>Wet Testing</i>		<i>Dry Testing</i>	
	σ [MPa]	Std. Dev. [MPa]	σ [MPa]	Std. Dev. [MPa]
0	880.8	118.0	880.8	118.0
4	760.6	69.9	811.8	77.2
8	759.5	112.8	801.0	83.5
12	690.3	86.4	770.1	26.9
16	680.8	41.2	-	-
26	677.0	54.8	756.0	175.6
35	620.4	70.8	771.5	74.0
52	651.7	104.7	774.3	91.4
78	623.1	103.0	749.9	74.0

Table 6.1c. Flexural Strength Determined After Immersion in 40°C Seawater (“Wet” Testing) and as a Result of Subsequent Drying (“Dry Testing”)

Time [weeks]	40°C			
	<i>Wet Testing</i>		<i>Dry Testing</i>	
	σ [MPa]	Std. Dev. [MPa]	σ [MPa]	Std. Dev. [MPa]
0	880.8	118.0	880.8	118.0
4	694.4	77.3	810.1	64.5
8	520.6	59.4	668.6	146.4
12	504.5	89.6	790.9	82.1
16	543.0	46.3	706.7	112.6
26	550.7	81.7	652.2	110.4
35	544.0	45.5	639.4	71.7
52	607.4	101.6	637.2	70.0
78	508.8	86.0	669.1	86.0

Table 6.1d. Flexural Strength Determined After Immersion in 60°C Seawater (“Wet” Testing) and as a Result of Subsequent Drying (“Dry Testing”)

Time [weeks]	60°C			
	<i>Wet Testing</i>		<i>Dry Testing</i>	
	σ [MPa]	Std. Dev. [MPa]	σ [MPa]	Std. Dev. [MPa]
0	880.8	118.0	880.8	118.0
4	616.4	79.4	779.6	89.6
8	540.3	60.4	689.7	94.3
12	493.5	64.2	683.4	54.8
16	487.4	126.4	683.4	54.8
26	422.9	88.6	542.9	88.7
35	453.7	31.0	500.4	77.9
52	404.2	29.7	518.3	31.1
78	393.2	76.2	503.1	46.8

Table 6.1e. Flexural Strength Determined After Immersion in -10°C Seawater (“Wet” Testing) and as a Result of Subsequent Drying (“Dry Testing”)

Time [weeks]	-10°C			
	<i>Wet Testing</i>		<i>Dry Testing</i>	
	σ [MPa]	Std. Dev. [MPa]	σ [MPa]	Std. Dev. [MPa]
0	880.8	118.0	880.8	118.0
4	798.1	114.2	808.6	81.2
8	733.1	120.5	832.0	86.5
12	749.4	68.5	808.6	59.0
16	683.2	138.2	792.8	56.8
24	683.2	138.2	767.2	44.3
35	700.7	53.8	770.8	79.2
48	667.2	111.7	806.2	110.9

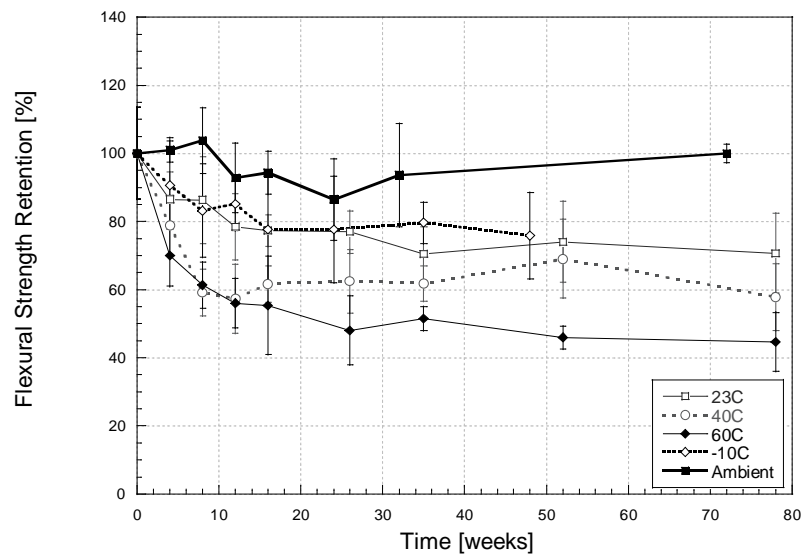


Figure 6.1. Change in Flexural Strength as a Function of Temperature and Time of Immersion in Seawater

As can be seen from Table 6.1 and Figure 6.1, immersion in seawater causes a decrease in flexural strength with the rate of decrease as well as the total amount of decrease increasing with the temperature of immersion. It is noted that a substantial portion of the decrease occurs in the first 16 weeks of immersion after which further changes are extremely slow. Figure 6.1 indicates that although immersion in seawater at 60°C environments is similar although it is slightly faster

at 60°C. This corresponds to the diffusion coefficients reported in Chapter 4, emphasizing the important and dominant role of moisture uptake on changes in flexural response.

Immersion in 23°C results in a decrease of 18% at the end of the 78 week period which compares well to results of Hodgkeiss et al. [48], Kootsookos and Mouritz [69], and Al-Bastaki and Al-Madani [76]. Previous research by Tucker [30] and Mazor et al. [87], however, indicated no change in flexural strength, whereas Liao et al [36], Macander and Silvergeit [67], and Gutierrez et al. [80] show smaller drops. In contrast, Fried and Graner [24] and Takanyagi and Kimpara [86] showed significantly higher levels of degradation although the severity could be ascribed to a number of aspects including exposure to an actual marine environment, degree of postcure, biofouling, exposure to ultraviolet radiation, and partial submergence.

Immersion in seawater at 40°C results in a low at 12 weeks followed by a slight increase in strength and equilibrium thereafter. Losses are on the order of 43% at 12 weeks and do not appear to drop below that level after that time period. The apparent slight increase in mean values of flexural strength have to be considered in relation to the increasing amounts of scatter. Rege and Lakkad [70] found similar changes in flexural strength when immersing in 40°C saline solution.

Immersion in seawater at 60°C also shows slowly changing values of flexural strength with the largest drop occurring at 72 weeks. Changes are on the order of 50% from 24 to 72 weeks. Figures 6.3 and 6.4 show SEM micrographs comparing levels of degradation as a result of immersion in seawater at 40 and 60°C for 4 weeks. Figure 6.2 provides the unexposed baseline.

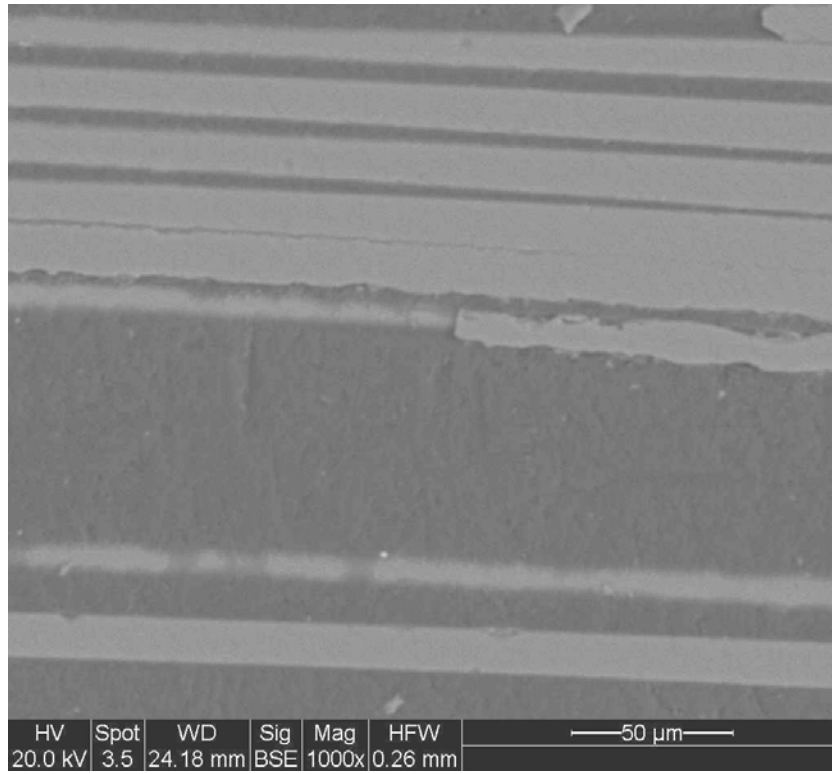


Figure 6.2. SEM Micrograph of E-glass/vinylester in As-Received State

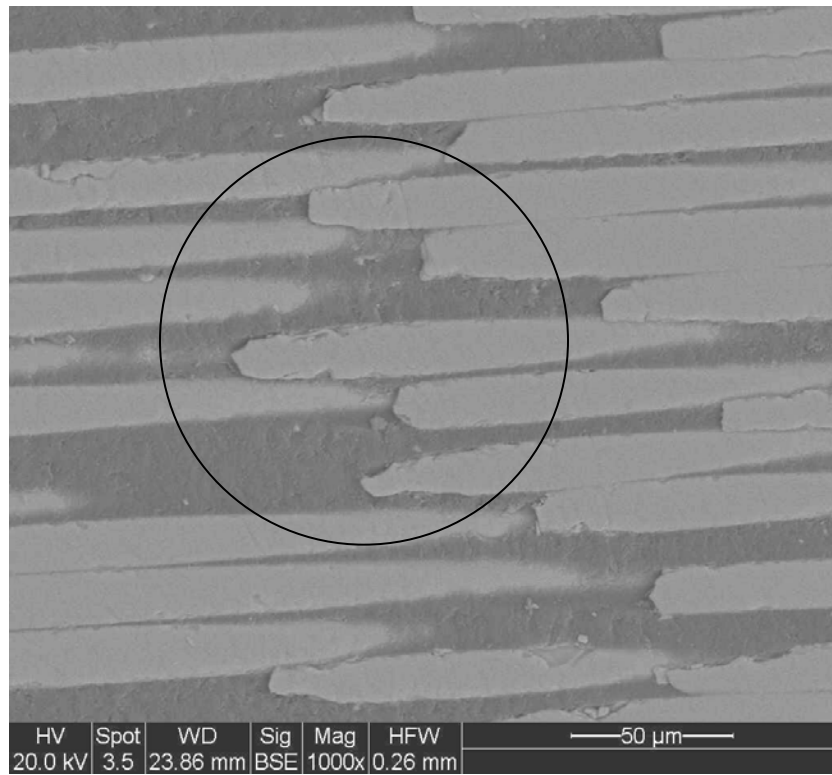


Figure 6.3. SEM Micrograph of E-glass/vinylester After Exposure to 40°C Seawater for 4 weeks

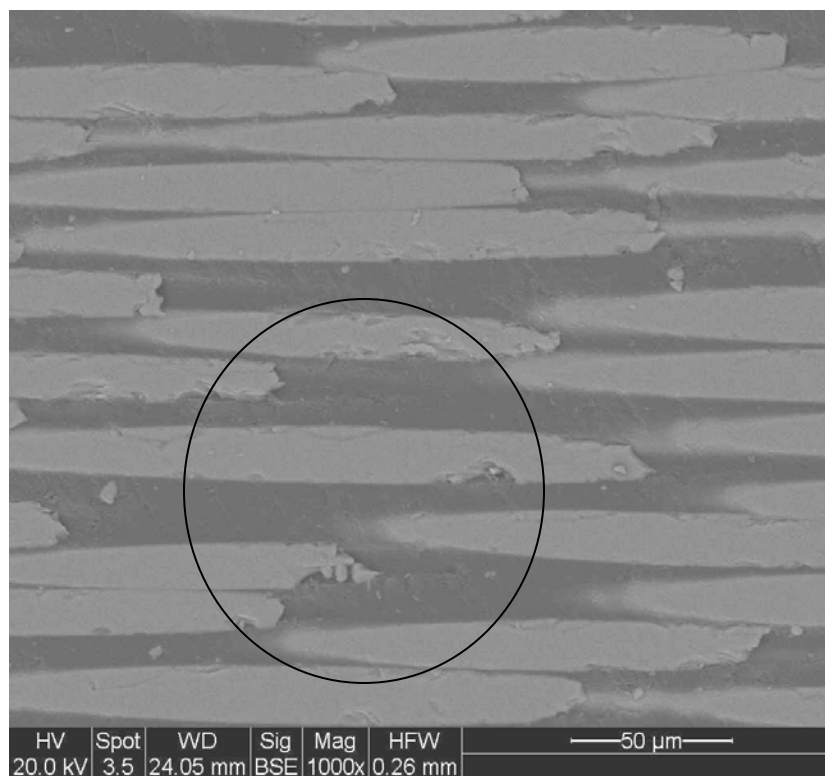


Figure 6.4. SEM Micrograph of E-glass/vinylester After Exposure to 60°C Seawater for 4 weeks

Figure 6.2 shows good adhesion between the fiber and the matrix, whereas in Figures 6.3 and 6.4 debond initiation can be noted with even fiber edge level degradation at the 60°C level.

Subramaniam et al. [33] hypothesized that the larger strength deterioration at elevated temperatures was due to the hydrophilic nature of glass, which has a tendency to sorb water on the surface, or due to the phenomenon of solvent crazing that occurs when solvent collects in cracks and voids [33]. Nakanishi and Shindo [17] noted that the larger amount of moisture that is in a sample, the larger the internal pressure that resides at the interface. At elevated temperatures, moisture diffusing at faster rates essentially causes interface cracks and premature failures.

A comparison of the effects due to immersion in seawater at 23°C and -10°C conditions after attainment of moisture uptake saturation shows that the overall response is similar emphasizing the dominating influence of moisture uptake. Changes in flexural strength reached

asymptotic behavior at 16 weeks. Jamond et al. exposed E-glass/vinyl ester composites subjected to a cold freezer (-13°C) for 9 months and did not find any changes in flexural strength [106].

Tables 6.2 and Figure 6.5 show the effect of cycling exposures on flexural strength.

Table 6.2a. Flexural Strength Determined After Exposure to Freeze/Thaw Cycling (“Wet” Testing) and as a Result of Subsequent Drying (“Dry Testing”)

Time [weeks]	Freeze/Thaw			
	<i>Wet Testing</i>		<i>Dry Testing</i>	
	σ [MPa]	Std. Dev. [MPa]	σ [MPa]	Std. Dev. [MPa]
0	880.8	118.0	880.8	118.0
4	726.0	56.9	794.6	176.8
8	680.1	118.7	737.4	46.5
12	682.1	100.7	694.1	154.3
16	622.4	111.1	803.1	63.2
24	686.2	81.0	905.2	30.5
35	717.9	14.3	752.2	79.0
54	719.8	39.9	774.6	98.9
72	722.5	36.7	-	-

Table 6.2b. Flexural Strength Determined After Exposure to Wet/Dry Cycling (“Wet” Testing) and as a Result of Subsequent Drying (“Dry Testing”)

Time [weeks]	Wet/Dry			
	Wet Testing		Dry Testing	
	σ [MPa]	Std. Dev. [MPa]	σ [MPa]	Std. Dev. [MPa]
0	880.8	118.0	880.8	118.0
4	771.0	102.1	781.1	77.3
8	749.6	100.2	846.5	110.4
12	695.4	77.3	820.8	100.0
16	649.3	41.6	807.3	86.1
24	675.4	31.2	870.5	62.4
35	689.2	92.5	755.0	54.0
54	661.2	143.1	771.2	141.5
72	629.3	69.3	798.7	77.7

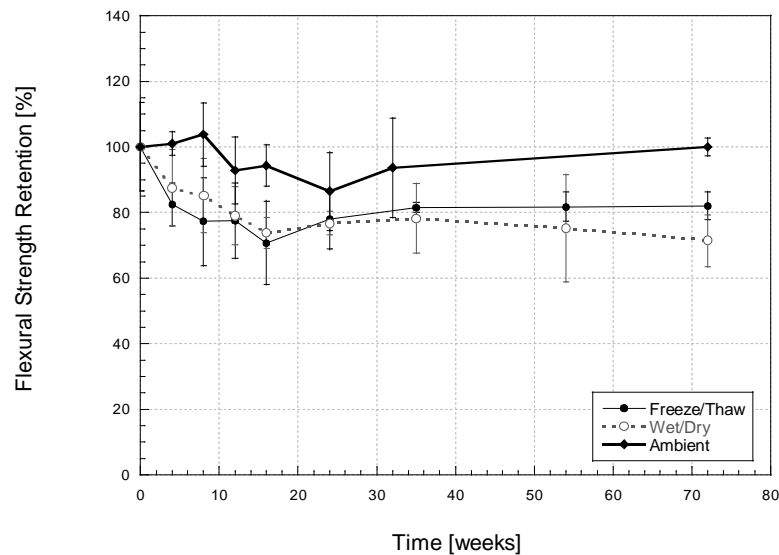


Figure 6.5. Change in Flexural Strength as a Function of Time and Type of Cyclic Exposure

When subjected to cycling conditions, freeze/thaw exposures result in a steady decrease between 4-16 weeks and reach equilibrium after about 24 weeks. Changes on an average of 20% occur from 4-72 weeks. Wet/dry cycling results in a larger level of standard deviations and a general retention of 75% from 16 to 72 weeks. The strength profiles are similar for flexural

strength properties although over longer periods there appear to be a slightly increasing level of degradation due to wet-dry cycling. Referring back to Chapter 5, the wet/dry condition was more severe than the freeze/thaw exposure for tensile properties. Tensile strength, however, is a fiber dominated property, and therefore the effect of microcracking due to cycling may not have been as prominent in tension as it is in flexure. Figures 6.6 and 6.7 show SEM micrographs of cross sections of the composite and similar levels of degradation for both cyclic exposures.

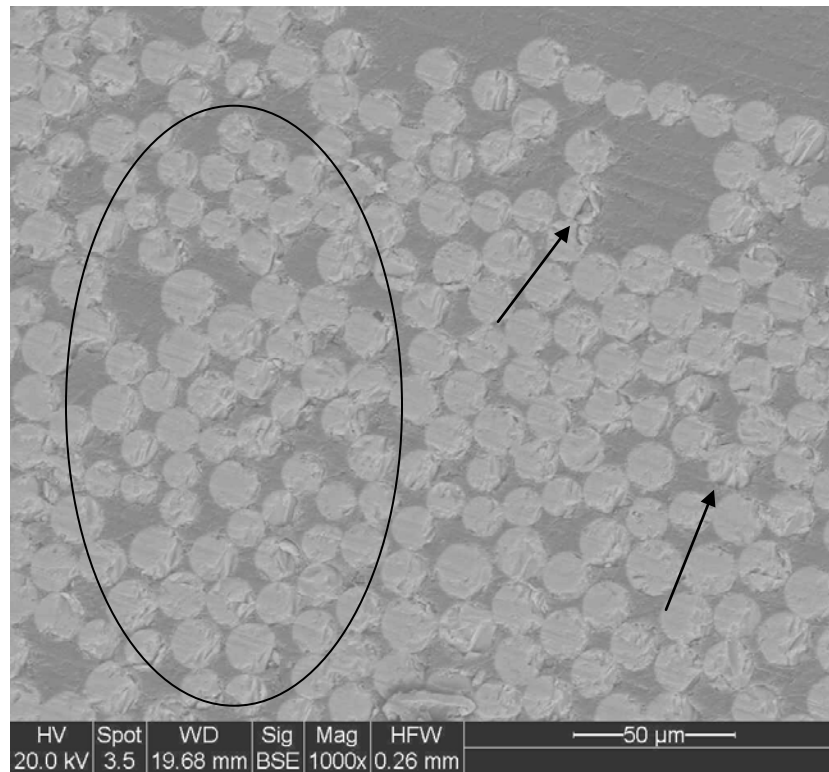


Figure 6.6. SEM Micrograph of E-glass/vinylester After Exposure to Freeze/Thaw Cycle for 72 weeks

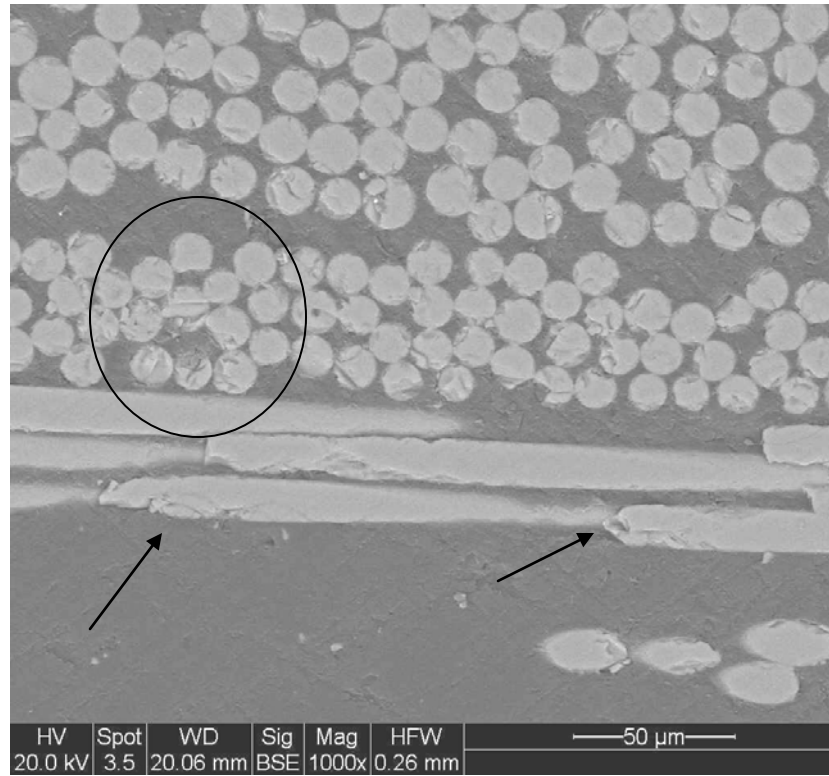


Figure 6.7. SEM Micrograph of E-glass/Vinylester After Exposure to Wet/Dry Cycle for 72 weeks

After exposure to immersion and cycling, specimens were tested after being redried in a conditioning chamber for 30 days at 23°C and 30%RH. Table 6.3 and Figures 6.5 and 6.6 demonstrate the effect of redrying.

Table 6.3a. Effect of Redrying for Flexural Strength After Immersion In Seawater

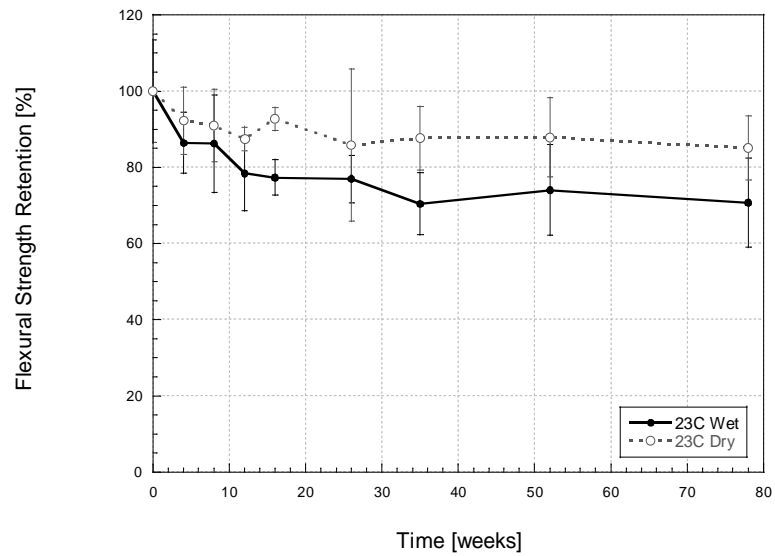
Time [weeks]	Regain [%]		
	23°C	40°C	60°C
0	100.0	100.0	100.0
4	42.6	62.1	61.7
8	34.2	41.1	43.9
12	41.9	76.1	49.0
16	67.9	48.5	49.8
26	38.8	30.8	26.2
35	58.0	28.3	11.0
52	53.5	10.9	23.9
78	49.2	43.1	22.5

Table 6.3b. Effect of Redrying for Flexural Strength After Exposure to Freezing Conditions

Time [weeks]	Regain [%]
	-10°C
0	100.0
4	12.8
8	67.0
12	45.0
16	55.5
26	42.5
35	38.9
52	65.1
78	

Table 6.3c. Effect of Redrying for Flexural Strength After Exposure to Cyclic Conditions

Time [weeks]	Regain [%]	
	Freeze/Thaw	Wet/Dry
0	100.0	100.0
4	44.3	9.2
8	28.6	73.9
12	6.0	67.7
16	69.9	68.3
26	-	95.0
35	21.1	34.4
52	34.0	50.1
78	-	67.4

**Figure 6.8a. Effect of Redrying on Flexural Strength Retention after Immersion at 23°C in Seawater**

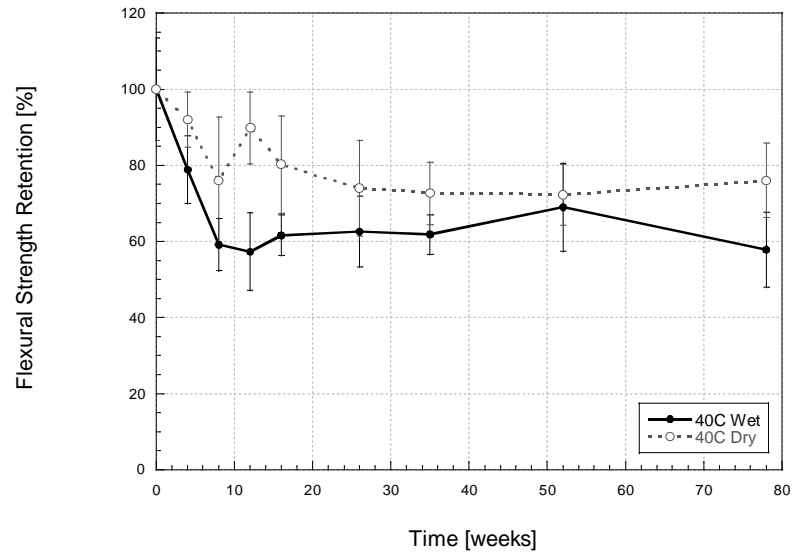


Figure 6.8b. Effect of Redrying on Flexural Strength Retention after Immersion at 40°C in Seawater

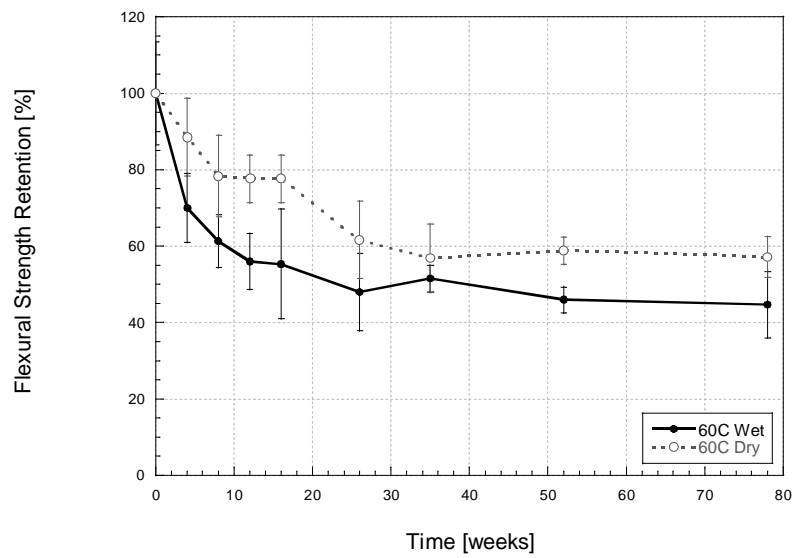


Figure 6.8c. Effect of Redrying on Flexural Strength Retention after Immersion at 60°C in Seawater

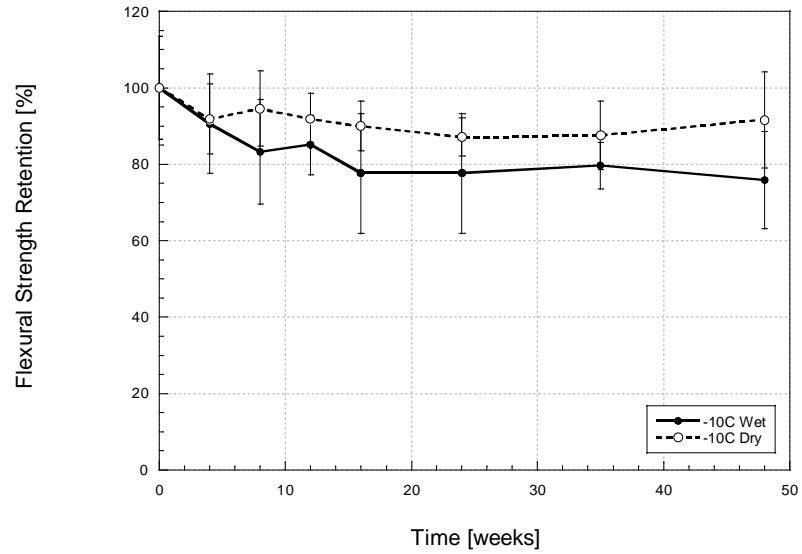


Figure 6.8d. Effect of Redrying on Flexural Strength Retention after Immersion at -10°C in Seawater

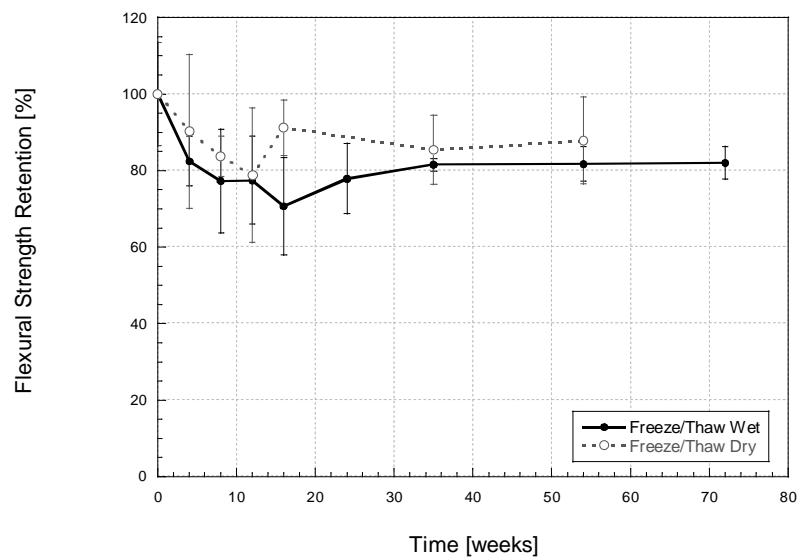


Figure 6.9a. Effect of Redrying on Flexural Strength After Exposure to Freeze/Thaw Condition

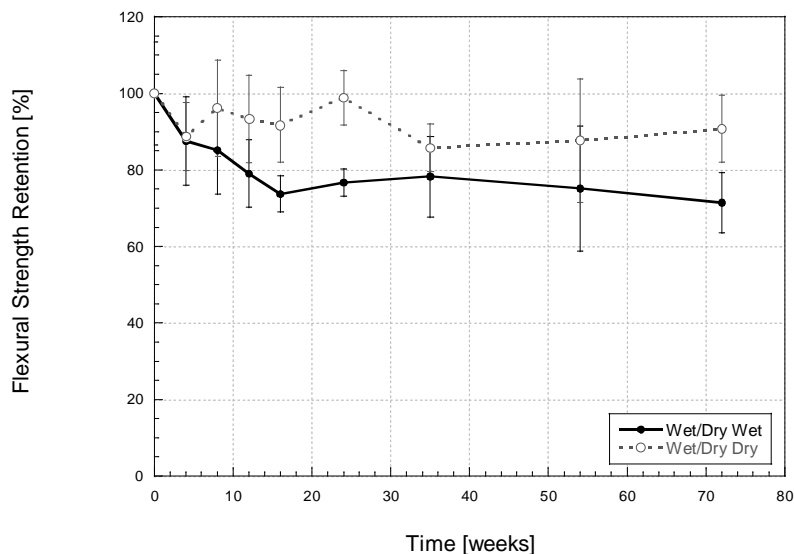


Figure 6.9b. Effect of Redrying on Flexural Strength After Exposure to Wet/Dry Condition

Redrying in a conditioning chamber at 23°C and 30% RH for thirty days results in partial regain as shown in Figure 6.8a. A plot of percent retention versus weight gain can provide indications of the periods of degradation can be attributed largely to plasticization. As described in Chapter 5, linear relationships can reflect the occurrence of plasticization once non-linearity in response as a function of moisture content is seen, other modes of degradation can be deemed present. As seen in Figure 6.10, plasticization may be dominant to 12 weeks in 23°C seawater. Trends for immersion in 40°C seawater and 60°C immersion show varying slopes, indicating that plasticization may be dominant only before 4 weeks. These conclusions are similar to those noted in Chapter 5. Application of this method towards cycling data shows a non-linearity, and therefore, the dominant degradation mechanism cannot be solely attributed to plasticization.

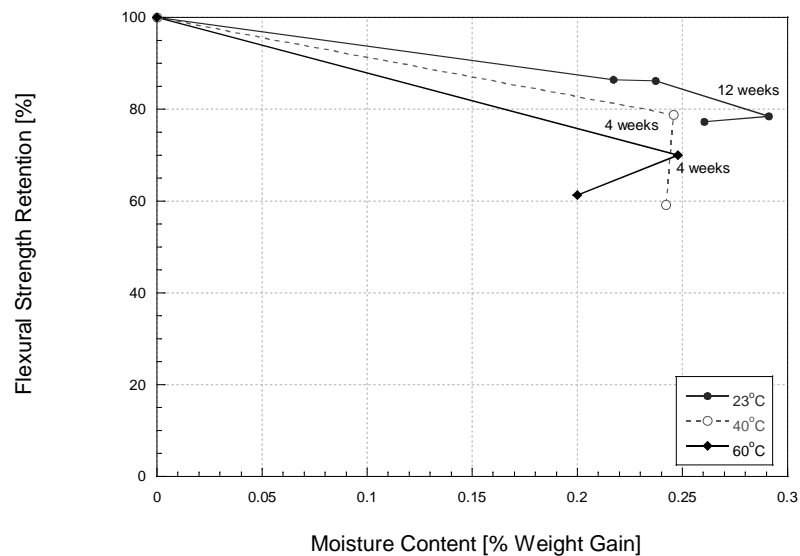


Figure 6.10. Relationship Between Moisture Content and Flexural Strength Retention for Specimens Immersed in 23°C, 40°C, and 60°C Seawater

6.2.2. Flexural Modulus

Changes in flexural modulus as a result of immersion in seawater, and after redrying are listed in Table 6.4 and Figure 6.11, whereas the corresponding results after cyclic exposure are shown in Table 6.5 and Figure 6.12. The effects of redrying are shown in Figures 6.13 and 6.14.

Table 6.4a. Flexural Modulus Determined At Ambient Conditions of 23°C and 30%RH

Time [weeks]	Ambient	
	E [GPa]	Std. Dev. [GPa]
0	26.9	1.3
4	29.5	1.7
8	29.5	2.7
12	24.0	2.0
16	24.0	3.3
24	30.8	3.2
32	28.8	2.5
48	33.8	1.1
72	29.6	2.0

Table 6.4b. Flexural Modulus Determined After Immersion in 23°C Seawater (“Wet” Testing) and as a Result of Subsequent Drying (“Dry Testing”)

Time [weeks]	23°C			
	<i>Wet Testing</i>		<i>Dry Testing</i>	
	E [GPa]	Std. Dev. [GPa]	E [GPa]	Std. Dev. [GPa]
0	26.9	1.3	26.9	1.3
4	24.4	1.3	26.0	2.0
8	27.5	0.9	30.0	1.6
12	29.9	1.3	25.4	1.4
16	23.8	1.5	26.0	2.3
26	23.8	2.9	26.3	1.0
35	22.4	0.3	25.3	1.3
52	-	-	28.6	2.1
78	24.4	1.9	23.8	1.6

Table 6.4c. Flexural Modulus Determined After Immersion in 40°C Seawater (“Wet” Testing) and as a Result of Subsequent Drying (“Dry Testing”)

Time [weeks]	40°C			
	<i>Wet Testing</i>		<i>Dry Testing</i>	
	E [GPa]	Std. Dev. [GPa]	E [GPa]	Std. Dev. [GPa]
0	26.9	1.3	26.9	1.3
4	27.4	2.6	26.8	3.4
8	24.2	1.4	23.3	1.9
12	23.0	2.1	28.2	2.1
16	29.9	5.3	26.2	3.0
26	24.2	1.1	26.4	2.8
35	26.3	1.9	25.1	1.3
52	26.2	2.4	27.2	6.2
78	25.6	2.8	24.8	1.7

Table 6.4d. Flexural Modulus Determined After Immersion in 60°C Seawater (“Wet” Testing) and as a Result of Subsequent Drying (“Dry Testing”)

Time [weeks]	60°C			
	<i>Wet Testing</i>		<i>Dry Testing</i>	
	E [GPa]	Std. Dev. [GPa]	E [GPa]	Std. Dev. [GPa]
0	26.9	1.3	26.9	1.3
4	25.5	1.0	25.1	0.9
8	24.0	2.5	23.9	1.0
12	24.1	0.9	23.9	1.7
16	25.2	1.8	23.9	1.7
26	22.4	2.6	23.5	4.6
35	24.4	2.4	24.4	2.0
52	24.9	3.6	24.1	1.0
78	25.7	2.6	25.8	1.3

Table 6.4e. Flexural Modulus Determined After Immersion in -10°C Seawater (“Wet” Testing) and as a Result of Subsequent Drying (“Dry Testing”)

Time [weeks]	-10°C			
	<i>Wet Testing</i>		<i>Dry Testing</i>	
	E [GPa]	Std. Dev. [GPa]	E [GPa]	Std. Dev. [GPa]
0	26.9	1.3	26.9	1.3
4	29.6	0.3	29.1	2.6
8	29.2	2.1	28.2	2.0
12	25.3	1.7	25.2	1.1
16	27.1	2.2	25.6	2.5
24	27.1	2.2	22.8	2.9
35	-	-	25.5	1.6
48	27.0	2.6	27.7	0.1
72				

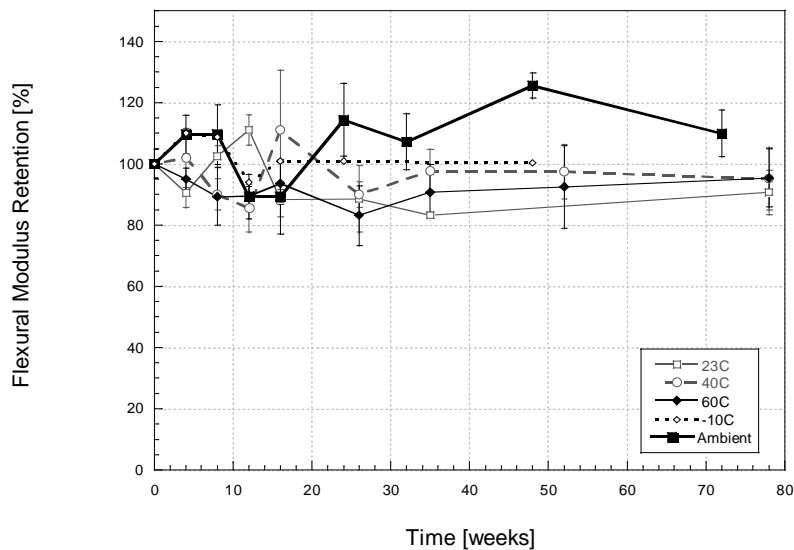


Figure 6.11. Change in Flexural Modulus as a Function of Temperature and Time of Immersion in Seawater

Similar to results reported earlier in [2,4,6,7,10,15] the reduction in modulus is less than that in strength with the maximum change over the 72 week period being 4-9%.

In contrast to changes in the flexural strength due to exposure, flexural modulus results showed immersion in seawater at -10°C did not reflect the trends typical of the initial saturation in room temperature seawater for 8 months. Modulus values exceeded as-received conditions and showed retention up to 109%. The increased brittleness of the network introduced by freezing conditions provided the modulus increase. Increases of 11% were observed by Jamond et al. [106] who exposed a glass/polyester composite to freezing conditions.

The following section reviews the changes in tensile modulus after exposure to cyclic conditions.

Table 6.5a. Flexural Modulus Determined After Exposure to Freeze/Thaw Cycle (“Wet” Testing) and as a Result of Subsequent Drying (“Dry Testing”)

Time [weeks]	Freeze/Thaw			
	<i>Wet Testing</i>		<i>Dry Testing</i>	
	E [GPa]	Std. Dev. [GPa]	E [GPa]	Std. Dev. [GPa]
0	26.9	1.3	26.9	1.3
4	22.5	1.6	35.9	2.9
8	-	-	24.5	3.0
12	24.0	3.2	32.0	3.0
16	30.8	0.7	26.9	4.2
24	23.8	2.2	25.5	1.6
35	24.7	1.1	25.4	1.6
54	26.3	1.8	23.0	1.7
72	25.9	3.0	28.4	-

Table 6.5b. Flexural Modulus Determined After Exposure to Wet/Dry Cycle (“Wet” Testing) and as a Result of Subsequent Drying (“Dry Testing”)

Time [weeks]	Wet/Dry			
	<i>Wet Testing</i>		<i>Dry Testing</i>	
	E [GPa]	Std. Dev. [GPa]	E [GPa]	Std. Dev. [GPa]
0	26.9	1.3	26.9	1.3
4	25.1	2.5	32.1	6.2
8	-	-	28.4	1.5
12	24.3	3.3	28.0	1.0
16	27.1	1.6	24.4	2.6
24	23.9	2.6	28.4	1.7
35	25.0	2.2	28.6	2.5
54	27.2	0.3	24.0	7.1
72	24.5	2.5	28.8	3.2

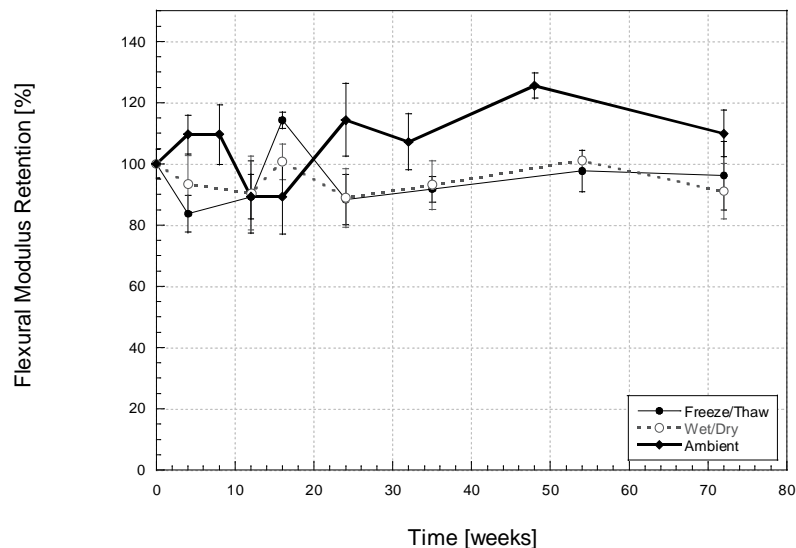


Figure 6.12. Change in Flexural Modulus as a Function of Time and Type of Cyclic Exposure

Cycling conditions also did not show any significant effects due to exposure. In general, flexural modulus values exceeded as-received conditions and initially provided fluctuating values as characteristic of cycling conditions.

Table 6.6 and Figures 6.13 and 6.14 show the effect of redrying in a conditioning chamber for 30 days at 23°C and 30% RH.

Table 6.6a. Effect of Redrying for Flexural Modulus After Immersion In Seawater

Time [weeks]	Regain [%]		
	23°C	40°C	60°C
0	100.0	100.0	100.0
4	64.9	129.3	-29.5
8	-392.4	-35.5	-5.7
12	149.2	133.7	-7.3
16	72.1	125.3	-77.3
26	79.6	81.7	25.7
35	65.1	-	191.7
52	-	138.7	-37.9
78	-25.3	-62.5	9.1

Table 6.6b. Effect of Redrying for Flexural Modulus After Exposure to Freezing Conditions

Time [weeks]	Regain [%]	
	-10°C	
0	100.0	
4	19.0	
8	46.3	
12	-4.0	
16	763.5	
26	2115.8	
35	-	
52	-851.6	
78		

Table 6.6c. Effect of Redrying for Flexural Modulus After Exposure to Cycling Conditions

Time [weeks]	Regain [%]	
	Freeze/Thaw	Wet/Dry
0	100.0	100.0
4	304.1	394.7
8	-	-
12	273.8	142.1
16	100.7	1694.5
26	55.5	149.8
35	32.2	189.4
52	-540.5	1047.9
78	238.8	179.6

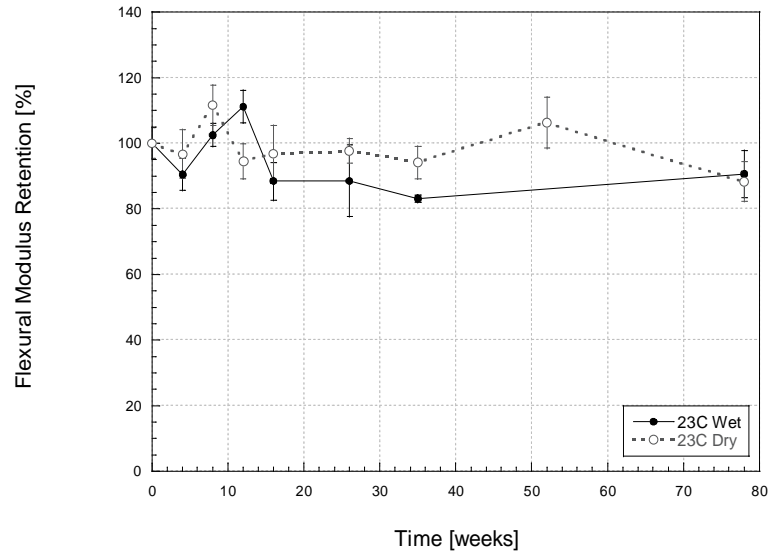


Figure 6.13a. Effect of Redrying on Flexural Modulus Retention after Immersion in 23°C Seawater

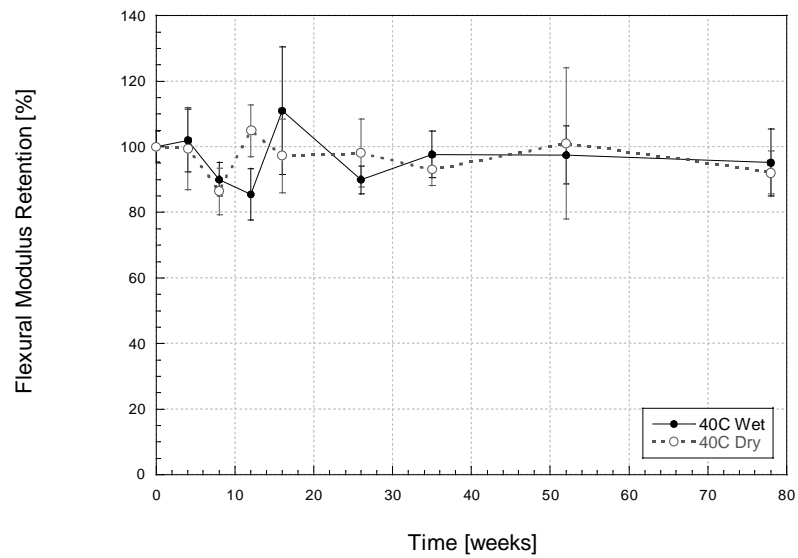


Figure 6.13b. Effect of Redrying on Flexural Modulus Retention after Immersion in 40°C Seawater

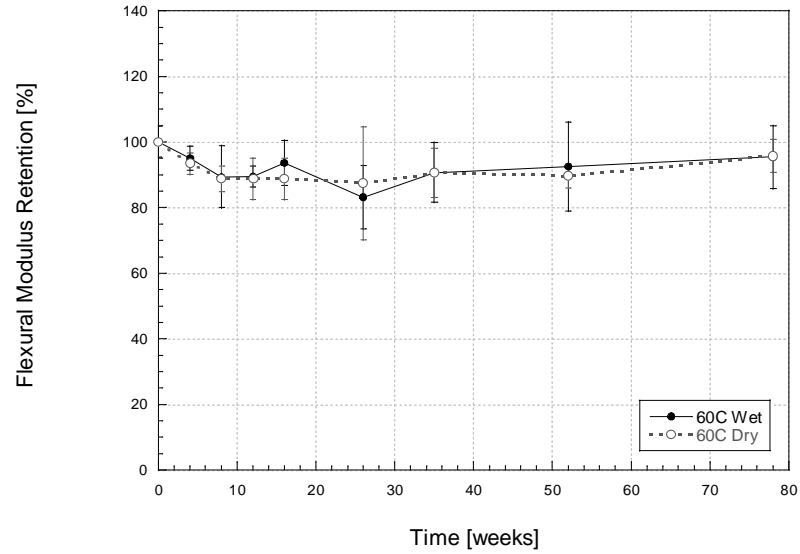


Figure 6.13c. Effect of Redrying on Flexural Modulus Retention after Immersion in 60°C Seawater

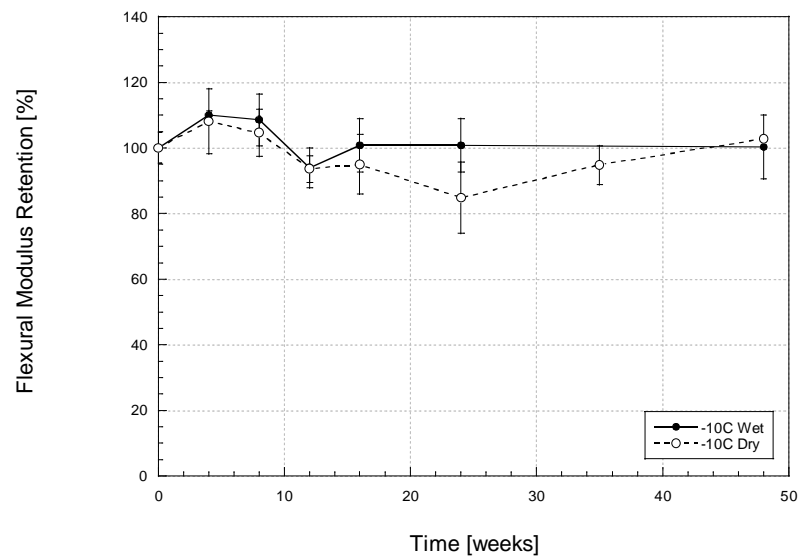


Figure 6.13d. Effect of Redrying on Flexural Modulus Retention after Immersion in -10°C Seawater

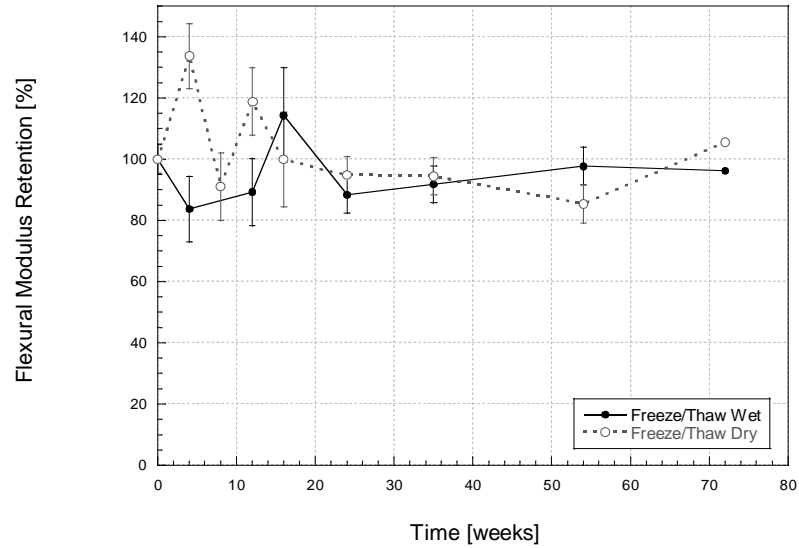


Figure 6.14a. Effect of Redrying on Flexural Modulus After Exposure to Freeze/Thaw Cycling

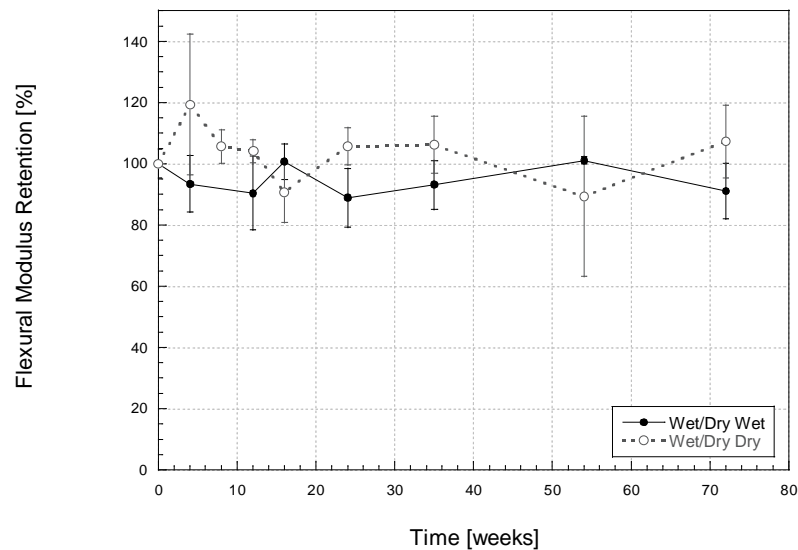


Figure 6.14b. Effect of Redrying on Flexural Modulus After Exposure to Wet/Dry Cycling

Referring to Figures 6.13 and 6.14, since values of flexural modulus were not adversely affected, redrying seemed to have no effect on the modulus. Dry values of flexural modulus fell within range of the wet values. A plot of percent retention versus weight gain did not show a linear relationship.

6.2.3. Failure Modes

Typical failure modes for three-point bending specimens include the delamination of the resin from the fiber. It is seen that exposure at elevated temperatures decreased the toughness of the composite. The as-received specimens show a high level of whitening at a concentrated area due to crazing and matrix microcracking. Because delamination and resin cracking absorb energy during the loading process and result in higher deflection, the whiter areas indicate a higher toughness [36]. Under immersion conditions, the whitening decreased with temperature due to flexibilization caused by plasticization. The freeze/thaw and wet/dry exposures have the same level of whiteness, and hence maintain the same level of toughness. Figure 6.15 shows the bottom surfaces of bending specimens in their as-received state as compared to specimens exposed to the seawater conditions at 72 weeks (23°C, 40°C, 60°C) and 78 weeks (Freeze/Thaw and Wet/Dry).

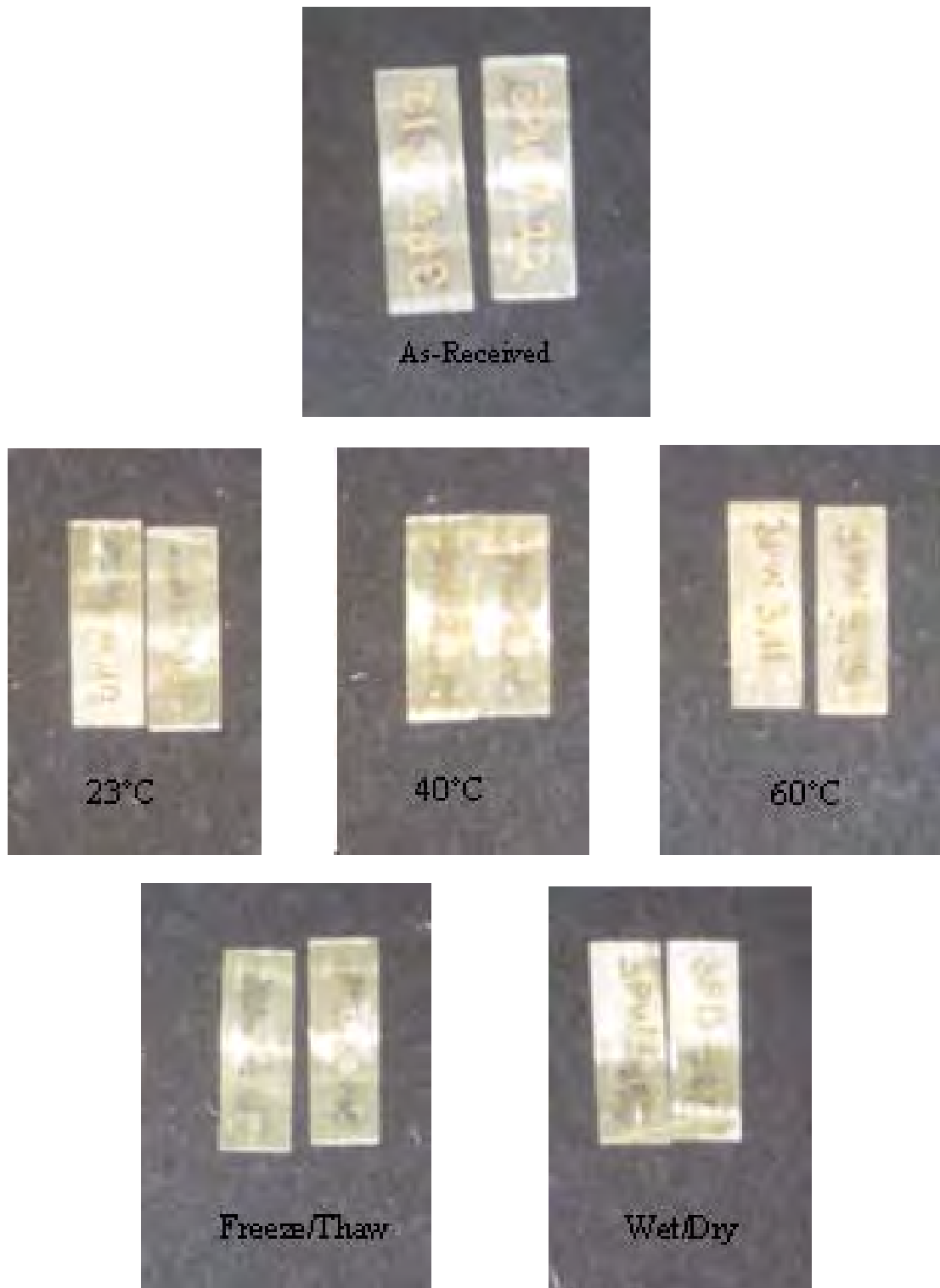


Figure 6.15. Bottom Surfaces of Failed 3-Point Bending Specimens For Different Conditions

The level of discoloration at 23°C immersion stays constant throughout the 78 weeks, while at 60°C immersion the level of whitening diminishes at 4 weeks and shows this through the 78 weeks. At 40°C immersion, the level of discoloration decreases with time. Figure 6.16 shows the bottom surfaces of failed three-point bending specimens subjected to 40°C immersion at 4, 26, 52, and 78 weeks. At 4 weeks, the level of discoloration is slightly affected, however at future periods of time, the whitening reduces to the point where it is only slightly visible at 78 weeks.

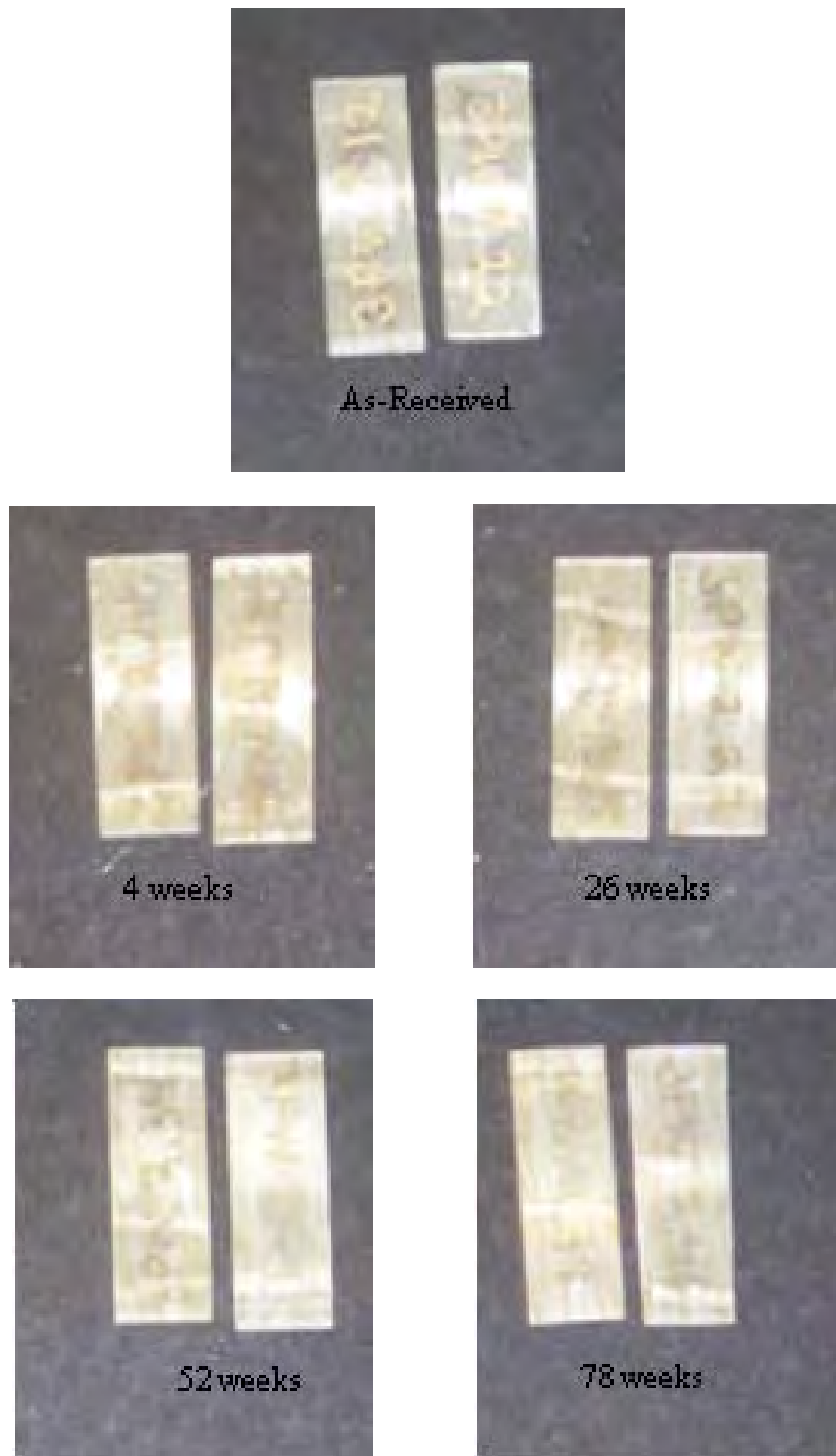


Figure 6.16. Bottom Surfaces of Failed Three-Point Bending Specimens Immersed in 60°C Seawater

6.3. SUMMARY

Moisture-induced degradation is prevalent in the results from flexure testing and the main conclusions are summarized as follows:

- Rates of degradation in flexural strength are low from 0-16 weeks in immersion conditions
- Initial degradation occurs at a similar rate for immersion at 40 and 60°C seawater in terms of flexural strength
- Cycling conditions have a small effect on the flexural strength
- Plasticization occurs from 0-12 weeks in 23°C, 0-4 weeks for 40°C immersion and before 4 weeks for 60°C immersion exposures
- Partial regain of flexural strength is experienced for immersion and cycling conditions
- No significant effects on the flexural modulus are observed
- Freezing conditions increased the brittleness of the network, and thus increased flexural modulus as compared to as-received conditions

CHAPTER 7 – SHORT BEAM SHEAR

7.1. INTRODUCTION

The intrinsic performance of a composite is predicated on the properties of the fiber reinforcement and the resin, and the efficiency of the interface between the two constituents. Laminate composites lack three-dimensional reinforcement and hence depend largely on resin characteristics for shear and through-thickness performance attributes. The short beam shear (SBS) test is a commonly used indicator of relative performance and quality of composites and due to the complexity of loading is fairly representative of local response encountered in composite structures [77]. The loading consists of a combination of tension-compression and shear. The short-beam shear test evaluates the characteristic strength between layers of a composite. This region is sensitive to the bond at the fiber/matrix interface and that between layers of the reinforcement. Previous research has shown that moisture can diffuse quickly through a composite and reach the midplane, degrading the SBS strength. However in seawater, the large Na particles often get blocked and this causes a low moisture content in a specimen. If moisture is retarded in reaching the midplane, then matrix degradation will be less apparent. Use of ambient cure in the manufacturing process can also directly affect the SBS strength. Since large structures are common in the marine industry, it is often difficult to post-cure boat decks and hulls. Due to conditions such as those listed above, the short-beam shear test is performed at intermittent periods for verification of properties.

The SBS strength is calculated according to equation 7-1 [93].

$$F^{sbs} = 0.75 \times \frac{P_m}{b \times h} \quad (7-1)$$

where:

F^{sbs} is the short beam shear strength in MPa,

P_m is the maximum load observed during the test in N,

b is the measured specimen width in mm, and

h is the measured specimen thickness in mm.

Percent regain is calculated according to equation 5-4.

7.2. RESULTS AND DISCUSSION

The following tables report the values of SBS strength as a function of time for specimens after immersion, after cyclic exposure, and after redrying. Results for ambient specimens are also reported.

7.2.1. Short Beam Shear Strength

Changes in SBS strength as a result of immersion in seawater, and after redrying are shown in Table 7.1 and Figure 7.1, whereas the corresponding results after cyclic exposure are shown in Table 7.2 and Figure 7.8. The effects of redrying are shown in Figures 7.11 and 7.12. In the figures percentage retention is determined by equation 7-3.

$$\% \text{ Retention} = \frac{P_t}{P_o} * 100 \quad (7-3)$$

where:

P_t is the property at time t and

P_o is the property at time $t = 0$.

Table 7.1a. SBS Strength Determined At Ambient Conditions of 23°C and 30%RH

Time [weeks]	Ambient	
	SBS Strength [MPa]	Std. Dev. [MPa]
0	49.1	2.0
4	46.6	1.3
8	47.2	1.0
12	50.7	3.2
16	42.2	2.8
24	49.2	1.0
32	49.2	4.1
48	50.2	2.1
72	48.5	2.4

Table 7.1b. SBS Strength Determined After Immersion in 23°C Seawater (“Wet” Testing) and as a Result of Subsequent Drying (“Dry Testing”)

Time [weeks]	23°C			
	<i>Wet Testing</i>		<i>Dry Testing</i>	
	SBS Strength [MPa]	Std. Dev. [MPa]	SBS Strength [MPa]	Std. Dev. [MPa]
0	49.1	2.0	49.1	2.0
4	46.3	3.2	48.3	2.8
8	42.2	3.7	43.8	1.5
12	40.1	5.0	42.0	2.4
16	38.7	4.1	43.3	6.0
26	37.6	1.9	43.5	3.0
35	38.4	9.1	41.0	2.6
52	36.6	6.0	41.5	2.7
78	37.7	3.3	40.2	1.5

Table 7.1c. SBS Strength Determined After Immersion in 40°C Seawater (“Wet” Testing) and as a Result of Subsequent Drying (“Dry Testing”)

Time [weeks]	40°C			
	<i>Wet Testing</i>		<i>Dry Testing</i>	
	SBS Strength [MPa]	Std. Dev. [MPa]	SBS Strength [MPa]	Std. Dev. [MPa]
0	49.1	2.0	49.1	2.0
4	37.3	3.0	40.5	1.4
8	35.8	2.3	43.0	4.2
12	31.0	5.7	42.6	2.3
16	31.7	1.4	38.0	2.0
26	29.5	7.9	39.5	7.2
35	30.1	4.7	41.9	1.6
52	31.2	1.3	42.2	3.3
78	31.0	3.1	41.6	4.6

Table 7.1d. SBS Strength Determined After Immersion in 60°C Seawater (“Wet” Testing) and as a Result of Subsequent Drying (“Dry Testing”)

Time [weeks]	60°C			
	<i>Wet Testing</i>		<i>Dry Testing</i>	
	SBS Strength [MPa]	Std. Dev. [MPa]	SBS Strength [MPa]	Std. Dev. [MPa]
0	49.1	2.0	49.1	2.0
4	33.8	2.4	39.0	3.8
8	24.5	2.6	41.2	1.4
12	25.1	6.2	31.7	3.8
16	20.3	5.6	30.0	1.3
26	19.3	2.8	27.1	6.5
35	17.8	3.7	28.1	3.8
52	16.3	2.1	24.6	2.2
78	17.7	0.6	24.8	1.7

Table 7.1e. SBS Strength Determined After Immersion in -10°C Seawater (“Wet” Testing) and as a Result of Subsequent Drying (“Dry Testing”)

Time [weeks]	-10°C			
	<i>Wet Testing</i>		<i>Dry Testing</i>	
	SBS Strength [MPa]	Std. Dev. [MPa]	SBS Strength [MPa]	Std. Dev. [MPa]
0	49.1	2.0	49.1	2.0
4	39.9	3.9	47.6	2.9
8	43.6	1.9	45.8	4.4
12	41.0	4.9	45.0	6.1
16	39.6	1.9	44.7	4.5
34	42.6	4.6	46.5	0.5
35	41.9	1.3	49.1	2.5
48	41.4	2.7	48.0	2.6
72				

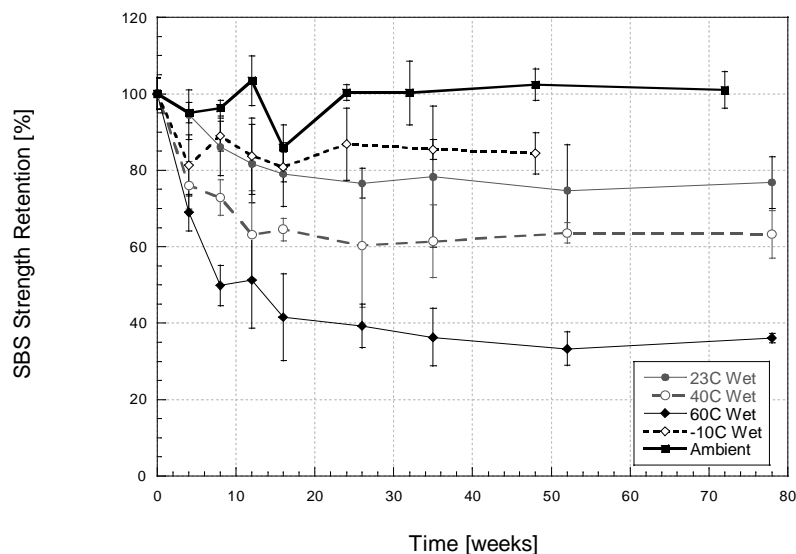


Figure 7.1. Change in SBS Strength as a Function of Temperature and Time of Immersion in Seawater

SBS strength retention of immersed specimens is in agreement with results found from previous studies that showed increasing reductions with increases in immersion temperature. The largest changes in strength correspond to the highest moisture content for that exposure. Since SBS strength is a resin dominated property, it is known to be sensitive to defects, voids, moisture, interfacial strength, hydrolysis of the matrix, and disruption of the fiber/matrix interface [40,87]. Mazor and Broutman stated that the SBS strength is affected by the presence of microcracks that result from moisture uptake [87]. Moisture uptake can cause cracks and debond sites through which moisture can wick and excess moisture can ultimately degrade the matrix [87]. Rege and Lakkad hypothesized that moisture collects at the interface and deteriorates SBS strengths [70]. Optical micrographs of specimens from the current investigation reveal the presence of these microcracks that can cause wicking as shown in Figure 7.2. Figure 7.2 represents the condition of the composite after immersion in seawater for 78 weeks at 23°C. The cracks originate at the region between layers where pressure differentials are created from the varying coefficients of expansion from the chopped strand mat and unidirectional fiber.

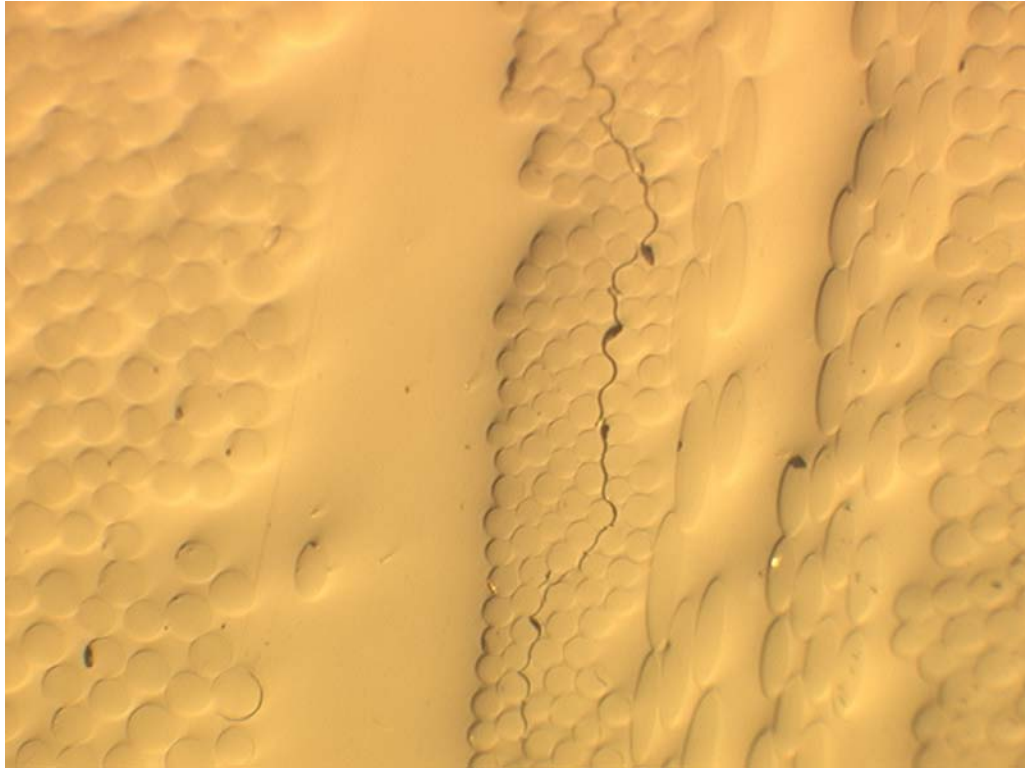


Figure 7.2. Optical Micrograph Showing Coalescence of Debonds Present at Chopped Strand Mat Layers (100X Magnification) After Immersion in Seawater at 23°C For 78 Weeks

Specimens immersed in 23°C seawater showed greatest losses at 48 weeks with a decline of 25%. Trends in strength loss at room temperature immersion showed a sharp decrease from 0-8 weeks followed by near asymptotic behavior after 12 weeks with very slow changes. Figure 7.3 is an optical micrograph showing the presence of interface degradation as early as 4 weeks that causes the 25% change in SBS strength.

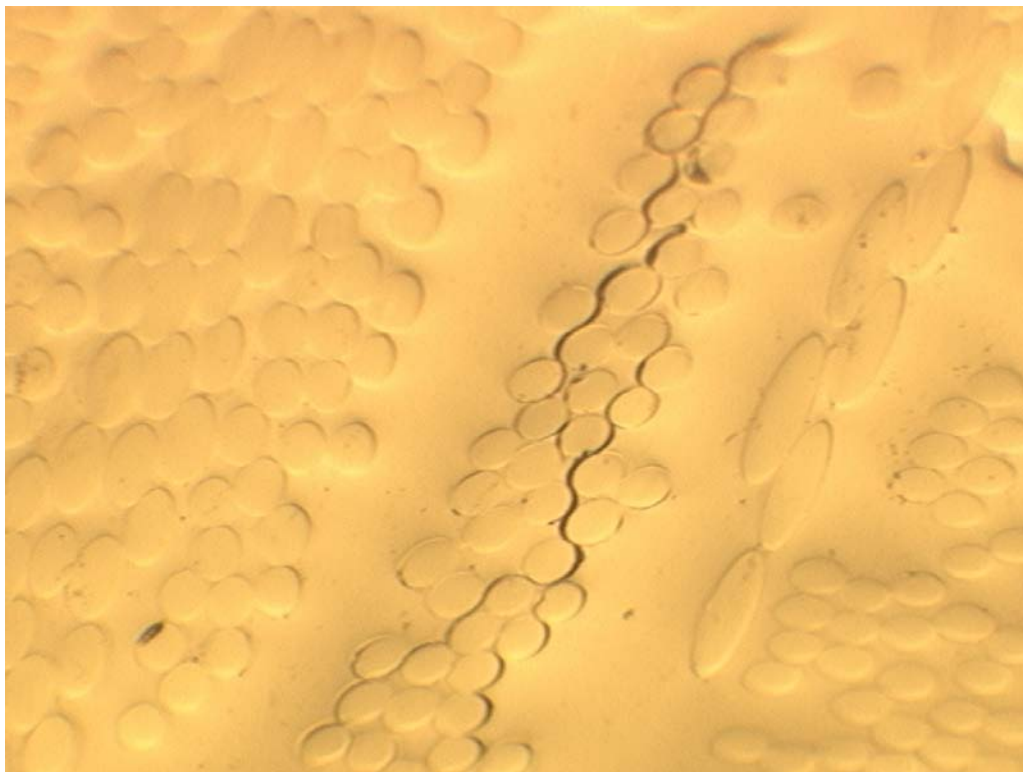


Figure 7.3. Optical Micrograph Showing Cracks Resulting from Immersion in 23°C Seawater after 4 weeks (100X Magnification)

Wu et al. studied a similar material exposed to 23°C seawater and suggested that the change in crosslinking density initiates postcure that causes an anomalous moisture diffusion to occur [18]. A boundary layer encompasses the swelling layers which can cause triaxial stresses that ultimately form microcracks at midplane (See Figure 7.2). This, in turn, directly affects SBS strength [18]. In the current study, measurements taken after the increase in SBS strength show anomalous moisture diffusion with weight gain increases at 78 weeks.

Changes in strength of the same magnitude from previous studies investigating the effects of saline solution at room temperature have been reported by Grant [32], Macander et al. [67], Steckel et al. [71], and Gutierrez et al. [80]. Other researchers found increases in SBS, or little changes [30,37,59]. Increases in SBS strength are caused by an increase in crosslinking density as a product of postcure [77].

Immersion at elevated temperatures showed a sharp decrease in levels of SBS strength from 0-8 weeks and a slower steady tendency from 12-78 weeks. Specimens immersed in 40°C seawater experienced greater losses at 26 weeks with a change of 40%. Microscopy reveals that the coalescence of debonds is prevalent at elevated temperatures. Figure 7.4 is an optical micrograph that shows cracks developing as early as 4 weeks in 40°C seawater. The cracks in Figure 7.4 representative of the condition of the composite at 4 weeks, while progression of microcracking seems to increase the microcracks in width and cause further damage with time, as shown in Figure 7.5. As can be noted on comparison with results in Figure 7.2, the effects of immersion in 40°C seawater are clearly accelerative.

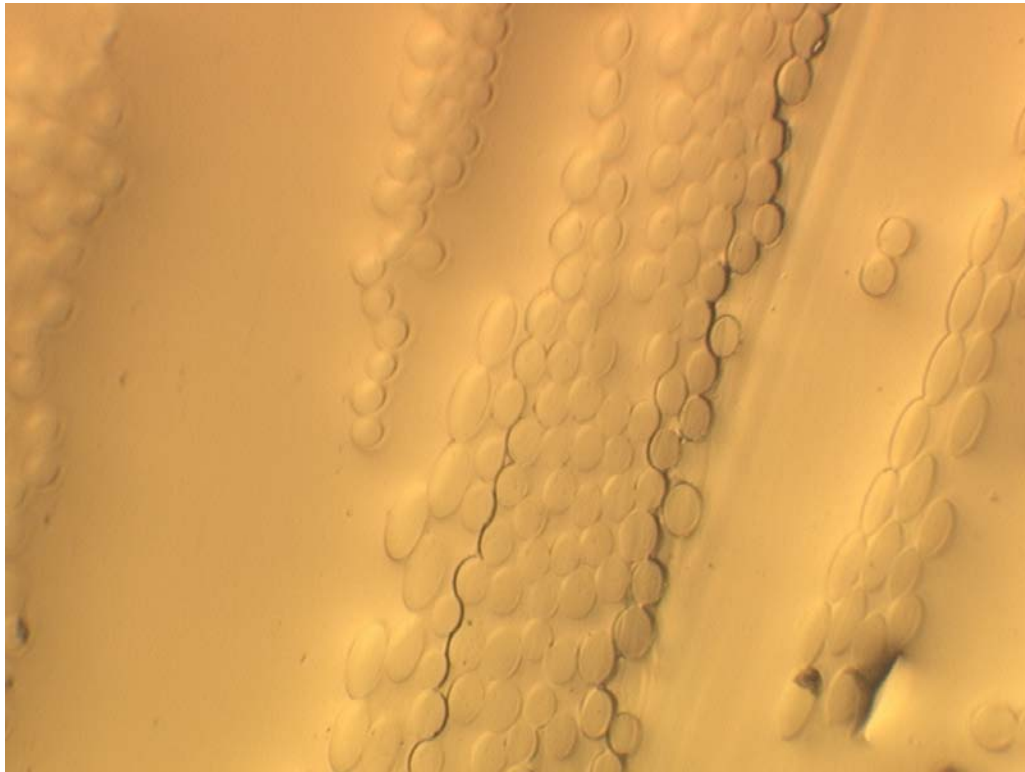


Figure 7.4. Optical Micrograph Revealing Coalescence of Debonds After Exposure to 40°C Seawater For 4 Weeks (100X Magnification)

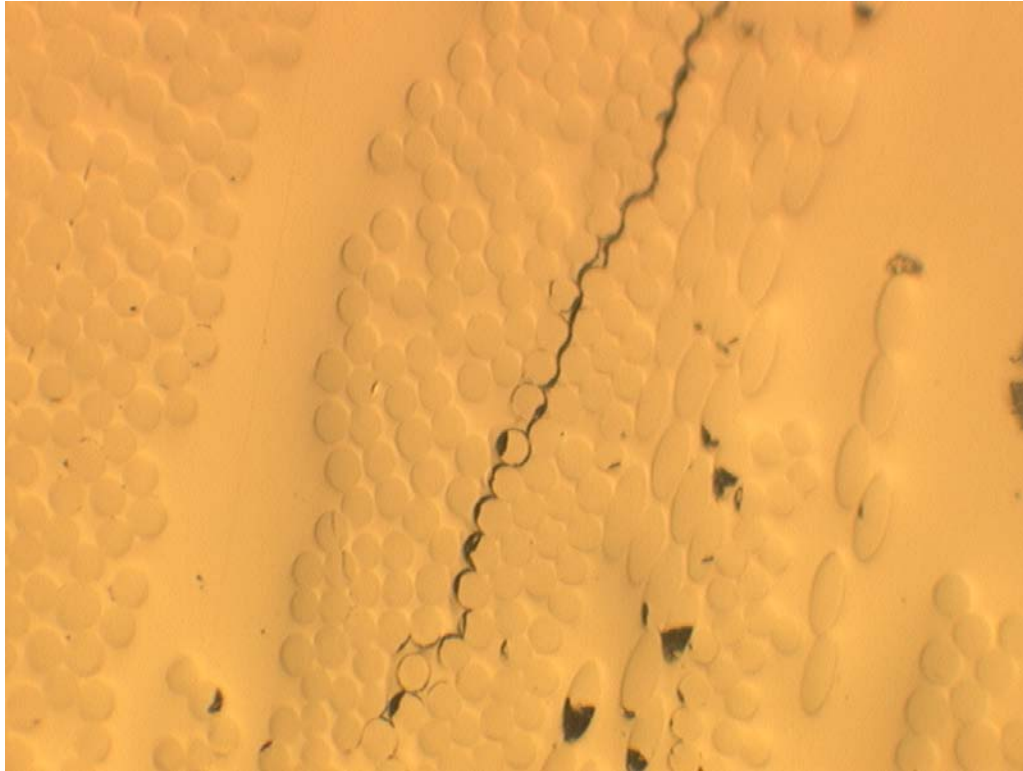


Figure 7.5. Optical Micrograph Showing Development of Cracks at 78 weeks in 40°C Seawater (100X Magnification)

Rege and Lakkad studied the durability of glass composites at elevated temperatures in salt solution and found much lower changes in strength (on the order of 10%) [70]. However, Chin et al. found concurring results studying an E-glass/Vinylester composite immersed in salt solution at 40°C [40].

Finally, specimens immersed in 60°C seawater showed substantial losses of 67% at 48 weeks. Agreement of these results were found by Gutierrez et al. [80] and Springer et al. [59] who immersed samples in elevated temperatures in salt water. Past evidence has shown that a strong correlation between shear strength reduction and diffusion rate exists [87]. The substantial losses in strength are validated by investigation through optical microscopy that show abundance of debonding and microcracking. Figure 7.6 is an optical micrograph that shows the increase in crack width as compared to immersion at room temperature and Figure 7.7 shows the amount of microcracking present in a specimen after exposure to 60°C seawater.

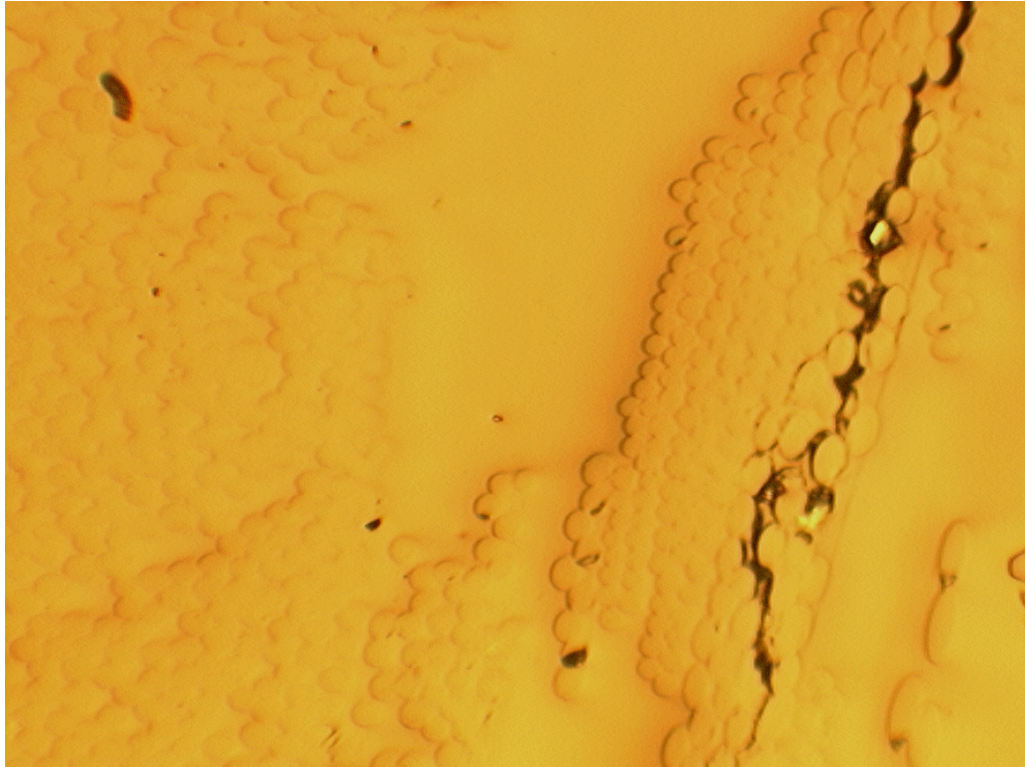


Figure 7.6. Optical Micrograph Showing Substantial Losses in ILSS Validated by Presence of Large Width Cracks after 60°C Seawater Immersion for 52 Weeks (100X Magnification)



Figure 7.7. Optical Micrograph Showing Large Amounts of Cracking and Debonding for E-glass/Vinylester After Immersion in 60°C Seawater Immersion for 52 Weeks (100X Magnification)

Freezing conditions validated the fact that moisture uptake was retarded by the exposure. Losses were minimal at 16 weeks with a 19% decline. Most losses were caused by the initial saturation period of 8 months in room temperature seawater. Comparison of strength profiles for freezing conditions and room temperature immersion show similar levels of degradation. The freezing condition seems to have retarded any degradation occurring after the 8 month immersion.

Table 7.2 and Figure 7.8 show the effect of cyclic exposure on SBS strength.

Table 7.2a. SBS Strength Determined After Exposure to Freeze/Thaw Cycling (“Wet” Testing) and as a Result of Subsequent Drying (“Dry Testing”)

Time [weeks]	Freeze/Thaw			
	<i>Wet Testing</i>		<i>Dry Testing</i>	
	SBS Strength [MPa]	Std. Dev. [MPa]	SBS Strength [MPa]	Std. Dev. [MPa]
0	49.1	2.0	49.1	2.0
4	41.5	2.9	44.9	3.5
8	39.2	3.8	47.2	2.2
12	41.9	2.6	44.6	5.8
16	39.3	5.6	47.5	4.1
24	42.4	3.6	47.9	2.8
35	39.5	5.9	47.9	3.9
54	42.7	1.6	44.7	5.9
72	42.7	3.5	47.1	1.8

Table 7.2b. SBS Strength Determined After Exposure to Wet/Dry Cycling (“Wet” Testing) and as a Result of Subsequent Drying (“Dry Testing”)

Time [weeks]	Wet/Dry			
	<i>Wet Testing</i>		<i>Dry Testing</i>	
	SBS Strength [MPa]	Std. Dev. [MPa]	SBS Strength [MPa]	Std. Dev. [MPa]
0	49.1	2.0	49.1	2.0
4	36.7	2.1	47.2	4.7
8	39.2	2.5	49.2	3.1
12	38.5	4.0	51.9	6.1
16	37.4	3.3	48.2	4.7
24	37.5	4.9	46.3	4.3
35	37.5	4.1	46.0	3.8
54	39.5	3.5	47.2	3.2
72	29.7	10.6	47.6	1.9

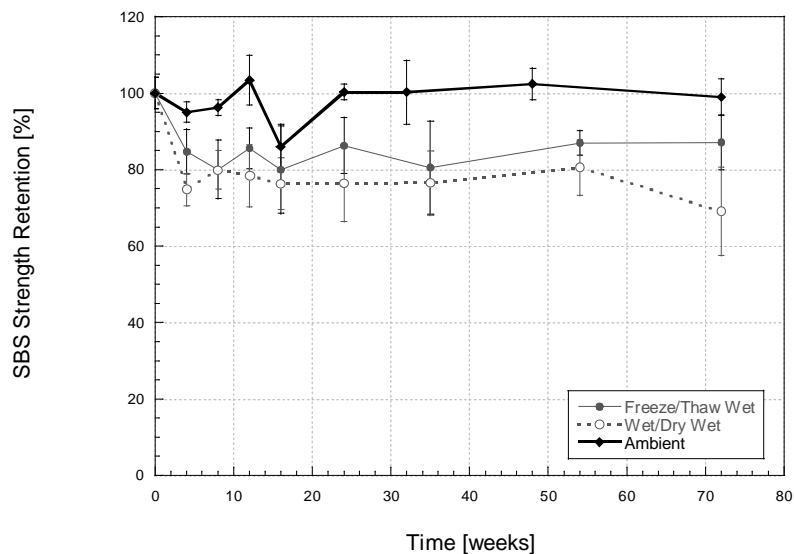


Figure 7.8. Change in SBS Strength as a Function of Time and Type of Cyclic Exposure

Cycling also confirmed the retardation of moisture uptake, especially in the freeze/thaw condition where data at 54 and 72 weeks showed a change of only 13%. Optical microscopy reveals that microcracking was less abundant than that seen at elevated temperatures. However at 72 weeks small amounts of microcracks (with large crack widths) were found. Figure 7.9 shows an optical micrograph showing cracks that are potential sites for wicking. Microscopy revealed that the presence of these microcracks is caused by the wet/dry cycle and propagate from resin rich areas caused by the manufacturing process. Because of their sporadic formation, they can cause large deviations in performance as measured through mechanical tests.

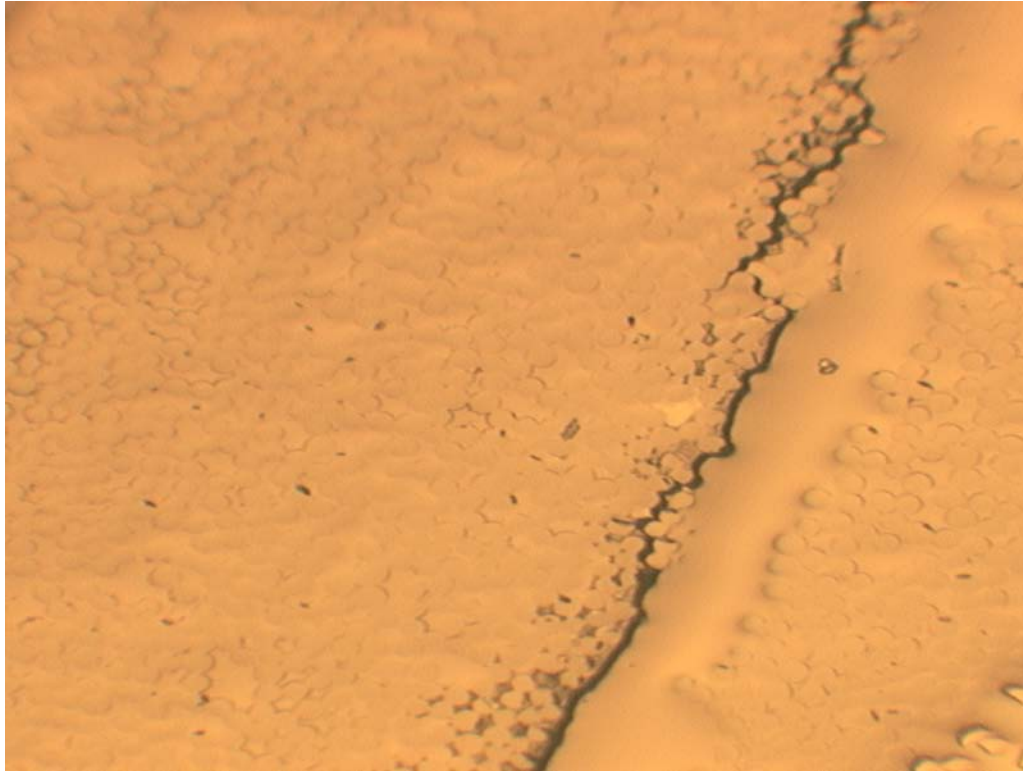


Figure 7.9. Optical Micrograph Showing Sites for Wicking After Exposure to Wet/Dry Cycles At 72 Weeks (100X Magnification)

Wet/dry cycling had a slightly more degradative effect on SBS strength with reductions of 31% at 72 weeks. Previous studies have found smaller reductions in strength (11%) when exposing E-glass/vinylester composites to a wet/dry cycle [18]. Microscopy reveals areas of debonding resulting from the wet/dry cycle. However cracking was found in relative small localized areas. Figure 7.10 shows an optical micrograph of a crack found after exposure of a specimen to the wet/dry cycles for 72 weeks. Microracks, such as those found in Figure 7.10, usually initiate from resin rich areas, as seen in the figure to the left of the crack. Similar to that experienced by the freeze/thaw cycle, microcracking was propagated from irregularities in the composite and resulted in large deviations in performance.



Figure 7.10. Optical Micrograph Showing Microcracking Characterized by Connection of Crescent Shaped Debonds at 72 Weeks in the Wet/Dry Cycle (500X Magnification)

Table 7.3 and Figures 7.11 and 7.12 show the effect of redrying specimens in a conditioning chamber for 30 days at 23°C and 30% RH.

Table 7.3a. Effect of Redrying for SBS Strength After Immersion In Seawater

Time [weeks]	Regain [%]		
	23°C	40°C	60°C
0	100.0	100.0	100.0
4	72.5	27.3	33.9
8	22.2	54.4	68.0
12	21.0	64.5	27.5
16	44.1	36.3	33.7
26	51.3	51.2	26.3
35	24.7	62.2	33.0
52	39.5	61.6	25.2
78	21.7	58.9	22.7

Table 7.3b. Effect of Redrying for SBS Strength After Exposure to Freezing Conditions

Time [weeks]	Regain [%]
	-10°C
0	100.0
4	84.0
8	39.6
12	49.8
16	54.1
26	60.3
35	100.6
52	86.1
78	

Table 7.3c. Effect of Redrying for SBS Strength After Exposure to Cyclic Conditions

Time [weeks]	Regain [%]	
	Freeze/Thaw	Wet/Dry
0	100.0	100.0
4	44.9	85.1
8	81.0	100.9
12	36.9	126.9
16	84.5	92.4
26	83.0	76.6
35	87.6	73.2
52	31.0	81.0
78	69.1	92.6

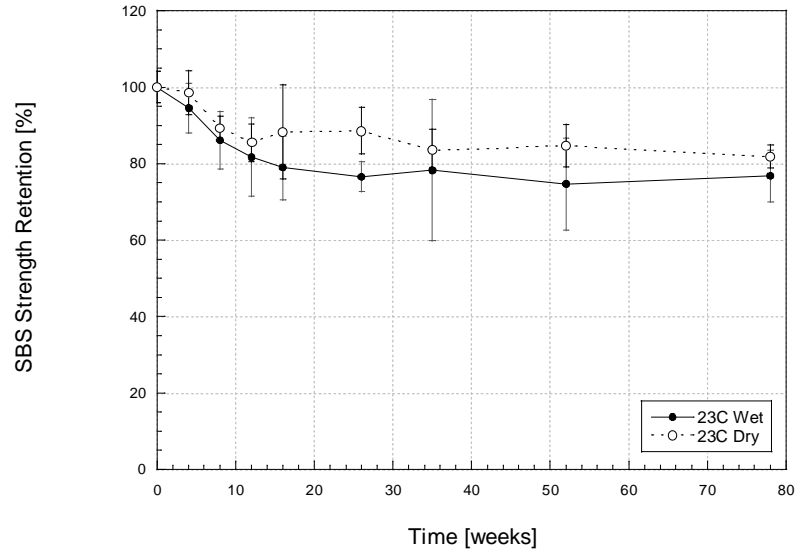


Figure 7.11a. Effect of Redrying on SBS Strength Retention after Immersion at 23°C in Seawater

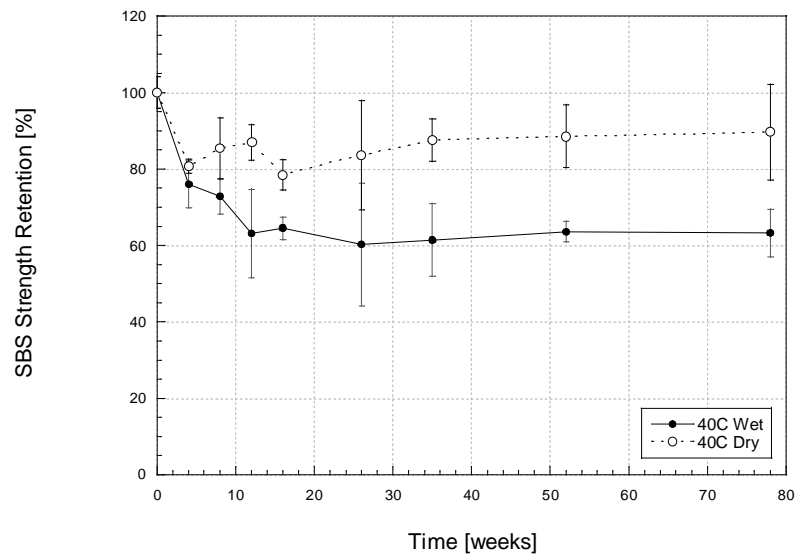


Figure 7.11b. Effect of Redrying on SBS Strength Retention after Immersion at 40°C in Seawater

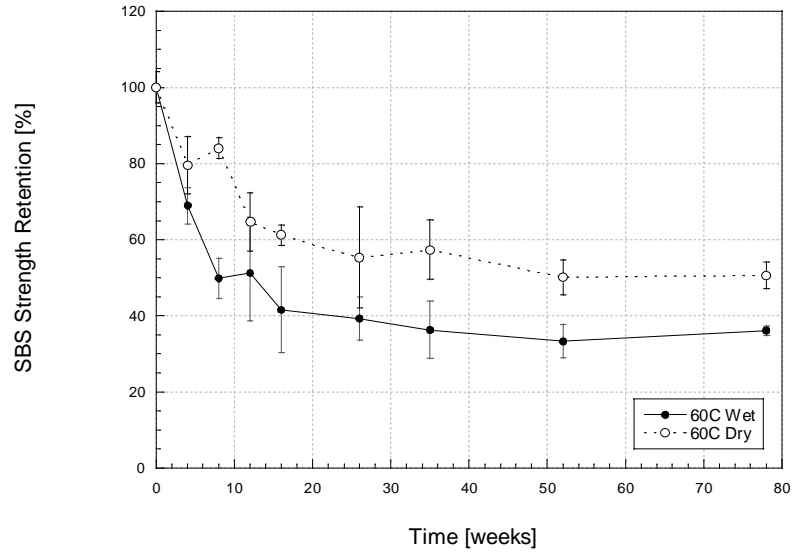


Figure 7.11c. Effect of Redrying on SBS Strength Retention after Immersion at 60°C in Seawater

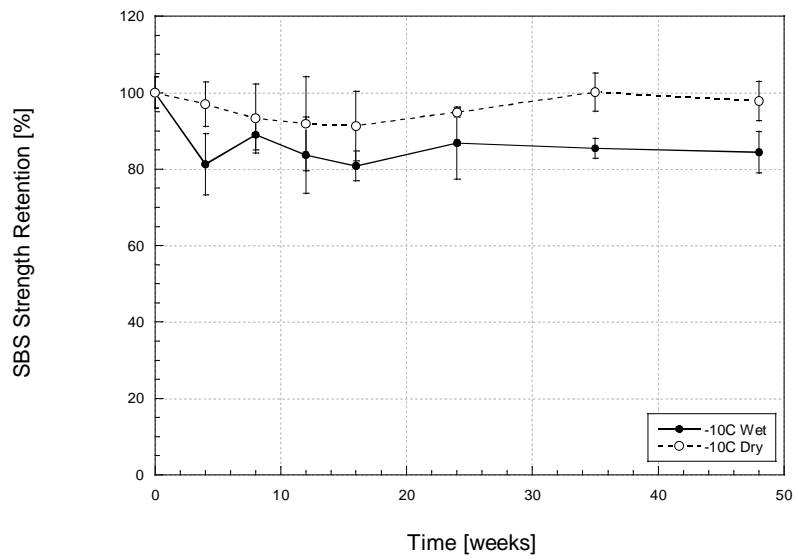


Figure 7.11d. Effect of Redrying on SBS Strength Retention after Immersion at -10°C in Seawater

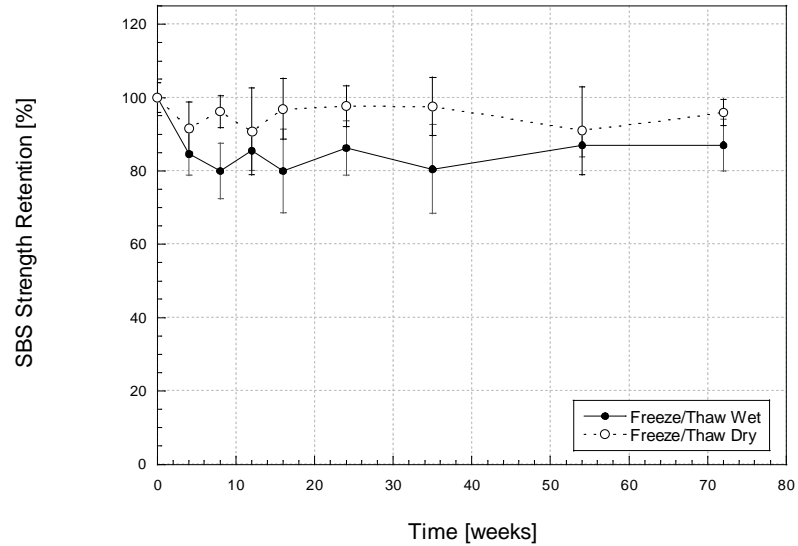


Figure 7.12a. Effect of Redrying on SBS Strength After Exposure to Freeze/Thaw Condition

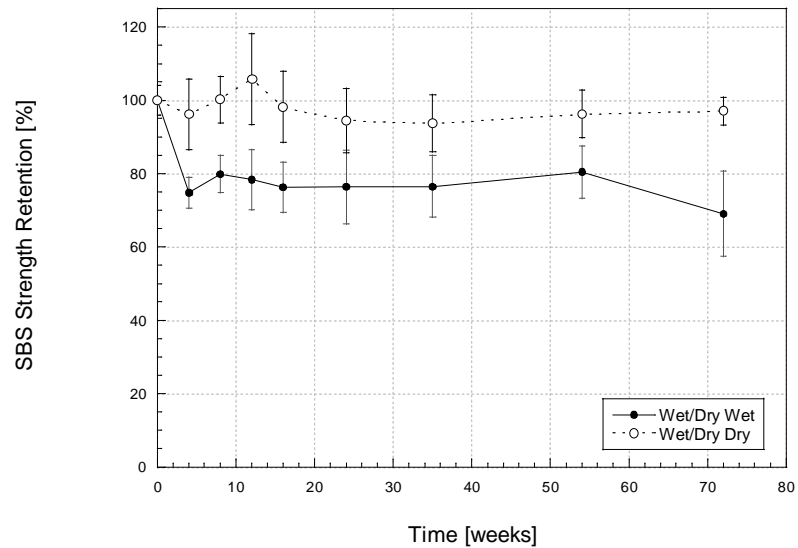


Figure 7.12b. Effect of Redrying on SBS Strength After Exposure to Wet/Dry Condition

Partial regain is experienced in all immersion conditions, with specimens exposed to freezing, freeze/thaw, and wet/dry cycling showed substantial amounts of regain. Irreversible degradation occurs because of matrix degradation, while reversible degradation is a result of matrix plasticization and swelling [87]. Since freezing and cycling impede moisture diffusion, less degradation at midplane occurs, resulting in larger relative values of reversible degradation.

According to moisture profiles for immersed specimens shown in Chapter 4, moisture reaches saturation after 4 weeks and shows signs of mass loss thereafter. The mass loss indicates the irreversible degradation, as reflected from redry strength profiles for immersion exposures.

A plot of percent retention versus moisture content reveals that plasticization may be the dominant mechanism from 0-12 weeks for specimens immersed in 23C seawater (Figure 7.13). The slopes vary for specimens immersed at higher temperatures, indicating that plasticization probably occurs only prior to 4 weeks. This same phenomenon was noted in tension and flexure, as explained in Chapters 5 and 6.

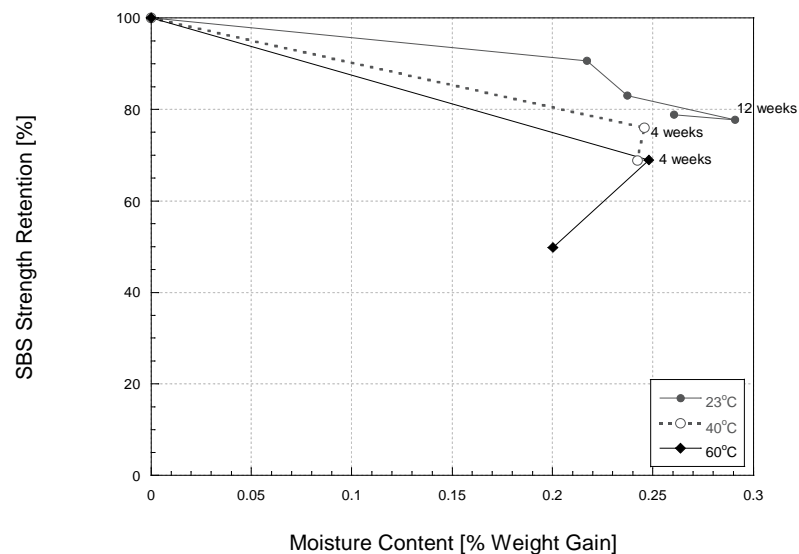


Figure 7.13. Relationship Between Moisture Content and SBS Strength Retention for Specimens Immersed in 23°C, 40°C, and 60°C Seawater

A similar plot can be generated for cycling exposures and is shown in Figure 7.14. According to the figure, plasticization may be the dominant mechanism between 0 and 12 weeks for the Freeze/Thaw cycle. In agreement with Figure 7.12, the upper bound of the SBS strength suggests full regain is possible for this specific exposure condition.

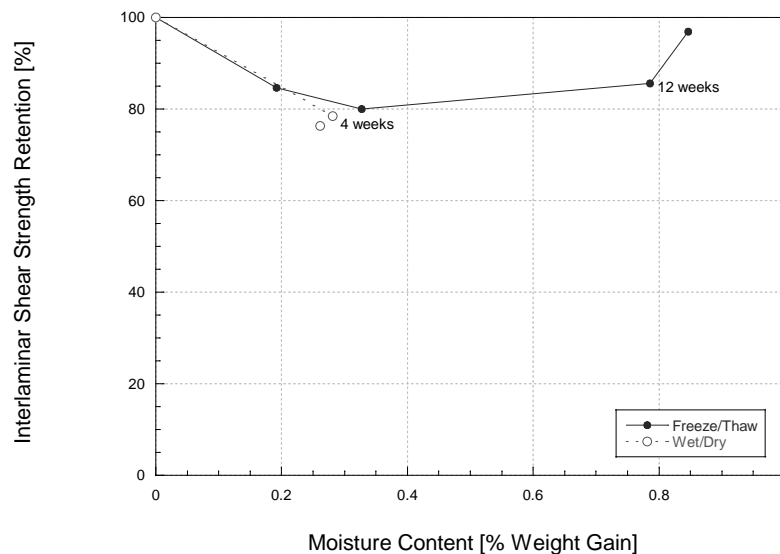


Figure 7.14. Relationship Between Moisture Content and SBS Strength Retention for Specimens Exposed to Cycling Conditions

7.2. COMPARISON OF MECHANICAL PROPERTIES

Changes in mechanical properties in the preceding chapters show similar trends in reduction. Tension characteristics reflect fiber-dominated properties, SBS strength reflects resin-dominated properties, and flexural characteristics are a representation of a combination. For comparison, strengths and modulus results are superimposed on the same plot in the following figures.

Figure 7.15 shows a strength retention comparison in room temperature seawater. In general, trends are similar for the three properties. Tensile strength properties are the least affected because it is a fiber dominated property and degradation associated with the fiber is minimal in terms of short-term immersion. Flexural and SBS strengths show very similar trends and any degradation noted is caused by degradation due to the matrix.

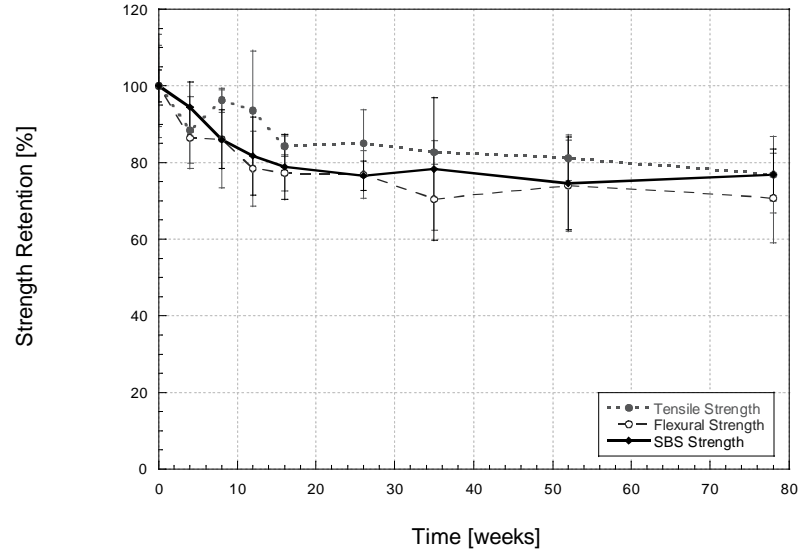


Figure 7.15. Comparison of Strength Retention Properties in 23°C Seawater

A similar plot is configured for specimens exposed to immersion in 40°C seawater (See Figure 7.16). Similar trends are observed throughout the 78 weeks. Tensile, flexural, and SBS strength profiles are closely followed at higher immersion exposures. The degradation that is characteristic of accelerated aging involving matrix and interface level properties.

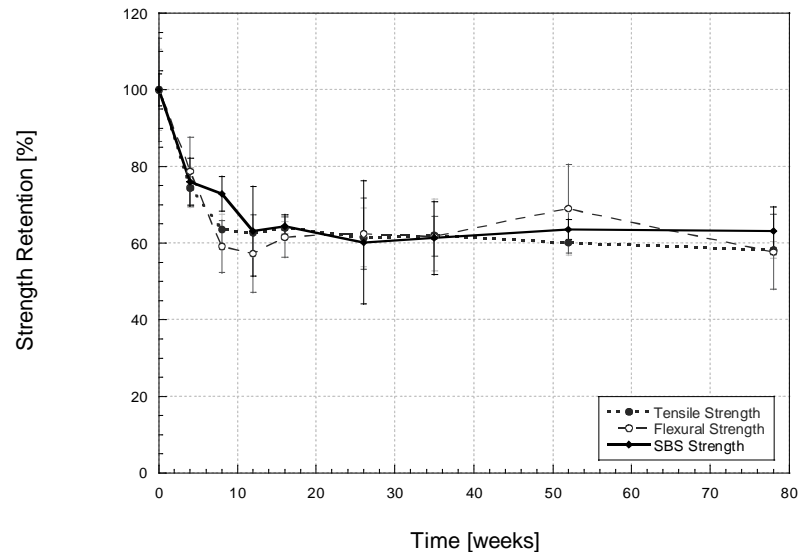


Figure 7.16. Comparison of Strength Retention Properties in 40°C Seawater

Figure 7.17 shows the strength profiles after exposure to immersion in 60°C seawater. The higher immersion temperature tends to differentiate damage at the interface and resin levels. The SBS strength profile deviates from the tensile and flexural strength profiles. This suggests a highly degraded matrix, while fiber dominated properties are retained better at this exposure level.

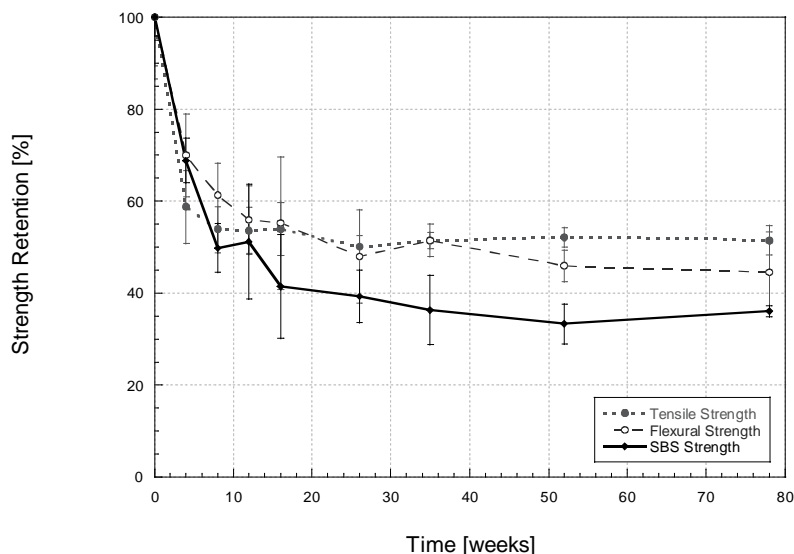


Figure 7.17. Comparison of Strength Retention Properties in 60°C Seawater

Figure 7.18 illustrates the trends in strength that occur when exposed to -10°C seawater. While not as clearly defined in trends as Figures 7.16 and 7.17 tensile, flexural, and SBS strength profiles follow similar trends. Tensile properties show less damage at the fiber level, while SBS strength shows more damage at the matrix and interface levels. Accordingly, flexural strength shows a combination of fiber and resin degradation.

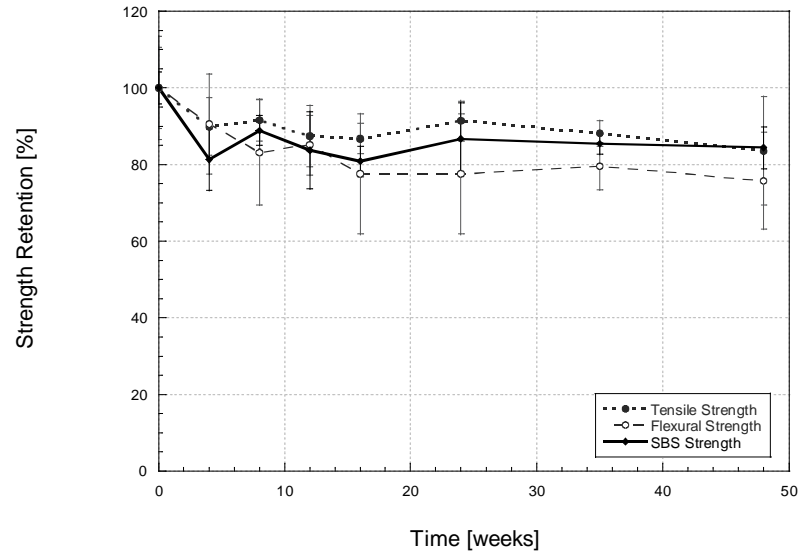


Figure 7.18. Comparison of Strength Retention Properties in -10°C Seawater

Freeze/thaw exposures (Figure 7.19) show that the freezing of the composite affects the resin dominated properties more than the fiber dominated properties. While SBS strength was found to be the most affected by the previous conditions, exposure to freeze/thaw showed that flexural strengths were the most affected according to freezing exposures. Most of the degradation as a result of cycling is caused by fiber/matrix debonding.

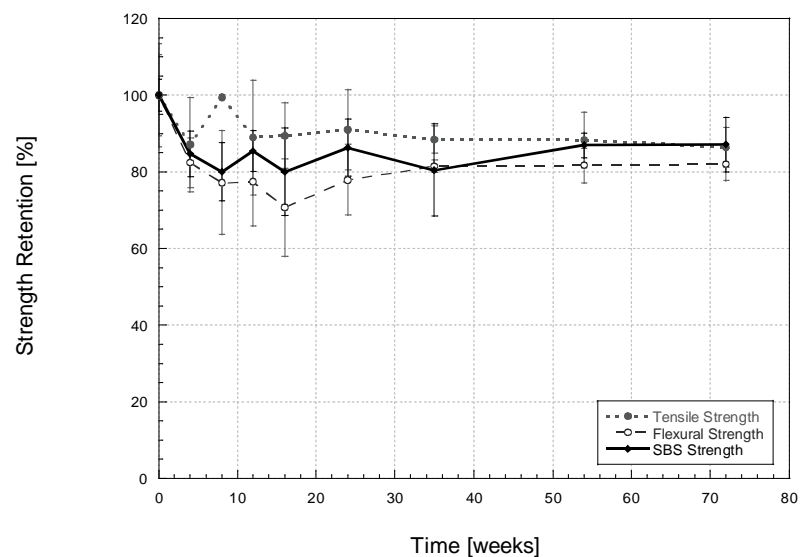


Figure 7.19. Comparison of Strength Retention Properties in Freeze/Thaw Cycle Exposure

Results of exposure to a wet/dry cycle (Figure 7.20) are in agreement with results shown in Figure 7.19. SBS strength and flexural strength are most affected from cycling, while tensile strengths are least affected.

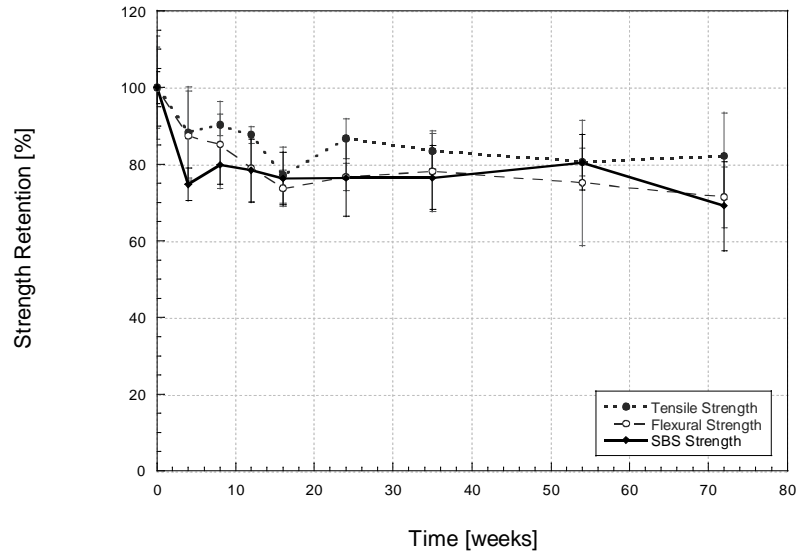


Figure 7.20. Comparison of Strength Retention Properties in Wet/Dry Cycle Exposure

Previous comparisons showed the effect of seawater on fiber and resin dominated strength properties; the following graphs show trends that are related to modulus. Only the tensile and flexural tests allow modulus values to be calculated, thus only these two profiles can be compared. Comparison of the following profiles is used to validate the modulus values obtained experimentally.

Figure 7.21 shows the effect of 23C seawater on modulus properties. Trends closely follow one another. Increases in modulus at 8 and 12 weeks are reflected in both characteristics. Initial observation suggests that the effect of postcure is commonly seen for the first 12 weeks of exposure.

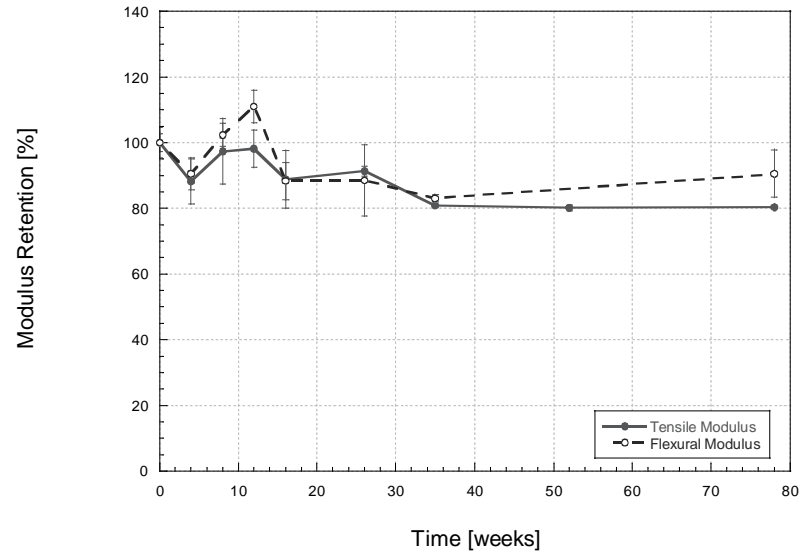


Figure 7.21. Comparison of Modulus Retention Properties in 23°C Seawater

Figure 7.22 relates the modulus profiles at 40°C seawater. In general the same trends are seen. However at 16 weeks, the value of flexural modulus retention falls below that of tensile modulus retention. It is likely that for the first 12 weeks, the effect of postcure is present. This may dominate the effect of initial degradation. After postcure is no longer a factor, the type of degradation has a clearer distinction. Because degradation occurs in the resin at higher immersion temperatures, degradation due to the matrix is more pronounced in flexural properties. Degradation in tension is not as clear because fiber degradation is not present.

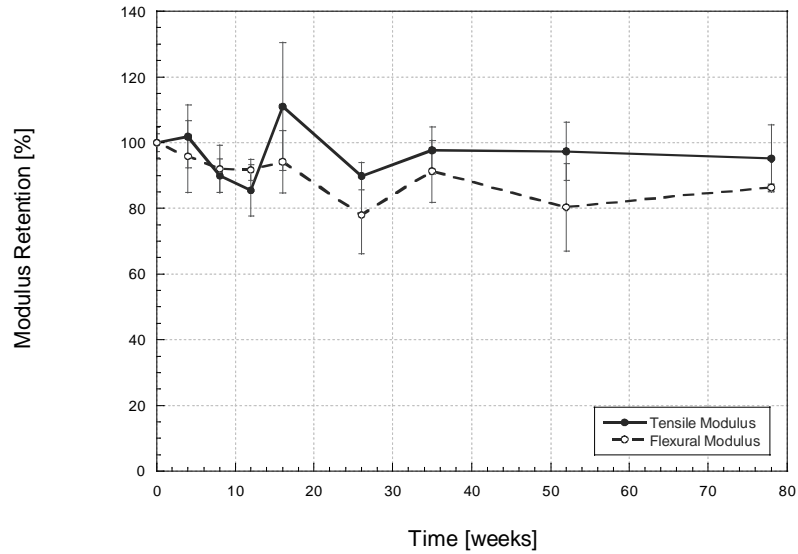


Figure 7.22. Comparison of Modulus Retention Properties in 40°C Seawater

In 60°C seawater (Figure 7.23), for the most part, trends in modulus are very similar.

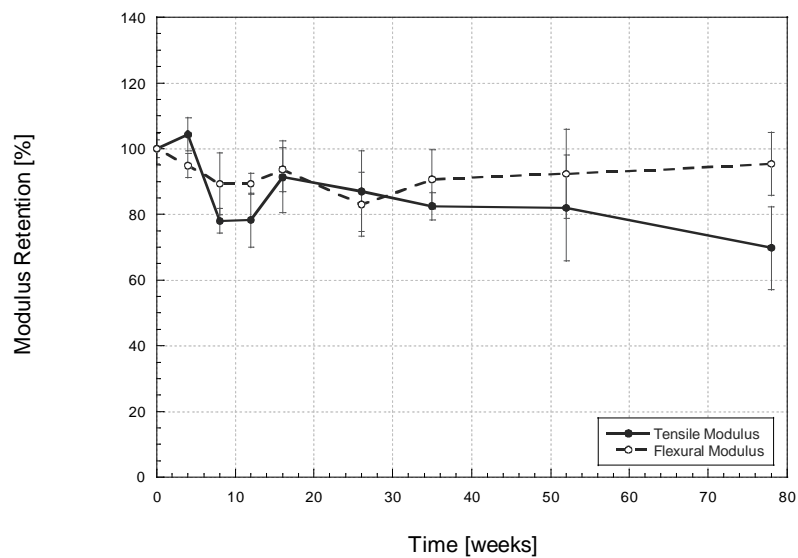


Figure 7.23. Comparison of Modulus Retention Properties in 60°C Seawater

Figure 7.24 shows an interesting observation in which modulus profiles differ when subjected to freezing. At four weeks, the flexural values increase and tensile properties decrease. Freezing causes embrittlement of the matrix, and thus the flexural modulus increases to over

100% retention. This embrittlement is unaffected by the fiber-dominated tensile test, and thus the properties are below 100% retention.

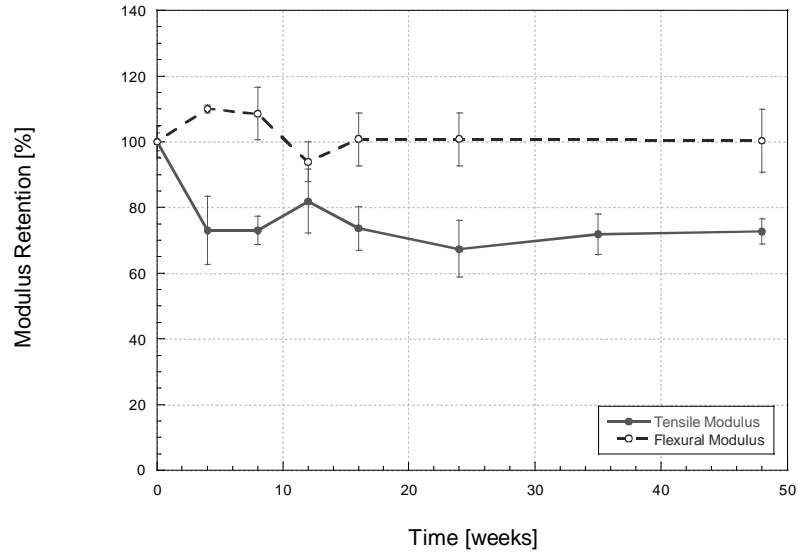


Figure 7.24. Comparison of Modulus Retention Properties in -10°C Seawater

When subjected to freeze/thaw exposures, modulus values seem to fluctuate between 0 and 12 weeks (Figure 7.25). In general, trends are very similar and standard deviation bounds fall within one another.

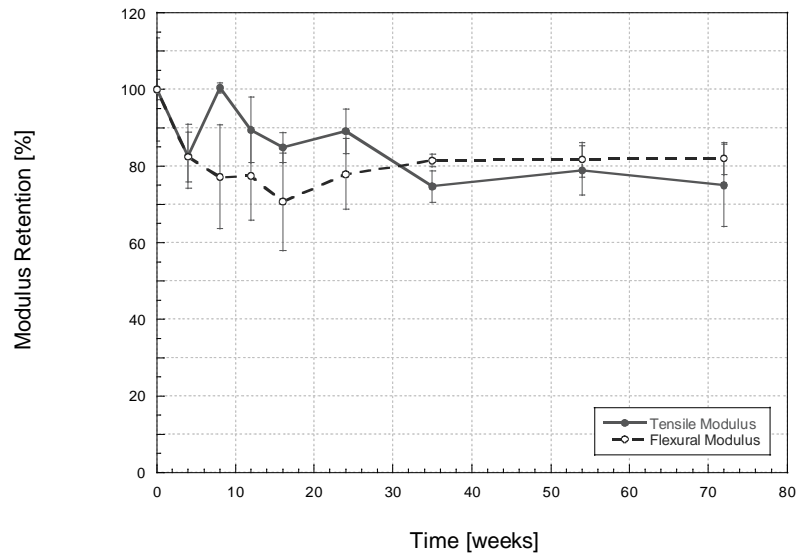


Figure 7.25. Comparison of Modulus Retention Properties in Freeze/Thaw Cycle Exposure

The wet/dry exposure shows similar trends up to 24 weeks. However, after this point, there is a clear distinction between tensile and flexure modulus values. This may suggest that long-term exposure to a wet/dry cycle can cause degradation that may alter the stiffness.

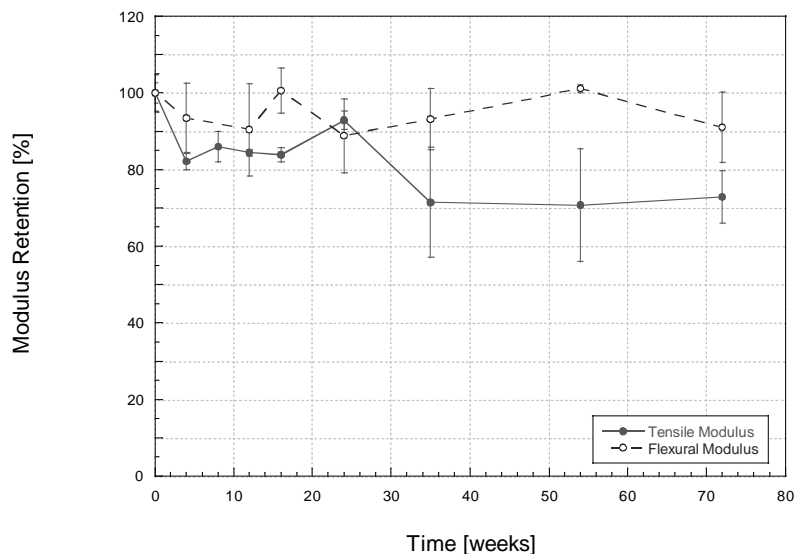


Figure 7.26. Comparison of Modulus Retention Properties in Wet/Dry Cycle Exposure

7.4. SUMMARY

Monitoring changes in SBS strength provides insight into the following items:

- Trends in SBS strength for immersion exposures show sharp decreases from 0-8 weeks, while asymptotic response is attained from 12-78 weeks
- Increases in SBS strength due to postcure are accompanied by anomalous moisture diffusion. This trend suggests the introduction of triaxial stresses in the composite
- Losses in SBS strength increase with increase in temperature of immersion
- Freezing introduces increased brittleness of the network
- Cycling shows initial decreases up to 4 weeks, with an average 20% change until 72 weeks

- Low changes in SBS strength from cycling conditions reflect that moisture uptake is retarded by the cycle and does not introduce significant damage at the interface over shorter periods of exposure
- Full regain is achieved after exposure to cyclic conditions that suggest minimal damage to the interface
- Partial regain is achieved from immersion at 40°C and 60°C seawater
- Plots of strength retention superimposed on the same plot reveal the effect of the exposure on fiber dominated and resin dominated properties

CHAPTER 8 – DYNAMIC MECHANICAL THERMAL ANALYSIS

8.1. INTRODUCTION

The use of Dynamic Mechanical Thermal Analysis (DMTA) is a commonly used tool for characterization and analysis of materials degradation. DMTA stems from the field of rheology involving the deformation and flow of materials [108]. Because of the fairly complicated background of DMTA, it has yet to be used extensively in the field of durability. DMTA provides insight into the viscoelastic response and molecular mobility of a material. As described in Chapter 3, a device is used to apply an oscillatory force on a sample in a temperature-controlled chamber. This force causes a sinusoidal stress, and in turn, a sinusoidal strain. The device then measures the amplitude of the peak deformation of the sine wave and the phase shift between them to determine values related to modulus, viscosity, and damping [108]. Analysis results from DMTA are often comprised of three characteristic curves: storage modulus, loss modulus, and tan delta. When looking at these properties, an analogy can be made to clarify their definitions. If a rubber ball is dropped from a level x , then it will bounce back a height y . The distance that the ball bounced back is the elastic energy in the ball and can be related to the storage modulus which is intrinsically the ability of a material to store energy [108]. The distance $x-y$ can be related to the amount of energy that is dissipated and is called the loss modulus, the ability of a material to lose energy [108]. Finally, tan delta is often termed as “damping” and is a ratio of the storage and loss moduli [108]. A technique that is sometimes used is called multifrequency testing. This method applies the simultaneous oscillatory forces over a wide range of frequencies during one test run. Use of the multifrequency testing is useful for calculating activation energies, which can reveal transitions in response and structural changes in the material.

The following sections describe results from various techniques used to analyze features of the storage modulus, loss modulus, and tangent delta profiles. Because of the high sensitivity of DMTA, slight variations in specific features can reveal the degree of cure, changes in molecular weight distribution, crystallization, irreversible degradation, and varying plasticization states.

8.2. RESULTS AND DISCUSSION

8.2.1. Tan Delta

Parameters derived from the tan delta profile are the most common feature analyzed by past researchers. Older instruments measured only phase angle, thus measurements from tan delta could only be inferred indirectly [108]. Another reason the tan delta profile is often analyzed is because it is a unit-less parameter and is independent of error due to measurement [108]. The tan delta curve provides information about the ability of a material to lose energy due to molecular rearrangements and internal friction [108]. It is calculated according to equation 8-1 [108].

$$\tan \delta = \frac{E''}{E'} \quad (8-1)$$

where:

E'' is the loss modulus, and

E' is the storage modulus

The high sensitivity of the DMTA can reveal changes in the various DMTA parameters that can reveal the varying degradation mechanisms occurring in a composite subjected to environmental exposure. Examining data in terms of durability involves discerning the types of degradation that occur simultaneously. When analyzing samples cured under ambient conditions, the effect of residual cure occurs in the short-term (i.e. 0-16 weeks). This effect is often countered by the effect of plasticization through moisture uptake when samples are immersed in aqueous solutions, which also typically occurs in the short-term. Changes in various DMTA

parameters during short-term immersion are the result of a competitive effect between these two factors. During long-term immersion, hydrolysis can occur in which low-weight molecular species are leached out of the material that can also affect DMTA parameters. The difficulty in examining results obtained from DMTA is in differentiating the separate effects of each of the factors described above. The following sections present values determined from DMTA tests and their change with time is analyzed in order to discriminate the effects of mechanisms such as residual cure, plasticization, and hydrolysis.

8.2.1.1. Glass Transition Temperature

DMTA measures the transition between the elastic and viscoelastic regimes [109]. The middle of the transition region is often measured by the peak position from the loss modulus [109]. The glass transition temperature (T_g) from the tan delta profile is denoted by its peak and marks the end of the transition period. The peak position of the loss modulus marks the middle portion of the transition region. Because specimens were tested in bending in the longitudinal direction, the dominance of the fiber is relevant and delays the T_g of the resin. This value of T_g determined from the peak of the tan delta curve is typically larger than that found from the loss modulus.

Results for the storage and loss modulus are provided in the Appendix. Trends typically are similar, therefore the analysis will solely concentrate on values of T_g based on tan delta.

The T_g is provided for four different frequencies (1, 5, 10, and 30 Hz) in Tables 8.1-8.7, however the variation is only plotted for the 1 Hz frequency in Figures 8.1-8.4. It should be noted that higher frequencies shift the T_g to higher temperature levels, but the overall response follows the same trends.

Table 8.1a. T_g Based on Tan Delta for Ambient Condition at 23°C and 30% RH

Time [weeks]	Ambient							
	1 Hz [°C]	Std. Dev. [°C]	5 Hz [°C]	Std. Dev. [°C]	10 Hz [°C]	Std. Dev. [°C]	30 Hz [°C]	Std. Dev. [°C]
0	117.1	0.3	122.0	0.3	128.0	0.5	128.9	0.1
4	118.1	0.9	123.7	0.9	130.0	0.6	130.4	0.4
8	119.8	0.3	125.4	0.1	131.6	0.1	132.1	0.4
12	119.3	1.2	124.8	1.0	126.2	0.5	131.1	0.5
16	120.1	0.1	125.5	0.0	127.5	1.4	132.3	1.1
24	121.4	0.8	128.0	0.0	129.0	2.5	134.5	1.7
32	-	-	-	-	-	-	-	-
48	120.9	-	126.6	-	129.4	-	134.9	-
72	123.1	0.7	128.9	1.1	131.1	0.7	136.7	0.7

Table 8.1b. T_g Based on Tan Delta Determined After Immersion in 23°C Seawater (“Wet Testing”) and as a Result of Subsequent Redrying (“Dry Testing”)

Time [weeks]	23°C Seawater “Wet Testing”							
	1 Hz [°C]	Std. Dev. [°C]	5 Hz [°C]	Std. Dev. [°C]	10 Hz [°C]	Std. Dev. [°C]	30 Hz [°C]	Std. Dev. [°C]
0	117.1	0.3	122.0	0.3	124.9	0.5	128.9	0.1
4	111.6	1.5	117.0	1.1	119.7	0.7	128.1	3.2
8	114.2	0.3	120.0	0.9	122.8	0.4	130.5	3.8
12	113.2	0.1	118.6	0.4	121.1	0.4	129.1	3.6
16	-	-	-	-	-	-	-	-
26	114.9	1.1	121.2	1.0	122.5	1.0	127.3	0.6
35	114.4	1.5	121.1	1.8	122.1	1.3	127.5	2.0
52	116.8	0.4	122.1	0.8	124.9	0.8	129.4	0.7
78	115.7	0.5	122.4	0.7	125.1	0.7	129.1	0.7

Time [weeks]	23°C Seawater “Dry Testing”							
	1 Hz [°C]	Std. Dev. [°C]	5 Hz [°C]	Std. Dev. [°C]	10 Hz [°C]	Std. Dev. [°C]	30 Hz [°C]	Std. Dev. [°C]
0	117.1	0.3	122.0	0.3	124.9	0.5	128.9	0.1
4	119.3	1.0	125.0	1.2	127.4	0.7	134.9	4.1
8	117.2	0.6	122.6	0.9	125.4	0.6	133.3	3.7
12	120.8	0.2	126.1	0.3	128.5	0.4	137.1	3.7
16	119.2	0.3	124.7	0.8	127.4	1.1	131.6	0.4
26	119.0	0.5	125.4	0.6	126.9	0.3	132.9	0.2
35	119.2	1.9	125.1	1.1	127.3	1.2	132.7	0.6
52	119.5	1.2	125.6	0.5	128.3	0.4	132.8	1.2
78	119.1	1.2	125.4	0.2	127.6	0.9	133.2	0.9

Table 8.1c. T_g Based on Tan Delta Determined After Immersion in 40°C Seawater (“Wet Testing”) and as a Result of Subsequent Redrying (“Dry Testing”)

Time [weeks]	40°C Seawater “Wet Testing”							
	1 Hz [°C]	Std. Dev. [°C]	5 Hz [°C]	Std. Dev. [°C]	10 Hz [°C]	Std. Dev. [°C]	30 Hz [°C]	Std. Dev. [°C]
0	117.1	0.3	122.0	0.3	124.9	0.5	128.9	0.1
4	114.5	0.6	120.3	0.6	122.4	0.6	130.5	3.7
8	109.0	0.4	114.0	0.5	116.8	0.5	124.4	3.1
12	112.6	0.7	118.1	0.7	120.9	0.3	128.8	3.7
16	113.9	0.7	119.4	0.7	121.8	0.7	126.0	0.6
26	115.2	0.8	120.2	0.0	123.2	0.0	128.2	0.0
35	113.8	1.0	119.8	0.8	122.1	0.4	127.0	1.5
52	116.6	0.1	121.9	1.2	124.7	1.2	129.7	0.3
78	117.2	0.5	124.0	0.5	126.2	1.0	130.6	0.4

Time [weeks]	40°C Seawater “Dry Testing”							
	1 Hz [°C]	Std. Dev. [°C]	5 Hz [°C]	Std. Dev. [°C]	10 Hz [°C]	Std. Dev. [°C]	30 Hz [°C]	Std. Dev. [°C]
0	117.1	0.3	122.0	0.3	124.9	0.5	128.9	0.1
4	113.8	0.6	119.6	0.7	122.1	0.5	130.1	3.4
8	115.6	1.5	120.9	1.8	123.4	1.8	131.8	4.1
12	118.7	0.8	123.9	0.2	126.3	1.1	134.5	3.7
16	118.7	1.1	124.3	1.0	127.3	1.2	131.8	1.0
26	118.9	1.6	124.7	1.3	126.1	3.9	130.9	3.8
35	118.8	0.9	124.2	1.4	126.9	1.4	132.0	1.0
52	120.8	0.8	127.5	0.9	128.5	0.9	133.7	0.6
78	121.2	0.4	127.8	0.4	128.8	0.4	133.9	0.5

Table 8.1d. T_g Based on Tan Delta Determined After Immersion in 60°C Seawater (“Wet Testing”) and as a Result of Subsequent Redrying (“Dry Testing”)

Time [weeks]	60°C Seawater “Wet Testing”							
	1 Hz [°C]	Std. Dev. [°C]	5 Hz [°C]	Std. Dev. [°C]	10 Hz [°C]	Std. Dev. [°C]	30 Hz [°C]	Std. Dev. [°C]
0	117.1	0.3	122.0	0.3	124.9	0.5	128.9	0.1
4	111.2	1.7	116.0	1.7	118.3	1.7	126.2	3.5
8	113.8	0.5	119.0	0.2	121.0	0.6	128.9	3.4
12	116.0	0.2	120.8	0.4	123.3	0.4	131.1	3.7
16	117.1	1.1	122.6	0.9	125.0	0.8	129.7	0.2
26	116.7	0.8	121.9	0.5	125.0	0.5	129.3	1.3
35	117.8	1.4	122.5	1.1	125.3	1.3	129.3	1.3
52	119.7	1.1	124.2	1.3	125.8	1.0	130.8	1.3
78	120.7	0.5	125.6	0.3	127.5	1.0	132.3	0.2

Time [weeks]	60°C Seawater “Dry Testing”							
	1 Hz [°C]	Std. Dev. [°C]	5 Hz [°C]	Std. Dev. [°C]	10 Hz [°C]	Std. Dev. [°C]	30 Hz [°C]	Std. Dev. [°C]
0	117.1	0.3	122.0	0.3	124.9	0.5	128.9	0.1
4	118.3	1.0	123.5	0.9	125.7	1.7	133.7	3.8
8	120.6	0.6	125.9	0.9	128.3	0.8	137.2	3.5
12	122.4	0.9	127.8	0.5	130.3	0.5	138.5	4.0
16	122.6	0.6	128.0	1.3	131.1	1.3	135.8	2.3
26	122.1	1.1	127.7	1.1	130.3	1.4	134.9	0.7
35	127.2	2.9	132.7	1.7	135.7	3.2	140.5	2.7
52	127.3	0.6	132.1	0.3	134.9	0.3	139.9	1.2
78	127.4	1.4	132.0	1.3	135.4	2.0	139.9	1.1

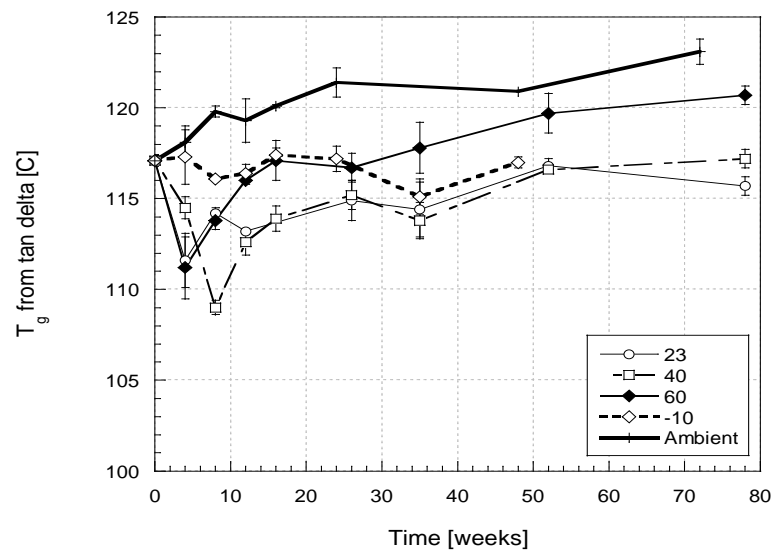


Figure 8.1. Change in T_g at 1 Hz Based on Tan Delta as a Function of Temperature and Time of Immersion in Seawater

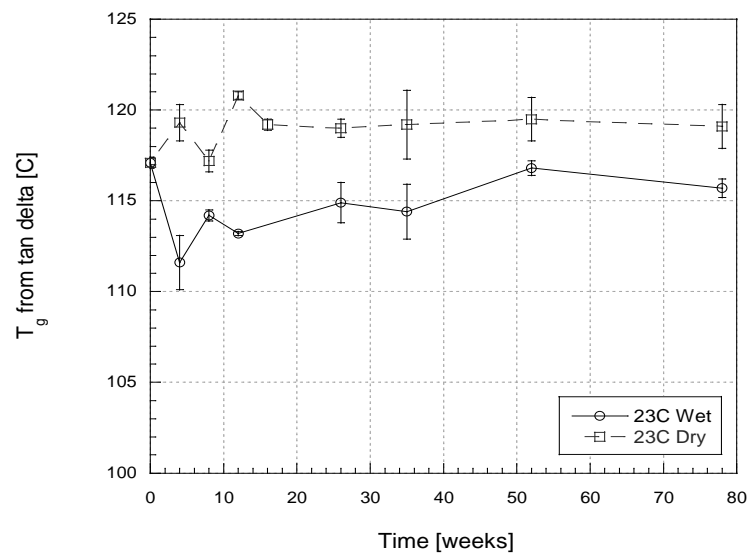


Figure 8.2a. Effect of Redrying on T_g at 1 Hz Based on Tan Delta After Immersion in 23°C Seawater

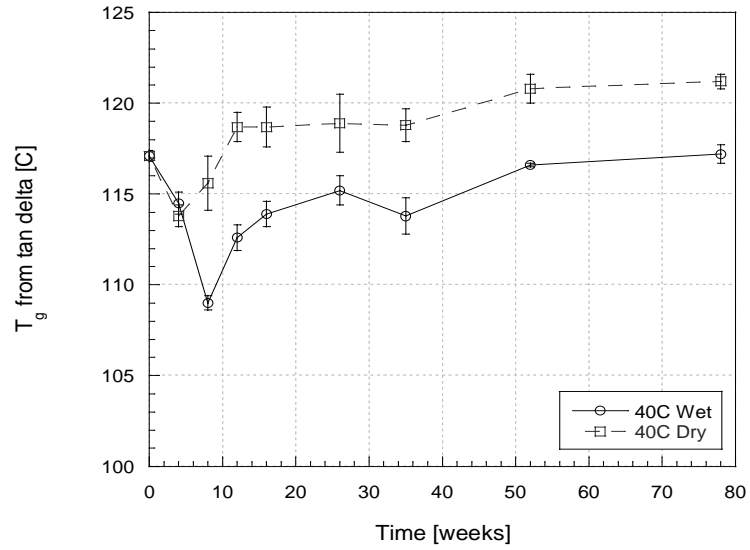


Figure 8.2b. Effect of Redrying on T_g at 1 Hz Based on Tan Delta After Immersion in 40°C Seawater

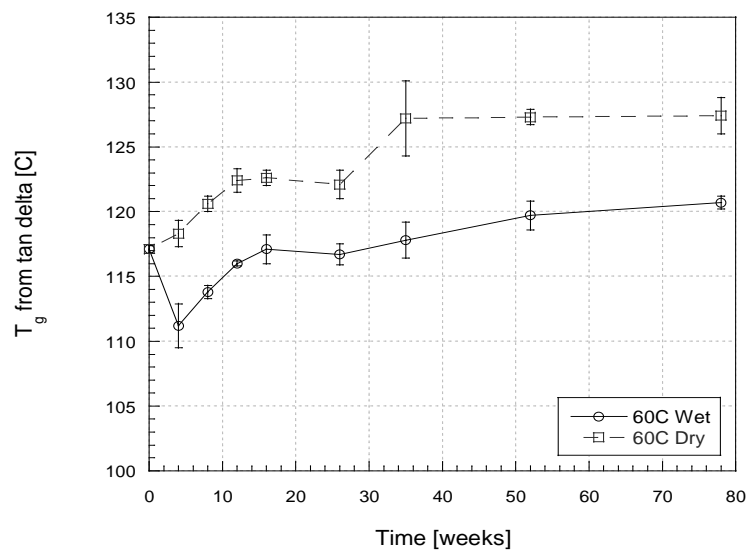


Figure 8.2c. Effect of Redrying on T_g at 1 Hz Based on Tan Delta After Immersion in 60°C Seawater

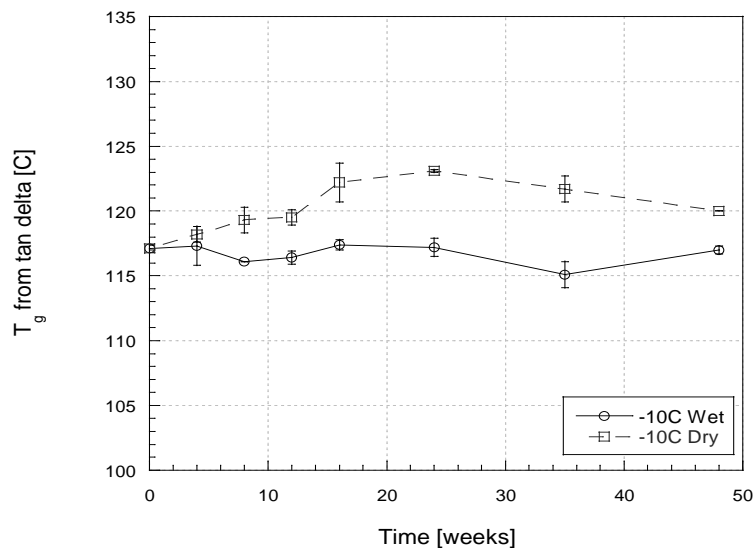


Figure 8.2d. Effect of Redrying on T_g at 1 Hz Based on Tan Delta After Immersion in -10°C Seawater

Typical analyses of T_g can represent the mobility of the polymer chain in the composite [109]. Figure 8.1 clearly shows the initial depression in the T_g that occurs at 4 weeks due to moisture uptake. This behavior is seen at all temperatures of immersion. An increase in moisture uptake accompanied by decreases in T_g is an indicator of moisture-initiated plasticization [55,109,111]. Others have suggested that a depression in T_g could be a result of the sorption in solution of free volume as unbound water [109]. This idea is based on the concept that water exists in two forms. The first form is described as free water that is absorbed through microcavities in the polymer [110]. The second form is a bound type of water that is absorbed through interactions between the polar segments in the polymer chain [110]. Noguiera et al. explained that moisture uptake affects the molecular structure through the hydrogen bonds between the water molecules and that the polar hydroxyl groups disrupt interchain hydrogen bonding [110]. It has also been noted that the reinforcing fibers in a composite have been found to enhance plasticization and hydrolysis, and delay T_g kinetics [18].

Specimens immersed in 23°C , 40°C , and 60°C seawater show an initial decrease in T_g between 0-4 weeks, which is then followed by either a noticeable increase in T_g (i.e. in the case

of 60°C) or a subtle increase in T_g (i.e. in the case of 23°C and 40°C). The depression is often caused by the initial effects of plasticization, while the elevation in T_g is due to leaching of molecular weight flexibilizing segments that occurs by processes such as hydrolysis and causes embrittlement of the matrix [18,40,109]. This hypothesis is reinforced by the moisture uptake profiles showed in Chapter 4 that show a continual decrease in weight gain after 4 weeks immersion in 23°C, 40°C, and 60°C seawater indicating loss in weight. The decrease in moisture uptake is most apparent at 60°C immersion and is present, but less obvious in 23°C and 40°C immersion cases.

Exposure of the specimens to a freezing environment reflects stable trends in a glass transition temperature of 117°C. While a depression in the T_g can be reasonably expected due to the 8-month period of saturation prior to freezing, a closer look at the results reveal that after 8 months exposure to 23°C seawater, the glass transition temperature is 116.8°C. The following exposure of the specimens to 12 months immersion in -10°C seawater shows that results stabilize around this value. The results are consistent with those reported by Jamond et al. who found insignificant changes on the T_g from freezing [106]. As seen in Figure 8.2d, the level of T_g exceeded as-received values upon redrying.

Redrying in an environmental chamber for 30 days at 23°C and 30% RH after immersion in 23°C, 40°C, and 60°C seawater showed increases in T_g that exceeded as-received values. As early as 12 weeks exposure to 40°C seawater immersion, the T_g was completely regained. In fact, a closer look at Table 8.1c shows that at 12 weeks, the T_g increased by 6.1°C at 1 Hz. Immersion in 60°C seawater revealed that the T_g was immediately regained at 4 weeks. Redrying after immersion in 60°C seawater resulted in an increase of 10°C in T_g at 35 weeks as compared to as-received data. For both these immersion conditions, the increase in T_g after redrying is caused by leaching of lower molecular weight species. The effect of drying eliminates the effect

of a depression in T_g due to moisture, therefore a prominent increase in T_g due to leaching is emphasized.

Table 8.2a. T_g Based on Tan Delta Determined as a Function of Time During Freeze/Thaw Exposure

Time [weeks]	Freeze/Thaw "Wet Testing"							
	1 Hz [°C]	Std. Dev. [°C]	5 Hz [°C]	Std. Dev. [°C]	10 Hz [°C]	Std. Dev. [°C]	30 Hz [°C]	Std. Dev. [°C]
0	117.1	0.3	122.0	0.3	128.0	0.5	128.9	0.1
4	116.6	0.6	122.4	0.4	128.4	0.4	128.9	0.4
8	116.5	1.7	122.6	1.2	128.8	1.5	129.3	1.4
12	-	-	-	-	-	-	-	-
16	114.8	0.4	121.0	0.8	123.8	1.2	128.3	0.9
24	115.4	0.8	121.4	0.7	123.5	1.2	128.7	1.1
35	116.6	1.8	123.2	1.7	125.4	1.2	131.0	1.2
54	116.9	3.1	124.0	2.1	125.6	2.6	130.6	3.6
72	115.8	2.7	122.7	0.9	124.4	1.8	130.0	1.8

Time [weeks]	Freeze/Thaw "Dry Testing"							
	1 Hz [°C]	Std. Dev. [°C]	5 Hz [°C]	Std. Dev. [°C]	10 Hz [°C]	Std. Dev. [°C]	30 Hz [°C]	Std. Dev. [°C]
0	117.1	0.3	122.0	0.3	128.0	0.5	128.9	0.1
4	114.0	0.6	119.6	0.0	125.8	0.6	126.6	0.6
8	120.9	1.4	126.6	2.0	132.9	2.0	132.9	2.1
12	119.6	0.6	125.7	0.8	128.6	0.7	133.0	0.7
16	-	-	-	-	-	-	-	-
24	120.9	0.8	126.9	0.8	129.6	0.7	134.6	1.6
35	120.4	-	126.8	-	131.3	-	135.3	-
54	121.8	1.0	127.2	0.7	128.9	1.6	135.7	0.8
72	121.1	0.7	127.1	0.5	129.9	0.5	134.9	1.6

Table 8.2b. T_g Based on Tan Delta Determined as a Function of Time During Wet/Dry Exposure

Time [weeks]	Wet/Dry "Wet Testing"							
	1 Hz [°C]	Std. Dev. [°C]	5 Hz [°C]	Std. Dev. [°C]	10 Hz [°C]	Std. Dev. [°C]	30 Hz [°C]	Std. Dev. [°C]
0	117.1	0.3	122.0	0.3	128.0	0.5	128.9	0.1
4	112.1	2.5	118.1	2.5	123.9	2.8	124.8	2.2
8	114.6	3.5	120.5	3.3	127.8	4.2	127.6	4.0
12	116.5	1.2	122.5	1.5	124.5	1.5	129.6	1.7
16	114.9	1.1	120.7	1.3	122.9	1.7	128.6	0.6
24	115.1	-	121.2	-	123.1	-	128.6	-
35	116.3	-	122.6	-	124.4	-	130.2	-
54	115.3	-	121.0	-	123.7	-	129.4	-
72	116.3	1.1	122.2	1.9	124.4	1.8	130.0	1.9

Time [weeks]	Wet/Dry "Dry Testing"							
	1 Hz [°C]	Std. Dev. [°C]	5 Hz [°C]	Std. Dev. [°C]	10 Hz [°C]	Std. Dev. [°C]	30 Hz [°C]	Std. Dev. [°C]
0	117.1	0.3	122.0	0.3	128.0	0.5	128.9	0.1
4	118.4	0.7	124.3	0.3	130.9	0.8	131.3	0.3
8	119.4	0.5	125.0	0.8	127.8	0.4	132.4	0.0
12	120.3	-	125.8	-	128.9	-	133.8	-
16	-	-	-	-	-	-	-	-
24	121.3	-	126.9	-	129.7	-	135.1	-
35	118.7	-	125.3	-	127.1	-	131.9	-
54	121.2	2.9	127.3	3.4	129.6	4.2	134.2	3.0
72	117.7	2.1	124.8	2.0	127.3	0.9	131.6	1.9

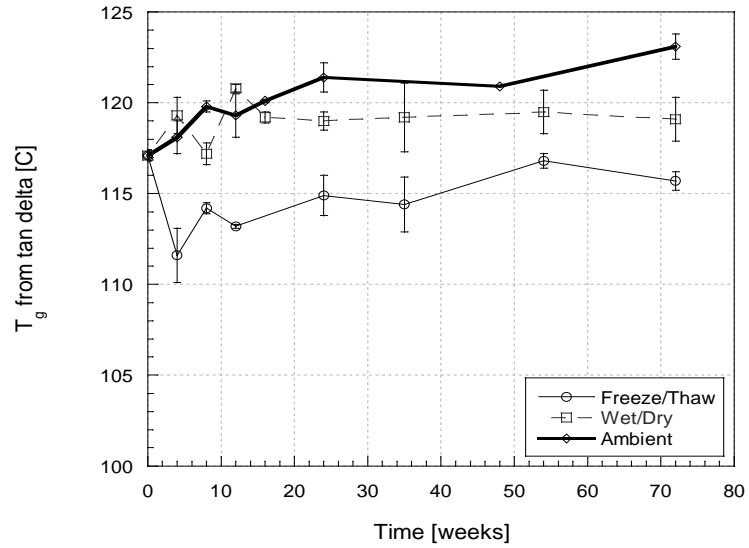


Figure 8.3. Change in T_g at 1 Hz Based on Tan Delta As a Function of Time and Type of Cyclic Exposure

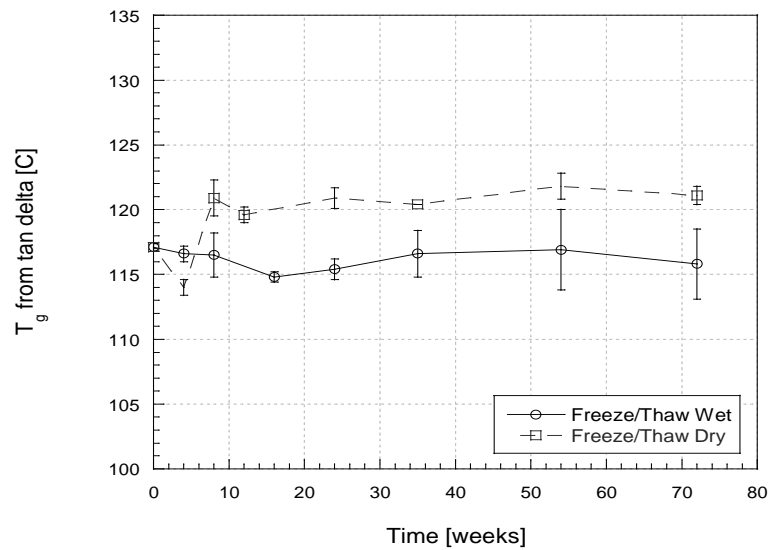


Figure 8.4a. Effect of Redrying on T_g at 1 Hz Based on Tan Delta as a Function of Freeze/Thaw Exposure

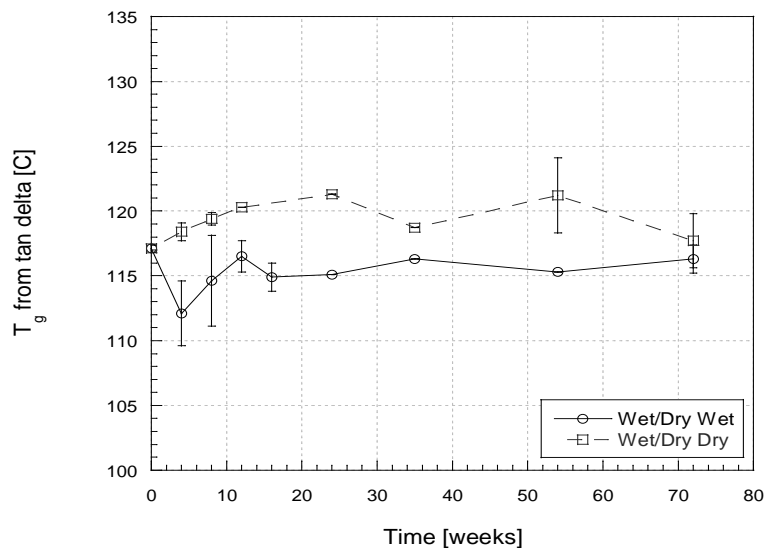


Figure 8.4b. Effect of Redrying on T_g at 1 Hz Based on Tan Delta as a Function of Wet/Dry Exposure

As seen in Figure 8.3, there is an initial depression in T_g after 4 weeks after exposure to the freeze/thaw cycle and after 8 weeks for the wet/dry cycle. Initial variations occur as a consequence of the cyclic exposure, however longer term exposure shows more stable trends. A stabilization of the T_g signifies the small amount of moisture in the composite, which is attributed to lower level of uptake in cyclic exposures. Values of the T_g are reflected as regainable (Figure 8.4), which is consistent with results found by Mazor, Broutman, and Eckstein [87].

8.2.1.2. Height of Tan Delta

The height of the tan delta (h_α) profile is an indicator of the amount of moisture ingress caused by exposure to various environments. A depression in h_α is often caused by moisture ingress. Subsequently, changes in h_α are an indicator of the competing effects of residual cure and degradation and an overall increase denotes an increasing level of cure.

The following tables summarize the values of h_α and are organized by environmental exposure.

Table 8.3a. Height of Tan Delta for Ambient Condition at 23°C and 30%RH - Values are Unitless

Time [weeks]	Ambient							
	1 Hz	Std. Dev.	5 Hz	Std. Dev.	10 Hz	Std. Dev.	30 Hz	Std. Dev.
0	0.278	0.027	0.302	0.031	0.313	0.031	0.331	0.034
4	0.293	0.004	0.314	0.004	0.324	0.005	0.339	0.006
8	0.287	0.010	0.309	0.010	0.320	0.009	0.337	0.009
12	0.317	0.011	0.335	0.010	0.352	0.007	0.367	0.006
16	0.312	0.013	0.332	0.012	0.348	0.006	0.364	0.005
24	0.317	0.015	0.341	0.017	0.369	0.027	0.387	0.030
32	-	-	-	-	-	-	-	-
48	0.288	0.010	0.305	0.010	0.322	0.008	0.336	0.008
72	0.289	0.017	0.304	0.019	0.319	0.023	0.330	0.024

Table 8.3b. Height of Tan Delta Determined After Immersion in 23°C Seawater (“Wet Testing”) and as a Result of Subsequent Redrying (“Dry Testing”) – Values are Unitless

Time [weeks]	23°C Seawater “Wet Testing”							
	1 Hz	Std. Dev.	5 Hz	Std. Dev.	10 Hz	Std. Dev.	30 Hz	Std. Dev.
0	0.278	0.027	0.302	0.031	0.313	0.031	0.331	0.034
4	0.244	0.006	0.263	0.008	0.271	0.008	0.286	0.010
8	0.297	0.006	0.316	0.006	0.326	0.005	0.339	0.006
12	0.309	0.017	0.328	0.019	0.337	0.020	0.353	0.022
16	-	-	-	-	-	-	-	-
26	0.320	0.010	0.334	0.010	0.361	0.025	0.374	0.030
35	0.326	0.030	0.343	0.029	0.365	0.024	0.378	0.025
52	0.308	0.032	0.324	0.033	0.340	0.037	0.350	0.040
78	0.314	0.008	0.329	0.010	0.347	0.012	0.358	0.015

Time [weeks]	23°C Seawater “Dry Testing”							
	1 Hz	Std. Dev.	5 Hz	Std. Dev.	10 Hz	Std. Dev.	30 Hz	Std. Dev.
0	0.278	0.027	0.302	0.031	0.313	0.031	0.331	0.034
4	0.270	0.001	0.291	0.000	0.302	0.000	0.317	0.001
8	0.293	0.002	0.311	0.002	0.320	0.002	0.333	0.001
12	0.315	0.009	0.336	0.007	0.345	0.006	0.360	0.005
16	0.306	0.006	0.331	0.007	0.341	0.007	0.360	0.007
26	0.321	0.007	0.342	0.008	0.363	0.010	0.379	0.011
35	0.319	0.000	0.335	0.002	0.352	0.001	0.365	0.004
52	0.306	0.002	0.322	0.001	0.340	0.004	0.352	0.005
78	0.303	0.013	0.320	0.014	0.338	0.016	0.351	0.018

Table 8.3c. Height of Tan Delta Determined After Immersion in 40°C Seawater (“Wet Testing”) and as a Result of Subsequent Redrying (“Dry Testing”) – Values are Unitless

Time [weeks]	40°C Seawater “Wet Testing”							
	1 Hz	Std. Dev.	5 Hz	Std. Dev.	10 Hz	Std. Dev.	30 Hz	Std. Dev.
0	0.278	0.027	0.302	0.031	0.313	0.031	0.331	0.034
4	0.306	0.021	0.325	0.022	0.335	0.022	0.350	0.023
8	-	-	-	-	-	-	-	-
12	0.294	0.012	0.314	0.013	0.323	0.014	0.337	0.015
16	0.333	0.007	0.357	0.007	0.366	0.008	0.384	0.007
26	0.315	0.016	0.331	0.017	0.344	0.017	0.353	0.018
35	0.317	0.019	0.332	0.020	0.345	0.021	0.355	0.022
52	0.326	0.001	0.341	0.003	0.358	0.007	0.367	0.008
78	0.310	0.006	0.326	0.006	0.339	0.009	0.349	0.009

Time [weeks]	40°C Seawater “Dry Testing”							
	1 Hz	Std. Dev.	5 Hz	Std. Dev.	10 Hz	Std. Dev.	30 Hz	Std. Dev.
0	0.278	0.027	0.302	0.031	0.313	0.031	0.331	0.034
4	0.293	0.000	0.312	0.001	0.323	0.002	0.339	0.005
8	0.323	0.009	0.347	0.009	0.358	0.009	0.375	0.009
12	0.311	0.002	0.332	0.002	0.342	0.003	0.356	0.004
16	0.319	0.003	0.341	0.004	0.351	0.004	0.367	0.004
26	0.335	0.013	0.351	0.017	0.376	0.016	0.390	0.019
35	0.321	0.011	0.339	0.010	0.357	0.013	0.368	0.013
52	0.311	0.011	0.326	0.012	0.339	0.014	0.350	0.013
78	0.341	0.014	0.356	0.013	0.374	0.015	0.385	0.014

Table 8.3d. Height of Tan Delta Determined After Immersion in 60°C Seawater (“Wet Testing”) and as a Result of Subsequent Redrying (“Dry Testing”) – Values are Unitless

Time [weeks]	60°C Seawater “Wet Testing”							
	1 Hz	Std. Dev.	5 Hz	Std. Dev.	10 Hz	Std. Dev.	30 Hz	Std. Dev.
0	0.278	0.027	0.302	0.031	0.313	0.031	0.331	0.034
4	0.284	0.015	0.305	0.016	0.314	0.016	0.330	0.016
8	0.295	0.023	0.314	0.023	0.323	0.023	0.336	0.023
12	0.328	0.008	0.350	0.008	0.358	0.007	0.371	0.007
16	0.333	0.008	0.352	0.014	0.360	0.014	0.374	0.014
26	0.303	0.016	0.320	0.015	0.329	0.014	0.338	0.014
35	0.299	0.010	0.316	0.009	0.326	0.008	0.337	0.006
52	0.317	0.024	0.340	0.023	0.351	0.024	0.363	0.023
78	0.277	0.008	0.297	0.009	0.307	0.010	0.316	0.012

Time [weeks]	60°C Seawater “Dry Testing”							
	1 Hz	Std. Dev.	5 Hz	Std. Dev.	10 Hz	Std. Dev.	30 Hz	Std. Dev.
0	0.278	0.027	0.302	0.031	0.313	0.031	0.331	0.034
4	0.338	0.017	0.363	0.016	0.379	0.019	0.394	0.019
8	0.348	0.017	0.369	0.016	0.378	0.015	0.392	0.015
12	0.354	0.009	0.372	0.008	0.380	0.008	0.392	0.008
16	0.335	-	0.353	-	0.376	-	0.390	-
26	0.312	0.018	0.332	0.014	0.343	0.013	0.355	0.010
35	0.316	-	0.332	-	0.344	-	0.353	-
52	0.323	0.011	0.342	0.012	0.354	0.014	0.365	0.013
78	0.327	0.011	0.347	0.013	0.359	0.014	0.370	0.015

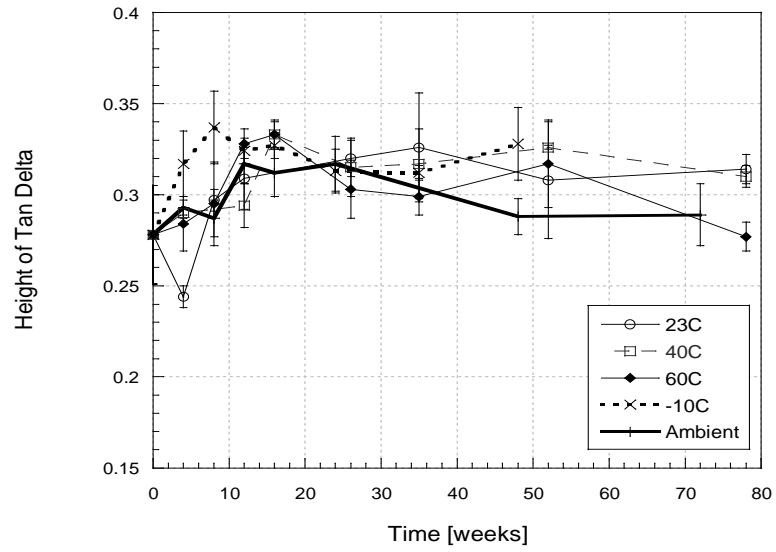


Figure 8.5. Change in Height of Tan Delta at 1 Hz as a Function of Temperature and Time of Immersion in Seawater

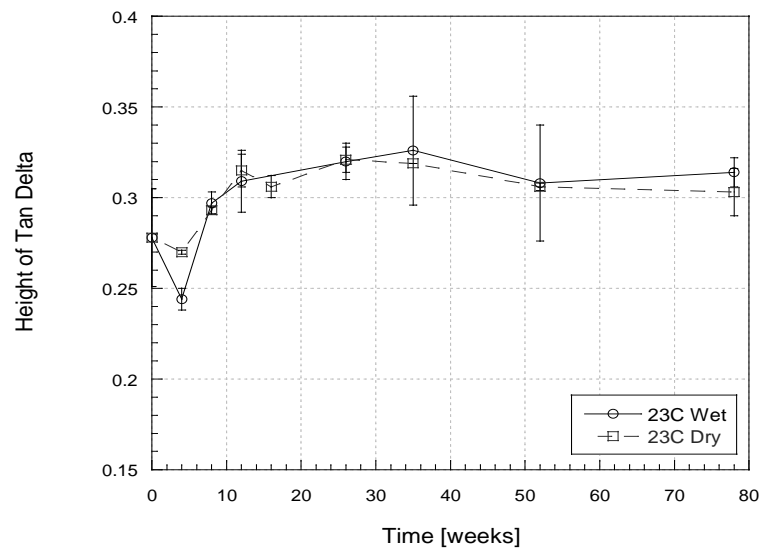


Figure 8.7a. Effect of Redrying on Height of Tan Delta after Immersion in 23°C Seawater

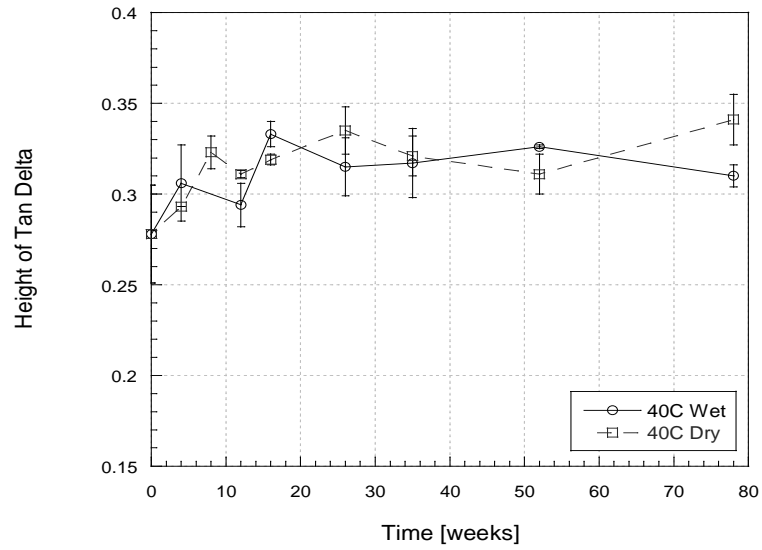


Figure 8.7b. Effect of Redrying on Height of Tan Delta after Immersion in 40°C Seawater

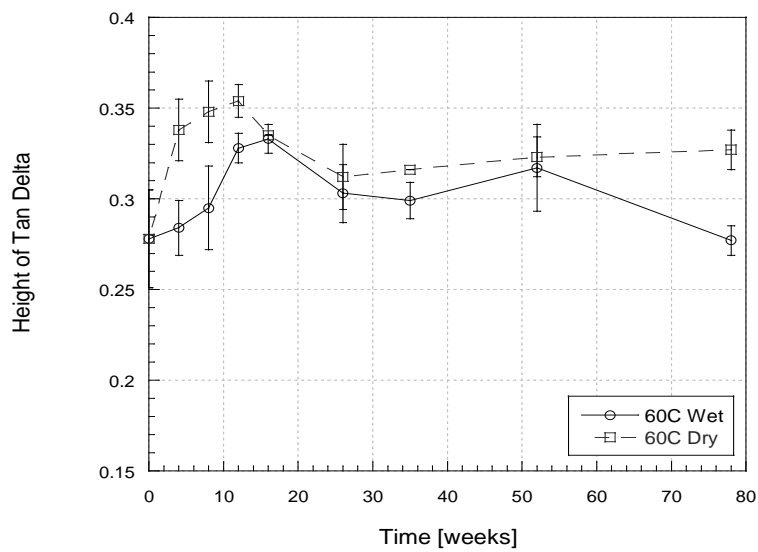


Figure 8.7c. Effect of Redrying on Height of Tan Delta after Immersion in 60°C Seawater

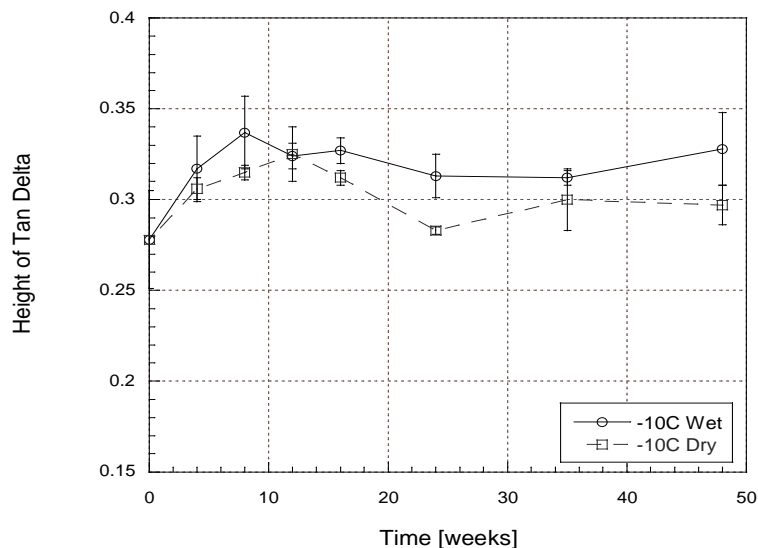


Figure 8.7d. Effect of Redrying on Height of Tan Delta after Immersion in -10°C Seawater

The height of the tan delta profile can be an indication of the competing effects of level of cure and moisture-induced degradation. This is a critical parameter for reviewing samples cured under ambient conditions. The level of cure is indicative of the molecular structure in a polymer, which is typically referred to as crosslinking density. This idea of crosslinking density is reviewed in a paper by Soles and Yee [111]. A fully crosslinked material has a broad β -relaxation peak [111]. As the material becomes more damaged with exposure or time, the crosslink density decreases and is reflected by a decrease in the peak breadth, position, and height [111]. The breadth position is often calculated by the width at 50% of the maximum height of tan delta, which is often denoted “full width at half maximum (fwhm)” [111].

As can be seen from Figure 8.5, the height of the tan delta profile shows overall increases (with slight initial variations) for all immersion conditions. For 23°C, 40°C, and 60°C immersion conditions, increases in height occur between 8-12 weeks. Between these periods of time, it is likely that for composites manufactured under ambient conditions, residual cure occurs. After 12 weeks, changes in height of tan delta show smaller changes, which indicates that the effects of

residual cure are no longer present. Because immersion conditions all result in increases in height, the increase in height is caused by residual cure rather than the exposure.

The initial increases in height of tan delta are greater due to freezing after saturation, as compared to any other immersion condition. The increase is caused by a combination of residual cure and increased brittleness of the matrix due to freezing.

Table 8.4a. Height of Tan Delta Determined as a Function of Time and Freeze/Thaw Exposure – Values are Unitless

Time [weeks]	Freeze/Thaw “Wet Testing”							
	1 Hz	Std. Dev.	5 Hz	Std. Dev.	10 Hz	Std. Dev.	30 Hz	Std. Dev.
0	0.278	0.027	0.302	0.031	0.313	0.031	0.331	0.034
4	0.311	0.022	0.331	0.025	0.340	0.026	0.355	0.028
8	0.285	0.008	0.305	0.008	0.315	0.008	0.331	0.008
12	0.317	0.002	0.335	0.004	0.356	0.007	0.369	0.008
16	0.313	0.014	0.333	0.013	0.355	0.012	0.370	0.012
24	0.317	0.007	0.335	0.009	0.358	0.014	0.374	0.015
35	0.322	0.010	0.337	0.010	0.361	0.021	0.371	0.015
54	0.323	0.001	0.338	0.003	0.355	0.003	0.367	0.004
72	0.325	0.005	0.340	0.010	0.366	0.002	0.378	0.001

Time [weeks]	Freeze/Thaw “Dry Testing”							
	1 Hz	Std. Dev.	5 Hz	Std. Dev.	10 Hz	Std. Dev.	30 Hz	Std. Dev.
0	0.278	0.027	0.302	0.031	0.313	0.031	0.331	0.034
4	0.316	0.005	0.341	0.008	0.363	0.012	0.381	0.014
8	0.300	0.009	0.320	0.008	0.330	0.006	0.346	0.004
12	0.302	0.029	0.325	0.031	0.344	0.031	0.364	0.033
16	0.304	0.021	0.320	0.021	0.337	0.018	0.349	0.018
24	-	-	-	-	-	-	-	-
35	0.328	0.006	0.332	0.023	0.356	0.029	0.370	0.029
54	0.294	0.014	0.309	0.015	0.329	0.018	0.342	0.022
72	0.310	0.011	0.328	0.011	0.346	0.009	0.360	0.009

Table 8.4b. Height of Tan Delta Determined as a Function of Time and Wet/Dry Exposure – Values are Unitless

Time [weeks]	Wet/Dry “Wet Testing”							
	1 Hz	Std. Dev.	5 Hz	Std. Dev.	10 Hz	Std. Dev.	30 Hz	Std. Dev.
0	0.278	0.027	0.302	0.031	0.313	0.031	0.331	0.034
4	0.320	0.008	0.342	0.011	0.370	0.017	0.386	0.017
8	0.305	0.025	0.326	0.025	0.338	0.025	0.354	0.025
12	0.349	-	0.365	-	0.385	-	0.394	-
16	0.314	0.011	0.333	0.008	0.355	0.003	0.370	0.006
24	0.316	0.028	0.332	0.029	0.352	0.028	0.362	0.028
35	0.327	0.021	0.343	0.023	0.365	0.022	0.379	0.028
54	0.330	0.018	0.346	0.018	0.362	0.015	0.377	0.018
72	0.303	0.022	0.321	0.023	0.338	0.029	0.348	0.029

Time [weeks]	Wet/Dry “Dry Testing”							
	1 Hz	Std. Dev.	5 Hz	Std. Dev.	10 Hz	Std. Dev.	30 Hz	Std. Dev.
0	0.278	0.027	0.302	0.031	0.313	0.031	0.331	0.034
4	0.285	0.024	0.305	0.025	0.315	0.025	0.332	0.025
8	0.282	0.009	0.302	0.009	0.317	0.014	0.332	0.015
12	0.297	0.012	0.317	0.008	0.335	0.011	0.350	0.005
16	-	-	-	-	-	-	-	-
24	0.297	-	0.316	-	0.336	-	0.355	-
35	0.321	0.020	0.339	0.022	0.504	0.277	0.371	0.025
54	0.317	0.032	0.332	0.034	0.344	0.037	0.356	0.039
72	0.315	0.013	0.333	0.013	0.353	0.008	0.365	0.008

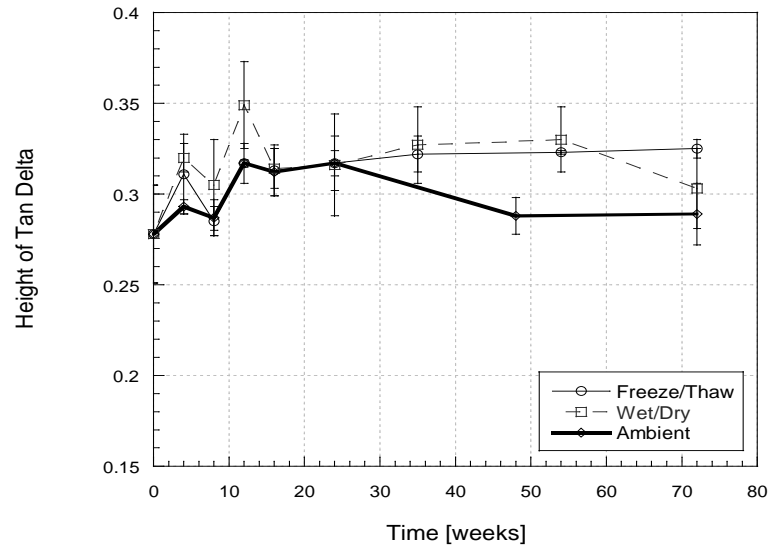


Figure 8.8. Change in Height of Tan Delta at 1 Hz As a Function of Time and Type of Cyclic Exposure

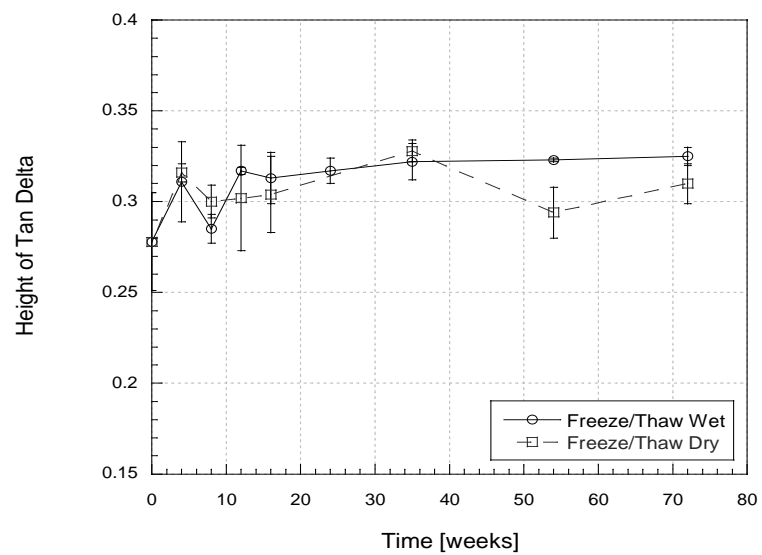


Figure 8.9a. Effect of Redrying on Height of Tan Delta as a Function of Freeze/Thaw Exposure

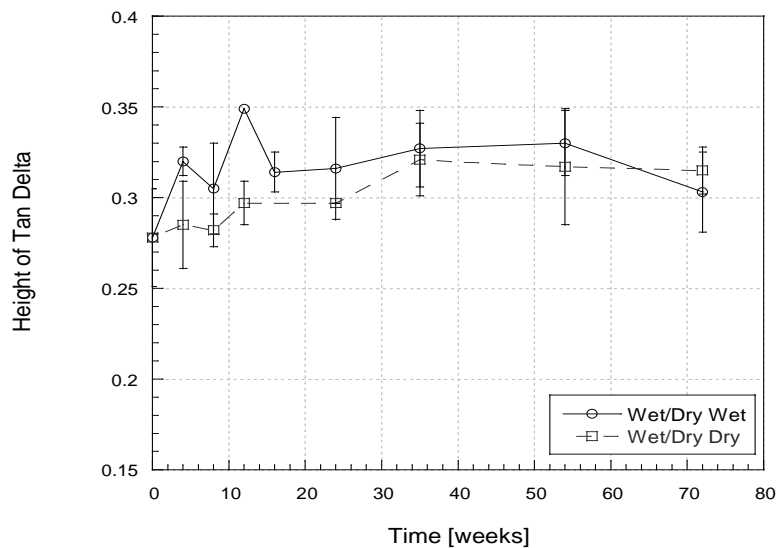


Figure 8.9b. Effect of Redrying on Height of Tan Delta as a Function of Wet/Dry Exposure

Exposure to freeze/thaw cycled showed an initially larger increase in height of tan delta from 0-12 weeks. Initial variations from 0-12 weeks could possibly be caused by microcracking due to the effects of the exposure and residual cure resulting from the manufacturing process. Figure 8.8b shows that the values of the height of the tan delta curve are within small scatter bounds from one another from 16-72 weeks, with the exception of the value resulting from exposure to the wet/dry cycle at 72 weeks. At this point, the value is lower than previous data, however a large amount of scatter is noted. Redrying showed indiscernible patterns in regards to the height of the tan delta profile.

8.2.1.3. Area Between Curves

Moisture ingress often causes the tan delta profile to shift with time. A measure of the level of degradation can be found by comparing results of an exposed sample to the as-received sample. This method was proposed by Nogueira et al. who stated that the effect of water interactions relates to the level of cure [110]. Calculating the area between the two curves can

track the change in molecular structure and be a good representation of the level of cure in the composite.

The following table summarizes the net area between the tan delta curve (calculated for selected periods of time) of an exposed sample to an as-received sample and is divided into immersion and cycling.

Table 8.5a. Area Between Tan Delta Curves at 1 Hz (Exposed Sample Compared to As-Received Sample) Determined as a Function of Temperature of Immersion in Seawater and Period of Exposure

Time [weeks]	Immersion in Seawater							
	23°C		40°C		60°C		-10°C	
	Area	Std. Dev.	Area	Std. Dev.	Area	Std. Dev.	Area	Std. Dev.
0	0.0	0.0	0.0	0.0	0.0	0.0	0.0	0.0
4	1.0	0.2	0.2	0.1	0.0	-	0.2	0.4
8	0.9	-	0.8	-	-0.1	-	0.4	-
16	-	-	-	-	-	-	0.2	0.3
26	0.3	-	0.6	-	-	-	0.1	0.5
52	0.3	-	0.5	-	-3.3	-	-0.4	0.4
78	0.4	-	0.5	0.4	-3.8	0.6		

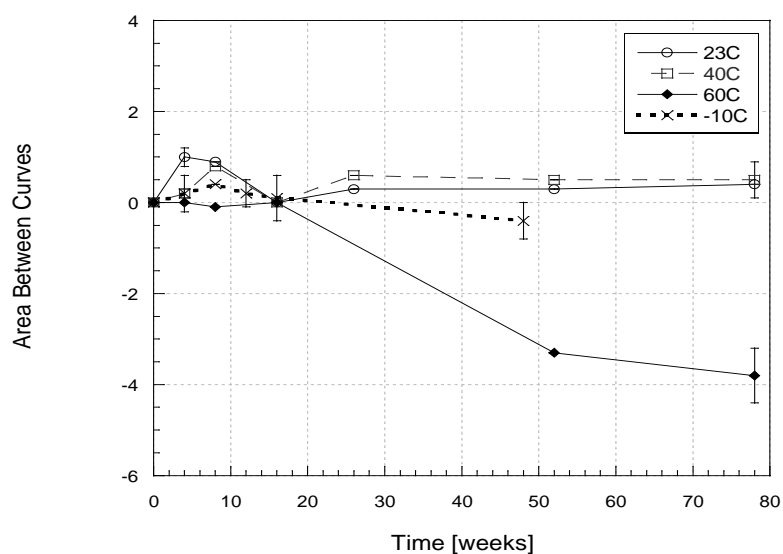


Figure 8.10a. Change in Area Between Tan Delta Curves at 1 Hz as a Function of Temperature of Immersion in Seawater and Period of Exposure

In order to analyze the area between curves, the general shift of the tan delta curve should be noted. The procedure used to calculate the areas between the curves is based on a study by Noguiera et al. [110]. Typically, if a tan delta profile shifts a large degree to the left from its as-received state, then this would indicate an ease in polymer chain mobility. High polymer chain mobility is often indicative of moisture-induced degradation. This causes the tan delta profile to shift to the left and provides a large net quantitative area. In this paper, this is denoted as a positive area, which follows the sign convention proposed by Noguiera et al. [110]. On the contrary, if a material exhibits an increased crosslinking density, this would cause less polymer chain mobility. If this is the case, the tan delta profile tends to shift very little. In cases where materials are under ambient cure conditions, initial periods of time may show an effect of cure which causes the tan delta profile to shift to the right. In cases such as these, the profile of the exposed specimen ends up shifting to the right of the as-received state. Consequently, this is noted as a negative area.

Referring to Figure 8.10a, exposure to 23°C seawater shows an increase in area at 4 weeks. An increase reflects high polymer chain mobility, which occurs as a result of plasticization. Plasticization is verified to occur between 0-12 weeks in 23°C seawater in Chapter 5 as well as in Section 8.2.1.1, which shows a depression in the T_g . After 26 weeks, the area stabilizes, which shows that polymer chain mobility is little affected by the exposure after this point. Changes in area after exposure to 40°C seawater show an increase in area at 8 weeks. This is caused by initial moisture-induced degradation. Changes from 26-78 weeks shows the value of the area between curves range from 0.5-0.6. This suggests that the effects of another type of degradation, such as hydrolysis is more prominent during long-term immersion. After exposure to seawater at 60°C, areas between curves do not change from 0-8 weeks and is followed by a dramatic decrease. The negative area is a consequence of the tan delta profile shifting to the right to a higher glass transition temperature. As explained in Section 8.2.2.1, leaching of low-weight molecular species

causes an increase in T_g . When this occurs, the composite structure changes and undergoes a brittle response.

The freezing condition shows a small change in area compared to immersion in 60°C seawater. The largest change occurs at 8 weeks with increase of 0.4 and at 52 weeks with a decrease of 0.4. As a result of the initial 8-month saturation, the area between the curves correspond to that level on the order of the value of the area between the curves reached under room temperature immersion at 52 weeks. As a result of freezing, little variation is observed. This level is maintained throughout the majority of testing, with the exception at 52 weeks, in which a slight drop in area is observed. An additional test at a period of 72 weeks would be optimal.

Table 8.5b. Area Between Tan Delta Curves at 1 Hz (Exposed Sample Compared to As-Received Sample) Determined as a Function of Type of Cyclic Exposure and Period of Exposure

Time [weeks]	Cyclic Exposure			
	Freeze/Thaw		Wet/Dry	
	Area	Std. Dev.	Area	Std. Dev.
0	0.0	0.0	0.0	0.0
4	0.2	0.5	-0.3	-
8	-0.1	0.6	-0.6	0.2
16	0.0	0.3	0.0	-
24	-0.2	0.0	-0.3	0.4
54	-0.2	0.3	-0.6	-
72	0.1	0.2	-0.6	-

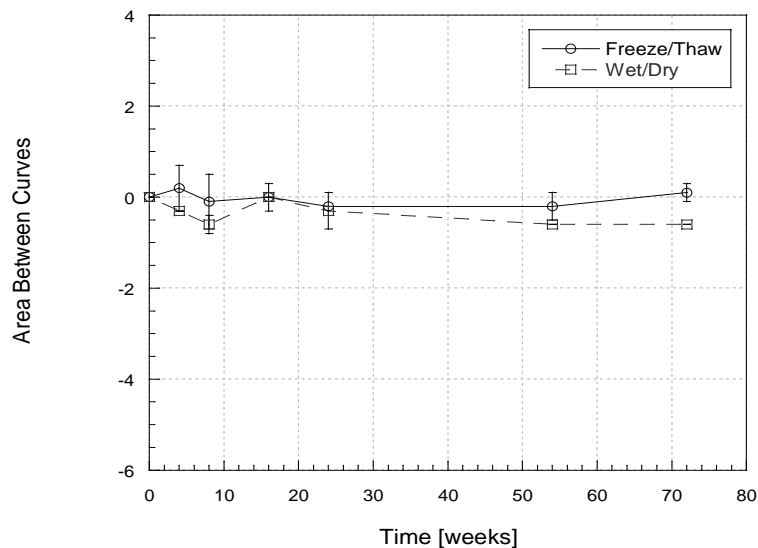


Figure 8.10b. Change in Area Between Tan Delta Curves at 1 Hz as a Function of Cyclic Exposure and Period of Exposure

Exposure to cycling conditions shows a small change in area as compared to immersion in 60°C seawater. This suggests that a different degradation mechanism, other than leaching and hydrolysis, occurs as a result of cyclic exposure. Exposure to the freeze/thaw cycle results in fluctuations in area from -0.2 to 0.1 during the 72-week immersion. Exposure to the wet/dry cycle results in fluctuations from -0.3 to -0.6 during the 72-week immersion. This implies that one degradation mechanism occurs for both cyclic exposures. As a result of cycling, microcracking of the matrix may result in the fluctuation during the 72-week exposure. Since the degree of microcracking varies from one specimen to another, this explains the fluctuations in area throughout the exposure period.

8.2.1.4. Activation Energy

The apparent activation energy (ΔE_a) based on the glass transition temperature is a measure of the energy barrier required for the transition between the elastic and viscoelastic regimes [109]. It is found by using the Arrhenius relationship, which is shown in equation 8-2.

$$f = f_o e^{-(\Delta E_a / RT)} \quad (8-2)$$

where:

f and f_o are frequencies,

ΔE_a is the Activation Energy,

R is the Universal Gas Constant, and

T is the temperature (in Kelvin).

The value ΔE_a can be found by plotting the natural logarithm of the frequency against the reciprocal of the temperature. The slope of this curve is multiplied by the universal gas constant and yields ΔE_a .

Activation energies are summarized in the following tables and are classified by immersion and cycling regimes.

Table 8.6a. Activation Energy Based on Tan Delta Determined After Exposure to Ambient Conditions at 23°C and 30% RH

Time [weeks]	Ambient	
	ΔE_a [kJ/mol]	Std. Dev. [kJ/mol]
0	357.3	10.7
4	349.6	18.0
8	354.2	12.4
12	365.6	2.2
16	344.2	-
24	332.3	6.1
35	-	-
48	332.2	23.2
72	340.2	28.9

Table 8.6b. Activation Energy Based on Tan Delta Determined After Immersion in 23°C Seawater (“Wet Testing”) and as a Result of Subsequent Redrying (“Dry Testing”)

Time [weeks]	23°C			
	“Wet Testing”		“Dry Testing”	
	ΔE_a [kJ/mol]	Std. Dev. [kJ/mol]	ΔE_a [kJ/mol]	Std. Dev. [kJ/mol]
0	357.3	10.7	357.3	10.7
4	340.9	-	351.0	1.2
8	337.1	-	350.9	5.8
12	338.1	5.1	359.1	17.9
16	-	-	348.0	7.7
26	334.2	10.7	327.6	15.7
35	334.2	14.9	-	-
52	333.2	1.0	336.1	4.0
78	329.2	4.0	320.7	23.0

Table 8.6c. Activation Energy Based on Tan Delta Determined After Immersion in 40°C Seawater (“Wet Testing”) and as a Result of Subsequent Redrying (“Dry Testing”)

Time [weeks]	40°C			
	“Wet Testing”		“Dry Testing”	
	ΔE_a [kJ/mol]	Std. Dev. [kJ/mol]	ΔE_a [kJ/mol]	Std. Dev. [kJ/mol]
0	357.3	10.7	357.3	10.7
4	341.8	3.9	343.4	1.8
8	345.6	6.8	339.5	3.2
12	337.7	-	347.6	2.8
16	336.6	1.5	326.8	15.0
26	348.4	4.9	336.4	4.7
35	334.2	15.4	336.7	1.4
52	336.0	5.5	349.9	11.8
78	331.3	9.0	345.8	-

Table 8.16d. Activation Energy Based on Tan Delta Determined After Immersion in 60°C Seawater (“Wet Testing”) and as a Result of Subsequent Redrying (“Dry Testing”)

Time [weeks]	60°C			
	“Wet Testing”		“Dry Testing”	
	ΔE_a [kJ/mol]	Std. Dev. [kJ/mol]	ΔE_a [kJ/mol]	Std. Dev. [kJ/mol]
0	357.3	10.7	357.3	10.7
4	368.4	0.7	372.2	27.8
8	360.2	9.9	356.2	15.7
12	371.3	15.9	364.8	14.6
16	367.1	-	370.9	30.1
26	388.8	3.8	356.7	12.8
35	378.4	13.3	346.7	6.3
52	398.2	1.5	353.5	9.2
78	389.8	19.8	352.0	3.7

Table 8.16e. Activation Energy Based on Tan Delta Determined After Immersion in -10°C Seawater (“Wet Testing”) and as a Result of Subsequent Redrying (“Dry Testing”)

Time [weeks]	-10°C			
	“Wet Testing”		“Dry Testing”	
	ΔE_a [kJ/mol]	Std. Dev. [kJ/mol]	ΔE_a [kJ/mol]	Std. Dev. [kJ/mol]
0	357.3	10.7	357.3	10.7
4	336.8	6.9	355.5	63.7
8	322.1	13.4	353.1	20.2
12	322.1	-	338.2	6.9
16	343.4	1.9	319.2	13.1
24	325.5	5.7	319.7	26.2
35	322.6	-	319.7	24.6
48	321.4	-	320.2	22.1
72	-	-	-	-

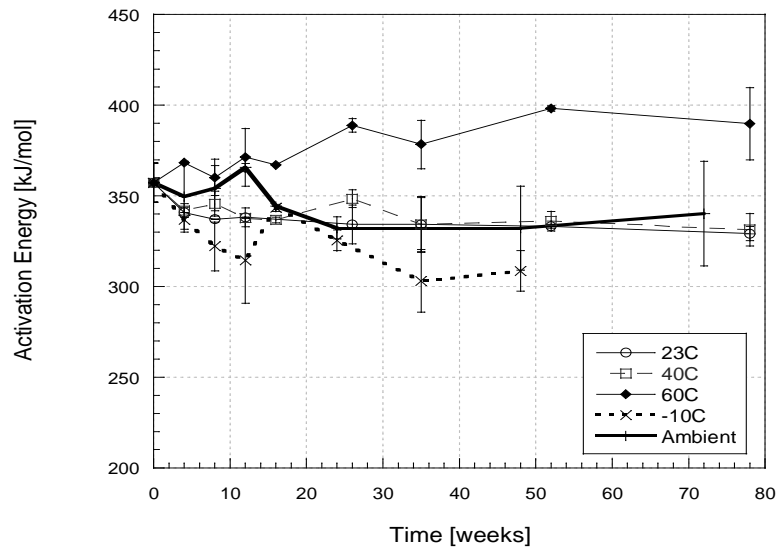


Figure 8.11. Change in Activation Energy Based on Tan Delta as a Function of Temperature and Time of Immersion in Seawater

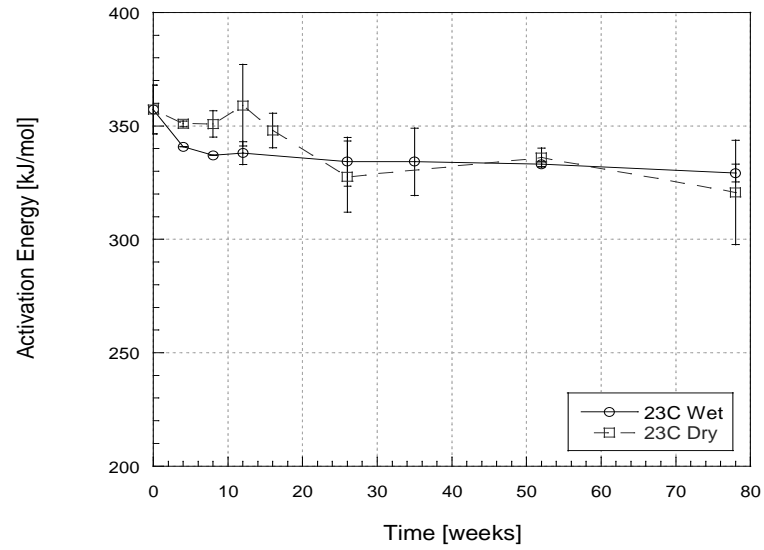


Figure 8.12a. Effect of Redrying on Activation Energy Based on Tan Delta After Immersion in 23°C Seawater

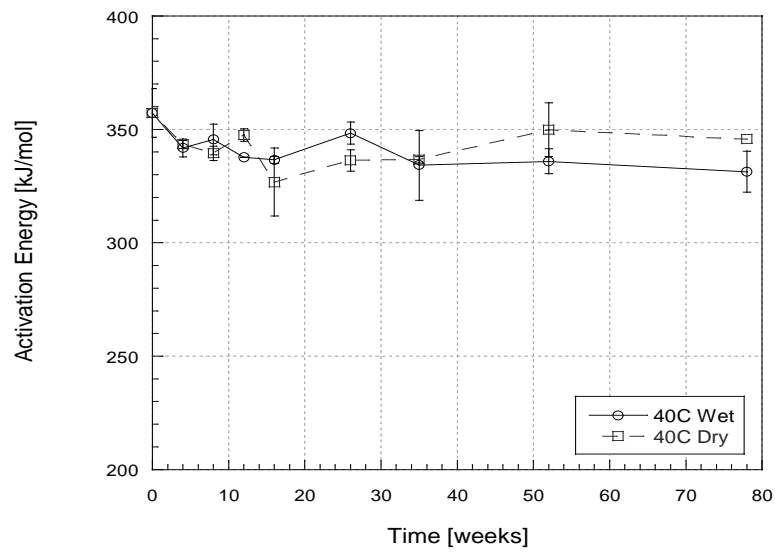


Figure 8.12b. Effect of Redrying on Activation Energy Based on Tan Delta After Immersion in 40°C Seawater

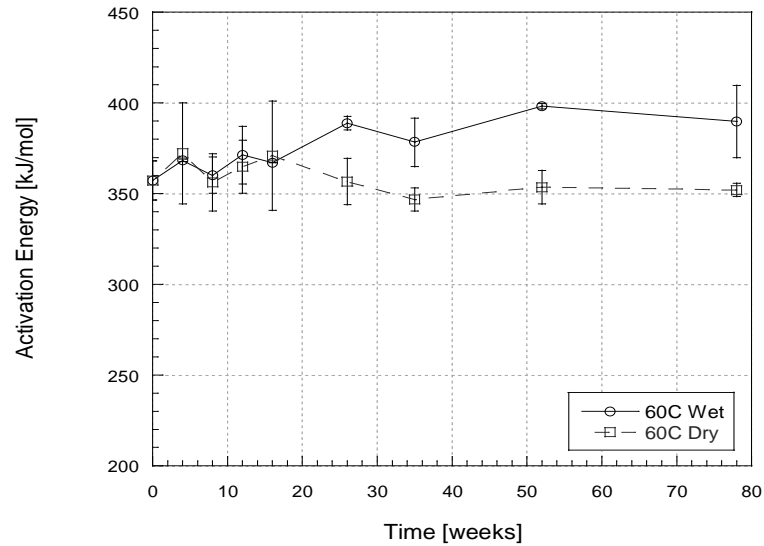


Figure 8.12c. Effect of Redrying on Activation Energy Based on Tan Delta After Immersion in 60°C Seawater

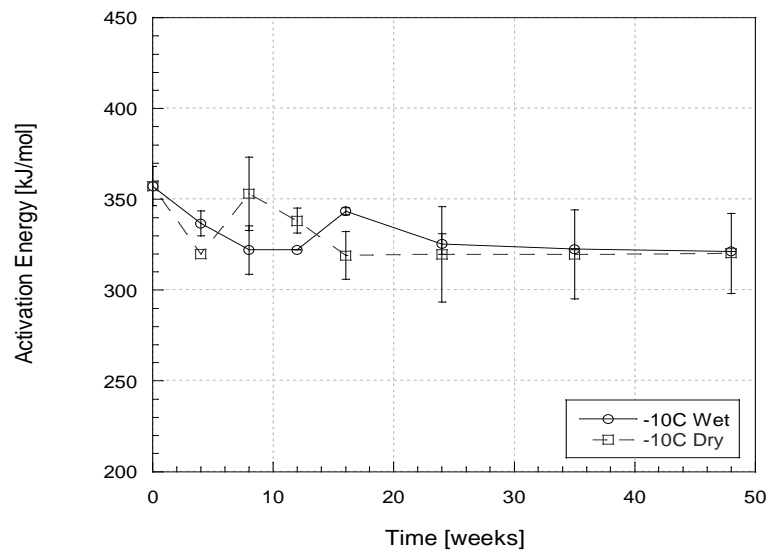


Figure 8.12d. Effect of Redrying on Activation Energy Based on Tan Delta After Immersion in -10°C Seawater

Review of the calculated activation energies from Chapter 4 show that 47.6 kJ/mol are required to initiate diffusion when submerged in seawater. This value is comparably less than the activation energy calculated based on the T_g at 1,5,10, and 30 Hz. However, the values are within reason because it requires much less energy for diffusion to occur once it is in contact with

moisture, however it takes much more energy to initiate the movement of polymer chains from a glassy to rubbery state.

The activation energies calculated in this study are comparable to those found by Karbhari and Wang [109] who tested an E-glass/vinylester composite and found an activation energy of 346.4 kJ/mol at ambient conditions. Low values of activation energy suggest that the shifting of the loss modulus can occur without much obstruction and shows a ductile response of the material [109]. Consequently, high values of activation energy depict that shifting of the loss modulus is much more difficult and represents a brittle response of the composite [109]. Increases in activation energy of 30 kJ/mol were found in the 60°C immersed specimens after 78 weeks immersion. The previous study by Karbhari and Wang at this exposure found an increase in activation energy of from 346.4 kJ/mol to 352.3 kJ/mol after immersion in 60°C deionized water for 6 months[109]. It was stated that the cause of this increase was attributed to materials degradation, brittleness, and sensitivity to defects [109].

While previous sections revealed freezing showed stable parameters, a decreasing trend in activation energy is reported. Since activation energy represents an energy barrier for transition from one state to another, the effect of freezing reflects an increase in the brittleness of the matrix and should increase the activation energy. However, it is uncertain why the activation energy shows a decreasing trend in the current investigation. It should be noted that because of the high sensitivity of the DMTA, thawing of the samples after removing them from their environment could alter the results.

Table 8.17a. Activation Energy Based on Tan Delta Determined as a Function of Freeze/Thaw Exposure

Time [weeks]	Freeze/Thaw			
	“Wet Testing”		“Dry Testing”	
	ΔE_a [kJ/mol]	Std. Dev. [kJ/mol]	ΔE_a [kJ/mol]	Std. Dev. [kJ/mol]
0	357.3	10.7	357.3	10.7
4	347.5	11.6	332.8	1.0
8	332.3	10.7	348.3	11.6
12	323.0	4.2	336.5	28.8
16	327.6	19.9	-	-
24	325.5	5.7	328.2	19.8
35	322.9	-	319.2	35.7
54	324.7	22.1	328.3	22.9
72	337.9	-	328.2	20.9

Table 8.17b. Activation Energy Based on Tan Delta Determined as a Function of Wet/Dry Exposure

Time [weeks]	Wet/Dry			
	“Wet Testing”		“Dry Testing”	
	ΔE_a [kJ/mol]	Std. Dev. [kJ/mol]	ΔE_a [kJ/mol]	Std. Dev. [kJ/mol]
0	357.3	10.7	357.3	10.7
4	327.4	16.0	334.8	17.2
8	324.5	9.9	340.2	12.5
12	342.0	15.0	337.4	3.3
16	335.0	12.6	-	-
24	328.1	1.1	332.3	-
35	323.7	14.6	333.9	11.9
54	324.7	22.1	350.1	8.1
72	325.3	18.7	335.2	3.3

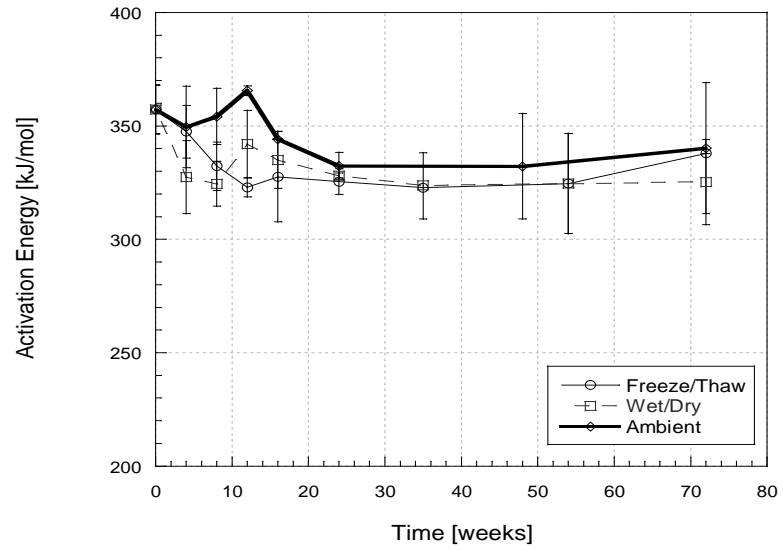


Figure 8.13. Change in Activation Energy Based on Tan Delta As a Function of Time and Type of Cyclic Exposure

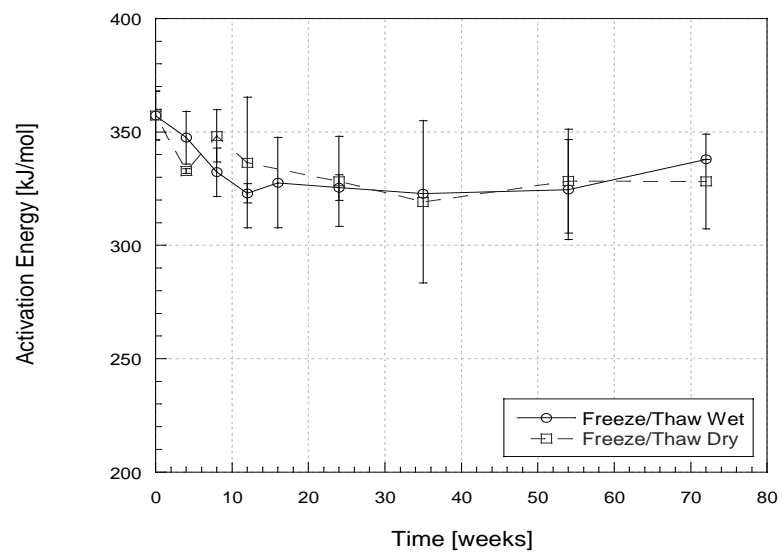


Figure 8.14a. Effect of Redrying on Activation Energy Based on Tan Delta as a Function of Freeze/Thaw Exposure

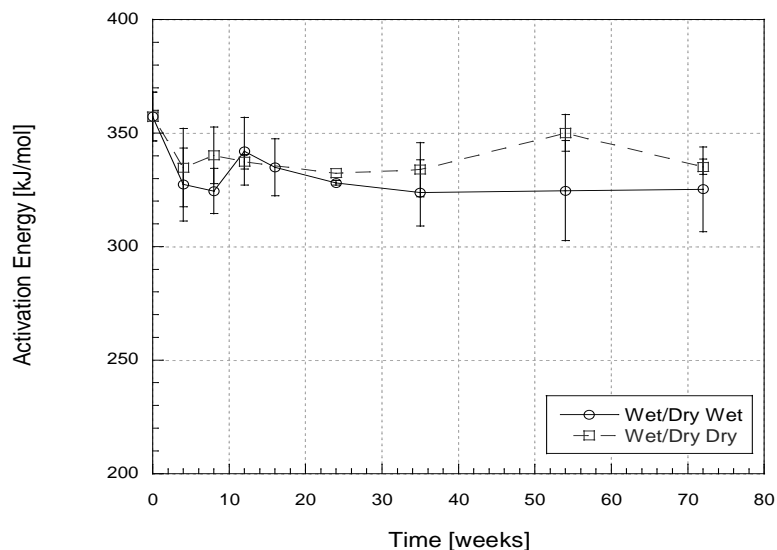


Figure 8.14b. Effect of Redrying on Activation Energy Based on Tan Delta as a Function of Wet/Dry Exposure

Exposures to freeze/thaw cycling conditions revealed that activation energies were depressed by small amounts of about 30 kJ/mol between 0-12 weeks. This is attributed to moisture induced plasticization. Asymptotic behavior is noted after this period of time, with the exception of an increase in the activation energy at 78 weeks, which is accompanied by a large scatter. Exposure to wet/dry cycling resulted in a decrease in activation energies at 8 weeks, followed by an increase at 12 weeks. Initial decreases in activation energy are caused by moisture induced plasticization, while the small increase at 12 weeks could be a factor of residual cure. After 12 weeks, the activation energy maintains a level of 325 kJ/mol. Results found by Karbhari and Wang who subjected an E-glass/Vinylester composite to 24 hour wet/dry cycling reported an initial decrease of 28 kJ/mol after 4 months exposure [109].

8.2.2. Storage Modulus

As mentioned previously, the ability of a material to store energy or the elasticity of a material, is the storage modulus or elastic modulus (E'). Analyzing E' can reveal shifts in the profile with exposure and time. It is calculated according to equation 8-3.

$$E' = \frac{\sigma^o}{\varepsilon^o} \cos \delta \quad (8-3)$$

where:

σ^o is the sinusoidal stress,

ε^o is the sinusoidal strain, and

δ is the phase angle.

8.2.2.1. Glass Transition Temperature

The T_g from E' is found by the inflection point in the middle portion of the storage modulus profile. An analysis program such as Rheometric Scientific Instruments Orchestrator can be used to find the first derivative of the E' curve, which is typically a parabolic curve. Analysis of the midpoint of the parabolic curve yields the T_g based on the storage modulus.

The value of T_g based on E' is summarized in the Appendix and is classified by environmental condition.

8.2.2.2. Verification of Flexural Modulus

Use of the parameters obtained from DMTA can verify material properties obtained from mechanical testing. DMTA samples were tested in a 3-point bend fixture, therefore a verification of flexural modulus values can be performed. The value of the flexural modulus can be verified by utilizing equation 8-4, which uses DMTA parameters to calculate flexural modulus

$$E_b = \sqrt{E'^2 + E''^2} \quad (8-4)$$

where:

E_b is the flexural modulus in GPa,

E' is the value of the storage modulus at 30°C, and

E'' is the value of the loss modulus at 30°C.

Table 8.19 and Figures 8.15-8.17 shows the flexural modulus calculated from DMTA parameters compared to experimental data. Table 8.20 calculates the percent difference between the two. Flexural modulus values are only calculated based on immersion at 23°C, 40°C, and 60°C. Exposures pertaining to freeze, freeze/thaw cycle, and wet/dry cycle involve embrittlement of the matrix and matrix microcracking, which could result in variations between calculated values of modulus based on DMTA parameters.

Table 8.18. Comparison of Flexural Modulus Calculated From DMTA and Experimental Data

Time [weeks]	Modulus Calculated From DMTA [GPa]			Experimental Flexural Modulus [GPa]		
	23°C	40°C	60°C	23°C	40°C	60°C
0	21.65	21.65	21.65	26.9	26.91	26.91
4	18.13	21.56	21.45	24.4	27.43	25.55
8	18.42	19.57	-	27.5	24.22	24.03
12	21.45	19.42	20.38	29.9	23.02	24.07
16	-	19.67	19.64	23.8	29.87	25.19
26	22.10	23.30	19.54	23.8	24.18	22.36
35	20.48	-	20.63	22.4	26.29	24.42
52	19.97	23.76	20.76	-	26.21	24.87
78	21.87	22.43	21.12	24.4	25.61	25.68

Table 8.19. Percent Difference Between Flexural Modulus Calculated From DMTA and Experimental Data

Time [weeks]	Difference [%]		
	23°C	40°C	60°C
0	24.30	24.30	24.30
4	34.34	27.27	19.10
8	49.54	23.73	-
12	39.40	18.53	18.09
16	-	51.90	28.25
26	7.78	3.80	14.40
35	9.24	-	18.34
52	-	10.31	19.82
78	11.50	14.18	21.58

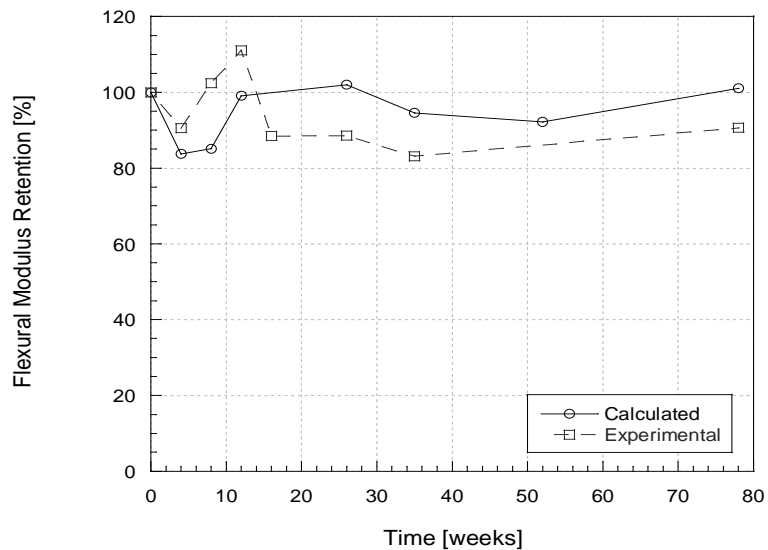


Figure 8.15. Comparison Between Calculated Flexural Modulus Based on DMTA Parameters and Experimental Data For Immersion in 23°C Seawater

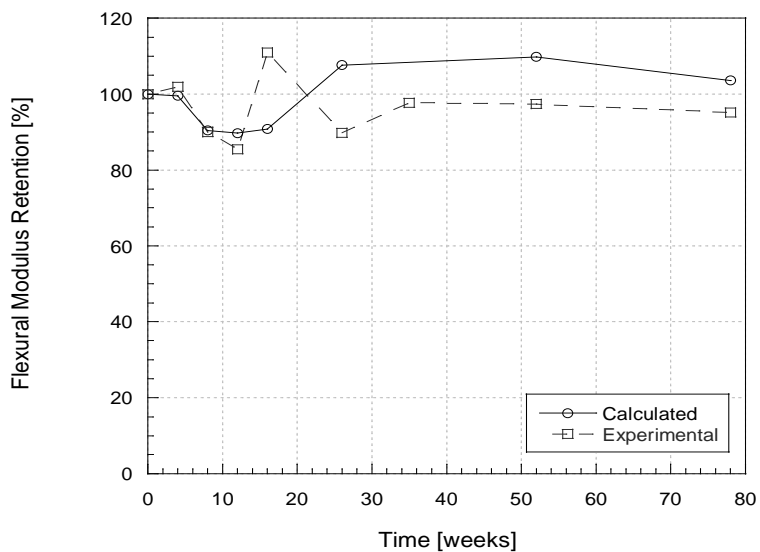


Figure 8.16. Comparison Between Calculated Flexural Modulus Based on DMTA Parameters and Experimental Data For Immersion in 40°C Seawater

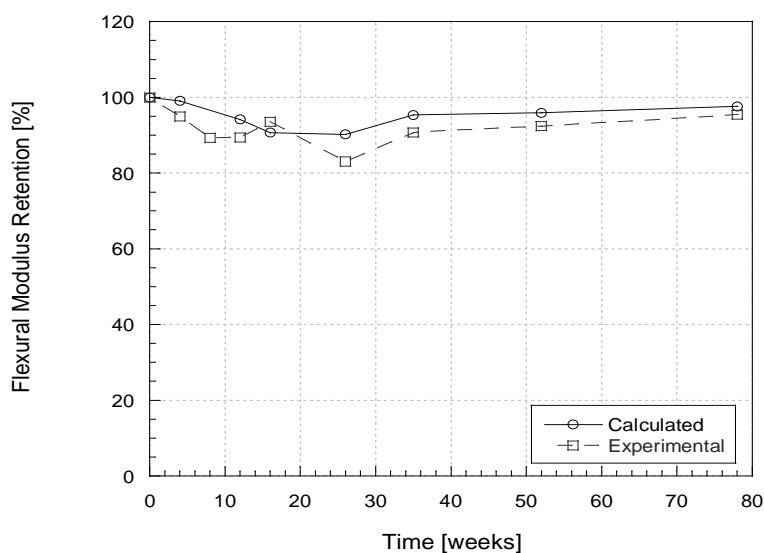


Figure 8.17. Comparison Between Calculated Flexural Modulus Based on DMTA Parameters and Experimental Data For Immersion in 60°C Seawater

Figures 8.15-8.17 show relationships between calculated flexural modulus values determined from DMTA parameters and experimental flexural modulus data. In order to compare the two, the figures are plotted percent retention versus time.

A study of Tables 8.18 and 8.19 shows there is a general correlation between the two values. Use of DMTA can offer a means of verifying mechanical test data at suspect data points

and provides a clear assessment of effects at the morphological and materials level on mechanical properties. Figure 8.15 shows that at room temperature immersion in seawater, flexural modulus values are in general agreement with those calculated.

8.2.2.3. Rubber Plateau

The rubber plateau region of the storage modulus is taken into account in order to determine the extent of chemical changes occurring within the composite. The tables below show the value of E'_r at a position of $T_g + 50^\circ\text{C}$ (T_g from tan delta).

Table 8.20a. Rubbery Modulus at $T_g + 50^\circ\text{C}$ At Ambient Conditions, 23°C and 30%RH

Time [weeks]	Ambient	
	E'_r [GPa]	Std. Dev [GPa]
0	4.15	0.10
4	4.54	0.16
8	3.83	0.60
12	2.37	0.52
16	2.59	0.46
24	3.35	2.74
35	-	-
48	2.82	0.87
78	3.23	0.97

Table 8.20b. Rubbery Modulus at $T_g + 50^\circ\text{C}$ After Immersion in Seawater

Time [weeks]	23°C		40°C		60°C	
	E_r' [GPa]	Std. Dev [GPa]	E_r' [GPa]	Std. Dev [GPa]	E_r' [GPa]	Std. Dev [GPa]
0	4.15	0.10	4.15	0.10	4.15	0.10
4	4.39	0.51	4.68	0.57	3.53	0.53
8	3.54	0.02	3.99	-	4.54	1.50
12	4.58	0.60	3.96	0.92	4.27	1.02
16	-	-	3.45	0.67	3.94	0.75
24	2.09	0.94	3.03	-	2.39	0.22
35	2.02	0.77	2.42	0.31	2.36	0.65
52	2.63	-	3.34	0.39	1.95	-
78	2.55	0.27	3.14	0.32	2.24	-

Table 8.20c. Rubbery Modulus at $T_g + 50^\circ\text{C}$ After Exposure to -10°C Seawater

Time [weeks]	-10°C	
	E_r' [GPa]	Std. Dev [GPa]
0	4.15	0.10
4	2.93	0.26
8	-	-
12	2.36	0.43
16	2.97	0.62
24	2.97	0.50
35	2.12	0.16
48	2.50	1.26
78		

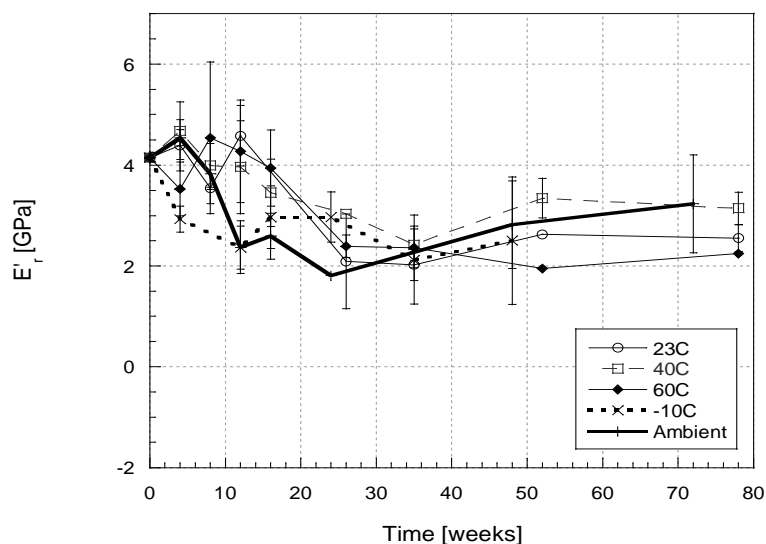


Figure 8.18. Change in Rubbery Modulus as a Function of Temperature and Time of Immersion in Seawater

The rubber plateau region has been found to change with time in past studies done by De'Neve et al. [112] and Noguiera et al. [110]. The rubber plateau can also be related by the degree of crystallinity in a material [108]. In the current study it is found by looking at the value of the storage modulus at a temperature of $T_g + 50^\circ\text{C}$ (where T_g is found from the peak position of the tan delta profile).

Figure 8.18 shows that immersion at 23°C and 40°C immersion follow close trends. The E'_r initially varies due to residual cure between 0 and 12 weeks, after which it reaches a low from 24-36 weeks, followed by an increase at 52 weeks. Immersion in 60°C seawater shows variation from 4-8 weeks followed by a decreasing behavior until 26 weeks after which it reaches equilibrium. It has been found that a change in E'_r is caused by the saturation of water and tends to drop the useful service temperature about 40°C [112].

Freezing exposures had a different initial reaction to the other immersion conditions. The initial change is much more drastic and drops to 2 Pa at a period of 4 weeks. Since a change in rubber modulus is reflected as the amount of moisture in a composite, this can be accounted for

by the long-immersion time. The increase between 16-24 weeks may be the result of variations involving thawing of frozen specimens before testing. It is noted the value of the rubber modulus reaches a value comparable to the value recorded at 12 weeks.

Table 8.21. Rubbery Modulus at $T_g + 50^\circ\text{C}$ Determined as a Function of Type and Period of Cyclic Exposure

Time [weeks]	Freeze/ Thaw		Wet/Dry		Ambient	
	E_r' [GPa]	Std. Dev. [GPa]	E_r' [GPa]	Std. Dev. [GPa]	E_r' [GPa]	Std. Dev. [GPa]
0	4.15	0.10	4.15	0.10	4.15	0.10
4	4.32	0.33	4.27	-	4.54	0.16
8	4.37	0.35	4.76	0.33	3.83	0.60
12	2.58	0.56	2.57	-	2.37	0.52
16	1.56	0.60	2.31	0.20	2.59	0.46
24	1.60	0.35	2.25	0.78	1.81	-
35	1.89	0.37	3.63	-	-	-
54	1.79	0.46	2.41	-	2.82	0.87
72	2.17	0.64	2.85	0.55	3.23	0.97

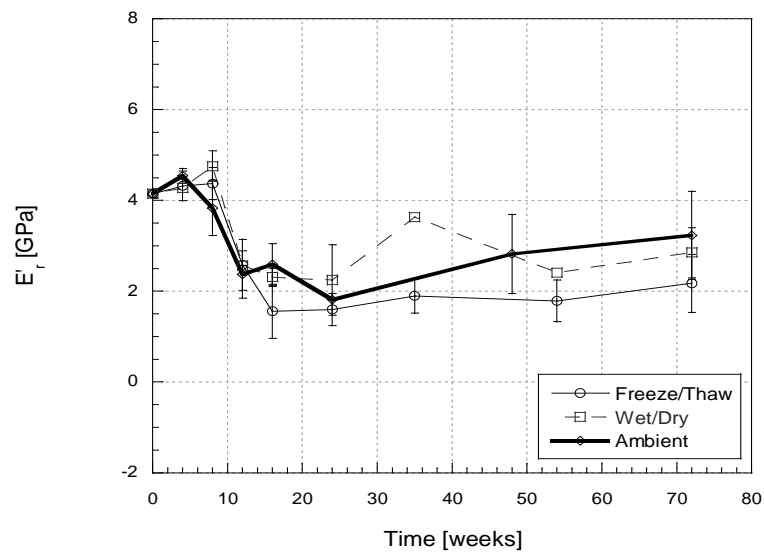


Figure 8.19. Change in Rubbery Modulus as a Function of Time and Type of Cyclic Exposure

8.2.2.4. Intercrosslink Molecular Weight

The intercrosslink molecular weight (M_c) is calculated according to a method proposed by De'Neve and Shanahan [112]. The M_c is calculated according to equation 8-5.

$$M_c = \frac{3\rho RT}{E_r(1-V_f^{1/3})} \quad (8-5)$$

where:

ρ is the density in kg/m^3

R is the Universal gas constant (8.3143 J/mol·K)

T is the Temperature in Kelvin (T_g based on $\tan \delta + 50^\circ\text{C}$)

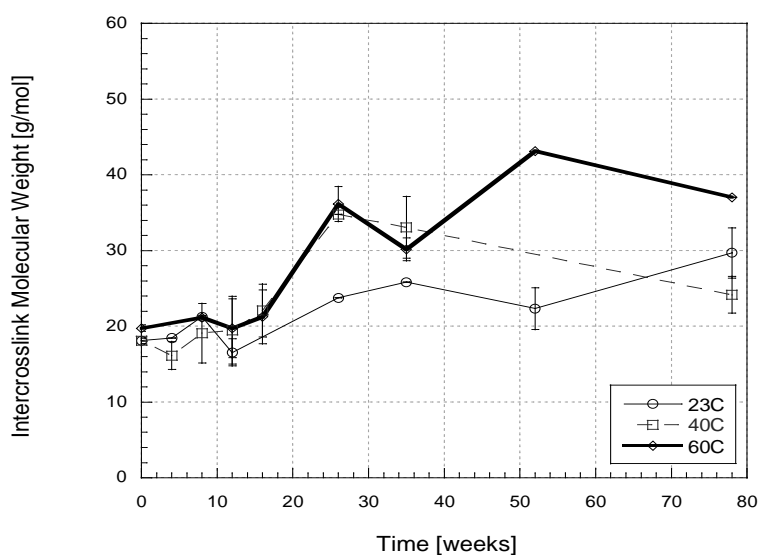
V_f is the fiber volume fraction

E_r is the rubber modulus corresponding to the temperature at T_g based on $\tan \delta + 50^\circ\text{C}$

It should be noted that the calculation itself involves assumptions and simplifications, and it's values should be analyzed in terms of trends rather than absolute values. The trends outlined in this section serve to verify the hypotheses stated in previous sections.

Table 8.22. Intercrosslink Molecular Weight Determined After Immersion in Seawater as a Function of Temperature

Time [weeks]	Immersion in Seawater					
	23°C [g/mol]	Std. Dev. [g/mol]	40°C [g/mol]	Std. Dev. [g/mol]	60°C [g/mol]	Std. Dev. [g/mol]
0	18.09	0.37	18.09	0.38	19.75	0.41
4	18.45	-	16.12	1.83	-	-
8	21.27	0.12	19.10	3.95	21.17	-
12	16.56	1.80	19.48	4.45	19.73	3.87
16	-	-	22.10	3.50	21.27	3.54
24	23.77	-	34.78	-	36.15	2.31
35	25.85	-	33.05	4.06	30.18	1.48
52	22.33	2.75	-	-	43.14	-
78	29.69	3.30	24.17	2.43	37.02	-

**Figure 8.20. Change in Intercrosslink Molecular Weight As a Function of Temperature and Time of Immersion in Seawater**

Changes in M_c are apparent in Figure 8.20 that describes E-glass/vinylester composites immersed in seawater. Up until 16 weeks, the molecular weight does not change with time. At this point in time, there is a differentiation in trends related to temperature of immersion. The room temperature immersion increases in height the smallest amount out of the three immersion temperatures. The increase in molecular weight relates to the crosslinking density and increases

with temperature of immersion. Interestingly, the molecular weight relating to immersion in 40°C seawater at 72 weeks falls below that of the molecular weight at room temperature immersion. This trend was also seen in the moisture uptake profiles for specimens immersed in 40°C seawater, which were presented in Chapter 4. The mass loss occurring at this exposure is shown through the reduction of molecular weight. The trends outlined here validate the hypotheses made in the previous sections that relate the period of time (24 weeks) at which molecular mobility is limited.

Table 8.23. Intercrosslink Molecular Weight Determined as a Function of Time and Type of Cyclic Exposure

Time [weeks]	Cyclic Exposure			
	Freeze/Thaw [g/mol]	Std. Dev. [g/mol]	Wet/Dry [g/mol]	Std. Dev. [g/mol]
0	19.11	0.40	18.09	0.38
4	18.41	1.22	17.52	-
8	-	-	-	-
12	-	-	-	-
16	43.50	-	32.54	-
24	44.22	0.22	27.76	0.37
35	-	-	22.96	-
54	34.86	-	31.18	-
72	32.17	5.74	29.41	4.35

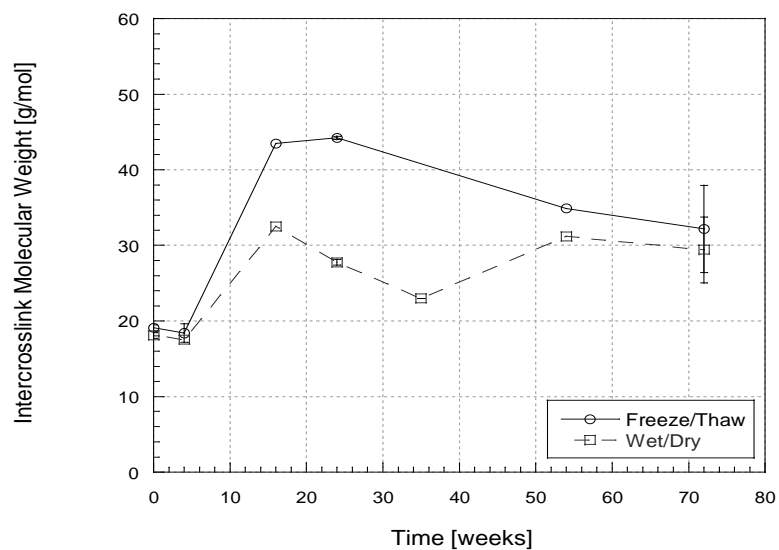


Figure 8.21. Change in Intercrosslink Molecular Weight As a Function of Time and Type of Cyclic Exposure

The change in M_c relating to exposure to cyclic conditions show increases as early as 4 weeks, followed by a gradual increase, until which it reaches equilibrium at 32 weeks. In general, molecular weight pertaining to the freeze/thaw exposure is much higher than the results from exposure to seawater immersion. This indicates a low level of degradation and resulting low levels of molecular mobility. Exposure to freeze/thaw cycling experienced a higher molecular weight, whereas the exposure to wet/dry cycling revealed a lower molecular weight. The molecular weight is more affected by the wet/dry cycle because of the varying coefficients of thermal expansion. The varying stress levels often result in swelling and cracking, which can initiate chain scission and reduce the molecular weight. The results are consistent with previous findings.

8.2.3. Loss Modulus

The loss modulus (E'') is a parameter that measures the level of dissipated energy [46]. It can also be commonly referred to as the viscous or imaginary modulus. It is calculated from the phase lag between the sinusoidal stress and strain and is represented in equation 8-6.

$$E'' = \frac{\sigma^\circ}{\varepsilon^\circ} \sin \delta \quad (8-6)$$

where:

σ° is the sinusoidal stress,

ε° is the sinusoidal strain, and

δ is the phase angle.

8.2.3.1. Glass Transition Temperature

The T_g can also be measured the peak of the loss modulus profile. This point denotes the middle of the transition period between the elastic and viscoelastic regimes. Because of this, the T_g based on E'' is always higher than the T_g based on $\tan \delta$. It has been found the T_g based on E'' has less variation because it marks the midpoint of the transition period.

The T_g based on E'' divided by environmental exposure and is provided in the Appendix.

8.2.3.2. Activation Energy

The ΔE_a is calculated as described in Section 8.2.1.4, however it is calculated from the T_g based on the loss modulus. Tables in the Appendix summarize the ΔE_a based on E'' divided into immersion and cycling.

8.3. SUMMARY

Use of the numerous techniques outlined in this chapter yields valuable information in the molecular state of the composite. While the information is abundant, it is useful to connect all of the ideas into a concise set of statements.

- Immersion in 23°C seawater has been shown to cause negligible effects on the material strength. However, it is noted that the effects of moisture-initiated plasticization occur between 0-4 weeks as evidenced by the drop in T_g and increase in area between curves. Following this drop in T_g , a slight increase follows which has been proven to be caused of leaching by low-weight molecular species. This is in agreement with findings found in Chapter 4 in which a decrease in weight gain occurs after 4 weeks. In general, since little degradation occurs at room temperature, analysis of residual cure may be beneficial. It has been found from the general increase in height of the tan delta profile that this occurs between 4-12 weeks.
- Immersion in 40°C seawater is slightly more complicated because the combined effects of plasticization, degradation, and residual cure occur simultaneously. Plasticization, as shown in previous chapters occurred between 0 and 4 weeks. Any degradation after that can be attributed to direct degradation at the resin or fiber/matrix interphase levels. As shown from the height of tan delta, there is a increase in height between 0-16 weeks caused by residual cure. Most of the mobility occurs before 8 weeks (as shown from the area between the curves) and reaches an equilibrium point after that. This is also validated by the stable behavior of the activation energies. At 24 weeks, the effect of cure is met with the typical types of degradation occurring at higher temperature immersion (typically hydrolysis and leaching). This is also confirmed with the change of the rubber plateau at 12 weeks and the increase in molecular weight at this time. The

amount of moisture in the sample is also indicated by examining at the glassy region of the storage modulus profile.

- Immersion in 60°C seawater shows slightly varied results as compared to 40°C immersion. There is an initial decrease in the T_g at 4 weeks that is validated by the sole effect of plasticization, which was determined to occur at this time in previous chapters. After that, there is an increase in T_g that is associated with the leaching of low molecular weight species and is also validated by the moisture profiles in Chapter 4. The height of tan delta is the greatest at 16 weeks, which shows that the increase in crosslink density from residual cure has reached its peak. This is consistent with the findings that the molecular weight starts to increase at 12 weeks. The activation energies have a generally increasing trend that also validates the level of degradation. The hypothesis of mobility of the polymer chains at 12 week is reinforced since the rubber modulus drops at this time also.
- The freezing condition shows quite interesting conclusions. As a result of the 8-month initial saturation in room temperature seawater in addition to the 12 months of freezing, these specimens underwent a total of 20 months exposure, longer than any of the other conditions. Most of the degradation resulted from the 8-month saturation in room temperature seawater. Analogous to previous studies [10], the effect of freezing served to stabilize the condition of the matrix. The T_g showed a stable trend throughout the exposure. The height of the tan delta profile increased due to the effect of the 8-month saturation in addition to the residual cure that took place in the initial 12 weeks during that saturation period. The increase in height also emphasize a brittle matrix, which is validated by the initial depression of the glassy plateau of the storage modulus profile. Similarly, the rubber plateau dropped immediately also due to the 8-month saturation.

- The effect of freeze/thaw and wet/dry cycling conditions experienced the same overall trends. There was a slight depression in T_g at initial periods of time (4 weeks for wet/dry). Small changes in activation energy also show that plasticization occurs early. The cycling conditions showed increases in height of the tan delta profile that showed a relatively small amount of moisture in the sample. This is also evidenced by the relatively stable behavior of the calculation of the area between the curves with time. As seen from molecular weight calculations, values are high throughout and validate the above findings.

CHAPTER 9 – MODELING AND LIFE PREDICTION

9.1. INTRODUCTION

The introduction of composites as new material in any application faces the hurdle of lack of substantial sets of validated data. It is often difficult to provide real-time data for components that are expected to last 25 years or more. In this respect, the concept of accelerated aging has been used to extrapolate long-term data from short-term data obtained from the laboratory. Accelerated life-testing uses the concept of applying a stimulus to accelerate a failure [113]. In the current investigation, temperature of immersion is used as the stimulus.

The specific details of an experiment are expected to be within means of the material being tested. Use of ASTM E-632 [114] aids in determining the framework for accelerated life-testing. After data is obtained, specific models can be applied to obtain a prediction of the service life for a mechanical characteristic. For the current investigation, the Arrhenius Rate Relationship and Time-Temperature Superposition have been applied to all mechanical properties tested for and details pertaining to these methods will be described in further detail in the following sections.

9.2. ARRHENIUS RATE RELATIONSHIP

The Arrhenius Rate Relationship is based on the Arrhenius reaction rate equation as displayed in equation 9-1 [113].

$$R(T) = Ae^{\frac{-E_A}{KT}} \quad (9-1)$$

where:

R(T) is the speed of the reaction,

A is an unknown non-thermal constant,

E_A is the activation energy,

K is the Boltzman's constant (1.38 x 10⁻²³ J/°K), and

T is the absolute temperature in degrees Kelvin.

Assuming that life is proportional to the inverse reaction rate of the process, the Arrhenius life-stress relationship is formulated can be shown in equation 9-2.

$$L(T) = Ce^{\frac{B}{T}} \quad (9-2)$$

where:

L is the quantifiable measure of life or the material property,

T is the temperature in degrees Kelvin, and

B and C are model parameters.

Taking the natural log of both sides of equation 9-2 results in a linear relationship as expressed in equation 9-3.

$$\ln(L(T)) = \ln(C) + \frac{B}{T} \quad (9-3)$$

where:

ln(L(T)) is the y variable,

ln(C) is the y-intercept,

B is the slope of the line, and

1/T is the x variable.

Equation 9-3 provides a prediction of service life based on a reference temperature.

9.2.1. Application to Data

Using data from the current investigation, the procedure to determine service life predictions will be displayed in detail for the tensile strength property. Other properties including tensile modulus, flexural strength, flexural modulus, and SBS strength will not be shown in detail, however their results will be presented.

Referring to Chapter 5, tensile strength retention results are repeated in Table 9.1.

Table 9.1. Tensile Strength Retention as a Function of Time (in months)

Time [months]	Tensile Strength Retention [%]		
	23°C	40°C	60°C
0	100.0	100.0	100.0
1	88.5	74.5	58.8
2	96.3	63.6	53.9
3	93.6	62.7	53.6
4	84.3	64.0	53.9
6	85.0	61.5	50.1
8	82.7	62.1	51.4
12	81.2	60.1	52.1
18	76.9	58.2	51.5

The values in Table 9.1 are plotted accordingly in Figure 9.1.

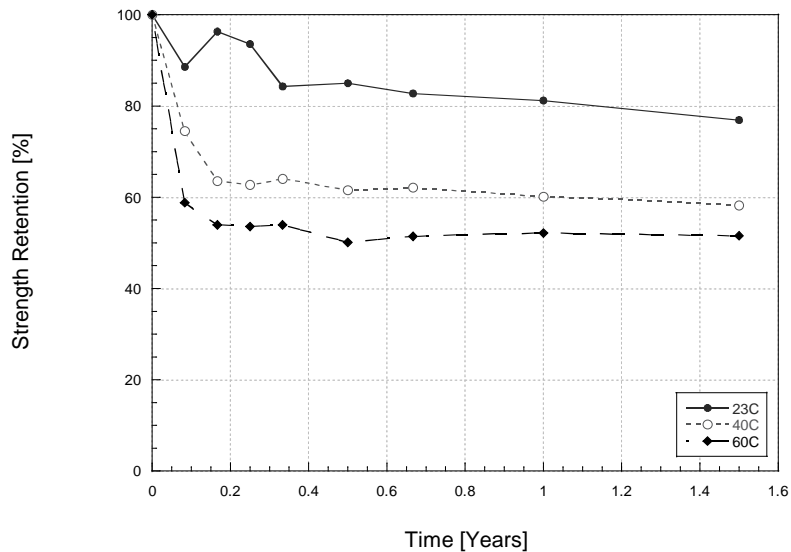


Figure 9.1. Tensile Strength Retention vs. Time

The relationship illustrated in Figure 9.1 is linearized by taking the natural log of time (x-axis) in days. It should be noted that the natural log at time zero yields a result of infinity. In this case, an estimate of as-received values is substituted with the natural log of 2 days, with the assumption that changes do not occur between 0 and 2 days. A least squares curve fit is applied to each of the trendlines resulting in linear relationships between tensile strength and the natural log of time. These results are displayed in Figure 9.2 and Table 9.2.

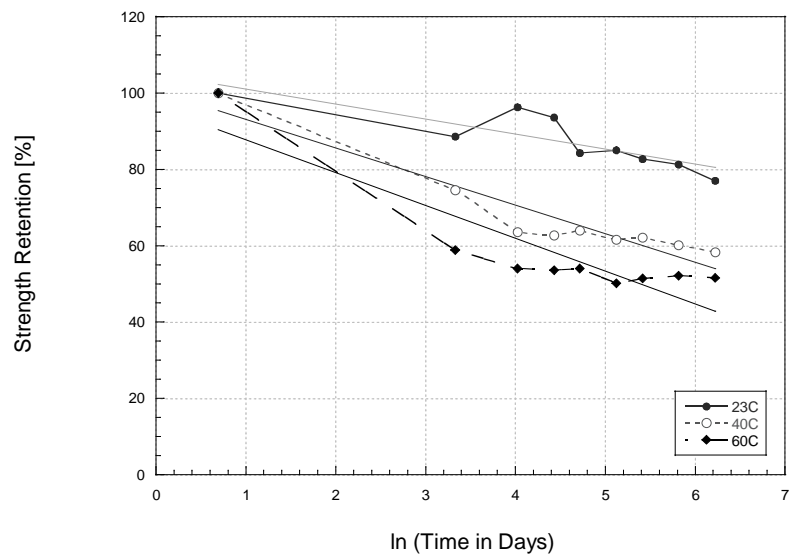


Figure 9.2. Tensile Strength Retention vs. ln (Time in Days)

Table 9.2. Linear Relationships Between Tensile Strength and Time

Temperature (°C)	Equation	R ²
23	$f_c(\tau) = f_c(1.0499 - 0.0393 \cdot \ln(\tau))$	0.74
40	$f_c(\tau) = f_c(1.0052 - 0.0749 \cdot \ln(\tau))$	0.91
60	$f_c(\tau) = f_c(0.9636 - 0.086 \cdot \ln(\tau))$	0.81

The time periods under consideration for prediction are 0, 0.5, 1, 1.5, 2, 3, 5, 10, 15, and 20 years. These values are labeled as τ and are converted into days. A ratio of $f_c(\tau)/f_c$ is obtained for equations listed in Table 9.2 at 40°C and 60°C immersion. Once these values are obtained, they are plotted against $1000/\text{Temperature (°K)}$. For 60°C and 40°C immersion, these values are 3.0017 and 3.1934, respectively. A least squares curve fit is applied for each time period and yields the results shown in Figure 9.3 and Table 9.3.

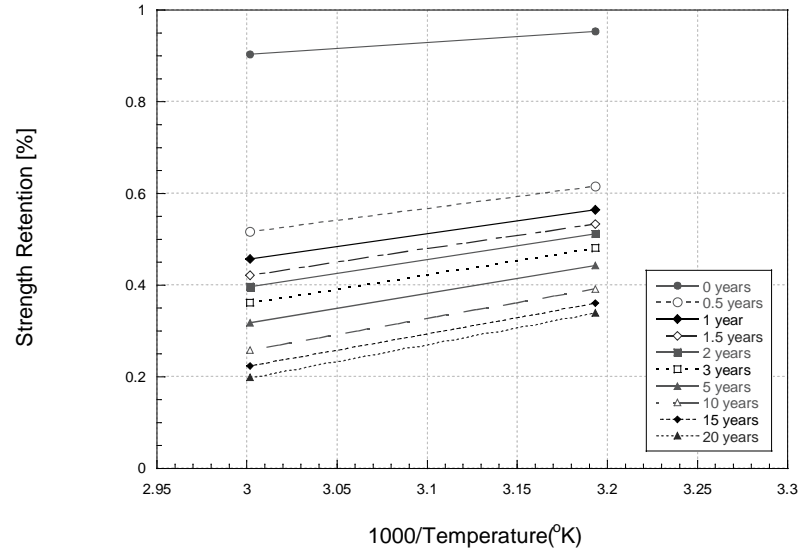


Figure 9.3. Tensile Strength Retention vs. Inverse Temperature

Table 9.3. Least Square Fit Between Strength and Inverse Temperature

Time [years]	Equation
0	$f_c(\tau)=f_c(0.1321+0.2571*1000/T)$
0.5	$f_c(\tau)=f_c(-1.0407+0.5185*1000/T)$
1	$f_c(\tau)=f_c(-1.2208+0.5587*1000/T)$
1.5	$f_c(\tau)=f_c(-1.3261+0.5821*1000/T)$
2	$f_c(\tau)=f_c(-1.4009+0.5988*1000/T)$
3	$f_c(\tau)=f_c(-1.506+0.6223*1000/T)$
5	$f_c(\tau)=f_c(-1.638+0.6519*1000/T)$
10	$f_c(\tau)=f_c(-1.819+0.692*1000/T)$
15	$f_c(\tau)=f_c(-1.9244+0.7155*1000/T)$
20	$f_c(\tau)=f_c(-1.9991+0.7321*1000/T)$

The equations displayed in Table 9.3 are used to obtain strength predictions at a specified temperature. In this case, we desire to determine the service life of a composite immersed at room temperature (23°C). Temperature (in degrees Kelvin) is used in the equations listed in Table 9.3 as the variable “T”. The results are listed in Table 9.4.

Table 9.4. Predicted Values of Strength Retention Based on Arrhenius Rate Relationship

Time [Years]	Predicted Retention [%]
0	100.0
0.5	71.0
1	66.6
1.5	63.9
2	62.1
3	59.5
5	56.3
10	51.8
15	49.2
20	47.3

Since the data sets being used are small and there is variation even within each time-exposure set, correction factors based on the relationship between theoretical and experimental retention are applied using a least squares fit. This can be done easily using short-term data. Figure 9.4 provides an estimation of retention comparison and Table 9.5 lists the differences between the predicted and experimental values. As can be seen the match is fairly good. It is noted that if the correction factor is not used, results can be fairly conservative since accelerated levels (higher temperatures) are used for prediction of lower temperature response rather than at a temperature between the extremes used in the investigation.

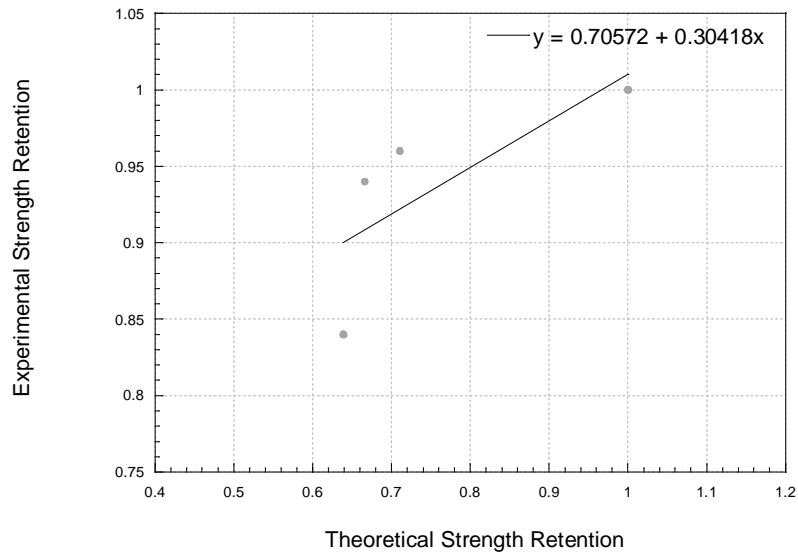


Figure 9.4. Determination of Correction Factor for Arrhenius Rate Relationship

Table 9.5. Values of Predicted Strength Retention Based on Modified Arrhenius Rate Relationship[%]

Time [Years]	Predicted Strength Retention [%]	Experimentally Obtained Strength Retention [%]	% Difference Between Predicted and Experimental Results
0	101.0	100.0	0.0
0.5	80.5	85.0	5.3
1	77.4	81.0	4.4
1.5	75.5	76.9	1.8
2	74.2		
3	72.4		
5	70.2		
10	66.9		
15	65.1		
20	63.8		

The experimental and predicted values are plotted in Figure 9.5 to enable comparison of values.

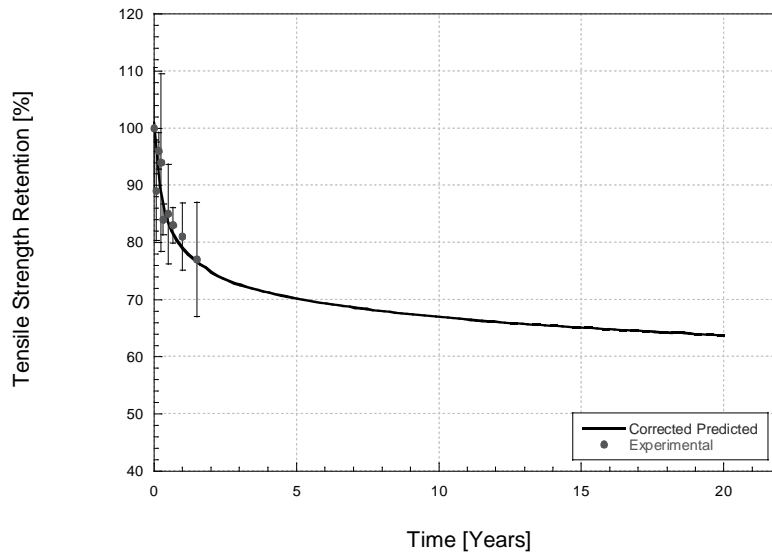


Figure 9.5. Comparison of Predicted and Experimental Values of Tensile Strength Retention Based on Arrhenius Rate Relationship

The same calculations are completed for tensile modulus, flexural strength, flexural modulus, and SBS strength. A complete set of predicted retention values for up to 20 years is provided in Table 9.6 and Figures 9.6 and 9.7.

Table 9.6. Retention [%] Values For Mechanical Properties Based on Modified Arrhenius Rate Relationship

Time [Years]	Property Retention [%]				
	Tensile Strength	Tensile Modulus	Flexural Strength	Flexural Modulus	SBS Strength
0	101.0	100	100.0	100.1	100.0
0.5	80.5	85.4	77.0	96.1	88.7
1	77.4	83.1	73.5	95.6	86.8
1.5	75.5	81.7	71.4	95.2	85.7
2	74.2	80.7	70.0	94.8	84.9
3	72.4	79.3	68.9	94.7	83.8
5	70.2	77.5	65.4	94.2	82.4
10	66.9	75.2	61.8	93.7	80.5
15	65.1	73.8	59.7	93.3	79.4
20	63.8	72.8	58.3	92.8	78.6

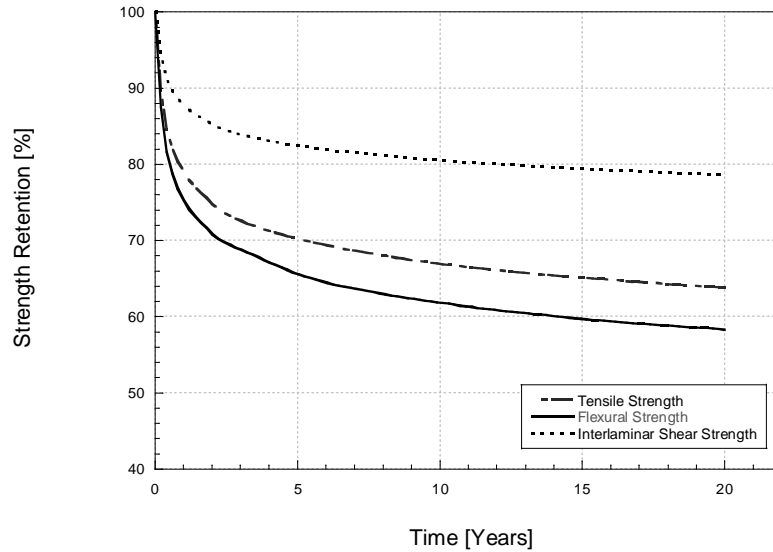


Figure 9.6. Predicted Strength Values Using Arrhenius Rate Relationship

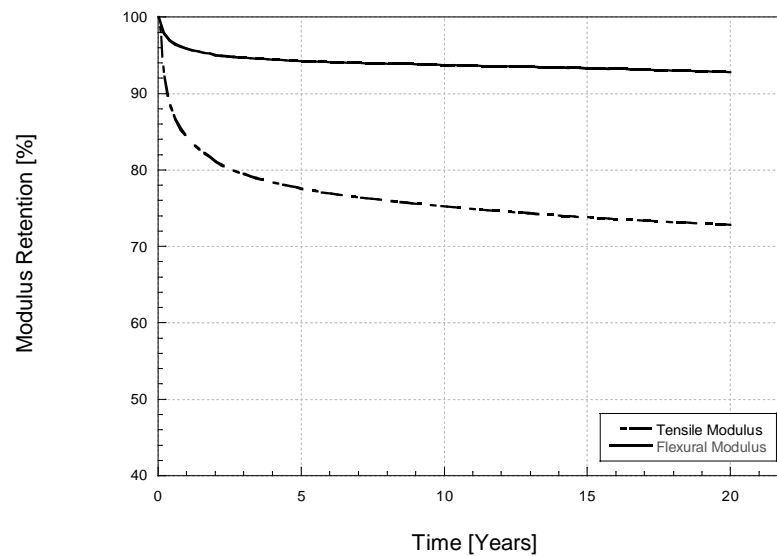


Figure 9.7. Predicted Modulus Values Using Arrhenius Rate Relationship

9.3. TIME-TEMPERATURE SUPERPOSITION

The Time-Temperature Superposition approach relates the effects of time and temperature on materials response based on viscoelastic theory [115]. In this method, data is measured at constant temperatures for different time periods. In order to shift the data, a reference temperature, usually denoted T_0 , is chosen. A master curve is generated by shifting the short-

term data on a logarithmic scale to the reference temperature [116]. The master curve results in a function of time and temperature [115]. The mathematical expression for the horizontal shift is expressed in equation 9-4.

$$f(T_o, t) = f(T_1, t / a_T) \quad (9-4)$$

where:

f is the property being considered in the model,

T_o is the reference temperature (in °K),

t is the time in weeks,

T₁ is the temperature that is being shifted (in °K), and

a_T is the shift factor.

Shifting the curves is dependent on two criteria based on the Williams-Landel-Ferry (WLF) model [116]. The first criterion is that the adjacent curves must match exactly over a reasonable distance [116]. The second criterion is that the same shift factor must be capable of use in superposition of all viscoelastic functions [116]. Because of the inherent changes in the property, it is often necessary to shift vertically in addition to the usual horizontal shift [116,117]. The vertical shift is based on the reference temperature, while the horizontal shift is based on the Arrhenius relation. The Arrhenius relation is shown in equation 9-5.

$$\text{Log}(a_T) = -\frac{\Delta E}{2.303R} \left(\frac{1}{T} - \frac{1}{T_{ref}} \right) \quad (9-5)$$

where:

Log (a_T) is the shift factor using the logarithmic scale,

ΔE is the Activation energy in Kcal/mol,

R is the gas constant (1.986 cal/mol/°K),

T is the temperature of the data being shifted in degrees Kelvin, and

T_{ref} is the reference temperature in degrees Kelvin.

Once the data is shifted accordingly, the master curve is generated in order to provide predictions of long-term data. The following section will outline procedures used to determine predictions based on the tensile strength. The results for models based on tensile modulus, flexural strength, flexural modulus, and SBS strength will be presented, however they will not be shown in detail.

9.3.1. Application to Data

Average values of tensile strength discussed in Chapter 5 are repeated for ease of reference in Table 9.7.

Table 9.7. Tensile Strength Values As a Result of Immersion in Seawater

Time [weeks]	Strength [MPa]		
	23°C	40°C	60°C
0	729.6	729.6	729.6
4	646.0	543.3	428.9
8	702.9	463.8	393.5
12	682.8	457.2	391.1
16	614.9	467.0	393.3
24	619.9	448.8	365.9
32	603.4	453.4	374.7
48	592.6	438.8	379.9
72	561.4	424.6	375.9

Using the values from Table 9.7, a plot of the log of strength versus the log of time (in weeks) is generated as the initial step before shifting the curves. This is shown in Figure 9.8.

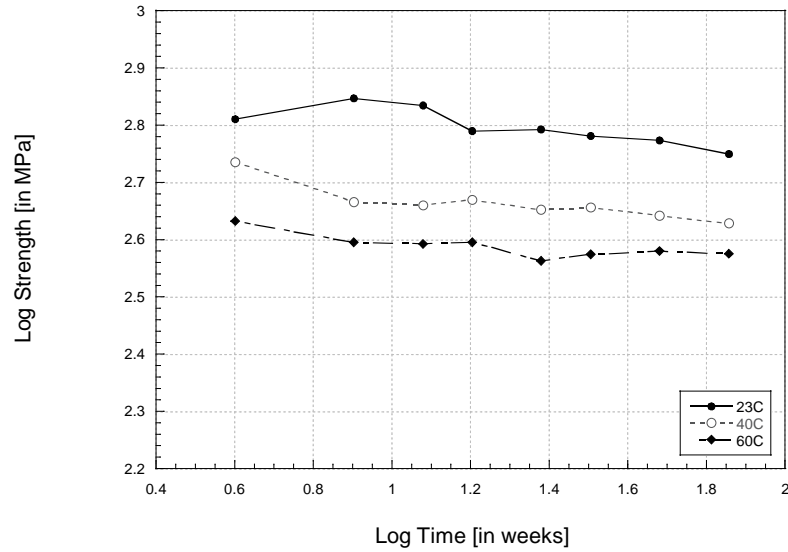


Figure 9.8. Plot of Log Strength versus Log Time

According to equation 9-5, the logarithmic horizontal shift for the 40°C and 60°C curves are 0.4 and 0.9, respectively. The vertical shift is with reference to the 23C curve. After all curves are shifted (see Figure 9.9), a master curve is completed and is shown in Figure 9.10.

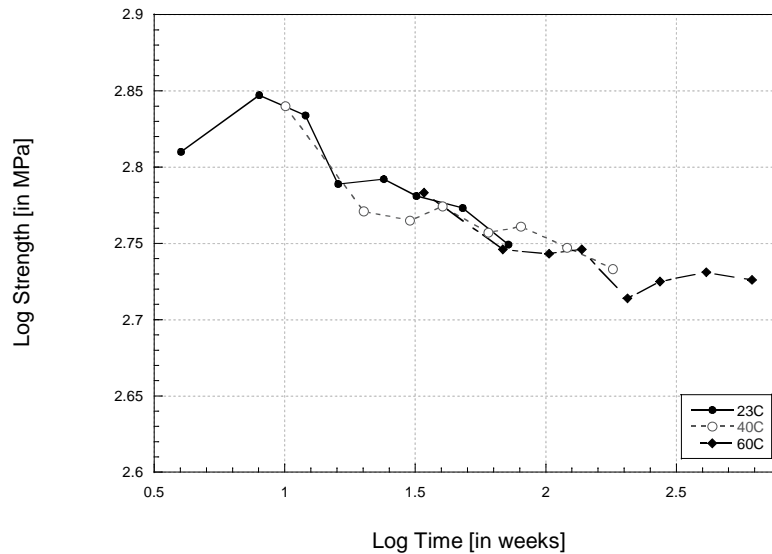


Figure 9.9. Shifted Curves to Generate Master Curve for Time-Temperature Superposition

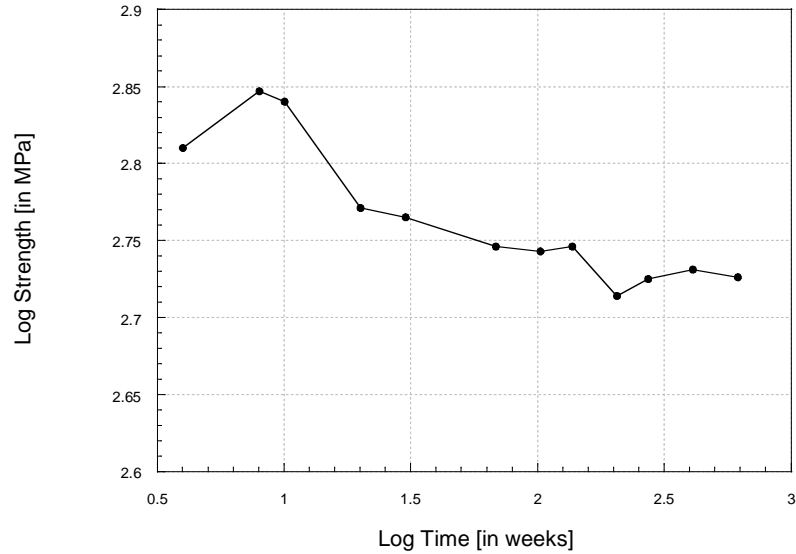


Figure 9.10. Master Curve for Time-Temperature Superposition

The master curve is then used to obtain values at future periods of time. A power curve fit is applied to the master curve in order to obtain a relationship for prediction. This prediction is based on samples immersed in room temperature seawater. Figure 9.11 shows the power curve fit to the data. Once the curve fit is determined, this equation is used to extrapolate values over extended periods of time.

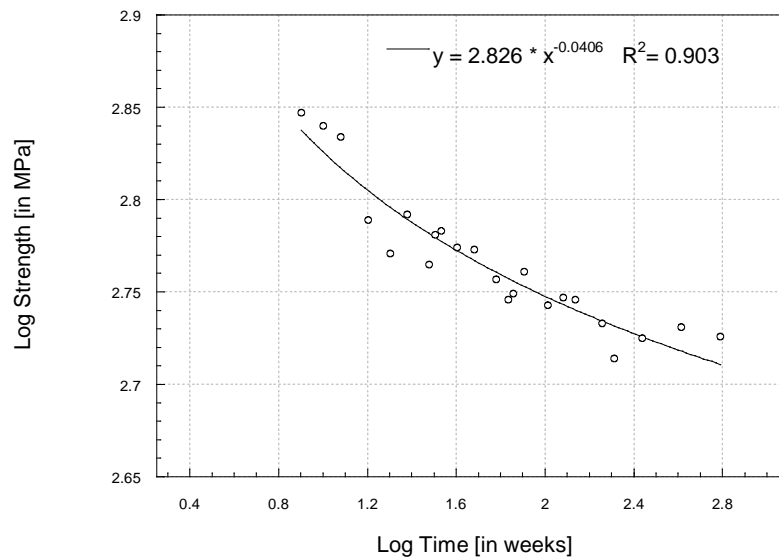


Figure 9.11. Power Curve Fit to Log of Strength Profile for Time-Temperature Superposition

Table 9.8 shows a comparison of predicted and experimental values. A calculation of differences between the two show percent differences less than 7%. To compare experimental data and data from the master curve, they are superimposed on the same plot in Figure 9.12 in terms of percent retention and years.

Table 9.8. Comparison of Predicted Values from Time-Temperature Superposition and Experimentally Obtained Values

Time	Predicted Strength Retention [%]	Experimentally Obtained Strength Retention [%]	% Difference Between Predicted and Experimental Results
0	100.0	100.0	0
0.5	83.8	85.0	1.4
1	79.7	81.2	1.9
1.5	77.8	76.9	-1.2
2	76.5		
3	74.9		
5	73.1		
10	70.9		
15	69.8		
20	69.0		

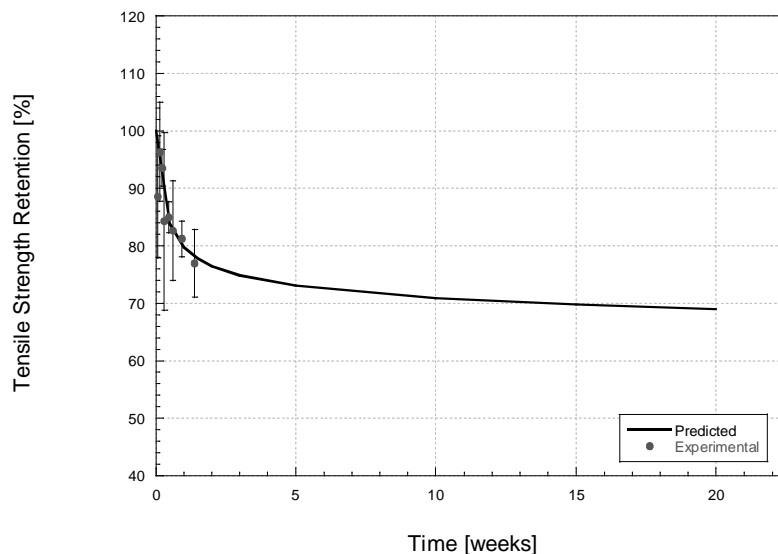


Figure 9.12. Comparison of Predicted and Experimental Values of Tensile Strength Retention Based on the Time-Temperature Superposition

Results for the other mechanical properties as derived from use of the Time-Temperature Superposition model are shown in Table 9.9 and Figures 9.13 and 9.14.

Table 9.9. Additional Mechanical Property Predictions Based on Time-Temperature Superposition

Time	Retention [%]				
	Tensile Strength	Tensile Modulus	Flexural Strength	Flexural Modulus	SBS Strength
0	100.0	100.00	100.0	100.0	100.0
0.5	83.8	88.55	70.9	93.8	69.7
1	79.7	86.13	66.5	93.0	62.1
1.5	77.8	84.94	64.4	92.6	58.6
2	76.5	84.17	63.1	92.4	56.5
3	74.9	83.18	61.4	92.0	53.8
5	73.1	82.05	59.5	91.7	51.0
10	70.9	80.70	57.3	91.2	47.8
15	69.8	80.00	56.2	91.0	46.2
20	69.0	79.53	55.4	90.8	45.1

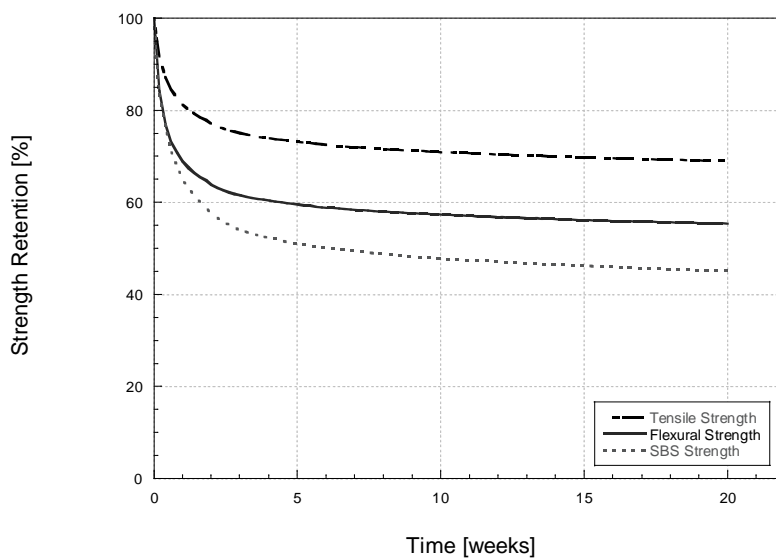


Figure 9.13. Strength Prediction Values Based on Time-Temperature Superposition

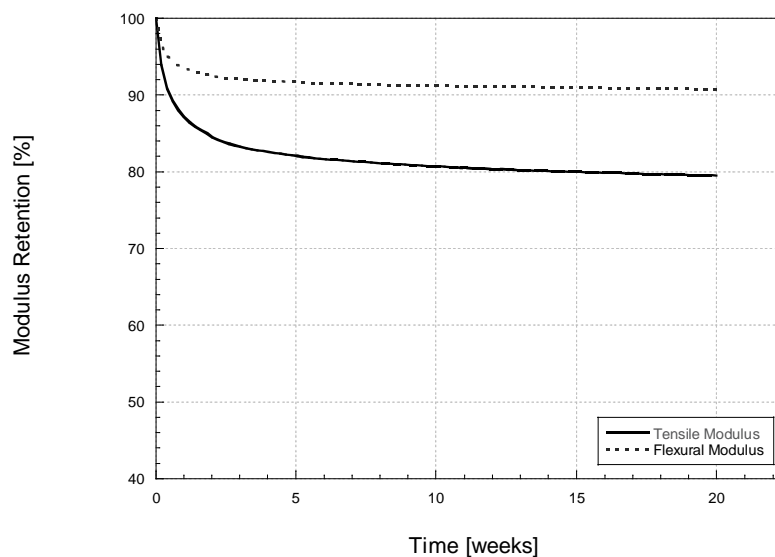


Figure 9.14. Modulus Prediction Values Based on Time-Temperature Superposition

9.4. COMPARISON OF PREDICTIVE MODELS

A direct comparison is made between the predictive models analyzed in the previous sections. Some major differences are apparent when applying both models. The Arrhenius Rate Relationship implicitly assumes that degradation occurs throughout and that increases in strength do not occur. However, from past studies and data from the current experiment, an increase in properties is expected because of the cure at ambient conditions. The Time-Temperature Superposition approach also does not account for post-cure, and similarly, does not take into account anomalies. One of the assumptions that the Time-Temperature Superposition imposes is that the same mechanism of degradation occurs across all temperatures [108]. This assumption is the main basis for shifting profiles at higher temperatures. Some other limitations exist in the Time-Temperature Superposition in that it is only valid for specific polymers and materials. In past studies, it has mainly been applied to fatigue S-N curves, however applications in other aspects has been studied [19,104,115,116,117,118].

Figure 9.15 illustrates the similarities in predictive values obtained for tensile strength retention for both models. The Time-Temperature Superposition appears to provide values closer

actual experimental data and predicted strength, as shown in Table 9.5 with minimal percent differences.

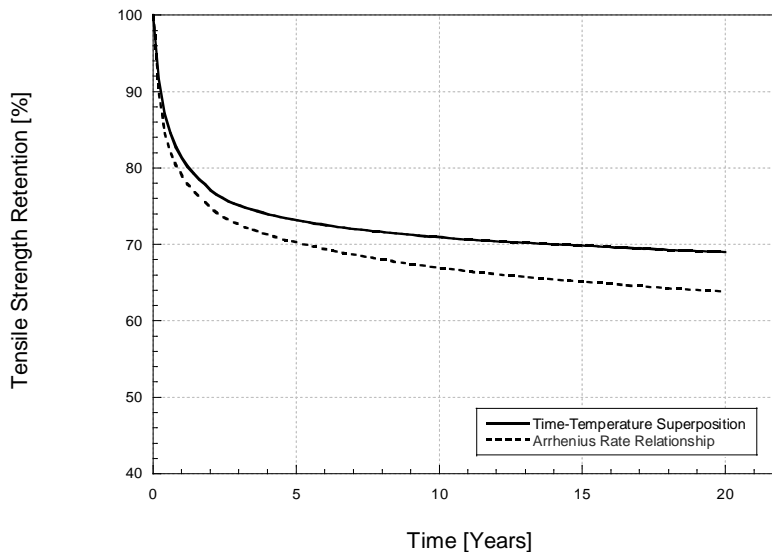


Figure 9.15. Comparison Between Prediction Results of Tensile Strength Retention for Time-Temperature Superposition and Arrhenius Rate Relationship

Figure 9.16 illustrates the comparison in predictive models for flexural strength. Both models appear to follow similar trends of deterioration. Slightly more conservative values result from the use of the Time-Temperature Superposition approach than the Arrhenius Rate Relationship. While, the Arrhenius Rate Relationship predicts slightly about 60% retention due to long-term immersion, the Time-Temperature Superposition approach predicts a retention on the order of 55%.

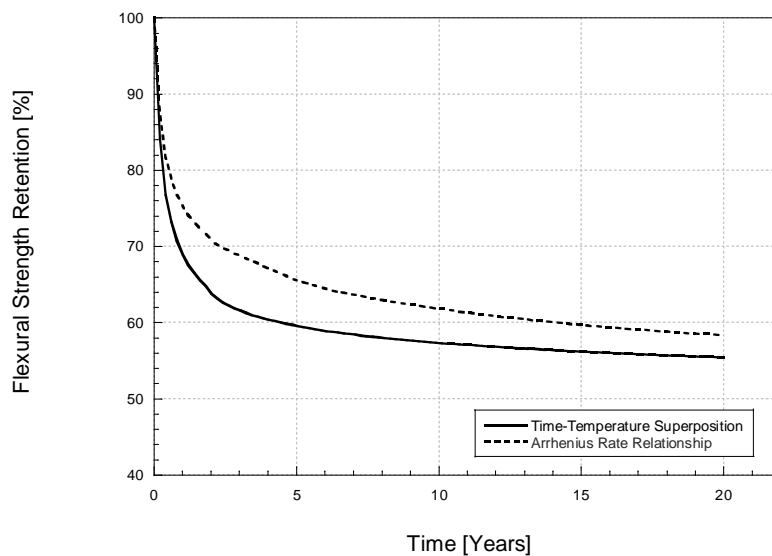


Figure 9.16. Comparison Between Prediction Results of Flexural Strength Retention for Time-Temperature Superposition and Arrhenius Rate Relationship

As seen in Figure 9.17, the Arrhenius Rate Relationship provides retention values on the order of 79% for SBS strength at 20 years. The Time-Temperature Superposition approach shows that the initial rate of decrease is significantly faster, and after 20 years, SBS strength retention is on the order of 45%.

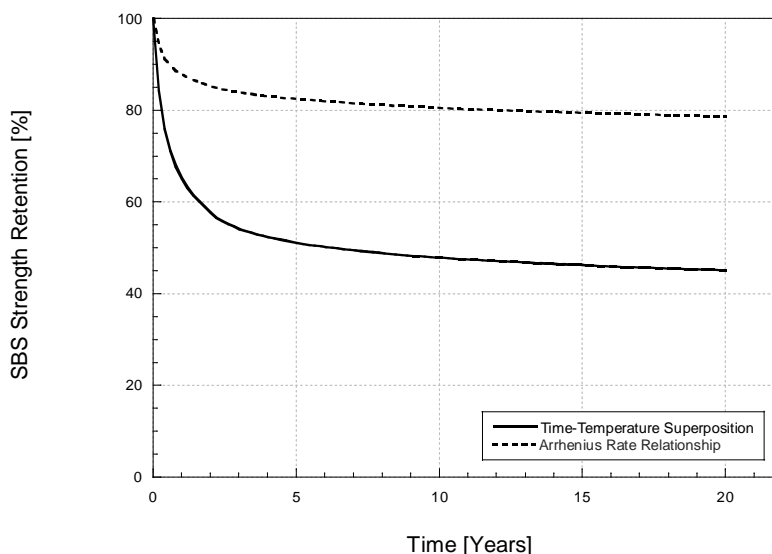


Figure 9.17. Comparison Between Prediction Results of SBS strength Retention for Time-Temperature Superposition and Arrhenius Rate Relationship

While previously examining the tensile modulus in Chapter 5, it was concluded that over the short term changes in tensile modulus were small and had insignificant adverse effects due to the exposure. Figure 9.18 shows a comparison of predictions provided by the two models. Both models predict retention on the order of 75-80% for long-term immersion at 23°C seawater.

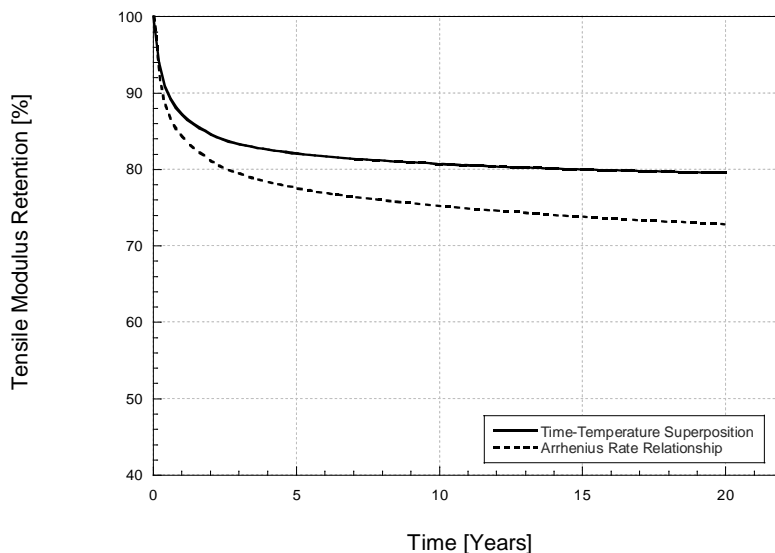


Figure 9.18. Comparison Between Prediction Results of Tensile Modulus Retention for Time-Temperature Superposition and Arrhenius Rate Relationship

Flexural modulus predictions are compared in Figure 9.19. Both models provide predictions of retention on the order of 90% at the 20-year level. Past studies have reported that increases in flexural modulus can be seen in room temperature synthetic seawater [67], while most researchers simply state that no significant changes occur [76,78,80,86,87,119].

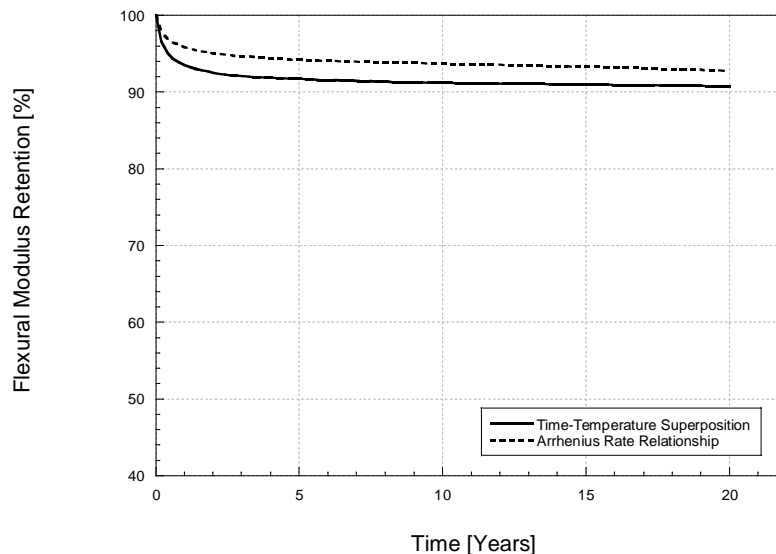


Figure 9.19. Comparison Between Prediction Results of Flexural Modulus Retention for Time-Temperature Superposition and Arrhenius Rate Relationship

9.5. SUMMARY

The appropriate use of predictive enables determination of long-term response from short-term environmental data. However, since extrapolation is involved it is essential that due thought be given to the choice of the method, and to the interpretation of results. Some major observations from the chapter are summarized below:

- Both models considered do not take into account effects of post-cure, and hence there is need for development of approaches that enable consideration of these effects. This is especially important over long periods of time where such effects could be important in offsetting deterioration.
- Both models provide similar results (with the exception for SBS strength) for long-term immersion
- Predictions for long-term strength retention are encouraging with the retention at the 20-year level being between 60-70%. It is also seen that changes in modulus over this time period are substantially less and often within the variation bounds of the material itself.

CHAPTER 10 – SUMMARY AND APPLICATION TO DESIGN

10.1. DEVELOPMENT OF A BASIS FOR DESIGN

The research provides an investigation into the durability characteristics of E-glass/vinyl ester composites subjected to a marine environment. A short summary is presented based on the relevant findings of this research.

Moisture studies show that the moisture uptake and kinetics of seawater immersion can vary substantially from moisture studies in deionized water. Seawater offers a complex composition that ultimately impedes moisture uptake through the large size of the sodium particles. This is demonstrated by relatively lower moisture contents measured in the samples. Moisture weight gain was found to be on the order of 0.3%. Immersion in elevated temperature seawater resulted in similar rates of diffusion, indicating similar degradation mechanisms. Initial periods of immersion show degradation due to plasticization, while longer-term immersion resulted in degradation due to leaching of low molecular weight species. It is however noted that the Na salts can cause degradation mechanisms and changes different from those seen through water immersion and thus a direct relationship of higher property retention due to lower moisture uptake cannot be made.

Tensile strength degradation after exposure to immersion in seawater and cycling resulted in a larger change in strength at higher immersion temperatures. Tensile modulus profiles did not show any significant effects during the entire exposure period. Plasticization was identified to have occurred between 0-12 weeks for samples immersed in room temperature water. The failure mode observed after testing in tension did not change with time. However, discoloration and the amount of explosive splitting behavior decreased with time and temperature of immersion indicating transition to a flexibilized state due to loss of matrix integrity. Failure modes observed after testing in tension associated with cycling did not change with time.

Changes in flexural strength with time showed an initial decrease followed by a state of equilibrium until the end of the exposure period. Rates of degradation for flexural strength occur slowly from 0-16 weeks in immersion conditions. This is attributed to the mechanical property's dependence on the fiber. Similar to what was observed regarding changes in tensile modulus, relatively low levels of deterioration were experienced in regards to changes in flexural modulus. The effect of postcure results in slight increases in the flexural strength during short-term immersion (i.e. 0-16 weeks). The effect of cycling in seawater shows that flexural strength is not severely affected. A closer look at the failure modes reveals that the toughness decreases with time and immersion temperature. Analysis of the failure modes of the flexural specimens show that the toughness in the composite is not affected significantly through cyclic exposure.

Changes in SBS strength revealed that the resin is severely degraded by elevated temperature levels of immersion. Microscopy shows the coalescence of debonds occurring at the interfaces. Cyclic exposures are noted to have lower effects on SBS strength deterioration as compared to immersion in seawater.

The high sensitivity of the DMTA reveals insight into the degradation mechanisms which occur in a composite exposed to environmental conditions. Immersion in 23°C seawater shows results that verify that plasticization occurs over the first 4 weeks, which is shown by a decrease in T_g . Subsequent increases in the height of tan delta until 12 weeks shows the effect of residual cure. An increase in the T_g after immersion for longer periods of time in both 23°C and 40°C seawater indicate that the leaching of low weight molecular species occurs and is supported by moisture uptake profiles reported in Chapter 4. Immersion in 60°C seawater results an initial decrease in T_g caused by moisture induced degradation. The material exhibits a brittle response after 12 weeks of exposure, which is reflected by a negative quantitative area between curves, increased activation energies, and increased T_g . The effect of leaching is most prevalent at this immersion temperature suggesting that this effect may realistically only be seen at very long time

scales. Cyclic exposures result in small amounts of moisture uptake which is reflected by the small changes in the area between the curves and minor reduction of activation energy after 72 weeks exposure.

Application of the data to life prediction models (Arrhenius Rate Relationship and Time-Temperature Superposition) shows promising results. The behavior of the material is characterized by an initial drop in properties followed by asymptotic behavior. Tensile strengths are predicted to have 70% retention at 20 years service. Flexural strength service life predictions show a 60% retention level. SBS strength predictions vary substantially between models with a 75% retention level being indicated by the Arrhenius Rate Relationship and a 50% retention level indicated by the Time-Temperature Superposition approach. Micrographs show that significant resin damage occurs at the interface and this leads to a range of potential damage mechanisms and progression paths.

10.2. MATERIAL OPERATIONAL LIMIT

Having obtained estimates of changes in material properties over periods of time, it is useful to assess the data from a design perspective. The use of the material operational limit (M.O.L.) principle enables the designer to estimate the useable service life of a material over time. Design guidelines often use a safety factor of 2 to account for inhomogeneities, construction defects, material flaws, unanticipated loads and various other factors. The material operational limit is calculated based on the safety factor as shown in equation 10-1.

$$M.O.L = \frac{1}{F.S.} * 100 \quad (10-1)$$

where:

M.O.L. is the material operational limit and

F.S. is the safety factor.

According to this equation, the M.O.L. for a F.S. of 2 is 50%. The M.O.L. is analyzed in the following sections for strength and modulus. The limits set forth provide an easy means of identifying critical periods of time at which performance characteristics fall below the M.O.L.

A study of the experimental results shows that even under the most severe regimes investigated, some characteristics do not approach the specified M.O.L. The patterns of strength degradation as represented in Chapters 5, 6, and 7 show equilibrium is often attained between 4-16 weeks of immersion after which further deterioration is extremely slow. Table 10.1 indicates the characteristics that reach the defined M.O.L. and the times at which this is attained.

Table 10.1. Characteristics that Reached M.O.L.

Environment	Tensile Strength	Tensile Modulus	Flexural Strength	Flexural Modulus	SBS Strength
23°C Seawater	*	*	*	*	*
40°C Seawater	*	*	*	*	*
60°C Seawater	6 months	*	6 months	*	2 months

It is clearly seen that the M.O.L. is only attained in the most severe condition of immersion in seawater at 60°C. Since this is an accelerated condition, it is useful to use the model results to assess the length of time at which M.O.L. would be reached in the non-accelerated case. The use of both the Arrhenius Rate Relationship and the Time-Temperature Superposition principle (TTSP) enables prediction of effects under the 23°C case. It is seen that the use of the TTSP predicts the SBS strength M.O.L. will be reached in 6 years and would be the only characteristic affected in a 25-year period. Table 10.2 indicates the level of characteristics at this time period as well as the time period at which the other characteristics can be expected to reach the defined M.O.L.

Table 10.2. M.O.L. Based on Predictive Models, Differing Values Based on TTSP are in Brackets

Characteristic	Tensile Strength	Tensile Modulus	Flexural Strength	Flexural Modulus	SBS Strength
% M.O.L Reached at 6 years	65% [73%]	75% [82%]	62% [59%]	94% [92%]	81% [50%]
Time M.O.L. Reached	> 100 years	> 100 years	> 100 years	> 100 years	>100 years [6 years]

10.3. CONFIDENCE LEVEL

Consideration of the M.O.L. in the previous section indicates that the durability of the composite under investigation will not degrade below a 50% allowable design value in typical marine environments for long periods of time. The current section provides a procedure to determine the confidence level which can be associated with a material property with respect to its service life as an aid in design. Typical designs require a “95/95” or “95/90” design value [120]. In this scheme, the first value describes the percent level of confidence in which at least a percent of all tests indicated by the second value will exceed a specified value [120]. Thus 95/95 indicates a 95% confidence level that 95% of all values will exceed the predefined value, usually the design limit or a predetermined allowable.

The procedure is based on ASTM E739, which provides a statistical analysis for linearized stress-life data [121]. The method is based on determining a that describes a data set. The following procedure follows ASTM E739 and the approach outlined by Sutherland and Veers [120]. As an example test data based on predicted service life for 20 years (using Time-Temperature Superposition) for tensile strength under immersion at 23°C is used in order to determine a design confidence level. Confidence levels based on other mechanical properties are then summarized.

A plot of normalized tensile strength versus the natural log of time is presented in Figure 10.1. As can be seen the data has a high degree of linearity.

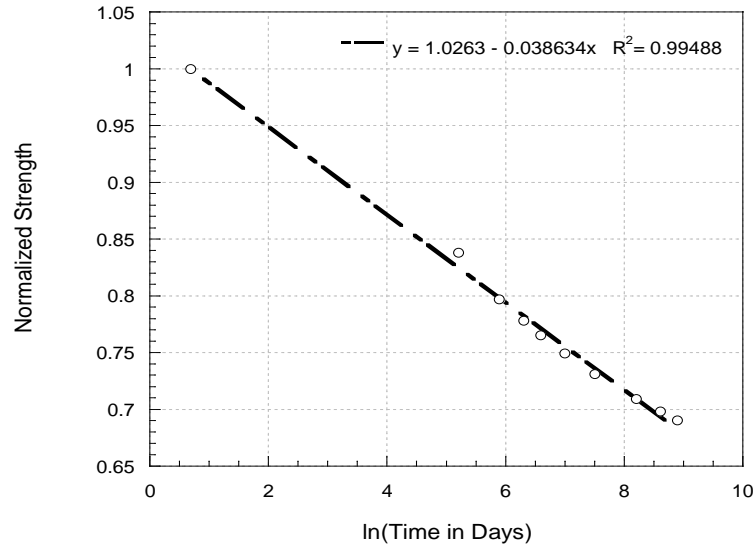


Figure 10.1. Log-Linear Fit of Strength-Life Data

In order to verify the “goodness of fit”, ASTM recommends calculating maximum likelihood estimators “A” and “m,” determined according to equation 10-2 and 10-3. Once calculated, it is expected that they match the values obtained by the linear curve fit in terms of the y intercept and slope in Figure 10.1.

$$\hat{A} = \bar{Y} - m\bar{X} \quad (10-2)$$

where:

\hat{A} and m are maximum likelihood estimators,

\bar{Y} is the mean value of the Y test data, and

\bar{X} is the mean value of the X test data.

$$m = \frac{\sum_{i=1}^n (X_i - \bar{X})(Y_i - \bar{Y})}{\sum_{i=1}^n (X_i - \bar{X})^2} \quad (10-3)$$

where:

n is the number of points in the data set,

X_i is the value of the X test data at i, and

Y_i is the value of the Y test data at i.

Confidence levels are based on the distribution about the mean line about the linear curve fit. This distribution is determined by equation 10-4, 10-5, and 10-6.

$$R_i = Y_i - \hat{Y}_i \quad (10-4)$$

where:

R_i are the residuals,

and \hat{Y}_i is defined in equation 10-5.

$$\hat{Y}_i = \hat{A} - mX_i \quad (10-5)$$

$$\sigma_y = \left[\frac{\sum_{i=1}^n (Y_i - \hat{Y}_i)^2}{n - 2} \right]^{\frac{1}{2}} \quad (10-6)$$

where:

σ_y is the standard deviation of the residuals.

It is essential that the residuals show that they are independent of the normalized strength. Figure 10.2 depicts a plot of residual life versus normalized strength and shows that there is no relationship between the two aspects, thus demonstrating the independence.

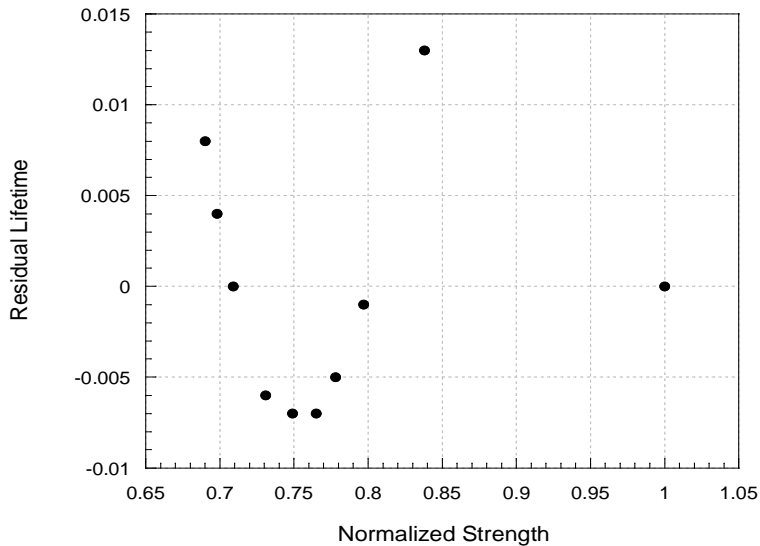


Figure 10.2. Distribution of Residuals

To verify the log-normal fit of the data to the normal distribution, an inverse normal distribution function is plotted versus the natural log of the residual lifetime. A linear relationship reveals that the use of the normal distribution is optimal. Figure 10.3 shows that the relationship between the inverse normal distribution function versus the natural log of time is linear with a high value of correlation ($R^2 = 0.95403$).

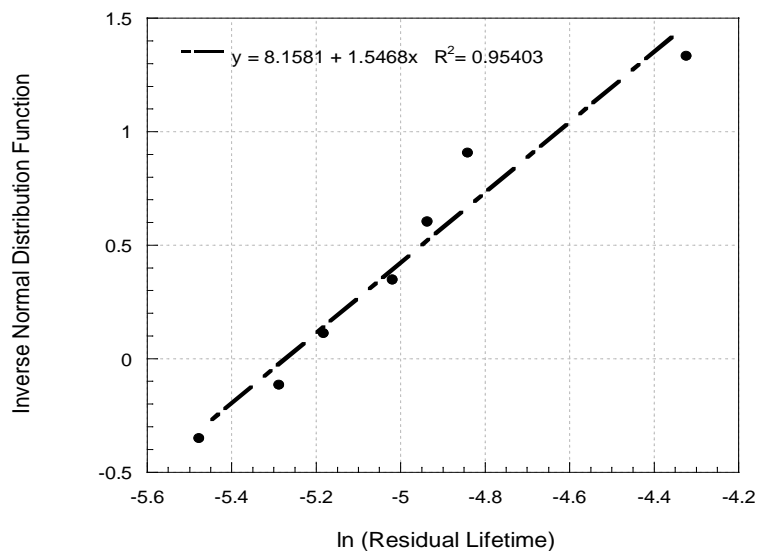


Figure 10.3. Inverse Normal Distribution of the Data

Once the distribution is established as inverse normal, a one-sided tolerance limit is computed according to equation 10-7. The one-sided tolerance limit is equivalent to the c-multiplier that will be used to calculate the confidence levels.

$$Y = \hat{A} + mX - c_{1-\alpha, \lambda} \sigma_y \quad (10-7)$$

where:

$c_{1-\alpha, \lambda}$ is the c-multiplier tabulated as a function of the confidence level, probability, and the number of data points.

After the c-multiplier is established, the confidence level can be calculated by equation 10-8.

$$X^* = \bar{X} - c_{1-\alpha, \gamma} \sigma_x \quad (10-8)$$

where:

σ_x is the standard deviation of the stress data.

Table 10.3 summarizes the maximum likelihood estimators and standard deviation of the residuals calculated for tensile strength, flexural strength, SBS strength, tensile modulus, and flexural modulus.

Table 10.3. Maximum Likelihood Estimators and Standard Deviation of the Residuals

Property	Maximum Likelihood Estimators, $\hat{A} = \bar{Y} - m\bar{X}$	R ²	Standard Deviation of Residuals, σ_y
Tensile Strength	$1.03 = \bar{Y} - 0.04 * \bar{X}$	0.95	0.02
Flexural Strength	$1.01 = \bar{Y} - 0.06 * \bar{X}$	0.97	0.04
SBS Strength	$1.04 = \bar{Y} - 0.07 * \bar{X}$	0.99	0.03
Tensile Modulus	$1.01 = \bar{Y} - 0.03 * \bar{X}$	0.99	0.01
Flexural Modulus	$1.00 = \bar{Y} - 0.01 * \bar{X}$	0.97	0.01

Table 10.4 summarizes the one-sided tolerance limit calculated for each property.

Table 10.4. One-Sided Tolerance Limit

Property	\hat{A}	m	$c_{1-\alpha,\gamma}$		σ_y	One-Sided Tolerance Limit, $Y = \hat{A} + mX - c_{1-\alpha,\lambda}\sigma_y$	R^2
			95/95	95/90			
Tensile Strength	1.03	0.04	1.61	1.52	0.02	$Y = 0.22*X + 2.06$	0.76
Flexural Strength	1.01	0.06	1.62	1.54	0.04	$Y = 0.85*X + 4.04$	0.76
SBS Strength	1.04	0.07	1.60	1.52	0.03	$Y = 0.66*X + 3.51$	0.82
Tensile Modulus	1.01	0.03	1.62	1.53	0.01	$Y = 0.72*X + 4.72$	0.83
Flexural Modulus	1.00	0.01	1.63	1.54	0.01	$Y = 0.99*X + 5.97$	0.74

Table 10.5 summarizes the variables used in equation 10-8 to determine the confidence level.

Table 10.5. Confidence Level Multipliers

Property	σ_x	Confidence Level, $X^* = \bar{X} - c_{1-\alpha,\gamma}\sigma_x$	
		95/95	95/90
Tensile Strength	66.7 MPa	$X^* = 565.8 - 1.61*\sigma_x$	$X^* = 565.8 - 1.52*\sigma_x$
Flexural Strength	115.1 MPa	$X^* = 576.6 - 1.62*\sigma_x$	$X^* = 576.6 - 1.54*\sigma_x$
SBS Strength	8.0 MPa	$X^* = 29.0 - 1.60*\sigma_x$	$X^* = 29.0 - 1.52*\sigma_x$
Tensile Modulus	2.3 GPa	$X^* = 31.8 - 1.62*\sigma_x$	$X^* = 31.8 - 1.53*\sigma_x$
Flexural Modulus	0.7 GPa	$X^* = 25.0 - 1.63*\sigma_x$	$X^* = 25.0 - 1.54*\sigma_x$

This procedure is performed based on predicted service life (using Time-Temperature Superposition) for tensile strength, flexural strength, tensile modulus, flexural modulus, and SBS strength for up to 20 years of immersion in seawater at 23°C. The table suggests, “With a 95 percent confidence level, I expect that at least 95 (or 90) percent of all tests up to 20 years environmental exposure will exceed X^* .” The values of X^* are summarized in Table 10.6. They are also repeated in terms of percent retention in Table 10.7.

Table 10.6. Confidence Levels Based on Predicted Service Life Using Time-Temperature Superposition After Exposure to 23°C Seawater For 20 Years

Material Property	Unexposed Value	Confidence Level	
		95/95	95/90
Tensile Strength	729.6 MPa	458.5 MPa	464.2 MPa
Flexural Strength	880.8 MPa	390.1 MPa	399.9 MPa
SBS Strength	49.1 MPa	16.2 MPa	16.9 MPa
Tensile Modulus	37.4 GPa	28.1 GPa	28.3 GPa
Flexural Modulus	26.9 GPa	23.8 GPa	23.9 GPa

Table 10.7. Confidence Levels Based on Predicted Service Life Using Time-Temperature Superposition After Exposure to 23°C Seawater For 20 Years

Material Property	Confidence Level	
	95/95 [%]	95/90 [%]
Tensile Strength	62.8	63.6
Flexural Strength	44.3	45.4
SBS Strength	33.0	34.4
Tensile Modulus	75.2	75.7
Flexural Modulus	88.5	88.7

Calculation of the confidence levels for material properties attained after seawater immersion at 23°C shows high confidence levels for most properties. The only property of concern is the SBS strength that shows a 95/90 confidence level that the property will not fall below 34.4% retention. This value is based on predicted service life data of low levels of SBS strength retention.

APPENDIX

Table A.4.1. Average Weight Gain for 23°C Immersion

Time (hr)	Hr ^{1/2}	Continuous		Non-Continuous	
		Average Weight gain, %	Std. Dev.	Average Weight gain, %	Std. Dev.
0	0.00	0.000	0.00	0.000	0.00
1	1.00	0.028	0.01	0.055	0.01
4	2.00	0.033	0.01	*	*
8	2.83	0.036	0.01	*	*
24	4.90	0.058	0.01	0.071	0.01
96	9.80	0.103	0.01	0.119	0.02
168	12.96	0.123	0.01	0.126	0.01
336	18.33	0.221	0.04	0.251	0.02
672	25.92	0.219	0.03	0.229	0.02
1344	36.66	0.241	0.03	0.234	0.02
2016	44.90	0.265	0.06	0.233	0.02
2688	51.85	0.266	0.03	0.228	0.01
4032	63.50	0.237	0.02	0.253	0.04
5376	73.32	0.230	0.03	0.246	0.04
8640	92.95	0.222	0.03	0.254	0.04
12960	113.84	0.262	0.03	0.293	0.02

Table A.4.2. Average Weight Gain for 40°C Immersion

Time (hr)	Hr ^{1/2}	Continuous		Non-Continuous	
		Average Weight gain, %	Std. Dev.	Average Weight gain, %	Std. Dev.
0	0.00	0.000	0.00	0.000	0.00
1	1.00	0.061	0.02	0.065	0.01
4	2.00	0.084	0.01	0.092	0.03
8	2.83	0.124	0.04	0.098	0.00
24	4.90	0.147	0.03	0.145	0.03
96	9.80	0.235	0.02	0.256	0.03
168	12.96	0.234	0.01	0.245	0.00
336	18.33	0.232	0.02	0.260	0.01
672	25.92	0.248	0.02	0.281	0.02
1344	36.66	0.268	0.02	0.276	0.01
2016	44.90	0.240	0.04	0.289	0.11
2688	51.85	0.204	0.04	0.265	0.03
4032	63.50	0.215	0.04	0.281	0.06
5376	73.32	0.198	0.03	0.248	0.05
8640	92.95	0.156	0.02	0.175	0.03
12960	113.84	0.125	0.02	0.115	0.02

Table A.4.3. Average Weight Gain for 60°C Immersion

Time (hr)	Hr ^{1/2}	Continuous		Non-Continuous	
		Average Weight gain, %	Std. Dev.	Average Weight gain, %	Std. Dev.
0	0.00	0.000	0.00	0.000	0.00
1	1.00	0.034	0.01	0.025	0.01
4	2.00	0.039	0.01	0.043	0.01
8	2.83	0.061	0.01	0.062	0.01
24	4.90	0.109	0.02	0.123	0.00
96	9.80	0.212	0.03	0.212	0.02
168	12.96	0.285	0.04	0.294	0.03
336	18.33	0.275	0.04	0.278	0.02
672	25.92	0.248	0.03	0.292	0.03
1344	36.66	0.200	0.04	0.266	0.01
2016	44.90	0.180	0.02	0.235	0.01
2688	51.85	0.199	0.03	0.253	0.03
4032	63.50	0.186	0.03	0.215	0.03
5376	73.32	0.177	0.02	0.237	0.03
8640	92.95	0.182	0.03	0.247	0.03
12960	113.84	0.185	0.04	0.215	0.04

Table A.4.4. Average Weight Gain for Freeze/Thaw Cycling

Time (hr)	Hr ^{1/2}	Continuous		Non-Continuous	
		Average Weight gain, %	Std. Dev.	Average Weight gain, %	Std. Dev.
0	0.00	0.000	0.00	0.000	0.00
1	1.00	0.061	0.04	0.048	0.01
4	2.00	0.119	0.06	0.121	0.03
8	2.83	0.142	0.05	0.294	0.06
24	4.90	0.192	0.05	0.124	0.01
144	12.00	0.193	0.03	0.220	0.02
192	13.86	0.184	0.03	0.233	0.06
360	18.97	0.192	0.03	0.192	0.04
696	26.38	0.327	0.15	0.953	1.10
2688	51.85	0.786	0.46	0.333	0.13
4056	63.69	0.846	0.52	0.272	0.05
4704	68.59	0.936	0.56	1.740	0.88
5856	76.52	0.401	0.09	0.345	0.08
9336	96.62	0.404	0.08	0.331	0.06
12192	110.42	0.428	0.07	0.604	0.52

Table A.4.5. Average Weight Gain for Wet/Dry Cycling

Time (hr)	Hr ^{1/2}	Continuous		Non-Continuous	
		Average Weight gain, %	Std. Dev.	Average Weight gain, %	Std. Dev.
0	0.00	0.000	0.00	0.000	0.00
1	1.00	0.026	0.02	0.022	0.00
4	2.00	0.156	0.04	0.054	0.00
8	2.83	0.187	0.05	0.113	0.01
24	4.90	0.23	0.05	0.151	0.03
192	13.86	0.163	0.00	0.135	0.02
360	18.97	0.263	0.04	0.210	0.01
696	26.38	0.223	0.03	0.218	0.02
2688	51.85	0.238	0.05	0.275	0.04
4056	63.69	0.222	0.03	0.283	0.04
4704	68.59	0.379	0.03	0.320	0.05
5856	76.52	0.258	0.03	0.213	0.02
9336	96.62	0.264	0.03	0.278	0.03
12192	110.42	0.294	0.03	0.319	0.00

Table A.8.1a. T_g Based on Storage Modulus for Ambient Condition at 23°C and 30%RH

Time [weeks]	Ambient							
	1 Hz [°C]	Std. Dev. [°C]	5 Hz [°C]	Std. Dev. [°C]	10 Hz [°C]	Std. Dev. [°C]	30 Hz [°C]	Std. Dev. [°C]
0	110.5	4.0	113.6	0.6	114.5	0.5	118.9	0.7
4	113.7	0.7	116.7	1.9	118.9	0.7	121.7	1.1
8	112.5	3.4	115.9	1.1	117.2	1.6	119.6	1.8
12	111.6	0.2	116.3	3.0	118.3	3.8	120.7	2.8
16	111.8	0.1	116.9	2.5	118.8	3.2	122.2	0.6
24	113.9	2.5	118.9	0.6	118.8	1.3	124.7	0.5
32	-	-	-	-	-	-	-	-
48	112.8	0.6	118.5	1.5	120.5	3.0	125.3	1.7
72	114.4	1.5	119.6	2.1	120.6	2.1	124.4	2.5

Table A.8.1b. T_g Based on Storage Modulus Determined After Immersion in 23°C Seawater (“Wet Testing”) and as a Result of Subsequent Redrying (“Dry Testing”)

Time [weeks]	23°C Seawater “Wet Testing”							
	1 Hz [°C]	Std. Dev. [°C]	5 Hz [°C]	Std. Dev. [°C]	10 Hz [°C]	Std. Dev. [°C]	30 Hz [°C]	Std. Dev. [°C]
0	110.5	4.0	113.6	0.6	114.5	0.5	118.9	0.7
4	108.3	1.0	112.0	1.7	113.7	1.7	116.1	0.7
8	111.8	1.1	115.1	3.4	117.4	1.6	118.7	2.5
12	109.1	0.6	112.2	0.8	113.3	1.9	116.4	0.8
16	-	-	-	-	-	-	-	-
26	113.1	0.1	116.5	2.6	115.2	1.1	121.0	2.3
35	114.0	-	115.2	7.8	111.6	5.4	115.1	7.8
52	108.4	1.6	110.6	0.9	113.0	1.1	118.8	1.8
78	108.5	0.6	112.8	1.0	113.8	0.9	119.0	1.9

Time [weeks]	23°C Seawater “Dry Testing”							
	1 Hz [°C]	Std. Dev. [°C]	5 Hz [°C]	Std. Dev. [°C]	10 Hz [°C]	Std. Dev. [°C]	30 Hz [°C]	Std. Dev. [°C]
0	110.5	4.0	113.6	0.6	114.5	0.5	118.9	0.7
4	112.9	2.7	115.6	0.1	117.8	2.7	120.1	0.6
8	111.9	1.4	115.3	1.1	117.2	0.5	120.6	0.4
12	115.3	0.4	117.1	1.1	118.7	1.3	122.5	1.0
16	113.0	0.4	117.3	0.4	118.6	1.6	122.1	0.9
26	110.1	1.0	114.3	1.0	116.6	0.6	121.5	1.1
35	112.0	2.2	115.6	2.1	117.8	1.7	122.3	2.1
52	112.0	0.4	115.6	3.0	118.1	1.7	122.7	0.8
78	111.3	3.7	117.9	1.6	117.1	0.7	121.2	1.9

Table A.8.1c. T_g Based on Storage Modulus Determined After Immersion in 40°C Seawater (“Wet Testing”) and as a Result of Subsequent Redrying (“Dry Testing”)

Time [weeks]	40°C Seawater “Wet Testing”							
	1 Hz [°C]	Std. Dev. [°C]	5 Hz [°C]	Std. Dev. [°C]	10 Hz [°C]	Std. Dev. [°C]	30 Hz [°C]	Std. Dev. [°C]
0	110.5	4.0	113.6	0.6	114.5	0.5	118.9	0.7
4	109.7	1.1	112.2	1.6	113.7	1.6	117.9	0.6
8	-	-	108.9	1.0	110.2	0.8	112.9	1.1
12	109.8	1.3	112.1	0.6	114.1	1.0	116.3	0.4
16	110.1	0.7	113.5	1.5	115.7	1.0	118.0	0.5
26	105.8	0.9	111.5	0.8	111.6	3.0	116.9	3.4
35	106.6	1.4	111.6	1.0	112.2	1.0	116.7	1.6
52	109.7	0.8	114.3	1.7	115.3	1.7	120.9	1.5
78	110.3	0.5	115.2	0.5	116.2	0.5	120.8	1.8

Time [weeks]	40°C Seawater “Dry Testing”							
	1 Hz [°C]	Std. Dev. [°C]	5 Hz [°C]	Std. Dev. [°C]	10 Hz [°C]	Std. Dev. [°C]	30 Hz [°C]	Std. Dev. [°C]
0	110.5	4.0	113.6	0.6	114.5	0.5	118.9	0.7
4	105.6	9.5	110.1	5.8	111.4	6.9	114.7	8.2
8	108.8	2.8	110.8	2.5	112.9	3.0	118.0	1.8
12	113.3	1.9	116.8	1.0	118.3	3.0	121.3	1.7
16	111.9	0.6	115.6	1.1	117.8	2.1	121.1	0.5
26	111.1	0.8	116.2	0.3	118.4	0.9	122.0	0.1
35	110.0	2.5	114.7	3.6	116.8	3.6	121.4	3.9
52	113.8	1.1	118.4	0.6	118.1	2.4	122.6	4.2
78	112.2	1.6	118.1	1.5	121.4	5.2	124.8	4.2

Table A.8.1d. T_g Based on Storage Modulus Determined After Immersion in 60°C Seawater (“Wet Testing”) and as a Result of Subsequent Redrying (“Dry Testing”)

Time [weeks]	60°C Seawater “Wet Testing”							
	1 Hz [°C]	Std. Dev. [°C]	5 Hz [°C]	Std. Dev. [°C]	10 Hz [°C]	Std. Dev. [°C]	30 Hz [°C]	Std. Dev. [°C]
0	110.5	4.0	113.6	0.6	114.5	0.5	118.9	0.7
4	108.9	1.5	111.3	0.4	112.7	0.9	115.0	1.2
8	110.4	1.9	112.5	2.1	112.7	3.3	116.9	0.1
12	111.6	0.6	115.4	1.4	116.1	0.9	118.4	0.3
16	112.5	1.4	113.9	1.9	117.0	3.9	120.3	1.1
26	109.1	1.3	114.5	1.8	116.9	1.7	119.9	1.0
35	110.7	1.3	115.8	1.0	118.3	1.0	123.6	2.1
52	109.6	1.1	116.4	1.3	117.9	1.8	123.8	2.4
78	111.7	2.2	120.9	1.4	121.5	2.0	125.1	3.5

Time [weeks]	60°C Seawater “Dry Testing”							
	1 Hz [°C]	Std. Dev. [°C]	5 Hz [°C]	Std. Dev. [°C]	10 Hz [°C]	Std. Dev. [°C]	30 Hz [°C]	Std. Dev. [°C]
0	110.5	4.0	113.6	0.6	114.5	0.5	118.9	0.7
4	111.4	3.0	114.8	1.9	115.8	2.1	118.3	2.7
8	114.0	3.6	117.5	2.1	120.3	0.7	121.2	1.0
12	115.8	1.0	118.8	1.2	120.4	0.9	122.8	0.2
16	119.4	0.3	122.5	0.3	125.3	1.5	129.5	3.9
26	114.8	0.4	119.7	0.0	121.3	1.4	125.7	0.8
35	120.4	2.0	124.3	1.5	125.9	2.4	132.0	1.5
52	118.7	0.8	123.3	1.2	125.3	1.9	130.4	1.4
78	117.7	0.7	124.9	1.0	125.9	1.0	131.0	1.1

Table A.8.2a. T_g Based on Storage Modulus Determined as a Function of Cyclic Exposure

Time [weeks]	Freeze/Thaw "Wet Testing"							
	1 Hz [°C]	Std. Dev. [°C]	5 Hz [°C]	Std. Dev. [°C]	10 Hz [°C]	Std. Dev. [°C]	30 Hz [°C]	Std. Dev. [°C]
0	110.5	4.0	113.6	0.6	114.5	0.5	118.9	0.7
4	112.4	1.2	115.6	1.9	117.4	1.5	120.0	2.3
8	111.4	1.1	114.9	1.6	116.0	1.0	119.2	2.8
12	107.4	1.8	109.7	0.9	110.2	1.7	113.2	4.1
16	107.6	1.5	110.5	1.8	115.2	1.9	118.2	1.5
24	107.6	1.6	111.4	0.6	114.5	1.6	117.2	2.9
35	107.5	3.5	111.5	4.0	112.9	4.3	118.0	4.0
54	110.0	2.5	114.2	0.4	116.0	0.6	113.3	0.5
72	110.0	1.3	114.4	1.9	111.6	2.2	117.9	0.3

Time [weeks]	Freeze/Thaw "Dry Testing"							
	1 Hz [°C]	Std. Dev. [°C]	5 Hz [°C]	Std. Dev. [°C]	10 Hz [°C]	Std. Dev. [°C]	30 Hz [°C]	Std. Dev. [°C]
0	110.5	4.0	113.6	0.6	114.5	0.5	118.9	0.7
4	109.0	2.1	111.8	2.3	113.1	1.1	116.4	1.2
8	110.2	5.9	112.9	5.9	118.0	0.3	121.6	0.5
12	112.7	1.5	116.4	3.2	119.1	3.3	121.7	2.5
16	-	-	-	-	-	-	-	-
24	113.2	1.9	117.6	1.2	120.0	2.6	124.7	1.9
35	111.9	2.8	116.1	3.2	116.8	3.5	121.0	3.2
54	114.1	2.8	118.2	3.0	119.8	1.5	123.2	2.5
72	113.2	0.8	118.8	0.7	120.4	0.6	124.9	1.3

Table A.8.2b. T_g Based on Storage Modulus Determined as a Function of Wet/Dry Exposure

Time [weeks]	Wet/Dry "Wet Testing"							
	1 Hz [°C]	Std. Dev. [°C]	5 Hz [°C]	Std. Dev. [°C]	10 Hz [°C]	Std. Dev. [°C]	30 Hz [°C]	Std. Dev. [°C]
0	110.5	4.0	113.6	0.6	114.5	0.5	118.9	0.7
4	107.6	3.7	110.2	6.6	111.7	5.2	114.1	6.4
8	109.2	1.0	112.6	1.5	116.5	0.1	118.4	2.6
12	109.6	2.3	115.0	2.4	116.8	4.9	120.6	3.8
16	107.3	2.3	112.0	4.5	114.3	3.4	117.2	1.7
24	106.7	2.2	111.5	2.6	113.1	3.0	117.7	2.7
35	108.6	2.2	114.5	2.4	116.2	3.0	119.1	2.4
54	105.3	3.5	109.5	2.7	109.1	6.5	114.6	4.8
72	105.9	3.1	112.0	0.8	114.1	0.9	118.2	1.2

Time [weeks]	Wet/Dry "Dry Testing"							
	1 Hz [°C]	Std. Dev. [°C]	5 Hz [°C]	Std. Dev. [°C]	10 Hz [°C]	Std. Dev. [°C]	30 Hz [°C]	Std. Dev. [°C]
0	110.5	4.0	113.6	0.6	114.5	0.5	118.9	0.7
4	110.8	5.6	115.8	1.8	117.2	1.6	119.5	5.4
8	111.4	3.5	112.7	4.3	114.7	4.9	120.7	5.2
12	109.2	5.5	113.0	4.8	116.5	4.1	120.3	4.2
16	-	-	-	-	-	-	-	-
24	116.0	3.0	119.0	2.0	120.8	0.7	125.6	0.6
35	110.7	0.9	115.7	2.9	116.5	0.6	121.3	0.6
54	114.7	2.1	120.0	3.0	121.0	4.1	125.6	4.3
72	111.6	3.5	115.4	0.8	115.7	3.0	120.8	5.1

Table A.8.3a. T_g Based on Loss Modulus for Ambient Condition at 23°C and 30%RH

Time [weeks]	Ambient							
	1 Hz [°C]	Std. Dev. [°C]	5 Hz [°C]	Std. Dev. [°C]	10 Hz [°C]	Std. Dev. [°C]	30 Hz [°C]	Std. Dev. [°C]
0	104.1	3.5	111.6	2.3	113.1	0.6	117.7	1.2
4	109.5	1.3	114.5	1.9	116.8	1.3	120.4	1.7
8	106.9	1.5	113.3	1.0	116.0	0.9	119.9	1.3
12	109.7	2.7	115.2	2.1	116.2	3.2	119.9	2.3
16	109.8	3.0	115.9	2.7	117.6	1.9	121.9	1.2
24	110.0	0.8	116.8	0.6	117.8	0.8	122.4	0.8
32	-	-	-	-	-	-	-	-
48	107.8	5.3	114.7	4.3	117.1	4.4	121.7	3.4
72	111.7	4.1	118.2	3.5	120.1	2.8	123.4	5.1

Table A.8.3b. T_g Based on Loss Modulus Determined After Immersion in 23°C Seawater (“Wet Testing”) and as a Result of Subsequent Redrying (“Dry Testing”)

Time [weeks]	23°C Seawater “Wet Testing”							
	1 Hz [°C]	Std. Dev. [°C]	5 Hz [°C]	Std. Dev. [°C]	10 Hz [°C]	Std. Dev. [°C]	30 Hz [°C]	Std. Dev. [°C]
0	104.1	3.5	111.6	2.3	113.1	0.6	117.7	1.2
4	102.7	1.2	108.1	0.2	110.3	0.4	114.0	0.3
8	105.9	1.5	110.4	1.3	113.2	1.7	116.1	1.0
12	104.6	1.1	109.3	0.9	111.8	0.4	115.2	1.1
16	-	-	-	-	-	-	-	-
26	107.3	0.9	112.6	1.3	113.3	2.2	118.1	1.4
35	107.3	0.6	113.4	0.0	114.1	0.0	118.8	2.0
52	107.2	1.4	112.9	2.4	114.5	1.4	119.1	2.4
78	106.1	0.6	111.2	0.8	113.8	0.9	119.0	0.4

Time [weeks]	23°C Seawater “Dry Testing”							
	1 Hz [°C]	Std. Dev. [°C]	5 Hz [°C]	Std. Dev. [°C]	10 Hz [°C]	Std. Dev. [°C]	30 Hz [°C]	Std. Dev. [°C]
0	104.1	3.5	111.6	2.3	113.1	0.6	117.7	1.2
4	106.3	1.0	113.1	1.0	115.7	2.1	119.6	1.6
8	107.6	2.1	113.2	1.4	115.8	1.3	119.3	1.2
12	110.1	2.0	115.9	1.2	118.0	1.2	121.9	0.8
16	108.6	1.9	114.8	2.0	116.7	2.2	120.9	2.2
26	107.7	0.4	114.5	0.9	115.5	0.5	120.7	0.5
35	109.3	2.2	115.6	2.1	117.8	3.2	122.3	2.1
52	109.2	1.6	115.6	1.6	117.6	1.6	122.1	1.7
78	109.2	0.8	115.4	1.0	116.4	1.9	121.2	1.9

Table A.8.3c. T_g Based on Loss Modulus Determined After Immersion in 40°C Seawater (“Wet Testing”) and as a Result of Subsequent Redrying (“Dry Testing”)

Time [weeks]	40°C Seawater “Wet Testing”							
	1 Hz [°C]	Std. Dev. [°C]	5 Hz [°C]	Std. Dev. [°C]	10 Hz [°C]	Std. Dev. [°C]	30 Hz [°C]	Std. Dev. [°C]
0	104.1	3.5	111.6	2.3	113.1	0.6	117.7	1.2
4	105.2	0.7	110.1	1.0	112.2	1.1	115.9	1.6
8	99.5	0.1	104.4	0.4	106.8	0.1	110.4	0.2
12	105.0	0.4	109.0	0.8	111.5	0.3	115.0	0.3
16	103.3	2.9	109.4	0.3	111.7	0.6	115.3	0.5
26	109.1	5.3	110.3	0.8	110.9	3.6	115.6	3.6
35	105.6	1.4	109.9	1.7	112.6	0.9	116.7	0.4
52	107.7	1.6	112.8	1.6	115.4	1.8	119.0	1.8
78	109.8	0.6	115.2	0.9	117.2	0.7	121.2	0.9

Time [weeks]	40°C Seawater “Dry Testing”							
	1 Hz [°C]	Std. Dev. [°C]	5 Hz [°C]	Std. Dev. [°C]	10 Hz [°C]	Std. Dev. [°C]	30 Hz [°C]	Std. Dev. [°C]
0	104.1	3.5	111.6	2.3	113.1	0.6	117.7	1.2
4	104.8	1.1	110.1	0.6	112.5	0.5	116.4	0.8
8	102.8	1.8	108.3	2.5	110.0	1.3	114.5	0.9
12	109.3	1.5	113.0	0.7	115.5	0.1	120.1	1.0
16	107.9	1.4	114.0	0.8	116.2	1.1	120.1	1.2
26	110.8	1.3	116.0	1.7	117.3	1.7	121.1	2.6
35	109.0	2.9	114.1	3.0	116.9	3.3	120.2	2.9
52	112.3	1.1	117.6	1.6	118.6	2.7	121.3	4.8
78	112.0	1.6	117.6	2.3	119.1	1.5	123.0	1.4

Table A.8.3d. T_g Based on Loss Modulus Determined After Immersion in 60°C Seawater (“Wet Testing”) and as a Result of Subsequent Redrying (“Dry Testing”)

Time [weeks]	60°C Seawater “Wet Testing”							
	1 Hz [°C]	Std. Dev. [°C]	5 Hz [°C]	Std. Dev. [°C]	10 Hz [°C]	Std. Dev. [°C]	30 Hz [°C]	Std. Dev. [°C]
0	104.1	3.5	111.6	2.3	113.1	0.6	117.7	1.2
4	104.5	0.4	108.0	0.7	109.4	0.4	112.4	0.7
8	106.7	0.7	110.4	0.4	112.4	0.4	115.8	0.7
12	109.4	0.6	112.9	0.3	115.0	0.4	117.4	0.9
16	109.5	1.0	113.7	1.2	116.2	1.0	119.4	1.0
26	110.0	1.4	115.4	0.4	117.7	0.7	120.3	1.3
35	112.2	1.1	116.3	1.8	118.3	1.0	122.4	1.1
52	113.3	0.5	117.0	0.3	118.9	1.2	122.6	1.0
78	114.7	2.3	118.9	1.8	121.5	2.0	124.3	1.8

Time [weeks]	60°C Seawater “Dry Testing”							
	1 Hz [°C]	Std. Dev. [°C]	5 Hz [°C]	Std. Dev. [°C]	10 Hz [°C]	Std. Dev. [°C]	30 Hz [°C]	Std. Dev. [°C]
0	104.1	3.5	111.6	2.3	113.1	0.6	117.7	1.2
4	108.8	0.8	112.9	0.9	113.9	0.8	117.2	2.2
8	113.0	1.5	117.0	0.8	118.9	1.2	122.6	0.6
12	114.7	1.0	118.4	0.7	120.5	0.8	124.0	0.8
16	116.3	1.2	120.6	1.2	122.1	1.2	126.4	2.0
26	114.3	2.0	119.2	1.3	120.2	2.2	123.9	2.4
35	120.0	2.1	123.8	2.0	125.9	2.4	130.5	2.0
52	120.1	0.9	124.7	1.2	126.2	0.7	130.4	1.4
78	119.7	0.7	124.3	0.7	126.3	1.4	129.2	1.2

Table A.8.4a. T_g Based on Loss Modulus Determined as a Function of Cyclic Exposure

Time [weeks]	Freeze/Thaw "Wet Testing"							
	1 Hz [°C]	Std. Dev. [°C]	5 Hz [°C]	Std. Dev. [°C]	10 Hz [°C]	Std. Dev. [°C]	30 Hz [°C]	Std. Dev. [°C]
0	104.1	3.5	111.6	2.3	113.1	0.6	117.7	1.2
4	107.2	1.6	112.7	1.3	114.8	1.1	118.9	1.0
8	106.5	0.6	112.8	0.4	114.3	0.9	118.6	1.1
12	101.2	1.4	105.8	1.6	106.8	3.9	110.7	3.0
16	104.1	1.6	110.5	1.8	112.0	1.1	116.2	1.8
24	105.2	1.0	111.4	0.6	113.1	0.7	117.6	0.4
35	106.0	3.4	112.3	3.5	114.0	2.5	119.3	3.0
54	108.8	-	112.6	-	114.9	-	119.8	-
72	107.0	1.8	112.4	2.2	112.8	1.0	117.1	1.6

Time [weeks]	Freeze/Thaw "Dry Testing"							
	1 Hz [°C]	Std. Dev. [°C]	5 Hz [°C]	Std. Dev. [°C]	10 Hz [°C]	Std. Dev. [°C]	30 Hz [°C]	Std. Dev. [°C]
0	104.1	3.5	111.6	2.3	113.1	0.6	117.7	1.2
4	102.7	2.3	108.6	1.9	110.0	1.8	114.0	1.8
8	105.1	5.6	111.3	4.1	115.3	2.7	119.4	2.6
12	108.7	2.1	115.3	2.0	117.5	1.8	121.4	3.0
16	-	-	-	-	-	-	-	-
24	110.8	3.3	116.7	2.8	119.2	2.9	123.5	2.4
35	107.7	3.6	113.8	4.2	115.9	4.5	119.7	4.3
54	110.8	3.6	116.4	4.2	116.9	4.2	121.4	3.7
72	111.4	1.6	118.3	1.2	119.9	1.4	124.9	1.3

Table A.8.4b. T_g Based on Loss Modulus Determined as a Function of Cyclic Exposure

Time [weeks]	Wet/Dry "Wet Testing"							
	1 Hz [°C]	Std. Dev. [°C]	5 Hz [°C]	Std. Dev. [°C]	10 Hz [°C]	Std. Dev. [°C]	30 Hz [°C]	Std. Dev. [°C]
0	104.1	3.5	111.6	2.3	113.1	0.6	117.7	1.2
4	101.6	4.0	106.6	4.5	108.0	4.9	111.4	5.8
8	100.3	5.1	107.1	7.4	109.1	7.2	113.1	6.6
12	108.6	2.7	114.2	3.0	116.0	2.6	121.0	2.5
16	105.8	2.7	111.8	3.0	113.6	2.8	117.6	3.1
24	105.2	2.4	111.5	2.6	111.8	4.3	116.2	4.1
35	104.8	3.1	111.4	3.3	113.3	2.5	117.9	3.4
54	106.3	-	112.7	-	115.5	-	119.5	-
72	105.4	1.4	111.0	1.4	112.5	0.7	118.8	0.9

Time [weeks]	Wet/Dry "Dry Testing"							
	1 Hz [°C]	Std. Dev. [°C]	5 Hz [°C]	Std. Dev. [°C]	10 Hz [°C]	Std. Dev. [°C]	30 Hz [°C]	Std. Dev. [°C]
0	104.1	3.5	111.6	2.3	113.1	0.6	117.7	1.2
4	105.9	6.8	110.9	7.1	114.1	5.6	118.6	5.0
8	106.4	3.3	113.4	4.0	115.5	3.7	120.1	3.6
12	107.4	6.7	113.6	5.7	115.3	5.8	119.7	5.0
16	-	-	-	-	-	-	-	-
24	107.0	9.5	113.6	8.2	115.9	7.0	120.3	7.6
35	102.0	8.9	107.5	9.4	109.5	9.1	114.0	8.0
54	111.9	1.8	117.0	1.5	119.5	2.7	123.8	2.6
72	108.3	4.3	114.6	4.9	115.7	4.8	119.2	4.8

Table A.8.5a. Activation Energy Based on Loss Modulus for Seawater Immersion

Time [weeks]	Ambient	
	ΔE_a [kJ/mol]	Std. Dev. [kJ/mol]
0	280.5	47.8
4	333.1	37.6
8	278.9	28.2
12	398.1	21.4
16	320.6	19.5
24	349.2	17.6
32	-	-
48	310.3	45.9
72	346.3	22.5

Table A.8.5b. Activation Energy Based on Loss Modulus for Seawater Immersion

Time [weeks]	23°C			
	“Wet Testing”		“Dry Testing”	
	ΔE_a [kJ/mol]	Std. Dev. [kJ/mol]	ΔE_a [kJ/mol]	Std. Dev. [kJ/mol]
0	280.5	47.8	280.5	47.8
4	330.5	27.4	286.9	14.5
8	364.1	13.5	330.3	34.8
12	354.7	22.6	335.1	32.1
16	-	-	315.3	8.6
26	390.7	34.6	327.4	8.4
35	376.1	79.6	329.0	1.5
52	340.4	32.0	330.5	3.2
78	322.9	5.8	333.4	4.4

Table A.8.5c. Activation Energy Based on Loss Modulus for Seawater Immersion

Time [weeks]	40°C			
	“Wet Testing”		“Dry Testing”	
	ΔE_a [kJ/mol]	Std. Dev. [kJ/mol]	ΔE_a [kJ/mol]	Std. Dev. [kJ/mol]
0	280.5	47.8	280.5	47.8
4	343.4	8.5	326.2	14.4
8	336.5	1.5	323.1	24.2
12	374.9	19.0	346.3	16.4
16	321.8	70.5	315.9	16.4
26	363.3	14.2	388.9	4.3
35	346.6	14.0	375.8	29.9
52	359.8	7.9	383.3	58.4
78	370.8	2.6	391.3	9.8

Table A.8.5d. Activation Energy Based on Loss Modulus for Seawater Immersion

Time [weeks]	60°C			
	“Wet Testing”		“Dry Testing”	
	ΔE_a [kJ/mol]	Std. Dev. [kJ/mol]	ΔE_a [kJ/mol]	Std. Dev. [kJ/mol]
0	280.5	47.8	280.5	47.8
4	474.8	13.5	469.7	80.8
8	420.0	41.4	414.2	31.6
12	478.9	69.7	424.8	10.5
16	390.0	41.2	448.3	80.7
26	398.4	38.8	454.4	11.3
35	400.7	27.3	420.5	20.4
52	448.7	22.3	437.8	23.9
78	441.6	23.8	430.0	-

Table A.8.5e. Activation Energy Based on Loss Modulus for Seawater Immersion

Time [weeks]	-10°C			
	“Wet Testing”		“Dry Testing”	
	ΔE_a [kJ/mol]	Std. Dev. [kJ/mol]	ΔE_a [kJ/mol]	Std. Dev. [kJ/mol]
0	280.5	47.8	280.5	47.8
4	367.0	50.8	371.6	53.1
8	380.3	35.1	356.9	11.5
12	367.6	46.0	348.7	36.7
16	346.4	22.9	317.3	18.3
24	336.5	18.7	303.5	38.9
35	367.6	29.0	336.5	12.7
48	377.5	17.0	338.4	2.5
72				

Table A.8.6a. Activation Energy Based on Loss Modulus After Exposure to Freeze/Thaw Cycling

Time [weeks]	Freeze/Thaw			
	“Wet Testing”		“Dry Testing”	
	ΔE_a [kJ/mol]	Std. Dev. [kJ/mol]	ΔE_a [kJ/mol]	Std. Dev. [kJ/mol]
0	280.5	47.8	280.5	47.8
4	330.6	22.0	333.5	19.0
8	318.4	10.6	358.9	-
12	359.0	12.5	347.8	30.1
16	343.1	1.9	-	-
24	336.5	18.7	354.3	17.6
35	317.4	11.1	351.3	22.2
54	354.4	33.0	382.2	4.9
72	327.6	-	320.2	10.4

Table A.8.6b. Activation Energy Modulus After Exposure to Wet/Dry Cycling Based on Loss

Time [weeks]	Wet/Dry			
	“Wet Testing”		“Dry Testing”	
	ΔE_a [kJ/mol]	Std. Dev. [kJ/mol]	ΔE_a [kJ/mol]	Std. Dev. [kJ/mol]
0	280.5	47.8	280.5	47.8
4	340.9	13.7	303.8	52.8
8	317.1	53.2	312.1	41.3
12	323.7	25.0	349.4	58.1
16	355.2	9.4	-	-
24	351.2	5.8	321.6	64.5
35	320.0	4.1	314.1	25.8
54	340.4	31.5	363.5	35.8
72	318.1	33.3	382.8	12.5

REFERENCES

- [1] Leiblein, S. (1981), "Survey of Long-Term Durability of Fiberglass-Reinforced Plastic Structures," NASA Report CR-165320, Rocky River, OH, 52 pages.
- [2] Searle, T.J. and Summerscales, J. (1999), "Review of the Durability of Marine Laminates," in Reinforced Plastics Durability, G. Pritchard: editor, Woodhead Publishing Ltd., Cambridge, UK, pp. 219-265.
- [3] Graner, W.R. and Della Rocca, R.J. (1971), "Evaluation of U.S. Navy GRP Boats for Material Durability," in 26th Annual Technical Conference, Reinforced Plastics/Composites Division, Society of Plastics Industry, Inc., pp. 7-F/1-7-F/10.
- [4] Pucini, G. (1993), "Environmental Aspects," in Composite Materials in Maritime Structures, Vol. 1, R.A. Shenoi and J.F. Wellicome: editors, Cambridge University Press, pp. 44.
- [5] Gibbs and Cox, Inc. (1960), Marine Design Manual for Fiberglass Reinforced Plastics, McGraw Hill, New York.
- [6] Cable, C.W. (1991), "The Effect of Defects in Glass-Reinforced Plastic," Marine Technology, Vol. 28 [2], pp. 91.
- [7] Potential for Composites Application in the Marine Industry, National Conference on the Use of Composite Materials in Load-Bearing Marine Structures, NAE, (1990), Arlington, VA.
- [8] Karbhari, V.M., Chin, J.W., and Reynaud, D. (2000), "Critical Gaps in Durability Data for FRP Composites in Civil Infrastructure," in Proceedings of the 45th International SAMPE Symposium, Long Beach, CA, pp. 549-563.
- [9] Harper, J.F. and Naeem, M. (1989), "The Moisture Absorption of Glass Fibre Reinforced Vinylester and Polyester Composites," Materials and Design, Vol. 10 [6], pp. 297-300.
- [10] Sagi-Mana, D., Narkis, M., Siegmann, A., Joseph, R. and Dodiuk, H. (1998), "The Effect of Marine Environment on a Vinyl Ester Resin and Its Highly Filled Particulate Quartz Composite," Journal of Applied Polymer Science, Vol. 69, pp. 2229-2234.
- [11] Apicella, A., Migliaresi, C., Nicolais, L., Iaccarino, L. and Roccotelli, S. (1983), "The Water Aging of Unsaturated Polyester-Based Composites: Influence of Resin Composite Structure," Composites, Vol. 14 [4], pp. 387-392.
- [12] Apicella, A., Migliaresi, C., Nicodemo, L., Nicolais, L., Iaccarino, L., and Roccotelli, S. (1982), "Water Sorption and Mechanical Properties of a Glass-Reinforced Polyester Resin," Composites, Vol. 13, pp. 406-410.
- [13] Marshall, J.M., Marshall, G.P., and Pinzelli, R.F. (1982), "The Diffusion of Liquids Into Resins and Composites," Polymer Composites, Vol. 13 [3], pp. 131-137.

- [14] Karbhari, V.M. and Zhang, S. (2000), "E-Glass/Vinylester Composites in Aqueous Environments-I: Experimental Results," *Applied Composite Materials*, in review.
- [15] Tai, R.C.L. and Szklarska-Smialowska, Z. (1993), "Effect of fillers on the degradation of automotive epoxy adhesives in aqueous solutions. Part I. Absorption of water by different fillers-incorporated automotive epoxy adhesives," *Journal of Materials Science*, Vol. 28 [22], pp. 6199-6204.
- [16] Tai, R.C.L. and Szklarska-Smialowska, Z. (1993), "Effect of fillers on the degradation of automotive epoxy adhesives in aqueous solutions. Part II. The microhardness change and delamination of automotive epoxy adhesives in distilled water and sodium chloride solutions," *Journal of Materials Science*, Vol. 28 [22], pp. 6205-6210.
- [17] Nakanishi, Y. and Shindo, A. (1982), "Deterioration of CFRP and GFRP in Salt Water," *Proceedings of the 4th International Conference on Composite Materials*, Vol. 2, Eds: T. Hayashi, K. Kawata and S. Umekawa, Tokyo, pp. 1009-1016.
- [18] Wu, L., Murphy, K., Karbhari, Vistasp, and Zhang, James M. (2002), "Short-term effects of sea water on E-glass/vinylester composites," *Journal of Applied Polymer Science*, Vol. 84 [14], pp. 2760-2767.
- [19] Chin, J. W., Nguyen, T., and Aouadi, Khaled. (1999), "Sorption and Diffusion of Water, Salt Water, and Concrete Pore Solution in Composite Matrices," *Journal of Applied Polymer Science*, Vol. 71, pp. 483-492.
- [20] Spaulding, K. B. (1966), "Fiberglass boats in naval service," *Naval Engineers Journal*, Vol. 78, pp. 333-340.
- [21] Hirose, K., Yamamoto, T., Kuroda, S., and Fujii, T. (1996), "A floating pier system for marinas using glass fibre mat-reinforced stampable sheets," *Journal of Advanced Materials*, Vol. 28 [1], pp. 32-41.
- [22] Mableson, A. R., R. J. Osborn, and Nixon, J.A. (1987), "Structural use of polymeric composites in ships and offshore," in *Proceedings 2nd International Conference Polymers in a Marine Environment*, London, Institute of Marine Engineers, Vol. 9, London, pp. 79-86.
- [23] Cobb, B. (1963), "A Report on the Long-term Durability of Resin Glass Boats," *Ship and Boat Builder*, pp. 41-42.
- [24] Fried, N. and Graner, W. R. (1966), "Durability of Reinforced-Plastic Structural Materials in Marine Service," *Marine Technology*, Vol. 3 [3], pp. 321-327.
- [25] Jones, F. R. (1994), *Handbook of Polymer-Fiber Composites*, Burnt Mill, Harlow, Essex, Longman Scientific & Technical.
- [26] Kaw, A. K. (2000), *Mechanics of Composite Materials*, Boca, Raton, Florida, CRC Press.

- [27] Wagner, P. A., Little, B. J., Hart, K.R., and Ray, Richard L. (1996), "Biodegradation of Composite Materials," *International Biodeterioration & Biodegradation*, pp. 125-132.
- [28] Garrison, Tom S. (2002), *Oceanography – An Invitation to Marine Science*, Pacific Grove, CA, Wadsworth -Brooks/Cole.
- [29] Grant, T. S. and Bradley, W. L. (1990), "Salt Water Degradation of Polymeric Composites, in *Proceedings of the International Offshore Mechanics and Arctic Engineering Symposium*," Vol. 3 [A], pp. 71-76.
- [30] Tucker, W. C. (1987), Master's Thesis, "Effects of Seawater on Graphite/Polymer Composites," Kingston, RI, University of Rhode Island.
- [31] Fried, N. (1967), "Degradation of Composite Materials: The Effect of Water on Glass-Reinforced Plastics," in *Proceedings of the Fifth Symposium on Naval Structural Mechanics*, Philadelphia, pp. 813-837.
- [32] Grant, T. S. (1991), Masters Thesis, "Seawater degradation of polymeric composites," Department of Mechanical Engineering, Texas A&M University, 88 pages.
- [33] Subramaniam, N., Blum, F. D., Dharani, L.R. (1993), "Effects of Moisture and Other Contaminants in Friction Composites," *Polymer Engineering and Science*, Vol. 33 [18], pp. 1204-1211.
- [34] Wood, C. A. (1996), Master's Thesis, "Determining the Effect of Seawater on the Interfacial Strength of an E-glass-Graphite/Epoxy Composite Using Observations for Transverse Cracking Made In-Situ and Environmental SEM," Mechanical Engineering Department, Texas A&M University, 103 pages.
- [35] Pomies, F. (1992), Master's Thesis, "Degradation of Composite Materials in a Marine Environment," Boca Raton, Florida Atlantic University.
- [36] Liao, K., Schultheisz, C. R., Hunston, D.L. (1999), "Effects of environmental aging on the properties of pultruded GFRP," *Composites: Part B*, Vol. 30, pp. 485-493.
- [37] Davies, P., Pomies, F., Carlsson, L.A. (1996), "Influence of Water and Accelerated Aging on the Shear Fracture Properties of Glass/Epoxy Composite," *Applied Composite Materials*, Vol. 3, pp. 71-87.
- [38] Soulier, J. P., Berruet, R., Chateauinois, A., Chabert, B, Gauthier, R. (1988), "Interactions of fibre-reinforced epoxy composites with different salt water solutions including isotonic liquid," *Polymer Communications*, Vol. 29, pp. 243-246.
- [39] Letton, A. and Bradley, W. L. (1991), "Studies in Long Term Durability of Composites in Seawater," in *Proceedings For Use of Composite Materials in Load-Bearing Marine Structures*, Washington DC, National Research Council, pp. 163-177.
- [40] Chin, J. W., Hughes, W. L., Signor, A. (2001), "Elevated Temperature Aging of Glass Reinforced Vinyl Ester and Isophthalic Polyester Composites in Water, Salt Water and

- Concrete Pore Solution,” in Proceedings of the American Society for Composites, Technical Conference, Vol. 16, pp. 572-583.
- [41] Tucker, W. C. and R. Brown (1989), "Moisture Absorption of Graphite/Polymer Composites Under 2000 Feet of Seawater," *Journal of Composite Materials*, Vol. 23, pp. 787-797.
- [42] Davis, R. J., T. Ghotra, Malhi, T.R., and Pritchard, G. (1983), “Blister Formation in Reinforced Plastics: The Origin of the Osmosis Process,” in 38th Annual Conference Reinforced Plastics/Composites Institute, Volume 17 [B].
- [43] Chiou, P.-L. and Bradley, W. L. (1997), "Seawater Effects on Strength and Durability of Glass/Epoxy Filament-Wound Tubes as Revealed by Acoustic Emission Analysis," *The American Society for Testing and Materials*, pp. 214-221.
- [44] Bradley, W., P. B. Chiou, and Grant, T. (1995), “The effect of sea water on polymeric composite materials,” in Proceedings of the first international workshop, NIST Special Publication 887.
- [45] Kajorncheappunngam, S., R. K. Gupta, Rakesh, K., and GangaRao, Hota V.S. (2002), "Effect of Aging Environment on Degradation of Glass-Reinforced Epoxy," *Journal of Composites for Construction*, Vol. 6 [1], pp. 61-69.
- [46] Karbhari, V. M., J. Rivera, and Zhang, J. (2002), "Low-Temperature Hygrothermal Degradation of Ambient Cured E-Glass/Vinylester Composites," *Journal of Applied Polymer Science*, Vol. 86, pp. 2255-2260.
- [47] Zhang, S., J. Rivera, and Karbhari, V.M. (2000), “Investigation of the Effects of Freeze-Thaw Exposure on Composites for Seismic Retrofit,” in Proceedings of the 45th International SAMPE Symposium, pp. 579-593
- [48] Hodgkiess, T., M. J. Cowling, and Mulheron, M. (1994), “Durability of glass reinforced polymer composites in marine environments,” in *Structural Materials in Marine Environments*, IoM/MTD/MechE/ImarE, pp. 58-72
- [49] Loos, A. C., G. S. Springer, Sanders, Barbara A., and Tung, Randy W. (1980), "Moisture Absorption of Polyester-E Glass Composites," *Journal of Composite Materials*, Vol. 14, pp. 142-154.
- [50] Larner, L., K. Speakman, and A. Majumdar (1976), "Chemical Interactions Between Glass Fibres and Cement," *Journal of Non-Crystalline Solids*, Vol. 20, pp. 43-74.
- [51] Carlsson, L. A. and F. Pomies (1995), “Influence of Seawater on Transverse Tensile Properties of PMC,” in NIST Special Publication 887, National Institute of Standards and Technology.
- [52] Sonawala, S. P. and R. J. Spontak (1996), "Degradation kinetics of glass-reinforced polyesters in chemical environments," *Journal of Materials Science*, Vol. 31[18], pp. 4757-4765.

- [53] Pomies, F., L. A. Carlsson, and Gillespie, John W. (1995), "Marine Environmental Effects on Polymer Matrix Composites," in ASTM Special Technical Publication, Composite Materials: Fatigue and Fracture, Vol. 5[1230], pp. 283-303.
- [54] Castaing, P. and L. Lemoine (1995), "Effects of Water Absorption and Osmotic Degradation on Long-Term Behavior of Glass Fiber Reinforced Polyester," Polymer Composites, Vol. 16 [5], pp. 349-356.
- [55] Zhang, S., V. M. Karbhari, Lin-Ye, Mai, and Yiu-Wing (2000), "Evaluation of Property Retention in E-Glass/Vinylester Composites after Exposure to Salt Solution and Natural Weathering," Journal of Reinforced Plastics and Composites, Vol. 19 [9], pp. 704-731.
- [56] Strait, L. H., M. L. Karasek, and Amateau, Maurice F. (1992), "Effects of Seawater Immersion on the Impact Resistance of Glass-Fiber Reinforced Epoxy Composites," Journal of Composite Materials, Vol. 26 [14], pp. 2118-2133.
- [57] Davies, P., F. Mazeas, and Casari, P. (2001), "Sea Water Aging of Glass Reinforced Composites: Shear Behaviour and Damage Modelling," Journal of Composite Materials, Vol. 35 [15], pp. 1343-1372.
- [58] Liao, K., R. I. Altkorn, Milkovich, Scott M., Gomez, Jose, Schultheisz, Carl R., Brinson, L. Catherine, Fildes, John M., and Brailsford, Bruce (1996), "Long-Term Durability of Composites in Secondary Infrastructure Applications," in Proceedings of the 28th International SAMPE Technical Conference, pp. 1278-1279.
- [59] Springer, G. S., B. A. Sanders, Tung, Randy W. (1980), "Environmental Effects on Glass Fiber Reinforced Polyester and Vinylester Composites," Journal of Composite Materials, Vol. 14, pp. 213-232.
- [60] Davies, P., F. Pomies, and Carlsson, L.A. (1996), "Influence of Water Absorption on Transverse Tensile Properties and Shear Fracture Toughness of Glass/Polypropylene," Journal of Composite Materials, Vol. 30 [9], pp. 1004-1019.
- [61] Pollard, A., R. Baggott, Wostenholm, G.H., and Yates, B. (1989), "Influence of hydrostatic pressure on the moisture absorption of glass fibre-reinforced polyester," Journal of Materials Science, Vol. 24, pp. 1665-1669.
- [62] Grant, T. S. and W. L. Bradley (1990), "Salt Water Degradation of Polymeric Composites," in Proceedings of the International Offshore Mechanics and Arctic Engineering Symposium, Vol. 3 [A], pp. 71-76.
- [63] Grant, T. S. and W. L. Bradley (1995), "In-situ Observations in SEM of Degradation of Graphite/Epoxy Composite Materials Due to Seawater Immersion," Journal of Composite Materials, Vol. 29 [7], pp. 852-867.
- [64] Tucker, W. C. (1990), "Degradation of Graphite/Polymer Composites in Seawater," American Society of Mechanical Engineers, Petroleum Division (Publication) PD, Vol. 32, pp. 95-99.

- [65] Kosuri, R. and Y. Weitsman (1995), "Sorption Process and Immersed-Fatigue Response of GR/EP Composites in Sea Water," in Proceedings ICCM-X, Whistler, BC, Canada, Cambridge, England, Woodhead, Vol. VI, pp. 177-184.
- [66] Loos, A. C. and Springer, G. S. (1979), "Moisture Absorption of Graphite-Epoxy Composites Immersed in Liquids and in Humid Air," *Journal of Composite Materials*, Vol. 13, pp. 131-147.
- [67] Macander, A. and M. Silvergleit (1977), "The Effect of the Marine Environment on Stressed and Unstressed Graphite/Epoxy Composites," *Naval Engineers Journal*, pp. 65-72.
- [68] Adams, R. D. and M. M. Singh (1995), "The effect of immersion in sea water on the dynamic properties of fibre-reinforced flexibilised epoxy composites," *Composite Structures*, Vol. 31, pp. 119-127.
- [69] Kootsookos, A. and Mouritz, A. P. (2004), "Seawater durability of glass- and carbon-polymer composites," *Composites Science and Technology*, Vol. 64 [10-11], pp. 1503-1511.
- [70] Rege, S. K. and Lakkad, S. C. (1983), "Effect of Salt Water on the Mechanical Properties of Fibre Reinforced Plastics," *Fibre Science and Technology*, Vol. 19, pp. 325-327.
- [71] Steckel, G. L., Hawkins, G. F., and Jerome L. Bauer, Jr (1999), "Durability Issues for Composites in Infrastructure," in Proceedings of the 44th International SAMPE Symposium, pp. 2194-2208.
- [72] Wood, C. A. and Bradley, W. L. (1997), "Determination of the effect of seawater on the interfacial strength of an interlayer e-glass/graphite/epoxy composite by in situ observation of transverse cracking in an environmental SEM," *Composites Science and Technology*, Vol. 57, pp. 1033-1043.
- [73] Weitsman, Y. J. (1995), "Effects of Fluids on Polymeric Composites-A Review," Knoxville, Department of Mechanical and Aerospace Engineering and Engineering Science, University of Tennessee, Report MAES 95-1.0 CM.
- [74] Faza, S. S., H. V. S. GangaRao, Hota V.S., Ajarapu, Seshagiri (1993), "Strength and Stiffness Degradation of Fiber Reinforced Polymers Under Accelerated Environmental Conditioning," in Proceedings of the 38th International SAMPE Symposium, pp. 1967-1977.
- [75] Grami, M. E., M. J. Moilanen, and Rosenow, Malcolm W.K, (1995), "Environmental Degradation of Glass Fibers in Polyurethane Matrix Composites," in Proceedings of ICCM-10, Whistler, B.C., Canada, pp. 207-214.
- [76] Al-Bastaki, N. M. S. and H. M. N. Al-Madani (1995), "Effect of Local Atmospheric Conditions in Bahrain on the Mechanical Properties of GRP," *Polymer Testing*, Vol. 14, pp. 263-272.

- [77] Baley, C., P. Davies, Grohens, Yves, and Dolto, Gregoire (2004), "Application of Interlaminar Tests to Marine Composites. A Literature Review," *Applied Composite Materials*, Vol. 11, pp. 99-126.
- [78] Gellert, E. P. and D. M. Turley (1999), "Seawater immersion ageing of glass-fibre reinforced polymer laminates for marine applications," *Composites: Part A*, Vol. 30, pp. 1259-1265.
- [79] Dukes, R. and D. L. Griffiths (1971), "Marine aspects of carbon fibre and glass-fibre/carbon-fibre composites," in *International Conference on carbon Fibers, their Composites and Applications*, London, Paper No. 28, pp. 1-6.
- [80] Gutierrez, J., F. L. Lay, and Hoarau, P. (1992), "A Study of the Aging of Glass Fibre-Resin Composites in a Marine Environment," in *Proceedings of the 3rd International Conference on Nautical Construction with Composite Materials*, Paris, IFREMER editions, Brest.
- [81] Bank, L. C., Gentry, T. R., Russell, T., and Barkatt, A. (1995), "Accelerated Test Methods to Determine the Long-Term Behavior of FRP Composite Structures: Environmental Effects," *Journal of Reinforced Plastics and Composites*, Vol. 14, pp. 559-587.
- [82] Liao, K., Schultheisz, C. R., Hunston, D., and Brinson, C.L. (1998), "Long-term Durability of Fiber-Reinforced Polymer-Matrix Composite Materials for Infrastructure Applications," *Journal of Advanced Materials*, Vol. 30 [4], pp. 3-40.
- [83] McBangonluri, F., Garcia, K., and Lesko, JJ. (2000), "Characterization of fatigue and combined environment durability performance of glass/vinyl ester composite for infrastructure application," *International Journal of Fatigue*, Vol. 22, pp. 53-64.
- [84] Meyer, M. R., Latour, R.A., and Shutte, H.D. (1994), "Long-term durability of fiber/matrix interfacial bonding in hydrothermal environments," *Journal of Thermoplastic Composite Materials*, Vol. 7 [July], pp. 180-91.
- [85] Katawaki, K. and I. Sasaki (1992), "Real Site Evaluation of Durability of Composite Materials Under Marine Environment," in *Proceedings of the 24th International SAMPE Technical Conference*, Vol. 24, pp. T143-T153.
- [86] Takanyagi, H., Kemmochi, K., and Kimpara, I. (2000), "Effect of marine exposure on weatherability of FRP laminates," in *Recent Developments in Durability Analysis of Composite Systems*, pp. 245-252.
- [87] Mazor, A. and L. J. Broutman (1978), "Effect of Long-Term Water Exposure on Properties of Carbon and Graphite Fiber Reinforced Epoxies," *Polymer Engineering and Science*, Vol. 18 [5], pp. 341-349.
- [88] Astrom, B. T. (1997). *Manufacturing of Polymer Composites*. London, Chapman & Hall, 469 pages.

- [89] Karbhari, V. M. (2004), "E-Glass/Vinylester Composites in Aqueous Environments: Effects on Short-Beam Shear Strength," *Journal of Composites for Construction*, Vol. 8 [2], pp. 148-156.
- [90] ASTM D5229, "Standard Test Method for Moisture Absorption Properties and Equilibrium Conditioning of Polymer Matrix Composite Materials," American Society for Testing and Materials, West Conshohocken, PA.
- [91] ASTM D3039, "Standard Test Method for Tensile Properties of Polymer Matrix Composite Materials," American Society for Testing and Materials, West Conshohocken, PA.
- [92] ASTM D790, "Standard Test Method for Flexural Properties of Unreinforced and Reinforced Plastics and Electrical Insulating Materials," American Society for Testing and Materials, West Conshohocken, PA.
- [93] ASTM D2344, "Standard Test Method for Short-Beam Strength of Polymer Matrix Composite Materials and Their Laminates," American Society for Testing and Materials, West Conshohocken, PA.
- [94] ASTM E1640, "Standard Test Method for Assignment of the Glass Transition Temperature By Dynamic Mechanical Analysis," American Society for Testing and Materials, West Conshohocken, PA.
- [95] Crank, J. (1975). *The Mathematics of Diffusion*, 2nd edition, Oxford, Clarendon Press.
- [96] Mouritz, A.P., Kootsookos, A. and Mathys, G. (2004), "Stability of Polyester-and Vinylester Based Composites in Seawater," *Journal of Materials Science*, Vol. 39, pp. 6073-6077.
- [97] Shen, C. H. and G. S. Springer (1976), "Moisture Absorption and Desorption of Composite Materials" *Journal of Composite Materials*, Vol. 10, pp. 2-20.
- [98] Carter, H. G. and Kibler, K.G. (1978), "Langmuir-Type Model for Anomalous Moisture Diffusion in Composite Resins," *Journal of Composite Materials*, Vol. 12, pp. 118-131.
- [99] Gonsalves, K. E., S. H. Patel, and Chen, X. (1989), "Development of Degradable Materials for Marine Applications," in *Proceedings of the 47th Annual Technical Conference-Society of Plastics Engineers*, pp. 1356-1361.
- [100] Hulatt, J., L. Hollaway, and Thorne, A. (2002), "Preliminary investigations on the environmental effects on new heavyweight fabrics for use in civil engineering," *Composites: Part B*, Vol. 33, pp. 407-417.
- [101] Phani, K. K. and Bose, N. R. (1987), "Temperature Dependence of Hygrothermal Ageing of CSM-Laminate During Water Immersion," *Composites Science and Technology*, Vol. 29, pp. 79-87.

- [102] Bonniau, P. and Bunsell, A.R. (1981), "Water absorption by glass fibre reinforced epoxy resin," *Composite Structures*, pp. 92-105.
- [103] Edwards, D. B. and Sridharan, N. S. (1982), *Polymer Composites*, Vol. 3[1], pp. 1.
- [104] Abanilla, A. (2004), Masters Thesis, Physico-mechanical characterization of T700 based carbon/epoxy systems for infrastructure rehabilitation. Department of Structural Engineering. La Jolla, University of California San Diego.
- [105] Matthewson, M. (1993), "Models for fiber reliability," in *Proceedings of SPIE*, pp. 128-137.
- [106] Jamond, R. M., T. A. Hoffard, Novinson, T., and Malvar, L.J. (2000), "Composites in Simulated Marine Environments," Port Hueneme, Naval Facilities Engineering Service Center, Special Publication SP-2083-SHR, pp. 1-25.
- [107] Karbhari, V., Personal Communication, February 26, 2004.
- [108] Menard, K. P. (1999). *A Practical Introduction to Dynamic Mechanical Analysis*. Boca Raton, Florida, CRC Press.
- [109] Karbhari, V. M. and Q. Wang (2004), "Multi-frequency dynamic mechanical thermal analysis of moisture uptake in E-glass/vinylester composites," *Composites: Part B*, Vol. 35, pp. 299-304.
- [110] Nogueira, P., C. Ramirez, Torres, A., Abad, M.J., Cano, J., Lopez, J., Lopez-Bueno, I., and Barral, L. (2000), "Effect of Water Sorption on the Structure and Mechanical Properties of an Epoxy Resin System," *Journal of Applied Polymer Science*, Vol. 80, pp. 71-80.
- [111] Soles, C. L. and A. F. Yee (1999), "A Discussion of the Molecular Mechanisms of Moisture Transport in Epoxy Resins," *Journal of Polymer Science: Part B: Polymer Physics*, Vol. 38, pp. 792-802.
- [112] De'Neve, B. and M. E. R. Shanahan (1993), "Water absorption by and epoxy resin and its effect on the mechanical properties and infra-red spectra," *Polymer*, Vol. 34 [24], pp. 5099-5105.
- [113] Reliasoft (2000), *Reliasoft's Life Data Analysis Reference*, Reliasoft Publishing, Tucson, Arizona.
- [114] ASTM E-632, "Standard Practice for Developing Accelerated Tests to Aid in the Prediction of the Service Life of Building Components and Materials," American Society for Testing and Materials, West Conshohocken, PA.
- [115] Kuraishi, A. (2001), Doctoral Dissertation, "Durability Analysis of Composite Structures Using the Accelerated Testing Methodology," Department of Aeronautics and Astronautics, Stanford, California, Stanford University, 143 pages.

- [116] Tissaoui, J. (1996), Doctoral Dissertation, "Effects of Long-Term Creep on the Integrity of Modern Wood Structures," Department of Civil Engineering, Blacksburg, Virginia, Polytechnic Institute and State University, 129 pages.
- [117] Chu, W. (2002), Master's Thesis, "Investigation of Short-Term Aqueous Exposure on Pultruded E-Glass/Vinylester Composites," Department of Structural Engineering, La Jolla, California, University of California, San Diego, 222 pages.
- [118] Fesko, D. G. (1971), Doctoral Dissertation, "Time-Temperature Superposition for Block Copolymers," Department of Materials Science, Pasadena, California, California Institute of Technology, 202 pages.
- [119] Liao, K., C. R. Schultheisz, Hunston, Donald L. (1999), "Long-term environmental fatigue of pultruded glass-fiber-reinforced composites under flexural loading," *International Journal of Fatigue*, Vol. 21, pp. 485-495.
- [120] Sutherland, H. and Veers, S., (2000), "The Development of Confidence Limits For Fatigue Strength Data," in *Wind Energy 2000*, pp. 1-11.
- [121] ASTM E739, "Standard Practice for Statistical Analysis of Linear or Linearized Stress-Life (S-N) and Strain-Life (ϵ -N) Fatigue Data," American Society for Testing and Materials, West Conshohocken, PA.

PART C

RELIABILITY BASED ASSESSMENT OF FRP DURABILITY FOR APPLICATION TO DESIGN

TABLE OF CONTENTS

List of Figures	x
List of Tables	xiii
Chapter	
1 Introduction	1
1.1 Introduction to Composite Materials	1
1.1.1 Common Applications of Composite Materials	1
1.2 Research Motivation	3
1.3 Overview of the Thesis	4
1.3.1 Introduction	4
1.3.2 Development of Analysis Methodologies	4
1.3.3 Testing	4
1.3.4 Analysis of Accelerated Degradation Test Data	5
1.3.5 Reliability Based Assessment of Long-Term Material Properties	5
1.3.6 Conclusions and Recommendations	5
2 Background	6
2.1 Rehabilitation with Fiber Reinforced Polymers	6
2.2 Accelerated Life Testing for FRPs	6
2.2.1 Eyring Relationship for Temperature Acceleration	9

2.2.2	Phani and Bose Method	9
2.2.3	Arrhenius Relationship	10
2.2.4	Reliability Based Assessment	11
2.2.4.1	The Gaussian Distribution	11
2.2.4.2	The Lognormal Distribution	12
2.2.4.3	The Exponential Distribution	12
2.2.4.4	The Gamma Distribution	13
2.2.4.5	The Weibull Distribution	13
2.2.5	Design Values	18
2.2.5.1	ACI 440	18
2.2.5.2	TR55	20
2.2.5.3	Canadian Bridge Highway Design Code	23
2.3	Gap Analysis	24
3	Material and Test Details	28
3.1	Materials	28
3.2	Sample fabrication	29
3.2.1	Composite Samples	29
3.2.1.1	Wet Layup Process	29
3.2.2	Resin Samples	29
3.2.3	Preconditioning	29
3.3	Exposure Conditions	30
3.4	Testing	30

3.5	Summary of test data	31
4	Data Analysis and Predictions	36
4.1	Overview	36
4.2	Determination of outliers	36
4.2.1	ASTM E178	37
4.2.1.1	Procedure	38
4.3	Normalization of Data	40
4.3.1	Normalization Procedure	40
4.3.2	Normalization results	40
4.3.3	Comparison of Neat Epoxy and Composite	49
4.4	Weibull distribution fit	52
4.4.1	Procedure for Weibull fit	52
4.4.2	Weibull fit results	52
4.4.3	ANOVA of Weibull Shape Parameters	61
4.4.4	Verification of Weibull fit	62
4.4.5	Comparison of Weibull Parameters with Published Values	63
4.5	Predictions of long-term material response	64
4.5.1	Accelerated Degradation Model Used for This Project	64
4.5.2	Procedure for predicting future response with an Arrhenius model	64
4.5.3	Arrhenius Predictive Results	71
4.6	Extended Arrhenius model	76
4.6.1	Comparison of Neat Resin and Composite	79

5	Reliability Based Assessment	83
5.1	Reliability	84
5.1.1	Methodology	84
5.2	Design values and Comparison	96
5.2.1	Comparison with Current Design Guidelines	96
5.3	Application to Design	100
6	Conclusions	102
6.1	Summary	102
6.2	Areas for additional research	103
	APPENDIX A: Test Data	105
	APPENDIX B: Weibull Parameters	107
	APPENDIX C: Minitab ANOVA Results	109
C.1	Glass Fiber Reinforced Polymer	115
C.1.1	Control Sample	115
C.1.1.1	Elastic Modulus Data	115
C.1.1.2	Ultimate Strength Data	115
	APPENDIX D: Arrhenius Details	117
	APPENDIX E: Additional Plots	118
	REFERENCES	119

LIST OF FIGURES

FIGURE	PAGE
2.1 Shape of Weibull Probability Density Function	15
2.2 Verification of Weibull Coefficient of Variation approximation	17
2.3 Verification of Weibull Mean approximation	17
4.1 Percent Modulus Retention for Epoxy	42
4.2 Percent Modulus Retention for Composite	44
4.3 Percent Ultimate Strength Retention for Epoxy	46
4.4 Percent Ultimate Strength Retention for Composite	48
4.5 Comparison of Modulus Retention for Neat Epoxy and Composite Im- mersed in Deionized Water	50
4.6 Comparison of Strength Retention for Neat Epoxy and Composite Im- mersed in Deionized Water	51
4.7 Weibull Shape Parameters for Modulus of Glass Fiber Reinforced Epoxy Samples	54
4.8 Weibull Shape Parameters for Ultimate Strength of Glass Fiber Rein- forced Epoxy Samples	56
4.9 Weibull Shape Parameters for Modulus of Neat Epoxy Samples	58
4.10 Weibull Shape Parameters for Ultimate Strength of Neat Epoxy Samples	60
4.11 Percent Retention of Modulus in Composite	65
4.12 Arrhenius step 1: Linear Regression of data for Composite Modulus .	67
4.13 Arrhenius step 2: Percent Retention versus inverse temperature for Composite Modulus	68

4.14	Arrhenius step 3: Arrhenius prediction for Composite Modulus	69
4.15	Revised Arrhenius Prediction for Composite Modulus, short term . .	70
4.16	Revised Arrhenius Prediction for GFRP Modulus After Immersion in Deionized Water at 22.8°C	72
4.17	Arrhenius Prediction for Ultimate Strength of GFRP After Immersion in Deionized Water at 22.8°C	73
4.18	Arrhenius Prediction for Modulus of Epoxy After Immersion in Deion- ized Water at 22.8°C	74
4.19	Arrhenius Prediction for Ultimate Strength of Epoxy After Immersion in Deionized Water at 22.8°C	75
4.20	Asymptotic Section for Modulus of GFRP	77
4.21	Asymptotic Section for Ultimate Strength of GFRP	78
4.22	Asymptotic Section for Modulus of Epoxy	79
4.23	Asymptotic Section for Ultimate Strength of Epoxy	80
4.24	Comparison of Predictive Models for Neat Resin Modulus and Com- posite Modulus	81
4.25	Comparison of Predictive Models for Neat Resin Ultimate Strength and Composite Ultimate Strength	82
5.1	Reliability Prediction	86
5.2	Reliability Prediction for Modulus of Neat Epoxy Immersed in Deion- ized Water at 22.8°C	88
5.3	Reliability Prediction for Ultimate Strength of Neat Epoxy Immersed in Deionized Water at 22.8°C	89
5.4	Reliability Prediction for Modulus of Glass Fiber Reinforced Epoxy Immersed in Deionized Water at 22.8°C	90
5.5	Reliability Prediction for Ultimate Strength of Glass Fiber Reinforce Epoxy Immersed in Deionized Water at 22.8°C	91

5.6	Reliability Prediction for Modulus of Neat Epoxy	92
5.7	Reliability Prediction for Ultimate Strength of Neat Epoxy	93
5.8	Reliability Prediction for Modulus of Glass Fiber Reinforced Epoxy .	94
5.9	Reliability Prediction for Ultimate Strength of Glass Fiber Reinforce Epoxy	95
5.10	Predictive Modulus Model with Current Design Guidelines	98
5.11	Predictive Ultimate Strength Model with Current Design Guidelines .	99

LIST OF TABLES

TABLE		PAGE
2.1	ACI 440 Environmental Reduction Factors	20
2.2	TR55 Partial Safety Factors for Modulus and Strain	22
2.3	TR55 Partial Safety Factors for Manufacturing Method and Application	22
2.4	CHBDC Partial Safety Factors for Manufacturing Method and Appli- cation	24
3.1	Summary Test Data: Modulus of Epoxy in <i>GPa</i>	32
3.2	Summary Test Data: Ultimate Strength of Epoxy	33
3.3	Summary Test Data: Elastic Modulus of Composite	34
3.4	Summary Test Data: Ultimate Strength of Composite	35
4.1	Possible Outliers	39
4.2	Average Percent Retention Results for Epoxy Modulus Data	41
4.3	Average Percent Retention Results for Composite Modulus Data	43
4.4	Average Percent Retention Results for Epoxy Ultimate Strength Data	45
4.5	Average Percent Retention Results for Composite Ultimate Strength Data	47
4.6	Weibull Parameters for Modulus of Glass Fiber Reinforced Epoxy Sam- ples	53
4.7	Weibull Parameters for Ultimate Strength of Glass Fiber Reinforced Epoxy Samples	55
4.8	Weibull Parameters for Modulus of Neat Epoxy Samples	57

4.9	Weibull Parameters for Ultimate Strength of Neat Epoxy Samples . . .	59
4.10	Analysis of Variance Summary for Comparison of Weibull Shape Parameters for Exposure Conditions	62
4.11	Analysis of Variance Summary for Comparison Weibull Shape Parameters Over Time	63
4.12	Comparison of Weibull Values for Ultimate Tensile Strength with Published Values	64
4.13	Arrhenius step 1: Regression equations for Composite Modulus	66
4.14	Arrhenius step 2: Regression equations for Retention versus inverse temperature Composite Modulus	66
4.15	Comparison of Arrhenius Predictions to Test data	68
4.16	Comparison of Arrhenius Predictions to Test data	70
4.17	Final Predictive Equations	76
4.18	Conversion Factors (C_{exp}) for Arrhenius extension to salt and alkaline environments.	78
A.1	Glass-reinforced epoxy composite control sample at 0 weeks	106
B.1	Glass-reinforced epoxy modulus Weibull parameters	108

CHAPTER 1

INTRODUCTION

1.1 Introduction to Composite Materials

Composite materials are a class of material created by the combination of multiple dissimilar materials in which at least one serves as the reinforcement and the other serves as the matrix. The combination of materials with differing material properties allows for the creation of a new composite material with different properties than the constituent materials. The dissimilar properties of the constituents work in conjunction to produce a final material with more advantageous properties than any of the constituent materials. Kaw [1] defines a composite as follows.

“A composite is a structural material that consists of two or more combined constituents that are combined at a macroscopic level and are not soluble in each other. One constituent is called the reinforcing phase and the other one in which it is embedded is called the matrix. The reinforcing phase material may be in the form of fibers, particles, or flakes. The matrix phase materials are generally continuous.”

1.1.1 Common Applications of Composite Materials

Composites are widely used in a large number of applications. Their applications include composite rebar as reinforcement in concrete, glass fiber reinforced

polymers in boat hulls, and metal matrix composites for high temperature engine components. The automotive industry regularly uses fiber reinforced polymer (FRP) composites with glass and carbon fiber as the reinforcement in epoxy, vinylester, and polyester resins to make body panels. FRPs are widely used in marine structures, and vessels. Wind turbines make extensive use of FRP materials for the blades, and housings. The aerospace industry is a large user of FRP materials for a wide array of parts ranging from structural fuselage components and control surfaces, to interior panels.

FRPs are useful for some naval applications due to their good fatigue resistance, good corrosion resistance, and good strength to weight ratio. One of the first major applications of FRPs for naval vessel hulls was for minesweepers. FRPs were chosen primarily because of their non-magnetic and corrosion resistance properties. The Royal Swedish Navy's Visby Class ships are some of the first ships of their size to use hulls made entirely of composites. These ships use a sandwich construction with a polyvinyl chloride foam core and carbon fiber reinforced vinyl-ester composites face sheets, producing a very strong, durable, and light weight hull. Small leisure and sporting vessel hulls are almost exclusively made of FRP materials. FRPs have taken over this industry due to their corrosion resistance and good strength and stiffness to weight ratio [2].

FRP materials are increasingly being used for a variety of civil applications; they are an excellent supplement to traditional materials such as steel, concrete, wood, and stone because of their high strength to weight ratio, relatively small material

thickness requirements, good corrosion resistance, and their ability to be bonded to an existing structure with relative ease [3–5].

FRPs have recently been used to strengthen and rehabilitate existing structures, such as bridge decks requiring increased load capacity, or bridge columns requiring increased seismic capacity [3, 5].

1.2 Research Motivation

Despite the extensive use of FRPs, there are still challenges related to the development of a validated database of material characteristics, as well as predictive methods for the determination of long term response.

Durability data is key for the engineer to effectively utilize composite materials in design. Over the past decade there has been significant focus in the area of civil and marine applications, to develop a database of properties for a variety of configurations. Testing for environmental effects over an extended period of time is needed to establish better databases related to the durability of FRPs. In addition there is a need for the development and validation of predictive models for material characteristics for a variety of material configurations and environments. The focus of this recent research is on “cheaper” non-aerospace materials, especially materials manufactured using non-autoclave cure processes. An added challenge is to develop a basis for reliability prediction and confidence intervals with minimal testing. [6, 7]

This thesis seeks to add to the knowledge developed by others in the aforementioned areas of research. Some of the specific issues this thesis seeks to address are: the lack of long term environmental test data for aqueous environments, the lack

of predictive models for aqueous environmental exposure validates by long-term data, and the need for durability data on wet-layup composites. In the context of the current research these issues will be addressed through accelerated degradation testing of a glass-fiber reinforced epoxy composite fabricated using a wet-layup process. The analysis of the test data includes the use of a predictive model for this material, and a reliability based assessment of material durability associated with the predictive model.

1.3 Overview of the Thesis

1.3.1 Introduction

The first chapter of this thesis seeks to lay the foundation for the rest of the thesis, by establishing the motivation for this research.

1.3.2 Development of Analysis Methodologies

Chapter 2 briefly reviews the background and methodologies used for this project. It introduces some recent work relating to rehabilitation with FRPs, accelerated degradation testing for FRPs, statistical methods applied to FRPs, and a summary gap analysis of the current research.

1.3.3 Testing

Chapter 3 provides a description of the test samples and the tests conducted on them. It introduces the exposure conditions, the testing procedures, and the associated standards.

1.3.4 Analysis of Accelerated Degradation Test Data

Chapter 4 provides an analysis of the accelerated degradation test results, the extrapolation of the material properties over longer periods of time, and elucidates fitting of the Weibull distribution to the data.

1.3.5 Reliability Based Assessment of Long-Term Material Properties

Chapter 5 elucidates the process used to determine reliability estimates for the results gained in Chapter 4. This chapter also presents the results of the reliability based assessment of the data.

1.3.6 Conclusions and Recommendations

Chapter 6 provides the conclusions from the research as well as recommendations for further work.

CHAPTER 2

BACKGROUND

2.1 Rehabilitation with Fiber Reinforced Polymers

FRP composites have been gaining popularity over the past two decades as an efficient means of rehabilitation of existing civil infrastructure. They have been gaining popularity due to several advantages FRPs have over traditional materials such as concrete, steel, and timber. Traditionally steel has been used to rehabilitate aging structures but steel is prone to corrosion, it is heavy, and difficult to handle [8]. FRPs are more desirable due to the fact that they are far more resistant to corrosion, they have a higher strength to weight ratio, they are easier to handle, and they have the potential for lower life-cycle costs. They also have highly tailorable properties, so they offer the flexibility to be used in a variety of applications and conditions. Despite the growing popularity and the advances of the past two decades there are still challenges related to the use of FRPs in the rehabilitation of civil infrastructure.

2.2 Accelerated Life Testing for FRPs

Accelerated degradation testing is a useful tool to understand the behavior of a material, component, or system over time using only a percentage of the time

period of interest. Accelerated testing is accomplished by submitting a test article to a severe simulation of the expected environmental condition of use. The environment is simulated by applying some or all of the factors expected in service, such as temperature, load, exposure to chemicals, moisture, UV, etc. The testing is accelerated by increasing the intensity of at least one of the factors beyond a level expected during normal use. For example increasing temperature is a common method of accelerating a test. The test article is exposed to the conditions for a pre-determined time and the degradation of the article is monitored. When the test is complete the results are used to build a mathematical model is used to predict the response of the test article over an extended period of time [9].

The choice of acceleration factor and the intensity of the factor are important components of an accelerated degradation test. The factor must accelerate the process in a predictable manner, and the intensity must not initiate any new failure modes. Some common acceleration factors are temperature, force, number of cycles, wear, UV exposure, and exposure to chemicals. There are a variety of acceleration models available based on what type of article is being tested, the acceleration factor used, and what the goal of the test is. Some common models are; the life-stress relationship, the Arrhenius time-temperature relationship, the inverse power relationship, and the Eyring relationship [9].

The primary focus of this project was to examine the effects of moisture on the material over an extended period of time so that the material could be better characterized for extended use. Moisture absorption by a FRP material is a diffusion

based process [10], which is temperature process. Diffusion processes can be modeled by Fick's Law [11] as shown in Equation 2.1.

$$\frac{\partial C}{\partial t} = \nabla \cdot [D [\vec{\nabla} C]] \quad (2.1)$$

Where t is time, D is the diffusion coefficient, and C is the concentration of the sorbate. It is known that the diffusion coefficient D is temperature dependent and can be modeled by the Arrhenius rate relationship [11], shown in Equation 2.2.

$$Rate = Ce^{-\frac{Q}{RT}} \quad (2.2)$$

Where $Rate$ is the rate of the reaction, C is a pre-exponential constant which is independent of temperature, Q is the activation energy for the reaction, R is the universal gas constant, and T is the absolute temperature [11].

Since the absorption of moisture by a FRP follows a diffusion process, and the rate of diffusion is temperature dependent; temperature was a natural choice for the acceleration factor.

A more detailed review of the models for the affect of moistue on FRPs was conducted by Stephanie L. Svetlik, in the PhD dissertation "An Investigation in the Hygrothermal Degradation of an E-glass/vinyl-ester Composite in Humid and Immersion Environments" [10].

2.2.1 Eyring Relationship for Temperature Acceleration

The Eyring relationship for temperature acceleration is a useful model for testing using temperature acceleration. It is presented as a reaction rate for chemical degradation based on quantum mechanics. The basic expression for the Eyring relationship is given in Equation 2.3.

$$\tau(T) = \left(\frac{A}{T}\right) \exp\left(\frac{B}{kT}\right) \quad (2.3)$$

Where, τ is the nominal life as a function of absolute temperature T , A and B are constants characteristic of the test article and test methods, and k is the Boltzman constant. The Eyring relationship is similar to the Arrhenius relationship and is considered an alternative to the Arrhenius relationship [9].

2.2.2 Phani and Bose Method

The Phani and Bose method is a model developed by K. K. Phani, and N. R. Bose, for predicting strength, σ , after exposure time t . The predicted strength is determined from Equation 2.4 [12, 13].

$$\sigma(t) = (\sigma_0 - \sigma_\infty) \left[-\frac{t}{\tau_0} \exp\left\{\frac{-E_d}{RT}\right\} \right] + \sigma_\infty \quad (2.4)$$

Where σ_0 is the unexposed strength, σ_∞ is the asymptotic strength after long term exposure, E_d is the activation energy, R is the universal gas constant, T is the absolute design temperature, and τ_0 is a constant determined from Equation 2.5.

$$\frac{1}{\tau} = \frac{1}{\tau_0} \exp\left(\frac{-E_d}{RT}\right) \quad (2.5)$$

Where, τ is the characteristic time, which is dependent on the exposure temperature.

The primary issue associated with the Phani and Bose method is that it explicitly requires the assumption of a predetermined asymptote, σ_∞ .

2.2.3 Arrhenius Relationship

The Arrhenius time-temperature relationship has been shown to be a good model for predicting material response in FRP materials for temperature accelerated tests [9,14]. This model is based on the Arrhenius rate relationship introduced above in Equation 2.2. The Arrhenius rate relationship is a rate relationship for the rate of diffusion or the rate of a temperature dependent chemical reaction. This model was developed by Savant August Arrhenius (1859-1927), a Swedish chemist. He developed and proved experimentally the relation known as the Arrhenius equation [11].

The Arrhenius time-temperature relationships useful for the analysis of accelerated degradation test data are derived from the Arrhenius rate relationship by first taking the natural logarithm of Equation 2.2 to give Equation 2.6.

$$\ln(\text{Rate}) = \ln(C) - \frac{Q}{R} \left(\frac{1}{T}\right) \quad (2.6)$$

The plot of the natural log of the rate, versus the inverse of absolute temperature is referred to as an Arrhenius plot. An Arrhenius plot can be useful in the

determination of the activation energy Q and the pre-exponential constant C from experimental data; the slope of the line is $-\frac{Q}{R}$, and extrapolating the line to $T = \infty$, or $\frac{1}{T} = 0$, gives the intercept $\ln(C)$ [11].

A few key assumptions associated with the Arrhenius degradation model are that, the degradation is not reversible, the model applies to a single degradation mode, and that the degradation before the beginning of the test is negligible [9].

The models presented above provide useful information about the mean performance of a material over time, but they lack any indication of data scatter. A mean value can be interesting, but holds limited use for design, thus the need for reliability data.

2.2.4 Reliability Based Assessment

The reliability of a material is a probabilistic characterization of the material properties [15]. Therefore a reliability based assessment of a material contains a probabilistic measure of the variability of the material properties for a given set of conditions. The use of a statistical probability distribution function allows for a reliability based characterization of a material. Some common distributions are introduced as follows.

2.2.4.1 The Gaussian Distribution

The Gaussian or normal distribution is the most commonly used probability distribution. It is a symmetric distribution with the location specified by the mean,

and the scale characterized by the standard deviation. The Gaussian distribution is very useful, but has a very rigid symmetric shape, thus limiting the applicability. The Gaussian probability density function is given by [16]:

$$f(x) = \frac{1}{\sigma\sqrt{(2\pi)}} \exp \left[-\frac{1}{2} \left(\frac{x - \mu}{\sigma} \right)^2 \right] \quad (2.7)$$

Where, μ is the arithmetic mean of of the sample population, and σ is the standard deviation of the sample population.

2.2.4.2 The Lognormal Distribution

The lognormal distribution is more versatile than the Gaussian distribution because it can take on a variety of shapes to fit a variety of data sets. It is very useful for the characterization of mechanical components subjected to fatigue stresses. The lognormal probability density function is given by [16]:

$$f(x) = \begin{cases} \frac{1}{\sigma x \sqrt{(2\pi)}} \exp \left[-\frac{1}{2} \left(\frac{\ln(x-\mu)}{\sigma} \right)^2 \right] & (for x \geq 0) \\ 0 & (for x < 0) \end{cases} \quad (2.8)$$

Where, μ is the arithmetic mean of of the sample population, and σ is the standard deviation of the sample population.

2.2.4.3 The Exponential Distribution

The exponential distribution is the traditional distribution used for reliability analysis, but it holds limited value for the characterization of material properties. It

is most useful for modeling the reliability of electronic components. The exponential probability density function is given by [16]:

$$f(x) = \begin{cases} \lambda \exp(-\lambda x) & (\text{for } x \geq 0) \\ 0 & (\text{for } x < 0) \end{cases} \quad (2.9)$$

Where, λ is the exponential distribution parameter, γ represents the mean of the population modeled by the exponential distribution.

2.2.4.4 The Gamma Distribution

The Gamma distribution, like the lognormal distribution, is also a versatile distribution because it can also take on a variety of shapes. In terms of reliability it is most useful for situations where partial failures can exist and the time to failure is exponentially distributed [15]. The Gamma probability density function is given by [16]:

$$f(x) = \begin{cases} \frac{\lambda^a}{\Gamma(a)} (\lambda x)^{a-1} \exp(-\lambda x) & (\text{for } x \geq 0) \\ 0 & (\text{for } x < 0) \end{cases} \quad (2.10)$$

Where, Γ is the gamma function, λ is the rate parameter, and a is the shape parameter.

2.2.4.5 The Weibull Distribution

The Weibull distribution has been shown to characterize well the mechanical response of composite materials [17–19], as well as lifetimes and reliabilities [9, 19, 20],

and is a highly adaptable distribution due to the ability to take on a variety of shapes [17, 21]. The Weibull probability distribution is a probability distribution function proposed by Waloddi Weibull, and published in 1951 [19]. It has also been proven to be very versatile [19], in that it can take on the shape of many different distributions, such as the gamma, normal, lognormal, and exponential distributions, [20] thus reducing the need to fit and compare several distributions.

The Weibull cumulative distribution function is defined as:

$$F(x) = 1 - e^{\left(-\frac{x}{\beta}\right)^\alpha} \quad (2.11)$$

The Weibull probability density function given by [16]:

$$f(x) = \frac{\alpha}{\beta} \left(\frac{x}{\beta}\right)^{(\alpha-1)} e^{-\left(\frac{x}{\beta}\right)^\alpha} \quad (2.12)$$

Where α is the Weibull shape factor, and β is the Weibull scale parameter.

Figure 2.1 illustrates the flexibility of the Weibull distribution. With a shape factor (α) of 1 the Weibull distribution takes on the shape of the exponential distribution, $\alpha = 2.5$ approximates the lognormal distribution, and $\alpha = 3.6$ approximates the Gaussian distribution [20].

A commonly used expression for the mean of the Weibull is given by [16]:

$$\mu = \beta \Gamma\left(1 + \frac{1}{\alpha}\right) \quad (2.13)$$

Where Γ is the gamma function.

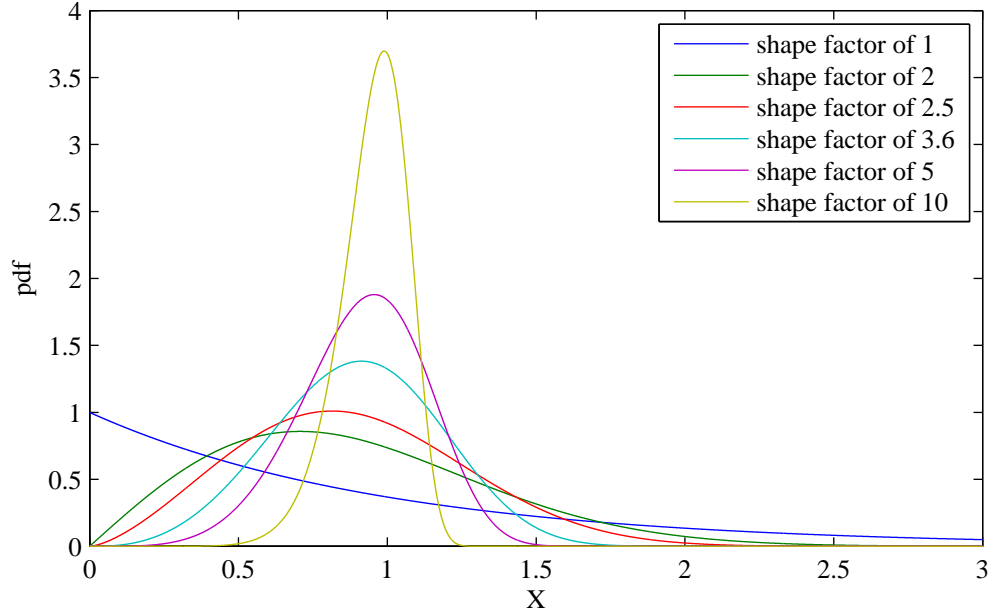


Figure 2.1: Shape of Weibull Probability Density Function

The sample variance can be estimated using the following expression [16]:

$$\sigma^2 = \beta^2 \left\{ \Gamma \left(1 + \frac{2}{\alpha} \right) - \Gamma^2 \left(1 + \frac{1}{\alpha} \right) \right\} \quad (2.14)$$

Equations 2.13 and 2.14 are used to derive the following expression for the coefficient of variation for the Weibull distribution. The coefficient of variation is defined as the sample standard deviation divided by the sample mean.

$$COV = \frac{\sigma}{\mu} = \left\{ \frac{\Gamma \left(1 + \frac{2}{\alpha} \right)}{\Gamma^2 \left(1 + \frac{1}{\alpha} \right)} - 1 \right\}^{\frac{1}{2}} \quad (2.15)$$

Weibull Fit Approximations According to He *et al.*, [22], the Weibull mean can be approximated by Equation 2.16.

$$\mu \approx \beta \tag{2.16}$$

The coefficient of variation in Equation 2.15 can be approximated by Equation 2.17 [22].

$$COV \approx \alpha^{-0.93} \tag{2.17}$$

This expression can be further simplified by Equation 2.18, [23].

$$COV \approx \frac{1.2}{\alpha} \tag{2.18}$$

Initially these approximations may appear to be very gross but, when the percent difference between Equations 2.15 and 2.18; and between Equations 2.13 and 2.16 are analyzed it turns out that as long as the shape factor is greater than five, the percent difference is less than six percent. The percent difference between Equations 2.15 and 2.18 is plotted in Figure 2.2. The approximation for the mean is similar, the percent difference between the actual mean and the approximation is less than thirteen percent as long as beta is greater than 1.5; and less than six percent when beta is greater than ten. The percent difference between Equations 2.13 and 2.16 is plotted in Figure 2.3 These approximations have been used to simplify the determination of the values of the Weibull shape and scale parameters [23].

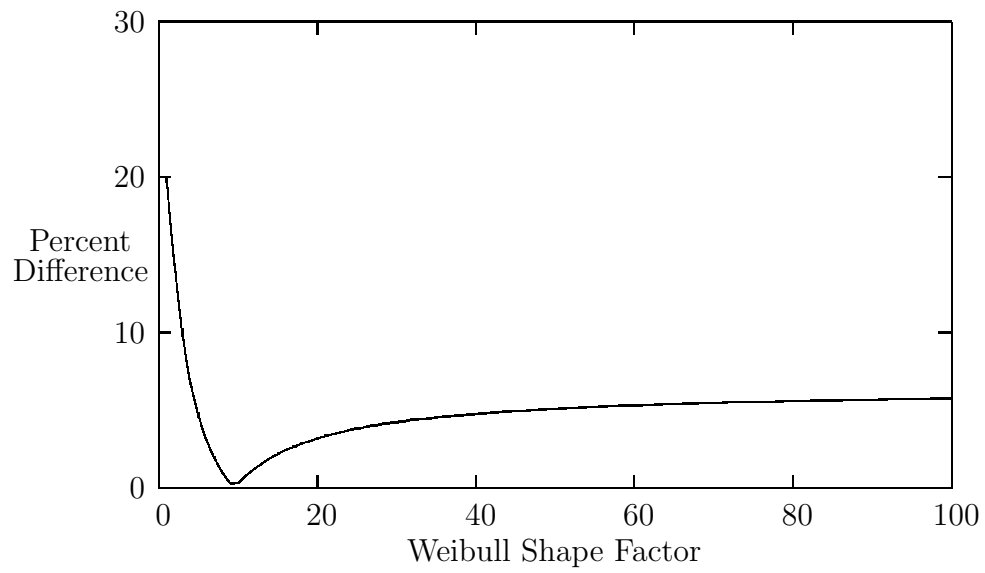


Figure 2.2: Verification of Weibull Coefficient of Variation approximation

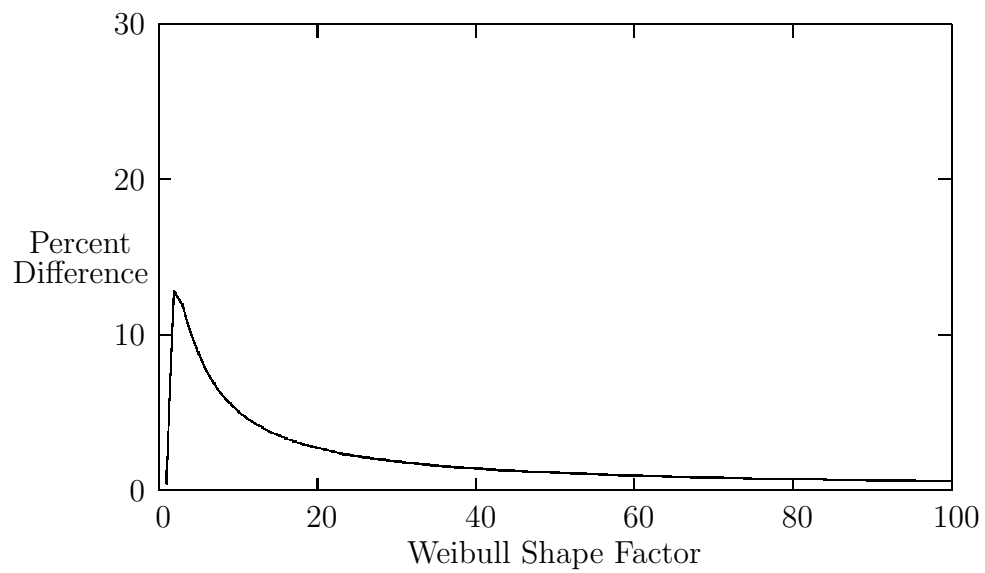


Figure 2.3: Verification of Weibull Mean approximation

2.2.5 Design Values

There are a number of current design guidelines for the application of FRPs in civil infrastructure. They all account for environmental degradation of the FRPs to an extent, but these guidelines do not account for time. Some of the primary guidelines are introduced here.

1. American Concrete Institute Committee 440, *Guide for the Design and Construction of Externally Bonded FRP Systems for Strengthening Concrete Structures (ACI 440.2R-02)*. Published 2009
2. The Concrete Society Technical Report 55, *Design Guidance for Strengthening Concrete Structures using Fibre Composite Materials 2nd Edition. (TR55)* Published 2004.
3. *Canadian Highway Bridge Design Code*. Published 2006

2.2.5.1 ACI 440

The American Concrete Institute committee 440 has published report 440.02R-02 detailing their design recommendations for using FRPs for external strengthening and rehabilitation of existing concrete structures [24]. Their recommendations for determining the design values for FRPs are as follows.

The ultimate strength is to be reported as follows.

$$f_{fu}^* = \overline{f_{fu}} - 3\sigma \quad (2.19)$$

Where f_{fu}^* is the reported ultimate strength of the material. $\overline{f_{fu}}$ is the mean value of the ultimate strength of the material, and σ is the standard deviation of the sample population.

The rupture strain is reported as follows.

$$\varepsilon_{fu}^* = \overline{\varepsilon_{fu}} - 3\sigma \quad (2.20)$$

Where ε_{fu}^* is the reported rupture strain, $\overline{\varepsilon_{fu}}$ is the mean rupture strain, and σ is the standard deviation of the sample population.

The design value for the ultimate strength is to be found as follows in Equation 2.21 to account for the environmental conditions the material is expected to experience.

$$f_{fu} = C_E (f_{fu}^*) \quad (2.21)$$

Where f_{fu} is the design ultimate strength, C_E is the environmental reduction factor to account for the environmental exposure over time.

The design rupture strain is found using Equation 2.22

$$\varepsilon_{fu} = C_E (\varepsilon_{fu}^*) \quad (2.22)$$

Where ε_{fu} is the design strain.

The design modulus is found using equation Equation 2.23

Table 2.1: ACI 440 Environmental Reduction Factors

Exposure Condition	Fiber/Matrix	C_E
Interior	Carbon/Epoxy	0.95
	Glass/Epoxy	0.75
	Aramid/Epoxy	0.85
Exterior	Carbon/Epoxy	0.85
	Glass/Epoxy	0.65
	Aramid/Epoxy	0.75
Aggressive	Carbon/Epoxy	0.85
	Glass/Epoxy	0.50
	Aramid/Epoxy	0.70

$$E_f = \frac{f_{fu}}{\varepsilon_{fu}} \quad (2.23)$$

Which makes the assumption that the modulus is unaffected by the environmental conditions, because C_E is canceled out.

2.2.5.2 TR55

The Concrete Society in the United Kingdom has published TR55 [25], detailing their design guidelines for the use of FRP composites for strengthening concrete structures. The approach outlined in this report utilizes partial safety factors to account for the differing environmental conditions, manufacturing methods, and materials. The procedure for determining design values according to this report are as follows. The modulus is to be reported as follows.

$$E_f = \bar{E} - 2\sigma \quad (2.24)$$

Where E_f is the reported modulus of the material. \bar{E} is the mean value of the modulus of the material, and σ is the standard deviation of the sample population.

Similarly, the rupture strain is reported as follows.

$$\varepsilon_f = \bar{\varepsilon} - 2\sigma \quad (2.25)$$

Where, ε_f is the reported rupture strain, $\bar{\varepsilon}$ is the mean rupture, and σ is the standard deviation for the sample population. The recommended design values are found using partial safety factors. The design value for modulus is found using Equation 2.26

$$E_{fd} = \frac{E_f}{\gamma_{mE}} \quad (2.26)$$

Where E_{fd} is the design value for the modulus, E_f is the characteristic value of the modulus, and γ_{mE} is the safety factor for the environmental conditions and the manufacturing process. For strain the design value is found using Equation 2.27

$$\varepsilon_{fd} = \frac{\varepsilon_f}{\gamma_{m\varepsilon}} \quad (2.27)$$

Where, ε_{fd} is the design strain value, ε_f is the reported rupture strain, and $\gamma_{m\varepsilon}$ is the safety factor to account for the effects of environmental conditions and manufacturing process on strain. The safety factors in Equations 2.26 and 2.27 are found using Equation 2.28.

Table 2.2: TR55 Partial Safety Factors for Modulus and Strain

Material	γ_{mE}	$\gamma_{m\varepsilon}$
Carbon FRP	1.1	1.25
E-Glass FRP	1.8	1.95
Aramid FRP	1.1	1.35

Table 2.3: TR55 Partial Safety Factors for Manufacturing Method and Application

Application	Manufacturing Method	γ_{mm}
Plates	Pultruded	1.05
	Prepreg	1.05
	Preformed	1.1
Sheets or Tapes	Machine-Controlled Application	1.05
	Vacuum Infusion	1.1
	Wet Layup	1.2
Prefabricated Shells	Filament Winding	1.05
	Resin Transfer Molding	1.1
	Hand Layup	1.2
	Hand Sprayup	1.5

$$\gamma_{mP} = (\gamma_{mE} \text{ OR } \gamma_{m\varepsilon}) * \gamma_{mm} \quad (2.28)$$

Where γ_{mP} is the final safety factor, γ_{mE} and $\gamma_{m\varepsilon}$ are the partial safety factors for modulus and strain respectively, based on the material, and where γ_{mm} is the partial safety factor for the method of manufacture and application.

The design tensile strength is found using Hooke's law as follows.

$$f_{fd} = E_{fd}\varepsilon_{fd} \quad (2.29)$$

2.2.5.3 Canadian Bridge Highway Design Code

The Canadian Bridge Highway Design Code is similar to the ACI 440 standard in that it utilizes a resistance factor based on conditions of use. The design strength is found using Equation 2.30

$$f_d = \phi_{FRP} (\bar{f} - 1.64\sigma) \quad (2.30)$$

Where f_d is the design strength, \bar{f} is the mean experimental strength, σ is the standard deviation of the sample population, and ϕ_{FRP} is the resistance factor based on the material, the manufacture process, and the environmental conditions. The design modulus follows the same procedure, using Equation 2.31.

$$E_d = \phi_{FRP} (\bar{E} - 1.64\sigma) \quad (2.31)$$

Where E_d is the design modulus, \bar{E} is the mean experimental modulus and σ is the standard deviation of the sample population.

The resistance factor ϕ_{FRP} is found using Equation 2.32.

$$\phi_{FRP} = (\phi_{pul} : or : \phi_{hl}) C_E \quad (2.32)$$

Where ϕ_{pul} and ϕ_{hl} are the resistance factors for factory or field manufactured FRP and C_E is the environmental factor.

Table 2.4: CHBDC Partial Safety Factors for Manufacturing Method and Application

Application	ϕ_{pul}	ϕ_{hl}	C_E
AFRP surface-mounted on concrete and exposed to moisture	0.8	0.6	0.5
AFRP surface-mounted on concrete or timber and not exposed to moisture and UV light	0.8	0.6	0.9
CFRP inside concrete or near-surface mounted	0.8	0.6	0.95
CFRP tendon	0.8	0.6	0.95
GFRP surface mounted on concrete and not exposed to moisture	0.8	0.6	0.8
GFRP surface mounted on concrete and exposed to moisture	0.8	0.6	0.7
GFRP tendon in concrete	0.8	0.6	0.6
GFRP tendon for stressed wood decks	0.8	0.6	0.8

2.3 Gap Analysis

Over the past two decades there has been increasing research to support the increased use of FRP composites in the civil infrastructure. Within the past decade there have been several reviews exploring the state of the available knowledge base for the durability of FRP composites in infrastructure. In the first of these Karbhari *et al.*, [7] investigates the availability and importance of durability data for a variety of environmental conditions including moisture or solution environments and alkaline environments. This study found that the durability data for external reinforcement

with exposure to moist or alkaline environments is very important and highly unavailable for non-autoclave materials. In the second study Karbhari *et al.*, [6] identified several specific needs within the durability knowledge base. One notable discrepancy identified for all the conditions investigated was the need for extended testing, that is testing over 18 months. Also, collection of data on continuous exposure to moisture was identified as a highly critical need. Since the publication of these studies much research has been done to rectify some of the gaps identified, the following paragraphs introduce a few key publications documenting the progress leading to this research.

In 2005 Atadero *et al.*, [21] published an investigation into material variability in FRP composites used for external strengthening. Samples of a carbon reinforced epoxy manufactured at the same time as a rehabilitation were tested and the data fit to several common statistical probability distributions. The accuracy of the fits was compared using the Pearson's Chi-squared test. It was found that the Weibull distribution was the best fit for strength and thickness data, and was suggested that the use of the mean minus two times the standard deviation would be a good design value as it represented a lower 95% confidence interval. It was found that the lognormal distribution best characterized the modulus data.

In 2006 Helbling *et al.*, [26] published the results of an investigation on the variability and durability of an E-glass reinforced vinyl-ester composite under exposure to deionized water at $23^{\circ}C$, $37.8^{\circ}C$ and $60^{\circ}C$ for a period of 100 weeks. The test results were extended using an Arrhenius relationship resulting in a 74.8% retention of tensile strength for a 30 year period.

In 2006 Abanilla *et al.*, [27] published a study investigating the durability characteristics of a carbon reinforced epoxy. The material was exposed to deionized water at 23°C , 37.8°C and 60°C , a 5% NaCl solution at 23°C , a pH 12 concrete leachate solution at 23°C , and daily freeze-thaw for a period of 100 weeks. The samples were characterized for moisture uptake, changes in glass transition temperature, tensile, and flexural response. The results of the tensile characterization were extended using an Arrhenius relationship and compared to the ACI 440 design standard. For a two layer specimen the predictive results indicate that the degradation will not exceed the allowable degradation within a 100 year span.

A study published in 2007 by Karbhari *et al.*, [23] developed a reliability based prediction for a carbon reinforced epoxy manufactured using a wet layup process, the material test conditions were presented in the previous paragraph. The study compared two prediction methods, the Arrhenius relationship and the method developed by Phani and Bose, for exposure to moisture at 23°C ; the material degradation was predicted to 100 years, and compared to the ACI 440 and TR55 design standards. The prediction was then extended to include the NaCl solution, the concrete leachate solution, and humid environments. It was found that the Arrhenius model provided a more accurate result than the Phani and Bose method for the material and environmental conditions tested. The test data was characterized for reliability by fitting the Weibull distribution to establish a characterization of scatter in the data.

In 2007 Jackson [28] published a master's thesis titled *Reliability-Based Durability Assessment of GFRP Bars for Reinforced Concrete* detailing a study to develop a reliability based model of the tensile strength of GFRP for 60 years using a Monte

Carlo method. This study utilized experimental data from Bhise [29], testing GFRP bars under exposure to water and alkaline environments at $30^{\circ}C$, $45^{\circ}C$ and $57^{\circ}C$ for a period of 180 days. This data was used to build a power law predictive model for the tensile strength of a GFRP to 60 years. The model predicts a percent retention of ultimate tensile strength after sixty years of exposure to be 41%.

In 2010 Cromwell *et al.*, [30] published an extensive study: *Environmental durability of externally bonded FRP material intended for repair of concrete structures*. The testing was performed on unidirectional CFRP plates, hand-layup unidirectional CFRP fabric, and hand-layup unidirectional GFRP fabric. This study utilized nine environmental conditions, including water at $38^{\circ}C$, salt water at $22^{\circ}C$, and an alkaline solution at $22^{\circ}C$. These three conditions were tested for 1000, 3000, and 10,000 hours. The specimens were subjected to tension tests according to ASTM D3039 [31], short beam shear tests according to ASTM D2344 [32], and concrete bond strength. In this study the GFRP showed higher levels of degradation than the CFRP for exposure to the aqueous environments, and was noted that the “GFRP was particularly affected by exposure to an alkaline environment” [30]. The conclusions of this study question the assertion of ACI 440.02R-02 [24] that the modulus of elasticity is unaffected by environmental exposure. Given this conclusion Cromwell *et al.*, has recommended that the ACI 440.02R-02 environmental reduction factor, C_E , be applied to the modulus as well.

CHAPTER 3

MATERIAL AND TEST DETAILS

Tests were conducted to assess the long term durability of FRP composites fabricated using the wet layup method as described in this section. Tests were conducted primarily at the University of California San Diego [33].

3.1 Materials

The material under investigation in this project was a unidirectional E-glass and epoxy composite. The fabric used was a “unidirectional E-glass fabric with hot melt adhesively bonded bi-component thermoplastic thread in the transverse direction,” with an areal weight of $913 \frac{g}{m^2}$ [33]. The matrix system used was a HEXCEL “high-tac, low VOC, 2 component one hundred percent solids, epoxy resin with a viscosity of 2500 *cps* at 23°C” [33]. The composite samples were fabricated using the wet layup process with a final fiber volume fraction, $V_f = 28\%$, which is equivalent to a weight fraction, $W_f \approx XX\%$

3.2 Sample fabrication

3.2.1 Composite Samples

3.2.1.1 Wet Layup Process

The wet layup fabrication method is an open mold manual process. This process inherently produces variability in the resulting composite. To mitigate the variability all the samples for this research were manufactured by the suppliers using a consistent manual process [33]. The resultant composite samples had a fiber volume fraction (V_f) of 28%. All of the samples were pre-conditioned prior to testing. The composites were fabricated in the form of panels which were then cut to the size specified in ASTM D3039 [31] with a nominal length of 254 mm, width of 12.5 mm, and thickness equivalent to two layers of fabric.

3.2.2 Resin Samples

The neat resin samples were fabricated in an aluminum mold, and cut to size, following ASTM D638 [34], using a water jet so as not to damage the samples.

3.2.3 Preconditioning

In order to ensure uniformity prior to exposure all samples were preconditioned for four weeks at 22.8°C at 40% relative humidity.

3.3 Exposure Conditions

For this series of tests there were six exposure conditions; (1) a control sample, kept in a humidity chamber at $22.8^{\circ}C$ ($73^{\circ}F$), and 40% relative humidity, (2) immersion in deionized water at $22.8^{\circ}C$ ($73^{\circ}F$), (3) immersion in deionized water at $37.8^{\circ}C$ ($100^{\circ}F$), (4) immersion in deionized water at $60^{\circ}C$ ($140^{\circ}F$), (5) immersion in a 5% *NaCl* salt water solution at $22.8^{\circ}C$ ($73^{\circ}F$), the salinity of which was monitored to maintain a consistent solution, and (6) immersion in a concrete-based alkaline solution to simulate the ionic content and concentration as would be seen in the case of ponding on concrete at $22.8^{\circ}C$ ($73^{\circ}F$). The alkaline solution had a *pH* between 11.5 – 12.5, formulated by running deionized water through concrete blocks until the desired level of alkalinity was achieved. All of the samples were monitored closely to maintain consistency. The temperature was controlled to $\pm 2^{\circ}C$ for all samples. The samples were not in contact with each other, to allow space for movement of solution between samples [33].

3.4 Testing

A random selection of five samples from each exposure condition were tested at predetermined, periodic, intervals. The samples were characterized for moisture uptake and uniaxial tension characteristics [33]. The moisture uptake characterization was performed by gravimetric means. The tension testing of unreinforced epoxy specimens was performed according to ASTM standard D638 [34], whereas that of the composite was conducted following ASTM D3039 [31].

3.5 Summary of test data

The following tables present a summary of the data collected from the testing.

Table 3.1: Summary Test Data: Modulus of Epoxy in *GPa*

Time in weeks	Control	Immersion in Deionized Water			Immersion in Alkaline	Immersion in Salt Water
	22.8°C	22.8°C	37.8°C	60.0°C	22.8°C	22.8°C
0	3.29 (0.10)	—	—	—	—	—
24	3.46 (0.31)	2.84 (0.32)	2.57 (0.24)	2.24 (0.21)	2.72 (0.12)	2.72 (0.21)
48	3.43 (0.32)	2.78 (0.57)	2.51 (0.17)	2.09 (0.20)	2.70 (0.12)	2.63 (0.24)
72	3.54 (0.16)	2.43 (0.21)	2.20 (0.10)	1.89 (0.16)	2.32 (0.29)	2.42 (0.13)
96	3.56 (0.27)	2.48 (0.11)	2.31 (0.10)	1.80 (0.38)	2.32 (0.28)	2.32 (0.25)
167	3.56 (0.21)	2.28 (0.23)	2.13 (0.06)	1.73 (0.27)	2.21 (0.17)	2.15 (0.16)
209	3.51 (0.18)	2.23 (0.08)	2.10 (0.09)	1.68 (0.27)	2.19 (0.10)	2.11 (0.08)
264	3.50 (0.29)	2.18 (0.02)	2.06 (0.13)	1.62 (0.21)	2.09 (0.22)	2.06 (0.18)
312	3.50 (0.17)	2.11 (0.09)	2.04 (0.12)	1.57 (0.15)	2.07 (0.07)	1.97 (0.17)

Values given as Mean (Standard Deviation)

Table 3.2: Summary Test Data: Ultimate Strength of Epoxy

Time in weeks	Control	Immersion in Deionized Water			Immersion in Alkaline	Immersion in Salt Water
	22.8°C	22.8°C	37.8°C	60.0°C	22.8°C	22.8°C
0	44.19 (1.81)	44.19 (1.81)	44.19 (1.81)	44.19 (1.81)	44.19 (1.81)	44.19 (1.81)
24	45.23 (2.59)	44.23 (1.31)	44.08 (3.00)	42.75 (1.39)	45.46 (1.43)	45.43 (2.46)
48	48.45 (4.11)	44.86 (5.53)	43.52 (4.62)	42.55 (2.37)	43.97 (8.09)	44.98 (3.89)
72	51.98 (2.81)	41.53 (5.72)	41.13 (2.45)	35.89 (4.51)	38.01 (1.46)	40.87 (4.99)
96	46.71 (4.02)	42.61 (0.75)	38.23 (3.43)	31.76 (2.76)	37.52 (3.43)	39.98 (3.51)
167	46.53 (2.60)	38.04 (1.94)	34.72 (3.72)	28.27 (1.97)	35.16 (4.37)	36.93 (2.53)
209	45.98 (3.69)	34.10 (7.85)	29.18 (4.75)	23.89 (5.04)	33.33 (7.36)	34.50 (7.18)
264	46.36 (2.21)	32.84 (5.78)	26.90 (2.86)	20.32 (3.28)	29.32 (3.90)	30.34 (9.05)
312	45.43 (3.49)	27.07 (3.63)	21.48 (5.77)	18.68 (1.75)	25.41 (5.17)	26.59 (5.42)

Values given as Mean (Standard Deviation)

Table 3.3: Summary Test Data: Elastic Modulus of Composite

Time in weeks	Control	Immersion in Deionized Water			Immersion in Alkaline	Immersion in Salt Water
	22.8°C	22.8°C	37.8°C	60.0°C	22.8°C	22.8°C
0	18.15 (2.68)	—	—	—	—	—
24	18.30 (1.08)	17.55 (0.47)	16.26 (0.76)	16.05 (1.48)	16.83 (0.24)	17.23 (0.43)
48	18.32 (0.40)	17.43 (2.19)	15.95 (1.46)	15.17 (0.47)	16.32 (0.55)	17.05 (0.62)
72	18.43 (0.82)	16.85 (0.15)	15.02 (1.07)	14.66 (1.37)	15.74 (0.86)	16.03 (0.95)
96	18.48 (1.39)	16.84 (0.99)	14.66 (0.64)	14.30 (3.90)	15.63 (0.33)	15.86 (1.00)
167	18.68 (0.76)	16.11 (0.61)	14.47 (0.58)	14.28 (0.43)	14.90 (0.47)	15.07 (0.52)
210	18.68 (0.45)	15.49 (0.41)	14.30 (0.40)	14.08 (0.49)	14.47 (0.35)	14.88 (0.29)
266	18.70 (0.26)	15.11 (0.32)	14.24 (0.21)	13.99 (0.33)	14.23 (0.36)	14.52 (0.31)
319	18.71 (0.66)	14.52 (0.20)	14.12 (0.39)	13.93 (0.60)	14.10 (0.36)	14.11 (0.28)

Values given as Mean (Standard Deviation)

Table 3.4: Summary Test Data: Ultimate Strength of Composite

Time in weeks	Control	Immersion in Deionized Water			Immersion in Alkaline	Immersion in Salt Water
	22.8°C	22.8°C	37.8°C	60.0°C	22.8°C	22.8°C
0	345.75 (25.57)	—	—	—	—	—
24	331.42 (35.67)	280.42 (23.47)	217.88 (28.43)	155.16 (6.57)	260.14 (6.81)	302.46 (7.66)
48	337.19 (41.32)	270.58 (12.41)	185.08 (17.69)	148.92 (6.03)	212.98 (16.72)	274.67 (13.36)
72	340.65 (12.91)	261.64 (17.37)	182.04 (6.03)	144.76 (12.03)	185.86 (15.35)	263.19 (23.76)
96	343.26 (11.11)	257.82 (30.25)	156.57 (15.86)	138.08 (22.72)	178.67 (25.05)	260.40 (22.16)
167	344.86 (17.99)	228.96 (14.20)	153.45 (15.05)	136.35 (8.20)	173.99 (16.08)	228.52 (22.93)
210	351.37 (19.84)	209.64 (12.38)	141.13 (11.51)	132.90 (6.13)	166.42 (6.16)	203.20 (5.23)
266	357.30 (21.02)	200.54 (3.12)	141.93 (3.47)	124.98 (4.68)	157.49 (9.96)	194.86 (17.18)
319	358.94 (27.04)	198.91 (10.88)	132.71 (8.41)	121.43 (11.61)	155.36 (9.44)	187.57 (8.31)

Values given as Mean (Standard Deviation)

CHAPTER 4

DATA ANALYSIS AND PREDICTIONS

4.1 Overview

This chapter details the analysis of the test data as well as the procedure used to fit the Weibull distribution to the data. The data analysis process begins with a check for outliers in the raw data following ASTM standard E178 [35]. After the check for outliers the data is normalized to allow for comparison between different sets of samples. The Weibull distribution is then fit to the normalized data sets to begin the reliability assessment of the material. The Arrhenius model is also applied to the data to enable prediction of the long term response of the samples based on the temperature accelerated test results. These predictions are used in conjunction with aqueous solution based data to predict long-term response for exposure to the salt water solution and the alkaline solution.

4.2 Determination of outliers

In any physical test or simulation where data is collected there is the possibility that one or more of the collected data points are outlying observations, that is they vary significantly from the behavior of the other data points in the sample, indicating

a possible error, unrelated to the subject of interest. When data is being characterized statistically it is recommended in ASTM standard E178 [35] that possible outliers be identified and removed from the sample.

4.2.1 ASTM E178

The American Society for Testing and Materials defines an outlying observation as “an observation that appears to deviate markedly in value from other members of the sample in which it appears”, [35]. The American Society for Testing and Materials has developed a standard procedure to identify possible outlying observations, this is standard ASTM E-178 [35]. This standard recommends the use of a calculated T statistic, as shown in Equation 4.1 or Equation 4.2.

$$T_n = \frac{\bar{x} - x_n}{s} \quad (4.1)$$

Where \bar{x} is defined as the arithmetic mean of all n values, and s is the estimated population standard deviation. The value of s is found using Equation 4.3, x_n is the value in question and T_n is the T statistic for the value in question. If the value in question is less than the sample mean Equation 4.1 should be used. Alternatively if the value in question is greater than the sample mean Equation 4.2 should be used.

$$T_n = \frac{x_n - \bar{x}}{s} \quad (4.2)$$

Where \bar{x} is defined as the arithmetic mean of all n values, and s is the estimated population standard deviation. The value of s is found using Equation 4.3 [35], x_n is the value in question and T_n is the T statistic for the value in question.

$$s = \sqrt{\frac{1}{n-1} \sum_{i=1}^n (x_i - \bar{x})^2} \quad (4.3)$$

4.2.1.1 Procedure

The procedure outlined in ASTM E-178 recommends calculating the T statistic for each value in question using Equation 4.1 or Equation 4.2, and comparing that value to a T critical value, T_{crit} , based on a desired level of significance, and the number of samples. T critical values are tabulated in [35]. If T_n is greater than T_{crit} then the value in question is likely to be an outlying observation. Each data set considered in the current investigation was checked for high and low outliers with 95% significance. The significance level is the probability of correctly identifying a possible outlier. Natuarally significance level should be as high as possible. Given the inherent variability in the data a significance level of 95% was chosen for this study. The critical value used for a significance of 95% with 5 samples was; $T_{crit} = 1.715$ [35]. The possible outliers identified through this procedure are for raw data listed in Appendix A are given in Table 4.1.

Table 4.1: Possible Outliers

Material	Exposure	Time	Property	High or Low	T value	Suspect Value
Epoxy	Control	0 Weeks	Modulus	High	2.018	4.492 GPa
Epoxy	Control	72 Weeks	Ultimate Strength	Low	1.726	31.97 MPa
Epoxy	23°C Water	96 Weeks	Ultimate Strength	Low	1.765	33.950 MPa
Epoxy	23°C Water	264 Weeks	Modulus	Low	1.727	2.060 GPa
Epoxy	38°C Water	96 Weeks	Modulus	Low	1.736	1.529 GPa
Composite	38°C Water	266 Weeks	Ultimate Strength	Low	1.759	105.630 MPa
Composite	Alkali	24 Weeks	Ultimate Strength	Low	1.721	213.650 MPa
Composite	Alkali	96 Weeks	Modulus	Low	1.729	13.234 GPa

4.3 Normalization of Data

Data normalization is a useful method to compare trends and patterns within data sets which contain information from different sources, for example comparing elastic modulus data from a composite, with elastic modulus data from a neat resin. This comparison can be seen in Section 4.4.

4.3.1 Normalization Procedure

In order to simplify comparisons between data sets, and to generalize the material response, the data was normalized. This was accomplished by finding the percent property retention.

$$R_{P_t} = \frac{P_{i_t}}{P_{0_t}} * 100 \quad (4.4)$$

Where R_{P_t} is the percent retention of property P , at exposure time t , P_{i_t} is the property of interest at exposure time t , and where P_{0_t} is the average property of the control sample at exposure time t . By comparing the control sample data at each exposure time to the property of interest at each corresponding time of exposure effects of post-cure and sample aging, even during the period of exposure, can be accounted for to an extent.

4.3.2 Normalization results

Tables 4.2, 4.3, 4.4 and 4.5 and Figures 4.1, 4.2, 4.3 and 4.4 show the percent retention results for the test data.

Table 4.2: Average Percent Retention Results for Epoxy Modulus Data

Time in weeks	Immersion in Deionized Water at			Immersion in	Immersion in
	22.8°C	37.8°C	60.0°C	Alkaline Solution at 22.8°C	Salt Water at 22.8°C
0	100.00 (2.89)	100.00 (2.89)	100.00 (2.89)	100.00 (2.89)	100.00 (2.89)
24	86.28 (11.39)	78.05 (9.43)	68.23 (9.51)	82.74 (4.38)	82.69 (7.67)
48	84.51 (20.46)	76.32 (6.64)	63.53 (9.48)	82.01 (4.58)	80.09 (9.19)
72	73.82 (8.54)	66.78 (4.44)	57.41 (8.30)	70.65 (12.40)	73.57 (5.47)
96	75.38 (4.29)	70.24 (4.33)	54.74 (21.31)	70.61 (12.03)	70.67 (10.89)
167	69.35 (10.27)	64.81 (2.86)	52.68 (15.38)	67.22 (7.85)	65.34 (7.36)
209	67.95 (3.36)	63.76 (4.50)	51.16 (16.31)	66.61 (4.78)	64.18 (3.56)
264	66.39 (0.78)	62.60 (6.55)	49.40 (13.01)	63.51 (10.68)	62.72 (8.75)
312	64.24 (4.17)	61.93 (5.94)	47.70 (9.61)	62.96 (3.58)	59.86 (8.65)

Values given as: Mean (Coefficient of Variation)

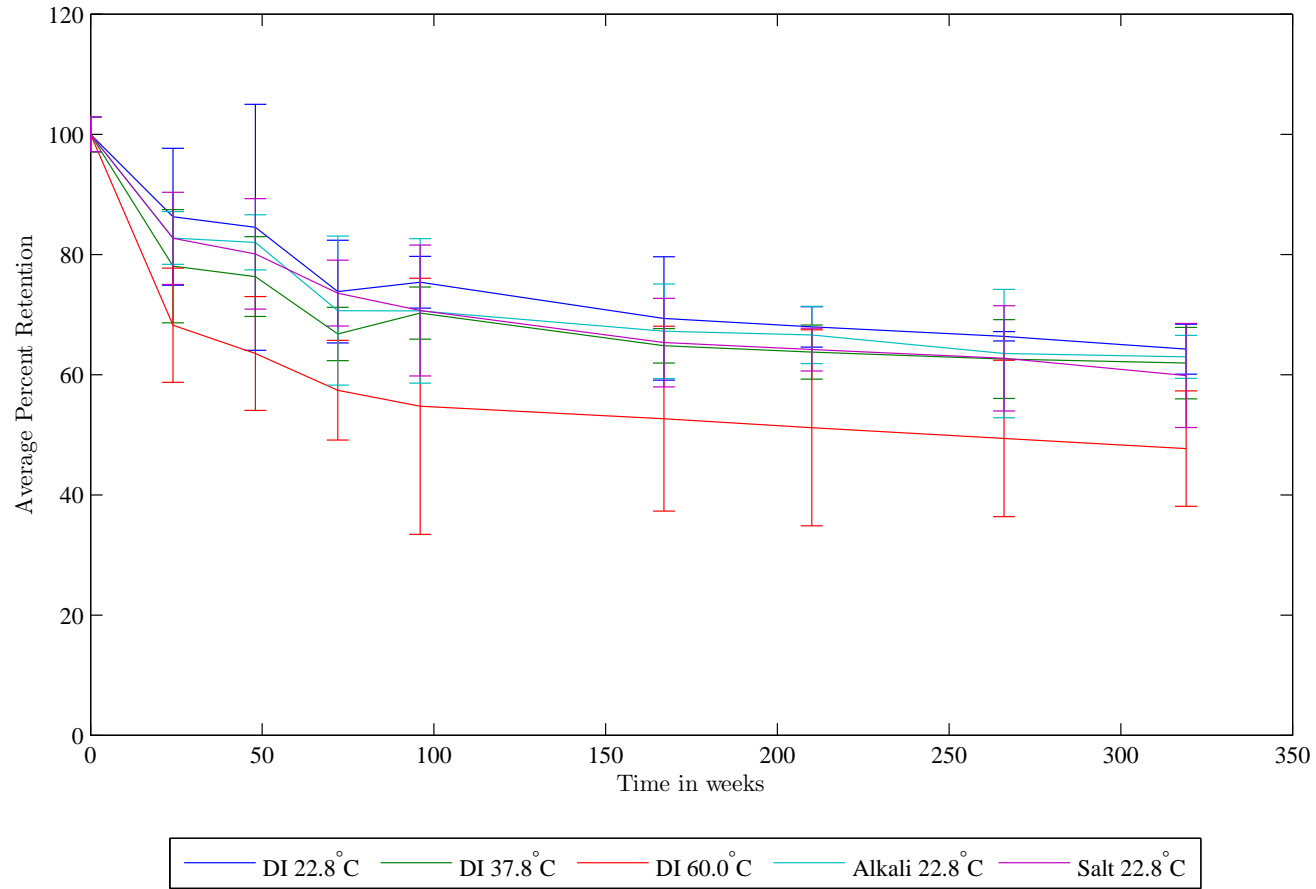


Figure 4.1: Percent Modulus Retention for Epoxy

Table 4.3: Average Percent Retention Results for Composite Modulus Data

Time in weeks	Immersion in Deionized Water at			Immersion in	Immersion in
	22.8°C	37.8°C	60.0°C	Alkaline Solution at 22.8°C	Salt Water at 22.8°C
0	100.00 (14.79)	100.00 (14.79)	100.00 (14.79)	100.00 (14.79)	100.00 (14.79)
24	96.71 (2.69)	89.60 (4.70)	88.41 (9.23)	92.75 (1.41)	94.93 (2.52)
48	96.05 (12.54)	87.88 (9.13)	83.56 (3.10)	89.94 (3.34)	93.94 (3.65)
72	92.83 (0.90)	82.75 (7.09)	80.78 (9.38)	86.72 (5.45)	88.33 (5.92)
96	92.77 (5.86)	80.80 (4.38)	78.80 (27.27)	86.10 (2.10)	87.41 (6.32)
167	88.75 (3.80)	79.76 (3.98)	78.70 (3.01)	82.11 (3.12)	83.06 (3.44)
210	85.34 (2.63)	78.81 (2.79)	77.56 (3.48)	79.75 (2.40)	81.97 (1.93)
266	83.27 (2.10)	78.45 (1.47)	77.11 (2.35)	78.40 (2.50)	79.99 (2.15)
319	80.03 (1.38)	77.79 (2.76)	76.76 (4.28)	77.67 (2.57)	77.77 (1.96)

Values given as: Mean (Coefficient of Variation)

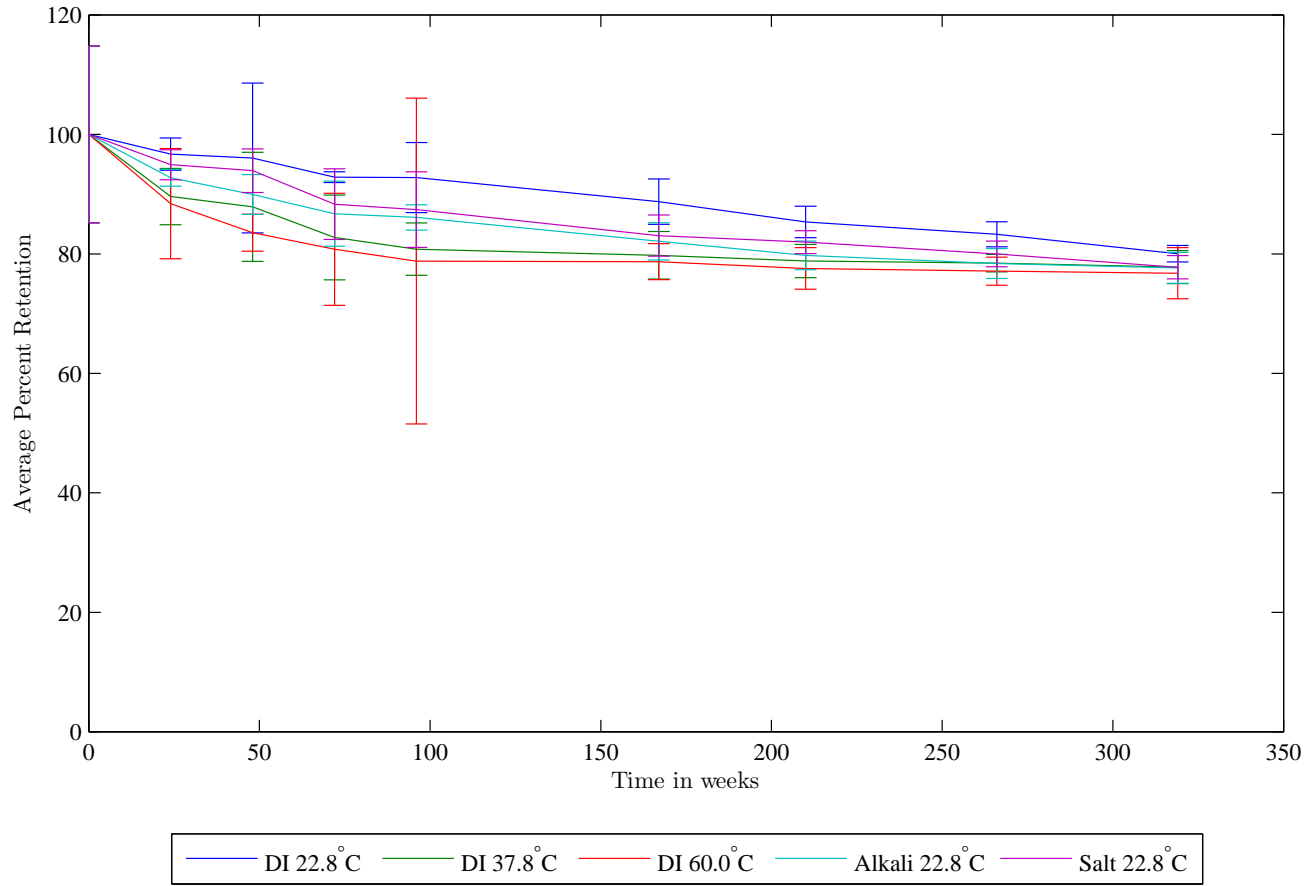


Figure 4.2: Percent Modulus Retention for Composite

Table 4.4: Average Percent Retention Results for Epoxy Ultimate Strength Data

Time in weeks	Immersion in Deionized Water at			Immersion in	Immersion in
	22.8°C	37.8°C	60.0°C	Alkaline Solution at 22.8°C	Salt Water at 22.8°C
0	100.00 (4.09)	100.00 (4.09)	100.00 (4.09)	100.00 (4.09)	100.00 (4.09)
24	100.08 (2.96)	99.75 (6.79)	96.75 (3.24)	102.88 (3.15)	102.80 (5.42)
48	101.51 (12.33)	98.49 (10.62)	96.28 (5.56)	99.49 (18.40)	101.78 (8.65)
72	93.98 (13.79)	93.07 (5.95)	81.22 (12.57)	86.01 (3.84)	92.49 (12.21)
96	96.42 (1.75)	86.51 (8.98)	71.86 (8.68)	84.91 (9.15)	90.48 (8.79)
167	86.09 (5.11)	78.58 (10.71)	63.98 (6.95)	79.57 (12.42)	83.56 (6.86)
209	77.16 (23.03)	66.03 (16.29)	54.06 (21.10)	75.42 (22.09)	78.08 (20.82)
264	74.32 (17.60)	60.87 (10.65)	45.98 (16.13)	66.35 (13.30)	68.65 (29.83)
312	61.26 (13.40)	48.60 (26.89)	42.28 (9.34)	57.50 (20.33)	60.17 (20.40)

Values given as: Mean (Coefficient of Variation)

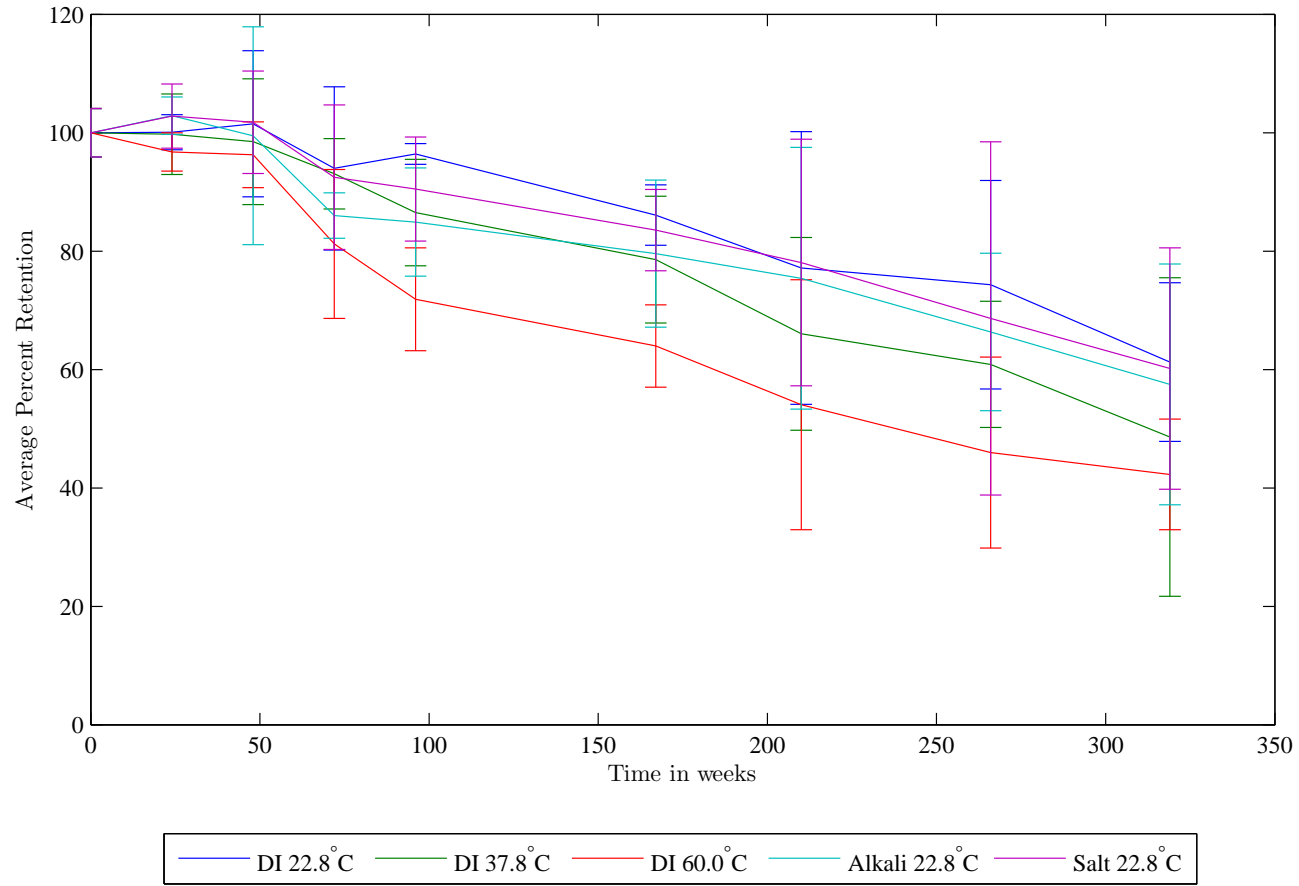


Figure 4.3: Percent Ultimate Strength Retention for Epoxy

Table 4.5: Average Percent Retention Results for Composite Ultimate Strength Data

Time in weeks	Immersion in Deionized Water at			Immersion in	Immersion in
	22.8°C	37.8°C	60.0°C	Alkaline Solution at 22.8°C	Salt Water at 22.8°C
0	100.00 (7.40)	100.00 (7.40)	100.00 (7.40)	100.00 (7.40)	100.00 (7.40)
24	81.10 (8.37)	63.02 (13.05)	44.87 (4.23)	75.24 (2.62)	87.48 (2.53)
48	78.26 (4.59)	53.53 (9.56)	43.07 (4.05)	61.60 (7.85)	79.44 (4.86)
72	75.67 (6.64)	52.65 (3.31)	41.87 (8.31)	53.76 (8.26)	76.12 (9.03)
96	74.57 (11.73)	45.28 (10.13)	39.94 (16.46)	51.68 (14.02)	75.31 (8.51)
167	66.22 (6.20)	44.38 (9.81)	39.43 (6.02)	50.32 (9.24)	66.09 (10.04)
210	60.63 (5.90)	40.82 (8.16)	38.44 (4.61)	48.13 (3.70)	58.77 (2.57)
266	58.00 (1.55)	41.05 (2.44)	36.15 (3.74)	45.55 (6.33)	56.36 (8.82)
319	57.53 (5.47)	38.38 (6.34)	35.12 (9.56)	44.93 (6.08)	54.25 (4.43)

Values given as: Mean (Coefficient of Variation)

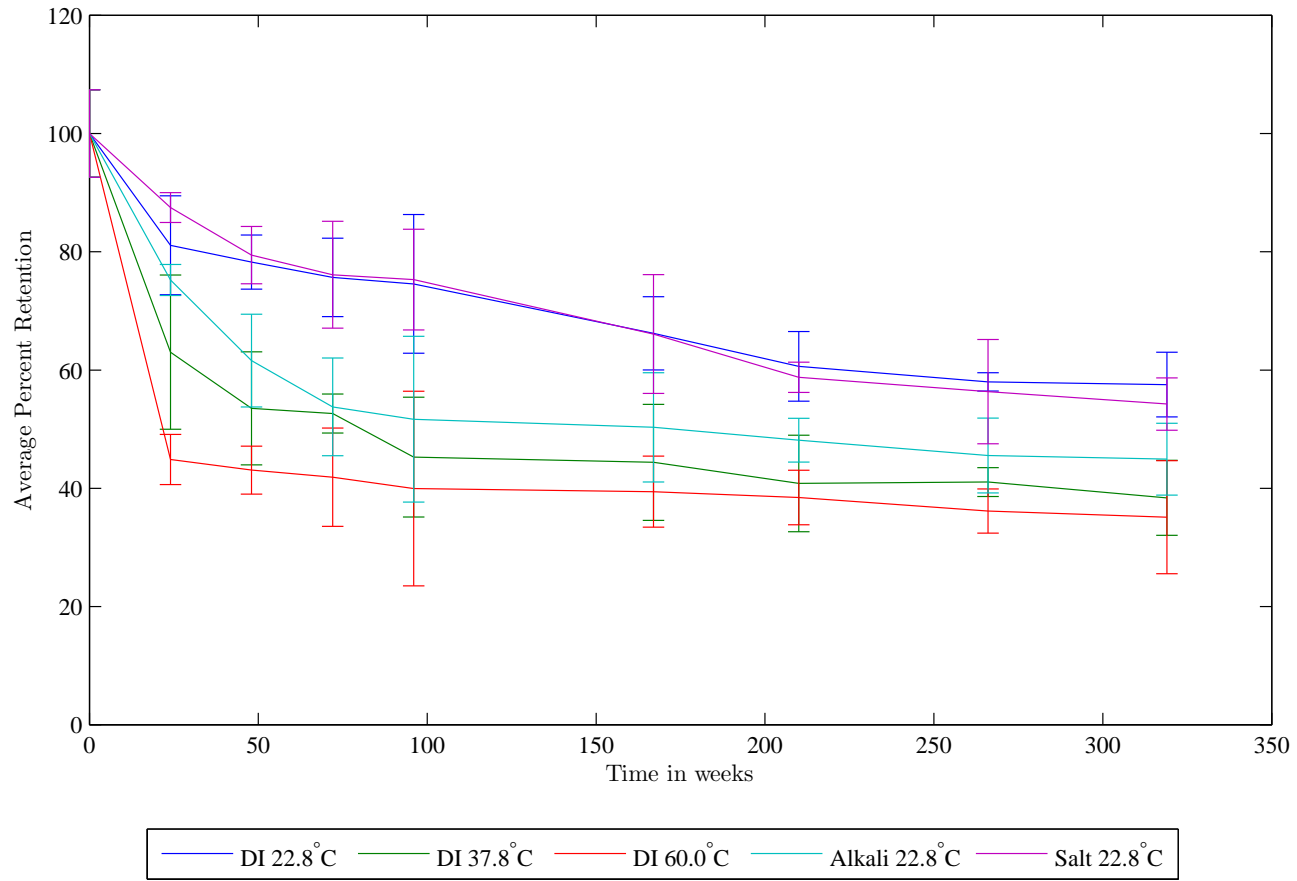


Figure 4.4: Percent Ultimate Strength Retention for Composite

4.3.3 Comparison of Neat Epoxy and Composite

Figures 4.5 and 4.6 show a comparison of the percent retention results between the neat epoxy samples and the fiber reinforced epoxy samples which were immersed in deionized water at 22.8°C. The error bars shown represent plus and minus the coefficient of variation. The coefficient of variation was used here because it is a normalized measure of dispersion. The comparison of modulus retention shown in Figure 4.5 indicates that fiber reinforced epoxy showed higher retention of modulus than the neat epoxy, indicating that the degradation of modulus is primarily a function of the epoxy. Alternatively the comparison of ultimate strength retention, shown in Figure 4.6, indicated the opposite. The neat epoxy retained more strength than the fiber reinforced epoxy indicating that the degradation in strength is primarily driven by the degradation of the fibers.

Please see Appendix E for additional comparisons.

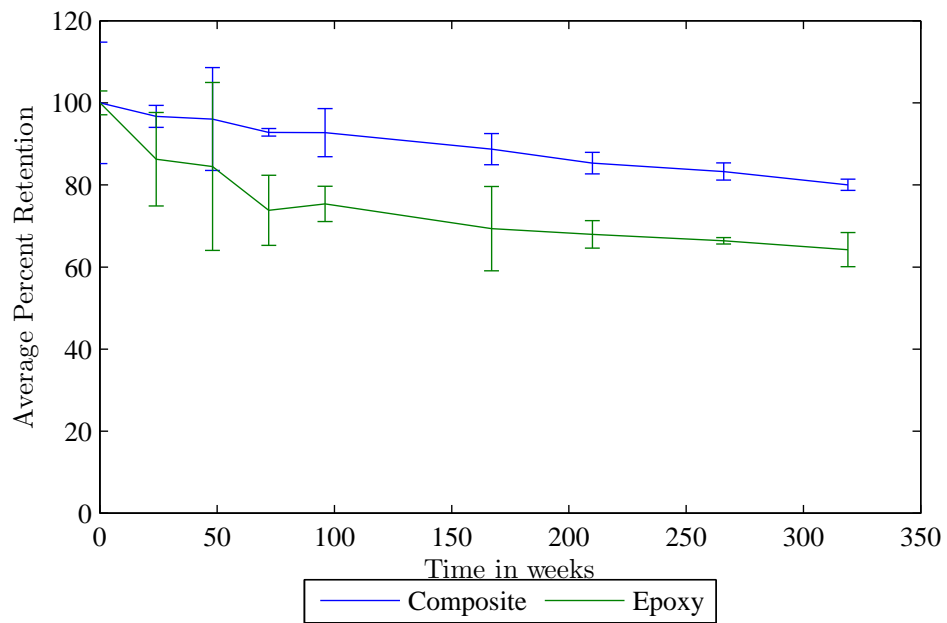


Figure 4.5: Comparison of Modulus Retention for Neat Epoxy and Composite Immersed in Deionized Water

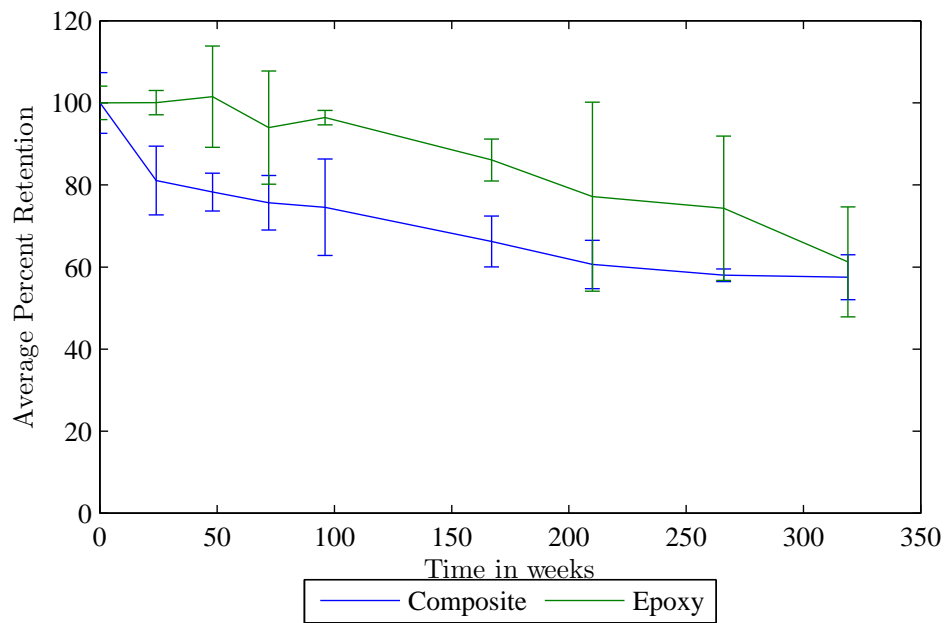


Figure 4.6: Comparison of Strength Retention for Neat Epoxy and Composite Immersed in Deionized Water

4.4 Weibull distribution fit

4.4.1 Procedure for Weibull fit

The Weibull distribution was fit to the test data for this project using the approximations introduced in Section 2.2.4.5. The Weibull shape parameter was found using Equation 2.18, and the Weibull scale parameter was found using Equation 2.16.

4.4.2 Weibull fit results

Tables 4.6, 4.7, 4.8 and 4.9 give the Weibull shape and scale parameters found for the experimental data given in Appendix A using the methods discussed above. Figures 4.7, 4.8, 4.9 and 4.10 show the Weibull shape parameters over exposure time with possible outliers removed. Possible outliers were identified according to ASTM standard E 178 [35], the procedure is outlined in Section 4.2.1. The inherent variability in the raw data prompted the removal of the possible outliers identified.

Table 4.6: Weibull Parameters for Modulus of Glass Fiber Reinforced Epoxy Samples

Time in weeks	Control Sample		Immersion in Deionized Water at						Immersion in Alkaline Solution at		Immersion in Salt Water at	
	22.8°C		22.8°C		37.8°C		60.0°C		22.8°C		22.8°C	
	α	β	α	β	α	β	α	β	α	β	α	β
0	8.11	18.15	8.11	18.15	8.11	18.15	8.11		8.11	18.15	8.11	18.15
24	20.40	18.30	44.62	17.55	25.55	16.26	13.01	16.05	84.93	16.83	47.56	17.23
48	54.89	18.32	9.57	17.43	13.15	15.95	38.70	15.17	35.94	16.32	32.90	17.05
72	27.03	18.43	133.80	16.85	16.92	15.02	12.80	14.66	22.03	15.74	20.26	16.03
96	16.00	18.48	20.49	16.84	27.41	14.66	4.40	14.30	57.02	15.63	18.97	15.86
167	29.54	18.68	31.54	16.11	30.16	14.47	39.85	14.28	38.44	14.90	34.88	15.07
210	49.93	18.68	45.68	15.49	43.02	14.30	34.45	14.08	50.08	14.47	62.10	14.88
266	86.31	18.70	57.24	15.11		14.24	51.04	13.99	47.94	14.23	55.85	14.52
319	33.96	18.71	86.95	14.52	43.50	14.12	28.01	13.93	46.75	14.10	61.26	14.11
Mean	36.24	18.50	48.67	16.45	25.98	15.24	25.60	14.56	43.47	15.60	37.99	15.88
Std. Dev.	24.05	0.21	40.42	1.22	13.00	1.33	16.52	0.72	21.70	1.34	19.80	1.37
Max	86.31	18.71	133.80	18.15	43.50	18.15	51.04	16.05	84.93	18.15	62.10	18.15
Min	8.11	18.15	8.11	14.52	8.11	14.12	4.40	13.93	8.11	14.10	8.11	14.11

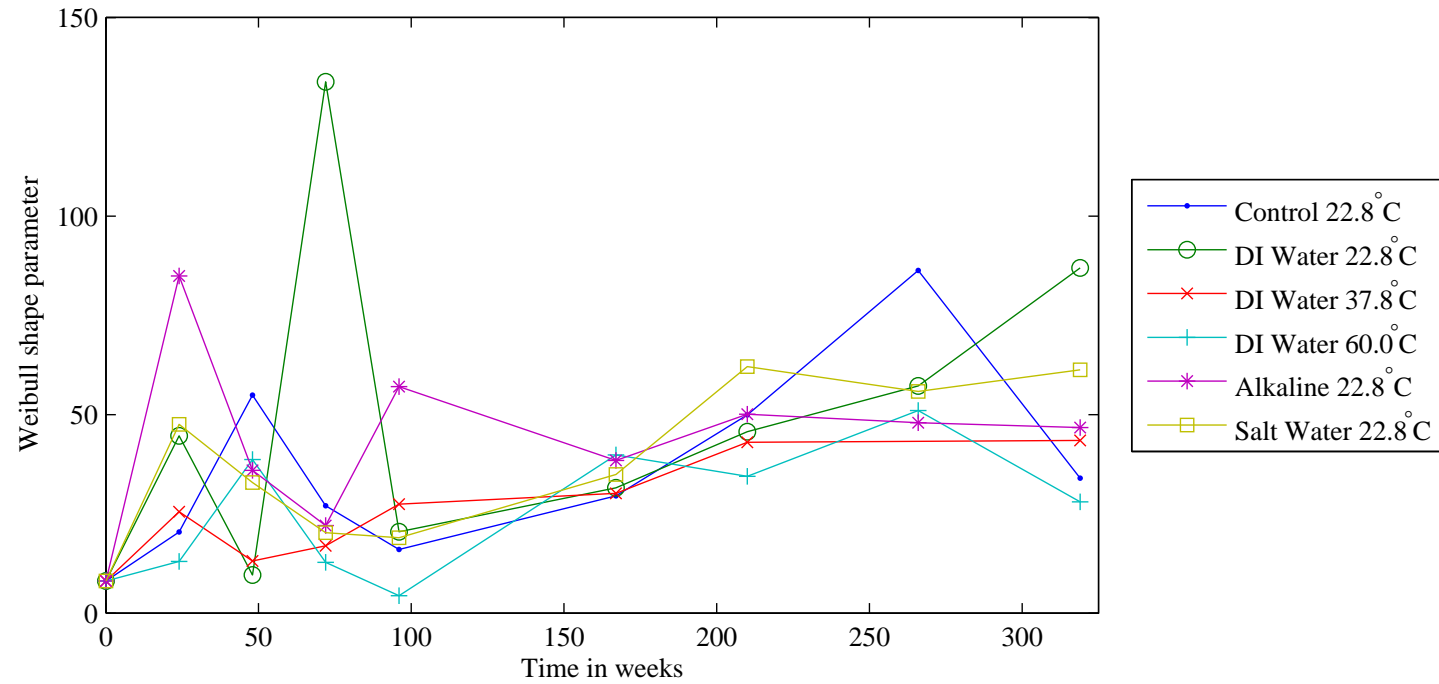


Figure 4.7: Weibull Shape Parameters for Modulus of Glass Fiber Reinforced Epoxy Samples

Table 4.7: Weibull Parameters for Ultimate Strength of Glass Fiber Reinforced Epoxy Samples

Time in weeks	Control Sample		Immersion in Deionized Water at						Immersion in Alkaline Solution at		Immersion in Salt Water at	
	22.8°C		22.8°C		37.8°C		60.0°C		22.8°C		22.8°C	
	α	β	α	β	α	β	α	β	α	β	α	β
0	16.22	345.75	16.22	345.75	16.22		16.22		16.22		16.22	345.75
24	11.15	331.42	14.34	280.42	9.20	217.88	28.35	155.16	45.86	260.14	47.40	302.46
48	9.79	337.19	26.16	270.58	12.56	185.08	29.65	148.92	15.29	212.98	24.67	274.67
72	31.66	340.65	18.08	261.64	36.25	182.04	14.44	144.76	14.53	185.86	13.29	263.19
96	37.08	343.26	10.23	257.82	11.85	156.57	7.29	138.08	8.56	178.67	14.10	260.40
167	23.01	344.86	19.35	228.96	12.23	153.45	19.94	136.35	12.98	173.99	11.96	228.52
210	21.26	351.37	20.32	209.64	14.71	141.13	26.03	132.90	32.43	166.42	46.63	203.20
266	20.40	357.30		200.54	49.10	141.93	32.05	124.98	18.97	157.49	13.61	194.86
319	15.93	358.94	21.93	198.91	18.94	132.71	12.55	121.43	19.75	155.36	27.08	187.57
Mean	20.72	345.64	18.33	250.47	20.12	163.85	20.73	137.82	20.51	186.36	23.88	251.18
Std Dev	8.99	9.02	4.86	47.22	13.48	28.86	8.67	11.54	11.56	34.96	14.12	52.90
Max	37.08	358.94	26.16	345.75	49.10	217.88	32.05	155.16	45.86	260.14	47.40	345.75
Min	9.79	331.42	10.23	198.91	9.20	132.71	7.29	121.43	8.56	155.36	11.96	187.57

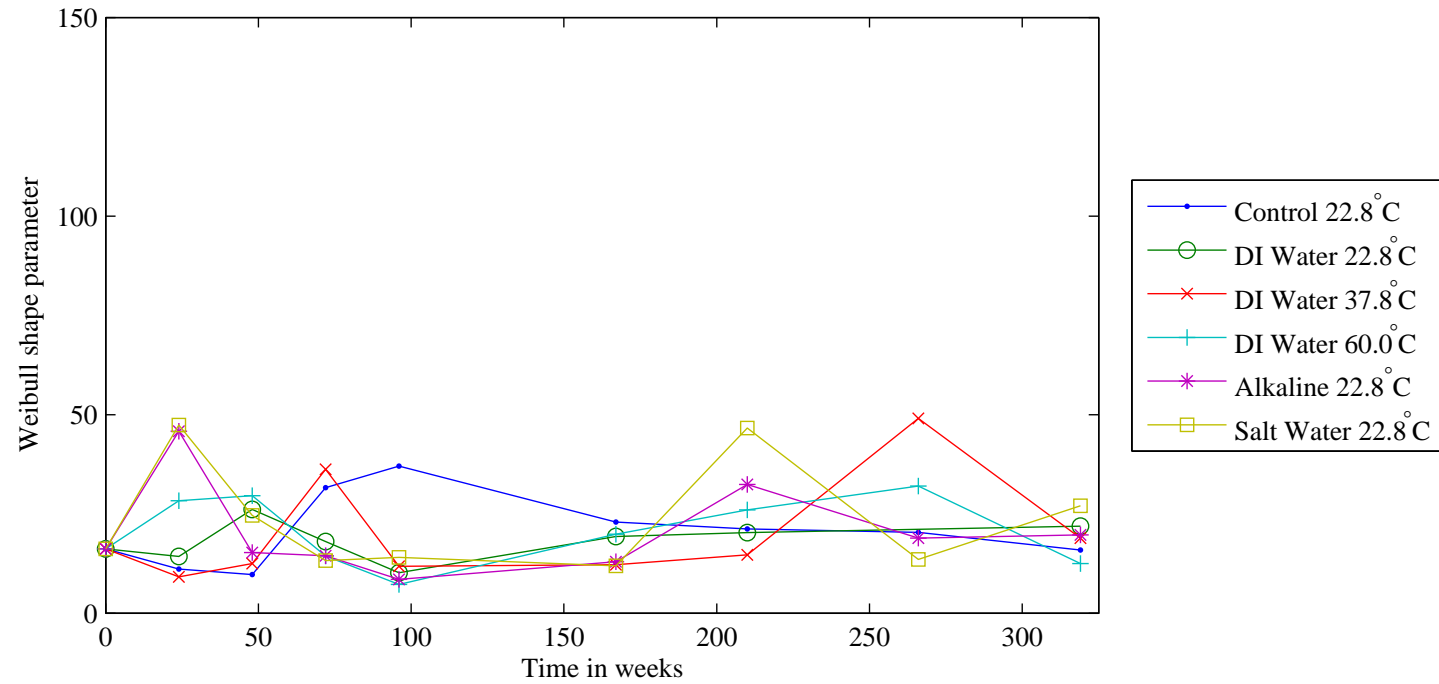


Figure 4.8: Weibull Shape Parameters for Ultimate Strength of Glass Fiber Reinforced Epoxy Samples

Table 4.8: Weibull Parameters for Modulus of Neat Epoxy Samples

Time in weeks	Control Sample		Immersion in Deionized Water at						Immersion in Alkaline Solution at		Immersion in Salt Water at	
	22.8°C		22.8°C		37.8°C		60.0°C		22.8°C		22.8°C	
	α	β	α	β	α	β	α	β	α	β	α	β
0			41.51	3.29	41.51				41.51	3.29	41.51	3.29
24	13.27	3.46	10.53	2.84	12.73	2.57	12.62	2.24	27.37	2.72	15.65	2.72
48	12.92	3.43	5.86	2.78	18.06	2.51	12.66	2.09	26.19	2.70	13.06	2.63
72	26.05	3.54	14.05	2.43	27.04	2.20	14.45	1.89	9.68	2.32	21.93	2.42
96	15.59	3.56	27.97	2.48	27.74	2.31	5.63	1.80	9.97	2.32	11.02	2.32
167	20.69	3.56	11.68	2.28	41.90	2.13	7.80	1.73	15.29	2.21	16.30	2.15
209	23.05	3.51	35.73	2.23	26.69	2.10	7.36	1.68	25.11	2.19	33.69	2.11
264	14.63	3.50		2.18	18.32	2.06	9.22	1.62	11.23	2.09	13.72	2.06
312	24.19	3.50	28.80	2.11	20.20	2.04	12.48	1.57	33.49	2.07	13.87	1.97
Mean	18.80	3.51	22.02	2.51	26.02	2.24	10.28	1.83	22.20	2.43	20.08	2.41
Std Dev	5.29	0.05	13.16	0.39	10.18	0.20	3.18	0.23	11.32	0.40	10.56	0.42
Max	26.05	3.56	41.51	3.29	41.90	2.57	14.45	2.24	41.51	3.29	41.51	3.29
Min	12.92	3.43	5.86	2.11	12.73	2.04	5.63	1.57	9.68	2.07	11.02	1.97

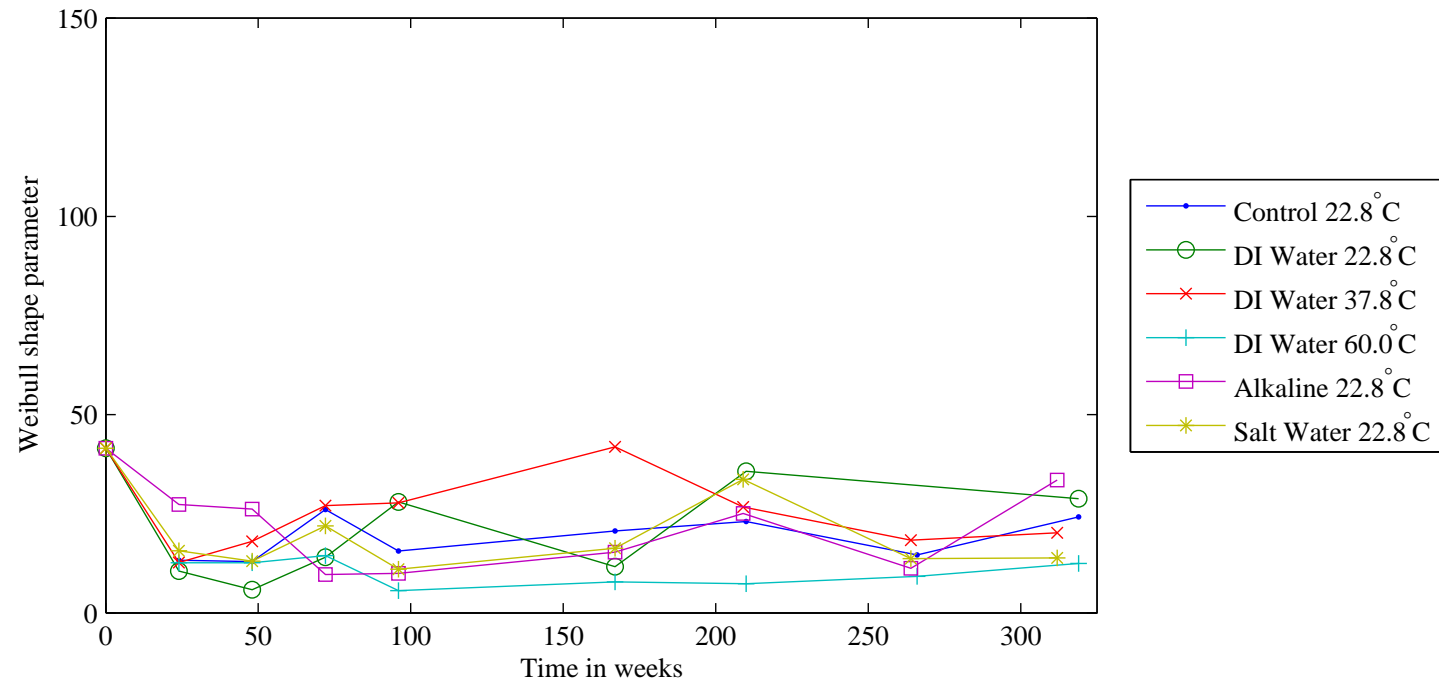


Figure 4.9: Weibull Shape Parameters for Modulus of Neat Epoxy Samples

Table 4.9: Weibull Parameters for Ultimate Strength of Neat Epoxy Samples

Time in weeks	Control Sample		Immersion in Deionized Water at						Immersion in Alkaline Solution at		Immersion in Salt Water at	
	22.8°C		22.8°C		37.8°C		60.0°C		22.8°C		22.8°C	
	α	β	α	β	α	β	α	β	α	β	α	β
0	29.37	44.19	29.37	44.19	29.37	44.19	29.37	44.19	29.37	44.19	29.37	44.19
24	20.92	45.23	40.60	44.23	17.66	44.08	37.01	42.75	38.07	45.46	22.12	45.43
48	14.15	48.45	9.74	44.86	11.30	43.52	21.58	42.55	6.52	43.97	13.87	44.98
72	22.17	0.00	8.70	41.53	20.18	41.13	9.55	35.89	31.29	38.01	9.83	40.87
96	13.96	46.71	68.58	42.61	13.36	38.23	13.83	31.76	13.12	37.52	13.65	39.98
167	21.52	46.53	23.48	38.04	11.20	34.72	17.26	28.27	9.66	35.16	17.48	36.93
209	14.97	45.98	5.21	34.10	7.37	29.18	5.69	23.89	5.43	33.33	5.76	34.50
264	25.22	46.36	6.82	32.84	11.27	26.90	7.44	20.32	9.02	29.32	4.02	30.34
312	15.62	45.43	8.95	27.07	4.46	21.48	12.84	18.68	5.90	25.41	5.88	26.59
Mean	19.77	46.11	22.38	38.83	14.02	35.94	17.17	32.03	16.49	36.93	13.56	38.20
Std Dev	5.45	1.26	21.16	6.25	7.47	8.38	10.47	9.90	12.74	6.92	8.39	6.67
Max	29.37	48.45	68.58	44.86	29.37	44.19	37.01	44.19	38.07	45.46	29.37	45.43
Min	13.96	44.19	5.21	27.07	4.46	21.48	5.69	18.68	5.43	25.41	4.02	26.59

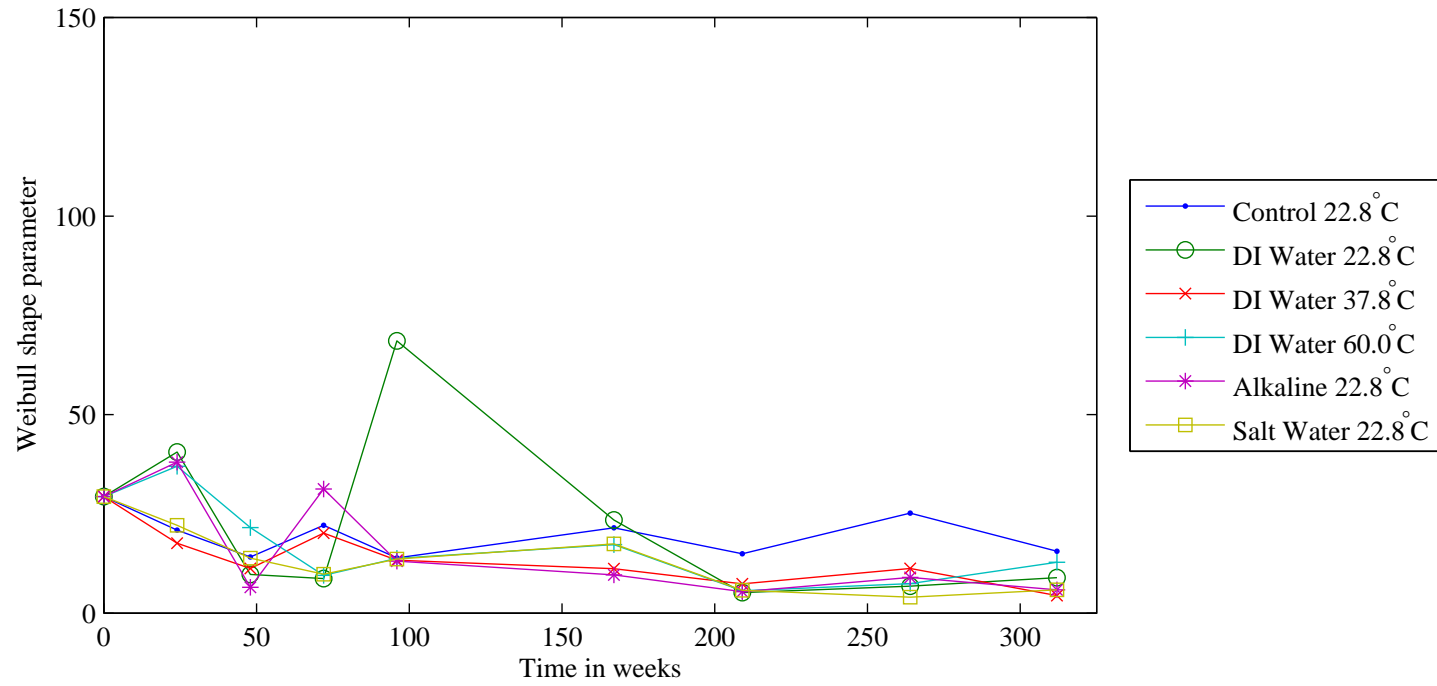


Figure 4.10: Weibull Shape Parameters for Ultimate Strength of Neat Epoxy Samples

4.4.3 ANOVA of Weibull Shape Parameters

An Analysis of Variance was performed in order to identify statistically significant differences in the values found for the Weibull shape parameter over time, and for the varying exposure conditions used for this research. Tables 4.10 and 4.11 provide a summary of the ANOVA results, complete details are provided in Appendix C.

Table 4.10 provides the results for the ANOVA comparing the Weibull shape parameter estimates for the five exposure conditions for the ultimate strength, and modulus for each the neat epoxy, and the glass fiber reinforced epoxy. These results indicate that there is not a statistically significant difference in Weibull shape parameters for the five exposure conditions, except in the case of the exposure to deionized water at $60.0^{\circ}C$ for the modulus of the neat epoxy. For this case the shape parameters tend to be lower than for the other exposure conditions. The lower values for the shape parameter indicate that there was more scatter in the data. The ANOVA was run a second time for the neat epoxy modulus with the values for exposure to deionized water at $60.0^{\circ}C$ removed, and the results indicate that there is not a statistically significant difference in the shape parameter values for the remaining four exposure conditions.

Table 4.11 provides the results for the ANOVA comparing the Weibull shape parameters over time. These results indicate that there is not a statistically significant difference in the shape parameters over time, with the exception of the shape parameters for the ultimate strength of the neat epoxy. The values of the shape

Table 4.10: Analysis of Variance Summary for Comparison of Weibull Shape Parameters for Exposure Conditions

ANOVA: Epoxy Modulus					
Source	DF	SS	MS	F	P
Factor	5	1169.8	234.0	2.49	0.045
Error	45	4227.4	93.9		
Total	50	5397.2			

ANOVA: Epoxy Strength					
Source	DF	SS	MS	F	P
Factor	5	516	103	0.71	0.621
Error	48	7002	146		
Total	53	7519			

ANOVA: Composite Modulus					
Source	DF	SS	MS	F	P
Factor	5	3746	749	1.26	0.298
Error	47	27975	595		
Total	52	31720			

ANOVA: Composite Strength					
Source	DF	SS	MS	F	P
Factor	5	139	28	0.24	0.944
Error	47	5531	118		
Total	52	5671			

parameters for the ultimate strength of the neat epoxy show a slight decrease over time, indicating an increase in the variability of the results over time.

4.4.4 Verification of Weibull fit

The Weibull parameters found using the method described previously were compared with parameter estimates generated by the statistical analysis software Minitab 15. The estimates generated by Minitab 15 were the result of a least squares estimation. This comparison showed good correlation between the two estimation methods. The calculated parameter values all fell within the ninety-five percent

Table 4.11: Analysis of Variance Summary for Comparison Weibull Shape Parameters Over Time

ANOVA: Epoxy Modulus versus Time					
Source	DF	SS	MS	F	P
Time	7	814.9	116.4	1.89	0.104
Error	31	1904.6	61.4		
Total	38	2719.6			

ANOVA: Epoxy Strength versus Time					
Source	DF	SS	MS	F	P
Time	8	2512	314	2.99	0.010
Error	40	4194	105		
Total	48	6706			

ANOVA: Composite Modulus versus Time					
Source	DF	SS	MS	F	P
Time	8	6140	768	1.42	0.220
Error	39	21126	542		
Total	47	27266			

ANOVA: Composite Strength versus Time					
Source	DF	SS	MS	F	P
Time	8	923	115	0.97	0.473
Error	39	4634	119		
Total	47	5557			

confidence interval for the parameter estimated generated by Minitab, indicating that the difference between the estimates is not statistically significant, with a significance level of ninety-five percent.

4.4.5 Comparison of Weibull Parameters with Published Values

Table 4.12: Comparison of Weibull Values for Ultimate Tensile Strength with Published Values

Specimen	α	β	Source
E-glass/epoxy	61.8	595.3	Bhise <i>et al.</i> , in Jackson []
E-glass/epoxy	10.2	938.4	Okeil <i>et al.</i> , in Jackson []
E-Glass single fiber	6.0	3690.0	Anderson <i>et al.</i> , []
E-glass fiber bundle	4.6	5235.0	Anderson <i>et al.</i> , []
E-glass/epoxy	20.5	875.9	Sun <i>et al.</i> , in Philippidis <i>et al.</i> , []
E-glass/epoxy	20.7	345.6	Table 4.7

4.5 Predictions of long-term material response

4.5.1 Accelerated Degradation Model Used for This Project

This thesis uses the Arrhenius time-temperature acceleration model, as introduced in Section 2.2.3, to predict the long-term material response of a glass-fiber and epoxy FRP after exposure to deionized water, salt water, and an alkaline solution.

4.5.2 Procedure for predicting future response with an Arrhenius model

The procedure used for applying the Arrhenius degradation model in this experiment is graphical. It utilizes linear regression techniques to find slope and intercept values for the data points. To illustrate the process details of applying the Arrhenius model to the modulus data for the composite sample will be explained. The process begins with the percent retention data for a series of temperatures, in this case, as an example, the data from exposure to deionized water at 22.8°C, 37.8°C, and 60.0°C, as can be seen in Figure 4.11.

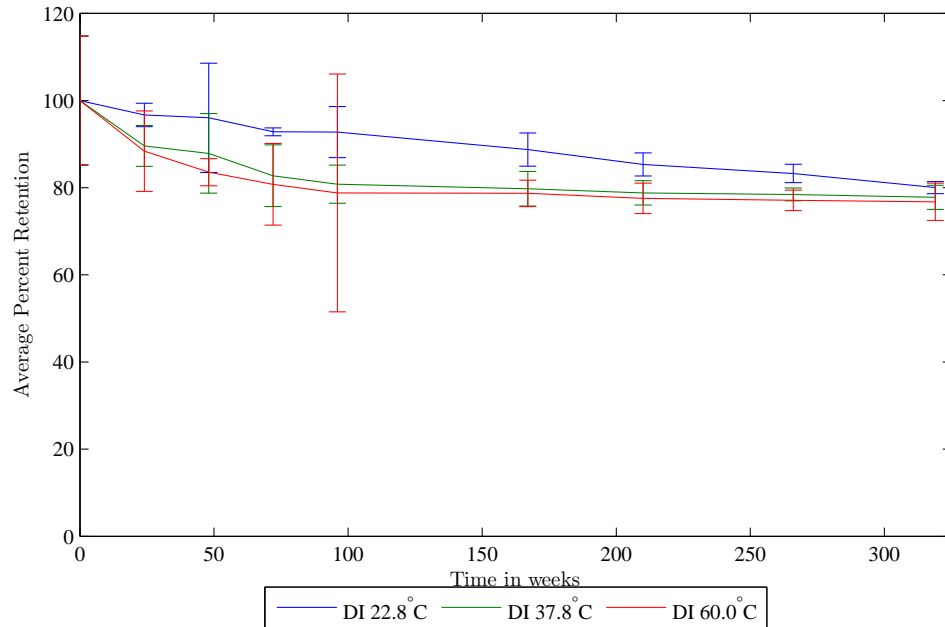


Figure 4.11: Percent Retention of Modulus in Composite

The first step is to plot the percent retention data on a semi-log scale, which should result in a linear relationship. This is one of the vital assumptions associated with the Arrhenius model, if this relationship is not linear than the accuracy of the predictions is greatly reduced. Then linear regression lines are found for each of the temperature exposures. This can be seen in Figure 4.12, and in Table 4.13. These equations give the percent retention of modulus of the FRP as a function of time for exposure due to immersion in deionized water at 22.8°C, 37.8°C, and 60.0°C.

The equations in Table 4.13 are then used to predict percent retention to the time of interest, in this case one hundred years, for each of the temperatures. These values are then plotted on an Arrhenius plot, and linear regression lines determined. The results of this step can be seen in Figure 4.13 and in Table 4.14.

Table 4.13: Arrhenius step 1: Regression equations for Composite Modulus

Temperature	Equation
22.8°C	$\frac{E}{E_0} = (-0.0220 \ln t + 1.0365)$
37.8°C	$\frac{E}{E_0} = (-0.0297 \ln t + 1.0154)$
60.0°C	$\frac{E}{E_0} = (-0.0313 \ln t + 1.0093)$

Table 4.14: Arrhenius step 2: Regression equations for Retention versus inverse temperature Composite Modulus

Time in years	Equation
0	$\frac{E}{E_0} = (0.0697(\frac{1000}{T}) + 0.7974)$
0.5	$\frac{E}{E_0} = (0.1936(\frac{1000}{T}) + 0.2571)$
1	$\frac{E}{E_0} = (0.2101(\frac{1000}{T}) + 0.1852)$
1.5	$\frac{E}{E_0} = (0.2198(\frac{1000}{T}) + 0.1431)$
2	$\frac{E}{E_0} = (0.2266(\frac{1000}{T}) + 0.1132)$
2.5	$\frac{E}{E_0} = (0.2319(\frac{1000}{T}) + 0.0901)$
5	$\frac{E}{E_0} = (0.2483(\frac{1000}{T}) + 0.0181)$
10	$\frac{E}{E_0} = (0.2649(\frac{1000}{T}) - 0.0538)$
15	$\frac{E}{E_0} = (0.2745(\frac{1000}{T}) - 0.0959)$
20	$\frac{E}{E_0} = (0.2814(\frac{1000}{T}) - 0.1257)$
25	$\frac{E}{E_0} = (0.2867(\frac{1000}{T}) - 0.1489)$
30	$\frac{E}{E_0} = (0.2910(\frac{1000}{T}) - 0.1678)$
35	$\frac{E}{E_0} = (0.2947(\frac{1000}{T}) - 0.1838)$
40	$\frac{E}{E_0} = (0.2979(\frac{1000}{T}) - 0.1976)$
45	$\frac{E}{E_0} = (0.3007(\frac{1000}{T}) - 0.2099)$
50	$\frac{E}{E_0} = (0.3032(\frac{1000}{T}) - 0.2208)$
55	$\frac{E}{E_0} = (0.3055(\frac{1000}{T}) - 0.2307)$
60	$\frac{E}{E_0} = (0.3075(\frac{1000}{T}) - 0.2397)$
65	$\frac{E}{E_0} = (0.3094(\frac{1000}{T}) - 0.2480)$
70	$\frac{E}{E_0} = (0.3112(\frac{1000}{T}) - 0.2557)$
75	$\frac{E}{E_0} = (0.3128(\frac{1000}{T}) - 0.2629)$
80	$\frac{E}{E_0} = (0.3144(\frac{1000}{T}) - 0.2696)$
85	$\frac{E}{E_0} = (0.3158(\frac{1000}{T}) - 0.2758)$
90	$\frac{E}{E_0} = (0.3172(\frac{1000}{T}) - 0.2818)$
95	$\frac{E}{E_0} = (0.3185(\frac{1000}{T}) - 0.2874)$
100	$\frac{E}{E_0} = (0.3197(\frac{1000}{T}) - 0.2927)$

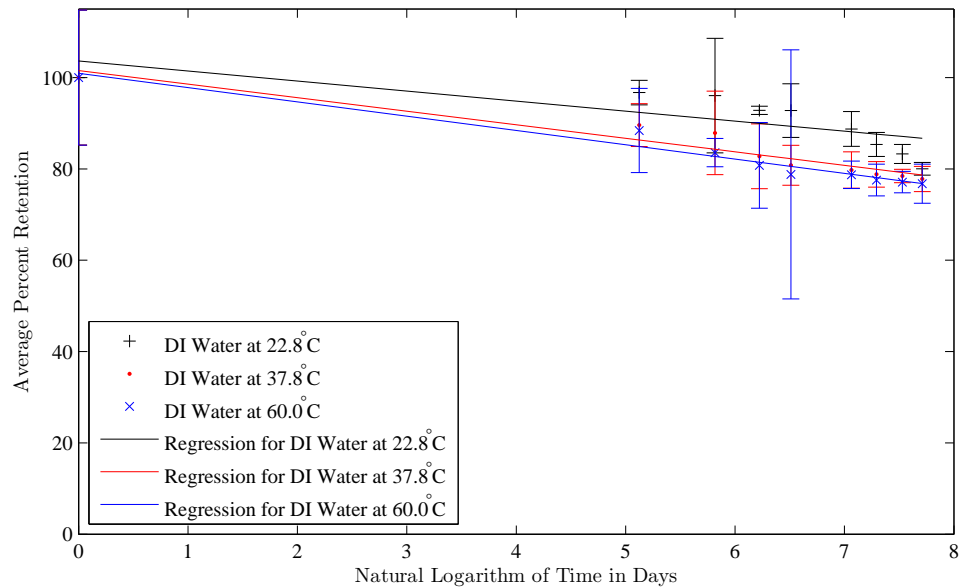


Figure 4.12: Arrhenius step 1: Linear Regression of data for Composite Modulus

The equations in Table 4.14 can be used to determine values at a desired temperature, these values can then be plotted to produce a predictive curve for the desired temperature, in this case the design temperature is 22.8°C . This plot is shown in Figure 4.14.

As can be seen in Figure 4.14 the test data indicates the material degradation is more severe than is indicated by the model. This inconsistency is most likely due to room temperature exposure results skewing the Arrhenius predictions to levels higher than was seen in the room temperature tests. Table 4.15 Shows a comparison between the experimental results and the initial predictive results, and the percent difference between. The last three percent difference entries in Table 4.15 also illustrate the inconsistency between the predictive model and the experimental data. In order to

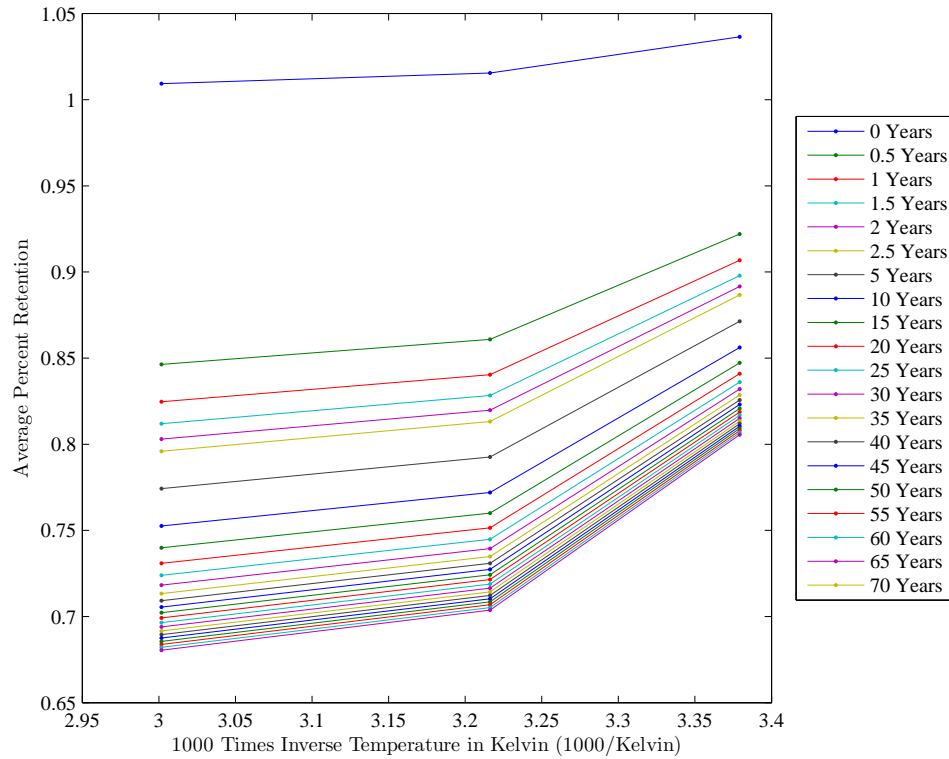


Figure 4.13: Arrhenius step 2: Percent Retention versus inverse temperature for Composite Modulus

Table 4.15: Comparison of Arrhenius Predictions to Test data

Time		Percent Retention		
Years	Weeks	Experimental	Theoretical	Percent Difference
0.00	0	100.00%	103.30%	3.30%
0.46	24	96.71%	91.33%	5.38%
0.92	48	96.05%	89.71%	6.34%
1.38	72	92.83%	88.76%	4.07%
1.85	96	92.77%	88.09%	4.68%
3.21	167	88.75%	86.80%	1.96%
4.04	210	85.34%	86.26%	-0.92%
5.12	266	83.27%	85.71%	-2.44%
6.13	319	80.03%	85.28%	-5.25%

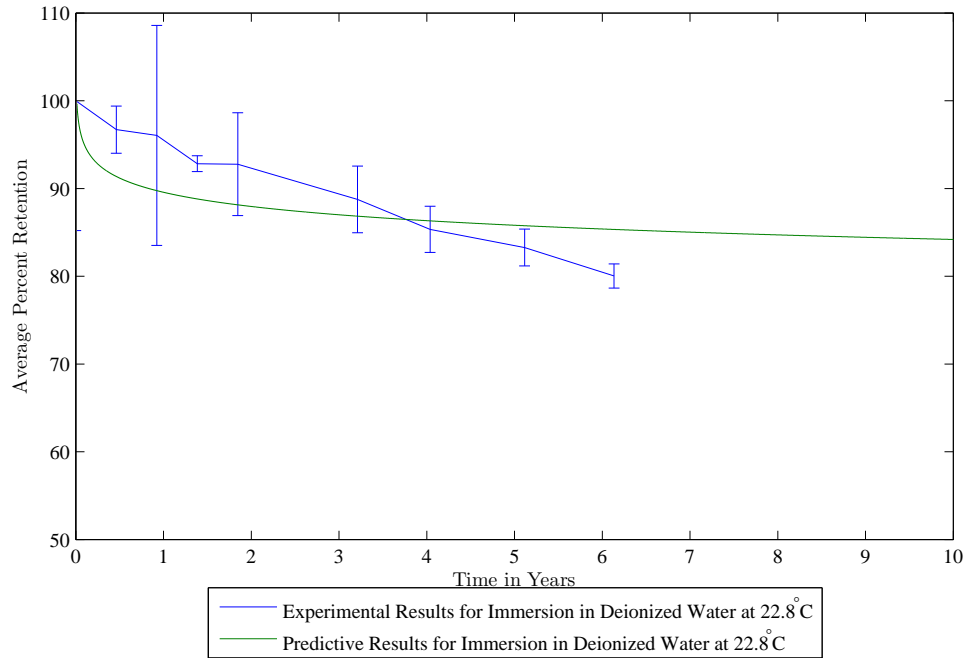


Figure 4.14: Arrhenius step 3: Arrhenius prediction for Composite Modulus

correct for this inconsistency, the room temperature results, 22.8°C , were removed and the Arrhenius prediction was performed again. The results of this revised prediction compared with the experimental results and the original prediction can be found in Figure 4.15; the revised prediction indicates a more extreme initial degradation than is seen in the experimental results, yielding a more conservative prediction. Table 4.16 gives a comparison of experimental and theoretical results for the revised Arrhenius prediction. Figure 4.16 gives the revised prediction results for the modulus of the E-glass reinforced epoxy to one hundred years.

Appendix D contains the details of the Arrhenius models for each the modulus and ultimate strength for the neat epoxy and the GFRP.

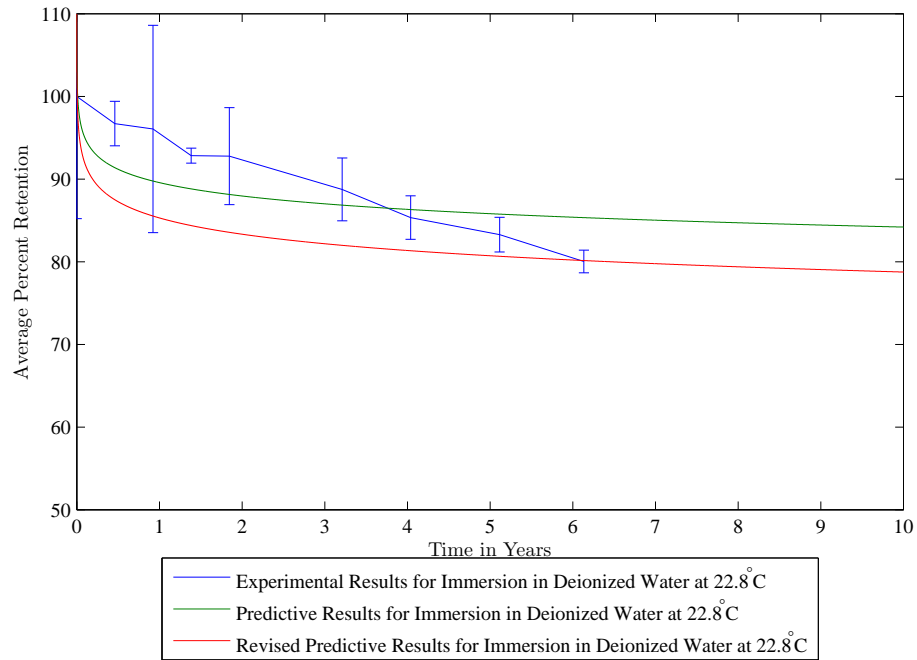


Figure 4.15: Revised Arrhenius Prediction for Composite Modulus, short term

Table 4.16: Comparison of Arrhenius Predictions to Test data

Time		Percent Retention		
Years	Weeks	Experimental	Theoretical	Difference
0.00	0	100.00%	102.01%	2.01%
0.46	24	89.60%	87.44%	2.16%
0.92	48	87.88%	85.47%	2.42%
1.38	72	82.75%	84.31%	1.56%
1.85	96	80.80%	83.50%	2.70%
3.21	167	79.76%	81.92%	2.17%
4.04	210	78.81%	81.27%	2.46%
5.12	266	78.45%	80.60%	2.15%
6.13	319	77.79%	80.08%	2.29%

4.5.3 Arrhenius Predictive Results

Figures 4.16, 4.17, 4.18 and 4.19 shown the Arrhenius predictions, the revised Arrhenius predictions, and the experimental data for the percent retention of modulus and ultimate strength for the neat epoxy, and for the GFRP. As the figures show the Arrhenius model gives a more conservative prediction for the experimental data for the composite samples than it does for the neat epoxy samples. The poor fit calls into question some of the assumptions made previously in this study. Specifically in the case of the ultimate strength of the neat epoxy, the assumption of the linearity of the semi-log plot of percent retention made in Section 4.5.2 is questionable. The linear regression for this step produced R^2 values between 35% and 55%, indicating that a linear fit is not ideal.

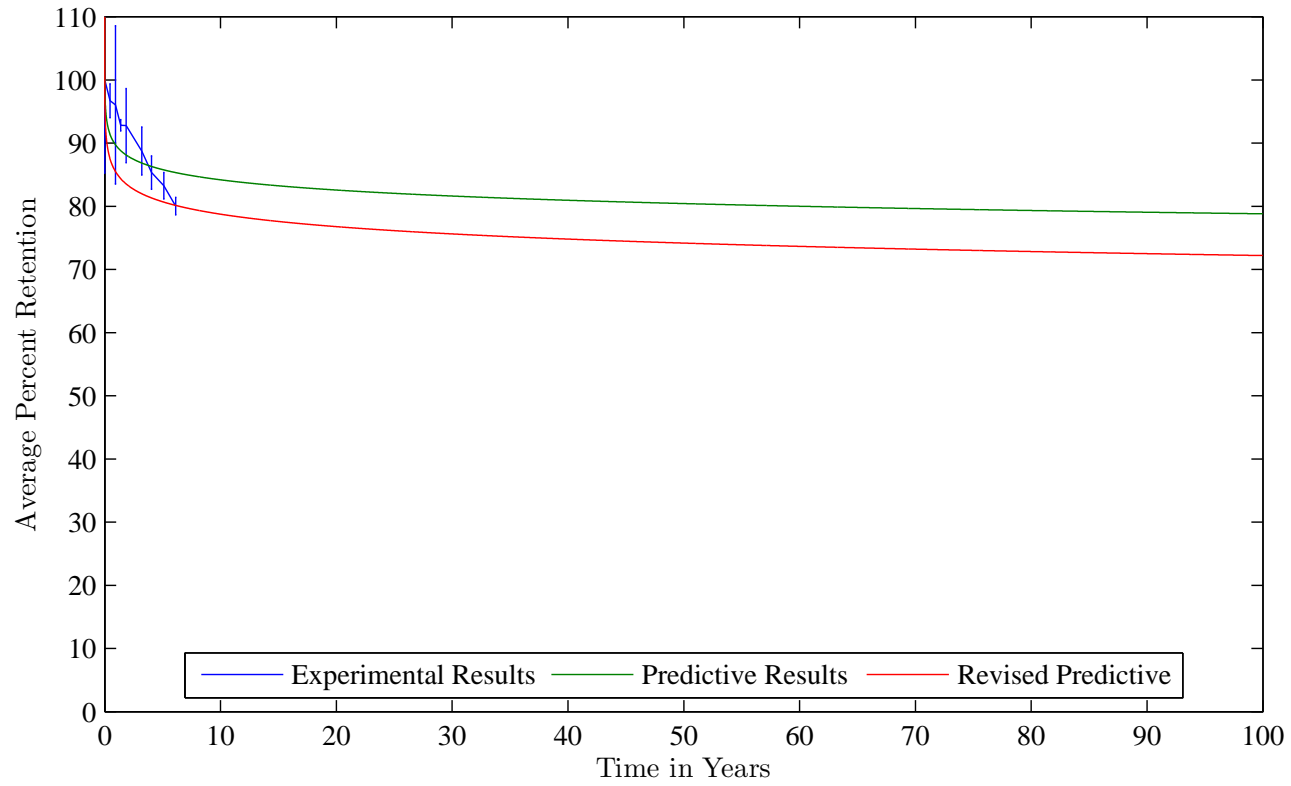


Figure 4.16: Revised Arrhenius Prediction for GFRP Modulus After Immersion in Deionized Water at 22.8°C

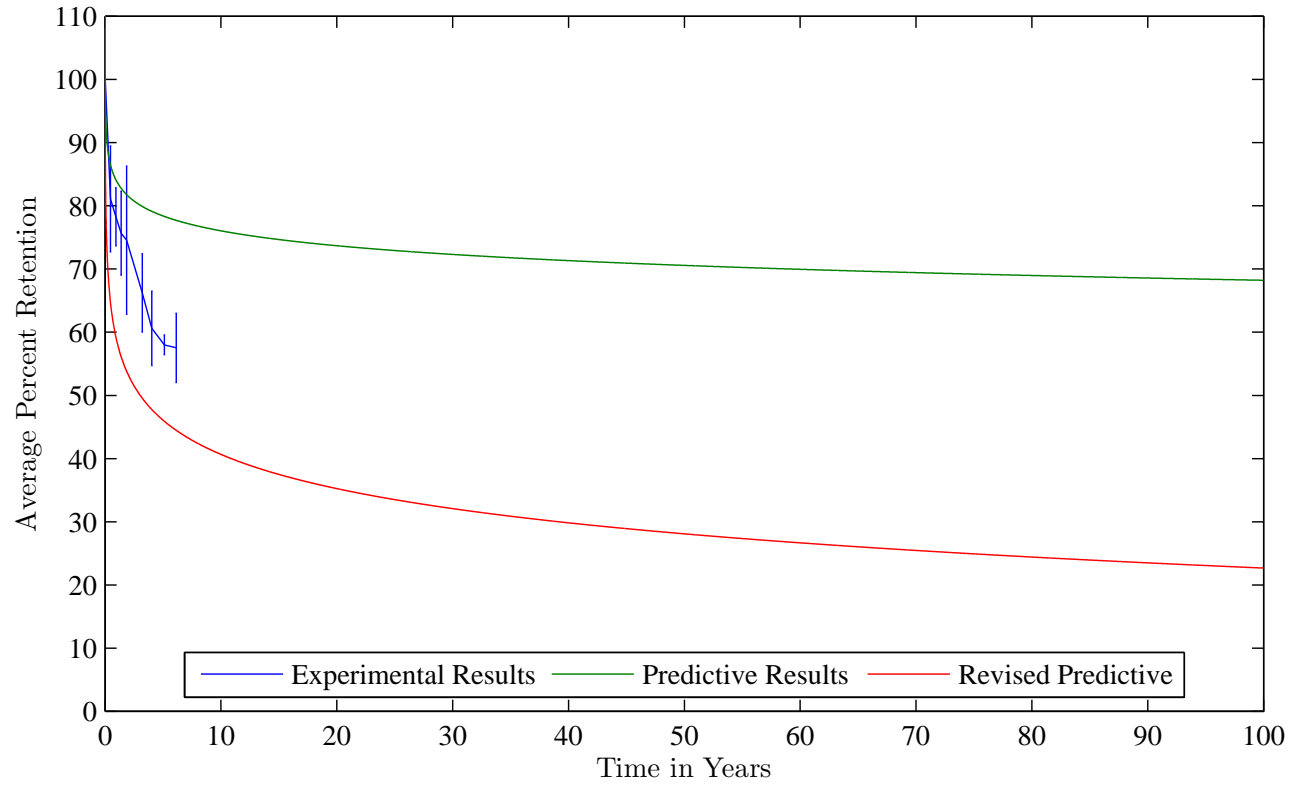


Figure 4.17: Arrhenius Prediction for Ultimate Strength of GFRP After Immersion in Deionized Water at 22.8°C

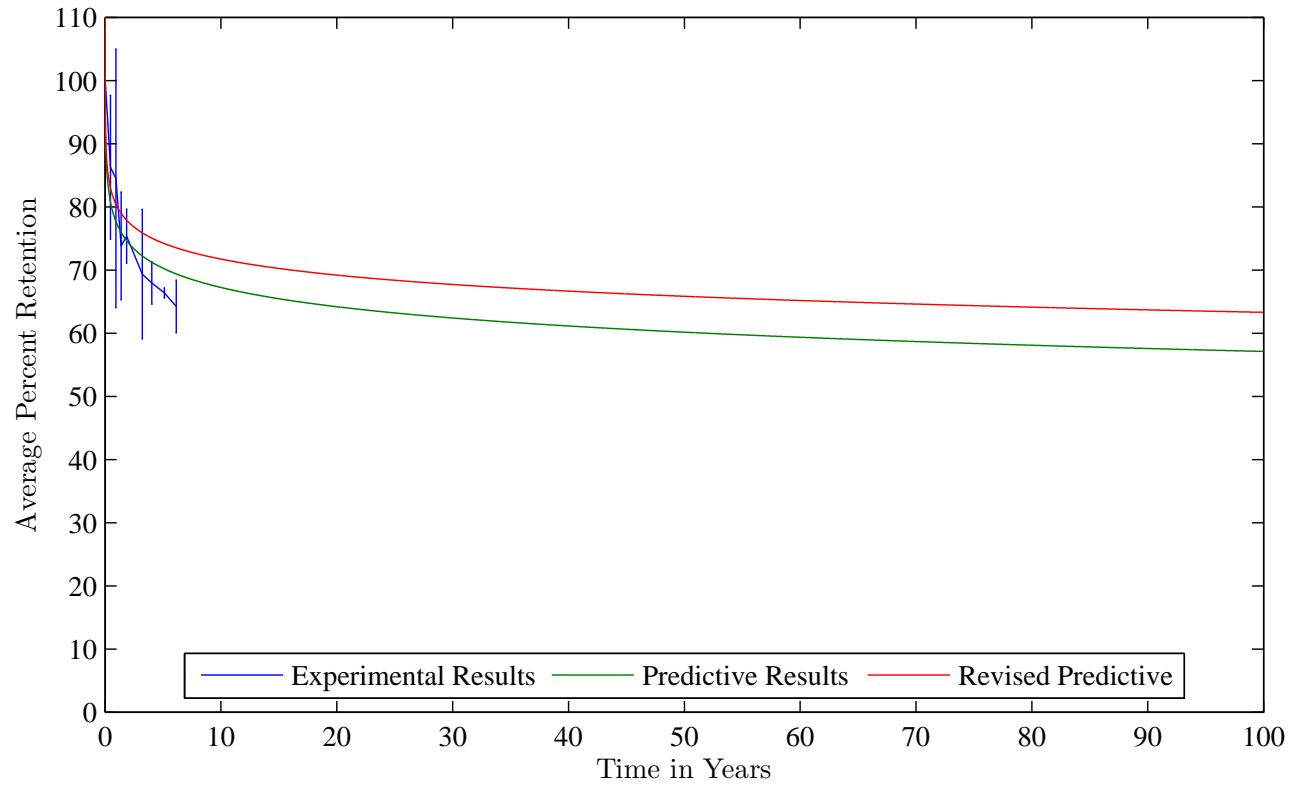


Figure 4.18: Arrhenius Prediction for Modulus of Epoxy After Immersion in Deionized Water at 22.8°C

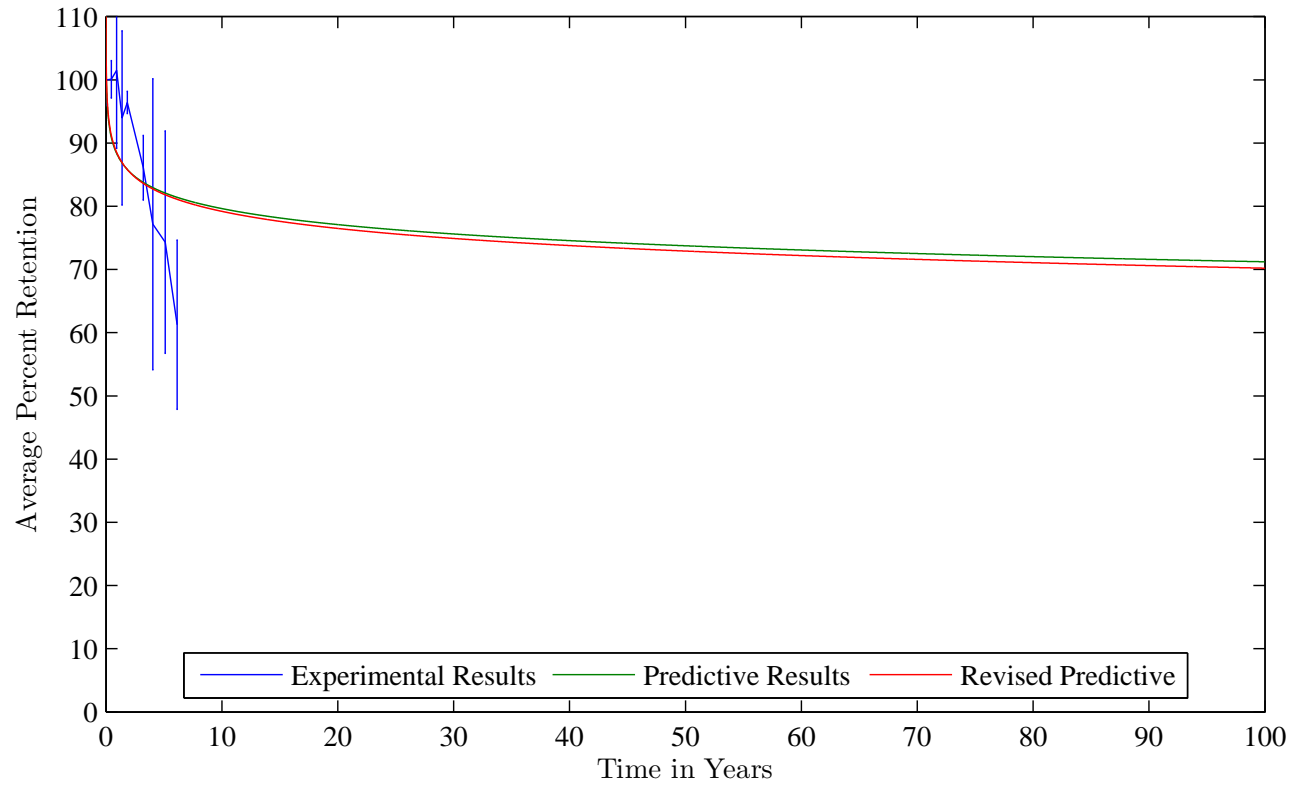


Figure 4.19: Arrhenius Prediction for Ultimate Strength of Epoxy After Immersion in Deionized Water at 22.8°C

Table 4.17: Final Predictive Equations

	Equation
Epoxy Modulus	$E = \frac{E_0}{100} (-0.0366 \ln t + 1.0166)$
Composite Modulus	$E = \frac{E_0}{100} (-0.0284 \ln t + 1.0201)$
Epoxy Ultimate Strength	$\sigma = \frac{\sigma_0}{100} (-0.0390 \ln t + 1.1113)$
Composite Ultimate Strength	$\sigma = \frac{\sigma_0}{100} (-0.0781 \ln t + 1.0457)$

4.6 Extended Arrhenius model

As can be seen in the plots of percent retention, Figures 4.1, 4.2, 4.3 and 4.4, the material degradation begins to show a near asymptotic stage as the exposure time increases. If the assumption is made that the degradation for each of the exposure conditions does approach an asymptote after an initial degradation period, then the results of one condition can be found from the results of another through the use of a constant multiplicative factor, the exposure correction factor $C_{exposure}$. By using this factor the predictive equations developed in Section 4.5.2 for exposure to deionized water can be extended to include exposure to alkaline and salt water solutions.

The extended predictive equations are of the form of Equation 4.5.

$$P_{exposure} = \frac{C_{exposure}P_0}{100}(B \ln t + C) \quad (4.5)$$

Where $P_{exposure}$ is the material property P under the given exposure condition, $C_{exposure}$ is the exposure correction factor, P_0 is the material property before exposure and $(B \ln t + C)$ is the predictive equation based on the accelerated test results from Table 4.14. The exposure correction factor, $C_{exposure}$, is found using Equation 4.6.

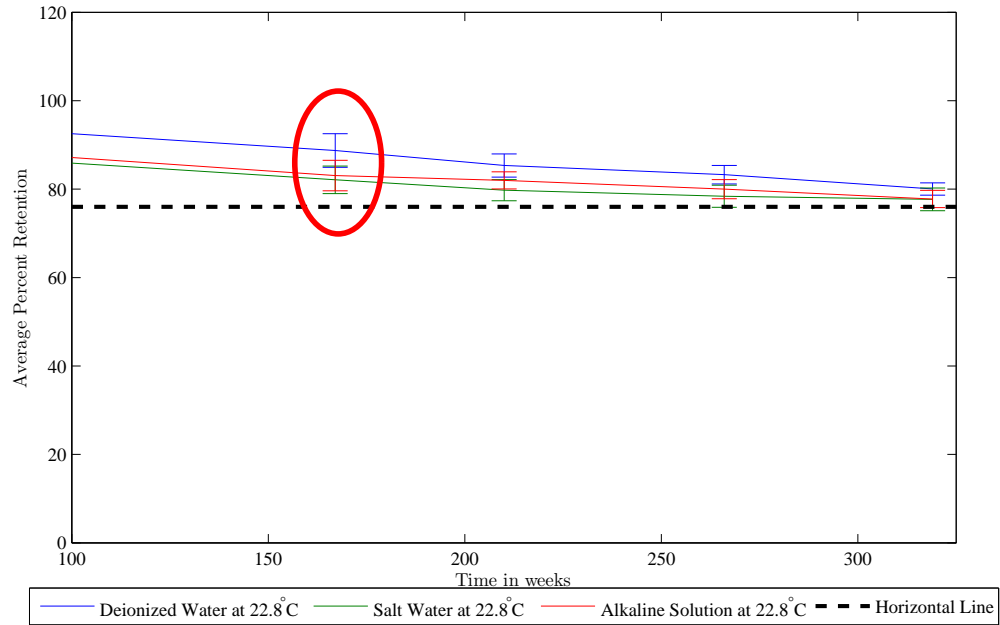


Figure 4.20: Asymptotic Section for Modulus of GFRP

$$C_{exposure} = \frac{\mu_{exposure}}{\mu_{water}} \quad (4.6)$$

Where $\mu_{exposure}$ is the mean percent retention of the ‘asymptotic’ section of the data, and μ_{water} is the mean percent retention of the ‘asymptotic’ section of the data for immersion in deionized water at 22.8°C. The asymptotic section was identified visually on the plots. Figures 4.20, 4.21, 4.22 and 4.23 illustrate where the asymptotic section was identified as beginning for the modulus and ultimate strength for the neat epoxy and the GFRP. These figures are focused versions of Figures 4.1, 4.2, 4.3 and 4.4 for the room temperature, 22.8°C, results in order to highlight the section determined as the asymptotic section.

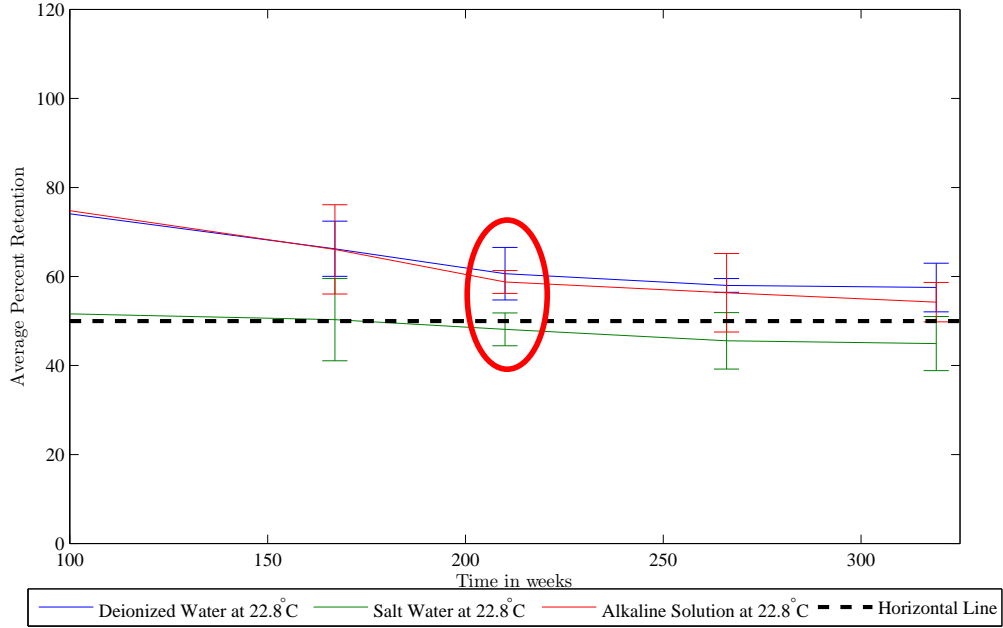


Figure 4.21: Asymptotic Section for Ultimate Strength of GFRP

Table 4.18: Conversion Factors (C_{exp}) for Arrhenius extension to salt and alkaline environments.

	Alkaline	Salt Solution
Epoxy Modulus	0.9724	0.9405
Composite Modulus	0.9485	0.9641
Epoxy Ultimate Strength	0.9366	0.9725
Composite Ultimate Strength	0.7869	0.9615

The regions identified in these figures were averaged for each exposure condition to find the exposure conversion factors, $C_{exposure}$, with Equation 4.6. The exposure conversion factors found are given in Table 4.18.

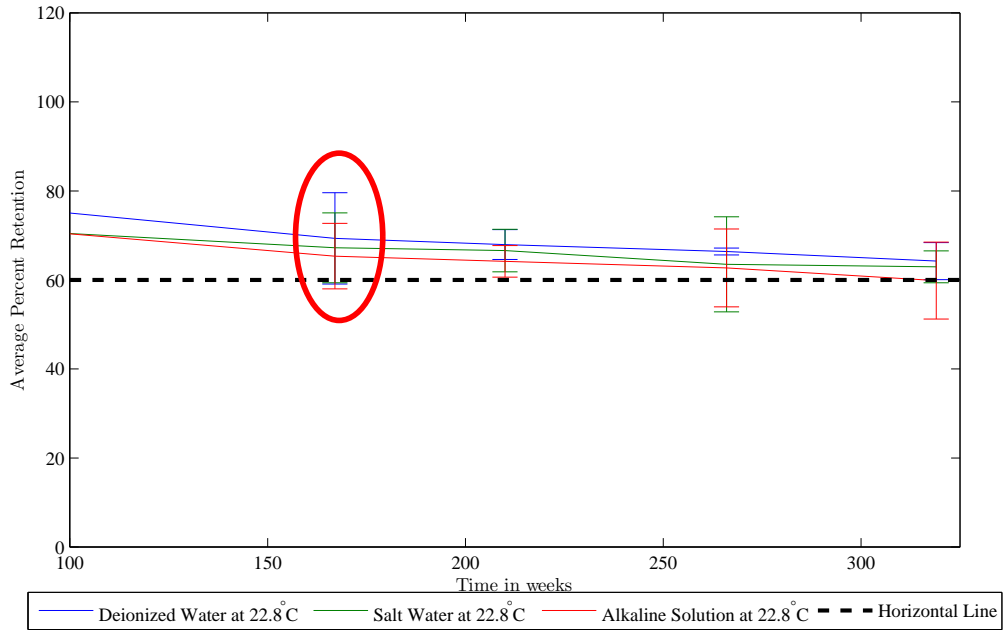


Figure 4.22: Asymptotic Section for Modulus of Epoxy

4.6.1 Comparison of Neat Resin and Composite

Figures 4.24 and 4.25 show the comparison of the percent retention between the neat resin and the composite for the modulus and ultimate strength respectively. This comparison provides interesting insight into the effects of the environment on the components of the composite. Figure 4.24 indicates that the degradation of the modulus due to moisture is primarily a function of the resin and is not significantly affected by the fibers. Alternatively, Figure 4.25 indicates that the ultimate strength of the composite degrades significantly more than the ultimate strength of the neat resin, suggesting that fiber degradation plays a significant role in the degradation of the ultimate strength of the material.

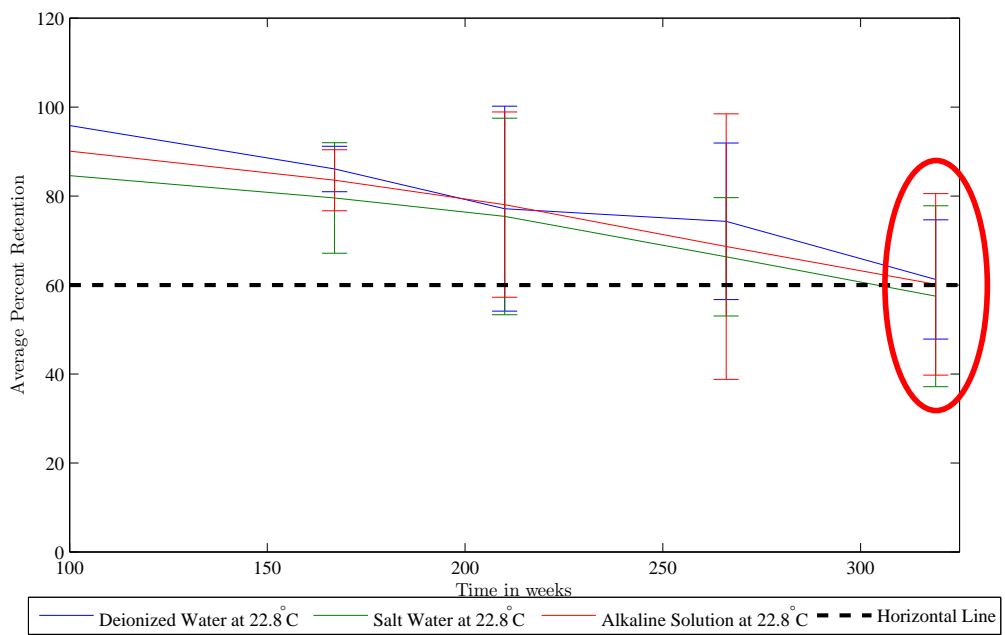


Figure 4.23: Asymptotic Section for Ultimate Strength of Epoxy

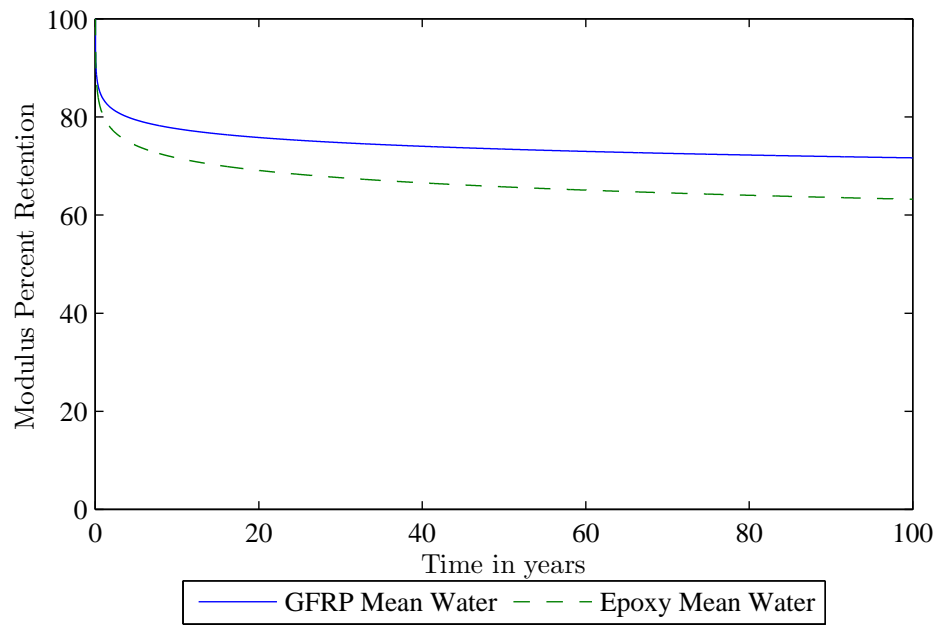


Figure 4.24: Comparison of Predictive Models for Neat Resin Modulus and Composite Modulus

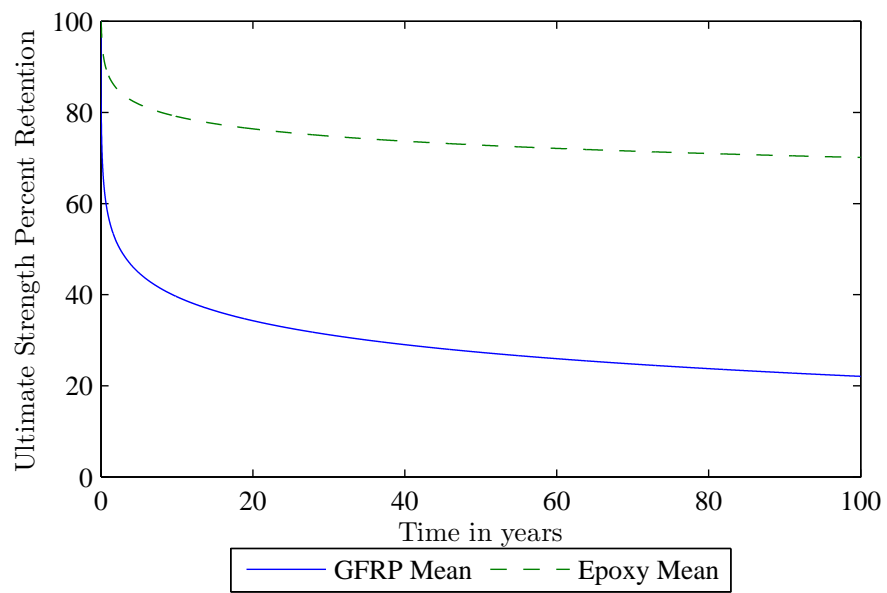


Figure 4.25: Comparison of Predictive Models for Neat Resin Ultimate Strength and Composite Ultimate Strength

CHAPTER 5

RELIABILITY BASED ASSESSMENT

In chapter 4 a model was developed to estimate the long-term mean values of ultimate strength and elastic modulus for a glass fiber reinforced epoxy, and a neat epoxy under exposure to aqueous environments. This chapter seeks to add an estimate of reliability to the models developed previously. The addition of a reliability metric to the predictive model will make the model more useful to the designer. By using the Weibull distribution, and the assumption of a constant shape parameter, an approximation of a probability distribution can be found to accompany the predicted mean values. The inclusion of probability distribution with a mean value allows for the determination of a more efficient design value for FRPs expected to see an extended service life with exposure to adverse environmental conditions (for example setting the design value as the mean minus n times the standard deviation, as is standard procedure for many FRP design guidelines). While many of the current design guidelines use a design value and a constant environmental degradation factor, this research suggests that a constant degradation factor may not be the most efficient or reliable method of accounting for long term exposure to adverse conditions. Sec-

tion 5.2 contains some comparisons of current design values with the data from this research.

5.1 Reliability

The determination of a predicted mean value, as has been done in the previous chapter, is extremely useful and provides valuable insight to the response of the material, but has limited value when used for design. To effectively design using predicted values some indication of the spread of the data is necessary. Without an indication of spread in the data the designer has no indication of the range of values represented by the given mean. Additionally, most design standards specify that when using test data a design value be found using the mean minus n times the standard deviation [24, 25, 36], requiring a measure of dispersion in the sample. A prediction of reliability will provide a measure of dispersion. Reliability is defined as “the probability that an item will preform a required function without failure under stated conditions for a stated period of time” [15]. For materials, reliability characterization reduces to a probabilistic characterization of the material properties over a specified time period. By including a reliability prediction with the predictive model for the mean, a measure of dispersion and a mean value are given to facilitate use in design.

5.1.1 Methodology

As introduced in Section 2.2.4.5, the Weibull probability distribution is well suited for the characterization of the reliability of materials, especially polymers and

FRP composites because of the flexibility of the distribution [17–19]. With the assumption of a constant shape parameter, the Weibull distribution fits found in Section 4.4.2 for the test data can be extended to accompany the predicted mean values. In accelerated life predictions it can be assumed that the Weibull shape parameter remains constant regardless the stress applied [9]. By utilizing this assumption and the approximation for the Weibull scale parameter, Equation 2.16, the Weibull distribution can easily be extended with the predicted means found in Section 4.6. The assumed constant shape parameter was taken to be the average of the values for each exposure condition. These values were chosen as representative values of the shape parameters for each, the ultimate strength and the modulus, of the neat epoxy and the FRP. The Weibull scale parameter can be found using an equation in the form of Equation 5.1, which is found by combining Equations 2.16 and 4.5.

$$\beta \approx \mu_{exp} = C_{exp} P_0 (B \ln t + C) \quad (5.1)$$

Figure 5.1 gives the predictive model for the composite sample under exposure to water with an associated 95% lower confidence limit, as an example case. The confidence limit is based on the extended Weibull parameters as discussed above. The lower confidence interval is found using Equation 5.2, which is derived from Equation 2.11. The derivation can be found in Appendix E.

$$Percentile = \beta (-\ln(1-p))^{1/\alpha} \quad (5.2)$$

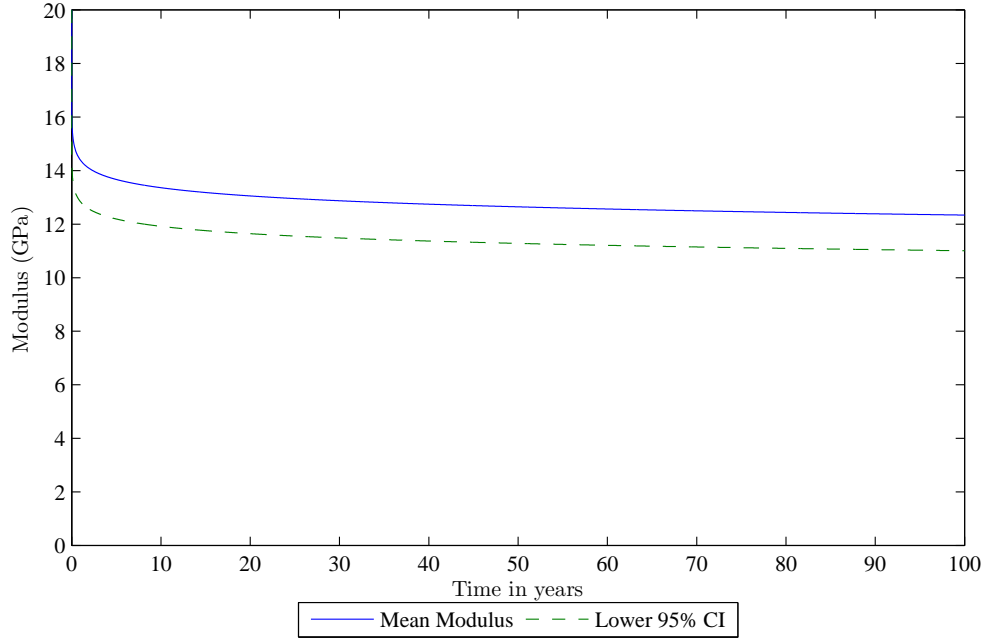


Figure 5.1: Reliability Prediction

Where p is the desired percentile of the distribution and α and β are the Weibull shape and scale parameters respectively. A more generic predictive reliability based equation can be found by combining Equations 5.1 and 5.2 to form Equation 5.3.

$$P_{design}(t) = C_{exp} P_0 (B \ln t + C) (-\ln(1-p))^{1/\alpha} \quad (5.3)$$

Where α and β are the Weibull shape and scale parameters respectively, C_{exp} is the exposure scale factor, t is time in weeks, B and C are constants found from the Arrhenius extensions, P_0 is the initial value of the property of interest, and p is the desired significance level as a percentage.

For example, the equation giving the design value for the modulus of an E-glass reinforced epoxy under exposure to immersion in an alkaline solution with a confidence level of 98% is given in Equation 5.4

$$E_{design}(t) = (0.9366)(18.15GPa)(-0.026 \ln t + 0.988) (-\ln(1 - 0.02))^{1/26} \quad (5.4)$$

Where $C_{exp} = 0.9366$ from Table 4.18, $E_0 = 18.15GPa$ from Table 3.3, $B = -0.0284$ and $C = 1.0201$ from the equation for modulus of the composite in Table 4.17, $\alpha = 43.47$ from Table 4.6 and $p = 0.02$ for the chosen 98% lower confidence level.

Figures 5.2, 5.3, 5.4 and 5.5 give a comparison of the predicted mean, the predicted lower 95% confidence limit, the mean of the samples at time zero minus the standard deviation of the same sample, the mean minus two standard deviations and the mean minus three standard deviations. The mean minus n standard deviation plots are from the control sample at time zero and therefore do not take into account any exposure conditions.

Figures 5.6, 5.7, 5.8 and 5.9 give a comparison of the predicted mean, the predicted lower 95% confidence limit for immersion in deionized water at $22.8^\circ C$, the predicted lower 95% confidence limit for immersion in an alkaline solution at $22.8^\circ C$ and the predicted lower 95% confidence limit for immersion in a salt water solution at $22.8^\circ C$; for each the modulus and ultimate strength, for the neat epoxy and the FRP.

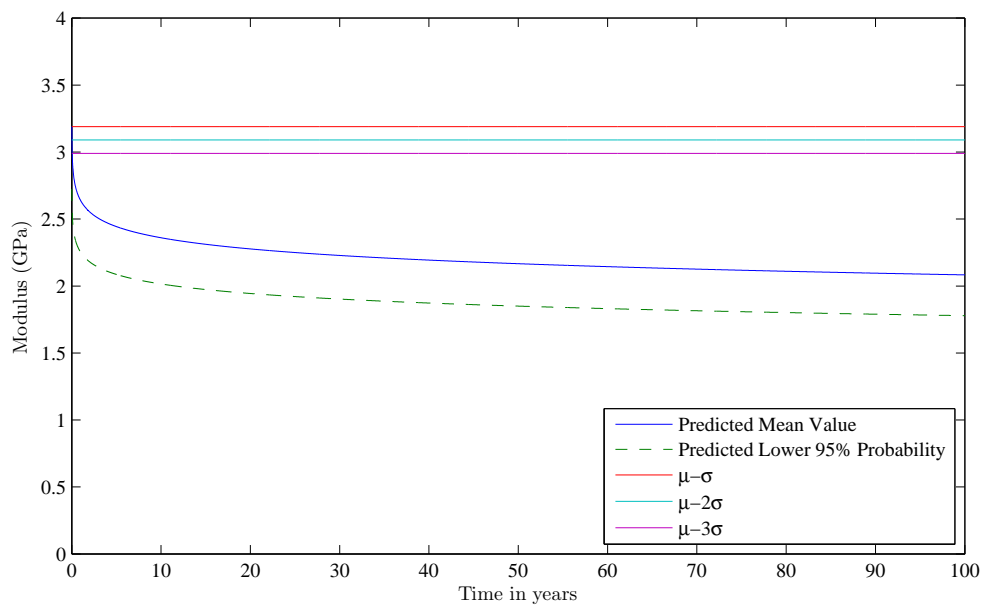


Figure 5.2: Reliability Prediction for Modulus of Neat Epoxy Immersed in Deionized Water at $22.8^{\circ}C$

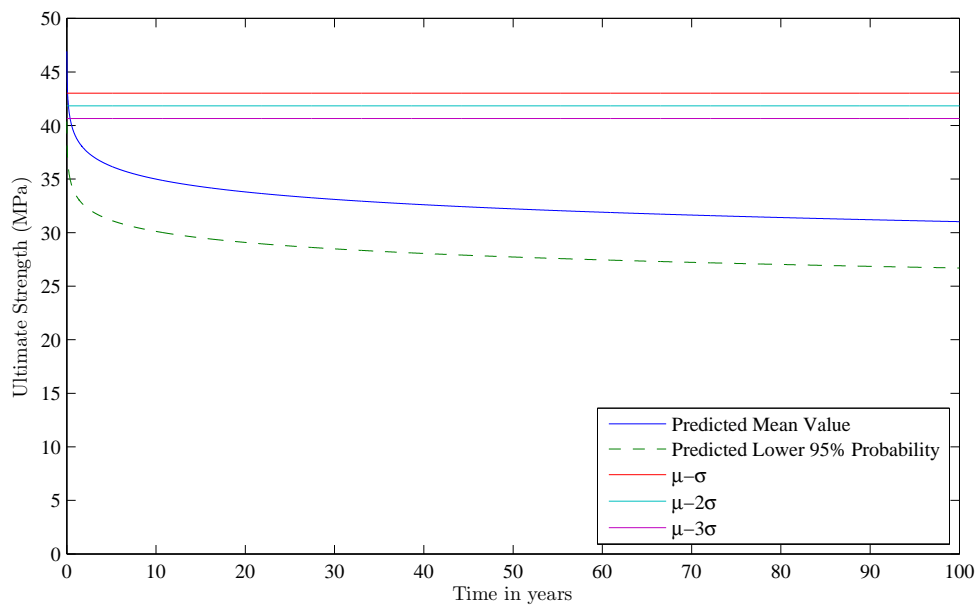


Figure 5.3: Reliability Prediction for Ultimate Strength of Neat Epoxy Immersed in Deionized Water at 22.8°C

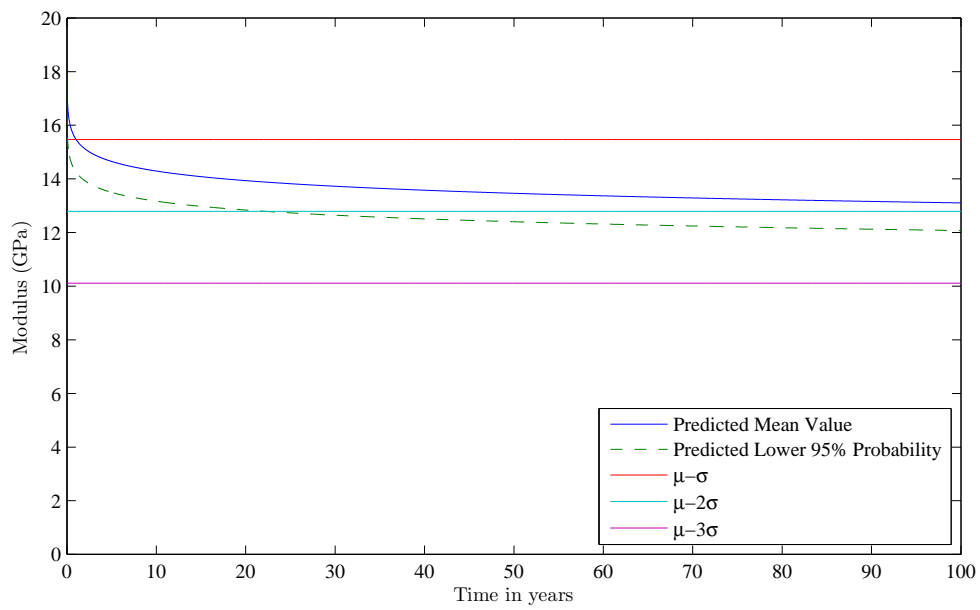


Figure 5.4: Reliability Prediction for Modulus of Glass Fiber Reinforced Epoxy Immersed in Deionized Water at 22.8°C

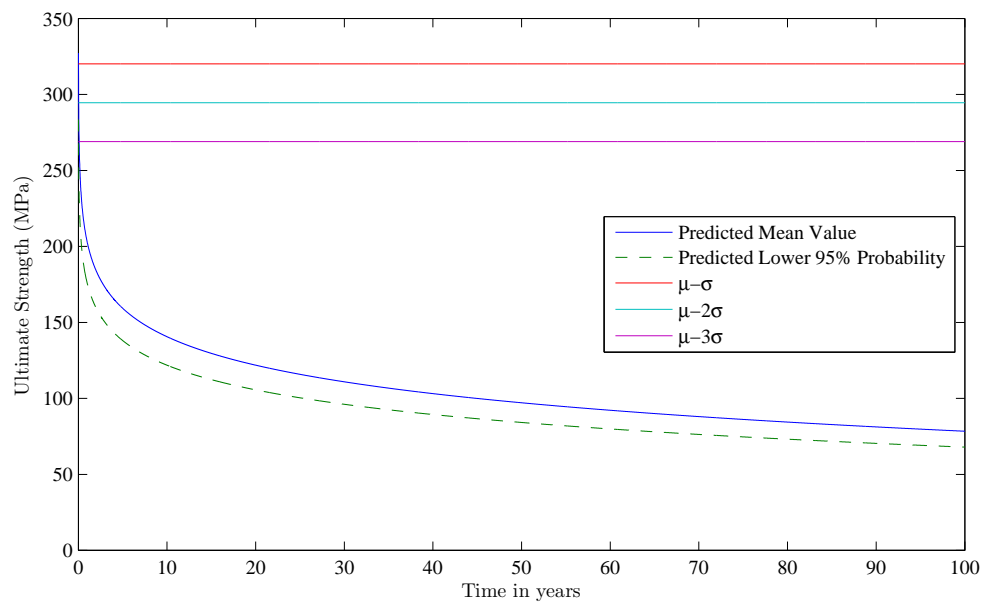


Figure 5.5: Reliability Prediction for Ultimate Strength of Glass Fiber Reinforce Epoxy Immersed in Deionized Water at 22.8°C

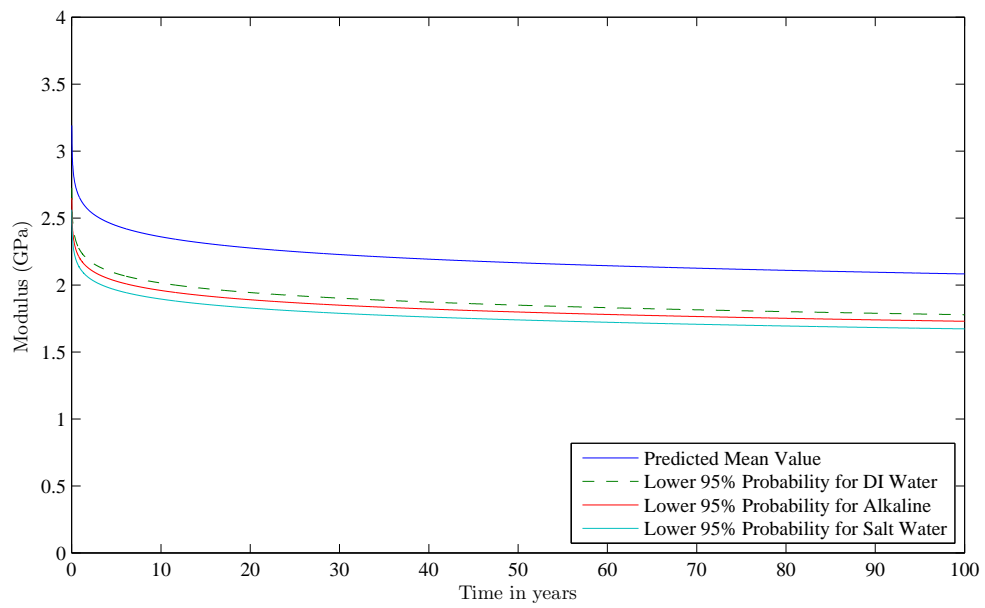


Figure 5.6: Reliability Prediction for Modulus of Neat Epoxy

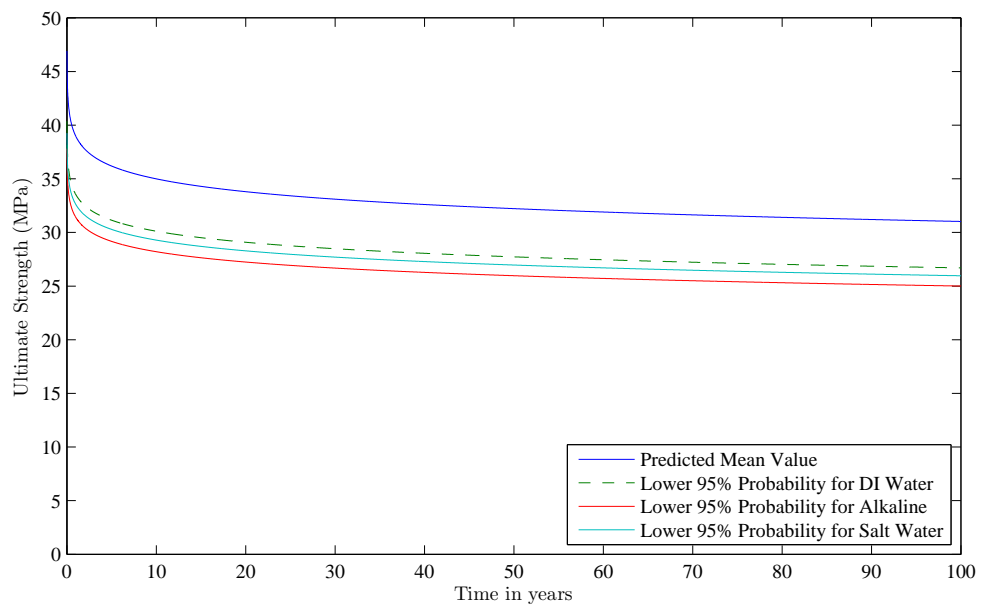


Figure 5.7: Reliability Prediction for Ultimate Strength of Neat Epoxy

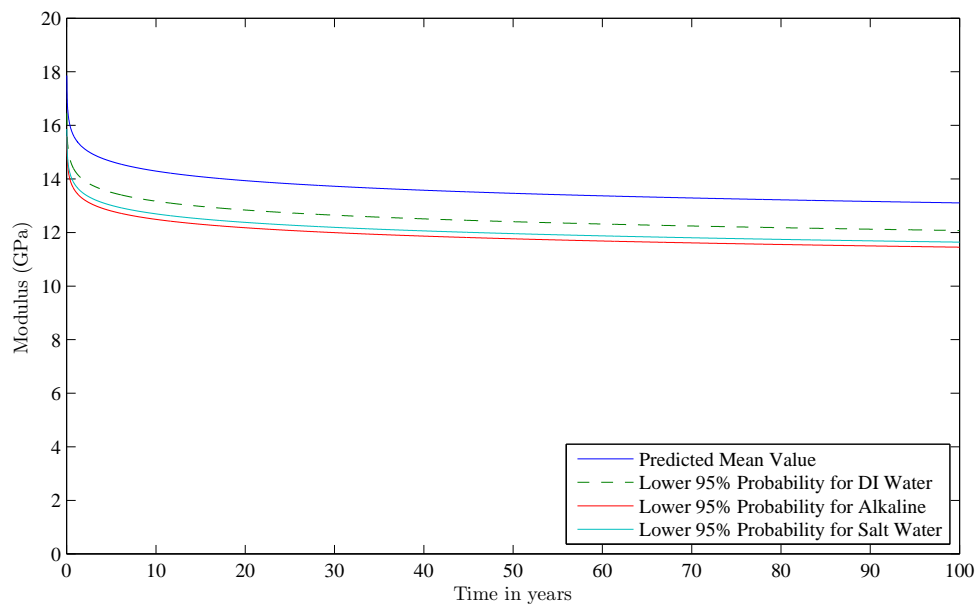


Figure 5.8: Reliability Prediction for Modulus of Glass Fiber Reinforced Epoxy

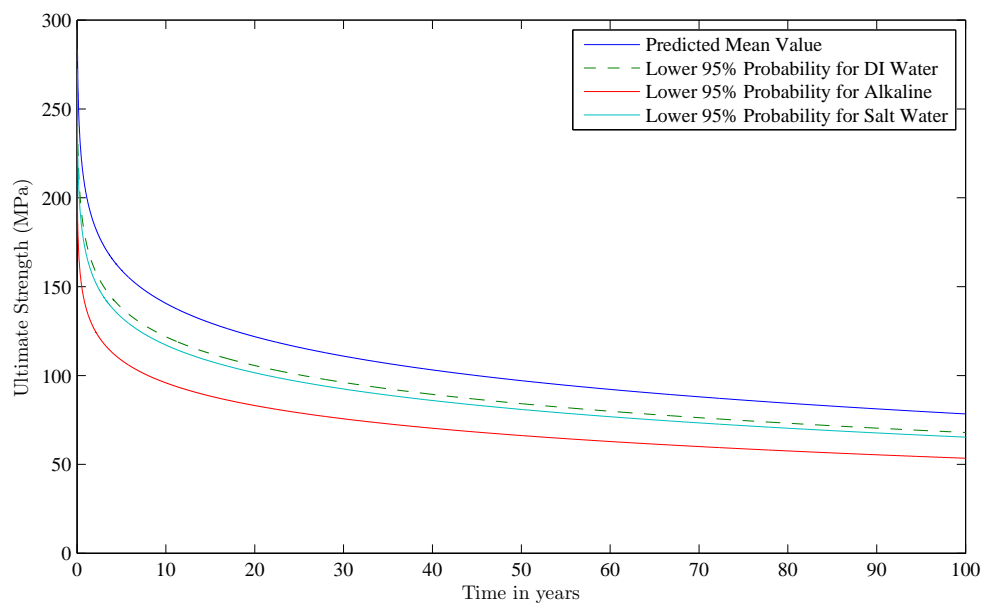


Figure 5.9: Reliability Prediction for Ultimate Strength of Glass Fiber Reinforce Epoxy

5.2 Design values and Comparison

5.2.1 Comparison with Current Design Guidelines

Figures 5.10 and 5.11 show a comparison between the predictive model developed in this thesis and some of the current design guidelines for the modulus and ultimate strength of the FRP respectively. In both figures, the predictive model shown is for exposure to the alkaline solution, due to the fact that this exposure produced the most severe degradation in the FRP seen in this research. This model was compared to three current design standards ACI440, TR55, and the Canadian Bridge Highway Design Code, as introduced in Section 2.2.5. The design standard values were determined assuming an externally bonded, hand layup, unprotected environmental conditions.

The values used for the ACI 440 standard were for a glass/epoxy exposed to exterior conditions. The values were found as follows. Equation 2.19 was used along with the control sample data from Table 3.4 to find the value for $f_{fu}^* = 269.04MPa$, which was then used in Equation 2.21 with an environmental correction factor of $C_E = 0.65$ from Table 2.1 resulting in a design value $f_{fu} = 174.87MPa$, for the stated conditions. The ACI 440 standard recommends using the reported value for the modulus, therefore the design modulus used in this case is the value for the control sample of the FRP at time zero from Table 3.3.

The values found for comparison from the TR55 standard were for hand layup, E-glass FRP, prefabricated shells. The TR55 standard specifies partial safety factors to account for various applications, materials, and manufacturing methods; it specifies

these partial safety factors for the modulus and rupture strain, it then recommends using Hooke's law to find the design tensile strength. In the absence of rupture strain data the determination of the design values becomes somewhat more complicated. Equations 2.24 and 2.25 are used to find the reported modulus and rupture strain, for this case a reported strength value, f_f , will be found similarly. The reported value for modulus is found using Equation 2.24 and the values for the FRP control sample at time zero from Table 3.3. Equation 2.28 is used to find the safety factors for the modulus and rupture strain. The safety factor for modulus was found to be $\gamma_{mE} = 2.16$ with a partial factor for material of $\gamma_{mE} = 1.8$ for E-glass FRPs, and a partial safety factor for the manufacturing method and application $\gamma_{mm} = 1.2$, from Tables 2.2 and 2.3 respectively. Equation 2.26 is then used with the partial safety value and the reported value for modulus to find the design value for modulus of $E_{fd} = 5.92GPa$. In order to find the design value for strength Equations 2.27, 2.28 and 2.29 are combined to form Equation 5.5.

$$f_{fd} = E_{fd}\varepsilon_{fd} = \frac{E_{fd}E_f}{f_f\gamma_{m\varepsilon}\gamma_{mm}} \quad (5.5)$$

Equation 5.5 was used to find the design value for strength, $f_{fd} = 109.69MPa$, with the rupture strain partial safety factors, $\gamma_{m\varepsilon} = 1.95$ for an E-glass FRP, and $\gamma_{mm} = 1.2$ for hand layup, prefabricated shells.

The values found using the Canadian Bridge Highway Design Code were found for a GFRP, surface mounted and exposed to moisture. The design values were found using Equations 2.30 and 2.31 for strength and modulus respectively, using

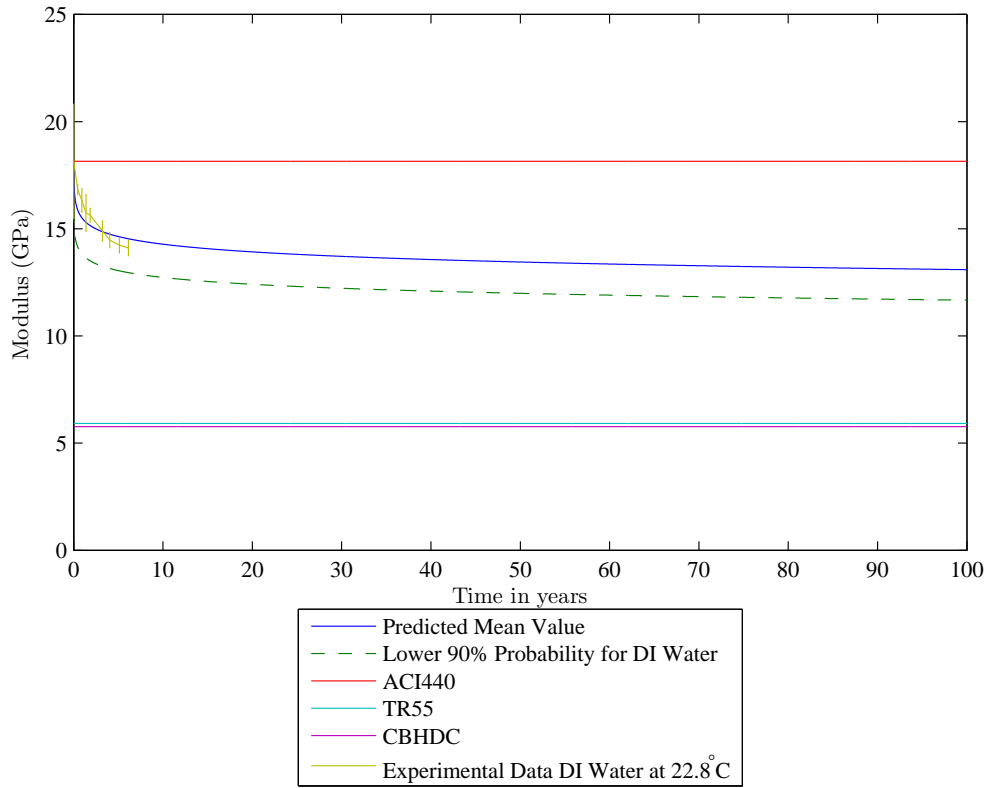


Figure 5.10: Predictive Modulus Model with Current Design Guidelines

Equation 2.32 with values for $\Phi_{hl} = 0.6$ and $C_E = 0.7$ from Table 2.4 to determine the resistance factor value $\Phi_{FRP} = 0.42$

For this comparison the predictive reliability model was calculated at a 90% lower confidence limit to align with the MIL handbook 17 standard for a B-basis material [37].

The comparison to standard design values suggests that the current design standards do not accurately account for exposure to a moist environment based on

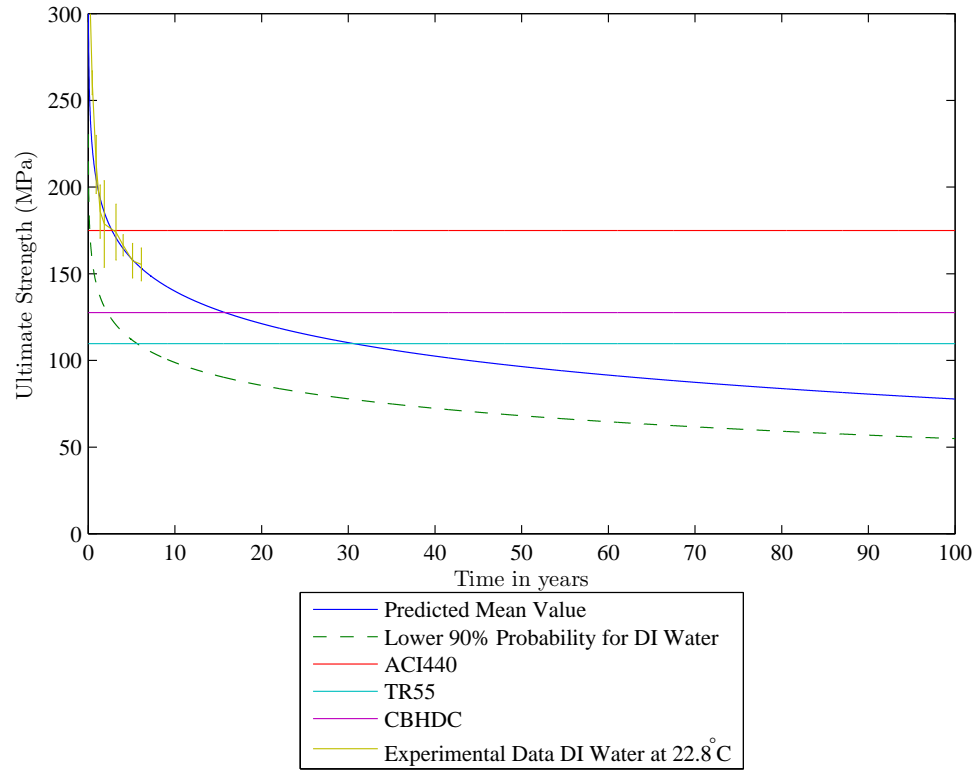


Figure 5.11: Predictive Ultimate Strength Model with Current Design Guidelines

the comparison with the experimental data from this research. The guideline design values for the modulus, with the exception of the ACI440 standard, are overly pessimistic when compared to the experimental data or the predictive model developed in this research, thereby inefficiently using the material by requiring more material to reach the required modulus. Conversely, the suggested design values for the ultimate strength are overly optimistic relative to the results of this research, primarily the ACI440 standard, the ultimate strength of the test samples falls below the ACI440 rec-

ommended value within three years. The strength predicted by the model developed in this research, falls below the Canadian Highway Bridge Design Code recommendation around fifteen years, and below the TR55 recommendation around thirty years. This indicates that the FRPs could experience greater degradation than is accounted for by the current design standards and therefore retain less strength than the current design standards allow for, thus potentially resulting in unexpected failures.

5.3 Application to Design

The models developed for this research can be used in the design process to provide a more precise estimate of material degradation due to exposure to moisture than the current design guidelines, when compared to the experimental data presented in this research, because these models allow for the determination of design values for a specific design life. Thus, allowing for more efficient and safer use of glass fiber and epoxy composite materials. The models developed allow the designer to estimate the material properties for the design life of the component, and to determine a specific design value at that time. The design value can be determined through the use of fitted Weibull distribution for a desired lower confidence limit. For example, consider a designer who needs a glass fiber and epoxy composite manufactured using a wet layup process for a salt water environment for a design life of sixty years. The designer would first use the equations in Table 4.14 for the composite modulus and ultimate strength, with the environmental conversion factors in Table 4.18 for exposure to a salt solution for the composite modulus and ultimate strength respectively. This would result in a mean modulus of 12.9 *GPa*, and a mean ultimate strength of

88.0 *MPa*. To determine an appropriate design value, the designer could use the lower 95% confidence limit for the fitted Weibull distribution at sixty years; this results in a modulus design value $E_d = 11.9 \text{ GPA}$, and an ultimate strength design value $\sigma_d = 77.7 \text{ MPa}$. This method will provide the designer with more accurate design values for the material than the current standards can provide, it also gives the designer the flexibility to use the desired confidence level and design life for the specific application, thus allowing for a more efficient and effective use of the material.

CHAPTER 6

CONCLUSIONS

The results of this research are a collection of equations indicating the effects of water, sea water, and an alkaline solution on a glass fiber and epoxy composite over a period of one hundred years, in addition to predictions of the mean ultimate strength and the elastic modulus are predicted Weibull distribution parameters. The combination of the predicted means and the predicted probability distributions provide the designer with the necessary information to design with these materials and achieve an acceptable level of reliability in the final design. Additionally, the comparison of the predictions from this experiment with the current design standards and guidelines indicate that the current standards may be overly optimistic for FRPs expected to have a very long service life.

6.1 Summary

While FRP composites are increasingly being used in a variety of applications, and the long term durability is relatively unknown, it is necessary to conduct research to determine the long term effects of environmental exposure on FRP composites. This thesis has undertaken a portion of this task by exploring the long term

effects of water, sea water, and an alkaline solution on a glass fiber and epoxy composite through the use of temperature induced accelerated degradation for a period of approximately six years. The accelerated degradation was accomplished by immersing samples in deionized water at room and increased temperatures, in a salt water, and an alkaline solution at room temperature. Samples were removed periodically and tensile tested. The results of these tests were normalized and the Weibull distribution was fit; then an Arrhenius degradation model was used to predict mean values for ultimate strength, and elastic modulus for one hundred years. The parameters of the Weibull distributions were extended by assuming that the Weibull shape parameter was a constant, the extended distribution parameters allow a predicted probability distribution to be associated with the predicted mean values. The combination of the predicted mean and the predicted probability distribution provides the designer with the necessary information to produce effective, efficient, and reliable designs with glass fiber reinforced epoxy composites.

6.2 Areas for additional research

Further research in this field could add greatly to the overall goal of finding a widely applicable method to determine long term material properties. Specific work that could be done, such as similar testing and analysis on additional materials, would add great value to the project. Also, the results of this project could be extended to other environments; for example humid environments, and exposure to higher and lower salinity and alkalinity levels.

APPENDICES

APPENDIX A

TEST DATA

This appendix contains the raw test data for each of the samples tested for this research. For each specimen the thickness and width of the test region is given, along with the modulus and the ultimate strength. For each of these values an average, standard deviation, minimum, maximum and coefficient of variation are given. Additionally the low and high T test statistic for the determination of outliers is given. Also, the percent retention for the modulus and ultimate strength is given as well as summary statistics for the percent retention results. Please see Chapter 4 for the procedure to find the percent retention and the T statistic.

Table A.1: Glass-reinforced epoxy composite control sample at 0 weeks

Specimen Number	Thickness <i>mm</i>	Width <i>mm</i>	Modulus <i>GPa</i>	Ultimate Strength <i>MPa</i>	Percent Retention of Modulus %	Percent Retention of Ultimate Strength %
G108	4.00	11.99	19.80	364.36	109.09%	105.38%
G183	3.65	12.28	16.10	379.18	88.73%	109.67%
G184	3.58	12.23	14.89	316.70	82.07%	91.60%
G111	3.31	12.35	18.45	338.95	101.64%	98.03%
G109	3.08	11.59	21.50	329.57	118.47%	95.32%
Average	3.52	12.09	18.1482	345.7511	100.00%	100.00%
Std. Dev.	0.35	0.31	2.6841	25.5719	14.79%	7.40%
Max	4.00	12.35	21.50	379.18	118.47%	109.67%
Min	3.08	11.59	14.89	316.70	82.07%	91.60%
C.V.	0.10	0.03	0.15	0.07	14.79%	7.40%
T_{high}	1.36	0.85	1.25	1.31		
T_{low}	1.28	1.61	1.21	1.14		

APPENDIX B

WEIBULL PARAMETERS

This appendix gives the Weibull parameter values for each set of samples tested with outliers removed and descriptive statistics. Also, the high and low T statistic values for the identification of outliers are given. The blank cells in the table indicate that an outlier was found, the alpha beta pair was removed in the case of an outlier.

Table B.1: Glass-reinforced epoxy modulus Weibull parameters

Time in weeks	Control		Immersion in Deionized Water						Immersion in Alkaline		Immersion in Salt Water	
	73° <i>F</i>		73° <i>F</i>		100° <i>F</i>		140° <i>F</i>		73° <i>F</i>		73° <i>F</i>	
	α	β	α	β	α	β	α	β	α	β	α	β
0	8.11	18.15	8.11	18.15	8.11	18.15	—	—	8.11	18.15	8.11	18.15
24	20.40	18.30	44.62	17.55	25.55	16.26	13.01	16.05	84.93	16.83	47.56	17.23
48	54.89	18.32	9.57	17.43	13.15	15.95	38.70	15.17	35.94	16.32	32.90	17.05
72	27.03	18.43	133.80	16.85	16.92	15.02	12.80	14.66	22.03	15.74	20.26	16.03
96	16.00	18.48	20.49	16.84	27.41	14.66	4.40	14.30	57.02	15.63	18.97	15.86
167	29.54	18.68	31.54	16.11	30.16	14.47	39.85	14.28	38.44	14.90	34.88	15.07
210	49.93	18.68	45.68	15.49	43.02	14.30	34.45	14.08	50.08	14.47	62.10	14.88
266	86.31	18.70	57.24	15.11	—	—	51.04	13.99	47.94	14.23	55.85	14.52
319	33.96	18.71	86.95	14.52	43.50	14.12	28.01	13.93	46.75	14.10	61.26	14.11
Average	36.24	18.50	48.67	16.45	25.98	15.24	25.60	14.56	43.47	15.60	37.99	15.88
Std Dev	24.05	0.21	40.42	1.22	13.00	1.33	16.52	0.72	21.70	1.34	19.80	1.37
Max	86.31	18.71	133.80	18.15	43.50	18.15	51.04	16.05	84.93	18.15	62.10	18.15
Min	8.11	18.15	8.11	14.52	8.11	14.12	4.40	13.93	8.11	14.10	8.11	14.11
T_{High}	2.08	1.03	2.11	1.39	1.35	2.19	1.54	2.05	1.91	1.90	1.22	1.66
T_{Low}	1.17	1.65	1.00	1.58	1.37	0.85	1.28	0.86	1.63	1.12	1.51	1.29

APPENDIX C

MINITAB ANOVA RESULTS

ANOVA Results from Minitab 15 statistical analysis software package.

Analysis of Variance to compare the Weibull Shape Parameters for each exposure condition over time.

1/13/2011 11:08:11 PM

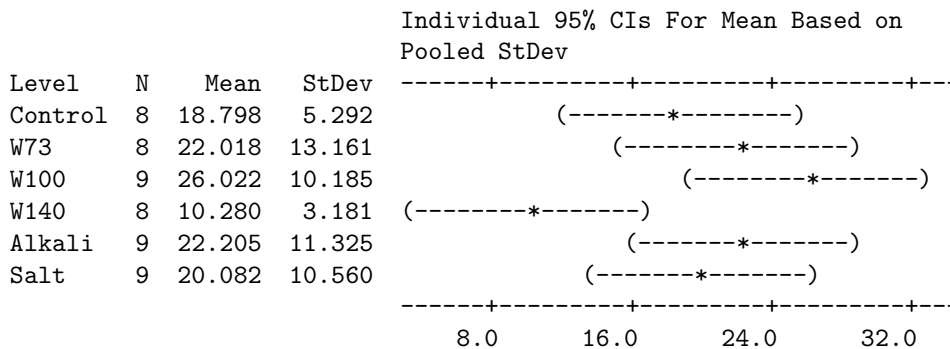
Welcome to Minitab, press F1 for help.

Results for: Epoxy Modulus

One-way ANOVA: Control, W73, W100, W140, Alkali, Salt

Source	DF	SS	MS	F	P
Factor	5	1169.8	234.0	2.49	0.045
Error	45	4227.4	93.9		
Total	50	5397.2			

S = 9.692 R-Sq = 21.67% R-Sq(adj) = 12.97%

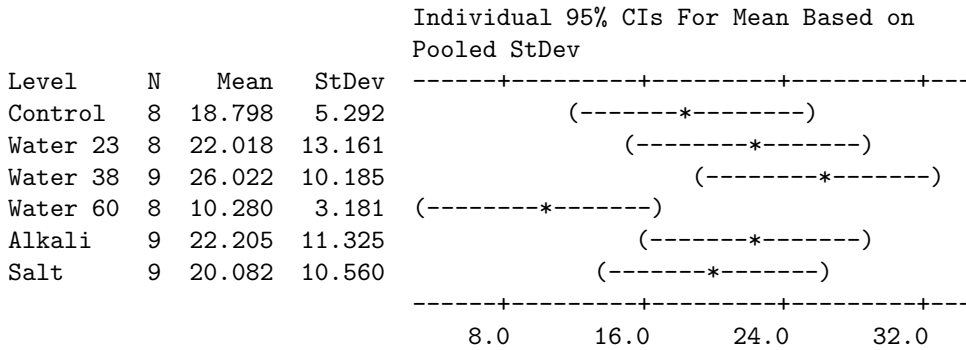


Pooled StDev = 9.692

One-way ANOVA: Control, Water 23, Water 38, Water 60, Alkali, Salt

Source	DF	SS	MS	F	P
Factor	5	1169.8	234.0	2.49	0.045
Error	45	4227.4	93.9		
Total	50	5397.2			

S = 9.692 R-Sq = 21.67% R-Sq(adj) = 12.97%



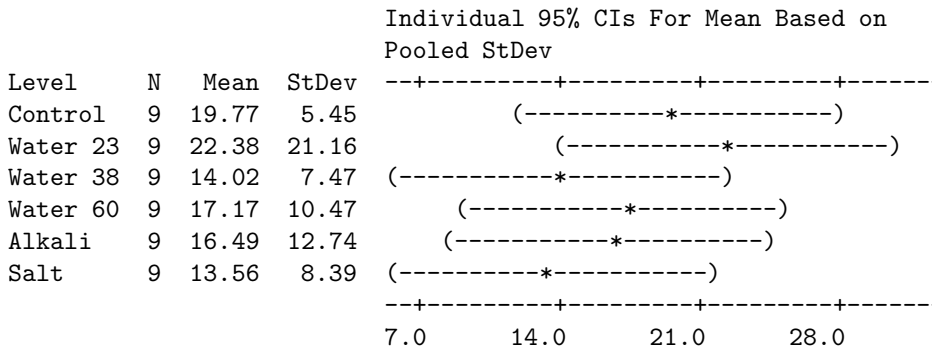
Pooled StDev = 9.692

Results for: Epoxy Strength

One-way ANOVA: Control, Water 23, Water 38, Water 60, Alkali, Salt

Source	DF	SS	MS	F	P
Factor	5	516	103	0.71	0.621
Error	48	7002	146		
Total	53	7519			

S = 12.08 R-Sq = 6.87% R-Sq(adj) = 0.00%



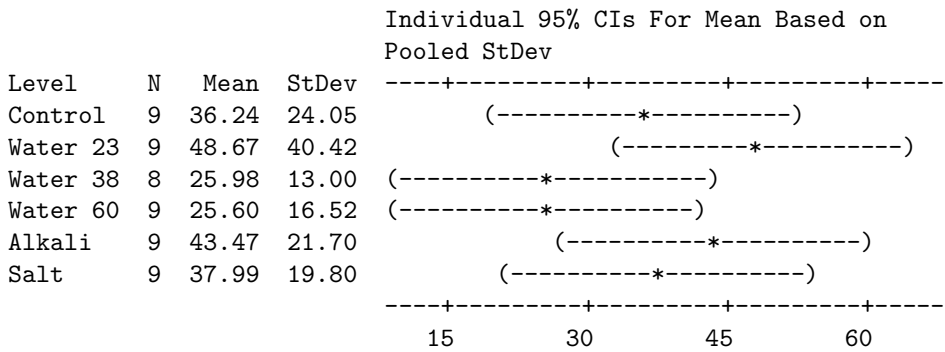
Pooled StDev = 12.08

Results for: Composite Modulus

One-way ANOVA: Control, Water 23, Water 38, Water 60, Alkali, Salt

Source	DF	SS	MS	F	P
Factor	5	3746	749	1.26	0.298
Error	47	27975	595		
Total	52	31720			

S = 24.40 R-Sq = 11.81% R-Sq(adj) = 2.43%



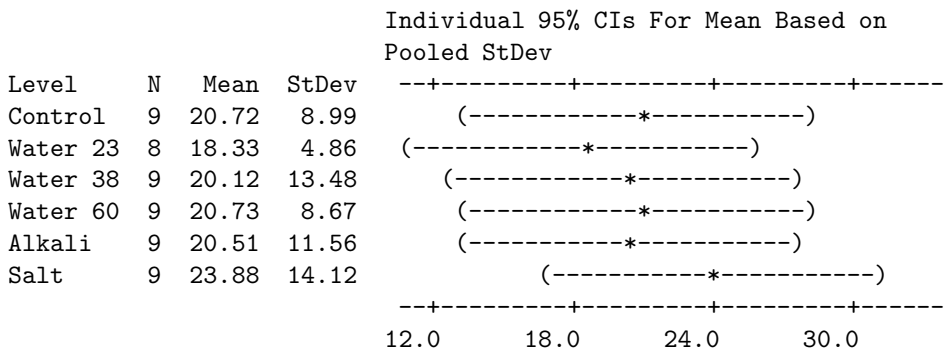
Pooled StDev = 24.40

Results for: Composite Strength

One-way ANOVA: Control, Water 23, Water 38, Water 60, Alkali, Salt

Source	DF	SS	MS	F	P
Factor	5	139	28	0.24	0.944
Error	47	5531	118		
Total	52	5671			

S = 10.85 R-Sq = 2.46% R-Sq(adj) = 0.00%



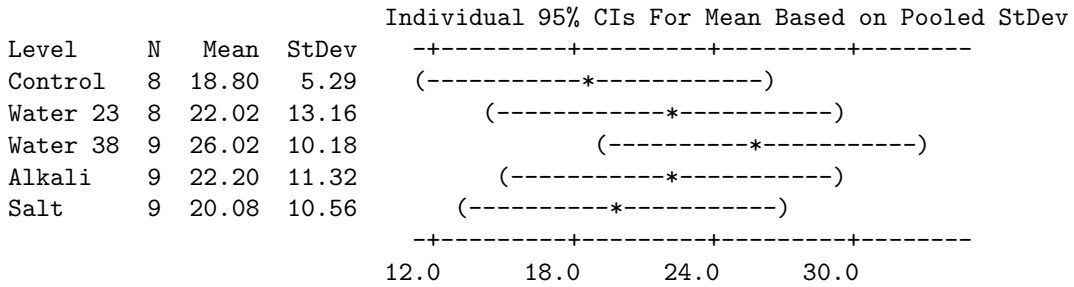
Pooled StDev = 10.85

Results for: Epoxy Modulus

One-way ANOVA: Control, Water 23, Water 38, Alkali, Salt

Source	DF	SS	MS	F	P
Factor	4	261	65	0.60	0.668
Error	38	4157	109		
Total	42	4417			

S = 10.46 R-Sq = 5.90% R-Sq(adj) = 0.00%

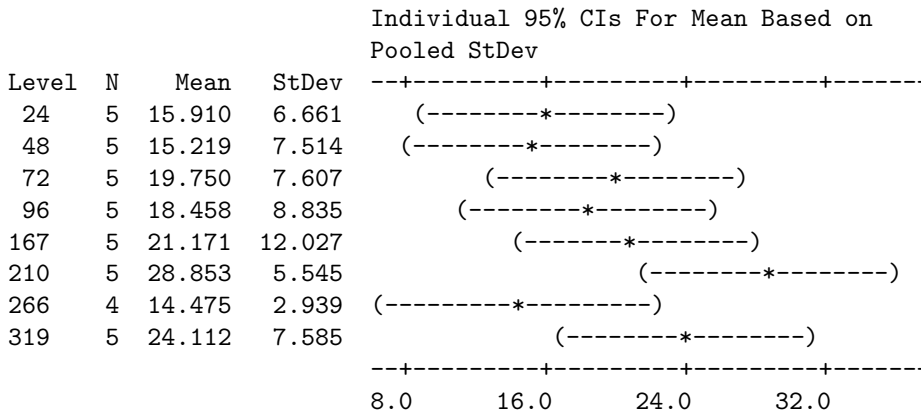


Pooled StDev = 10.46

One-way ANOVA: Epoxy Modulus versus Time

Source	DF	SS	MS	F	P
Time	7	814.9	116.4	1.89	0.104
Error	31	1904.6	61.4		
Total	38	2719.6			

S = 7.838 R-Sq = 29.96% R-Sq(adj) = 14.15%

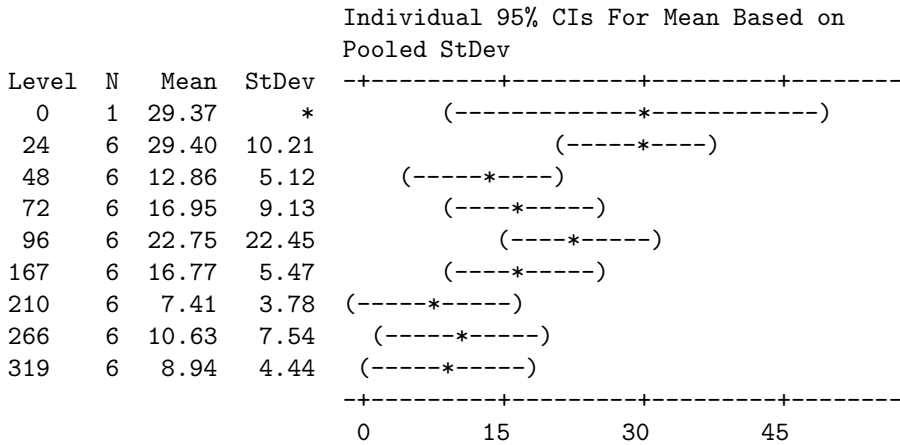


Pooled StDev = 7.838

One-way ANOVA: Epoxy Strength versus Time

Source	DF	SS	MS	F	P
Time	8	2512	314	2.99	0.010
Error	40	4194	105		
Total	48	6706			

S = 10.24 R-Sq = 37.46% R-Sq(adj) = 24.95%

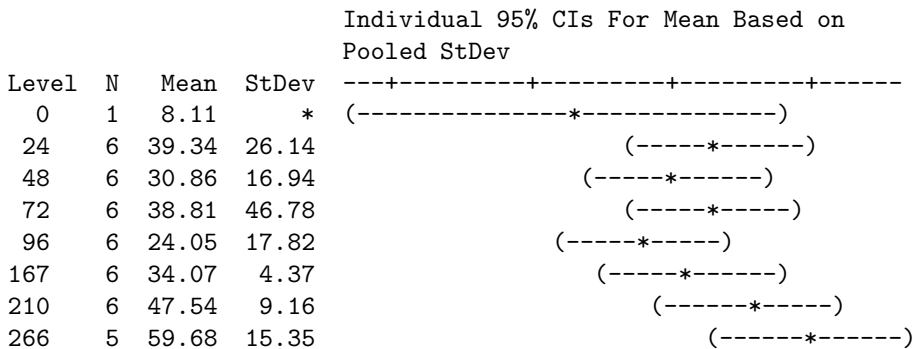


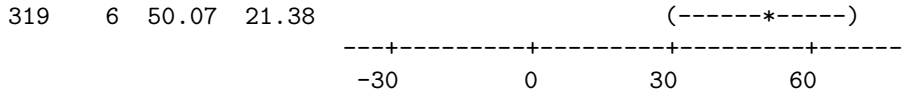
Pooled StDev = 10.24

One-way ANOVA: Composite Modulus versus Time

Source	DF	SS	MS	F	P
Time	8	6140	768	1.42	0.220
Error	39	21126	542		
Total	47	27266			

S = 23.27 R-Sq = 22.52% R-Sq(adj) = 6.63%



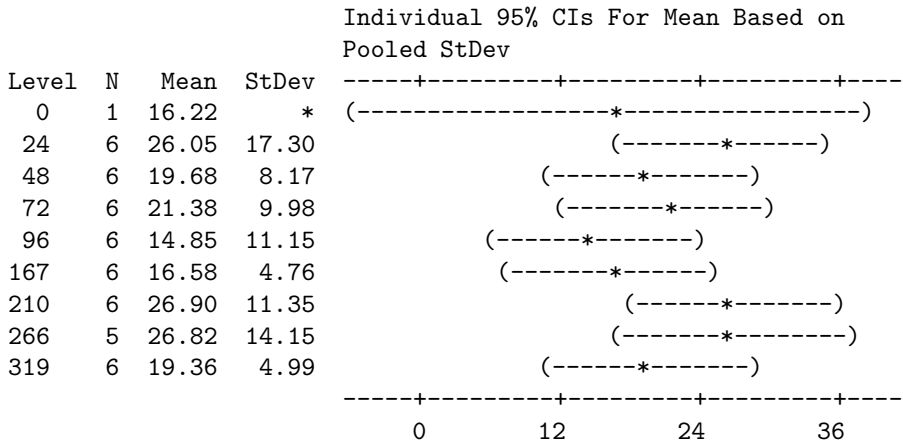


Pooled StDev = 23.27

One-way ANOVA: Composite Strength versus Time

Source	DF	SS	MS	F	P
Time	8	923	115	0.97	0.473
Error	39	4634	119		
Total	47	5557			

S = 10.90 R-Sq = 16.61% R-Sq(adj) = 0.00%



Pooled StDev = 10.90

In order to statistically illustrate the existence of trends in the data an Analysis of Variance was done on the data to test the null hypothesis that there does not exist a statistically significant difference in the means for each of the factors.

All of the tests were 2-factor ANOVA with replication, with a level of significance; $\alpha = 0.05$.

C.1 Glass Fiber Reinforced Polymer

C.1.1 Control Sample

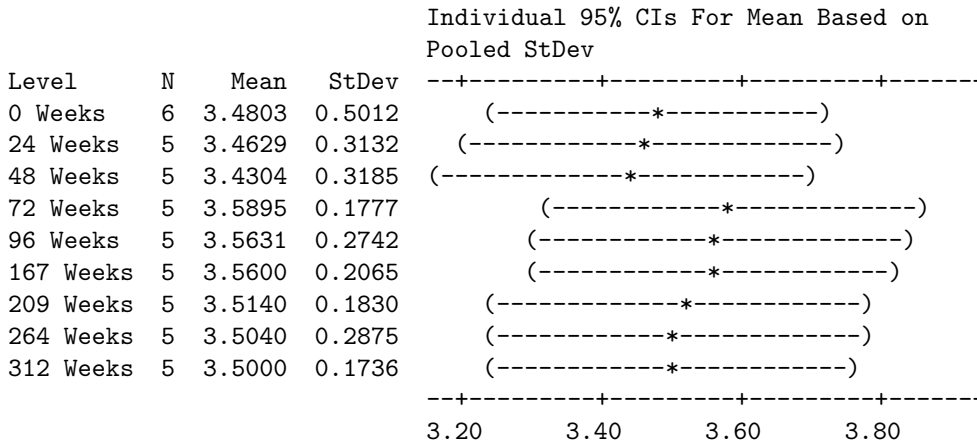
C.1.1.1 Elastic Modulus Data

ANOVA for GFRP modulus control samples

One-way ANOVA: 0 Weeks, 24 Weeks, 48 Weeks, 72 Weeks, 96 Weeks, 167 Weeks, ...

Source	DF	SS	MS	F	P
Factor	8	0.1070	0.0134	0.15	0.996
Error	37	3.2369	0.0875		
Total	45	3.3439			

S = 0.2958 R-Sq = 3.20% R-Sq(adj) = 0.00%



Pooled StDev = 0.2958

C.1.1.2 Ultimate Strength Data

Composite ultimate strength, basic statistics and ANOVA

Descriptive Statistics: 0 Weeks, 24 Weeks, 48 Weeks, 72 Weeks, 96 Weeks, ...

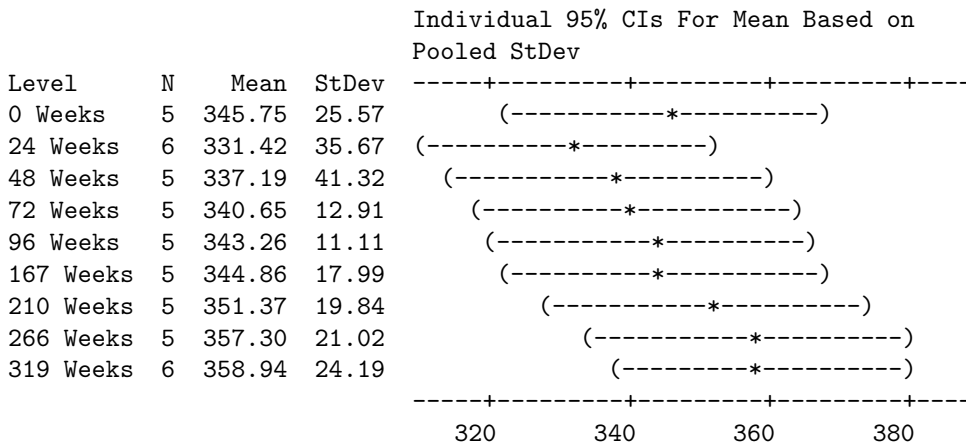
Variable	N	N*	Mean	SE Mean	StDev	CoefVar	Minimum	Q1	Median
0 Weeks	5	0	345.8	11.4	25.6	7.40	316.7	323.1	338.9
24 Weeks	6	0	331.4	14.6	35.7	10.76	291.5	298.5	330.1
48 Weeks	5	0	337.2	18.5	41.3	12.25	290.0	294.1	351.1
72 Weeks	5	0	340.65	5.77	12.91	3.79	324.01	327.18	345.34
96 Weeks	5	0	343.26	4.97	11.11	3.24	329.12	333.92	340.55
167 Weeks	5	0	344.86	8.04	17.99	5.22	319.29	328.70	346.89
210 Weeks	5	0	351.37	8.87	19.84	5.65	321.73	334.31	354.89
266 Weeks	5	0	357.30	9.40	21.02	5.88	325.92	340.34	357.89
319 Weeks	6	0	358.94	9.87	24.19	6.74	315.29	347.03	358.95

Variable	Q3	Maximum	Range	Skewness	Kurtosis
0 Weeks	371.8	379.2	62.5	0.37	-1.71
24 Weeks	364.6	374.9	83.3	0.08	-2.65
48 Weeks	373.3	385.3	95.3	-0.21	-2.43
72 Weeks	351.78	354.40	30.39	-0.46	-2.17
96 Weeks	353.96	358.25	29.13	0.21	-0.40
167 Weeks	360.00	368.12	48.83	-0.29	0.66
210 Weeks	366.66	376.54	54.81	-0.53	1.48
266 Weeks	373.96	384.47	58.55	-0.48	1.70
319 Weeks	380.45	383.34	68.06	-1.27	2.27

One-way ANOVA: 0 Weeks, 24 Weeks, 48 Weeks, 72 Weeks, 96 Weeks, 167 Weeks, ...

Source	DF	SS	MS	F	P
Factor	8	3631	454	0.70	0.687
Error	38	24526	645		
Total	46	28156			

S = 25.41 R-Sq = 12.89% R-Sq(adj) = 0.00%



Pooled StDev = 25.41

REFERENCES

- [1] A. K. Kaw, *Mechanics of Composite Materials*, 2nd Edition, CRC Press, 2006.
- [2] A. Mouritz, C. Gardiner, *Composites*, Vol. 21 of *ASM Handbook*, ASM International, 2001, Ch. Marine Applications, pp. 1085–1090.
- [3] V. M. Karbhari, *Composites*, Vol. 21 of *ASM Handbook*, ASM International, 2001, Ch. Civil Infrastructure Applications, pp. 1091–1100.
- [4] L. C. Hollaway, P. R. Head, *Advanced Polymer Composites and Polymers in the Civil Infrastructure*, Elsevier Science, 2001.
- [5] V. M. Karbhari.
- [6] V. M. Karbhari, J. W. Chin, D. Hunston, B. Benmokrane, T. Juska, R. Morgan, J. J. Lesko, U. Sorathia, D. Reynaud, Durability gap analysis for fiber-reinforced polymer composites in civil infrastructure, *Journal of Composite Construction* 7 (3) (2003) 238–247.
- [7] V. M. Karbhari, J. W. Chin, D. Reynaud, Critical gaps in durability data for frp composites in civil infrastructure, *SAMPE Proceedings* 45 (2000) 549–563.
- [8] J. W. Chin, Material aspects of fiber-reinforced polymer composites in infrastructure, NIST.
- [9] W. Nelson, *Accelerated Testing, Statistical Models, Test Plans, and Data Analyses*, John Wiley and Sons, 1990.
- [10] S. L. Svetlik, An investigation in the hygrothermal degradation of an e-glass/vinyl-ester composite in humid and immersion environments, Ph.D. dissertation, Department of Structural Engineering, University of California, San Diego (2008).
- [11] J. F. Shackelford, *Introduction to Material Science for Engineers*, 6th ed, Pearson Prentice Hall, 2005.
- [12] K. K. Phani, N. R. Bose, Hydrothermal ageing of csm-laminate during water immersion an acousto-ultrasonic study, *Journal of Materials Science* 21 (1986) 3633–3637, 10.1007/BF00553810.
URL <http://dx.doi.org/10.1007/BF00553810>

- [13] K. Phani, N. Bose, Temperature dependence of hydrothermal ageing of csm-laminate during water immersion, *Composites Science and Technology* 29 (2) (1987) 79 – 87. doi:DOI: 10.1016/0266-3538(87)90050-9.
- [14] S.-J. Jin, Reliability-based characterization of prefabricated frp composites for rehabilitation of concrete structures, Master’s thesis, Department of Structural Engineering, University of California, San Diego (2008).
- [15] P. D. T. O’Connor, *Practical Reliability Engineering*, 4th ed, John Wiley & Sons, 2002.
- [16] W. Navidi, *Statistics for Engineers and Scientists*, McGraw-Hill, 2008.
- [17] M. R. Wisnom, Statistical aspects of failure of fibre-reinforced composites, *Proceedings of the Institution of Mechanical Engineers, Part G: Journal of Aerospace Engineering* 212 (3) (1998) 189–192.
- [18] R. Bullock, Strength Ratios of Composite Materials in Flexure and in Tension, *Journal of Composite Materials* 8 (2) (1974) 200–206. doi:10.1177/002199837400800209.
- [19] W. Weibull, A statistical distribution function of wide applicability, *Journal of Applied Mechanics* (1951) 293–297.
- [20] B. Dodson, *Weibull Analysis*, American Society for Quality, 1994.
- [21] R. Atadero, L. Lee, V. M. Karbhari, Consideration of material variability in reliability analysis of frp strengthened bridge decks, *Composite Structures* 70 (2004) 430–443.
- [22] X. He, S. O. Oyadiji, Application of coefficient of variation in reliability-based mechanical design and manufacture, *Journal of Materials Processing Technology* 119 (2001) 374–378.
- [23] V. M. Karbhari, M. A. Abanilla, Design factors, reliability, and durability prediction of wet layup carbon/epoxy used in external strengthening, *Composites Part B: Engineering* 38 (1) (2007) 10 – 23. doi:DOI: 10.1016/j.compositesb.2006.06.001.
- [24] ACI Committee 440, *ACI Manual of Concrete Practice*, Vol. 5, American Concrete Institute, 2008, Ch. Guide for the Design and Construction of Externally Bonded FRP Systems for Strengthening Concrete Structures (ACI 440.2R-02).
- [25] C. Arya, J. Clarke, E. Kay, P. O’Regan.

- [26] C. Helbling, M. Abanilla, L. Lee, V. Karbhari, Issues of variability and durability under synergistic exposure conditions related to advanced polymer composites in the civil infrastructure, *Composites Part A: Applied Science and Manufacturing* 37 (8) (2006) 1102 – 1110, the 2nd International Conference: Advanced Polymer Composites for Structural Applications in Construction. doi:DOI: 10.1016/j.compositesa.2005.05.039.
- [27] M. A. Abanilla, Y. Li, V. M. Karbhari, Durability characterization of wet layup graphite/epoxy composites used in external strengthening, *Composites Part B: Engineering* 37 (2-3) (2006) 200 – 212. doi:DOI: 10.1016/j.compositesb.2005.05.016.
- [28] N. D. Jackson, Reliability-based durability assessment of gfrp bars for reinforced concrete, Master's thesis, Department of Engineering Mechanics, Virginia Polytechnic Institute and State University, Blacksburg, Virginia (November 2007).
- [29] V. Bhise, Strength degradation of gfrp bars, Via Department of Civil and Environmental Engineering, Virginia Polytechnic Institute and State University.
- [30] Environmental durability of externally bonded frp materials intended for repair of concrete structures, *Construction and Building Materials* In Press, Corrected Proof. doi:DOI: 10.1016/j.conbuildmat.2010.11.096.
- [31] American Society for Testing and Materials, ASTM D 3039-08: Standard Test Method for Tensile Properties of Polymer Matrix Composite Materials, ASTM International, 100 Bar Harbor Dr., West Conshohcken, PA 19428, United States.
- [32] American Society for Testing and Materials, ASTM D 2344-00: Standard test method for short-beam strength of polymer matrix composite materials and their laminates, ASTM International, 100 Bar Harbor Dr., West Conshohcken, PA 19428, United States.
- [33] V. M. Karbhari, Communication (2009).
- [34] American Society for Testing and Materials, ASTM D 638-03: Standard Test Method for Tensile Properties of Plastics, ASTM International, 100 Bar Harbor Dr., West Conshohcken, PA 19428, United States.
- [35] American Society for Testing and Materials, ASTM E178-08: Standard Practice for Dealing with Outlying Observations, ASTM International, 100 Bar Harbor Dr., West Conshohcken, PA 19428, United States.
- [36] New canadian highway bridge design code design provisions for fiber-reinforced structures, *Canadian Journal of Civil Engineering*.
- [37] Materials Science Corporation in Cooperation with ASTM, Lancaster, PA, *The Composite Materials Handbook (HDBK-MIL17), Guidance for Characterization of Structural Materials, Vol. 2 Edition* (2002).

PART D

APPLICATION OF TIME-BASED DURABILITY TO DESIGN OF JACKETS FOR SEISMIC RETROFIT

TABLE OF CONTENTS

Abstract.....	2
1. Introduction.....	3
2. Materials Systems and Test Methods.....	4
3. Results of Durability Testing and Arrhenius Analysis.....	8
4. Comparison With ACI-440 Recommendations.....	15
5. Background to Jacket Design.....	18
6. Application to Jacket Design.....	23
7. Summary and Conclusions.....	45
References.....	47

ABSTRACT

Although FRP composites are increasingly being used for the rehabilitation of civil infrastructure, there is still a lack of well documented long-term durability data, and of design methodologies that explicitly consider effects of deterioration over time at a structural level. This paper provides results of an investigation aimed at assessing the effect of deterioration over time, at the materials level, on the effectiveness of FRP jackets used for seismic retrofit. Three different systems are investigated and results of accelerated testing are used to provide predictive equations for long-term performance of the material, which are then used to analyze effectiveness at the level of seismic retrofit through four specific cases. The effect of deterioration is expressed, for ease in comparison, to an increase in the required thickness of the jacket with expected service-life. Results using unexposed values for materials performance are compared to those obtained using the values recommended by ACI-440 procedures, as well as through the use of time-dependent materials degradation models. It is shown that the ACI recommendations for durability may be excessively conservative for the 50 year period considered herein. The use of the proposed predictive methodology for materials durability combined with the analytical tools for design of FRP jacket thickness are shown to not only enable a better assessment of required jacket thickness but can also enable assessment of the dominant mechanism controlling selection of thickness which can change with time of exposure. Results of the accelerated tests are also linked to field exposure results providing a set of correlation factors.

1. INTRODUCTION

Concrete columns that need to be retrofit are commonly deficient in flexural ductility, shear strength, bar buckling restraint, and/or lap splice clamping. The use of jackets around existing deficient columns induces lateral confining stresses in the concrete as it expands laterally as a function of the high axial compressive strains, or in the tension zone as a function of dilation of lap splices, or through the development of diagonal shear cracks. Jacketing has been effected through the application of steel shells, additional reinforced concrete, and the wrapping of fiber reinforced polymer (FRP) composites around the deficient column. While all three methods provide the required retrofit efficiency FRP composites offer significant advantages as related to speed of application, substantially less disruption of traffic, reduced weight, insignificant change to dimensions and the overall configuration, potentially lower life-cycle maintenance, and directional anisotropy. Since the efficacy of the jacket is dependent on hoop confinement FRP composites offer tremendous tailorability since they can be designed to have fibers oriented primarily in the hoop direction to provide constraint without substantially increasing stiffness over the height of the column.

The effectiveness of FRP jacketing has been extensively validated through large and full-scale laboratory tests [1-3], field applications [4] and in-situ field tests and assessment [5, 6]. In addition significant research has been conducted in developing an understanding of the mechanisms of interaction between the FRP jacket and the concrete and the overall retrofit response. To date advances have also been made in the development of design

guidelines and specifications including for construction [7-10]. While the structural effectiveness of FRP jackets has been widely accepted by the community there is still some reservation regarding its use due to concerns related to cost and long-term durability in field environments.

In recent years, durability of FRP jacketing materials has been assessed through laboratory tests [11-14] and limited field tests [15] and a detailed set of evaluation criteria and durability test protocols have been established by the Civil Engineering Research Foundation under the aegis of the Federal Highway Administration [16]. This research has, however, largely been at the level of materials deterioration and has not been linked to the design, or assessment of deterioration, at the structural level. This link is crucial both for purposes of safe design and to assess life of jacket systems. If deterioration rates for a specific FRP composite were known jackets could be designed with an appropriate safety factor, accomplished through use of “sacrificial” thickness, to ensure their reliability over expected periods of field use. This paper reports on the results of an investigation aimed at providing a means for this as well as a basis for the future development of reliability based design tools that incorporate materials deterioration.

2. MATERIALS SYSTEMS AND TEST METHODS

Three different systems, representative of commercially available products that have been used extensively in the field were investigated. System A is representative of the

prefabricated class wherein a hollow circular cross-sectional shell is first fabricated under carefully controlled factory conditions, including elevated temperature cure over an extended period of time. This cylinder is then slit down the length to create an opening and after the addition of adhesive to the inner surface is pulled over a column. Subsequent layers are added with the position of the slit being staggered to enable good overlap with the overall configuration being akin to that of an onionskin. Bonding is achieved under ambient conditions with external pressure applied by separate circumferential straps tightened manually and removed after a period of time. Systems B and C are representative of the extensively used wet layup process wherein fabric is impregnated with an appropriate resin system in the field, then wrapped around the column and cured under ambient conditions. The primary difference between these systems was that system B used Aramid tows in the transverse direction whereas system C was completely constituted of E-Glass fibers. The volume fraction of transverse direction fibers in both cases was extremely small with the fibers essentially serving to hold the warp direction fibers in place. All three systems considered in this investigation were primarily of unidirectional orientation with the reinforcing fibers being of E-glass.

Following earlier investigations on the development of an appropriate test method that would capture materials, manufacturing and structural aspects in a single coupon [15, 16] the ring burst test was used in this investigation. The 510 mm (20" internal diameter) rings allowed the stressing of the material in a fashion closely simulating the actual structural system during dilation of concrete during a seismic event. Following procedures detailed by Reynaud et al. [16], as part of the HITEC specifications,

specimens were fabricated by manufacturers as in the field, in the form of blanks of 178 mm (7") height, to enable the system to be exposed to environmental conditions in the jacket, rather than ring, configuration. All blanks were coated in the same manner as would be applied in the field to provide protection against environmental exposure and all edges were sealed using the same coating. Specimens were immersed in water at 15°C, 23°C, 40°C and 60°C for extended periods of time to enable use of time-temperature superposition principles for prediction of long-term durability. Base-line specimens were also stored under controlled conditions of 23°C and 55% relative humidity (RH). Once exposures were completed, 4 rings each of 25.4 mm (1") height were cut from the central portion of each blank (Figure 1) with a fifth ring being also cut from the same section for specimens to be tested in short-beam-shear (SBS) using specimens of nominal span-to-depth ratio of 5:1, assessment of glass transition temperature (T_g), moisture content, and microscopic investigations.

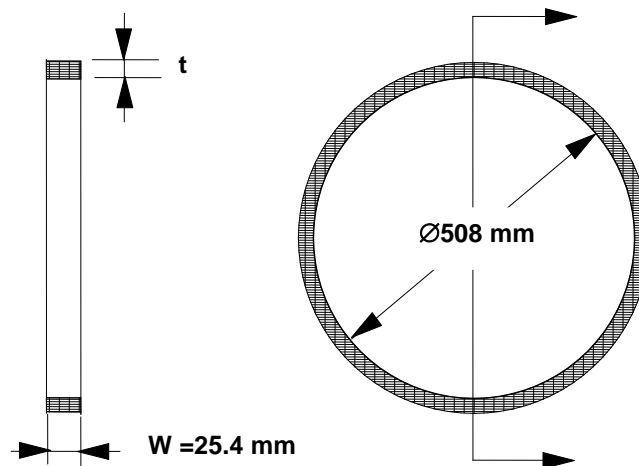


Figure 1(a): Dimensions of NOL Ring Test Unit

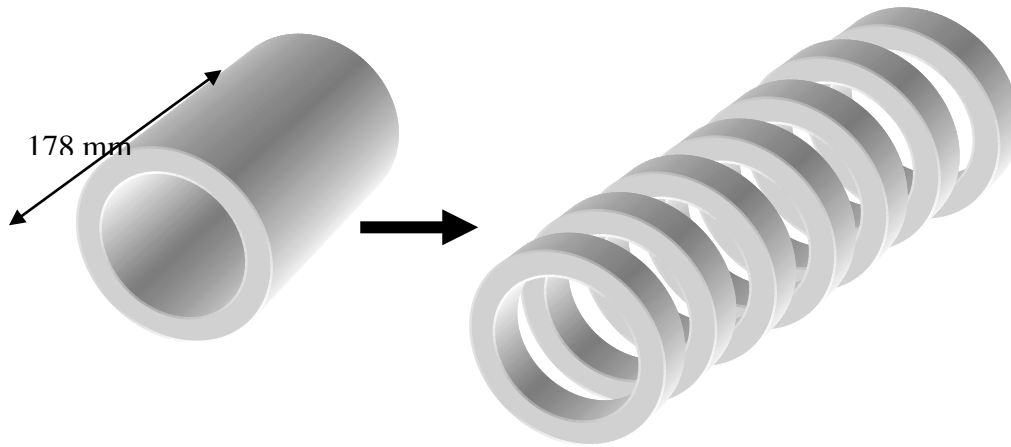


Figure 1(b): Schematic of Test Blank and Ring Specimens Obtained From a Blank

A set of 5 samples was tested in each of these cases. In order to provide ease of comparison and to reduce uncertainty due to operator judgment the glass transition temperature was determined from the peak of the $\tan \delta$ curve resulting from Dynamic Mechanical Thermal Analysis (DMTA) conducted on specimens. The use of test specimens from the central region of each test blank, rejecting edge areas, enabled almost complete elimination of edge effects during environmental exposure which could, otherwise, have resulted in non-uniformity; and testing of specimens with moisture contents and attendant damage not likely to be encountered by the overall jacket in the field. In order to provide a standard baseline for design of test specimens for purposes of durability assessment, manufacturers were asked to fabricate blanks to meet a predetermined internal pressure rating of 17.2 MPa (2500 psi) with a maximum thickness constraint of 11.5 mm (0.45") following specifications prescribed by the California Department of Transportation [8].

3. RESULTS OF DURABILITY TESTING AND ARRHENIUS ANALYSIS

Details related to dominant damage mechanisms for each of the systems were reported earlier by Karbhari et al. [11] and are hence not repeated herein. Results of the exposures for each of the systems are summarized in Tables 1-3.

Since the reinforcing shells in system A were fabricated under controlled conditions with elevated temperature cure the weak link in terms of degradation due to environmental exposure is the ambient cured adhesive. Failures were seen in all cases within the adhesive layer as shown in Figure 2, with very little damage to the prefabricated layer surfaces. This mechanism of deterioration was common to all specimens with the loss of adhesive integrity being noticed from the 6-month level of exposure and increasing with time of exposure. In some specimens the failures were also seen in the adhesive plug formed between ends of the shells (Figure 2(b)).

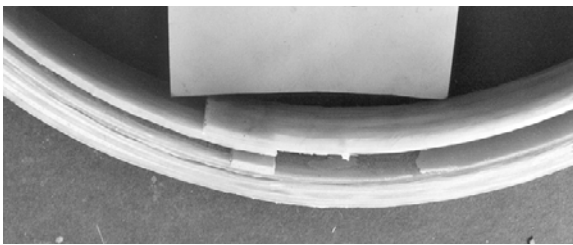


Figure 2(a): Separation of plies through failure at the bond-line and within the adhesive.



Figure 2(b): Failure within the adhesive in the joint region between shell ends

As a result of exposure, system B samples showed mechanisms of delamination between fabric layers with significant hoop splitting and tearing of fabric accompanied by pull-out

Table 1: Properties as a Function of Time and Exposure Period for System A

Exposure: Immersion in Deionized Water		Hoop Strength	Std. Dev.	Hoop Modulus	Std. Dev.	Strain	Std. Dev.	SBS	Std. Dev.	Tg
Unexposed Baseline		386.00 MPa	13.79 MPa	40.70 GPa	1.03 GPa	9250 μ strain	546 μ strain	23.4 MPa	2.41 MPa	158.00 $^{\circ}$ C
		% Retention	Std. Dev (MPa)	% Retention	Std. Dev (GPa)	% Retention	Std. Dev (μ strain)	% Retention	Std. Dev (MPa)	% Retention
15 $^{\circ}$ C	6 months	94%	6.90	99%	3.00	96%	216	99%	1.46	100%
	12 months	93%	6.90	98%	4.43	97%	317	98%	1.39	101%
	18 months	90%	27.58	98%	0.89	94%	478	95%	1.29	102%
	24 months	85%	13.79	97%	2.32	91%	135	90%	1.45	99%
23 $^{\circ}$ C	6 months	89%	6.90	96%	0.91	100.2%	182	93%	1.05	101%
	12 months	89%	13.79	91%	3.84	106.6%	473	90%	1.39	101%
	18 months	89%	20.69	93%	2.14	99.7%	283	89%	1.56	98%
	24 months	77%	13.79	90%	1.63	87%	351	84%	0.94	97%
40 $^{\circ}$ C	6 months	79%	6.90	93%	1.00	88%	312	86%	2.15	100%
	12 months	45%	13.79	75%	2.98	66%	417	60%	1.90	98%
	18 months	32%	13.79	66%	2.15	51%	631	31%	1.46	92%
	24 months	0%	-	0%	-	0%	-	0%	-	88%
60 $^{\circ}$ C	6 months	79%	13.79	90%	3.85	99.5%	641	55%	0.65	101%
	12 months	32%	41.37	30%	4.23	82%	1011	35%	0.92	98%
	18 months	0%	-	0%	-	0%	-	0%	-	92%
	24 months	0%	-	0%	-	0%	-	0%	-	84%

Table 2: Properties as a Function of Time and Exposure Period for System B

Exposure: Immersion in Deionized Water		Hoop Strength	Std. Dev.	Hoop Modulus	Std. Dev.	Strain	Std. Dev.	SBS	Std. Dev.	Tg
Unexposed Baseline		468.90 MPa	27.58 MPa	28.80 GPa	0.97 GPa	17992 μ strain	1658 μ strain	26.30 MPa	1.10 MPa	72.00 $^{\circ}$ C
		% Retention	Std. Dev (MPa)	% Retention	Std. Dev (GPa)	% Retention	Std. Dev (μ strain)	% Retention	Std. Dev (MPa)	% Retention
15 $^{\circ}$ C	6 months	91%	34.48	100%	2.19	96%	1251	70%	2.21	100%
	12 months	80%	20.69	95%	2.21	85%	936	65%	1.14	98%
	18 months	66%	6.90	92%	1.33	75%	431	59%	0.64	99%
	24 months	64%	7.09	91%	1.50	72%	418	57%	0.64	98%
23 $^{\circ}$ C	6 months	89%	41.37	104%	1.86	96%	2970	61%	1.12	94%
	12 months	76%	27.58	94%	2.43	72%	1431	65%	3.56	108%
	18 months	65%	13.79	89%	1.08	68%	1437	54%	1.37	100%
	24 months	61%	12.28	91%	1.06	67%	1448	51%	1.22	98%
40 $^{\circ}$ C	6 months	70%	27.58	103%	0.93	68%	1360	66%	0.99	99%
	12 months	66%	20.69	92%	2.97	64%	451	66%	1.05	106%
	18 months	54%	13.79	95%	0.43	56%	346	64%	2.21	110%
	24 months	46%	10.71	90%	0.41	53%	351	63%	1.97	110%
60 $^{\circ}$ C	6 months	50%	6.90	104%	2.15	43.5%	444	67%	2.83	119%
	12 months	50%	13.79	104%	1.17	43.5%	743	68%	1.61	128%
	18 months	46%	13.79	94%	0.52	42.9%	188	67%	1.57	128%
	24 months	40%	13.45	90%	0.48	41%	179	66%	1.49	119%

Table 3: Properties as a Function of Time and Exposure Period for System C

Exposure: Immersion in Deionized Water		Strength	Std. Dev.	Modulus	Std. Dev.	Strain	Std. Dev.	SBS	Std. Dev.	Tg
Unexposed Baseline		606.80 MPa	6.89 MPa	26.30 GPa	0.48 GPa	22343 μ strain	668 μ strain	31.00 MPa	1.31 MPa	73.00 $^{\circ}$ C
		% Retention	Std. Dev (MPa)	% Retention	Std. Dev (GPa)	% Retention	Std. Dev (μ strain)	% Retention	Std. Dev (MPa)	% Retention
15 $^{\circ}$ C	6 months	98%	6.90	100%	0.78	99.0%	2156	99%	1.08	100%
	12 months	95%	20.69	99%	0.63	98.0%	1021	98%	1.46	101%
	18 months	90%	13.79	97%	1.28	95.0%	357	96%	0.45	100%
	24 months	88%	6.90	96%	2.15	92.0%	423	92%	0.43	99%
23 $^{\circ}$ C	6 months	85%	27.58	92%	1.10	88.3%	2139	93%	1.45	96%
	12 months	83%	27.58	92%	1.01	90.7%	760	90%	2.25	105%
	18 months	81%	27.58	93%	0.81	86.4%	1011	92%	0.92	92%
	24 months	78%	20.69	91%	0.83	86.1%	352	90%	0.68	93%
40 $^{\circ}$ C	6 months	66%	27.58	94%	1.75	70.2%	3124	85%	1.06	98%
	12 months	65%	6.90	93%	0.80	62.1%	215	76%	1.48	97%
	18 months	60%	13.79	90%	0.77	56.3%	107	74%	0.68	98%
	24 months	46%	6.90	88%	2.17	55.0%	456	71%	0.77	99%
60 $^{\circ}$ C	6 months	38%	6.90	92%	0.72	37.9%	372	60%	1.06	112%
	12 months	37%	20.69	94%	0.93	38.1%	217	60%	0.76	128%
	18 months	37%	6.90	98%	0.61	35.5%	255	62%	0.79	111%
	24 months	33%	13.79	90%	1.12	31.1%	452	55%	0.85	108%

of the aramid tows (Figure 3(a)) at lower temperatures and upto the 12 month period at 60°C, after which failure was due to fiber rupture (Figure 3(b)) indicating deterioration of fiber-matrix bond and even of the fiber.

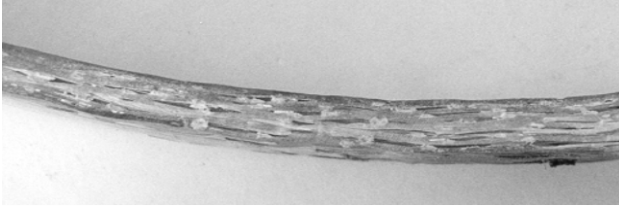


Figure 3(a): Hoop splitting, tearing, and interface deterioration around aramid tows

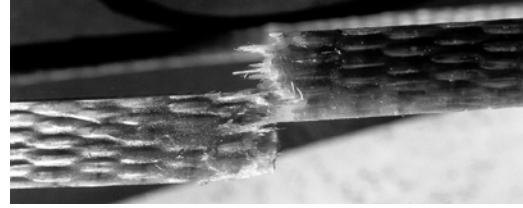


Figure 3(b): Fiber rupture after extended exposure

Although the level of degradation in terms of hoop strength increases both with temperature and period of immersion it is of interest to note that the exposure to water at the two highest temperatures also resulted in a progression of cure as seen through the increase in the glass transition temperature. This is further highlighted through the almost asymptotic level of deterioration in short-beam-shear strength attained as a result of immersion in water at both 40°C and 60°C, as can be seen in Table 2. Although one may be tempted to relate the increase in glass transition temperature solely to residual curing it is noted that this phenomena has been shown to also result from the leaching of low molecular weight flexibilizing segments leading to embrittlement of the network which is borne out by the change in dominant mechanisms with time of exposure in the current case.

In comparison to system B, the transverse tows in system C fabric were also from E-glass which could be expected to result in less swelling and moisture uptake as compared to that resulting from the aramid fibers. Levels of deterioration are seen to be slightly less than that of system B at the two lower temperatures of 15°C and 23°C but are higher with

a faster rate of deterioration at the two higher levels of 40°C and 60°C. In all cases failure was through a combination of separation between layers and tensile rupture (Figure 4) with some degradation at the longer time periods at the fiber and fiber-matrix interphase level. It is noted that a detailed study of the fiber-matrix interphase in a similar system was reported by Zhang et al [12] wherein fiber level degradation was seen. Unlike system B, in system C it is noted that with the exception of samples immersed in water at the highest temperature of 60°C there is no indication of post-cure due to the temperature of immersion and that there is a slow but progressive deterioration in short-beam-shear strength with temperature and time of immersion.

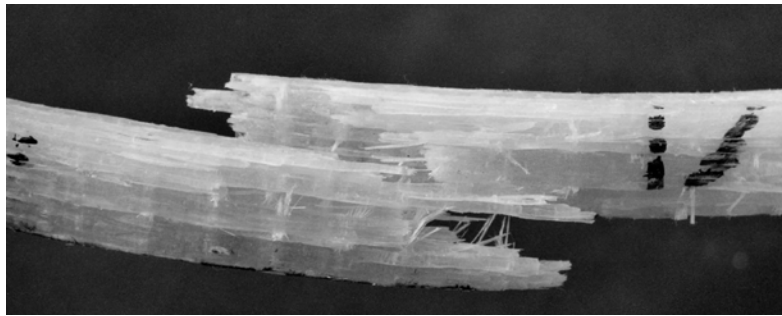


Figure 4: Failure in system C through a combination of separation between layers and fiber rupture.

Following the procedure in Litherland et al [17], Proctor et al [18] and as recently used for E-glass vinylester systems by Chin et al. [19] and Karbhari [20], the Arrhenius method was used to predict changes in performance over time. In this method the logarithm of time to reach a set of levels of percentage retention versus $1/T$ (where T is the temperature in Kelvin) is used to predict service life at a given temperature (normally assumed to be the ambient level). This follows from the Arrhenius rate equation which shows first-order effects, wherein it is assumed that the rate at which degradation occurs follows the form

$$k = A \exp\left(\frac{-E_a}{RT}\right) \quad \dots(1)$$

where k is a variable representing the rate of degradation, E_a is the activation energy, R is the universal gas constant, and T is the exposure temperature in degrees Kelvin. The validity of the primary assumption, that the material has a set of dominant mechanisms which do not change with time and temperature, but are accelerated by increase in temperature, is borne out through a linear relationship between the diffusion coefficients for the materials immersed at various temperatures and the temperature of immersion. Using data from tests conducted at 15, 40 and 60°C, predictions were made for property retention as a function of time for the 23°C immersion case, and are seen to compare well with the experimental results for this exposure within the overall scatter bounds. Equations for time dependent change in properties for the three material systems are given in Table 4.

Table 4: Predictive Equations (expressed as $\frac{P(t)}{P_0} = A + B \ln(\tau)$ where $P(t)$ is the property at any time $t > 0$, P_0 is the unexposed value at $t = 0$ as listed in Tables 1-3, A and B are constants, with B representing the rate of degradation with time, and τ is the time in days)

Characteristic	System A	System B	System C
Strength, $f_i(\tau)$	=1.0339-0.0403 ln(τ)	=1.0029-0.0525 ln(τ)	=1.0363-0.0375 ln(τ)
Modulus, $E_i(\tau)$	= 1.0014-0.0163 ln(τ)	= 1.0012-0.0097 ln(τ)	=1.0110-0.0089 ln(τ)
Strain, $\epsilon_j(\tau)$	= 1.0031-0.0250 ln(τ)	= 1.0022-0.0439 ln(τ)	= 1.0294-0.0318 ln(τ)

It is noted that immersion in water represents a single exposure condition which may not represent exposure in the field. The results of the durability of system A and B materials through field exposure adjacent to actual wrapped bridge columns in Tacoma,

Washington, were reported earlier by Zhang et al. [15]. The exposure for the period of 89 weeks included temperature variation between -2°C and 35.6°C, with precipitation, freeze-thaw cycles, and salt exposure from road salt. A comparison of data from field exposure and the predictions for immersion in water at 23°C (based on equations in Table 4) shows that for system A the rate coefficients due to field exposure for strength and modulus need to be modified by 0.625 and 1.129, respectively, and those for system B by 0.646 and 1.877, respectively. This shows that the specific field environment considered in that study is replicated rather closely by the immersion environment considered herein with the strength deterioration being slightly slower in the field than as indicated by acceleration, and the modulus deterioration actually being faster in the field than indicated by deterioration.

4. COMPARISON WITH ACI-440 RECOMMENDATIONS

The American Concrete Institute guidelines [7] suggest that the design ultimate strength, f_{fu} , be determined by modifying the reported strength, f_{fu}^* , by an environmental reduction factor, C_E , such that

$$f_{fu} = C_E f_{fu}^* \quad \dots\dots\dots (2)$$

where

$$f_{fu}^* = (\bar{f}_{fu} - 3\sigma) \quad \dots\dots\dots (3)$$

\bar{f}_{fu} is the mean ultimate strength and σ is the standard deviation of the test population. For cases of exterior exposure and aggressive environments, $C_E = 0.65$, indicating that the threshold to which the FRP composite can degrade prior to being considered as below the reported value is $0.65 f_{fu}^*$. A similar restriction exists for design rupture strain. ACI-440 [17], however, assumes that modulus is not affected by environmental conditions and hence the design allowable is taken to be the value reported by the manufacturer, i.e. the average determined through testing. A comparison of the ACI recommended values with predictions from the equations determined through accelerated testing are shown in Table 4 for the three systems considered in the current investigation. Since the thickness of FRP composite jackets can be shown to relate directly to the modulus of the composite in the cases of shear strength retrofit and lap-splice clamping [21] and the modulus in the case of the systems considered herein does degrade over time (even over the short-term) the approach listed in equations (2) and (3) is used for modulus as well in this report. It is noted that the guidelines from the Concrete Society in the UK [10] do consider factors for the degradation of FRP modulus in their approach.

As can be seen from Table 5, the ACI-440 [7] values are significantly lower than the nominal values determined from the as-received (i.e. without exposure) tests on the three systems. Use of the predictive equations determined through accelerated testing also shows that in the case of modulus and ultimate strain the ACI-440 values are not reached for extremely long periods of time. Since there is intrinsically a concern related both to the use of accelerated tests and the extrapolation of short-term data to extremely long periods of time the values are simply given as “> 100 years.” It should, however, be

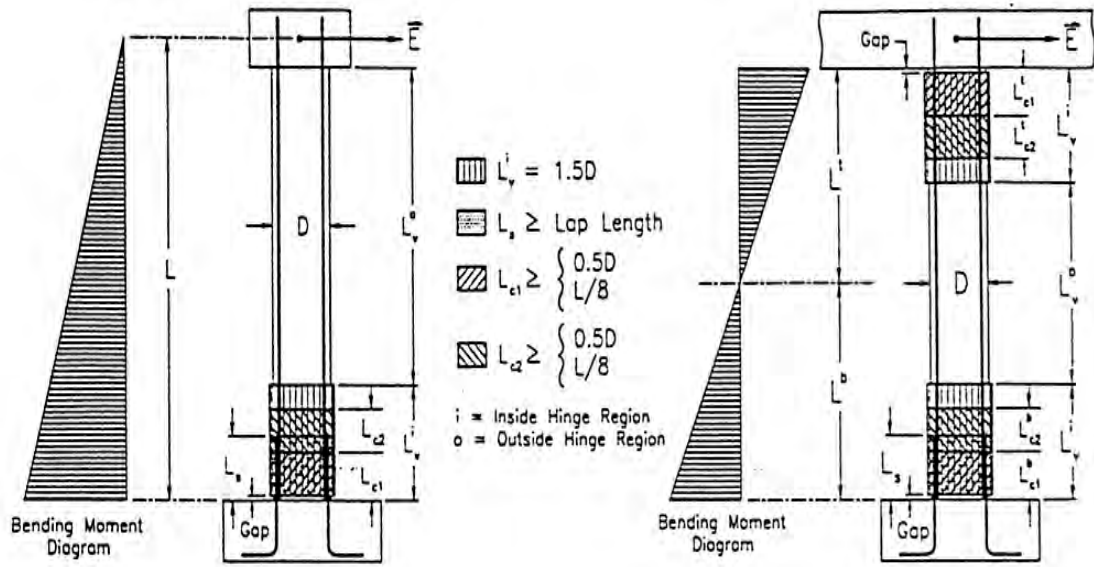
emphasized that these predictions are made based on the assumption of continuation of self-similar behavior without changes in damage mechanisms over time. As can be seen, system A shows the least amount of time required to reach the ACI value for strength, whereas system C does not show deterioration to that level within the nominal 100 year period. As noted previously the presence of the aramid fibers causes both increased moisture wicking and degradation along the interface which explains why system B takes a significantly lower time to reach the ACI value than system C. It should be mentioned that these values are determined from the perspective of immersion in water at 23 C. In reality exposure conditions in the field would consist of variation in environment, resulting, in general, in a slightly different rate of deterioration. A comparison based on the use of factors determined from the limited field data reported by Zhang et al. [15] and reported in the previous section indicates that the ACI values for strength would be reached in the field in 23.68 years and 31.74 years for systems A and B, respectively.

Table 5: Characteristic Values for Material Parameters

Characteristic	Material System	Hoop Strength f_{ju} (MPa)	Hoop Modulus E_{ju} (GPa)	Ultimate Strain ϵ_{ju} (μ Strain)
“Unexposed”	A	386	40.7	9250
	B	468.9	28.8	17992
	C	606.8	26.3	22343
ACI-440 at $C_E = 0.65$	A	224.01	24.45	4947.8
	B	251.00	16.83	8461.7
	C	380.98	16.16	13220.4
Time in years to reach the ACI 440 Values	A	14.8	> 100	> 100
	B	20.5	> 100	> 100
	C	> 100	> 100	> 100

5. BACKGROUND TO JACKET DESIGN

Reinforced concrete columns with insufficient transverse reinforcement and/or seismic detailing show three primary failure modes. Shear failure is the first and most critical mode. It may lead to the development and opening of inclined cracks, cover concrete spalling, opening of transverse reinforcement, buckling of the longitudinal reinforcement, and disintegration of the concrete core. The most vulnerable areas are in the column end regions, potential plastic hinge regions, and in the central portion between hinges. Confinement failure of the flexural plastic hinge region is the second column failure mode. It may lead to flexural cracking, cover concrete crushing and spalling, buckling of the longitudinal reinforcement or plastic hinge deterioration. These failures are considered less critical because of their large inelastic deformations. The area most vulnerable to this failure mode is the plastic hinge region [22]. Lap splice failure is the third failure mode. When vertical cracks develop in the cover concrete and dilation increases, lap splice debonding may occur. This generally occurs where lap splices are located at the lower end of the column, forming the connection between the footing and the column. The vulnerable sections are at the lower end of a column in the lap splice region. Six design regions can be defined based on these modes, as shown in Figure 5. They are L_s , the lap splice length, L_{c1} , the primary confinement region for plastic hinge, L_{c2} , the secondary confinement region adjacent to the plastic hinge, L_v , the shear strengthening region where L_v^I is the shear retrofit inside the plastic hinge zone and L_v^O is the shear retrofit outside the plastic hinge zone [21].



(a) Single Bending

(b) Double Bending

Figure 5: Jacket Regions in Column Retrofit jacket regions for seismic retrofit of columns ($L_v^i=1.5D$, $L_v^o=L-2 L_v^i$, $L_{c1}^i = L_{c1}^b=0.5D$, $L_{c2}^i = L_{c2}^b=0.5D$)

To date a significant number of approaches have been proposed for the design of FRP jackets for column retrofit and reviews have been recently reported by Teng et al. [23] and will hence not be repeated herein. For the purposes of the current study, which is the investigation of durability on jacket thickness, the approach detailed by Seible and Karbhari [21] and Seible et al. [1] will be used as an example. It is emphasized that the time dependent change in material properties (as listed in Table 4) could just as easily be used with other design approaches. Since the design approach and equations are detailed in previously published work [1, 21] they are not repeated herein. Rather only the pertinent final equations are provided to facilitate ease of reference. In each case the time dependent material properties $f_j(\tau)$, $E_j(\tau)$ and $\epsilon_j(\tau)$, for the strength, modulus and strain, respectively, will be used.

The jacket thickness for shear retrofit is determined as

$$t_j^v = \frac{\frac{V_o}{\phi_v} - (V_c + V_s + V_p)}{\frac{\pi}{2} \times 0.004 E_j(\tau) D} \quad \dots(4a)$$

for circular columns, and

$$t_j^v = \frac{\frac{V_o}{\phi_v} - (V_c + V_s + V_p)}{2 \times 0.004 E_j(\tau) D} \quad \dots(4b)$$

for rectangular columns, where V_o is the column shear demand based on full flexural over-strength in the potential plastic hinge regions, ϕ_v is the shear capacity reduction factor, assumed to be 0.85 in this study, V_c , V_s , and V_p are the shear capacity contributions related to concrete, horizontal steel reinforcement and axial load, respectively, as formulated in the three component shear model [24], $E_j(\tau)$ is the time dependent value of the composite jacket modulus in the hoop direction (as described in Table 4), and D is the column dimension in the loading direction. The increase in shear strength in the section is achieved by constraining the opening of inclined cracks and with it the loss of aggregate interlock within these cracks through limiting the column dilation in the loading direction to less than 0.4% [24].

In the case of flexural hinge confinement, for circular columns, the confinement effects are provided by the radial pressure forces generated by the jacket curvature and the tensile hoop strains in the jacket generated by the dilation of the plastic hinge. For rectangular columns with a side aspect ratio of depth/width <1.5 and for columns with

side dimensions of depth/width =0.75/0.5 m, composite jackets with twice the theoretical thickness derived for an equivalent circular column of diameter D_e have performed well [21]. Ductility of the flexural plastic hinge may also be increased through confinement of the region. The required jacket thickness for confinement of the flexural plastic hinge for circular columns is determined from

$$t_j^{cl} = 0.09 \frac{D(\varepsilon_{cu} - 0.004)f'_{cc}}{\phi_f f_{ju}(\tau)\varepsilon_{ju}(\tau)} \quad \dots(5)$$

where f'_{cc} is the confined concrete compression strength (while a number of empirical formulae have been proposed for this, a conservative value can be estimated as $1.5 f'_c$ [24], $f_{ju}(\tau)$ is the time dependent strength capacity of the composite jacket in the hoop direction, $\varepsilon_{ju}(\tau)$ is the time dependent strain of the composite jacket in the hoop direction (as described in Table 4), ϕ_f is the flexural capacity reduction factor (assumed to be 0.9), ε_{cu} is the ultimate concrete strain which depends on the confinement provided by the jacket and for purposes of design is determined by moment-curvature analysis as the product of ultimate section curvature and the corresponding neutral axis depth. These can both be determined from a sectional moment-curvature analysis and can be related to the ductility factor, μ_Δ , as

$$\mu_\Delta = 1 + 3 \left(\frac{\Phi_u}{\Phi_y} - 1 \right) \frac{L_p}{L} \left(1 - 0.5 \frac{L_p}{L} \right) \quad \dots(6)$$

where L is the shear span to the plastic hinge, Φ_y is the section yield curvature and L_p is the semi empirical plastic hinge length, assumed as

$$L_p = 0.08L + 0.022 f_{sy} d_b \quad \dots(7)$$

where f_{sy} is the yield strength of the main column reinforcement and d_b is the bar diameter of the main column reinforcement, such that

$$\varepsilon_{cu} = \mu_{\Delta} \Phi_y c_u \quad \dots(8)$$

The jacket thickness in the secondary confinement region, t_j^{c2} , is taken as half the value determined in the primary region through equation (5). It is noted that in the case of a rectangular jacket the thicknesses are approximated by doubling those determined for an equivalent circular column of diameter D_e .

The relative slippage of concrete that adheres to the starter bars and the column reinforcement can be controlled with lap splice clamping using increased confinement to raise the shear-type friction. Experimental tests show an onset of debonding between 1,000 $\mu\varepsilon$ and 2,000 $\mu\varepsilon$ [24]. The dilation strain levels are often therefore conservatively limited to 1,000 $\mu\varepsilon$, and the required jacket thickness is given by

$$t_j^s = 500 \frac{D(f_l - f_h)}{E_j(\tau)} \quad \dots(9)$$

where f_h is the horizontal stress level provided by the existing hoop reinforcement in a circular column at a strain of 0.1% given by

$$f_h = \frac{0.002 A_h E_h}{D_s} \quad \dots(10)$$

f_l is the lateral clamping pressure over the lap splice length, L_s and is determined as

$$f_l = \frac{A_s f_{sy}}{\left[\frac{p}{2n} + 2(d_b + c_c) \right] L_s} \quad \dots(11)$$

where p is the perimeter of the cross-section determined by the location of the lap-spliced steel reinforcement, n is the number of starter bars, d_b is the bar diameter, c_c is the concrete cover and L_s is the lap splice length provided in the steel reinforcement.

Since the intent of this investigation is to assess the effect of FRP material deterioration over time, rather than the equations used for design, two options are incorporated for the determination of the confined concrete strength, f'_{cc} . The first option uses the conservative estimate as $1.5 f'_c$ following Priestley et al. [24], whereas the second uses the empirical form proposed by Lam and Teng [25] where

$$f'_{cc} = f'_c \left(1 + 2 \frac{f_l}{f'_c} \right) \quad \dots(12a)$$

wherein the lateral confinement provided by the composite jacket is estimated as

$$f_l = \frac{2 f_{ju}(\tau) t}{d} \quad \dots(12b)$$

where t and d are the appropriately selected jacket thickness and diameter respectively.

6. APPLICATION TO JACKET DESIGN

For purposes of elucidation of the effect of environmental deterioration on assessment of jacket thickness, 4 different specimen configurations are used, some of which have been previously described in Seible and Karbhari [21] and Seible et al. [1], and were tested on 40% scale models as reported by Innamorato and Karbhari [26]. The specimen geometry

and reinforcement details are provided in Table 6 and Figures 6(a)-(d). For purposes of jacket design a displacement ductility level of at least 8 was required.

Table 6: Summary of Material and Configuration Details and Specifications for Columns

	Seismic Deficiency Characteristic	Shear in Double Bending	Shear in Double Bending	Flexure	Lap Splice in Flexure
Column Section	Cross-Section	Circular	Rectangular	Rectangular	Circular
	Column height, H (mm)	2438	2438	3658	3658
	Shear span, L (mm)	1219	1219	3658	3658
	Column depth, D (mm)	609.6	609.6	730	609.6
	Column width, B (mm)	609.6	406	489	609.6
	Concrete cover, cc (mm)	20.32	19	19	19
	Concrete strength, f'_c (MPa)	34.45	34.45	34.45	34.45
Long. Reinf. (Grade 40)	Bar diameter, d_b (mm)	19 (#6)	19 (#6)	25 (#8) 22 (#7)	19 (#6)
	Number of bars, n	26	22	14 28	26
	Bar area, A_s (mm ²)	284	284	510	284
	Yield strength, f_{sy} (MPa)	303.16	303.16	303.16	303.16
Trans. Reinf. (Grade 40)	Bar diameter, d_b (mm)	6 (#2)	6 (#2)	6 (#2)	6 (#2)
	Bar area, A_h (mm ²)	32	32	32	32
	Spacing, s (mm)	127	127	127	127
Column Section Properties	Axial load, P (kN)	591.85	507	1780	1780
	Moment capacity, M_{yi} (kN.m)	647	619	2165	815
	Yield curvature, Φ_y (1/mm)	5.984×10^{-6}	5.472×10^{-6}	4.685×10^{-6}	6.339×10^{-6}
	Neutral axis depth, c_u (mm)	152.4	116	208	211

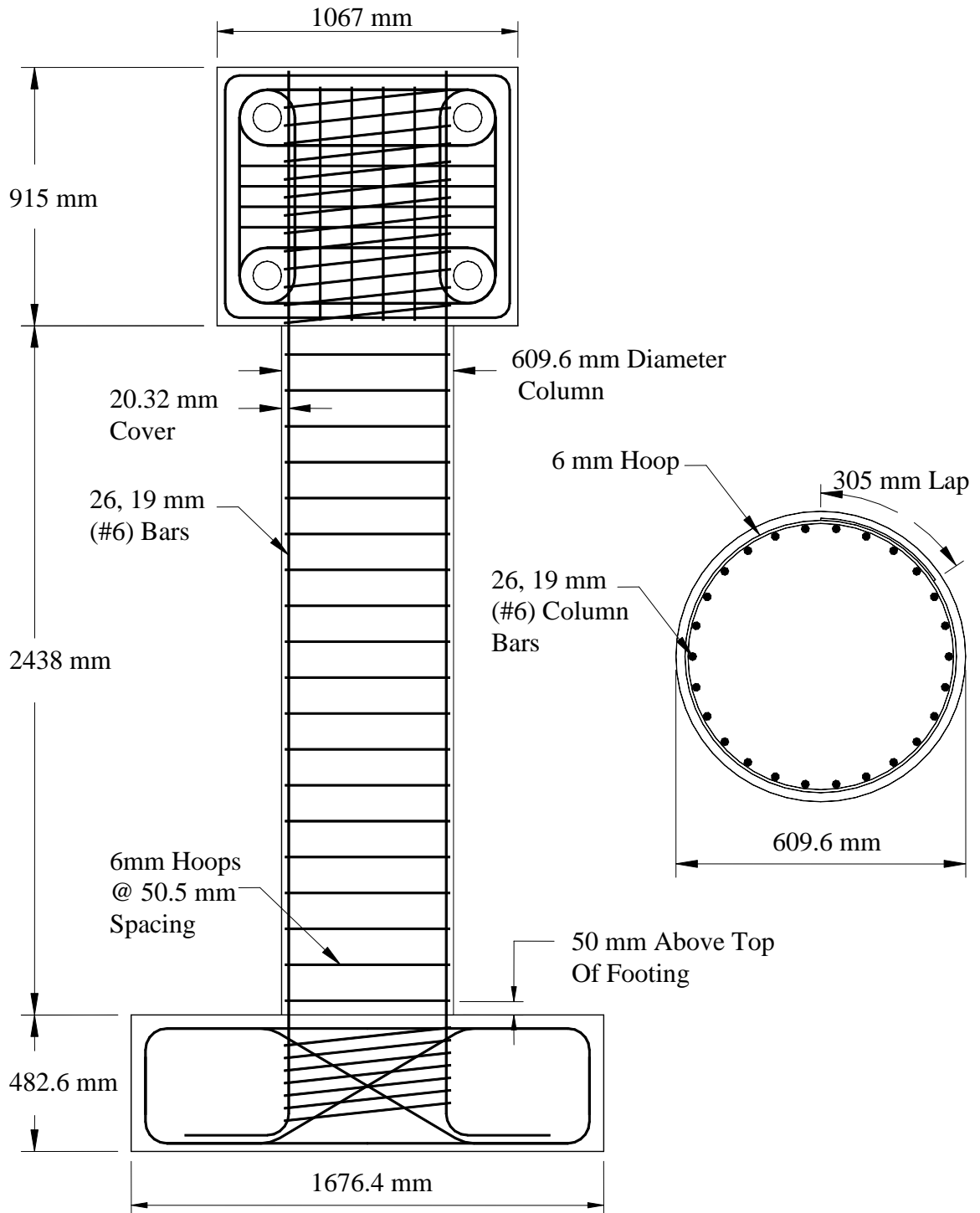


Figure 6(a): Schematics showing details of the circular column to be retrofit for shear in double bending

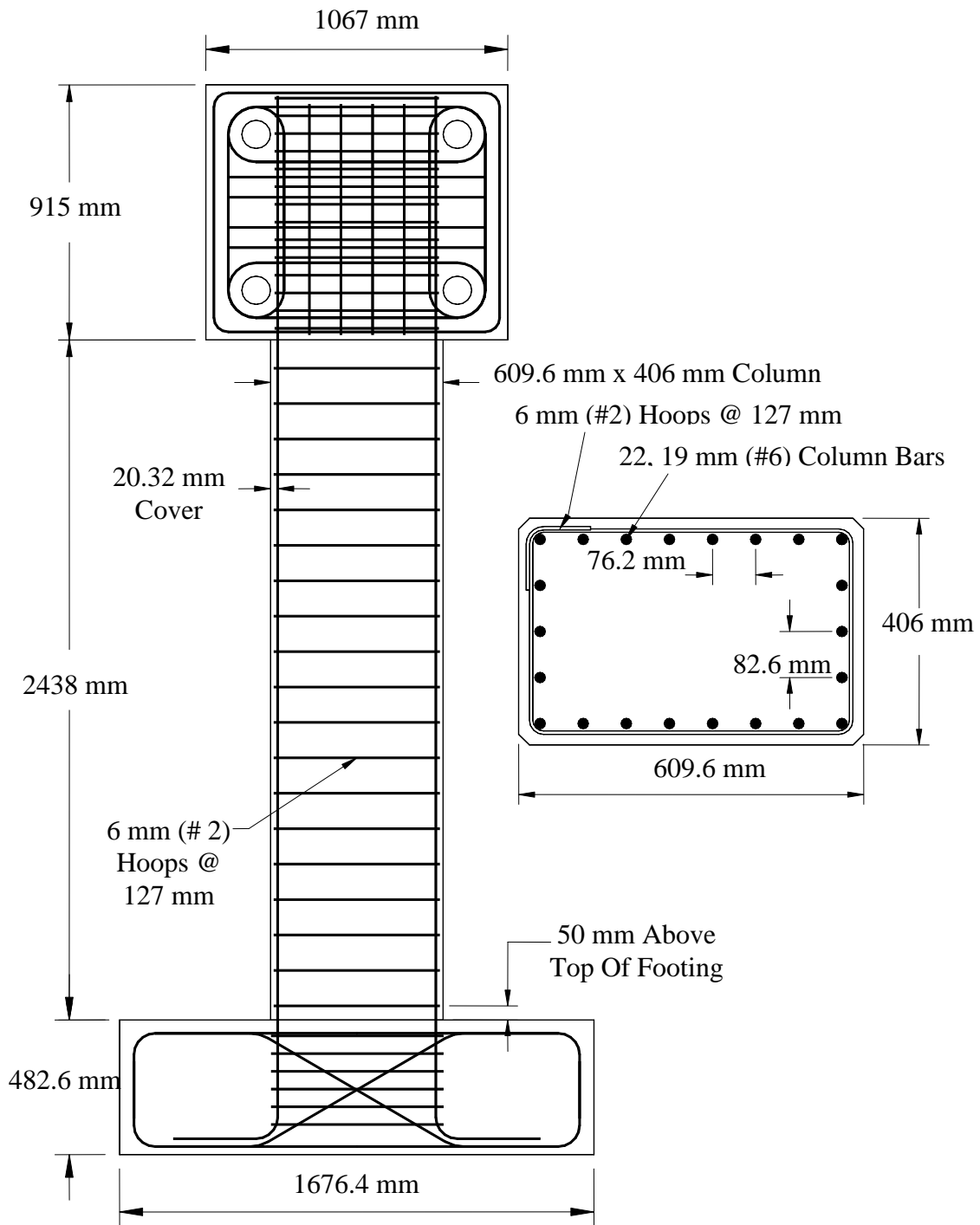


Figure 6(b) Schematics showing details of the rectangular column to be retrofit for shear in double bending

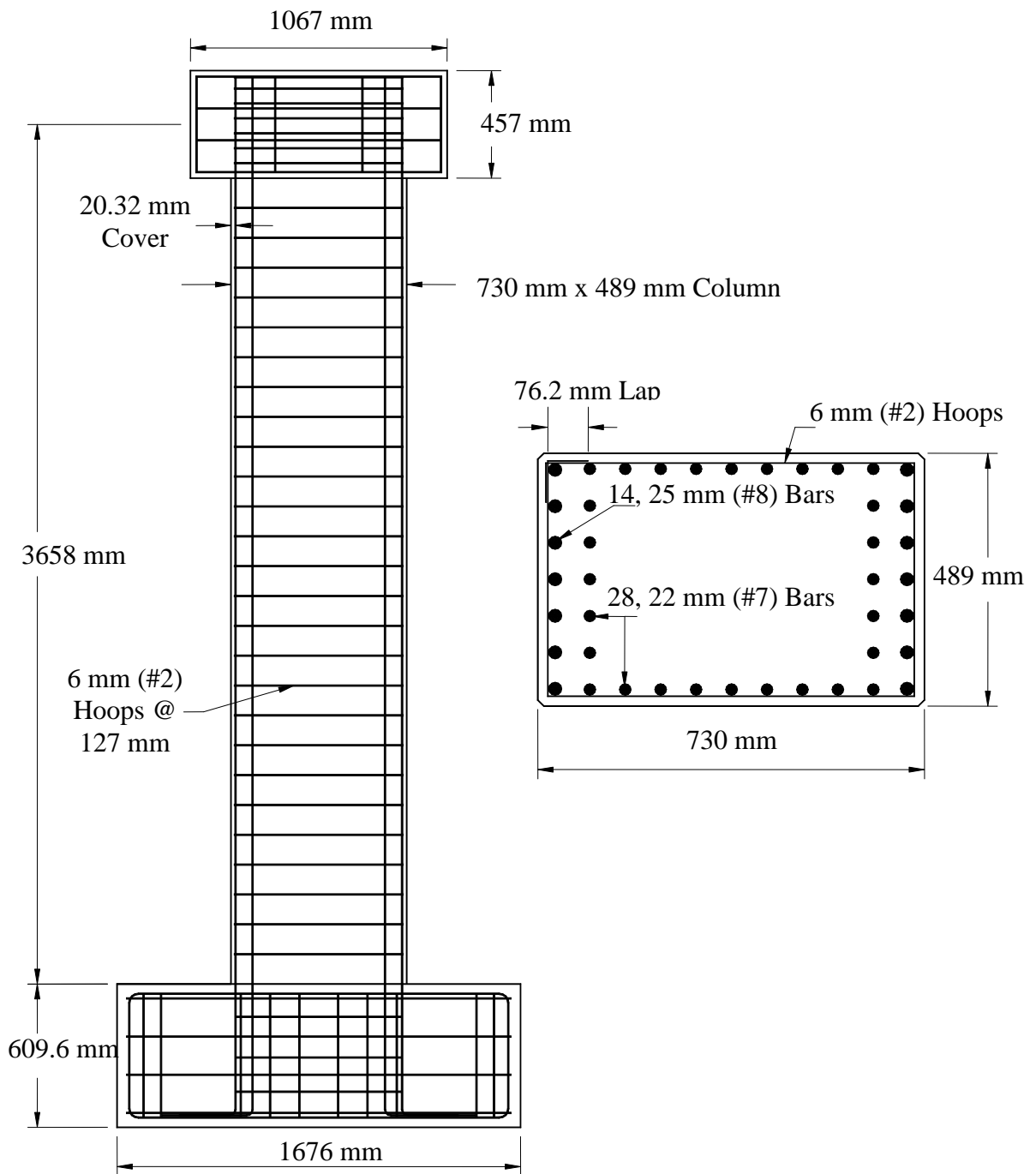


Figure 6(c): Schematics showing details of the rectangular column to be retrofit for flexure

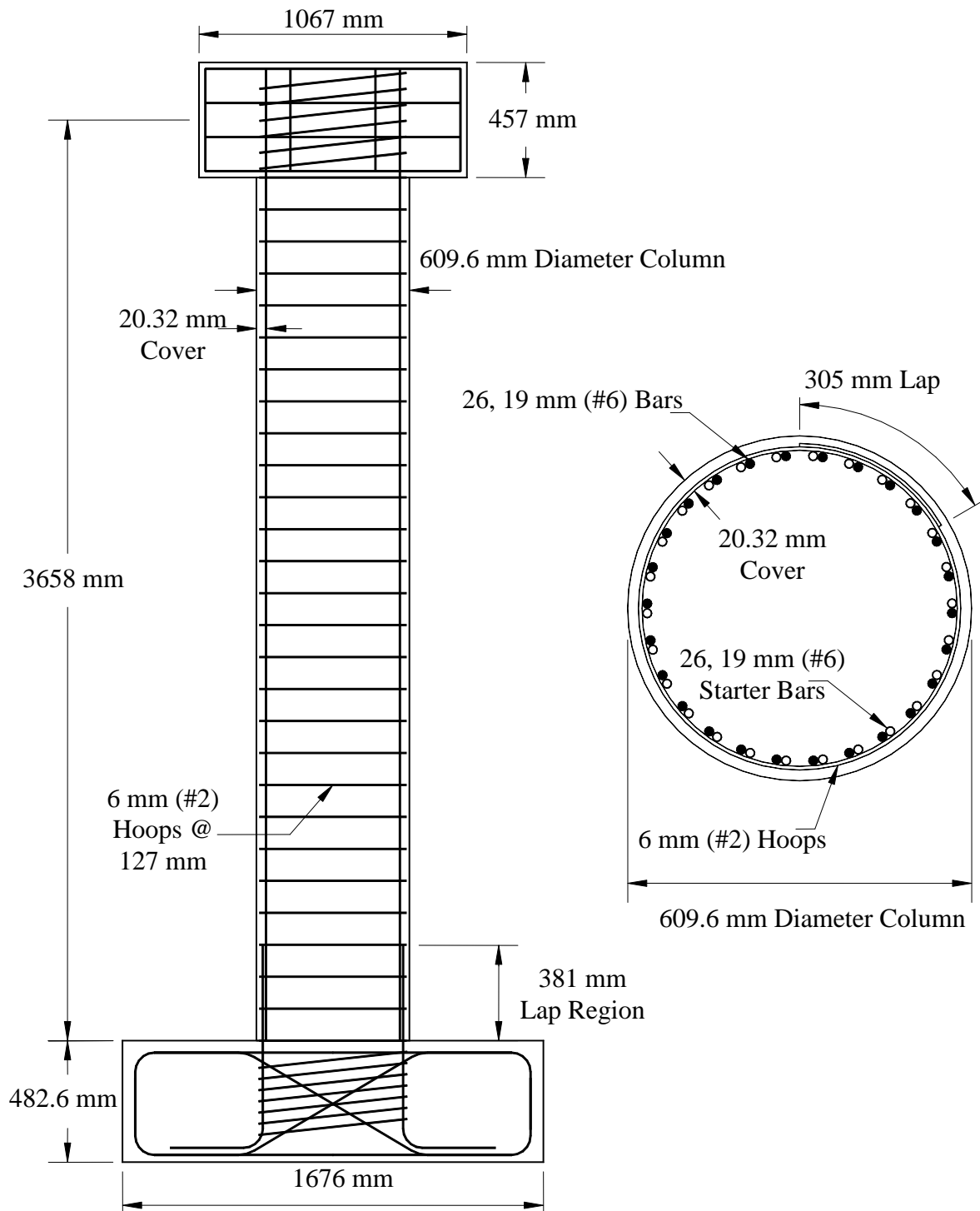


Figure 6(d): Schematics showing details of the circular column to be retrofit for lap splice clamping deficiency in flexure

Table 7: Jacket Thickness (mm) by Retrofit Zone (As Shown in Figure 5)

Case†	Material System	Design Aspect	Shear Retrofit		Flexural Confinement				Lap Splice Clamping
			f'_{cc} Using Equations 12(a) and 12(b)		$f'_{cc} = 1.5f'_{c0}$		f'_{cc} Using Equations 12(a) and 12(b)		f'_{cc} Using Equations 12(a) and 12(b)
			t_j^{vi}	t_j^{vo}	t_j^{c1}	t_j^{c2}	t_j^{c1}	t_j^{c2}	t_s
1	A	Unexposed *	4.5	2.8	8.8	4.4	5.9	2.9	-
		ACI-440 **	7.5	4.6	28.4	14.2	18.9	9.5	-
		50 Years ***	5.4	3.3	-	-	12.1	6.1	-
	B	Unexposed	6.4	3.9	3.7	1.9	2.5	1.2	-
		ACI-440	10.9	6.7	14.8	7.4	9.9	4.9	-
		50 Years	7.0	4.3	-	-	8.9	4.5	-
	C	Unexposed	7.0	4.3	2.3	1.2	1.6	0.8	-
		ACI-440	11.4	6.9	6.3	3.1	4.2	2.1	-
		50 Years	7.6	4.6	-	-	3.2	1.6	-
2	A	Unexposed	3.3	2.1	12.2	6.1	8.1	4.1	-
		ACI-440	5.5	3.5	39.3	19.7	26.2	13.1	-
		50 Years	3.9	2.5	-	-	16.8	8.4	-
	B	Unexposed	4.7	2.9	5.2	2.6	3.4	1.7	-
		ACI-440	8.0	5.0	20.1	10.3	14.1	7.0	-
		50 Years	5.2	3.3	-	-	12.3	6.2	-
	C	Unexposed	5.1	3.2	3.2	1.6	2.1	1.1	-
		ACI-440	8.3	5.3	8.7	4.3	5.8	2.9	-
		50 Years	5.5	3.5	-	-	4.5	2.2	-

3	A	Unexposed	3.1	1.7	42.9	2.5	28.6	14.3	-
		ACI-440	5.2	2.7	138.2	69.1	92.2	46.1	-
		50 Years	3.7	2.0	-	-	59.1	29.5	-
	B	Unexposed	4.4	2.3	18.2	9.1	12.1	6.1	-
		ACI-440	7.5	4.0	72.1	36.1	48.1	24.1	-
		50 Years	4.9	2.6	-	-	43.3	21.7	-
	C	Unexposed	4.8	2.6	11.3	5.7	7.5	3.8	-
		ACI-440	7.8	4.2	30.4	15.2	20.3	10.1	-
		50 Years	5.2	2.8	-	-	15.7	7.9	-
4	A	Unexposed	1.1	-	23.1	11.6	15.4	7.7	14.4
		ACI-440	1.8	-	74.5	37.2	49.6	24.8	24.0
		50 Years	1.3	-	-	-	31.8	15.9	17.1
	B	Unexposed	1.5	-	9.8	4.9	6.5	3.3	20.4
		ACI-440	2.6	-	38.9	19.4	25.9	12.9	34.8
		50 Years	1.7	-	-	-	23.3	11.7	22.5
	C	Unexposed	1.7	-	6.1	3.0	4.1	2.0	22.3
		ACI-440	2.7	-	16.4	8.2	10.9	5.5	36.3
		50 Years	1.8	-	-	-	8.5	4.2	24.1

†: represents the retrofit cases outlined in Table 6 and Figures 6(a) – 6(d)

*: Baseline prior to environmental exposure

** : Pursuant to ACI-440 procedures for consideration of durability as given in equation (2)

***: After 50 years of exposure following the predictive equations listed in Table 4

For purposes of comparison results for jacket thickness are determined in each case using three different sets of materials design values, namely

- (i) Values for hoop strength, modulus and strain as determined through testing prior to exposure;
- (ii) Values for hoop strength, modulus and strain determined using the ACI 440 (2002) criterion as listed in equations (2) and (3) with the approach applied to strength, modulus and ultimate strain; and
- (iii) Time dependent values for hoop strength, modulus and strain determined using the accelerated test determined equations reported in Table 4.

Results from the first two conditions, for each of the 4 cases of retrofit, are reported in Table 7, with the results from the time-dependent case being shown through figures for each case. It is noted that the equations (12a) and (12b) were used to determine the value of the confined concrete strength, f'_{cc} in the time-dependent case to enable changes to be made in this value as well due to deterioration in hoop strength. Details are discussed for each retrofit case separately.

Case 1: Shear Retrofit of a Circular Column in Double Bending

From Table 6 and Figure 6(a) the maximum expected plastic shear demand, V_0 , with contributions from the shear mechanisms associated with concrete in the plastic hinge region, V_c^i and outside the plastic hinge region, V_c^o , the transverse reinforcement, V_s , and the axial load, V_p , can be determined as 796 kN, 54.79 kN, 328.74 kN, 67.47 kN and 111 kN, respectively. Using a shear capacity reduction factor of $\phi_v = 0.85$, the required jacket thickness inside and outside the plastic hinge region can be calculated from

equations (4a) and (4b), respectively, using the time-dependent equations for each of the three material systems, and are shown in Table 7 and Figures 7(a)-(c) for the three material systems. To develop the full column capacity at the required displacement ductility of $\mu_{\Delta} = 8$, the required curvature ductility following equation (6) is 14.87, leading to an ultimate concrete strain, following equation (8) of 0.014 mm/mm. The jacket thickness required to provide this level of ultimate concrete strain can be determined from equation (5) using the time-dependent equations for each of the three material systems, with the thickness in the secondary confinement region, t_j^{c2} , being half the thickness, and are shown in Table 7 and Figures 7(a)-(c) for the three materials systems. Since $M/(VD) = L/D$ is less than 4 no anti-bar buckling thickness has to be added.

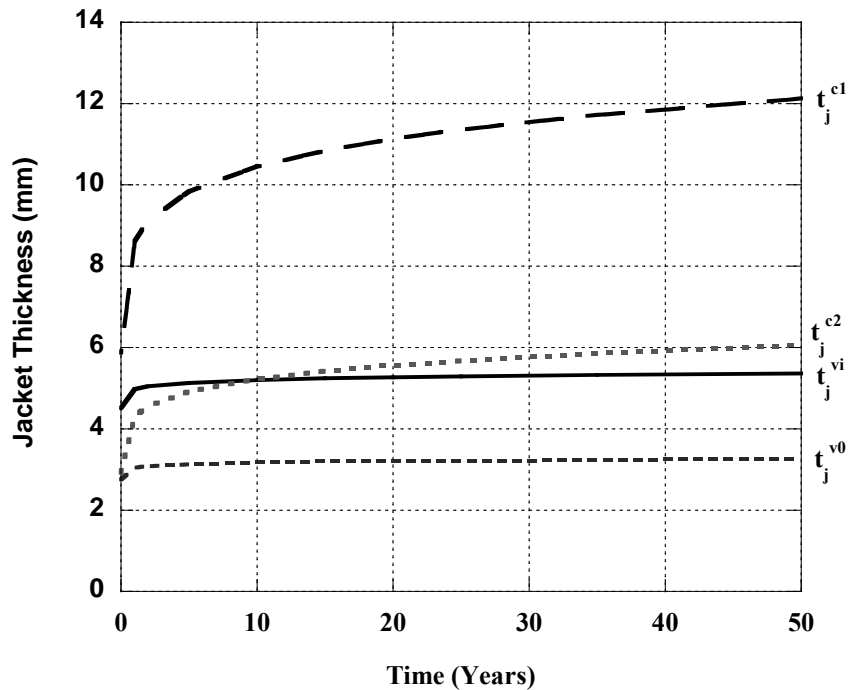


Figure 7(a) Jacket thicknesses required for circular column to be retrofit for shear in double bending for Material System A

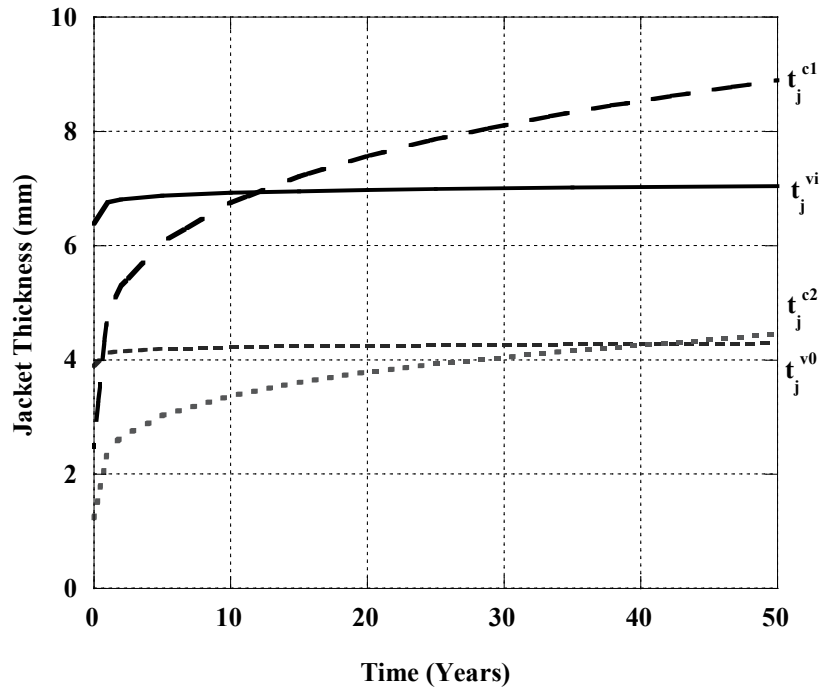


Figure 7(b) Jacket thicknesses required for circular column to be retrofit for shear in double bending for Material System B

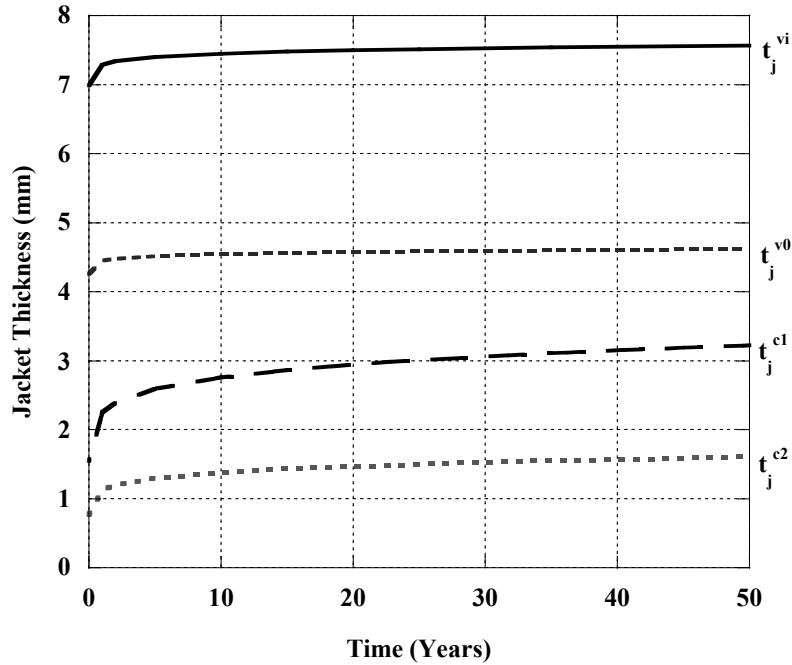


Figure 7(c) Jacket thicknesses required for circular column to be retrofit for shear in double bending for Material System C

As can be seen from Table 7 and Figures 7(a)-(c) in all cases the effects of deterioration as related to the thickness required for shear retrofit are more pronounced in the first few years, with changes being relatively small after the initial period of time. However, the change in thickness required for flexural confinement is significantly greater, indicating the faster rate of deterioration in hoop strength and strain as compared to modulus. As shown in Figure 5(b) there are essentially 4 distinct zones along the height of the column as related to requirements for FRP jacket thickness: (1) L_{c1}^b and L_{c1}^t , the primary confinement regions for the plastic hinge, at the bottom and top of the column, respectively, extending a distance of 0.5D (or 304.8 mm in this case) each, (2) L_{c2}^b and L_{c2}^t , the secondary confinement regions for the plastic hinge, at the bottom and top of the column, respectively, extending a distance of 0.5D (or 304.8 mm in this case) each, (3) L_v^i , the shear strength region inside the plastic hinge region, both at the top and the bottom extending a distance of 1.5D (or 914.4 mm in this case), which essentially overlaps and extends past the confinement region for the plastic hinge, and (4) L_v^o , the region of shear retrofit outside the plastic hinge region, spanning a distance of $H - 2L_v^i$ (or 609.2 mm in this case). Thus within the plastic hinge region the design thickness will be the larger of t_j^{c1} , t_j^{c2} and t_j^{vi} in the overlap region. As seen in Figure 7(a) in the case of Material A t_j^{c1} is always greater than t_j^{vi} , whereas t_j^{c2} is less than t_j^{vi} for a period of 9.3 years (at which point the required jacket thickness is 5.19 mm), after which the levels of material deterioration cause t_j^{c2} to be the operative thickness. In the case of Material B (Figure 7(b)) t_j^{c1} is less than t_j^{vi} for 11.8 years (at which point the required thickness is

6.93 mm) after which t_j^{c1} is the operative thickness. The thickness required in the secondary confinement region for the plastic hinge, t_j^{c2} , is always less than that required for shear retrofit, t_j^{vi} , and hence t_j^{vi} is used as the required thickness. In the case of Material C, the requirements for t_j^{vi} always dominate and hence this thickness is used over the entire plastic hinge region.

It is noted that the overall change in thickness as related to shear retrofit outside the plastic hinge region over even the extended period of 50 years is fairly small and the required increase is essentially less than the thickness of a single layer of additional material. Considering that the initial thickness of the jacket in the field is predicated by the number of layers of material used it is highly likely that the as-built thickness would more often than not be greater than that required even considering deterioration over the 50 year time period considered as an example in this investigation. As noted earlier, this however, does not hold true for jacket thickness required in regions of plastic hinge confinement. System C shows the best overall performance (i.e. the minimum change in thickness with time) whereas system A is the worst as related to the areas requiring shear retrofit, and system B is the worst in areas requiring flexural confinement. A comparison of values for thicknesses in Table 7 clearly shows the conservatism associated with the use of the ACI criteria even as compared to the 50-year predictions. In addition, it is clear that the incorporation of equations 12(a) and 12(b) rather than the simplistic form of $f'_{cc} = 1.5f'_{c0}$ as suggested by Priestley et al (1996) results in a much smaller and more

realistic (as validated through testing and limited field data) assessment of jacket thickness for flexural confinement.

Case 2: Shear Retrofit of a Rectangular Column in Double Bending

From Table 6 and Figure 6(b) the maximum expected plastic shear demand, V_0 , with contributions from the shear mechanisms associated with concrete in the plastic hinge region, V_c^i and outside the plastic hinge region, V_c^o , the transverse reinforcement, V_s , and the axial load, V_p , can be determined as 761.4 kN, 48.8 kN, 209.7 kN, 88.3 kN and 102.7 kN, respectively. Using a shear capacity reduction factor of $\phi_v = 0.85$, the required jacket thickness inside and outside the plastic hinge region can be calculated from equations (4a) and (4b), respectively, using the time-dependent equations for each of the three material systems, and are shown in Table 7 and Figures 8(a)-(c) for the three material systems. To develop the full column capacity at the required displacement ductility of $\mu_\Delta = 8$, the required curvature ductility following equation (6) is 15, leading to an ultimate concrete strain, following equation (8) of 0.0095 mm/mm. The jacket thickness required to provide this level of ultimate concrete strain can be determined from equation (5) with the modification of multiplying the equation by 2 in consideration of the rectangular cross-section with the equivalent diameter dimension being determined through ovalization as 766 mm. Using the time-dependent equations for each of the three material systems results for thicknesses are shown in Table 7 and Figures 8(a)-(c) for the three materials systems. Since $M/(VD) = L/D$ is less than 4 no anti-bar buckling thickness has to be added.

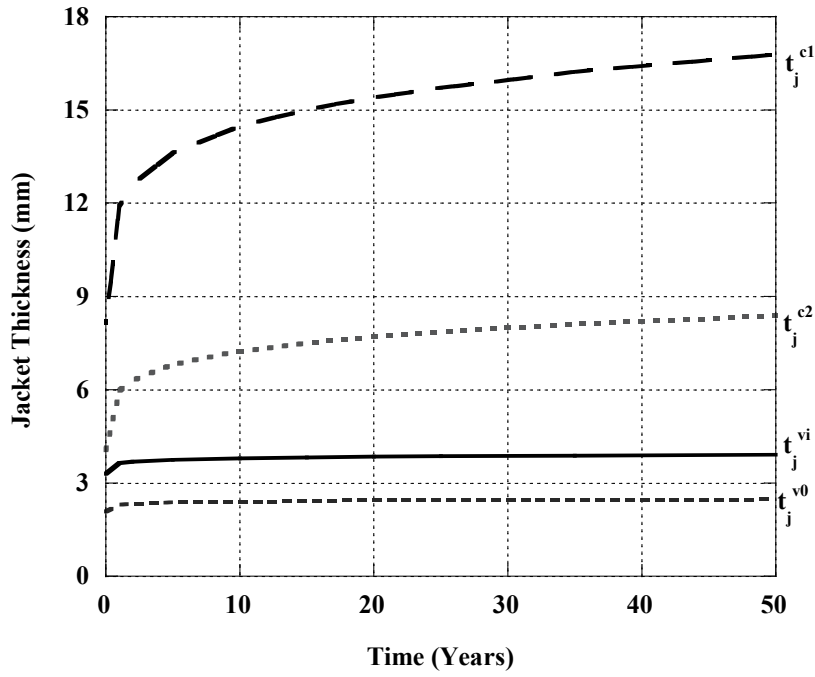


Figure 8(a): Jacket thicknesses required for rectangular column to be retrofit for shear in double bending for Material system A

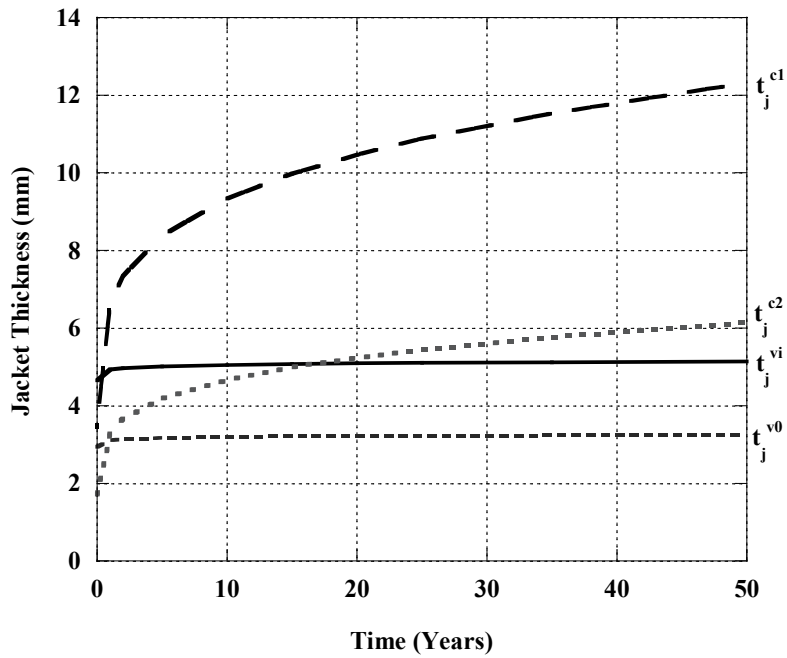


Figure 8(b): Jacket thicknesses required for rectangular column to be retrofit for shear in double bending for Material system B

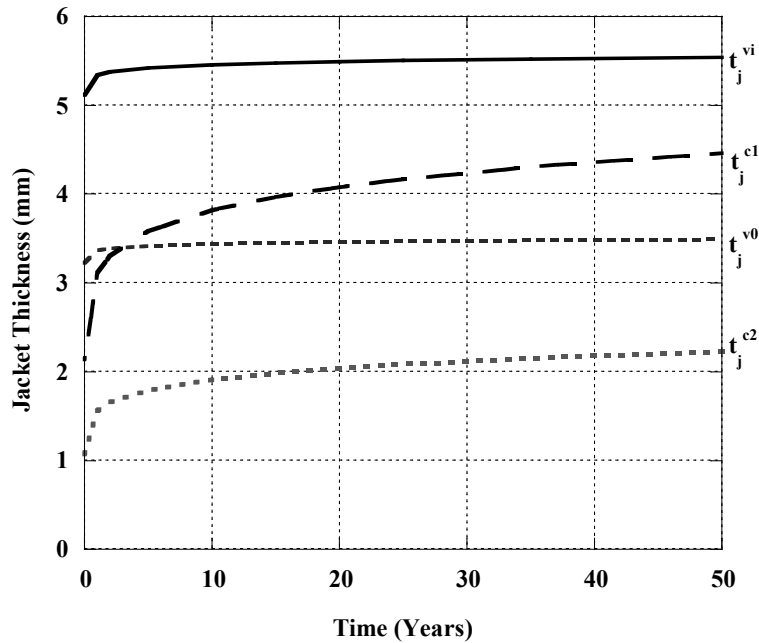


Figure 8(c): Jacket thicknesses required for rectangular column to be retrofit for shear in double bending for Material system C

As seen in Figure 8(a) in the case of Material A, in the plastic hinge region t_j^{c1} and t_j^{c2} are always greater than t_j^{vi} . In the case of Material B (as seen in Figure 8(b)) t_j^{vi} has a larger requirement than t_j^{c1} only for a very short period of time of 0.1 year, at which point the required jacket thickness is 4.8 mm, whereas t_j^{c2} is less than t_j^{vi} for a period of 16.9 years (at which point the required jacket thickness is 5.09 mm). As in the case of the circular column, discussed previously in Case 1, the requirements for jacket thickness resulting from shear retrofit demands dominate even in the plastic hinge region for Material C.

Case 3: Flexural Retrofit of a Rectangular Cantilever Column

From Table 6 and Figure 6(c) the maximum expected plastic shear demand, V_0 , with contributions from the shear mechanisms associated with concrete in the plastic hinge region, V_c^i , and outside the plastic hinge region, V_c^o , the transverse reinforcement, V_s , and the axial load, V_p , can be determined as 887.6 kN, 70.4 kN, 419 kN, 106.6 kN and 127 kN, respectively. Using a shear capacity reduction factor of $\phi_v = 0.85$, the required jacket thickness inside and outside the plastic hinge region can be calculated from equations (4a) and (4b), respectively, using the time-dependent equations for each of the three material systems, and are shown in Table 7 and Figures 9(a)-(c) for the three material systems.

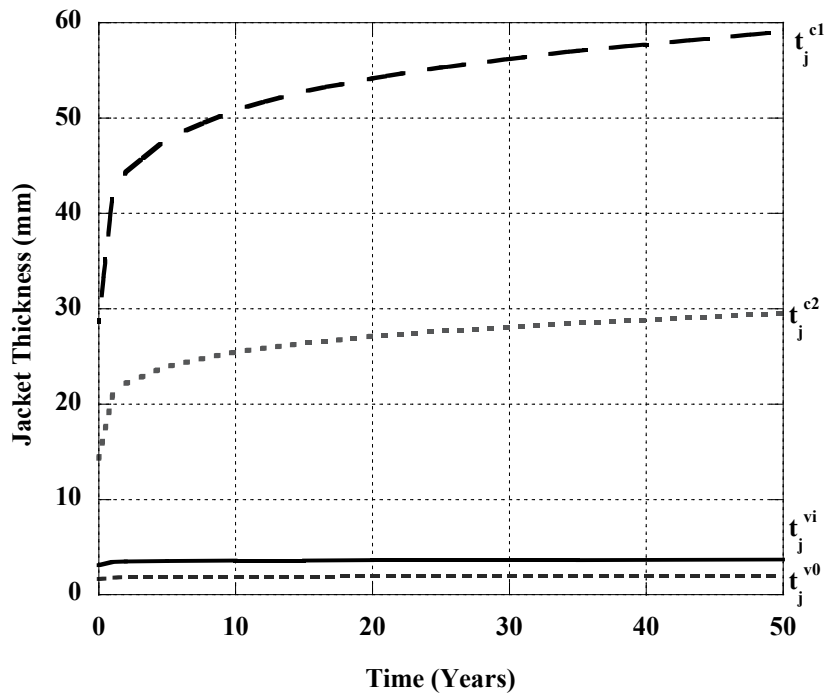


Figure 9(a): Jacket thicknesses required for rectangular column to be retrofit for flexure for Material System A

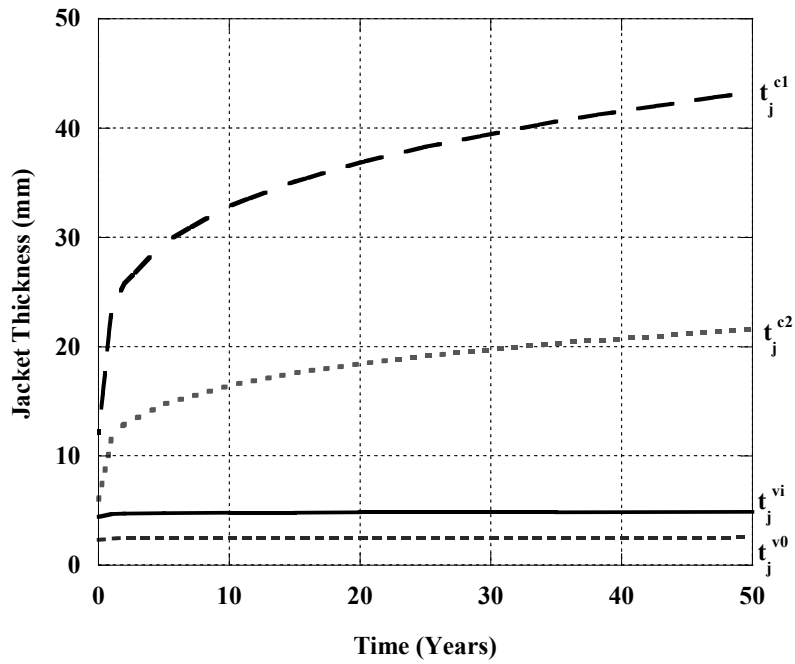


Figure 9(b): Jacket thicknesses required for rectangular column to be retrofit for flexure for Material System B

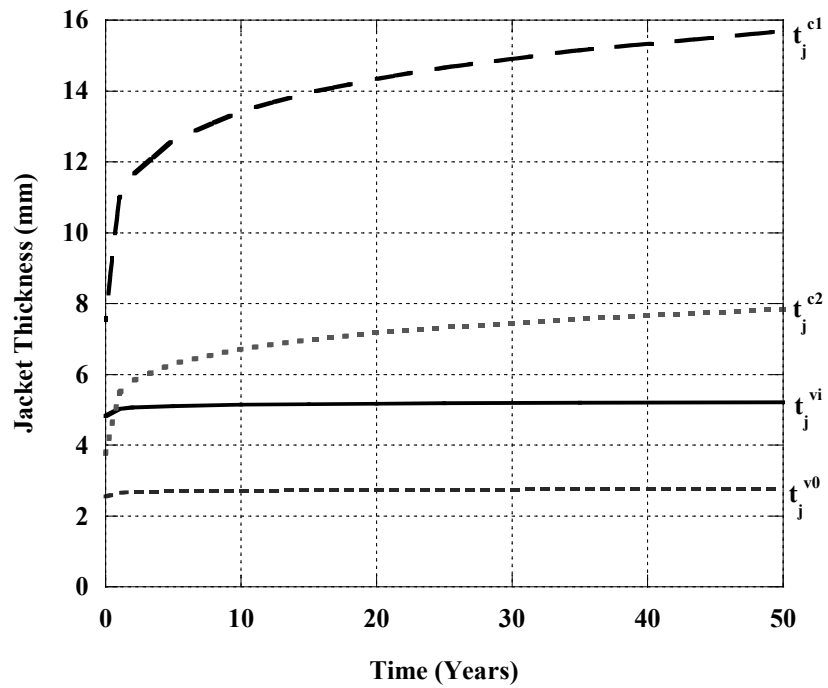


Figure 9(c): Jacket thicknesses required for rectangular column to be retrofit for flexure for Material System C

To develop the full column capacity at the required displacement ductility of $\mu_{\Delta} = 8$, the required curvature ductility following equation (6) is 20.7, leading to an ultimate concrete strain, following equation (8) of 0.0202 mm/mm. The jacket thickness required to provide this level of ultimate concrete strain can be determined from equation (5), with the modification of multiplying the equation by 2 in consideration of the rectangular cross-section with the equivalent diameter dimension being determined through ovalization as 915 mm. Using the time-dependent equations for each of the three material systems results are shown in Table 7 and Figures 9(a)-(c).

In this case, both Materials A and B show the clear dominance of flexural confinement demands in the plastic hinge region (as seen in Figures 9(a) and 9(b)), with t_j^{c1} and t_j^{c2} always being greater than t_j^{vi} . However, in the case of Material C the jacket requirements in the secondary confinement region within the plastic hinge region, t_j^{c2} , is less than that required for shear retrofit, t_j^{vi} , in that region for the short period of 0.3 years (at which point the required thickness is 4.97 mm).

From a practical perspective, the thickness required in the plastic hinge region for Materials A and B are significant and may in fact cause problems in ensuring adequate quality of performance in the field. In the case of Material A this concern is related to the excessive number of adhesive bonds required and the problems with ensuring compaction and uniform bond-line formation across that thickness, whereas in the case of Material B the concerns are associated with the larger number of inter-layer interfaces which have been shown in previous research [27] to result in faster deterioration due to

environmental exposure. In this case, the significantly lower jacket requirements of Material C are a tremendous advantage from multiple perspectives.

Case 4: Lap-Splice Clamping of Circular Flexural Cantilever Column

From Table 6 and Figure 6(d) the maximum expected plastic shear demand, V_0 , with contributions from the shear mechanisms associated with concrete in the plastic hinge region, V_c^i and outside the plastic hinge region, V_c^o , the transverse reinforcement, V_s , and the axial load, V_p , can be determined as 334.3 kN, 57.6 kN, 343.1 kN, 69.4 kN and 97.1 kN, respectively. Using a shear capacity reduction factor of $\phi_v = 0.85$, the required jacket thickness inside and outside the plastic hinge region can be calculated from equations (4a) and (4b), respectively, using the time-dependent equations for each of the three material systems, and are shown in Table 7 and Figures 10(a)-(c) for the three material systems. To develop the full column capacity at the required displacement ductility of $\mu_\Delta = 8$, the required curvature ductility following equation (6) is 22.6, leading to an ultimate concrete strain, following equation (8) of 0.0302 mm/mm. The jacket thickness required to provide this level of ultimate concrete strain can be determined from equation (5). Using the time-dependent equations results are shown in Table 7 and Figures 10(a)-(c) for the three materials systems. Since L/D is greater than 4 in this case, the anti-bar buckling criteria needs to be checked, but can be shown to result in no additional jacket thickness. The available lateral clamping pressure provided by the hoop reinforcement can be calculated from equation (10) to be 0.165 MPa, and the required clamping pressure to prevent lap splice debonding can be found from equation (11) as 2.089 MPa. The jacket thickness can then be determined from equation (9) using the

time-dependent values for modulus for each of the three material systems, and is shown in Table 7 and Figures 10(a)-(c) for the three materials systems.

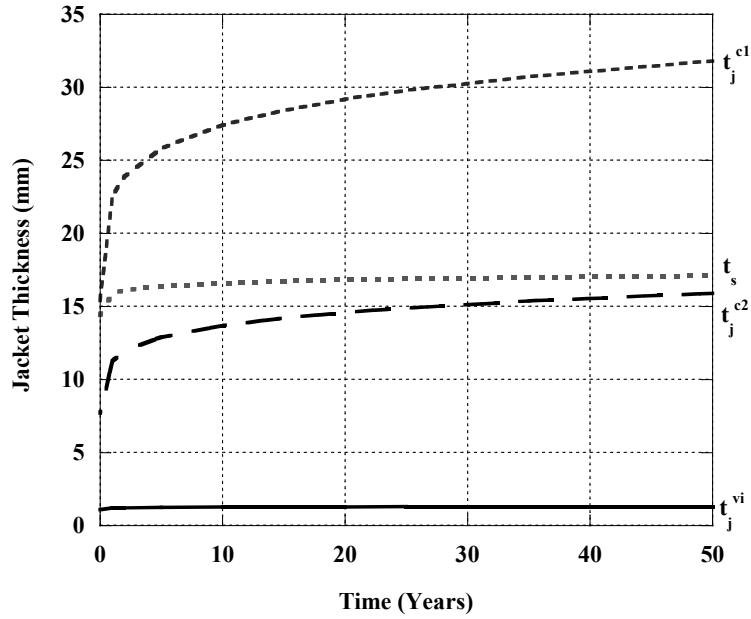


Figure 10(a): Jacket thicknesses required for circular column to be retrofit for lap-splice clamping deficiency in flexure for Material System A

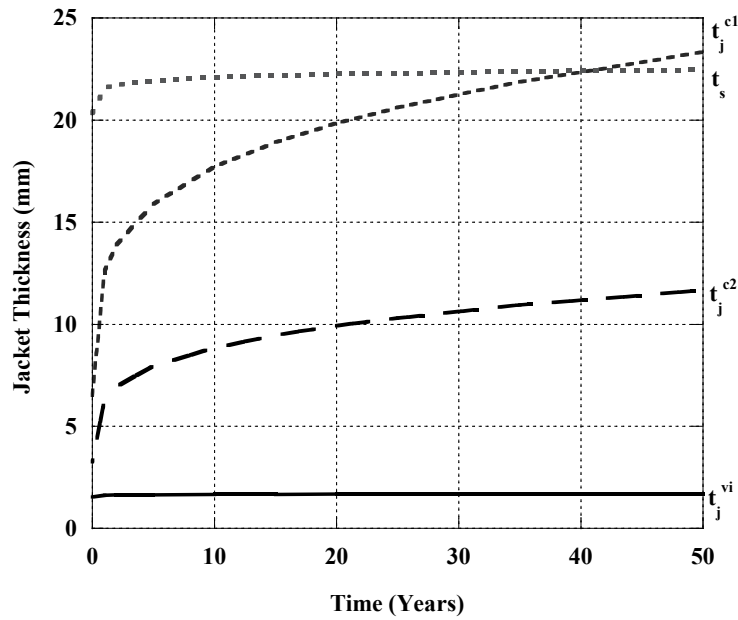


Figure 10(b): Jacket thicknesses required for circular column to be retrofit for lap-splice clamping deficiency in flexure for Material System B

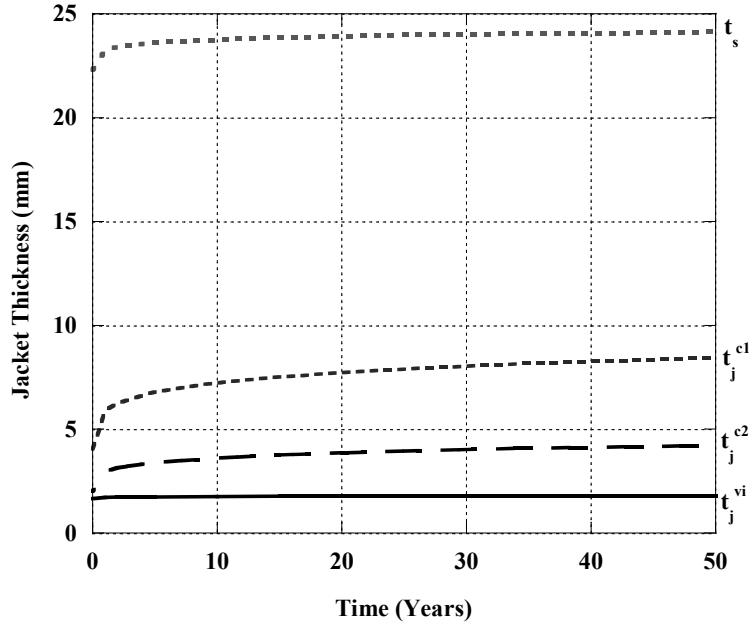


Figure 10(c): Jacket thicknesses required for circular column to be retrofit for lap-splice clamping deficiency in flexure for Material System C

In the case of lap-splice clamping retrofit of the circular flexural column, a further region of the jacket pertaining to lap-splice clamping, t_s , has to be considered. As shown in Figure 5, this region extends beyond the primary confinement region and into the secondary confinement region. Thus at the bottom of the column considered in this example, the designer has to consider jacket requirements in terms of four thicknesses, namely, t_s , t_j^{c1} , t_j^{c2} , and t_j^{vi} . As seen in Figure 10(a), for Material A, the requirement for jacket thickness pertaining to primary confinement in the plastic hinge dominates over the lap splice clamping requirement (i.e. $t_j^{c1} > t_s$) whereas the opposite is true in the secondary confinement region (i.e. $t_j^{c2} < t_s$). The thickness required for shear retrofit in the plastic hinge region is the least of the four, and can be seen to be significantly smaller at all levels than the other thickness requirements. It is noted that it is only 7.1% of the thickness required for primary confinement in the plastic hinge region at the “unexposed” level and 4.1% at the 50-year level. As shown in Figure 10(b), in the case of Material B, $t_s > t_j^{c1}$ for a period of 40.1 years (at which point the jacket thickness is 22.42 mm in this region) and $t_s > t_j^{c2}$ over the entire 50-year period considered. In fact the thickness

requirement for lap-splice clamping dominates over all others. This is also true in the case of Material C.

7. SUMMARY AND CONCLUSIONS

The durability of 3 FRP composite systems used for seismic retrofit of columns is investigated through tests conducted on ring-type specimens which have been shown to enable an assessment of both materials and structural level characteristics. Accelerated aging is enabled through the immersion of specimens in water at 4 different temperatures, three of which are used to determine predictions for long-term durability in terms of tensile strength, modulus and ultimate strain. To enable ease of use in design the predictions are developed as equations in the form

$$\frac{P(t)}{P_0} = A + B \ln(\tau) \quad \dots(13)$$

where $P(t)$ and P_0 are the characteristic at time t and 0 , respectively, A and B are constants, with B representing the rate of degradation with time, τ , in days. Comparisons of predicted data at an immersion temperature of 23°C with field exposure results from Seattle-Tacoma are used to derive correlation factors between the laboratory and field. For the specific field exposure considered the two are fairly close. The time-dependent equations for materials response are then used in conjunction with equations for determination of FRP jacket thickness for seismic retrofit, and it is shown that the use of the time-dependent approach provides a better estimate of thickness in the different regions of the columns and even enables an assessment of periods in which one set of demands may override others. This approach thus allows designers to appropriately

detail jackets based on estimated service-life requirements, and also provide ease of comparison between material systems. Results are elucidated through 4 different retrofit scenarios, and the efficacy of each of the three material systems is demonstrated and compared.

It is noted, as an aside, that the approach is amenable to extension to estimates of reliability since the material parameters can be reformulated in terms of Weibull distributions. Comparison of thicknesses resulting from the use of the time-dependent approach with the thicknesses resulting from the use of the ACI-440 recommendations for durability suggest that the ACI approach is overly conservative in this case, which could result in the development of inefficient and cost-prohibitive designs.

REFERENCES

- [1] Seible, F., Priestley, M.J.N., Hegemier, G.A. and Innamorato, D., “Seismic Retrofit of RC Columns With Continuous Carbon Fiber Jackets,” *ASCE Journal of Composites for Construction*, 1997; 1[2], pp. 40-52.
- [2] Xiao, Y. and Ma, R., “Seismic Retrofit of RC Circular Columns Using Prefabricated Composite Jacketing,” *ASCE Journal of Structural Engineering*, 1997; 123[10], pp. 1357-1364.
- [3] Saiidi, M.S., Martinovic, F., McElhaney, B., Sanders, D. and Gordaninejad, F., “Assessment of Steel and Fiber Reinforced Plastic Jackets for Seismic Retrofit of Reinforced Concrete Columns With Structural Flares,” *ASCE Journal of Structural Engineering*, 2004; 130[4], pp. 609-617.
- [4] Pantelides, C.P., Alameddine, F., Sardo, T. and Imbsen, R., “Seismic Retrofit of State Street Bridge on Interstate 80” *ASCE Journal of Bridge Engineering*, 2004; 9[4], pp. 333-342.
- [5] Pantelides, C.P., Gergely, J. and Reaveley, L.D., “Retrofit of RC Bridge Pier With CFRP Composites,” *ASCE Journal of Structural Engineering*, 1999; 125[10], pp. 1094-1099.
- [6] Pantelides, C.P. and Gergely, J., “Carbon-Fiber-Reinforced Polymer Seismic Retrofit of RC Bridge Bent: Design and In Situ Validation,” *ASCE Journal of Composites for Construction*, 2002; 6[1], pp. 52-60.
- [7] American Concrete Institute, “Guide for the Design and Construction of Externally Bonded FRP Systems for Strengthening Concrete Structures,” ACI

- Committee 440, Report 440.2R-02, 2002, American Concrete Institute, Farmington Hills, MI.
- [8] California Department of Transportation, Caltrans Memorandum to Designers, 20-4, Attachment B: Composite Column Casing, and Standard Specification. I.48_AENC.DOC, 1996.
- [9] Mirmiran, A., Shahawy, M., Nanni, A. and Karbhari, V.M., “Bonded Repair and Retrofit of Concrete Structures Using FRP Composites: Recommended Construction Specifications and Process Control Manual, “NCHRP-514, 2004, Transportation Research Board, National Academy Press.
- [10] TR-55, “Design Guidance for Strengthening Concrete Structures Using Fibre Composite Materials,” The Concrete Society, UK, 2000.
- [11] Karbhari, V.M., Zhang, J., Wu, L. and Reynaud, D., “Materials and Durability Characterization of Composite Wrap Systems Using NOL Ring Tests,” in *Composite Materials: Testing and Design Fourteenth Volume, ASTM STP 1436*, C. E. Bakis, Ed., American Society for Testing and Materials, West Conshohocken, PA, 2003, pp. 151-165.
- [12] Zhang, J.S., Karbhari, V.M., Isley, F. And Neuner, J., “Fiber-Sizing-Based Enhancement of Materials Durability for Seismic Retrofit,” *ASCE Journal of Composites for Construction*, 2003; 7[3], pp. 194-199.
- [13] Saenz, N., Walsh, E.J., Pantelides, C.P. and Adams, D.O., “Long Term Durability of FRP Composites for Infrastructure Rehabilitation,” *Proceedings of the SAMPE Conference*, Long Beach, Ca, 2005, 12 pp.

- [14] Saenz, N., Pantelides, C.P. and Reveley, L.D., "Long Term Durability of Strengthened Concrete With Externally Applied FRP Composites," Proceedings of the SAMPE Conference, Long Beach, Ca, 2005, 12 pp.
- [15] Zhang, J.S., Karbhari, V.M., Wu, L. and Reynaud, D., "Field Exposure Based Durability Assessment of FRP Column Wrap Systems," *Composites B*, 2003; Vol. 34[1], pp. 41-50.
- [16] Reynaud, D., Karbhari, V.M. and Seible, F., "The HITEC Evaluation Program for Composite Column Wrap Systems for Seismic Retrofit," International Composites Exposition '99, Cincinnati, OH, 1999, pp. 4A/1-6.
- [17] Litherland, K.L., Oakley, D.R. and Proctor, B.A., "The Use of Accelerated Ageing Procedures to Predict the Long-Term Strength of GRC Composites," *Cement and Concrete Research*, 1981; 11, pp. 455-466.
- [18] Proctor, B.A., Oakley, D.R. and Litherland, K.L., "Developments in the Assessment and Performance of GRC Over 10 Years," *Composites*, 1982; 13[2], 73
- [19] Chin, J.W., Hughes, W.L. and Signor, A., "Elevated Temperature Aging of Glass Fiber Reinforced Vinyl Ester and Isophthalic Polyester Composites in Water, Salt Water and Concrete Pore Water Solutions," Proceedings of the 16th ASCE Conference, American Society of Composites, Dayton, OH, 2001.
- [20] Karbhari, V.M., "E-Glass/Vinylester Composites in Aqueous Environments: Effects on Short-Beam Shear Strength," *ASCE Journal of Composites for Construction*, 2004; 8[2], pp. 148-156.

- [21] Seible, F. and Karbhari, V.M., “Seismic Retrofit of Bridge Columns Using Advanced Composite Materials,” The National Seminar on Advanced Composite Material Bridges, May 5-7, 1997, Washington, D.C., 1-29 pp.
- [22] Priestley, M.J.N. and Seible, F., “Design of Seismic Retrofit Measures for Concrete and Masonry Structures,” *Construction and Building Materials*, 1995; 9[9], pp. 365-377.
- [23] Teng, J.G., Chen, J.F., Smith, S.T. and Lam, L., *FRP Strengthened RC Structures*, Wiley, 2002.
- [24] Priestley, M.J.N., Seible, F. and Calvi, M., *Seismic Design and Retrofit of Bridges*, John Wiley & Sons Inc., New York, 1996.
- [25] Lam, L. and Teng, J.G., Strength Models for FRP-Confined Concrete, *ASCE Journal of Structural Engineering*, 2002; 128[5], pp. 612-623.
- [26] Innamorato, D. and Karbhari, V.M., “FRP Composite Wrap Durability Evaluation: Volume 2 – Structural Test Results Summary,” University of California San Diego, Structural Systems Research Project, Report No. TR-2001/11, 2002.
- [27] Abanilla, M.A., Karbhari, V.M. and Li, Y (2006, in press), “Interlaminar and Intralaminar Durability Characterization of Wet Layup Carbon/Epoxy Used in External Strengthening, *Composites B*.